UNIVERSITÀ DI SIENA 1240

Dipartimento di Scienze fisiche, della Terra e dell'ambiente

Dottorato in Scienze e tecnologie ambientali, geologiche e polari

30° Ciclo

Coordinatore: Prof. Roberto Bargagli

Provenance of late-Quaternary sediments from Ross Sea region (Antarctica)

Settore scientifico disciplinare: *GEO/07*

Candidato/a

Matteo Perotti

Università di Siena

Firma del candidato

Tutore

Prof. Franco Maria Talarico

Università di Siena

Firma del tutore

Prof. Franco Talarico

Eventuale/i co-tutore/i

Prof. Massimiliano Zattin

Università di Padova

Anno accademico di conseguimento del titolo di Dottore di ricerca

2017/2018

Università degli Studi di Siena
Dottorato in Scienze della Terra, ambientali e polari
30° Ciclo

Componenti del Collegio dei docenti

Personale di ruolo nelle università italiane	***Personale non accademico dipendente di altri enti e di università straniere***
Bargagli Roberto, Università di Siena Boscato Paolo, Università di Siena Carmignani Luigi, Università di Siena Corsi Ilaria, Università di Siena Corsolini Simonetta, Università di Siena Delmonte Barbara, Università di Milano Bicocca Foresi Luca Maria, Università di Siena Fossi Maria Cristina, Università di Siena Leonzio Claudio, Università di Siena Manganelli Giuseppe, Università di Siena Mantovani Enzo, Università di Siena Marchettini Nadia, Università di Siena Masini Maria Angela, Università di Genova Sandrelli Fabio, Università di Siena Talarico Franco, Università di Siena Tavarnelli Enrico, Università di Siena Viti Cecilia, Università di Siena	Brugnoli Enrico, CNR – Dip. Terra Ambiente Calamandrei Gemma, Istituto Superiore di Sanità Depledge Michael H., Universities of Exeter and Plymouth, Plymouth UK Frezzotti Massimo, ENEA Roma Gambi Maria Cristina, Stazione Zoologica Anton Dohrn, Napoli Antonio Meloni, INGV Roma

Data dell'esame finale
08/03/2018

Commissione giudicatrice
Lisa Borgatti, Università di Bologna, DICCAM
Ester Colizza, Università di Trieste, DMG
Ilaria Corsi, Università di Siena, DSFTA

Esperto/i
Nicoletta Ademollo, CNR IRSA Roma
Fabio Florindo, INGV Roma
Daniele Giordan, CNR IRPI Torino

Supplenti
Luca M. Foresi, Università di Siena, DSFTA
Marco Nigro, Università di Pisa, DMCS

Abstract

In this thesis the application of multi-disciplinary provenance methods to the study of late Quaternary sediments deposited along the edge of the continental shelf of Ross Sea and in the coastal area of McMurdo Sound (Southern Victoria Land) is treated.

In particular, petrographic analysis of gravel fraction (clasts of different grain size) has been applied to glacimarine intervals related to the last advance and consequent retreat of the Antarctic Ice Sheet on the continental shelf at the Last Glacial Maximum. The sediments were analyzed using a petrographic approach, with logging and classification of gravel-sized clasts of various lithologies in cores distributed along an E-W transect along the entire Ross Embayment. The classification and quantitative approach applied on the gravel fraction, coupled with geo and thermo- chronological techniques on sandy fractions from the same stratigraphic intervals, allowed to refine the existing data in the region dealing with drainage pattern of paleo-ice flows during the Last Glacial Maximum. In particular, in the region of Eastern Ross Sea, the acquired new data allowed to better constrain the contribution of West Antarctica Ice Sheet to the ice drainage in the Ross Embayment, while in the Central and Western Ross Sea the contribution of East Antarctic Ice Sheet has been revealed by new petrographic data that have qualitatively refined existing provenance models.

In addition, a petrographic approach on onshore unconsolidated sediments (Ross Sea Drift) transported by a grounded Ice Sheet in the McMurdo Sound region (Southern Victoria Land) has been carried out, applying a quantitative approach to various granulometric fractions. Deposits have been classified according to the lithological composition of clasts that composed these sediments. The data obtained allowed to refine the existing ice transport models in the region and to hypothesize paleo ice flow depending on the provenance of glacial erratics.

Riassunto

In questa tesi è presentata l'applicazione di metodi multi disciplinari allo studio di sedimenti tardo Quaternari deposti lungo il margine di piattaforma continentale del Mare di Ross e nella zona costiera del McMurdo Sound (Terra Vittoria Meridionale).
In particolare sono stati applicati metodi petrografici di analisi della frazione ghiaiosa (clasti di varia granulometria) in intervalli glaciomarini relativi all'ultima avanzata della calotta Antartica sulla piattaforma continentale, avvenuta nell'Ultimo Massimo Glaciale. I sedimenti sono stati analizzati con un approccio petrografico di log, mappatura e classificazione di clasti di varia natura litologica in carote distribuite lungo un transetto E-W lungo tutta la baia di Ross. L'approccio classificativo e quantitativo sulla frazione ghiaiosa, accoppiato ad indagini di natura geo- e termo-cronologica su frazioni sabbiose provenienti dagli stessi intervalli stratigrafici, ha consentito di raffinare i dati esistenti nella regione sull'andamento dei paleo flussi glaciali durante l'ultima glaciazione. In particolare nella regione del Mare di Ross orientale i nuovi dati acquisiti hanno consentito di meglio caratterizzare il contributo della Calotta Antartica Occidentale, mentre nella zona del Mare di Ross centrale e occidentale i dati petrografici evidenziano un contributo della Calotta Antartica Orientale, raffinando in questo modo i modelli di provenienza esistenti che avevano ipotizzato un contributo al trasporto glaciale da parte di entrambe le calotte, convergente nel Mare di Ross centrale.
Inoltre è stato effettuato uno studio petrografico su sedimenti terrestri trasportati dalla calotta antartica ancorata al continente nella regione del McMurdo Sound (Terra Vittoria Meridionale), applicando un approccio quantitativo su varie frazioni granulometriche di tali sedimenti sciolti, in modo da classificare i depositi a seconda della litologie che li compongono. I dati ottenuti hanno consentito di raffinare i modelli esistenti di trasporto glaciale nella regione e di ipotizzare paleo flussi glaciali a seconda della composizione litologica dei depositi e della provenienza di tali litologie.

Table of Contents

Chapter I.
Introduction

Evaluating global sea level change in the future is one of the most challenging issues for the Earth Sciences community. One of the key topic to deal with in assessing this purpose is the reconstruction of the ice sheets dynamics and the understanding of factors influencing ice flows and melting processes. Constraining the models of ice melting in the future requires an excellent comprehension of the past evolution of ice sheets in response to climate changes. Indeed, several studies dealing with evolution of ice sheets focus on the past behavior of these ice masses to somehow understand and predict their future attitude in response of climatic forcing.

With this perspective, one of the most studied area of the world is represented by the Ross Sea Embayment in Antarctica. At present, Ross Sea is hosting an extensive ice shelf, but during past glacial cycles was occupied by an ice sheet (Ross Ice Sheet, RIS) that, during the Last Glacial Maximum (LGM), grounded in proximity to the continental shelf break (Anderson et al., 2014 and references therein). This is a key area in understanding ice sheets dynamics, as it drains about one third of the Antarctic ice, discharged both by West Antarctic Ice Sheet (WAIS) and East Antarctic Ice Sheet (EAIS).

Discriminating the contribution of the WAIS and EAIS to the drainage pattern of the Ross Ice Sheet and their evolution trough time since the formation of Antarctic Ice Sheet has been the subject of several studies during the past decades. This is of fundamental importance, since the two Ice Sheets have different features and could behave differently to abrupt climate forcing. In fact, WAIS is more unstable as it is grounded below sea level and drained by fast moving Ice Streams, while EAIS is grounded on the continent and considered more stable.

In order to provide evidence on WAIS and/or EAIS contribution to ice drainage in the Ross Sea Embayment, several geomorphologic, stratigraphic, chronologic and sediment provenance studies have been carried out (Anderson et al., 1983, 1980, 1992; Shipp et al., 1999; Domack et al., 1999; Mosola and Anderson, 2006; Licht et al., 2005, 2006, 2014; Licht and Palmer, 2013; Farmer et al., 2006). At least three ice drainage models for LGM Ross Embayment have been proposed during the last decades, shown in figure 1.1. The first, made by Stuiver et al. (1981), accounts for a main contribution of WAIS to the flow lines pattern in the Ross Embayment, with a scenario of expanding west Antarctica Ice Streams and only a minor contribution of ice discharged by outlet glaciers along the Transantarctic Mountains (TAM, figure 1.1C). More recently, most of provenance studies revealed an almost even contribution of WAIS and EAIS to the ice drainage into the Ross Sea, with a more important role given to the outlet glaciers of the Transantarctic Mountains (Licht et al., 2005, 2014; Licht and Palmer, 2013; Farmer et al., 2006, figure 1.1D). In these models the confluence of the two

Ice Sheets is located approximately around 180°W longitude. In spite of the general agreement about this second model, some other hypotheses based on numerical modeling slightly differ from the latter (Golledge et al., 2012, figure 1.1E and 1.2). Recently, enhanced models has led to a more precise fitting between provenance studies and numerical models, applying a time-dependent approach instead of a steady-state model (Golledge et al., 2013).

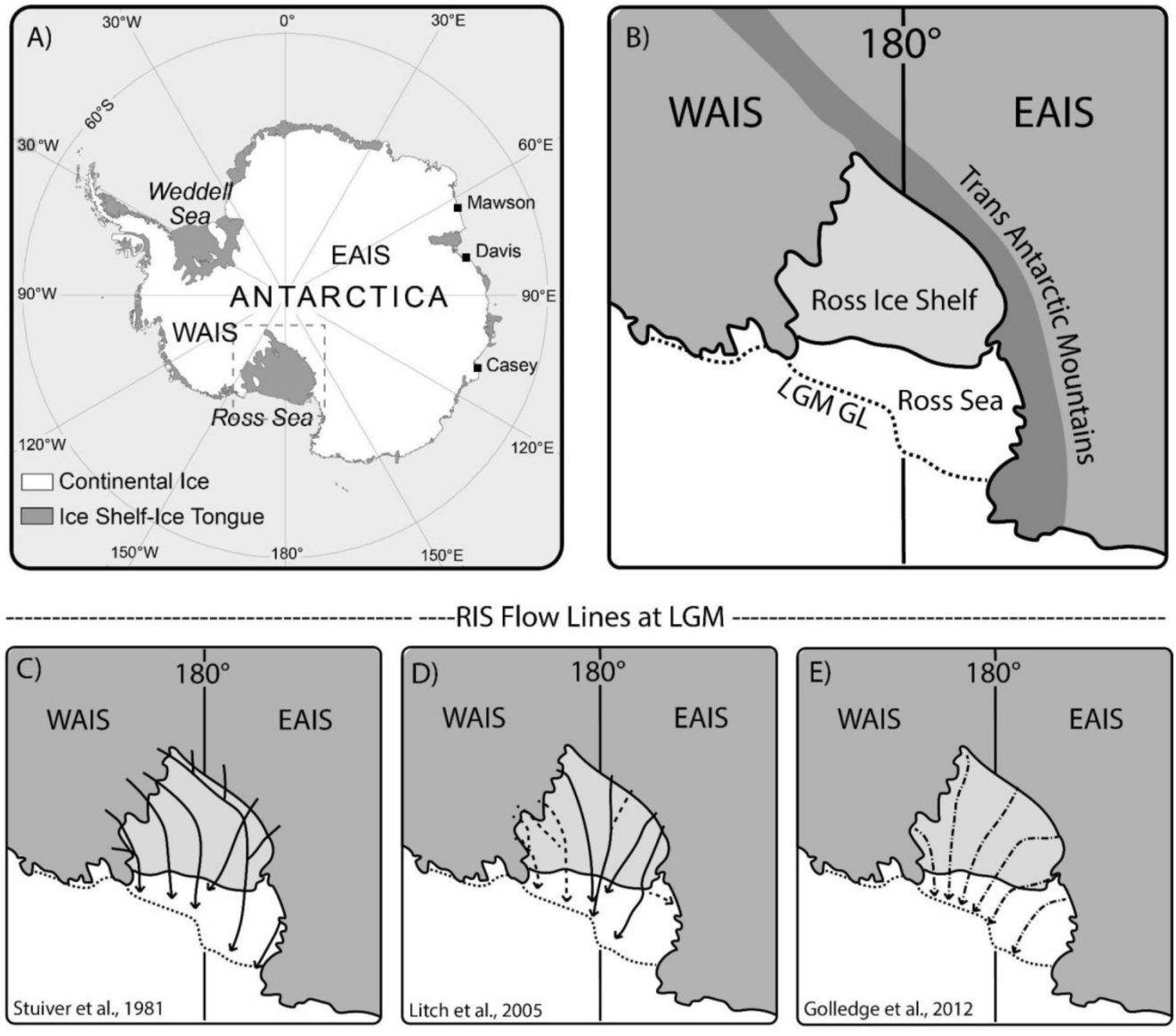

Figure 1.1 A) Antarctica maps, with location of the main study area (Ross Sea) shown by the dashed grey perimeter. B) detail map of the Ross Sea, with limit of the grounding line (GL) of the Ross Ice Sheet at LGM shown by the dotted line. C), D), E) are three different LGM ice drainage models, C and D based on sediment provenance studies, while E based on numerical modeling. Basemap of B, C, D, and E are from Licht et al. (2005).

However, despite the results obtained by previous authors, a need for more sediment provenance data through a more densely spatial coverage is still highly recommended, since so far only few samples from the region have been studied. The main objective of this thesis is providing more data and reliable evidences to support these interpretations, applying a multi-proxies provenance study based both on gravel sized and sand-sized detritus recovered from LGM sediments across the Ross Embayment and from onshore deposits in McMurdo Sound region. The relationships between detrital sediments and source areas allowed to better constrain paleo-ice flows during LGM, and discriminate different contributions both from WAIS and EAIS, also in the light of existing models from different approaches (sediment provenance, numerical models, geomorphic features).

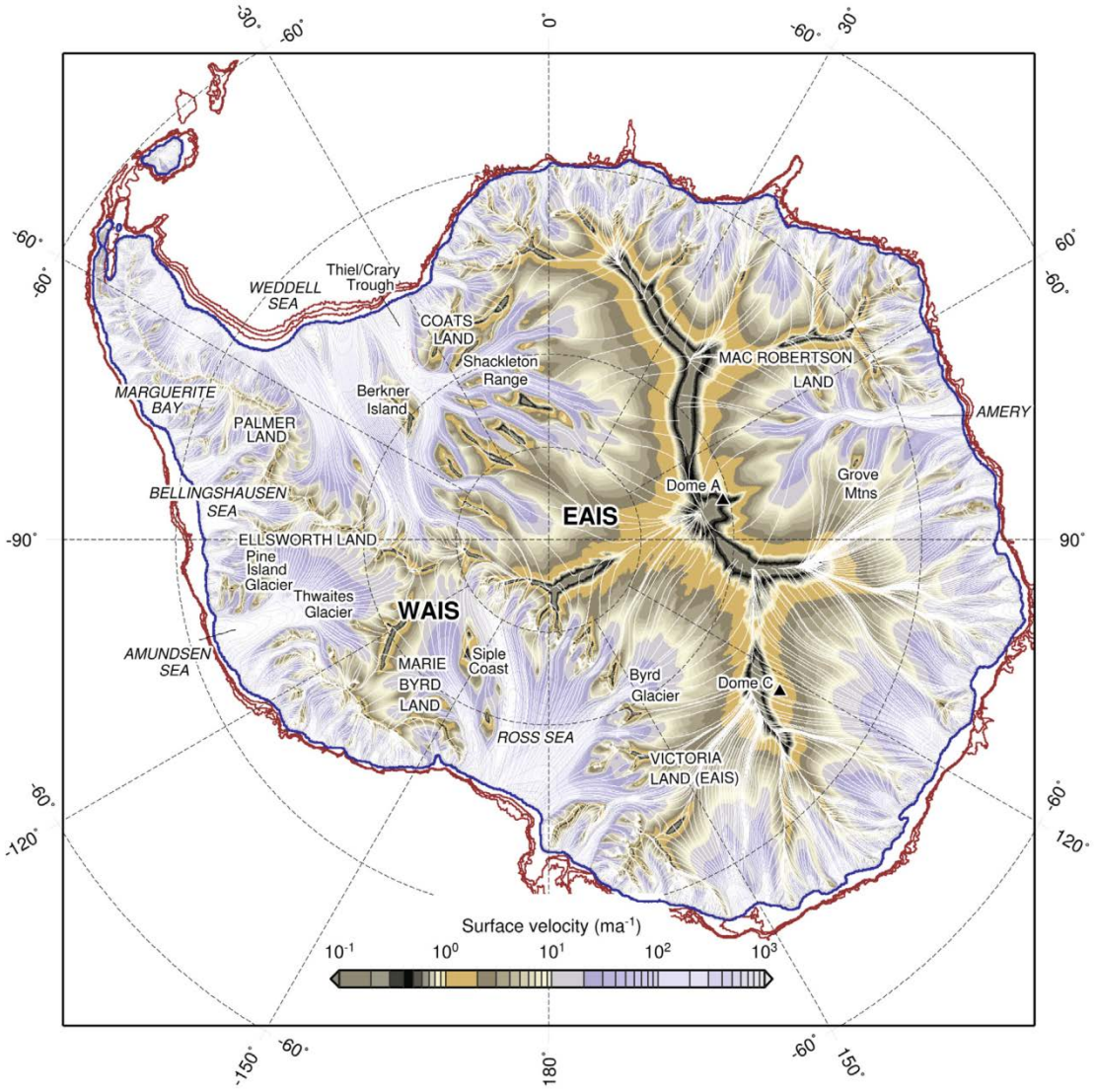

Figure 1.2 Numerical model of surface velocity distribution of glacial maximum ice sheet configuration, with flowlines showing steady-state surface transport route. Red lines indicate the continental shelf break, while blue lines indicate the limit of the modeled ice sheet (after Golledge et al., 2013).

This study was aimed to apply a multi-proxy approach in order to study provenance of LGM sediments in the Ross Embayment (offshore samples) and in McMurdo Sound region (onshore samples). The main objective was to refine existing models referring LGM ice-flows pattern in the Ross Sea with particular focus on the gravel fraction of sediments, which has been so far the less studied material from known literature. The study area has been divided into three main sector: Eastern Ross Sea, Central/Western Ross Sea, and McMurdo Sound Coast.

In the following sections an overview of the geological and glaciological setting of the Ross Sea at the LGM, as well as results obtained by previous provenance studies, are briefly introduced. Data are mainly sourced from a recent review about the LGM deglacial history of the region (Anderson et al., 2014, The RAISED Consortium et al., 2014) and from references therein.

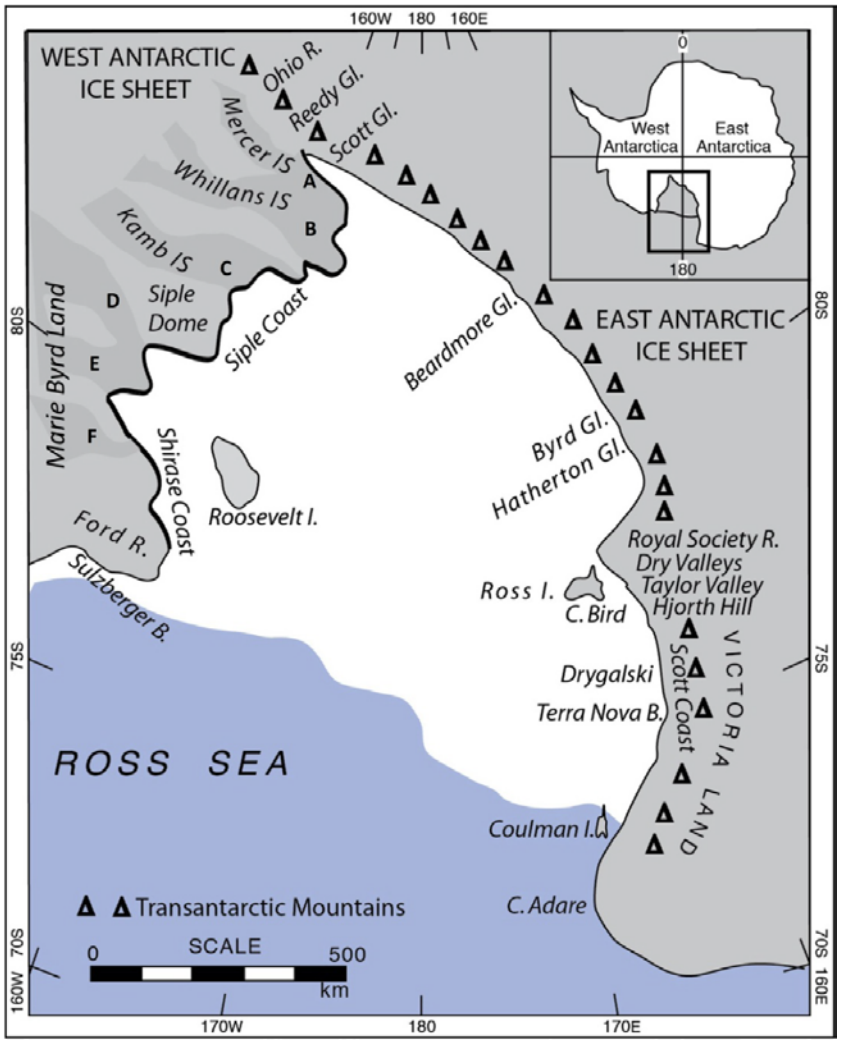

Figure 1.3. Geographic map of the Ross Sea (modified after Anderson et al., 2014), with some of the geographic names cited in the text.

1.1 Ross Sea LGM ice-sheet configuration

The Ross Sea Embayment is bordered by the 3500 km-long mountain chain of the Transantarctic Mountains to the west and Marie Byrd Land to the east (figure 1.3).

Almost one third of the ice of Antarctica is currently drained to the Ross Sea Embayment, both from East Antarctic Ice Sheet (EAIS) and West Antarctic Ice Sheet (WAIS). EAIS ice flows come from big outlet glaciers through the TAM, while most of the West Antarctica ice flows from fast moving ice streams (labelled with letters A-F in figure 1.3), without any significant rock exposures. Ice streams are originated prevalently in West Antarctica, even if some of them (Whillans Ice Stream and Mercer Ice Stream, Licht et al., 2014) could drain ice also from the southern Transantarctic Mountains sector. In this thesis, as in several previous studies, Ross Sea has been divided in three sectors, Western Ross Sea (WRS) that borders the Transantarctic Mountains area, Central Ross Sea (CRS) and Eastern Ross Sea (ERS), close to Marie Byrd Land in West Antarctica.

Several marine geological evidences support the fact that during LGM a grounded ice-sheet advanced in the Ross Embayment to the continental shelf-break (figure 1.2). The term Last Glacial Maximum is here used to indicate the period of global ice-sheet expansion occurred between ~26.5 and 19 ka BP (Clark et al., 2009), even if maximum expansion of grounded ice-sheet in part of the Ross Sea persisted longer than this time interval (Anderson et al., 2014). To reconstruct late Quaternary glacial history in the Ross Sea, hundreds of sediment cores have been studied with a sedimentological approach in order to distinguish glacimarine facies and tills (Kellogg et al., 1979; Anderson et al., 1980, 1983, 1992; Domack et al., 1999; Licht et al., 1999; Licht and Andrews, 2002; Mosola and Anderson, 2006; McKay et al., 2008, 2016). The early studies defined tills facies on the basis of the presence of over-consolidated diamicton in analyzed cores, but with the appearance of the first concept of deformation till (Alley et al., 1986), also soft-water-sediments were considered as tills. The combined data of the cited studies provided evidences of the widespread presence of glaciomarine sediments and tills on the continental shelf of the Ross Embayment, thus demonstrating that a grounded ice-sheet was present in this region in the past (Anderson et al., 2014).

The typical stratigraphic sequence of the sediment cores recovered from the western Ross Sea shows an upward succession from a basal till facies to proximal and distal glaciomarine facies, with an increasing diatomaceous material at the top of the sequence (Anderson et al., 1992; Domack et al., 1999; Licht et al., 1999; McKay et al., 2008, 2016). This succession records a progressive retreat of the grounding line at site of deposition, that passed from a sub-glacial condition to progressively sub ice shelf conditions and eventually to an open marine environment, with primary productivity and diatomaceous ooze deposition. Domack et al. (1999) identified a pelletized sub-ice shelf facies typical of the lift-off phase of the ice-sheet from the sea bottom, overlain by a mud facies lacking coarse material, associated to the so called sub-ice shelf “null zone”. This stratigraphic model is shown in figure 1.4. Other authors found different sub-ice shelf facies from cores located at present below the

Ross ice shelf, with a clast-rich diamicton overlain by laminated sand and massive mud (McKay et al., 2008). In western Ross Sea, the studied stratigraphic sequences end up with a glaciomarine diatomaceous ooze or mud with sparse ice rafted debris, that is informative about seasonally open marine conditions (Domack et al., 1999; Licht et al., 1999; McKay et al., 2008). On the contrary, in the central and eastern Ross Sea, terrigenous glaciomarine sediments lie sharply on tills, generally without a diatomaceous upper level, indicating that an almost persistent ice cover was present that limited primary productivity (Licht and Andrews, 2002; Mosola and Anderson, 2006).

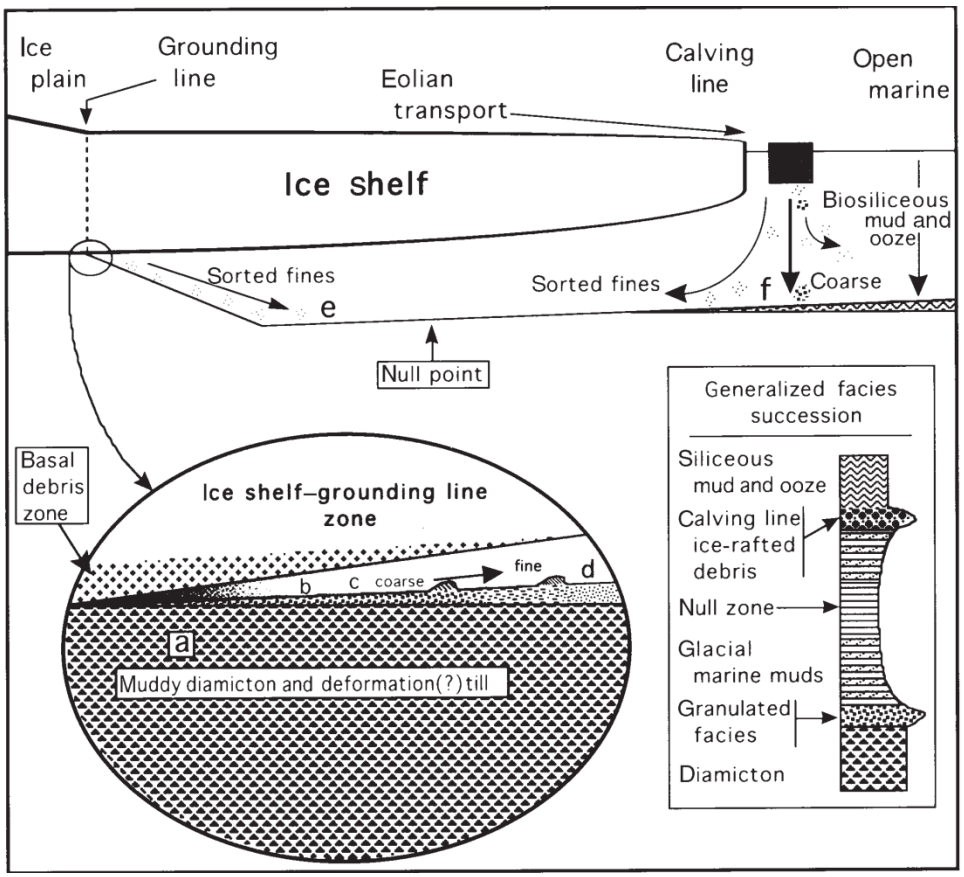

Figure 1.4. Stratigraphic model and generalized facies succession for LGM sediments in western Ross Sea (after Domack et al., 1999).

With the development of multibeam swath bathymetry, a series of geomorphic features were mapped in the Ross Sea floor, such as mega-scale glacial lineations, grounding zone wedges, drumlins, grooves, megaflutes, iceberg furrows, both from western Ross Sea (Shipp et al., 1999) and central/eastern Ross Sea (Mosola and Anderson, 2006; Bart and Cone, 2012; Bart and Owolana, 2012). These features are interpreted to be formed during the most recent glacial advance onto the continental shelf.

1.2 Paleodrainage reconstructions of LGM in the Ross Sea

Paleo-drainage reconstruction of LGM ice sheets were firstly proposed by Hughes (1973) on the basis of the presence of large bathymetric troughs on the Ross Sea floor.

The hypothesis of an expanded WAIS developed during one of the early studies of Stuiver et al. (1981) centered on the correlation between ice-sheet expansion and continental shelf morphology. Stuiver et al. (1981) led to the conclusion that LGM Ice Streams occupied the ocean floor troughs as they advanced on the Ross Sea continental shelf. Clay minerals data obtained by Balshaw (1981) gave support to the hypothesis of Stuiver et al. (1981). Based on the smectite content of analyzed tills, Balshaw (1981) assumed a western Ross Sea sediment source from the A-C Ice Streams (Mercer, Whillans, Kamb, figure 1.3) and a source of Central Ross Sea and Eastern Ross Sea sediments from D-F (Bindshadler, McAyeal and Echelmeyer) Ice Streams.

Similarly to what happened to the clay minerals of tills, Anderson et al. (1983), Anderson et al. (1992) and Tokuhashi et al. (1996) noted significant east-west variations in the composition of heavy minerals, coarse sand and pebbles of diamictons recovered in the Quaternary sequence of the Ross Sea. These authors defined seven petrological provinces (increasingly numbered from west to east) correlated to onshore rock outcrops. The petrographic limits that divide the WRS from the CRS and ERS, according to these authors, coincide with the drainage dividing the A-B (TAM receptors) ice streams from the C-D-E-F (draining MBL) ice streams.

For the reconstruction of LGM paleo ice-flows Shipp et al. (1999) used geomorphological features such as megascale glacial lineations, drumlins, etc., indicating an ice-flow direction trending to north-east in the CRS. These CRS lines are consistent with both the reconstructions of Licht and Fastook (1998) and Denton and Hughes (2000) which imply a convergence of WAIS and EAIS, and with the model of a dominant WAIS expansion.

In the past, provenance studies gave few direct evidences of correlation between Ross Sea sediments and onshore rock outcrops, in particular in West Antarctica where rock exposures are sparse and rare. The first petrographic analysis of tills recovered beneath Whillans and Kamb Ice Streams were made by Tulaczyk et al. (1998). Later, for the first time Licht et al. (2005) analyzed with petrographic point counting techniques LGM tills from Ross Sea and from beneath the main Ice Streams, thus allowing a precise correlation between detrital sediments deposited offshore and at the head of the main Ice Streams and along the Transantarctic Mountains. Moreover, isotopic analysis were carried out on the same samples by Farmer et al. (2006). More recently, other geochronological and petrographic studied were carried out by Licht and Palmer (2013), Licht et al. (2014) and Farmer and Licht (2016).

In particular Licht and Palmer (2013) studied the influence of Byrd Glacier ice in the Ross Sea and found that it split into two flows divided by Ross Bank, one in WRS and in one in western-CRS. Moreover they found that the confluence of EAIS and WAIS occurred between troughs 3 and 4 (figure 1.5). These conclusions were obtained with a three provenance tracers analysis comprising particle size analysis, sand petrography and detrital zircon geochronology. The combined results of these studies demonstrated the contribution of LGM drainage in the Ross Sea both from EAIS and WAIS,

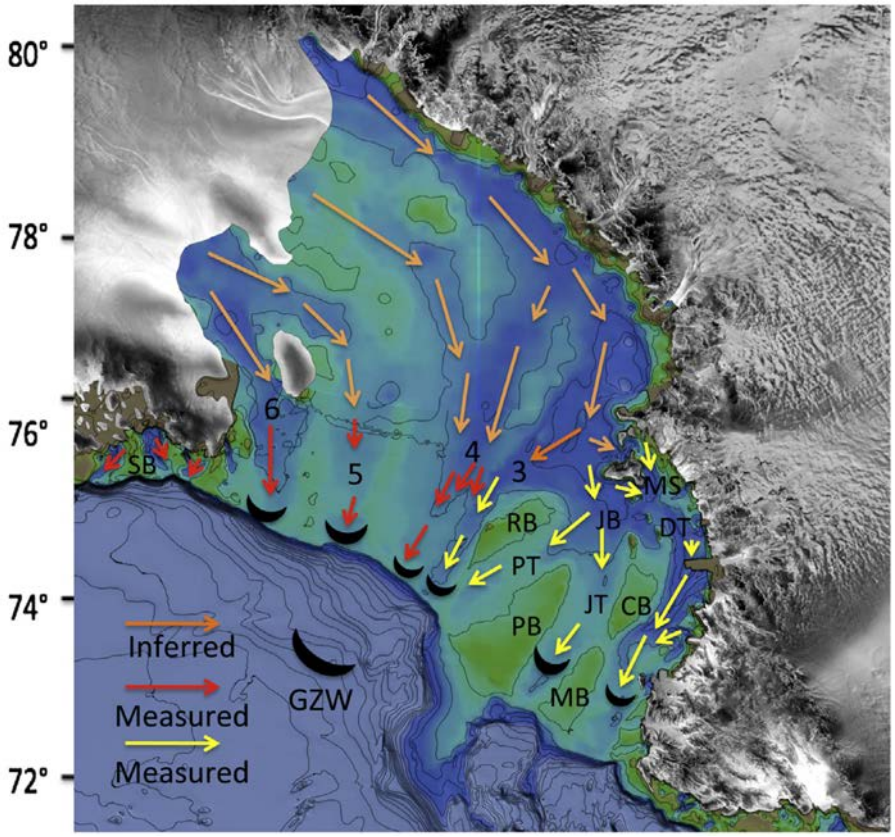

Figure 1.5. Ross Sea LGM paleo-drainage reconstruction based on combined sediment provenance analysis and orientation of linear sub-glacial geomorphic features. The boundary between EAIS and WAIS flows is located approximately at 180°W. MS = McMurdo Sound, DT = Drygalski Trough, CB = Crary Bank, GZW=Grounding zone wedges, JB = JOIDES Basin (Trough), JT = JOIDES Trough, MB = Mawson Bank, PB = Pennell Bank, PT = Pennell Trough, RB = Ross Bank, SB = Sulzberger Bay and the numbers 3, 4, 5 and 6 correspond to the numbering system used by Mosola and Anderson (2006) to designate troughs. After Anderson et al. (2014).

with the convergence of the two ice flows into the Ross Sea at about 180° longitude. The results of these combined research are summarized in figure 1.5.

In the region of McMurdo Sound, volcanic islands and peninsulas (Minna Bluff, Ross Island, Black and White Isalnds etc.) exerted strong influence on the ice flow pattern during LGM (Stuiver et al., 1981; Denton and Marchant, 2000; Hall et al., 2013). Ice flowed north and south Ross Island and from the east toward the west, as shown in the model of Denton and Hughes (2000) in figure 1.6. Moreover, high resolution swath bathymetry provided more data about the paleo-glacial drainage in McMurdo Sound (Greenwood et al., 2012) with at least four stages of evolution of the ice-sheet: (i) north-eastward flow into the Ross Sea from McMurdo Sound; (ii) westward flow from the Ross Sea around Ross Island and onto the Victoria Land coast; (iii) a deglacial phase with minor shifts in flow and grounding-line retreat into McMurdo Sound; (iv) grounding-line pinning on Ross Island during regional retreat.

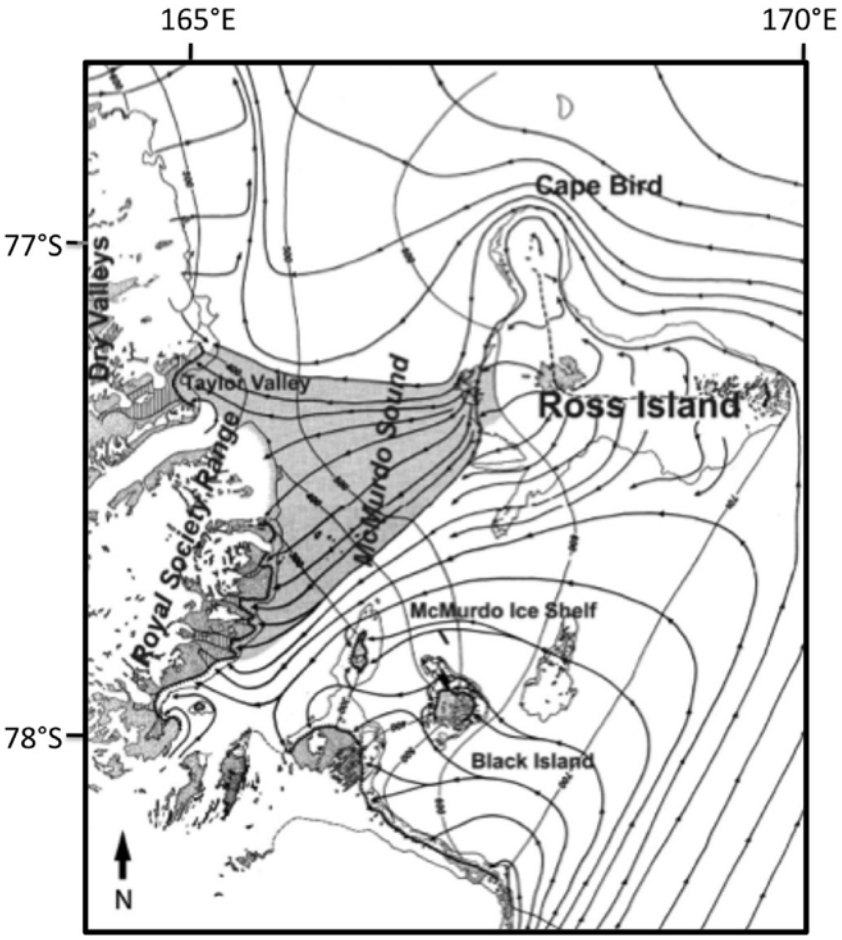

Figure 1.6. Reconstruction of ice-flow lines in the McMurdo Sound region at the LGM (modified from Denton and Marchant, 2000).Ice flowed north and south around Ross Island from the East toward the West into the Dry Valleys.

1.3 Terrestrial geologic evidences of LGM ice-sheet extent in the Ross Sea

Terrestrial evidence of ice-sheet thickness and extent during the LGM comes from (i) a widespread drift sheet (Ross Sea drift) with far-travelled erratics located on islands and peninsulas in the Ross Embayment, along the southern Scott Coast, and in the mouths of the Dry Valleys and the valleys fronting the Royal Society Range (Stuiver et al., 1981; Denton and Marchant, 2000; Hall et al., 2000a, 2013; Anderson et al., 2014); (ii) the occurrence of discontinuous, but correlative, drift sheets alongside EAIS outlet glaciers in the Transantarctic Mountains (TAM) from Reedy Glacier to Terra Nova Bay (Mercer, 1968; Bockheim et al., 1989; Orombelli et al., 1990; Denton and Marchant, 2000; Hall et al., 2013; Anderson et al., 2014); (iii) relatively unweathered drift sheets deposited on nunataks in Marie Byrd Land and inland West Antarctica (Ackert et al., 1999, 2007; Stone et al., 2003);

(iv) results from glaciological models constrained by data from ice cores, radar-detected internal stratigraphy from ice rises, and visible flow features such as flow-stripes and crevasse patterns, that are often well preserved in the Ross ice streams and in the Ross Ice Shelf (Conway et al., 1999; Parizek et al., 2003; Parizek and Alley, 2004; Hall et al., 2013).

Along the Northern Victoria Land coast, EAIS outlet glaciers merged with RIS in the Ross Embayment and left a widespread drift sheet (Terra Nova drift) that has been correlated with the Ross Sea Drift because of its weathering, elevation, morphology and ages (Stuiver et al., 1981; Orombelli et al., 1990). Geomorphological mapping of the LGM longitudinal profiles of the ice sheet near Terra Nova Bay demonstrated that elevation of RIS was nearly 400 m above sea level at the intersection of the present day coastline (Orombelli et al., 1990).

Instead, in Southern Victoria Land and in particular in the Dry Valleys region, EAIS outlet glaciers did not contribute to the RIS. In fact, LGM Ross Ice Sheet tongues of west-ward flowing ice penetrated into the mouths of Taylor Valley and in the other valleys fronting Royal Society Range (Clayton-Greene et al., 1988; Denton and Hughes, 2000; Denton and Marchant, 2000; Hall et al., 2000a; Anderson et al., 2014). Thickness of the LGM ice in McMurdo Sound region is based on the geomorphology of drift and moraines deposited in the coastline and it ranges from ~720 m above sea level on eastern Ross Island to >590 m above sea level at Cape Bird (figure 1.5), to 350-400 m asl at the mouth of Taylor Valley, and 250 m asl in the Royal Society Range foothills (Stuiver et al., 1981; Denton and Marchant, 2000; Dochat et al., 2000; Hall et al., 2000a). Reconstruction of the moraine slopes and distribution of volcanic erratics of anorthoclace-phyric phonolite in the region of McMurdo Sound show that LGM ice flowed westward around northern Ross Island and then westward and southward into the ice-free valleys (Stuiver et al., 1981; Denton and Marchant, 2000; Hall et al., 2000a; figure 1.5).

In the southern and central Transantarctic Mountains region, an unweathered, in places ice-cored, drift sheet exists adjacent to many EAIS outlet glaciers; on the basis of its appearance and absence of soil development, it has been attributed to the LGM and Holocene deglaciation (Mercer, 1968; Bockheim et al., 1989; Denton et al., 1989; Bromley et al., 2010, 2012).

In the coastal Marie Byrd Land, at the easternmost portion of Ross Embayment, Ford Ranges were overrun by an ice sheet during the LGM, with an ice sheet elevation of more than 800 m asl than present close to the coast and less thickening farther inland (Stone et al., 2003; Anderson et al., 2014).

In the inland regions of the WAIS, LGM deposits have been reported from Mt Waesche (Ackert et al., 1999) and in the Ohio Range region (Ackert et al., 2007; 2011).

1.4 Timing of LGM ice sheet advance and retreat in the Ross Sea

Acid Insoluble Organic Fraction (AIO) dates from diatomaceous and glacimarine facies have been used to date the retreat history of the RIS from the continental shelf. In spite of their uncertainties (reservoir correction, reworking of old carbon etc.), AIO ages have confirmed that geomorphic features on the floor of the Ross Sea were formed during the last advance(s) of the ice-sheet onto the

continental shelf, confirming the results of high resolution seismic stratigraphic studies (Shipp et al., 1999; Mosola and Anderson, 2006; Bart and Cone, 2012).

On the basis of AIO radiocarbon ages distribution in WRS, Licht et al. (1996) argued that the LGM grounding line was located immediately south of Coulman Island (figure 1.2), while on the basis of mega scale glacial lineations within the Drygalski Trough, Shipp et al. (1999) placed the LGM grounding line north of Coulman Island, ~50 km north of that of Licht et al. (1996). Results from the chronological study of Cunningham et al. (1999) show that the grounding line shifted south from its Coulman Island position by ~13.0 ka BP (corrected age), while by ~11.0 ka BP (corrected age) it was located close to the Drygalski Ice Tongue, suggesting a slow retreat in this time interval (Licht et al., 1996, 1999; Cunningham et al., 1999; Domack et al., 1999; McKay et al., 2008; Anderson et al., 2014). Later, it retreated faster to a location south of Ross Island ~7.8 ka BP (Licht et al., 1996; McKay et al., 2008). Recently, a minimum age of grounding line migration of 8.6 ± 0.2 cal. Kyr BP has been measured by McKay et al. (2016) from Coulman High site, nearly 60 km east of Ross Island, indicating glacial retreat and open marine conditions at this site.

Within the ERS, Mosola and Anderson (2006) acquired AIO ages from glacimarine sediment cores and argued that RIS retreated from the ERS prior than in the WRS, most likely during LGM. These hypothesis has been supported by the ages found by Licht and Andrews (2002), that show that glacimarine sedimentation in the continental shelf began as early as ~22 ka BP (corrected age). Moreover, in CRS, a middle shelf grounding zone wedge (GZW) has been dated at ~30.8 ka BP (corrected age, Bart and Cone, 2012), suggesting retreat of the grounding line from the outer shelf prior to this time and a grounding line pause sufficiently long for GZW formation (Anderson et al., 2014).

Terrestrial ages for ice retreat come from relative sea level curves derived from ages of organic material in raised beaches (Baroni and Orombelli, 1991; Baroni and Hall, 2004; Hall et al., 2004, Anderson et al., 2014). At Terra Nova Bay, radiocarbon dates of shell, seal skin, and penguin remains bracket the age of the marine limit and the timing of complete unloading of grounded ice to ~8.2 ka BP (Baroni and Hall, 2004). This is somewhat later than the timing inferred from marine records, which indicate that the grounding line shifted to about this location after ~11.0 ka (Domack et al., 1999; Licht and Andrews, 2002; McKay et al., 2008). In McMurdo Sound region, a large suite of ^{14}C dates are available from organic materials, algae within moraines deposited in ponds and glaciolacustrine sediments (Stuiver et al., 1981; Denton et al., 1989; Denton and Marchant, 2000; Hall and Denton, 2000a, 2000b). Ages from Taylor Valley LGM moraines range from ~18 to ~13 ka BP (Hall and Denton, 2000a).

South of McMurdo Sound at the Darwin/Hatherton Glacier system, analysis of development and availability of ^{14}C ages, indicate that the maximum ice thickness there was maintained until at least 13.0 ka BP, and present-day elevations were reached by 6.8 cal ka BP (Bockheim et al., 1989; Anderson et al., 2014).

Within the ERS, the emergence of nunataks in the Ford Ranges of coastal Marie Byrd Land began before ~11 ka BP (Stone et al., 2003).
As a whole, these terrestrial and marine datasets show a well defined scenario of advance and retreat of the grounding line in the WRS, with the latter, located north of Coulman Island, that began to retreat by ~13 ka BP and at ~11 ka BP was located within the trough close to the Drygalski Ice Tongue. Then, the grounding line retreated to a location north of Ross Island by ~7.8 ka BP and south to Hatherton Glacier by ~6.8 ka BP, reaching its present position around 2-3 ka BP. However, in CRS and ERS, timing of retreat remains problematic, because of the limiting number and unreliability of available ages; if the marine ages collected by Bart and Cone (2012) are corrected, these data would mean that the grounding line was farther inland from the margin of the continental shelf already by the LGM and possibly formed a sort of embayment in CRS. Thus, retreat of RIS from CRS and ERS would be synchronous in respect of that occurred in WRS. However, this hypothesis needs more ages and data from the CRS to be tested and validated (Anderson et al., 2014).

1.5 Thesis outline

The structure of this thesis is the following: **Chapter II** shows a brief introduction to the applied methods and the studied materials. **Chapter III** is a multi-proxy study of LGM tills from Eastern Ross Sea carried out in collaboration with the University of Padova (Italy): it is a paper accepted and published in 2017 in the journal Geochemistry, Geophysics, Geosytems. **Chapter IV** shows preliminary results and interpretation of petrographic data from LGM sediments in the Central and Eastern Ross Sea: it has the body of a paper that is in preparation but should be integrated with other data before submission. **Chapter V** illustrate results of a provenance analysis carried out on detrital samples collected during the XXXth Italian Expedition to Antarctica from the McMurdo Sound coastal area (Southern Victoria Land). A petrographic approach has been applied in this chapter, that has the body of a paper in preparation. Each of the single Chapter III, IV and V has its own data presentation, discussion and conclusion. **Chapter VI** summarizes the main conclusions of the three previous chapters.
In **Appendix** the petrographic descriptions and the mineral chemistry data that are not in the text are listed.

Chapter II.
Materials and methods

2.1 Introduction

In this chapter the investigated materials and the applied methods will be presented and briefly discussed. In each of the following chapters (i.e. III, IV, V) methods and sampling strategy will be presented in depth. Petrographic analyses have been the most applied analytical technique of this thesis, comprising optical microscopy and mineral chemistry analyses via scanning electron microscopy. In Chapter III also thermochronology (Apatite Fission Track) and geochronology (Zircon UPb dating) have been applied and their data have been discussed, so these analytical techniques will be briefly introduced in the following sections.

2.2 Materials

2.2.1 Ross Sea

The study area of this thesis is represented by the Ross Sea and the investigated materials are the sediments deposited into the inner continental shelf by the last advance (and consequent retreat) of the Antarctic Ice Sheet. The sedimentological signature of this processes has been described in the Introduction and more in detail in several stratigraphic studies carried out in the last decades (Kellogg et al., 1979; Anderson et al., 1980, 1983, 1992; Domack et al., 1999; Licht et al., 1999; Licht and Andrews, 2002; Mosola and Anderson, 2006; McKay et al., 2008). In particular the stratigraphic models of Domack et al. (1999) and McKay et al. (2008) are considered reliable for sediments deposited on the sea floor during and after a glacial advance.
For the purposes of this thesis, a total amount of 42 gravity piston cores collected from different scientific cruises across the Ross Sea was chosen. Applied criteria for this choice have been:

- Sediment recovery: only cores with a complete sediment recovery have been chosen.
- Apparent completeness of the sedimentary sequence: it was attempted to understand through the description of the reports of oceanographic campaigns and previous studies, if there were transitional glaciomarine deposits and diatomaceous ooze, in order to sample from a complete glacial-interglacial cycle.
- Presence of sand-size intervals in order to sample for thermochronology and geochronology dating methods.

Area	Cruise	Core	Label	Latitude	Longitude	Water depth (m)	Core length (cm)	Clast Log	N° Clasts	Sampled clasts
Sulz.Bay	NBP96-01	011-PC	96-11	-76.78	-155.44	392	389	x	259	9
Sulz.Bay	NBP96-01	014-PC	96-14	-76.59	-155.55	369	154	x	48	5
Sulz.Bay	NBP96-01	016-PC	96-16	-76.91	-155.93	1273	65	x	172	2
ERS	NBP96-01	010-PC	96-10	-77.23	-160.11	493	190	x	13	1
ERS	NBP96-01	008-PC	96-08	-77.56	-160.94	650	202	x	163	12
ERS	NBP96-01	009-PC	96-09	-77.61	-160.85	643	210	x	58	8
ERS	ELT32	027-PC	32-27	-77.78	-160.63	670	148	x	185	14
ERS	NBP99-02	017-PC	99-17	-77.72	-161.86	715	205	x	33	14
ERS	ELT32	026-PC	32-26	-78.07	-162.39	605	247	x	29	13
ERS	DF83	014-PC	83-14	-78.48	-164.14	601	277	x	40	14
ERS	DF62-01	016-PC	62-16	-77.97	-165.83	467	229			
ERS	NBP94-07	056-PC	94-56	-77.33	-166.66	441	362	x	60	15
ERS	ELT32	024-PC	32-24	-78.40	-169.13	565	433			
ERS	NBP94-07	057-PC	94-57	-77.34	-167.36	525	89	x	23	4
ERS	NBP94-07	058-PC	94-58	-77.35	-167.46	525	315	x	53	8
ERS	NBP94-07	061-PC	94-61	-77.23	-168.04	548	36	x	8	1
ERS	NBP94-07	063-PC	94-63	-77.33	-169.18	582	292	x	53	9
ERS	NBP94-07	065-PC	94-65	-77.47	-168.44	587	116	x	13	8
ERS	NBP99-02	004-PC	99-4	-78.15	-168.58	618	104	x	18	8
CRS	DF76	003-PC	76-3	-78.2	-174.183	558	671	x	49	7
CRS	DF76	008-PC	76-8	-77.533	-175.933	576	351	x	24	4
CRS	DF78	012-PC	78-12	-78.267	175.25	538	271	x	36	6
CRS	ELT27	014-PC	27-14	-77.627	175.377	720	394	x	99	4
CRS	NBP93-08	007-PC	93-7	-77.131	-175.671	388	262	x	47	9
CRS	NBP93-08	013-PC	93-13	-77.369	-177.987	676	217	x	44	9
CRS	NBP94-07	008-PC	94-8	-77.713	-178.083	544	292	x	12	10
CRS	NBP94-07	043-PC	94-43	-77.917	-178.822	725	241	x	35	10
CRS	NBP94-07	45-PC	94-45	-77.633	-179.391	661	172	x	13	5
CRS	NBP94-07	049-PC	94-49	-77.534	-177.775	670	316	x	40	8
CRS	NBP94-07	055-PC	94-55	-77.726	-177.798	676	312	x	66	6
CRS	NBP94-07	073-PC	94-73	-76.586	-178.758	644	135	x	10	7
CRS	NBP94-07	078-PC	94-78	-76.493	-179.963	375	270	x	53	8
CRS	NBP94-07	079-PC	94-79	-76.487	179.949	295	151	x	11	4
CRS	NBP94-07	090-PC	94-90	-76.76	178.535	298	359	x	115	9
CRS	NBP96-01	002-JPC	96-2	-76.452	179.881	373	419	x	112	15
WRS	DF78	014-PC	78-14	-76.5	164.0	424	334	x	98	22
WRS	DF80	133-PC	80-133	-77.083	166.167	897	258	x	9	3
WRS	DF80	134-PC	80-134	-77.15	166.183	869	260	x	26	3
WRS	DF80	189-PC	80-189	-77.2	167.883	907	193	x	34	5
WRS	ELT32	013-PC	32-13	-74.955	172.163	536	207	x	20	8
WRS	NBP94-01	002-PC	94-2	-76.284	169.704	679	174	x	37	2
WRS	NBP95-01	025-PC	95-25	-77.115	168.815	978	172	x	9	5

Table 2.1. List of sampled piston cores investigated within this thesis. Clast log includes identification, classification and counting of the granule size fraction from the analyzed intervals (>4mm). Cores are shown labeled with the label name elsewhere in the text. Abbreviations: Sulz.Bay=Sulzberger Bay; ERS= Eastern Ross Sea; CRS=Central Ross Sea; WRS=Western Ross Sea.

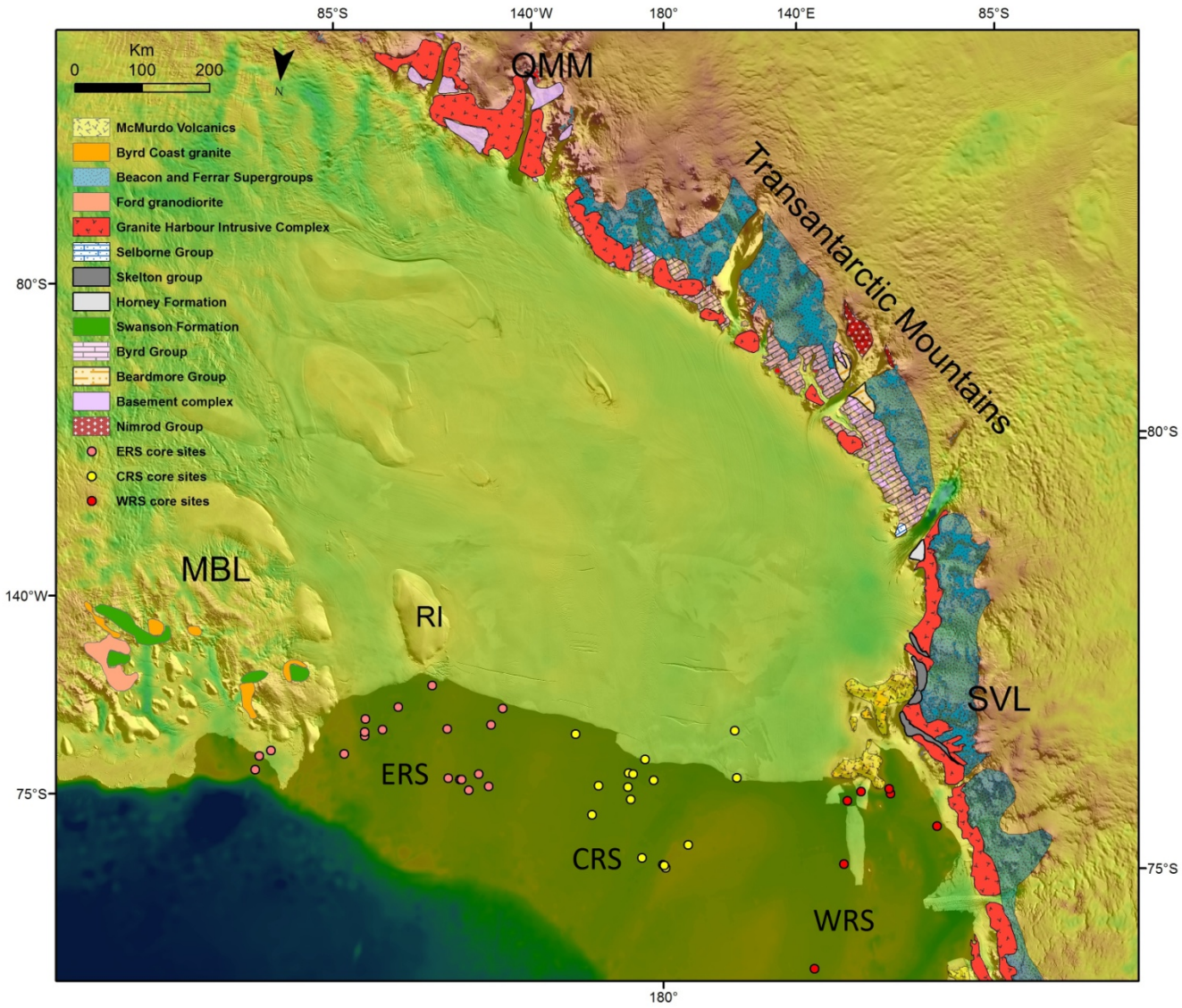

Figure 2.1. Bedmap overview of the Ross Sea region with core sites locations and geologic sketch map of the two sides of the Ross Sea Embayment. Basement rocks in the Queen Maud Mountains correspond to the outboard formations correlatives of the Byrd Group (Goodge et al., 2002) and associated Liv Group rocks (Stump, 1985). Abbreviations are the following: MBL: Marie Byrd Land; QMM: Queen Maud Mountains; RI: Roosevelt Island; ERS: Eastern Ross Sea; CRS: Central Ross Sea; WRS: Western Ross Sea; SVL: Southern Victoria Land. Geological maps are simplified from: Bushnell and Craddock (1970), Borg et al. (1989), Davis and Blakenship (2006), McGregor and Wade (1969), Carosi et al. (2007), Cox et al. (2012), Wade et al. (1977a, 1977b, 1977c, 1978).

- Geographic distribution of core sites: selected cores are distributed along an E-W transect parallel to the ice shelf margin all along the Ross Embayment, from the easternmost cores located in Sulzberger Bay (Marie Byrd Land) to the westernmost ones located in McMurdo Sound (figure 2.1).

Table 2.1 shows the list of analyzed piston cores; these have been recovered during oceanographic campaigns in the Ross Sea carried out in the past decades with different ships: the name of the cores are identified by a progressive number associated to the name of the ship (R/V Nathaniel Palmer, USCGC Glacier, USNS Eltanin) followed by the year of expedition and the number of the cruise during one particular year. These cores are taken by gravity piston core method and they sampled just the surface of the sea bottom sediments (approximately from 30 cm to few meters, see core length in Table 2.1). All of the analyzed cores are stored at the Antarctic Research Facility of the Florida State University (Tallahassee). The investigated materials have been the gravel-size fraction (i.e. granule to cobble) present within these glacimarine sediments and associated sand-sized intervals.

2.2.2 McMurdo Sound Coast

Onshore materials investigated in the chapter V of this thesis belong to the deposits called Ross Sea Drift, which is a widespread drift sheet with far-travelled erratics located on islands and peninsulas

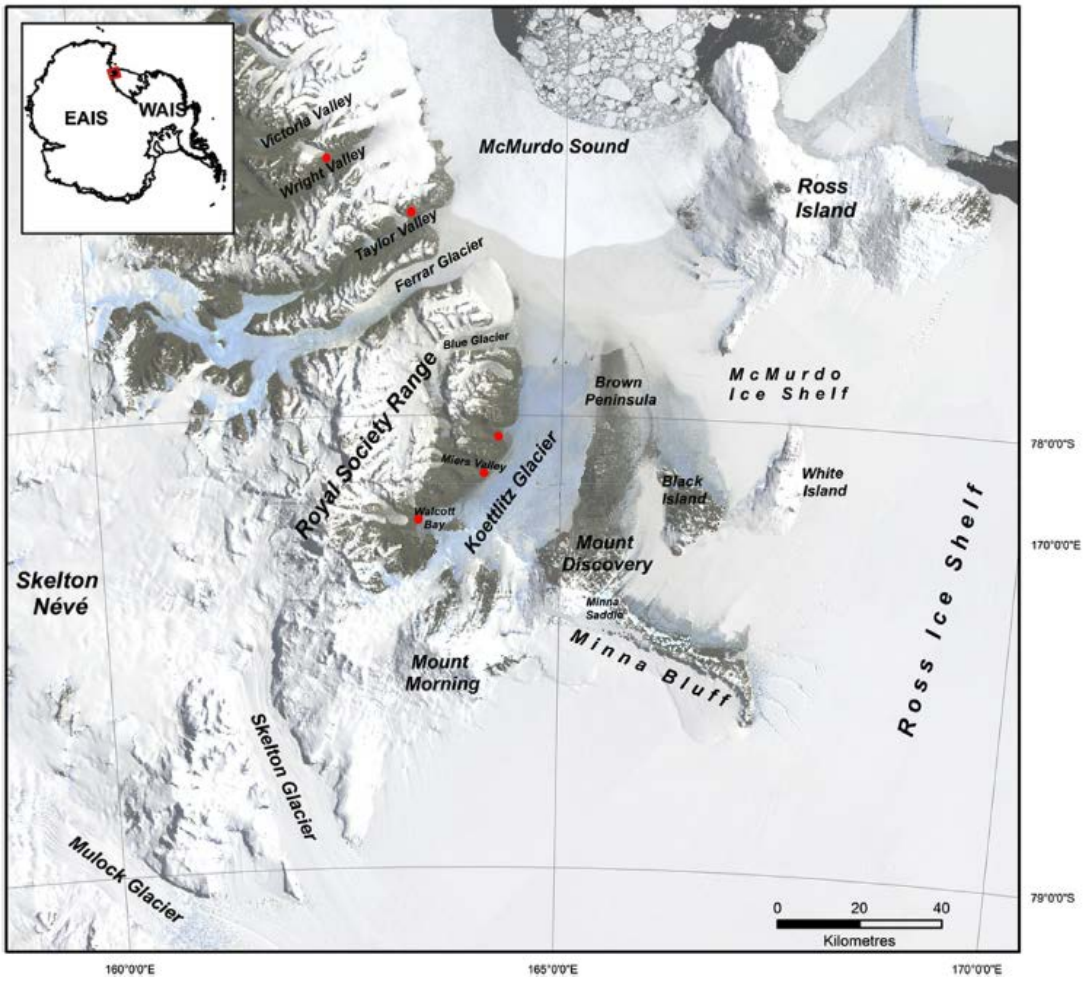

Figure 2.2. Satellite view of McMurdo Sound and Dry Valleys regions (Southern Victoria Land), with location of onshore sampling sites from Ross Sea Drift deposits (red dots, modified after Anderson et al., 2017).

of the Ross Embayment and in particular in McMurdo Sound region, in the mouths of the Dry Valleys and in the coastal foothills fronting the Royal Society Range (Figure 2.2). These bulk loose glacial sediments were analyzed with a petrographic approach, counting and classifying each lithology present from different granulometric fractions, focusing on the gravel-size clasts (i.e. granule to cobbles).

2.3 Methods

2.3.1 Petrography

The applied methods of analysis for petrographic characterization of gravel-sized clasts follow the procedure already used for CRP and ANDRILL projects (see Cape Roberts Science Team, 1998a,b and Panter et al., 2008). For each analyzed core, a clast logging was performed. Indeed, glaciomarine sequences usually are rich of coarse clasts of glacially eroded rocks, deposited in the sea bottom as ice rafted debris (IRD) or as result of massive processes in proximity of the grounding line of a marine ice sheet. The distribution and types of coarse clasts (>2mm) present in the glaciomarine sequences was examined visually in each working-half split of the core and on selected samples using thin sections. Sampling, macroscopic observations and petrographical analysis were carried out following a preliminary subdivision of clasts into two main grain-size group: pebbles with diameter larger than 8 mm, suitable for sampling for further petrological investigations; and granules and small pebbles with diameter <8mm, which were examined in the core using a hand lens. Clast logging included visual classification and counting of granules to boulder clasts all along the entire length of each core, usually with a number of clasts per 10 centimeters; clasts were grouped into 6 major rock types: sedimentary rocks (intrabasinal and extrabasinal), granitoid rocks, volcanic rocks, metamorphic rocks, dolerite and quartz. Table 2.2 shows the amount of counted granule to boulder clasts and the amount of sampled clasts from each core. The latter were sampled with a strategy focused on representativeness: clasts were taken from each of the identified lithologic group in order to carry out detailed petrological investigation with optical microscopy and mineral chemistry analysis. Moreover, sampling strategy involved the geographic distribution of cores in order to sample homogeneously the entire E-W transect of the Ross Embayment. A total amount of 314 clasts were sampled and from this group, 107 thin sections were made. Detailed sample preparation for optical microscopy and mineral chemistry analysis will be presented in each of the third, fourth and fifth Chapter.

Ross Sea Drift from McMurdo Sound region were chosen on the basis of their geographic distribution, trying to represent each of the sub-areas of the region (Wright and Taylor Valleys, Miers and Marshall Valleys, Walcott Bay); samples taken from Wright Valley belong to a drift older than LGM, at least early-middle Quaternary (Hall and Denton, 2005), while other samples refer to the LGM period. Samples were taken as bulk till sediments (preferentially from diamicton deposits, but in some cases from glaciolacustrine facies, see Chapter V). A total amount of 19 bulk till samples were dried and

sieved in order to obtain different granulometric fraction for each sample. For specific petrographic analysis the fraction >4 mm was analyzed macroscopically and some thin sections were made for representative pebble to cobble-sized clasts. Broad lithological groups were made for macroscopic analysis, and each clast was classified and counted for each sample. Moreover the granulometric fractions between 4 to 2 mm (granule-sized) and 2mm-425 µm (very coarse to coarse sand-sized) were impregnated with epoxy and made into thin sections following the standard preparation, taking care about putting as much grains as possible in the thin section plane. Thus, at least two thin sections containing lithics and minerals of two different grain sizes were made for each collected sample. The granule (2-4 mm) fraction was analyzed with the objective of identifying and classifying each lithic grains on the mount. The coarse sand fraction (425 µm-2.0 mm) was analyzed with the Indiana Point Counting method (Suttner, 1974) with an Olympus BX51 polarizing microscope equipped with an Olympus U-Fmp graduated point counting stage. The Indiana point counting method (Suttner, 1974; Suttner et al., 1981) identifies individual minerals and rock fragments (a rock-fragment consists of two or more minerals or mineral phases) and was chosen over the Gazzi–Dickinson Method (Gazzi, 1966; Dickinson, 1970) because it accounts for both lithology and mineralogy. Classifying both lithic grains and individual minerals increases the number of descriptive categories, thus allowing for a more detailed characterization of the samples. Systematic parallel transects were made with graduated stage across the thin sections, counting each grains. When a number of 300 or more counts was reached, the samples was considered statistically characterized. Not every thin section reached 300 counts, for the limited amount of available grains (for detail see Chapter V).

2.3.2 U-Th-Pb geochronology

The radiometric system U-Th-Pb is based on the decay of multiple parent isotopes to stable isotopes of Pb, each with different half-lives. Each of the parent isotopes decays following a sequence of alpha and beta decays, creating a series of intermediate daughter isotopes and eventually leading to the formation of the stable isotope of Pb. The decay reactions are:

$^{238}U \rightarrow {}^{206}Pb^*$ with $\lambda_{238} = 1.55125e^{-10}$ year^{-1}
$^{235}U \rightarrow {}^{207}Pb^*$ with $\lambda_{235} = 9.8485e^{-10}$ year^{-1}
$^{232}Th \rightarrow {}^{208}Pb^*$ with $\lambda_{232} = 4.9475e^{-10}$ year^{-1}

Where * stands for radiogenic isotope of Pb, while λ_{238}, $\lambda_{235,}$ and λ_{232} are the decay constants of ^{238}U, ^{235}U and ^{232}Th, respectively. Treating these three decay systems separately permits to build three different age equations; the latter, in minerals where the contribution of initial Pb is negligible compared to the radiogenic component, like zircon and monazite, are the following:

$$\left(\frac{^{206}\mathrm{Pb}^{*}}{^{238}U}\right) = (e^{\lambda_{238}t} - 1)$$
$$\left(\frac{^{207}\mathrm{Pb}^{*}}{^{235}U}\right) = (e^{\lambda_{235}t} - 1)$$
$$\left(\frac{^{208}\mathrm{Pb}^{*}}{^{232}Th}\right) = (e^{\lambda_{232}t} - 1)$$

Where t are the times since the system closed (e.g. the crystallization of a mineral). Since the ratio $^{235}U/^{238}U$ is considered constant in terrestrial rocks (137.88; Steiger and Jager, 1977), when the initial Pb is negligible there is no need to measure U but only the ratio ($^{207}Pb/^{206}Pb$)* can be used to calculate a date. Anyway, by measuring only isotopes of U and Pb, with these equations and ($^{207}Pb/^{206}Pb$)* ratio one can calculate three different isotopic ages (t) and, in closed system, all three would agree.

Data are usually plotted in the Concordia diagram (Figure 2.3, Wetherill, 1956), which plots $^{206}Pb^*/^{238}U$ versus $^{207}Pb^*/^{235}U$ from the same analyses. Points on the Concordia curve are where $^{207}Pb^*/^{235}U$ and $^{206}Pb^*/^{238}U$ both correspond to the same date. On the concordia plot, all samples that remained a closed system since the time of formation fall on the concordia curve; those that do not are called discordant and have experienced some form of open-system behavior.

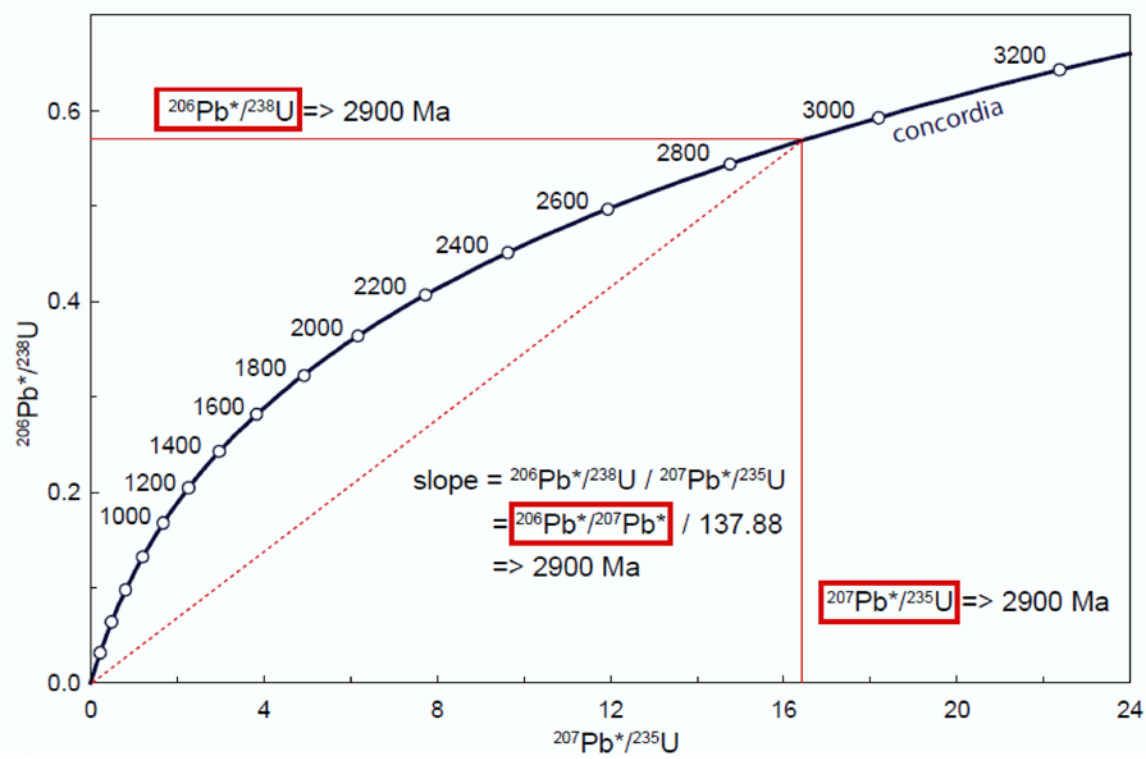

Figure 2.3. Concordia diagram showing three dates $^{207}Pb^*/^{235}U$, $^{206}Pb^*/^{238}U$ and $^{206}Pb^*/^{207}Pb^*$ for a concordant analysis. If the three dates are not equivalent, points would plot outside the curve and the analysis will be discordant (Gehrels, 2010)

Since the ratio $^{235}U/^{238}U$ is a constant value, an age could be determined also measuring $^{206}Pb^*$ and $^{207}Pb^*$, which is the slope of the straight line joining the origin with the point on the Concordia curve (figure 2.3). Practically, to plot an ages in the Concordia diagram, $^{206}Pb^*/^{238}U$ and $^{206}Pb^*/^{207}Pb^*$ ratios are measured, since these two values are calculated with an high degree of accuracy. $^{207}Pb^*/^{235}U$ value is more difficult to calculate since ^{235}U is always less abundant than ^{238}U, and can be calculated with equation $^{235}U=^{238}U/137.88$.

The system Pb/Th is not directly linked to the system Pb/U since U and Th have different chemical behavior. Usually Pb/Th measures are not reported since Pb/Th is more difficult to calculate than Pb/U, and the smaller abundance of Th compared to U make it less susceptible as chronometer in the majority of minerals. An exception is represented by monazite, where Pb/Th is preferable to Pb/U since Th is more abundant than U in such mineral.

The system Pb/U can give discordance (i.e. data plotted outside Concordia curve) results for different reasons, the most important are Pb loss and mixing. The discordance arrays have a lower intercept date which could be meaningful. In the case of Pb loss, minerals at high temperature tend to lose Pb, while U remains fixed, so Pb*/U lowers and the ages result younger. The trajectory of the Pb loss in the Concordia space remains a straight line which join the crystallization age with the event of Pb loss (figure 2.4).

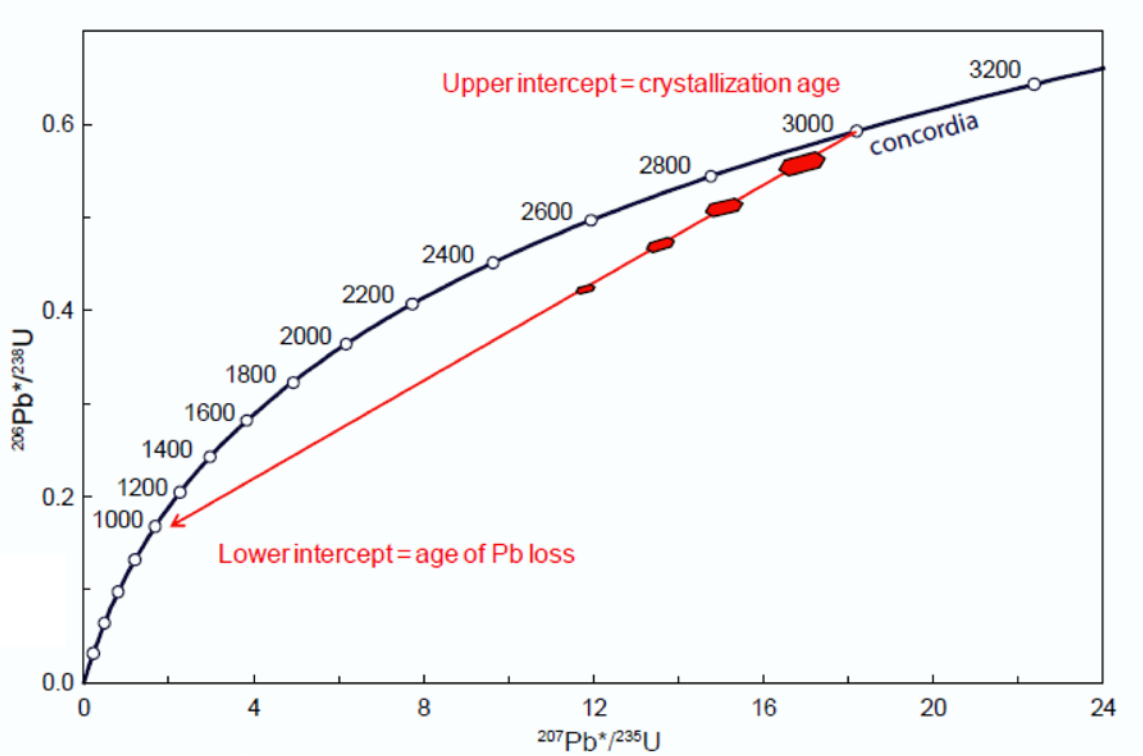

Figure 2.4. Concordia Diagram with Pb loss effect (Gehrels, 2010).

The other effect which can produce discordance arrays is the mixing process: in fact, zircon and other minerals can contain old cores and one or more generations of younger overgrowths that, if analyzed together, can lead to discordance arrays in concordia space (figure 2.5).

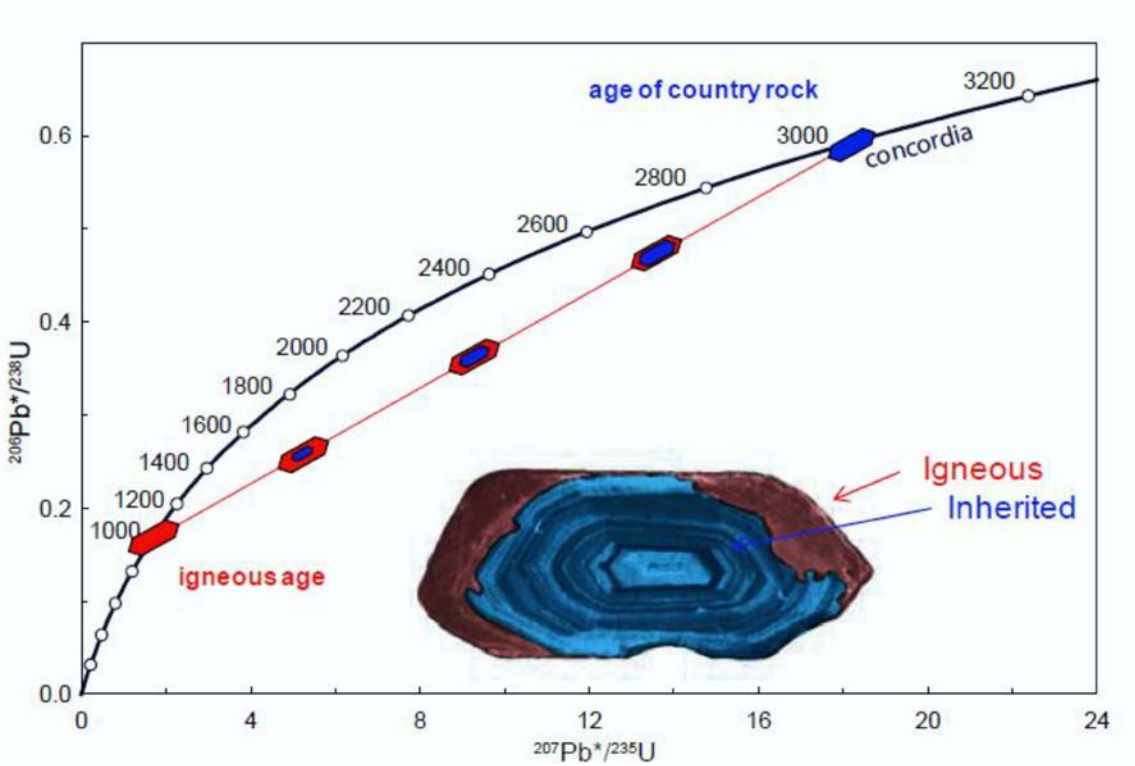

Figure 2.5. Mixing process in Concordia diagram (Gehrels, 2010)

The development of in situ high spatial resolution analytical techniques has avoided this issue.
The analytical methods usually applied in U-Th-Pb geochronology are isotope dilution thermal ionization mass spectrometry (ID-TIMS), secondary ion mass spectrometry (SIMS) and laser ablation inductively coupled plasma mass spectrometry (LA-ICP-MS).

2.3.2.1 Zircon U-Th-Pb geochronology

Zircon is a suitable mineral for U-Th-Pb geochronology since it has the following properties: high U concentration (usually 100-1000 ppm); moderate Th content (usually 10-100 ppm); low Pb content during crystallization (ppt); it is common in felsic and intermediate magmatic rocks; it is mechanically and chemically resistant.
One of the main application of zircon U-Th-Pb geochronology is in detrital studies, with at least three major motivation (Gehrels, 2011) : 1) provenance of sediments compared with known sources; 2) correlation of sedimentary units, assuming identical provenance; 3) quantify the maximum depositional age of strata in absence of other age data.

In the third Chapter of this thesis, detrital zircon UPb data will be discussed to interpret provenance source rocks of glaciomarine sediments from the Ross Sea and to correlate different source areas with zircon age populations found from offshore samples.

2.3.3 Apatite Fission Track (AFT) thermochronology

Thermochronometry techniques are based on the sensitivity to a low range of temperature (ca 30 °C to 550 °C) of some radioactive systems (thermochronometers) in order to obtain information on the thermal histories of rocks and minerals in that temperature range. Three groups of thermochronometers are in common use in Earth science: the (U-Th)/He, the fission tracks, based on the production of respectively He and lattice damage by decay of U in U-Th-bearing minerals (e.g. zircon and apatite) and the $^{40}Ar/^{39}Ar$ systems based on the production of ^{40}Ar from ^{40}K in K-bearing minerals (feldspar, mica, hornblende).

In this case detrital thermochronometry, and in particular AFT dating, has been applied to sedimentary samples. When sedimentary samples has been hold at low temperature (below the closure temperature of the thermochronometer, i.e. the temperature of a rock at its thermochronometric cooling age), the system remained closed. Thus the samples yield a wide range of ages, which represent the cooling ages of the source rocks/terrains. This is used to reveal sediment source areas and to unravel thermal histories of those source. A discrimination of the age populations present in a detrital sediment is based on the distribution of the grain ages, that is treated statistically (Andreucci, 2013).

Fission track thermochronometry is based on lattice damages produced by the spontaneous fission of U. The method is based on the radioactive system of ^{238}U and linear lattice damages (fission tracks) produced by its spontaneous fission in minerals such zircon and apatite (Price and Walker, 1963, Fleischer et al., 1975). The heavy unstable isotope which decays by spontaneous fission splits into two nuclear fragments that are pushed away to each other by a combination of energy released by the nuclear fission and the repulsion Coulomb forces. The passage through the crystal lattice of the two positively charged particles induces dislocation of atoms from their original positions due to a change in the electrostatic charge of the surrounding lattice region; the result is the formation of high density linear defect of the lattice, the fission tracks (Ion Explosion Spike theory of Fleischer et al., 1975, figure 2.6).

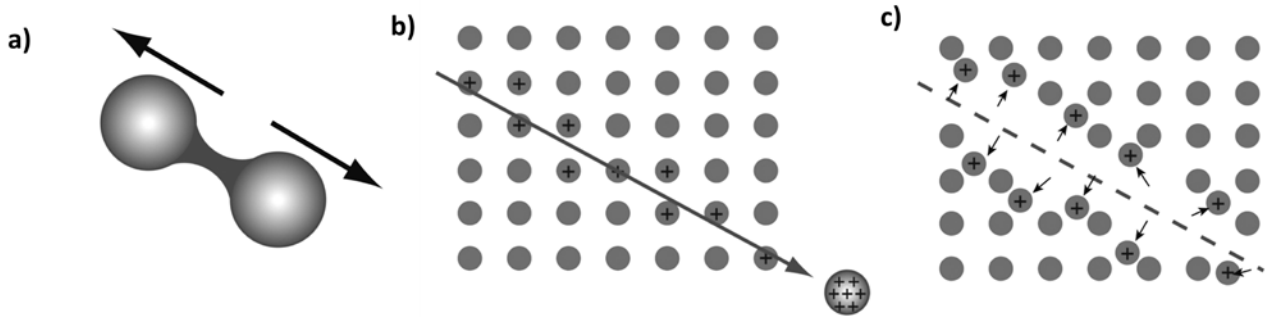

Figure 2.6. The Ion Explosion Spike model of Fleischer et al. (1975) for the formation of Fission Tracks. a) splitting of the heavy nucleus into two nuclear fragments. b) the two fragments along their track tear off electrons from the surrounding atoms of the lattice. c) the positively charged atoms move from their original position because of repulsion electrostatic forces.

Fission tracks accumulate in time (t) in the crystal lattice and their quantity is described in the decay equation (Tagami and O'Sullivan, 2005):

$$N_s = \frac{\lambda_f}{\lambda_\alpha} {}^{238}N\left(e^{\lambda_\alpha t} - 1\right)$$

Where λ_f is the constant decay of spontaneous fission of ^{238}U (λ_f =8.5 10^{-17} yr^{-1}), λ_α is the α decay constant of ^{238}U (λ_α =1.5 10^{-10} yr^{-1}), N_s is the number of spontaneous fission track per unit volume, ^{238}N is the number of ^{238}U atoms per unit volume.

To calculate single crystal age from a sample the most common used method is the External Detector Method (EDM), which is shown in figure 2.7. The samples are mounted in epoxy resin, polished and then chemically etched. Chemical etching is needed because the tracks etch more rapidly than the crystal lattice and so they become visible for counting. The spontaneous track density on a single mineral grain surface can be determined after etching. To determine the unknown concentration of ^{238}U atoms (^{238}N) in the crystal, the EDM is used, since it is based on the constant natural ratio ^{235}U/^{238}U (7.252x10^{-3}). A sheet of U-free mica is placed in contact with the polished mount. Neutron irradiation in a nuclear reactor induces fission of ^{235}U in the samples: nuclear fragments irradiating from the polished surface of the sample are injected in the mica sheet causing the formation of fission tracks in its lattice (induced fission tracks). After chemical etching of mica sheet, also induced fission tracks can be measured, thus obtaining the value of ^{235}U from which is possible to calculate the ^{238}U content. The induced tracks are present also in the sample mount, but since the etching of the sample is done before neutron irradiation, they are not revealed on the surface of crystals. The sample and the related mica are then placed together in a single slide and analyzed with an optical microscope associated to a sliding table and proper software. The operator then is able to count the density of spontaneous fission tracks on the sample mount and the induced fission tracks on the mica sheet (Reiners and Brandon, 2006).

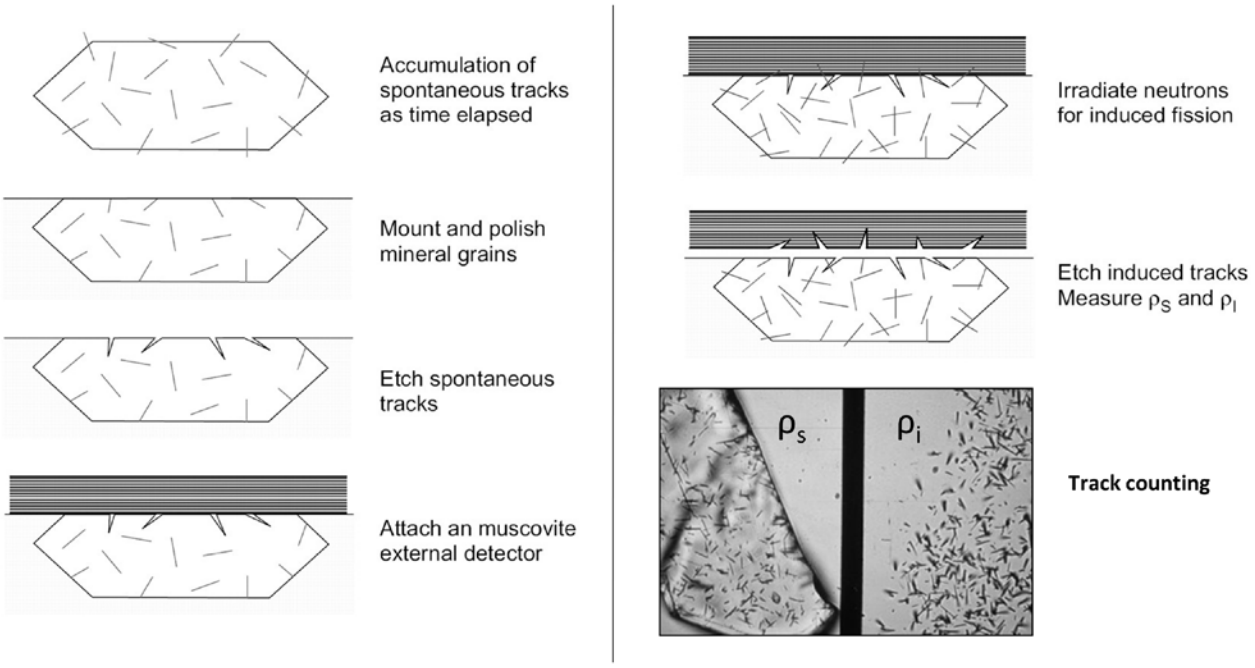

Figure 2.7 Schematic procedure for fission track analysis with the EDM method (Tagami and O'Sullivan 2005). Picture taken from Andreucci (2013).

The AFT age of a single apatite grain determined by EDM method can be calculated with the age equation:

$$t_i = \frac{1}{\lambda_d} ln\left(1 + \lambda_d \zeta g \rho_d \frac{\rho_{s,i}}{\rho_{i,i}}\right)$$

where *i* stands for the generic grain *i*, t_i is the age of grain *i*, λ_d is the total decay constant of ^{238}U, ζ is the calibration factor based on EDM of fission track age standards, depending on the microscope and the operator, *g* is the geometric factor for spontaneous fission track registration, ρ_d is the induced fission track density for a uranium standard which depends on the sample position during neutron irradiation, $\rho_{s,I}$ is the spontaneous fission track density for grain *i*, $\rho_{i,I}$ is the induced fission track density for grain *i* (Donelick et al., 2005).

Usually track density are measured on 20 to 40 grain from the same sample: the measured parameters are the number of induced tracks, the number of spontaneous tracks, the area of the crystals, the mean D_{par} of the tracks (i.e. the means width of fission track etch pits, a value informative for track retentivity), the lengths of the tracks. Counted data are then processed with dedicated softwares and plotted usually in radial plots. In sedimentary samples grain ages are usually distributed in different population of ages. To establish the age components in a mixed grain age

distribution, the binomial peak fitting algorithm (Galbraith and Green, 1990; Galbraith and Laslett, 1993) is usually applied, using dedicated software such as BINOMFIT (Brandon, 2002, figure 2.8).

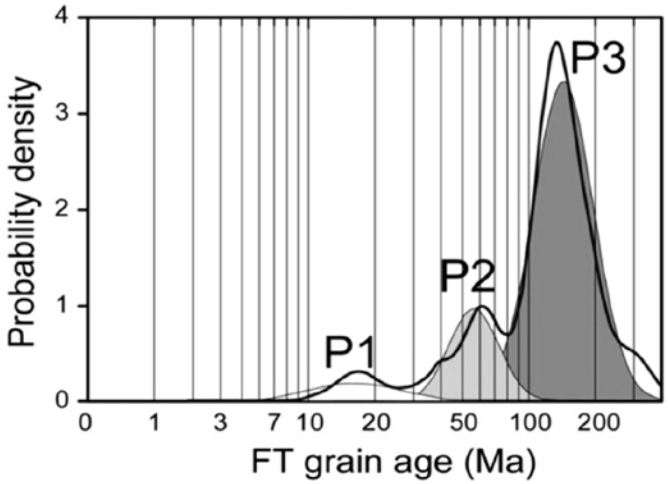

Figure 2.8. Estimate of the components of a mixed grain age distribution (the case of a sedimentary sample) made with the BINOMFIT software (Brandon, 2002). Picture taken from Andreucci (2013).

In the third Chapter of this thesis, detrital AFT data will be discussed to interpret provenance source rocks of glaciomarine sediments recovered from Ross Sea and to correlate different source areas with AFT age populations found from offshore samples.

Chapter III.
Multi analytical provenance analysis of Eastern Ross Sea LGM till sediments (Antarctica): petrography, geochronology and thermochronology detrital data.

3.1 Chapter Overview

The present chapter is a paper accepted and published in the journal Geochemistry, Geophysics, Geosystems in 2017 (published online, volume 18, 30 pp.). A multi-proxy study of LGM sediments from Eastern Ross Sea has been carried out, applying petrographic analysis to the gravel sized clasts and a double dating technique (ZrnUPb and AFT) to the sand sized fraction. This paper has been produced within an active collaboration with University of Padova (Italy). The writer has produced petrographic data, while ZrnUPb data have been collected by Dr. Langone and AFT data by Dr. Andreucci. Data interpretation and discussion has involved professors Franco Talarico and Massimiliano Zattin and has been written and reviewed together with other co-authors.

3.1 Paper

Matteo Perotti[1], Benedetta Andreucci[2], Franco Talarico[1], Massimiliano Zattin[2], Antonio Langone[3]

[1] University of Siena, Department of Physical Sciences, Earth and Environment, Strada Laterina 8, 53100 Siena, Italy

[2] University of Padova, Department of Geosciences, Via Gradenigo 6, 35131 Padova, Italy

[3] Consiglio Nazionale della Ricerche–Istituto di Geoscienze e Georisorse, Unita` di Pavia, Via Ferrata 1, 27100, Pavia, Italy

3.2 Abstract

In order to reveal provenance of detrital sediments supplied by West Antarctic Ice Sheet (WAIS), 19 glaciomarine cores of Last Glacial Maximum age were analyzed from Eastern Ross Sea and Sulzberger Bay. Analytical techniques included petrographic analysis of gravel-sized clasts, geochronology (zircon U-Pb: Zrn-UPb) and thermochronology (apatite fission track: AFT) of sand-sized fractions. Petrographic analysis revealed a similarity with the lithologies presently exposed in western Marie Byrd Land (MBL), with major roles played by low grade metamorphic rocks and granitoids. Furthermore Zrn-UPb and AFT data allowed to identify the ages of formation and cooling of sedimentary source area, consisting of Cambrian-Precambrian basement (i.e. Swanson Formation in western MBL) which underwent at least two episodes of magma intrusion, migmatization and cooling during Devonian-Carboniferous and Cretaceous-Paleocene times. Scarcity of volcanic clasts in the region of Ross Sea along the front of West Antarctica Ice Streams in association with the occurrence of AFT Oligocene-Pliocene dates suggests a localized tectonic exhumation of portions of MBL, as already documented for the opposite side of West Antarctic Rift System in the Transantarctic Mountains. Furthermore, a Zrn-UPb and AFT population of Late Triassic-Jurassic age

indicates the presence of unexposed rocks that formed or metamorphosed at that time in the sedimentary source area, which could be identified in McAyeal Ice Stream and Bindschadler Ice Stream catchment areas.

3.3 Introduction

Glaciated regions such as Antarctica are often characterized by areas with poor rock exposures, so studies of glacial sediments are crucial in revealing glacier dynamics and providing important information about concealed source rocks.

The Ross Sea, hosting at present an extensive ice shelf, is a key area for studying the ice sheets dynamics of Antarctica as it drains about one third of the Antarctic ice, both from the East Antarctic Ice Sheet (EAIS) and West Antarctic Ice Sheet (WAIS, Fig. 3.1). This embayment was occupied, during the Last Glacial Maximum (LGM), by an ice sheet that grounded in proximity of the continental shelf break, leaving stratigraphic and geomorphological traces on the sea bottom sediments (Domack et al., 1999, Shipp et al., 1999, Licht et al., 1999, Licht and Andrews, 2002, Mosola and Anderson, 2006). Soon after the LGM the grounding line retreated to the current position (Anderson et al., 2014).

Information about ice sheet dynamics have been provided by provenance analysis of glaciomarine sediments in the works of Licht et al. (2005 and 2014), Licht and Palmer (2013), Farmer et al. (2006). Although the above cited studies have been carried out on LGM till fractions from the eastern Ross Sea, knowledge about the catchment areas of West Antarctic Ice Streams feeding this marine region (i.e. Kamb, Bindschadler and McAyeal Ice Streams) is not complete. Here we present a multi-analytical provenance study of eastern Ross Sea LGM sediments, based on detrital geochronology, thermochronology and petrographic techniques.

Provenance studies commonly take advantage of detrital geochronology and thermochronology, as they allow inferences to be made about the location, age, and exhumation history of source terrains. Comparison between age populations found in sedimentary samples versus regional bedrock ages allows the identification of possible source areas, that may be used to determine ice flow drainage patterns. In addition, petrography of a gravel-sized fraction can give a complete microstructural and lithological picture of the rocks involved in the erosional framework, thus allowing a robust interpretation of geology of the source area. This methodology has been successfully used in Antarctica to track provenance changes and unravel paleo ice-flow patterns evolution through time (e.g. Talarico and Sandroni, 2011). Provenance studies in the eastern Ross Sea have so far provided petrographic data only from medium and coarse sand fraction analysis (Anderson et al., 1992; Licht et al., 2005).

In this work we present a geo- and thermochronological provenance study of eastern Ross Sea LGM sediments, combined with a gravel-sized clasts petrographic analysis. The methodology allowed us to identify distinct different eroded source rock units, consisting of metamorphic basement, metasediments, volcanic and plutonic rocks, and to obtain information about crystallization, metamorphism and exhumation history of source rock units. The combined dataset obtained with this study well matches the western Marie Byrd Land geology, therefore illuminating the ice drainage patterns during LGM.

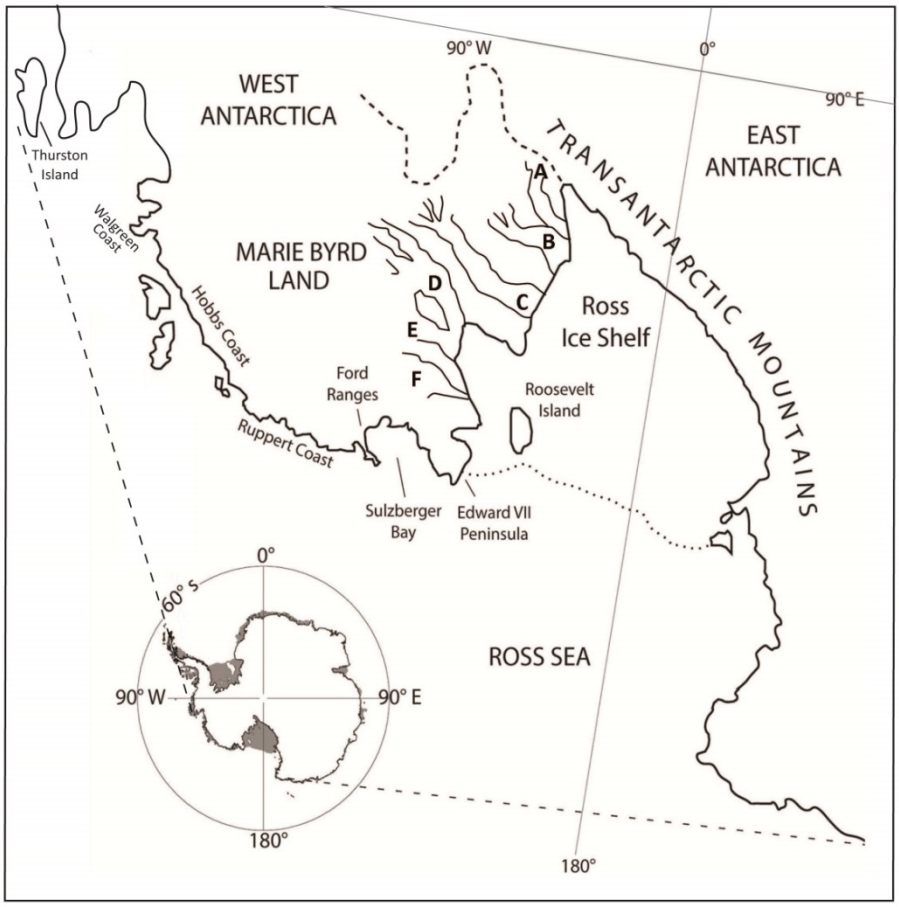

Figure 3.1 – Geographic sketch map of the study area: Eastern Ross Sea and Marie Byrd Land. Also schematic pattern of Siple coast Ice Streams is shown (labeled A-F: A: Mercer Ice Stream; B: Whillans Ice Stream; C: Kamb Ice Stream; D: Bindschadler Ice Stream; E: MacAyeal Ice Stream; F: Echelmeyer Ice Stream.)

3.4 Geological Setting

3.4.1 Geology of Western Marie Byrd Land

The Ross Sea Embayment is bordered by the 3500 km-long mountain chain of the Transantarctic Mountains to the west and Marie Byrd Land to the east. The modern West Antarctic Ice Sheet occupies part of the West Antarctic Rift System, formed in the Mid-Cretaceous to Cenozoic with a total horizontal displacement of several hundreds to thousand kilometers between Marie Byrd Land and East Antarctica (Di venere et al., 1994; Luyendyk et al., 2003; Siddoway, 2008; Storti et al., 2008).

The best-exposed rock outcrops in West Antarctica are in Marie Byrd Land. The oldest unit is the Neoproterozoic-Cambrian Swanson Formation (Bradshaw et al., 1983; Adams, 1986; Pankhurst et al., 1998); it is a folded and cleaved low-grade metaturbidite sequence which has been correlated on the basis of U-Pb detrital zircon ages to the Robertson Bay Group in North Victoria Land and Greenland Group in Western New Zealand (Adams et al., 2013; Ireland et al., 1998). It crops out mainly in the Ford Ranges in Western Marie Byrd Land. Low grade-metasedimentary rocks are also exposed in small outcrops in eastern Marie Byrd Land (Brand, 1979).

The Swanson Formation was intruded by Devonian-Carboniferous Ford Granodiorite suite, which records a major pulse of calc-alkaline magmatism along the Antarctica-Zealandia-Australia segment of Gondwana continental margin (Weaver et al., 1991). The Ford Granodiorite is a suite of grey to black and white

metaluminous to peraluminous I-type biotite-hornblende granodiorites-tonalites (Weaver et al., 1991). Two hypotheses have been proposed for this event: subduction (Weaver et al., 1991) or back-arc extension (Tulloch et al., 2009). It is unclear if plutons of Ford Granodiorite were emplaced in Ford Ranges during short-lived pulses or prolonged magmatism during the Devonian-Carboniferous (Pankhurst et al., 1998; Siddoway and Fanning, 2009; Yakymchuk et al., 2015).

The inboard area of a calc-alkaline Jurassic-Cretaceous magmatic arc along the east Gondwana margin was involved in the emplacement of alkaline Byrd Coast Granite suite occurred in Cretaceous time, with ages of 124-95 Ma (Weaver et al., 1992). The Byrd Coast granite intruded both the Swanson Formation and the Ford Granodiorite suite and chemically derived from the latter in a setting of back-arc extension (Weaver et al., 1992) or intracontinental extension (Korhonen et al., 2010). This is a pinkish coarse equigranular to porphyritic A-type leucogranite and monzogranite variety. This igneous activity involved Ruppert and Hobbs Coast (110-101 Ma) (Mukasa and Dalziel, 2000) and Ford Ranges-Edward VII Peninsula region (Weaver et al., 1992; Pankhurst et al., 1998). Crustal extension in Cretaceous produced also the emplacement of mafic dykes throughout the Ford Ranges (Siddoway et al., 2005; Saito et al., 2013). Within the Ford Ranges, a migmatite-granite complex is exposed in the Fosdick Mountains (Siddoway et al., 2004a), with ortho-gneisses and para-gneisses which underwent at least two high-grade metamorphic events, in Devonian-Carboniferous and Cretaceous time respectively (Korhonen et al., 2010, 2012; Yakymchuk et al., 2015). The granulite facies gneisses consist of migmatitic paragneisses with discrete domains of melanosome which typically contains cordierite, sillimanite, biotite, quartz, plagioclase, and k-feldspars, with or without garnet, and coarser grained leucosome containing quartz, k-feldspar, anti-perthite and biotite, with or without garnet (Kohronen et al., 2010a,b). On the other hand migmatitic orthogneisses are mainly composed by quartz, plagioclase, k-feldspar, biotite, iron oxides and in some cases may contain garnet (Kohronen et al., 2010a,b).

Other migmatites are exposed in the Alexandra Mountains (Edward VII Peninsula, Smith, 1996) and in Demas Range, eastern Marie Byrd Land (Mukasa and Dalziel, 2000).

The emplacement of youngest components of the Byrd Coast Granite coincides with the onset of regional extension to transtension and to the development of the West Antarctic Rift System (Siddoway, 2008).

During the Cenozoic, starting from about 35 Ma, the region was affected by an intense alkaline volcanism and uplift of Marie Byrd Land Dome, which today has an area of 800x500 km and an altitude reaching 2700 m above sea level (LeMasurier et al., 2011). Eighteen major volcanoes and many smaller centers are known in the region, and are composed of felsic alkaline lavas (phonolite, trachyte, rhyolite and intermediate differentiates) (Panter et al., 2000). They are distributed as linear ranges in central Marie Byrd Land, such as the Flood Range and Executive Committee Range. Moreover, several volcanic centers are believed to exist sub-glacially beneath the WAIS, as demonstrated during the Central West Antarctica aerogeophysical survey carried out from 1991-1997 over the region (Behrendt et al., 1994, 1996 and 2004).

Starting from about Oligocene time (Ivany et al., 2006 in Antarctic Peninsula), West Antarctica was involved in the first development of an ice sheet which enlarged further forming the West Antarctic Ice Sheet in Middle to Late Miocene time (Barker and Camerlenghi, 2006). In this scenario, on the basis of geomorphological evidences, Marie Byrd Land was affected since ~ 15 Ma by a cold-based glaciation (Rocchi et al., 2006). The WAIS collapsed several times during Pliocene (Naish et al., 2009; Pollard and DeConto, 2009). Currently, almost one third of the ice of Antarctica is drained to the Ross Sea Embayment, both from the EAIS and the WAIS. EAIS ice flows come from big outlet glaciers through the Transantarctic Mountains , while most of the West Antarctica ice flows from fast moving Ice Streams, without any significant rock exposures. Some of the Ice Streams (Whillans and Mercer Ice Streams, Licht et al., 2014)

could drain ice also from the southern sector of the Transantarctic Mountains. The current ice-flow pattern is different from that occurring during last glaciation, according to indicators of flow of ovverriding ice across some mountain ranges in Western Marie Byrd Land during LGM (Sugden et al., 2005 for the Ford Ranges). These authors demonstrated that some regional LGM ice flows have changed to radial flows affected by local glaciers following deglaciation during Holocene time.

The sampling area of this study, the eastern basin of the Ross Sea, has a bathymetry characterized by two north trending troughs, separated by ridges. These geomorphic features were at LGM occupied by grounded ice fed by WAIS Ice Streams (Mosola and Anderson, 2006; Anderson et al., 2014). This study follows the nomenclature given by Mosola and Anderson (2006) for these easternmost troughs of the Ross Sea Embayment (5 and 6, respectively). Other offshore sampling areas are located close to the coast of Marie Byrd Land, in the glacially eroded Colbeck Trough fronting Edward VII Peninsula, and in the western Sulzberger Bay, in the region east of Cape Colbeck (Fig. 3.2).

3.4.2 Provenance studies in eastern Ross Sea and bedrock geochronology and thermochronology of MBL

Paleo-drainage reconstruction of LGM ice sheets was first proposed by Hughes et al. (1973) based on the presence of large bathymetric troughs on the Ross Sea floor. Later, Anderson et al. (1983 and 1992) used heavy minerals and clays from tills to reconstruct paleo ice-flows on the continental shelf. Petrographic coarse sand data from Anderson et al. (1992) revealed an Eastern Ross Sea detrital composition made up mainly by metamorphic and felsic granitoid lithic grains. More recently, provenance studies on a till sand fraction by means of petrographic (point counting), isotopic (Sm-Nd; Pb-Pb) and geochronological (U-Pb; Ar-Ar) techniques were carried out by Licht et al. (2005 and 2014), Farmer et al. (2006), and Licht and Palmer (2013). The combined results of these studies demonstrated that the Ross Sea has a contribution of drainage both from EAIS and WAIS, with the convergence of the two ice flows into the Ross Sea at about 180° longitude (Licht et al., 2005; Licht et al., 2014; Anderson et al., 2014). In particular Licht et al. (2014) provide detrital zircon U-Pb (Zrn-UPb) data from the Ross Sea and from some of the Ice Streams draining the West Antarctica Ice Sheet. Their data show an abundance of Neoproterozoic and older dates for both the Ross Sea and the Ice Stream samples. Minor populations with Cenozoic and Upper Triassic-Jurassic ages are also present. Close to our study area, Siddoway et al. (2004b) provide Cretaceous Zrn-UPb ages for dredged mylonites from Colbeck Trough, interpreted to be derived from Byrd Coast granite in Edward VII peninsula. The same authors found also late Cretaceous AFT ages for the same samples.

Taking in consideration previous provenance studies carried out in the region, this study focus on marine piston cores distributed spatially in four main groups across eastern Ross Sea, facing the coastal area of western Marie Byrd Land and Roosevelt Island: the easternmost group comprises 3 cores located close to the coast in Sulzberger Bay; the second group comprises 1 core in Colbeck Trough, the third group comprises 6 cores located in the bathymetric trough number 6 of Mosola and Anderson (2006); the fourth group comprises 8 cores located in trough number 5 of Mosola and Anderson (2006) (Fig. 3.2).

Considering this geographical setting and sampling sites distribution, an overview of previous geochronological and thermochronological studies carried out on bedrock geology of the area is necessary. Making use of available exposures (Fig. 3.2), several works define formation, metamorphism and exhumation timing of the Marie Byrd Land outcropping rocks (Pankhurst et al., 1998; Mukasa and Dalziel, 2000; Siddoway and Fanning, 2009; Kohronen et al., 2010a) . Knowledge of the geological history of potential source rocks is key to detrital geochronology and thermochronology. Diagnostic criteria for age of origin of offshore sediments, gleaned from these studies, are here summarized as follows (from E to W).

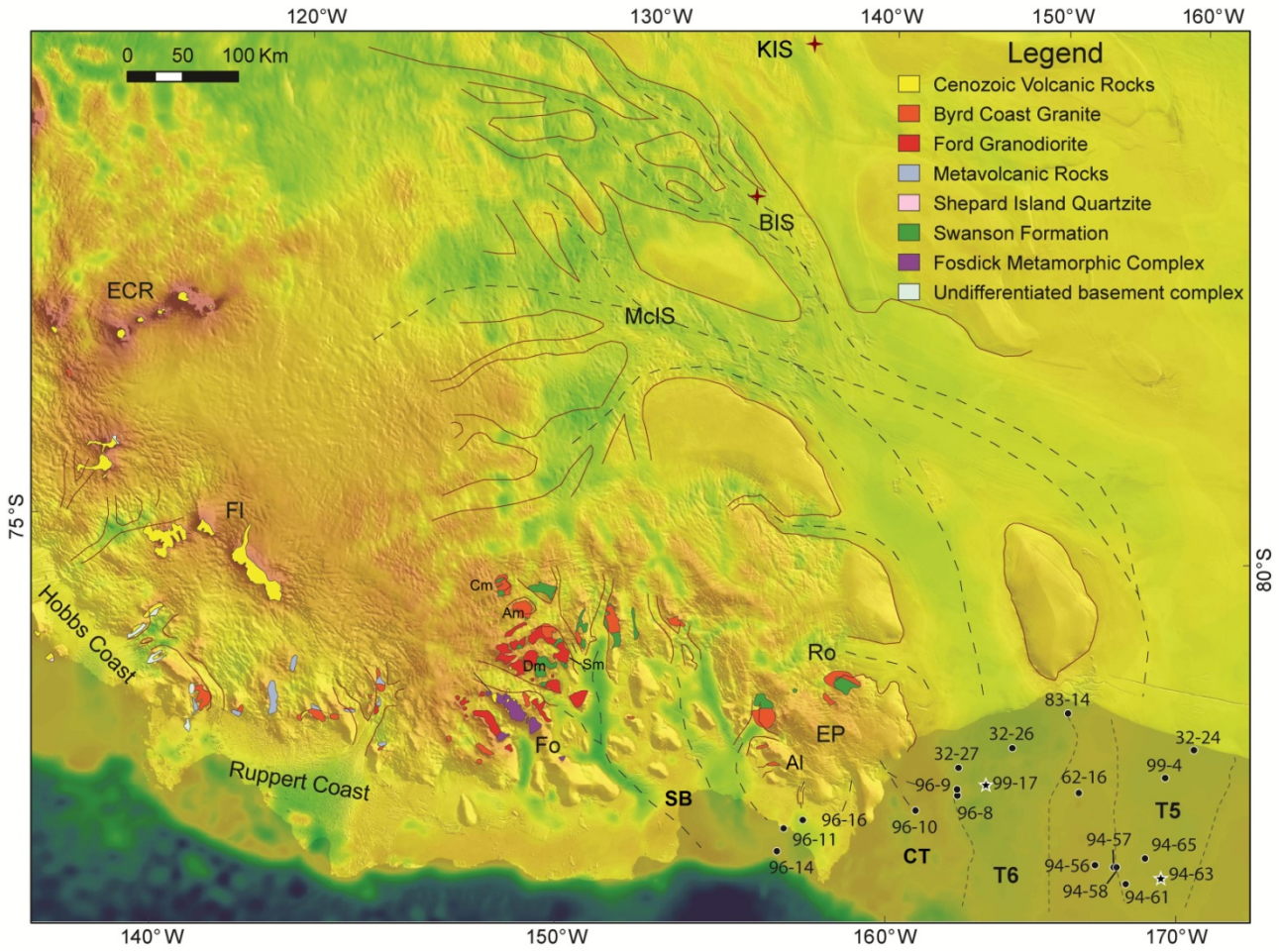

Figure 3.2– Bedmap geology of Marie Byrd Land, with sample locations in Eastern Ross Sea. Offshore cores labelled with a black star were studied also by Licht et al. (2014) as well as onshore red cross samples from Ice Streams. SB-Sulzberger Bay; Ct-Colbeck Trough; Ro-Rockfeller Mts; Al-Alexandra Mts; EP-Edward VII Peninsula; Fo- Fosdick Mts, Fl-Flood Range; ECR-Executive Committee Range; Dm- Denfield Mts; Sm- Sarnoff Mts; Am- Allegheny Mts; Cm- Clark Mts; McIS-MacAyeal Ice Stream; BIS-Bindschadler Ice Stream; KIS- Kamb Ice Stream. T5 and T6 are troughs 5 and 6 of Mosola and Anderson (2006), contoured by short-dashed lines. Long-dashed lines trace hypothetical flow lines. Geologic map from Wade et al. (1977a,b,c) and Wade et al. (1978).

Mukasa and Dalziel (2000) provide Late Paleozoic and mainly Cretaceous Zrn-UPb ages in granitoids from Ruppert and Hobbs coast. Hart et al. (1997) infer K-Ar ages for volcanic rocks in the Hobbs Coast ranging between 12 and 2 Ma.

On the basis of geochronological Zrn data, Pankhurst et al. (1998) divided Marie Byrd Land in two provinces, the westernmost one being characterized by Cambrian and Devonian-Carboniferous ages.

Yakymchuck et al. (2015) uncover detrital UPb ages of the sedimentary Swanson Fm., in the Ford Ranges, with a major Neoproterozoic-Cambrian (500-750 Ma) and minor Mesoproterozioc (930-1180 Ma), Paleoproterozoic (1560-1930 Ma) and Paleozic (387±22 Ma) age populations.

Zrn-UPb ages of the Fosdick Mountains migmatite–granite complex (Siddoway and Fanning, 2009; Brown et al., 2016) define intervals of 370 to 355 Ma and 118-90 (McFadden et al., 2010a,b; Brown et al., 2016) for plutonism and migmatization.

McFadden et al. (2010a,b), Saito et al. (2013) and Brown et al. (2016) present UPb ages for zircons and titanite in the Fosdick Mountains plutons, mafic dykes and migmatites, yielding Cretaceous crystallization

ages (Byrd Coast Granite age). Richard et al. (1994) provide AFT, Ar/Ar, and Monazite UPb data for high grade metamorphic rocks in the Ford Ranges, yielding Cretaceous to Eocene ages.

Contreras et al. (2012) present zircon UPb and U-Th/He dates on metasedimentary gneisses and granites between Alexandra (Edward VII Peninsula) and Fosdick Mountains (Ford Ranges), yielding major detrital populations of 1000-1100 and 500 Ma, and Middle-Late Cretaceous crystallization-cooling ages.

Adams et al. (1995) carried out a geo-thermochronometric study of the Edward VII Peninsula (Alexandra and Rockfeller Mountains), revealing regional metamorphism at 421-432 Ma (Rb-Sr dates of the Swanson Formation), emplacement of granites and thermal metamorphism in the Cretaceous (95-105 Ma, K-Ar dates of granites). Upper Cretaceous-Paleocene (98-55 Ma) zircon fission track and AFT data from this work and Siddoway et al. (2004b) indicate the period of regional cooling and uplift started concurrently to granite emplacement.

Lisker and Olesch (1998) infer from AFT data three distinct periods of cooling for the Edward VII Peninsula and the Ford Ranges (100-85; 70-65 and since the Oligocene), attributed to a pulsing mantle plume. Spiegel et al. (2016) provide zircon fission track data (108-80 Ma), AFT (93-28 Ma), and apatite (U-Th)/He (128-5 Ma) data for the Hobbs Coast and eastern Marie Byrd Land.

As a whole these data describe a Precambrian-Cambrian basement, undergoing several episodes of magma intrusion, metamorphism, migmatization and regional uplift and cooling (Devonian-Carboniferous; Cretaceous-Paleocene), and a major volcanic and localized uplift-cooling stage since the Oligocene. From such a bedrock picture single grain detrital samples are expected to be mainly Neoproterozoic, Devonian-Carboniferous, Triassic-Jurassic or Cretaceous for the Zrn-UPb, and mainly late Cretaceous-Cenozoic for the AFT.

3.5 Materials, Methods and Results

3.5.1 Sampling strategy

A total of 19 LGM and post-LGM piston cores collected by different scientific cruises across the Eastern Ross Sea was logged and sampled at the Marine Geology Antarctic Research Facility of Tallahassee, Florida. Distribution map and list of samples are shown in Fig. 3.2 and Table 3.1. The rationale of the choice of these piston cores is based on their geographic distribution, sediment recovery, and presence of clast rich glacial till sedimentary facies. Figure 2 shows geographic location of sites, which are distributed over the eastern Ross Sea and can be grouped in four different sub-areas: Sulzberger Bay on the east, Colbeck Trough close to the coast of Edward VII Peninsula, trough 6 in the central sub-area and trough 5 on the west of the study area (following the nomenclature applied by Mosola and Anderson, 2006, Fig. 3.2).

Logging was aimed to identify the distribution and the features of the gravel fraction (i.e. granule to cobble size clasts) along the entire length of each core. The size, shape and features of each clast >2mm was determined for each 10 cm interval of the working half split surface of the core. On the basis of distinctive macroscopic features, clasts were grouped into six major lithological groups (volcanic rocks; intrusive rocks; metamorphic rocks; sedimentary rocks; quartz; dolerite). Data acquisition also involved subdivision and counting of clasts occurrence in each group for each 10 cm interval of the cores. A summation of all clasts from different lithological groups was carried out for each core. Table 3.1 shows also number of logged clasts for each half split surface of cores. A total amount of 1118 clasts were counted and measured from

Table 3.1. List of sample sites from Eastern Ross Sea and analytical techniques carried out. The same sites are shown labelled in Figure 2 and elsewhere in the text. Clast log includes gravel-size clasts identification, classification and sampling of selected clasts for detailed petrographic analysis. Also the sampling depths in cm for Upb and AFT analysis are shown. Abbreviations: Sulz.Bay: Sulzberger Bay; T5 and T6: trough 5 and trough 6 from Mosola and Anderson (2006).

Area	Cruise	Core	Label	Latitude	Longitude	Water depth (m)	Core length (cm)	Clast Log	N° Clasts	Sampled clasts	UPb	AFT
Sulz.Bay	NBP96-01	011-PC	96-11	-76.78	-155.44	392	389	x	259	9		x (40-43)
Sulz.Bay	NBP96-01	014-PC	96-14	-76.59	-155.55	369	154	x	48	5		
Sulz.Bay	NBP96-01	016-PC	96-16	-76.91	-155.93	1273	65	x	172	2		x (2-6)
Colbeck Trough	NBP96-01	010-PC	96-10	-77.23	-160.11	493	190	x	13	1	x (188-190)	x (9-14; 25-29; 188-190)
T6	NBP96-01	008-PC	96-08	-77.56	-160.94	650	202	x	163	12		
T6	NBP96-01	009-PC	96-09	-77.61	-160.85	643	210	x	58	8		
T6	ELT32	027-PC	32-27	-77.78	-160.63	670	148	x	185	14		x (55-60; 105-110)
T6	NBP99-02	017-PC	99-17	-77.72	-161.86	715	205	x	33	14		x (134-139)
T6	ELT32	026-PC	32-26	-78.07	-162.39	605	247	x	29	13		
T6	DF83	014-PC	83-14	-78.48	-164.14	601	277	x	40	14	x (231-236)	x (81-86; 183-190; 231-236)
T6/T5	DF62-01	016-PC	62-16	-77.97	-165.83	467	229					x (111-117; 151-156)
T6/T5	NBP94-07	056-PC	94-56	-77.33	-166.66	441	362	x	60	15		
T5	ELT32	024-PC	32-24	-78.40	-169.13	565	433				x (142-146)	x (416-420)
T5	NBP94-07	057-PC	94-57	-77.34	-167.36	525	89	x	23	4		
T5	NBP94-07	058-PC	94-58	-77.35	-167.46	525	315	x	53	8		x (170-173)
T5	NBP94-07	061-PC	94-61	-77.23	-168.04	548	36	x	8	1		
T5	NBP94-07	063-PC	94-63	-77.33	-169.18	582	292	x	53	9		
T5	NBP94-07	065-PC	94-65	-77.47	-168.44	587	116	x	13	8		
T5	NBP99-02	004-PC	99-4	-78.15	-168.58	618	104	x	18	8		

the 19 cores and from these 210 representative clasts (granule to cobble size) were sampled for petrographic analysis. Furthermore, 15 bulk till sand rich intervals (2-5 cm thick) were sampled for geochronological and thermochronological analysis on the granulometric fraction comprised between 63 µm and 2 mm. Sampling depths for geo- and thermochronological analysis are listed in Table 3.1.

3.5.2 Petrography

3.5.2.1 Analytical Details

A selection of 51 representative pebble sized clast thin sections was examined under a polarizer microscope in order to establish a detailed mineralogical and textural analysis for each sample. The identification of possible source rocks for pebbles was carried out thanks to a representative collection of Marie Byrd Land rocks stored at the Polar Rock Repository at the Byrd Polar and Climate Research Center (Ohio State University).

3.5.2.2 Petrographic results

On the basis of detailed petrographic analysis, clasts recovered from the piston cores can be grouped in the following 4 main lithological groups (Table 3.2 and Fig. 3.3):

-Igneous plutonic rocks, including undeformed biotite-hornblende granodiorite and tonalite, biotite monzogranite, alkaline feldspar quartz-syenite, leucocratic biotite syeno-granite (334 total clasts)

- Igneous sub-volcanic and minor volcanic rocks, including syeno-granite, monzonitic and mafic porphyries, dolerites, trachyte and rare felsic volcanics (25 total clasts).

- Low grade metamorphic rocks, including biotite hornfels, biotite ± white mica schists, biotite-actinolite schists, quartzites, metasiltstones, metasandstones, phyllites, slates (604 total clasts).

- Sedimentary rocks, including lithic graywackes, impure quartz-arenites, siltstones and mudstones (85 total clasts).

Two main types of granitoids were distinguished among the samples: black and white biotite ± hornblende monzogranite, granodiorite and tonalite (type A in Table 3.2 and Fig. 3.3) are slightly foliated inequigranular, medium to coarse grained, with hypidiomorphic texture. Biotite is sometimes replaced by chlorite, while feldspars present a light to strong alteration in sericite; quartz is anhedral and interstitial to euhedral plagioclase. Accessory phases are titanite, apatite, zircons, allanite, and opaque minerals. The second variety is composed by slightly foliated pinkish, inequigranular to slightly equigranular, medium to coarse grained, porphyritic biotite monzogranite and leuco syeno-granites (type B in Table 3.2 and Fig. 3.3), with hypidiomorphic texture. Ortoclase is perthitic and slightly altered in sericite. Accessory phases comprise apatite, zircon/monazite and opaque minerals.

Light grey syeno-granite porphyry (Thin section 14) consists of inequigranular porphyritic texture, with mm sized euhedral phenocrysts of K-feldspar, sub-rounded quartz and plagioclase set in a fine grained quartz and feldspar groundmass. Dolerite (Thin section 17) has inequigranular fine to medium grained sub-ophitic texture, with small plagioclase laths intergrowth with larger clinopyroxene crystals and small altered olivine crystals. In another thin section (23), dolerite has a slightly spherulitic texture, with crystals of plagioclase and clinopyroxene set in a matrix of opaque minerals. Mafic rocks include doleritic porphyries, characterized by holocrystalline fine to medium grained porphyritic textures, with phenonocrysts of plagioclase and clinopyroxene set in a microcrystalline plagioclase-clinopyroxene-opaque minerals groundmass. In one case (i.e. Thin section 16), clinopyroxenes appear to be completely altered.

Among volcanic rocks, one sample (60) of dark grey trachyte was found: it has a finely porphyritic holocrystalline trachytic texture with oriented microliths of K-feldspar set in a groundmass of opaque minerals and altered clinopyroxene. Other samples of volcanic rocks are a basaltic vescicular scoria (Thin section 69), a very altered olivine basalt (Thin section 66) with aphanitic hypocrystalline texture, and a rhyolitic volcanic rock with flow texture and phenonocrysts of embayed quartz and alkaline-feldspar (thin section 68).

The group of low grade metamorphic rocks comprises metasiltstones, metasandstones, phyllites, slates, quartzite, biotite hornfels, biotite ± amphibole schists and rare gneisses. Metasandstones are fine to medium grained, with well preserved bedding and clastic texture. Grains are composed mainly of quartz, with minor amount of feldspars, which are set in recrystallized matrix composed of chlorite, muscovite and calcite, and sometimes oxides. Phyllites display of a very weak fine grained foliation defined by orientation of white mica, chlorite and rare biotite flakes, set in a mainly quartzose and carbonate equigranular matrix. Slate is characterized by a well defined quartz and opaque minerals cleavage, with a spotted texture formed by Fe-oxides porphyroblasts (Thin section 52). Hornfels are mainly of sedimentary origin: they preserve clastic texture, with fine to medium grained granoblastic quartz domains and randomly oriented biotite and chlorite flakes, which sometimes form spotted structures. Biotite schists show fine to medium grained grano-lepidoblastic texture, with foliation defined by orientation of biotite and poikiloblastic actinolite, and granoblastic domain defined by interlobate quartz and plagioclase aggregates (Thin section 20). In some cases, amphibole is absent and the foliation is defined by biotite and rare white mica (Thin section21).

Table 3.2. Petrographic characteristics of sampled gravel-sized clasts recovered from Eastern Ross Sea piston cores[a]

Thin Section	Cruise	Core	Top	Bottom	Lithology	Pl (%)	Cam (%)	Bt (%)	Qtz (%)	Opm (%)	Kfs (%)	Cal (%)	Cpx (%)	Ol (%)	Grt (%)	Czo-Ep (%)	Ttn (%)	Ap (%)	Zrn (%)	Chl (%)	Wm (%)	Lithics (%)	Matrix (%)	Groundmass (%)	Glass (%)	Grain Size
1	NBP96-01	11-PC	261	262	Bt-granodiorite/tonalite	40		10	40	<1	10							<1	<1	<1						mg
2	NBP96-01	11-PC	291	292	Bt-granodiorite	38		4	41	<1	16					<1		<1	<1	<1	<1					fg-mg
3	NBP96-01	11-PC	295	297	Bt-cam-schist	32	8	21	36	<1						<1		<1		2						fg-mg
4	NBP96-01	11-PC	310	312	Bt-monzogranite	27		10	30		32					<1		<1	<1		<1					mg-cg
5	NBP96-01	14-PC	43	44	Alcaline feldspar quartz-sienite	5		7	18	<1	69							<1	<1	<1						mg-cg
6	NBP96-01	14-PC	84	85	Sub-litharenite	2			78	3		9				<1				<1	1	6				mg
7	NBP96-01	16-PC	62	65	Bt-bearing leucocratic syeno-granite	18		1	22	1	57							<1		<1	<1					mg
8	NBP96-01	16-PC	62	65	Graywacke	3			81	1		5							<1	3	1	5				mg
9	ELT32	27-PC	117	118	Bt-pl schist	25		8	65	<1								<1	<1							fg
10	NBP96-01	08-PC	99	100	(meta) Sandstone	1			79	1		15								<1	3					fg
11	NBP96-01	08-PC	111	112	Meta sandstone (hornfels)	1		6	70			4								12	7					mg
12	NBP99-02	17-PC	16	19	Cataclasite				35			49				<1				2				13		fg-mg
13	NBP99-02	17-PC	1	3	Bt-tonalite	40		8	42	1	8							<1	<1	<1						mg
14	DF83	14-PC	23	25	Leucocratic syeno-granite porphyry	15		<1	40		45								<1	<1	<1					mg-cg
15	DF83	14-PC	241	245	Bt-Hbl-tonalite	57	15	2	20	1	5						<1		<1	<1						mg
16	DF83	14-PC	252	256	Meta-pl-cpx-porphyry	45			8	3		2	4			1				5				31		mg
17	NBP 94-07	057-PC	15	16	Dolerite	48				1			35	4						12						mg
18	NBP 94-07	057-PC	36	37	Bt-Hbl-tonalite	63	7	5	18	1	2						<1	<1	<1	3						mg
19	NBP 94-07	058-PC	113	117	Meta-vulcano-clastite	4			15	1		23				12				12		21		12		mg-cg
20	NBP 94-07	063-PC	213	214	Bt-Act-schist	12	4	28	49			3						<1		2	1					fg-mg
21	NBP99-02	04-PC	8	9	Bt-Wm-gneissic schist	21		12	61	1								<1			5					mg
22	NBP99-02	04-PC	34	35	Wm-opm rich-metasandstone				68	15						3				2	12					vfg-mg
23	NBP99-02	04-PC	92	93	Dolerite	45			2	1			34			3				15						fg-mg
42	ELT32	27-PC	49	52	Qtz arenite	3			80			1								5	1	1	9			fg-mg
43	ELT32	27-PC	68	72	Meta-siltstone																					fg
44	ELT32	27-PC	135	138	Medium grained graywacke	2			76			18									2	2	12			mg
45	NBP99-02	17-PC	77	82	Qtz-arenite				93	1		1								<1	2	3				mg-cg
46	NBP99-02	17-PC	176	180	Impure arenite/graywacke				46	3		50										1	50			fg-mg
47	ELT32	26-PC	140	146	Bt-gneiss	34		12	51	1								<1			1					mg
48	ELT32	26-PC	237	238	Siltstone																					vfg-fg
49	DF83	14-PC	208	210	Meta-siltstone																					fg
50	DF83	14-PC	31	33	Coarse grained sub-litharenite				88	2		3									1	5	7			mg-cg
51	DF83	14-PC	269	273	Medium grained qtz-arenite				98	1											1	<1	<1			mg
52	NBP 94-07	058-PC	55	57	Slate																					vfg
53	NBP 94-07	058-PC	121	125	Quartzite	1			89	1										7	2					fg-mg
54	NBP 94-07	063-PC	222	223	Hbl-gneiss	2	7	4	72	2		4			2		<1	<1		4	2					mg-cg
55	NBP 94-07	063-PC	11	14	Meta-vulcano-clastite	4	12		53	1										30						mg
56	NBP 94-07	056-PC	140	142	Wm-metasandstone	2			80	4											8					fg-mg
57	NPP 94-07	056-PC	216	217	Qtz-arenite	<1			95	1	1	<1										<1				mg
58	NBP 94-07	056-PC	234	235	Siltstone																					vfg
59	NBP 94-07	056-PC	305	308	Bt-Hbl-tonalite	59	5	4	24	1	5						1	<1	<1							mg-cg
60	NBP 94-07	065-PC	31	34	Trachyte	10				14	63		12	1												fg
61	NBP 94-07	065-PC	16	18	Qtz-siltstone					3		1									1					vfg
62	NBP96-01	09-PC	5	6	Bt-Wm-granofels	11		37	46	1								<1			5					mg
63	NBP96-01	09-PC	122	124	Calc-schist	2			53	1		35									9					fg
64	NBP96-01	09-PC	145	150	Medium grained (meta)arenite	2			81	1		10									4	1				fg-mg
65	NBP 94-07	058-PC	225	226	Mafic porphyry (altered)	15			8(s)			45(s)												32		
66	DF83	14-PC	90	94	Olivine basalt (altered)	25				10			2	7											56	vfg
67	ELT32	27-PC	34	36	Cpx-porphyry	10							35							5(s)	2(s)			47		fg-mg
68	NBP 94-07	065-PC	17	20	Felsic volcanic	5			22		12						<1							61		mg
69	NBP 94-07	063-PC	227	228	Basaltic scoria	2								1											97	

[a]Also geographic areas referring to piston cores location and labels of sampling sites, as shown elsewhere in the text and in Figures 2 and 7, are listed. Mineral abbreviations according to *Kretz* [1983] except for Wm: white mica and Opm: opaque minerals. Petro type—IP: igneous plutonic; S: sedimentary; M: metamorphic; IV: igneous volcanic; ISv: igneous subvolcanic. Grain size—Cg: coarse grained; mg: medium grained; fg: fine grained; vgf: very fine grained. Top and bottom refer to sampling depth along the cores, expressed in centimeters. T5 and T6 are trough 5 and trough 6 from *Mosola and Anderson* [2006].

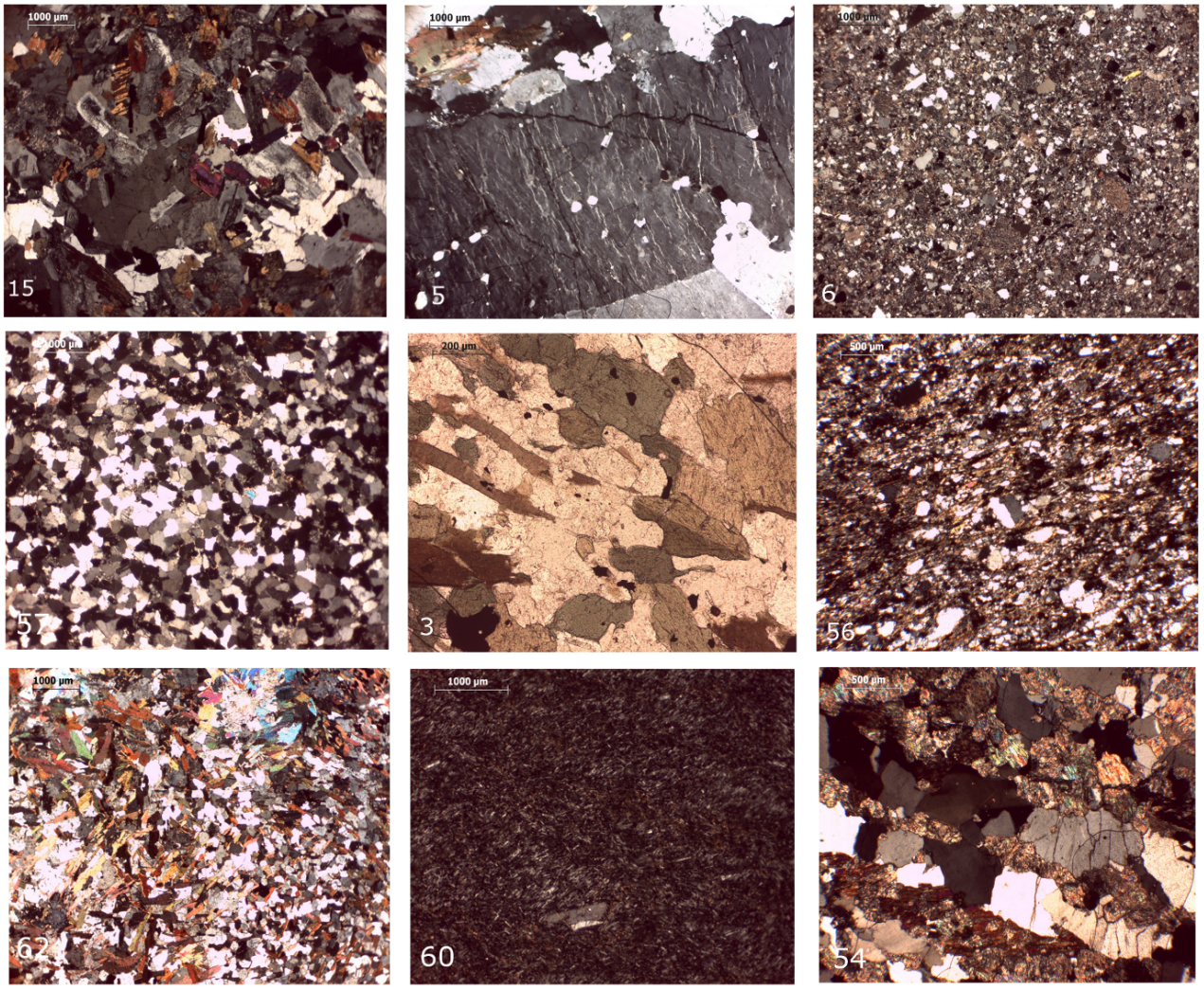

Figure 3.3– Photomicrographs of representative clasts recovered in Eastern Ross Sea cores: Thin section 15 (core 83-14, crossed polarizers): bt-hbl tonalite showing medium grained hypidiomorphic texture (type A granitoid); Thin section 5 (core 96-14, crossed polarizers): coarse grained alkali feldspar quartz-syenite (type B granitoid); Thin section 6 (core 96-14, crossed polarizers): fine to medium grained heterogranular sub-litharenite; Thin section 57 (core 94-56, crossed polarizers): medium grained qtz-arenite; Thin section 3 (core 96-11, planed polarizers): bt-hbl schist with foliation defined by orientation of mica and amphibole; Thin section 56 (core 94-56, crossed polarizers): white mica metasandstone; Thin section 62 (core 96-9, crossed polarizers): biotite-white mica hornfels; Thin section 60 (core 94-65, crossed polarizers): trachyte with holocrystalline oriented fine grained texture; Thin section 54 (core 94-63, crossed polarizers): biotite-hornblende gneiss.

One sample (Thin section 54) is characterized by gneissic layering defined by granoblastic interlobate quartz and plagioclase domains associated to nematoblastic hornblende and rare garnet.

Sedimentary rocks are mainly siltstones, graywackes and medium grained quartz-arenite. Dark grey to black siltstones are composed of very fine grained quartz grains set in a matrix of clay and opaque minerals. Graywackes consist of fine to medium grained sands composed by quartz and minor amount of feldspars. Low grade metamorphic and siliceous lithic fragments are prevalent, set in a matrix of clay, calcite, and sometimes chlorite. Brown to pinkish quartz arenites are heterogranular, medium to coarse grained, with prevalent sub-rounded quartz grains and minor amount of feldspars, chert and low grade metamorphic lithic fragments. The cement consists sometimes of authigenic quartz overgrowth and sometimes of carbonates.

3.5.2.3 Clasts distribution

The Sulzberger Bay cores are characterized by a distinct clast assemblage, with core 96-14 dominated by low-grade metamorphic rocks (81%), followed by granitoids and subordinate sedimentary rocks; on the other side, core 96-11 shows a prevalent granitoid lithology of clasts (79%) and a minor metamorphic component. Core 96-16 has a mixed composition with prevalent granitoids (40%), with subordinate metamorphic (27%) and sedimentary clasts (17%). Considering all the counted clasts together as a single group, these three cores have a overall composition consisting of dominant granitoids rock fragments (66%), and minor low-grade metamorphic rocks (15%) , quartz (10%) and sedimentary rocks (9%).

Trough 6 cores have an overall clasts distribution more homogeneous than the Sulzberger Bay group (Fig. 3.2 and 3.7). In every core, the predominant lithology among the counted clasts is low grade metamorphic rock, followed in general by sedimentary clasts and granitoids; only in one case (core 83-14) do granitoids prevail over sedimentary rock fragments in counted clasts. Volcanic and sub-volcanic clasts are rare and occur only in the westward 3 cores, distributed from the centre of the trough to its border, close to the Ice Shelf margin. The minor amount of granitoid clasts is reflected also in the overall composition of this group, with 75% clasts composed of low grade metamorphic rock fragments, 12% of sedimentary rock fragments and 5% of granitoids, with minor amount of volcanic and sub-volcanic clasts.

Also in the case of trough number 5 of Mosola and Anderson (2006) (fig. 3.2 and 3.7), low-grade metamorphic rocks are the most widespread lithologies among the counted clasts in the cores, with a percentage range of 50 and 72%. Granitoids are the second most represented lithology in all but one of the cores (99-04), followed by sedimentary clasts and minor mafic porphyries, dolerites and volcanic rocks. In this trough, granitoids are more abundant than sedimentary clasts, ranging from 50% in 94-61 core to 6% in 99-04 core. Volcanic rocks are minor, but are present in 4 out of 8 cores, with a peak occurrence in core 99-04 with 17% of the total. Sub-volcanic mafic porphyries and dolerites are present in minor amount in 5 out of 8 cores, with the maximum occurrence of 8% in 94-65 PC. Counting all the clasts together as a single group, the Trough 5 cores have a overall clast assemblage including 64% of metamorphic clasts, 24% of granitoids, 4% of sedimentary clasts and minor amounts of sub-volcanic and volcanic rocks.

3.5.3 Mineral Chemistry

3.5.3.1 Analytical details

Mineral chemistry analyses were carried out on 10 representative clasts. They were chosen on the basis of the presence of minerals such as amphiboles and white micas and considering also their lack of alteration. Only samples with fresh mineral surfaces were chosen. They include biotite amphibole schist (Thin sections 3 and 20), fine to medium grained metasandstones (Thin sections 11 and 56), biotite hornblende tonalite (Thin section 59), biotite-white mica gneissic schist (Thin section 21), biotite gneiss (Thin section 47), biotite-hornblende gneiss (Thin section 54), biotite-white mica hornfels (Thin section 62) and fine-grained calc-schist (Thin section 63). Chemical analysis of the main mineral phases identified via petrographic microscope were carried out with an X-ray energy dispersive system EDAX DX4 attached to a Scansion Electron Microscope Philips XL30 at the Department of Physical Sciences, Earth and Environment of Siena (Italy). Selected thin sections have been polished and carbon coated before carrying out measurements. Analytical conditions were 20 kV of accelerating voltage, 25 μA of emission current, and a beam spot size of 0.2 Am. Natural minerals were used as standards. Fe^{3+} concentration in clinoamphiboles and clinopyroxenes was estimated by the equation of Droop (1987), assuming charge balance.

3.5.3.2 Mineral chemistry results

Chemical analysis of bulk-rock samples from western Marie Byrd Land are available in literature (Weaver et al., 1991, 1992; Korhonen et al., 2010b; Yakymchuk et al., 2015; Brown et al., 2016). However, published mineral chemistry analyses from the region are sparse. One example is Smith C.H. (1996) in which mineral data of migmatitic paragneiss from Scott Nunataks (Alexandra Mountains) are presented.

In this work, also minerals from one sample of biotite-hornblende Ford granodiorite from Lewis Rocks (Phillips Mountains) and one sample of Swanson formation phyllite from Bailey Ridge (Sarnoff Range), both stored at the Polar Rock Repository at the Byrd Polar And Climate Research Center (Ohio State University), were analyzed. The latter were chosen because they showed similar petrographic features with some of the detrital clasts recovered offshore and to better check the possibility of a comparison with some bedrock sources.

Clinoamphiboles, biotites and white micas composition are shown in Fig. 3.4. All analyzed amphiboles are members of the calcic-amphibole group (Fig. 3.4a, Leake et al., 1997). Clinoamphiboles in biotite-amphibole schist (Thin section 20) are actinolitic hornblendes to actinolites in composition, with X_{Mg} varying from 0.63 to 0.80, and they are slightly zoned, with a Fe-richer core and a Mg-richer rim. In gneiss (Thin section 54),

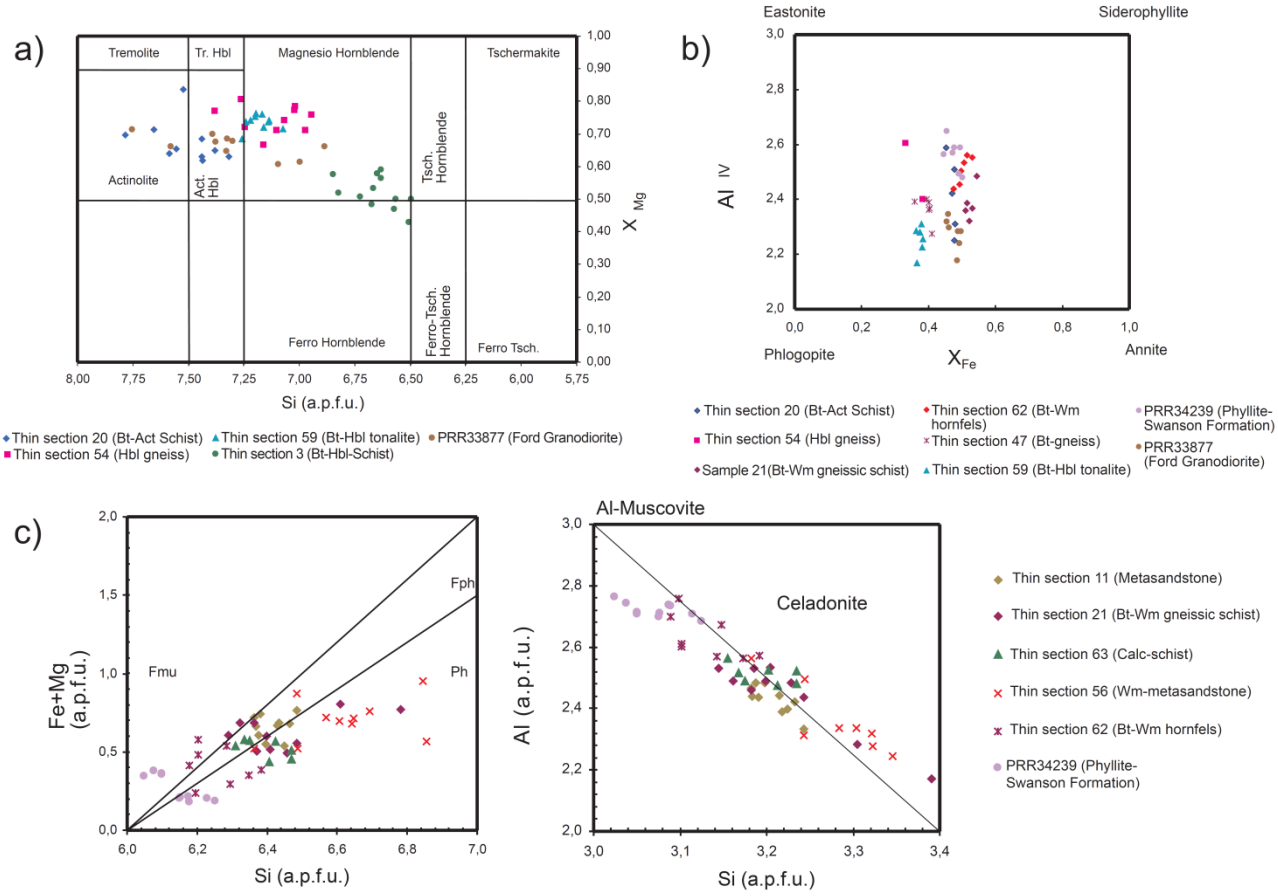

Figure 3.4- Representative chemical analysis of minerals from Eastern Ross Sea detrital clasts: a) Ca-amphibole classification from Leake et al. (1997), in terms of X_{mg} vs Si (atoms per formula unit); b) biotite composition in terms of Al^{IV}vs Fe/(Fe+Mg); c) white mica composition in terms of Fe + Mg vs SI and Al vs Si (atoms per formula unit). PRR33877 and PRR34239 are samples from bedrock, respectively from Ford Granodiorite and Swanson Formation, stored at the Polar Rock Repository, Ohio State University. Mineral abbreviation from Kretz (1983) except for Wm=White mica.

amphiboles are mostly Mg-hornblendes to actinolitic hornblendes (X_{Mg} ranging from 0.67 to 0.82), having a weak zonation, with Fe-richer rim and Mg-richer core in most cases. In tonalite (Thin section 59) amphiboles are mainly Mg-hornblendes (X_{Mg} 0.68-0.76), in some cases zoned, with a Mg-richer core and a Fe-enriched rim. In biotite schist (Thin section 3), amphiboles are distributed around the boundary between Mg- and Fe-hornblende fields (X_{Mg} 0.43-0.59).

Biotite representative compositions are listed in Figure 4b. In some samples (e.g. Thin section 62), biotites have a wide compositional range (X_{Fe} from 0.45 to 0.55) and exhibit a strong zonation, with Fe enrichment and Mg depletion from core to rim. In tonalite (Thin section 59), biotites show the lowest X_{Fe} values (0.37-0.39). Biotite-white mica schist (Thin section 21) and biotite-amphibole schist (Thin section 20) show a compositional range, with X_{Fe} ranging from 0.50 to 0.55 and 0.45 to 0.48, respectively.

White mica representative compositions are listed in Figure 4c. White micas in metasandstone (Thin section 11), calc-schist (Thin section 63), biotite-white mica hornfels (Thin section 62) and gneissic schist (Thin section 21) are all muscovite, with a wider and more phengitic composition in the latter. White micas in the other analyzed metasandstone (Thin section 56) show a wide and prevalently phengitic composition, with Si (a.p.f.u.) ranging from 6.36 to 6.86.

3.5.4 Zircon U-Pb geochronology

3.5.4.1 Analytical Details

Zircon U-Pb dating was performed on 3 piston core samples (96-10; 83-14; 94-63, sampling depths are listed in Table 3.1) at the LA-ICP-MS lab at the Consiglio Nazionale della Ricerche (CNR)–Istituto di Geoscienze e Georisorse Unità di Pavia (Italy), following the analytical conditions described in Langone et al. (2014). Samples were taken from sand-rich intervals in order to obtain as much datable grains as possible; the choice of cores was determined by their geographic location, which cover an extensive area from Colbeck Trough (core 96-10) close to Cape Colbeck in Edward VII Peninsula to trough 6 close to the coast of Roosevelt Island (core 83-14) and trough 5 (core 94-63). Sampling site locations are shown in Figure 2.

Zircon grains were separated from 100 cc bulk samples after careful crushing using heavy liquids and magnetic separation techniques. Zircon grains were then mounted in 1-inch epoxy-filled mount, and polished to obtain even surfaces suitable for cathodoluminescence (CL) imaging and LA-ICP-MS analyses. Prior to age determination, the internal structure of the zircons was investigated with backscattered electron (BSE) microscopy and CL using a Philips XL30 electron microscope equipped with a Centaurus CL detector. Prior to the CL imaging, the samples were carbon coated and the images were obtained using 15 kV acceleration voltage and a working distance of 26 mm. Age determinations were performed using a 193 nm ArF excimer laser microprobe (GeoLas200QMicrolas) coupled to a magnetic sector ICP-MS (Element 1 from ThermoFinnigan). Analyses were carried out in single spot mode and with a spot size fixed at 25 µm. The laser was operated with a frequency of 5 Hz, and with a fluence of 8 J/cm2. Sixty seconds of background signal and at least 30 s of ablation signal were acquired. The signals of masses ^{202}Hg, ^{204}(PbHg), ^{206}Pb, ^{207}Pb, ^{208}Pb, ^{232}Th, and ^{238}U were acquired in magnetic scan mode. ^{235}U is calculated from ^{238}U based on the mean ratio ^{238}U/^{235}U of 137.818, as recently proposed by Hiess et al. (2012). The 202 and 204 masses were collected in order to monitor the presence of common Pb in zircon (more analytical details in Tiepolo et al., 2003; Paquette and Tiepolo, 2007), with the signal of ^{202}Hg acquired to correct the isobaric interference of ^{204}Hg on ^{204}Pb (Horn et al., 2000). Mass bias and laser-induced fractionation were corrected

by adopting external standards, the GJ-1 zircon standard (608.5 ± 0.4 Ma; Jackson et al., 2004). During an analytical run of zircon analyses, a reference zircon (02123, 295 Ma; Ketchum et al., 2001) was analyzed together with unknowns for quality control. Data reduction was carried out through the GLITTER software package (Van Achterbergh et al., 2001). Time-resolved signals were carefully inspected to detect perturbation of the signal related to inclusions, cracks, or mixed-age domains. Within the same analytical run, the error associated with the reproducibility of the external standards was propagated to each analysis of sample (see Horstwood et al., 2003), and after this procedure each age determination was retained as accurate within the quoted error. The Concordia test was performed for each analytical spot from $^{206}Pb/^{238}U$ and $^{207}Pb/^{235}U$ ratios using the function in the software package Isoplot/Ex 3.00 (Ludwig, 2003). Percentage of discordance has been calculated as {[1(206Pb/238U age/207Pb/235U age)] * 100}, and only the U-Pb ages with a percent of discordance <±1.5% were considered reliable. Errors in the text and figures are reported as 2σ. Discordant data were not taken into consideration because of doubtful interpretation. The Isoplot software was also used to draw concordia diagrams and probability density plots. U-Pb isotope analyses and calculated ages of zircons are reported in the data repository.

3.5.4.2 Zircon U-Pb geochronology results

Zircon U-Pb results are reported in Table 3.3 and in figure 3.5. This figure displays the data from three new samples together with the data of Licht et al. (2014), in geographic order from East to West.

Sample from core 96-10 is characterized by zircon with various crystal shapes, from elongated to short, rounded and abraded, with internal features, as shown by CL imaging, varying from continuous oscillatory zoning to homogenous low CL core and rims, separated by high CL bands/domains. Eighty-one analyses were carried out, and 44 concordant ages were obtained.

Sample from core 83-14 yields generally zircon grains in a good state of conservation, with shapes varying from elongated to short. CL imaging highlights different kinds of zonation, from continuous oscillatory to high CL core and rims separated by low CL bands. Ninety-two analyses were performed and 52 concordant ages were obtained.

Sample from core 32-24 shows zircon grains with variable crystal shapes, from elongated to short, and several grains appear rounded and abraded. Zonation is very variable, with some crystals showing continuous oscillatory zonation, and others showing alternating homogeneous high and low CL bands and oscillatory zonation bands. Eighty-two concordant dates were obtained from 106 analyses.

Among the three analyzed samples five age populations could be identified.

A significant **Cretaceous-Paleocene** (63-139 Ma) population is present in samples from cores 96-10 (Colbeck Trough) and 83-14 (Roosevelt Island), whereas it is minor in sample 32-24 (Trough 5).

A **Devonian-Carboniferous** (311-360 Ma) population is present in samples from cores 96-10 and 83-14. This population is absent in sample from core 32-24, where a **Late Triassic** (201 Ma) population is instead present.

A **Neoproterozoic-Cambrian** (492-566 Ma) population is minor in sample from core 96-10 and major in samples from cores 83-14 and 32-24.

Subordinate Precambrian (987-1039; 1457; 2155 Ma) populations are present only in samples from cores 83-14 and 32-24.

These results resemble the data of Licht et al. (2014) in most respects (Figure 3.5).

Table 3.3 Isotopic data and U-Pb ages of zircon from samples 96-10, 83-14 and 32-24. Continues in the next pages.

			Data for Wetherill Plot					Ages							Concordant Ages	
Sample	$^{207}Pb/^{206}Pb$	1σ abs	207Pb/^{235}U	1σ abs	$^{206}Pb/^{238}U$	1σ abs	Rho	$^{207}Pb/^{206}Pb$	1σ abs	$^{207}Pb/^{235}U$	1σ abs	$^{206}Pb/^{238}U$	1σ abs	% U-Pb disc	2σ abs	
NBP96–01-10																
Ju24c006	0.04812	0.00205	0.10124	0.00452	0.01520	0.00028	0.4	105	4	98	4	97	2	0,7	97	4
Ju24c007	0.47275	0.05707	2.81583	0.28924	0.04320	0.00328	0.7	4158	502	1360	140	273	21	79,9		
Ju24c008	0.05287	0.00336	0.41783	0.02678	0.05681	0.00123	0.3	323	21	354	23	356	8	−0,5	356	15
Ju24c009	0.08423	0.00314	3.59811	0.14222	0.30914	0.00617	0.5	1298	48	1549	61	1,736	35	−12,1		
Ju24c010	0.06023	0.00576	0.91774	0.08702	0.10951	0.00309	0.3	612	59	661	63	670	19	−1,3	670	36
Ju24c011	0.04746	0.00696	0.11918	0.01740	0.01822	0.00048	0.2	72	11	114	17	116	3	−1,8	116	6
Ju24c013	0.04772	0.00319	0.10889	0.00733	0.01655	0.00032	0.3	85	6	105	7	106	2	−0,8	106	4
Ju24c014	0.04632	0.00204	0.10724	0.00490	0.01679	0.00028	0.4	14	1	103	5	107	2	−3,8		
Ju24c015	0.05641	0.00244	0.43750	0.01963	0.05637	0.00108	0.4	469	20	368	17	354	7	4,1		
Ju24c016	0.04784	0.00597	0.11848	0.01469	0.01797	0.00046	0.2	91	11	114	14	115	3	−1,0	115	6
Ju24c017	0.04836	0.00245	0.11545	0.00600	0.01732	0.00032	0.4	117	6	111	6	111	2	0,2	111	4
Ju24c018	0.79643	0.05074	8.90714	0.46764	0.08095	0.00381	0.9	4915	313	2329	122	502	24	78,5		
Ju24c019	0.04828	0.00234	0.11413	0.00568	0.01715	0.00030	0.4	113	5	110	5	110	2	0,1	110	4
Ju24c020	0.04730	0.00852	0.10676	0.01913	0.01637	0.00047	0.2	64	12	103	18	105	3	−1,6	105	6
Ju24c021	0.04677	0.00379	0.11172	0.00905	0.01733	0.00038	0.3	37	3	108	9	111	2	−3,0		
Ju24c022	0.77456	0.04336	7.67018	0.35705	0.07167	0.00293	0.9	4876	273	2193	102	446	18	79,7		
Ju24c023	0.19107	0.00808	0.64240	0.02690	0.02440	0.00055	0.5	2751	116	504	21	155	4	69,2		
Ju24c024	0.04765	0.00277	0.11118	0.00651	0.01694	0.00033	0.3	82	5	107	6	108	2	−1,2	108	4
Ju24c025	0.05451	0.00460	0.49118	0.04124	0.06544	0.00164	0.3	392	33	406	34	409	10	−0,7	409	20
Ju24c026	0.07019	0.00264	0.15452	0.00612	0.01597	0.00029	0.5	934	35	146	6	102	2	30,0		
Ju24c030	0.07454	0.00263	1.86818	0.07013	0.18211	0.00335	0.5	1056	37	1070	40	1,078	20	−0,8		
Ju24c031	0.76567	0.04094	432.45984	438.15154	4.09573	4.14873	1.0	4859	260	6165	6246	10,497	10,633	−70,3		
Ju24c032	0.05569	0.00412	0.13753	0.01016	0.01790	0.00038	0.3	440	33	131	10	114	2	12,6		
Ju24c033	0.05862	0.00206	0.13641	0.00509	0.01688	0.00028	0.4	553	19	130	5	108	2	16,9		
Ju24c034	0.05085	0.00716	0.23600	0.03241	0.03339	0.00110	0.2	234	33	215	30	212	7	1,6	212	14
Ju24c035	0.10233	0.00465	4.12272	0.18671	0.29335	0.00648	0.5	1667	76	1659	75	1,658	37	0,0	1658	59
Ju24c036	0.04796	0.00449	0.13504	0.01261	0.02043	0.00046	0.2	97	9	129	12	130	3	−1,4	130	6
Ju24c037	0.07814	0.00222	2.07500	0.06474	0.19297	0.00339	0.6	1150	33	1141	36	1,137	20	0,3	1138	35
Ju24c038	0.05003	0.00426	0.14273	0.01209	0.02070	0.00047	0.3	196	17	135	11	132	3	2,5	132	6
Ju24c039	0.29417	0.00827	0.94265	0.02764	0.02322	0.00046	0.7	3440	97	674	20	148	3	78,1		
Ju24c040	0.07840	0.00245	2.00370	0.06559	0.18614	0.00315	0.5	1157	36	1117	37	1,100	19	1,5	1104	33
Ju24c041	0.05373	0.00308	0.41583	0.02399	0.05628	0.00112	0.3	360	21	353	20	353	7	0,0	353	14
Ju24c042	0.36433	0.01398	1.73529	0.06349	0.03451	0.00084	0.7	3768	145	1022	37	219	5	78,6		
Ju24c043	0.29489	0.01442	1.08758	0.04966	0.02670	0.00073	0.6	3444	168	747	34	170	5	77,3		
Ju24c044	0.04946	0.00445	0.16793	0.01501	0.02460	0.00055	0.3	170	15	158	14	157	4	0,6	157	7
Ju24c045	0.04726	0.00330	0.10056	0.00694	0.01543	0.00032	0.3	62	4	97	7	99	2	−1,5	99	4
Ju24c046	0.08743	0.00698	1.53138	0.11971	0.12718	0.00349	0.4	1370	109	943	74	772	21	18,2		
Ju24c047	0.07691	0.00391	1.93481	0.09883	0.18256	0.00372	0.4	1119	57	1093	56	1,081	22	1,1		
Ju24d006	0.73272	0.03208	8.06137	0.28038	0.0798	0.00264	1	4796	210	2238	78	495	16	77,9		
Ju24d007	0.04967	0.01235	0.15379	0.03775	0.02239	0.00098	0.2	180	45	145	36	143	6	1,7	143	12
Ju24d008	0.04933	0.00219	0.14921	0.0065	0.02188	0.00038	0.4	164	7	141	6	140	2	1,2	140	5
Ju24d009	0.04943	0.00375	0.11192	0.00835	0.01643	0.00033	0.3	168	13	108	8	105	2	2,5	105	4
Ju24d010	0.08389	0.01058	0.20253	0.02467	0.01743	0.00064	0.3	1290	163	187	23	111	4	40,5		
Ju24d011	0.05236	0.00659	0.10792	0.0133	0.01524	0.00047	0.2	301	38	104	13	98	3	6,3		
Ju24d012	0.08967	0.00210	0.27716	0.0064	0.02241	0.00035	0.7	1419	33	248	6	143	2	42,5		
Ju24d013	0.04846	0.00529	0.11856	0.01265	0.01772	0.00048	0.3	122	13	114	12	113	3	0,5	113	6
Ju24d014	0.17770	0.00541	1.74246	0.05007	0.07112	0.00131	0.6	2632	80	1024	29	443	8	56,8		
Ju24d015	0.04818	0.00274	0.11791	0.00657	0.0178	0.00032	0.3	108	6	113	6	114	2	−0,5	114	4
Ju24d016	0.04810	0.00261	0.1117	0.00597	0.01684	0.0003	0.3	104	6	108	6	108	2	−0,1	108	4
Ju24d017	0.05182	0.00579	0.15746	0.01725	0.02286	0.00065	0.3	277	31	148	16	146	4	1,9	146	8
Ju24d018	0.05300	0.00687	0.13189	0.01674	0.01909	0.00061	0.3	329	43	126	16	122	4	3,1		

			Data for Wetherill Plot					Ages							Concordant Ages	
Sample	$^{207}Pb/^{206}Pb$	1σ abs	207Pb/^{235}U	1σ abs	$^{206}p_{b/U}^{238}$	1σ abs	Rho	$^{207}_{pb/}{}^{206}_{pb}$	1σ abs	$^{207}Pb/^{235}U$	1σ abs	$^{206}_{pb/}{}^{238}_{U}$	1σ abs	% U-Pb disc	2σ abs	
Ju24d019	0.09781	0.00492	0.21921	0.01061	0.01626	0.00034	0.4	1583	80	201	10	104	2	48,3		
Ju24d020	0.05434	0.00216	0.42226	0.0165	0.05715	0.00097	0.4	385	15	358	14	358	6	−0,2	358	12
Ju24d021	0.04924	0.00208	0.12144	0.00501	0.01793	0.0003	0.4	159	7	116	5	115	2	1,6	115	4
Ju24d022	0.04824	0.00291	0.1064	0.00628	0.01612	0.00031	0.3	111	7	103	6	103	2	−0,4	104	4
Ju24d023	0.06480	0.00306	0.21161	0.00978	0.02369	0.00043	0.4	768	36	195	9	151	3	22,6		
Ju24d024	0.20253	0.04199	0.47512	0.09079	0.01953	0.00161	0.4	2847	590	395	75	125	10	68,4		
Ju24d025	0.04819	0.00123	0.11646	0.003	0.01761	0.00028	0.6	109	3	112	3	113	2	−0,6	113	4
Ju24d026	0.04739	0.00327	0.15049	0.01019	0.02303	0.00047	0.3	69	5	142	10	147	3	−3,1		
Ju24d027	0,07665	0,00330	1,85064	0,078	0,17695	0,00346	0,5	1112	48	1064	45	1,050	21	1,3		
Ju24d032	0,13112	0,00719	0,11963	0,00623	0,00662	0,00015	0,4	2113	116	115	6	43	1	62,9		
Ju24d033	0,13351	0,00195	7,31453	0,10443	0,39511	0,00549	1	2145	31	2151	31	2,146	30	0,2	2154	11
Ju24d034	0,05845	0,00140	0,73906	0,01729	0,09161	0,00131	0,6	547	13	562	13	565	8	−0,6	564	15
Ju24d035	0,05921	0,00399	0,76221	0,05028	0,09367	0,00202	0,3	575	39	575	38	577	12	−0,3	577	24
Ju24d036	0,07115	0,00123	1,59366	0,02782	0,16248	0,00241	0,8	962	17	968	17	971	14	−0,3	967	22
Ju24d037	0,33504	0,01526	1,32588	0,05269	0,02871	0,00078	0,7	3640	166	857	34	182	5	78,7		
Ju24d038	0,06183	0,00148	0,67829	0,0161	0,07962	0,00122	0,6	668	16	526	12	494	8	6,1		
Ju24d039	0,73196	0,06492	22,21374	2,75323	0,22048	0,02707	1	4795	425	3193	396	1,284	158	59,8		
Ju24d040	0,04838	0,00384	0,11313	0,00876	0,01699	0,00037	0,3	118	9	109	8	109	2	0,2	109	5
Ju24d041	0,04830	0,00382	0,12234	0,00949	0,01838	0,00041	0,3	114	9	117	9	117	3	−0,2	117	5
Ju24d042	0,04762	0,00323	0,10902	0,00726	0,0168	0,00036	0,3	80	5	105	7	107	2	−2,2	107	5
Ju24d043	0,04888	0,00142	0,11107	0,0032	0,01649	0,00025	0,5	142	4	107	3	105	2	1,4	106	3
Ju24d044	0,04973	0,00226	0,15423	0,00686	0,02258	0,0004	0,4	182	8	146	6	144	3	1,2	144	5
Ju24d045	0,05049	0,00135	0,12026	0,00318	0,01728	0,00027	0,6	218	6	115	3	110	2	4,2		
Ju24d046	0,05352	0,00130	0,41637	0,01	0,05644	0,00085	0,6	351	8	353	8	354	5	−0,1	354	10
Ju24d047	0,05802	0,00215	0,69651	0,02522	0,08718	0,00146	0,5	531	20	537	19	539	9	−0,4	539	17
Ju24d048	0,24641	0,01135	0,73239	0,03049	0,02152	0,00054	0,6	3162	146	558	23	137	3	75,4		
Ju24d050	0,04861	0,00264	0,11794	0,00627	0,01762	0,00031	0,3	129	7	113	6	113	2	0,5	113	4
Ju24d051	0,04770	0,00222	0,11246	0,00514	0,01711	0,00029	0,4	84	4	108	5	109	2	−1,1	110	4
Ju24d052	0,05163	0,00435	0,11189	0,00921	0,01571	0,00037	0,3	269	23	108	9	100	2	6,7		
DF83–014																
Ju25e006	0.07663	0.00289	1.89073	0.08115	0.17908	0.00341	0.4	1112	42	1078	46	1,062	20	1,5		
Ju25e007	0.04767	0.00772	0.14795	0.02367	0.02254	0.00086	0.2	83	13	140	22	144	5	−2,6		
Ju25e008	0.08022	0.00886	0.22583	0.02453	0.02045	0.00069	0.3	1202	133	207	22	130	4	36.9		
Ju25e009	0.06970	0.00543	0.16619	0.01305	0.01732	0.00044	0.3	920	72	156	12	111	3	29.1		
Ju25e010	0.41504	0.02194	3.12259	0.15601	0.05476	0.00185	0.7	3964	210	1438	72	344	12	76.1		
Ju25e011	0.08333	0.00787	0.26811	0.02524	0.02337	0.00067	0.3	1277	121	241	23	149	4	38.3		
Ju25e012	0.05459	0.00324	0.39457	0.02436	0.05259	0.00115	0.4	395	23	338	21	330	7	2.2	331	14
Ju25e014	0.04963	0.00452	0.12437	0.01138	0.01825	0.00049	0.3	178	16	119	11	117	3	2.0	117	6
Ju25e015	0.04881	0.00363	0.10928	0.00832	0.01619	0.00036	0.3	139	10	105	8	104	2	1.7	104	5
Ju25e016	0.04705	0.00206	0.10035	0.00484	0.01549	0.00027	0.4	52	2	97	5	99	2	−2.0	99	4
Ju25e017	0.05885	0.00259	0.73612	0.03553	0.09083	0.00168	0.4	562	25	560	27	560	10	−0.1	560	20
Ju25e018	0.05862	0.00223	0.70439	0.03042	0.08727	0.00158	0.4	553	21	541	23	539	10	0.4	540	19
Ju25e019	0.05639	0.00176	0.61203	0.02307	0.07884	0.00135	0.5	468	15	485	18	489	8	−0.9	489	16
Ju25e020	0.04775	0.00175	0.11516	0.00485	0.01751	0.00031	0.4	87	3	111	5	112	2	−1.1	112	4
Ju25e021	0.06153	0.00277	0.90585	0.04448	0.10670	0.00198	0.4	658	30	655	32	654	12	0.2	654	23
Ju25e022	0.05121	0.00743	0.11889	0.01719	0.01686	0.00050	0.2	250	36	114	16	108	3	5.5		
Ju25e023	0.06167	0.00152	1.36421	0.04452	0.16069	0.00259	0.5	663	16	874	29	961	15	−9.9		
Ju25e024	0.05871	0.00211	0.73198	0.03035	0.09054	0.00160	0.4	556	20	558	23	559	10	−0.2	559	19
Ju25e025	0.07608	0.00216	1.93261	0.06859	0.18443	0.00314	0.5	1097	31	1092	39	1,091	19	0.1	1091	33
Ju25e026	0.06406	0.00213	1.06193	0.04142	0.12066	0.00223	0.5	744	25	735	29	734	14	0.1	734	25
Ju25e027	0.05872	0.00160	1.19944	0.04143	0.14847	0.00248	0.5	557	15	800	28	892	15	−11.5		
Ju25e028	0.05716	0.00322	0.63172	0.03688	0.08045	0.00183	0.4	498	28	497	29	499	11	−0.3	499	22
Ju25e029	0.04904	0.00316	0.09900	0.00651	0.01468	0.00035	0.4	150	10	96	6	94	2	2.0	94	5

			Data for Wetherill Plot					Ages							Concordant Ages	
Sample	$^{207}Pb/^{206}Pb$	1σ abs	207Pb/^{235}U	1σ abs	$^{206}p_{b/U}^{238}$	1σ abs	Rho	$^{207}_{pb/}{}^{206}_{pb}$	1σ abs	$^{207}Pb/^{235}U$	1σ abs	$^{206}_{pb/}{}^{238}_{U}$	1σ abs	% U-Pb disc	2σ abs	
Ju25e030	0.18379	0.00461	1.48129	0.04881	0.05850	0.00097	0.5	2687	67	923	30	366	6	60.3		
Ju25e031	0.06907	0.00231	1.44448	0.05716	0.15172	0.00260	0.4	901	30	908	36	911	16	−0.3	910	29
Ju25e032	0.06772	0.00190	1.34569	0.04715	0.14421	0.00236	0.5	860	24	866	30	868	14	−0.3	868	26
Ju25e033	0.07544	0.00286	1.90099	0.08152	0.18284	0.00339	0.4	1080	41	1081	46	1,082	20	−0.1		
Ju25e037	0.04911	0.00184	0.12891	0.00552	0.01904	0.00032	0.4	153	6	123	5	122	2	1.2	122	4
Ju25e038	0.05743	0.00186	0.63985	0.02462	0.08077	0.00134	0.4	508	16	502	19	501	8	0.3	501	16
Ju25e039	0.07465	0.00186	1.38099	0.04529	0.13412	0.00214	0.5	1059	26	881	29	811	13	7.9		
Ju25e040	0.05536	0.00173	0.55221	0.02076	0.07228	0.00124	0.5	427	13	446	17	450	8	−0.8	450	15
Ju25e041	0.05834	0.00187	0.72184	0.02757	0.08969	0.00149	0.4	543	17	552	21	554	9	−0.4	554	17
Ju25e042	0.05050	0.00230	0.20787	0.01032	0.02983	0.00054	0.4	218	10	192	10	189	3	1.2	189	7
Ju25e043	0.06299	0.00200	0.74018	0.02810	0.08523	0.00138	0.4	708	22	563	21	527	9	6.3		
Ju25e044	0.04670	0.00227	0.13694	0.00717	0.02125	0.00038	0.3	34	2	130	7	136	2	−4.0		
Ju25e045	0.06912	0.00198	1.43724	0.05115	0.15052	0.00252	0.5	902	26	905	32	904	15	0.1	904	28
Ju25e046	0.07788	0.00216	0.66339	0.02311	0.06169	0.00100	0.5	1144	32	517	18	386	6	25.3		
Ju25e047	0.05016	0.00631	0.10960	0.01378	0.01584	0.00042	0.2	202	25	106	13	101	3	4.1		
Ju25e048	0.05298	0.00264	0.41489	0.02222	0.05676	0.00106	0.3	328	16	352	19	356	7	−1.0	356	13
Ju25e049	0.05661	0.00164	0.61162	0.02196	0.07816	0.00128	0.5	476	14	485	17	485	8	−0.1	485	15
Ju25e050	0.09015	0.00224	2.14094	0.06995	0.17212	0.00266	0.5	1429	35	1162	38	1,024	16	11.9		
Ju25e051	0.06386	0.00557	0.13812	0.01216	0.01565	0.00037	0.3	737	64	131	12	100	2	23.8		
Ju25e052	0.04914	0.00248	0.10900	0.00591	0.01606	0.00028	0.3	155	8	105	6	103	2	2.2	103	4
Ju25e053	0.05326	0.00139	0.37930	0.01279	0.05155	0.00080	0.5	340	9	327	11	324	5	0.8	324	10
Ju25e054	0.07849	0.00243	2.17402	0.08035	0.19879	0.00343	0.5	1159	36	1173	43	1,169	20	0.3	1170	36
Ju25e055	0.37190	0.02549	6.64725	0.42214	0.12862	0.00560	0.7	3799	260	2066	131	780	34	62.2		
Ju25e056	0.07894	0.00204	2.17142	0.07267	0.19888	0.00314	0.5	1171	30	1172	39	1,169	18	0.2	1170	32
Ju25e057	0.06652	0.00223	1.31273	0.05138	0.14241	0.00245	0.4	823	28	851	33	858	15	−0.8	857	27
Ju25e058	0.05701	0.00280	0.64171	0.03355	0.08085	0.00156	0.4	492	24	503	26	501	10	0.4	501	19
Ju25e059	0.06516	0.00188	0.58702	0.02092	0.06512	0.00104	0.4	780	22	469	17	407	6	13.3		
Ju25e060	0.26389	0.01508	0.99013	0.05474	0.02690	0.00080	0.5	3270	187	699	39	171	5	75.5		
Ju25e061	0.05520	0.00272	0.52178	0.02692	0.06843	0.00124	0.4	420	21	426	22	427	8	−0.1	427	15
Ju25e062	0.25789	0.01669	4.48268	0.28580	0.12560	0.00424	0.5	3234	209	1728	110	763	26	55.9		
Ju25e063	0.06931	0.00188	1.42350	0.04857	0.14892	0.00229	0.5	908	25	899	31	895	14	0.4	895	25
Ju25e064	0.04783	0.00383	0.10342	0.00829	0.01558	0.00036	0.3	91	7	100	8	100	2	0.3	100	5
Ju25c005_91500	0.07538	0.00401	1.87954	0.09612	0.17943	0.00467	0.5	1079	57	1074	55	1,064	28	0.9		
Ju25c006	0.04939	0.01191	0.13329	0.03163	0.01980	0.00094	0.2	166	40	127	30	126	6	0.5	126	12
Ju25c007	0.07829	0.01359	0.26142	0.04432	0.02424	0.00104	0.3	1154	200	236	40	154	7	34.5		
Ju25c008	0.08615	0.00377	0.18207	0.00765	0.01536	0.00036	0.6	1342	59	170	7	98	2	42.1		
Ju25c009	0.07713	0.00596	0.17172	0.01276	0.01620	0.00047	0.4	1125	87	161	12	104	3	35.6		
Ju25c010	0.13442	0.00284	7.40510	0.15024	0.39987	0.00822	1.0	2157	46	2162	44	2,168	45	−0.3	2155	10
Ju25c011	0.07215	0.00204	1.61677	0.04427	0.16314	0.00348	0.8	990	28	977	27	9,74	21	0.3	976	34
Ju25c012	0.07514	0.00173	1.85792	0.04125	0.17945	0.00367	0.9	1072	25	1066	24	1,064	22	0.2	1068	26
Ju25c013	0.17255	0.00617	0.44130	0.01458	0.01859	0.00044	0.7	2583	92	371	12	119	3	68.0		
Ju25c014	0.05201	0.00190	0.28301	0.01004	0.03956	0.00086	0.6	286	10	253	9	250	5	1.2	250	11
Ju25c015	0.05789	0.00139	0.67547	0.01589	0.08462	0.00175	0.9	526	13	524	12	524	11	0.1	524	19
Ju25c016	0.64850	0.02156	8.94317	0.25083	0.10009	0.00283	1.0	4621	154	2332	65	615	17	73.6		
Ju25c017	0.04702	0.02891	0.12551	0.07646	0.01933	0.00167	0.1	50	31	120	73	123	11	−2.8		
Ju25c018	0.03746	0.00849	0.12552	0.02816	0.02430	0.00093	0.2	−523	−119	120	27	155	6	−28.9		
Ju25c019	0.07665	0.00220	1.97291	0.05429	0.18695	0.00394	0.8	1112	32	1106	30	1,105	23	0.1	1106	37
Ju25c020	0.35612	0.01403	1.67001	0.05782	0.03403	0.00093	0.8	3733	147	997	35	216	6	78.4		
Ju25c021	0.06806	0.00154	1.33494	0.02913	0.14217	0.00292	0.9	870	20	861	19	857	18	0.5	865	23
Ju25c022	0.04879	0.00351	0.12473	0.00870	0.01849	0.00047	0.4	138	10	119	8	118	3	1.0	118	6
Ju25c028	0.07570	0.00173	1.95465	0.04272	0.18713	0.00385	0.9	1087	25	1100	24	1,106	23	−0.5	1094	24
Ju25c029	0.07755	0.00366	2.08569	0.09493	0.19444	0.00469	0.5	1135	54	1144	52	1,145	28	−0.1	1145	48
Ju25c030	0.06063	0.00165	0.85666	0.02244	0.10253	0.00211	0.8	626	17	628	16	629	13	−0.1	629	23

			Data for Wetherill Plot					Ages							Concordant Ages	
Sample	$^{207}Pb/^{206}Pb$	1σ abs	207Pb/^{235}U	1σ abs	$^{206}Pb/^{238}U$	1σ abs	Rho	$^{207}Pb/^{206}Pb$	1σ abs	$^{207}Pb/^{235}U$	1σ abs	$^{206}Pb/^{238}U$	1σ abs	% U-Pb disc	2σ abs	
Ju25c031	0.11648	0.00972	0.34729	0.02731	0.02165	0.00075	0.4	1903	159	303	24	138	5	54.4		
Ju25c032	0.07094	0.00202	1.57165	0.04267	0.16069	0.00335	0.8	956	27	959	26	961	20	−0.2	960	33
Ju25c033	0.05907	0.00173	0.75431	0.02111	0.09258	0.00189	0.7	570	17	571	16	571	12	0.0	571	22
Ju25c034	0.07520	0.00238	1.87339	0.05676	0.18051	0.00389	0.7	1074	34	1072	32	1,070	23	0.2	1071	38
Ju25c035	0.05755	0.00133	0.67029	0.01482	0.08449	0.00170	0.9	513	12	521	12	523	10	−0.4	521	18
Ju25c036	0.04768	0.01616	0.14223	0.04782	0.02170	0.00105	0.1	83	28	135	45	138	7	−2.5		
Ju25c037	0.18861	0.01772	0.47584	0.04130	0.01833	0.00076	0.5	2730	256	395	34	117	5	70.4		
Ju25c038	0.02325	0.00401	0.06230	0.01068	0.01944	0.00051	0.2	−2024	−349	61	11	124	3	−102.3		
Ju25c039	0.05637	0.00214	0.57112	0.02059	0.07383	0.00159	0.6	467	18	459	17	459	10	−0.1	459	19
Ju25c040	0.64151	0.02764	12.93097	0.47426	0.14666	0.00523	1.0	4605	198	2675	98	882	31	67.0		
Ju25c041	0.04806	0.00469	0.12430	0.01188	0.01878	0.00053	0.3	102	10	119	11	120	3	−0.8	120	7
Ju25c042	0.07589	0.00250	0.42228	0.01328	0.04045	0.00086	0.7	1092	36	358	11	256	5	28.5		
Ju25c043	0.09983	0.00239	0.22404	0.00508	0.01633	0.00034	0.9	1621	39	205	5	104	2	49.1		
Ju25c044	0.10239	0.00221	0.89830	0.01830	0.06392	0.00133	1.0	1668	36	651	13	399	8	38.6		
Ju25c045	0.07305	0.00189	1.71279	0.04159	0.16973	0.00354	0.9	1015	26	1013	25	1,011	21	0.3	1014	31
Ju25c046	0.38961	0.02026	1.77963	0.07868	0.03334	0.00115	0.8	3869	201	1038	46	211	7	79.6		
E LT 32–024																
Ma21a005	0.05854	0.00208	0.71942	0.02288	0.08874	0.00371	0.6	550	20	550	17	543	11	0,4	548	20
Ma21a006	0.05029	0.00351	0.20841	0.01397	0.03005	0.00056	0.3	203	15	132	13	191	4	0,7	131	8
Ma21a007	0.05699	0.00134	0.63556	0.01144	0.08111	0.00343	1.0	491	12	500	9	503	9	−0,6	493	12
Ma21a0D8	0.05826	0.00177	0.68025	0.01762	0.08480	0.00153	0.7	540	16	527	34	525	9	0,4	525	18
Ma21a009	0.09327	0.00202	1.11206	0.01719	0.08664	0.00355	1.2	1493	32	759	32	536	10	23,4		
Ma21a012	0.05733	0.00133	0.62186	0.01030	0.07887	0.00339	3.0	504	12	431	9	489	9	0,3	436	9
Ms21a013	0.09158	0.00205	3.23315	0.05478	0.25580	0.00459	3.0	1461	33	1465	25	1,463	27	−0,2	1462	8
Ma21a014	0.08634	0.00202	2.77391	0.04918	0.23205	0.00421	1.0	1357	32	1343	24	1,345	24	0,2	1353	9
Ma21a015	0.05726	0.00165	0.62924	0.01534	0.07383	0.00346	0.3	502	14	436	32	495	9	0,1	435	17
Ma21a016	0.06087	0.00622	0.84117	0.08339	0.10018	0.00287	0.3	635	65	620	61	615	18	0,7	616	34
Ma21a017	0.05703	0.00158	0.62610	0.01444	0.07970	0.00345	0.8	493	14	494	31	494	9	−0,1	434	17
Ma21a018	0.05676	0.00189	0.59464	0.01752	0.07598	0.00344	0.6	482	16	474	34	472	9	0,4	472	17
Ma21a013	0.09350	0.00241	3.92779	0.07553	0.28579	0.00540	1.0	1617	39	1613	31	1,620	31	−0,1	1618	13
Ma21a021	0.08802	0.00345	1.23061	0.04345	0.10146	0.00202	0.6	1383	51	815	29	623	12	23,5		
Ma21a022	0.05713	0.00211	0.63814	0.02118	0.08105	0.00354	0.6	437	18	501	37	502	10	−0,2	502	18
Ma21a024	0.05552	0.00167	0.21292	0.00548	0.02787	0.00050	0.7	433	13	196	5	177	3	9,6		
Ma21a026	0.08652	0.00164	1.02619	0.01217	0.08607	0.00152	1.5	1352	26	717	9	532	9	25,8		
Ma21a027	0.05760	0.00170	0.62657	0.01544	0.07914	0.00342	0.7	515	15	434	32	491	9	0,6	432	17
Ma21a028	0.07286	0.00289	0.81747	0.02330	0.08141	0.00352	0.6	1010	40	607	22	505	10	16,8		
Ma21a023	0.07755	0.00228	2.06016	0.05152	0.19253	0.00373	0.3	1138	33	1136	28	1,135	22	0,1	1136	34
Ma21a030	0.05992	0.00157	0.73214	0.01650	0.09474	0.00359	0.8	601	16	587	32	534	10	0,5	586	18
Ma21a031	0.07559	0.00204	1.91646	0.04253	0.13409	0.00339	0.3	1084	29	1037	24	1,083	20	0,2	1087	30
Ma21a032	0.07584	0.00269	1.89108	0.05961	0.18080	0.00358	0.6	1091	39	1078	34	1,071	21	0,6		
Ma21a036	0.06058	0.00437	0.24787	0.01709	0.02959	0.00073	0.4	624	45	225	35	189	5	16,1		
Ma21a037	0.05048	0.00616	0.23125	0.02778	0.03325	0.00079	0.2	217	26	213	25	211	5	0,2	211	10
Ma21a038	0.06051	0.00139	0.66999	0.01183	0.08036	0.00345	1.0	622	14	521	9	438	9	4,3		
Ma21a039	0.05745	0.00219	0.66877	0.02329	0.08444	0.00368	0.6	509	19	520	38	523	10	−0,5	522	20
Ma21a040	0.05181	0.00267	0.29789	0.01446	0.04172	0.00087	0.4	277	14	265	33	263	5	0,5	264	11
Ma21a041	0.04956	0.00600	0.11968	0.01410	0.01752	0.00053	0.3	174	21	115	34	112	3	2,5		
Ma21a042	0.06112	0.00232	0.86809	0.02987	0.10304	0.00205	0.6	643	24	635	22	632	13	0,4	633	24
Ma21a043	0.04694	0.00209	0.20322	0.00802	0.03013	0.00058	0.5	145	6	188	7	138	4	−1,9	131	7
Ma21a044	0.13734	0.00623	0.32614	0.01328	0.01722	0.00040	0.6	2194	39	287	32	110	3	61,6		
Ma21a045	0.05068	0.00372	0.23918	0.01696	0.03426	0.00074	0.3	226	17	218	35	217	5	0,3	217	9
Ma21a046	0.05792	0.00171	0.66583	0.01681	0.08338	0.00353	0.7	527	16	518	33	516	9	0,4	517	18
Ma21a047	0.07755	0.00221	2.04361	0.04301	0.19106	0.00368	0.3	1138	32	1130	27	1,127	22	0,3	1130	33
Ma21a048	0.05893	0.00210	0.71681	0.02295	0.08832	0.00369	0.6	565	20	549	38	546	10	0,6	546	20

			Data for Wetherill Plot					Ages							Concordant Ages	
Sample	$^{207}Pb/^{206}Pb$	1σ abs	207Pb/^{235}U	1σ abs	$^{206}p_{b/U}^{238}$	1σ abs	Rho	$^{207}_{pb/}{}^{206}_{pb}$	1σ abs	$^{207}Pb/^{235}U$	1σ abs	$^{206}_{pb/}{}^{238}_{U}$	1σ abs	% U-Pb disc	2σ abs	
Ma21a049	0.07237	0.D0341	1.67075	0.07235	0.16808	0.00375	0.5	996	47	997	43	1,002	22	−0,4	1001	40
Ma21a050	0.07742	0.00201	2.06705	0.04326	0.19359	0.00354	0.3	1132	29	1138	24	1,141	21	−0,2	1137	28
Ma21a051	0.07095	0.00175	1.55857	0.02336	0.15356	0.00285	0.3	956	24	954	33	954	17	0,0	354	21
Ma21a052	0.06006	0.00173	0.83133	0.02024	0.10041	0.00383	0.7	606	17	614	35	617	11	−0,4	616	20
Ma21a053	0.05892	0.00149	0.73737	0.01438	0.09072	0.00357	0.3	564	14	561	31	560	10	0,2	561	17
Ma23a054	0.11930	0.00262	1.25012	0.01332	0.07599	0.00338	1.3	1946	43	823	33	472	9	42,7		
Ma21a055	0.05905	0.00191	0.72717	0.02057	0.08942	0.00372	0.7	569	18	555	36	582	11	0,5	553	20
Ma21a056	0.05722	0.00185	0.6113D	0.01750	0.07816	0.00351	0.7	500	16	484	34	485	9	−0,2	485	18
Ma21a057	0.05386	0.00217	0.46279	0.01685	0.06257	0.00339	0.5	365	15	336	34	331	7	−1,3	331	14
Ma21a058	0.25172	0.02299	0.05149	0.00425	0.00149	0.00006	0.5	3196	232	51	4	10	0	31,2		
Ma21a059	0.05820	0.00258	0.68279	0.02803	0.08542	0.00376	0.5	537	24	528	22	523	11	0,0	528	31
Ma21a060	0.06545	0.00155	1.14308	0.02056	0.12711	0.00223	1.0	783	19	774	34	771	14	0,3	778	14
Ma21a061	0.05084	0.D0323	0.25633	0.01549	0.03682	0.00084	0.4	234	15	232	14	233	5	−0,6	233	10
Ma21aOG2	0.05221	0.00306	0.31318	0.01740	0.04354	0.00091	0.4	295	17	277	15	275	6	0,5	275	11
Ma21a065	0.08320	0.00437	2.51919	0.12386	0.21953	0.00491	0.5	1274	67	1273	63	1,279	29	−0,1	1273	50
Ma21a06B	0.07398	0.00170	1.73666	0.03055	0.17038	0.00323	1.0	1041	24	1022	38	1,018	13	0,5	3030	8
Ma21a067	0.04725	0.00664	0.03934	0.00542	0.00602	0.00015	0.2	62	3	33	5	39	1	0,8	33	2
Ma23a068	0.05750	0.00155	0.67061	0.01439	0.08443	0.00352	0.3	515	14	521	32	523	9	−0,3	522	17
Ma21b005	0.07590	0.00329	1.86493	0.07396	0.17810	0.00300	0.4	1092	47	1063	42	1,057	13	1,1		
Ma21b006	0.02098	0.00309	0.05126	0.00746	0.01772	0.00039	0.2	−2431	−358	51	7	113	2	−123,1		
Ma21h007	0.05958	0.00157	0.73354	0.01645	0.08926	0.00328	0.6	588	16	559	33	551	8	1,3	553	15
Ma21b008	0.05747	0.00227	0.68756	0.02493	0.08675	0.00338	0.4	510	20	531	39	536	9	−0,9	536	16
Ma21b009	0.05819	0.00198	0.72161	0.02229	0.08989	0.00339	0.5	537	18	552	37	555	9	−0,6	555	16
Ma21b010	0.07155	0.00340	0.25133	0.01119	0.02542	0.00044	0.4	976	46	228	30	162	3	28,3		
Ma21b0Jl	0.05830	0.00259	0.68972	0.02863	0.08556	0.00345	0.4	541	24	533	22	530	9	0,5	530	17
Ma21b012	0.10714	0.00672	0.38401	0.02264	0.02601	0.00056	0.4	1751	110	330	39	166	4	43,8		
Ma21b013	0.07622	0.00230	1.97950	0.05277	0.18818	0.00285	0.6	1101	33	1109	30	1,112	17	0,3	1111	29
Ma21b014	0.06617	0.00195	1.22674	0.03214	0.13446	0.00200	0.6	812	24	813	21	813	12	0,0	313	22
Ma21b015	0.05850	0.00183	0.69846	0.01358	0.08646	0.00330	0.5	552	17	538	35	535	8	0,6	535	15
Ma21b016	0.05859	0.00213	0.70340	0.02326	0.08711	0.00333	0.5	552	20	541	38	533	8	0,4	539	16
Ma21b017	0.04728	0.00287	0.11313	0.00660	0.01735	0.00030	0.3	53	4	109	6	111	2	−1,3	111	4
Ma21b018	0.07057	0.00177	1.55805	0.03249	0.16010	0.00226	0.7	945	24	954	20	957	14	−0,4	956	23
Ma21b019	0.06003	0.00400	0.78965	0.05085	0.09536	0.00380	0.3	605	40	591	38	587	11	0,6	587	21
Ma21b02G	0.06028	0.D0154	0.85249	0.01829	0.10259	0.00345	0.7	614	16	626	13	630	9	−0,6	629	16
Ma21b021	0.05158	0.01457	0.29683	0.08272	0.04165	0.00389	0.2	271	77	264	74	263	12	0,3	263	23
Ma21b022	0.04908	0.00144	0.18903	0.00483	0.02794	0.00040	0.6	152	4	176	4	173	3	−1,0	178	5
Ma21b023	0.06194	0.00449	0.93594	0.06510	0.10954	0.00237	0.3	672	49	671	47	671	15	0,0	671	27
Ma21b024	0.06307	0.00335	1.00963	0.05119	0.11612	0.00203	0.3	711	38	709	36	708	12	0,1	708	23
Ma21b025	0.07456	0.00228	1.81132	0.04307	0.17604	0.00255	0.6	1059	32	1050	28	1,045	16	0,4	1047	28
Ma21b02G	0.04829	0.00339	0.11545	0.00785	0.01734	0.00030	0.3	114	8	111	8	111	2	0,1	111	4
Ma21b027	0.05031	0.D0253	0.20551	0.00982	0.02965	0.00048	0.3	209	11	190	9	188	3	0,7	188	6
Ma21b028	0.06044	0.00239	0.49769	0.01816	0.05975	0.00094	0.4	613	24	410	35	374	6	8,8		
Ma21b029	0.049B3	0.00327	0.19955	0.01257	0.02307	0.00054	0.3	187	12	185	32	185	3	0,0	185	7
Ma21b030	0.03356	0.00203	0.26072	0.01513	0.05619	0.00093	0.3	−819	−43	235	34	352	6	−19,8		
Ma21b031	0.08866	0.00283	1.34980	0.05679	0.15968	0.00250	0.6	1397	45	1038	32	955	16	13,1		
Ma21b032	0.07303	0.00203	1.70674	0.04061	0.16951	0.00246	0.6	1015	28	1011	24	1,009	15	0,2	1010	26
Ma21h033	0.04935	0.00393	0.18039	0.01397	0.02652	0.00052	0.3	164	13	168	33	169	3	−0,2	169	7
Ma21b035	0.07457	0.00201	1.82303	0.04123	0.17713	0.00248	0.6	1060	29	1054	24	1,051	15	0,2	1052	25
MB21KJ39	0.05059	0.00300	0.23845	0.01354	0.03418	0.00052	0.3	222	13	217	32	217	4	0,2	217	8
Ma21b040	0.07340	0.00244	0.75720	0.02275	0.07486	0.00315	0.5	1025	34	572	37	465	7	18,7		
Ma21b041	0.05705	0.00194	0.64089	0.01386	0.08147	0.00322	0.5	433	17	503	35	505	8	−0,4	505	14
Ma21b042	0.13252	0.00298	4.70048	0.03404	0.25732	0.00358	0.3	2132	48	1767	32	1,476	21	16,5		
Ma21b043	0.08054	0.D0242	2.32140	0.06154	0.20874	0.00313	0.6	1213	36	1219	32	1,222	18	0,3	1221	31

			Data for Wetherill Plot					Ages							Concordant Ages	
Sample	$^{207}Pb/^{206}Pb$	1σ abs	207Pb/^{235}U	1σ abs	$^{206}p_{b}^{238}{}_{U}$	1σ abs	Rho	$^{207}{}_{pb}{}^{206}{}_{pb}$	1σ abs	$^{207}Pb/^{235}U$	1σ abs	$^{206}{}_{pb}{}^{238}{}_{U}$	1σ abs	% U-Pb disc	2σ abs	
Ma21b044	0.07453	0.00234	0.83065	0.02310	0.08039	0.00120	0.5	1067	33	614	17	493	7	18,8		
Ma21b045	0.05753	0.00234	0.67158	0.02541	0.08445	0.00133	0.4	516	21	522	20	523	8	−0,2	523	15
Ma21b046	0.05930	0.00403	0.72483	0.04743	0.08855	0.00187	0.3	578	39	554	36	548	12	1,1	548	22
Ma21b047	0.07941	0.00321	2.21243	0.08172	0.20185	0.00340	0.5	1182	48	1185	44	1,185	20	0,0	1185	35
Ma21b048	0.06107	0.00208	0.90140	0.02777	0.10706	0.00153	0.5	642	22	652	20	656	10	−0,5	655	19
Ma21b049	0.04996	0.00647	0.19523	0.02475	0.02848	0.00080	0.2	193	25	181	23	181	5	0,0	181	10
Ma21b050	0.05018	0.00342	0.21821	0.01436	0.03154	0.00058	0.3	203	14	200	13	200	4	0,1	200	7
Ma21b051	0.07824	0.00304	2.05539	0.07370	0.19157	0.00335	0.5	1153	45	1134	41	1,130	20	0,4	1131	35
Ma21b052	0.04877	0.02037	0.16646	0.06875	0.02439	0.00159	0.2	137	57	156	65	158	10	−1,4	158	20
Ma21b053	0.07380	0.00218	1.91048	0.04975	0.18771	0.00280	0.6	1036	31	1085	28	1,109	17	−2,2	1100	28
Ma21b054	0.05224	0.00285	0.31683	0.01650	0.04420	0.00080	0.3	296	16	279	15	279	5	0,2	279	10
Ma21b055	0.05855	0.00348	0.71325	0.04035	0.08814	0.00157	0.3	554	33	547	31	545	10	0,4	545	20
Ma21b056	0.06891	0.00230	0.67937	0.02045	0.07134	0.00110	0.5	896	30	526	16	444	7	15,6		
Ma21b057	0.08447	0.00323	0.89888	0.03129	0.07708	0.00127	0.5	1303	50	651	23	479	8	26,5		
Ma21b059	0.06580	0.00194	1.14429	0.02965	0.12722	0.00195	0.6	800	24	775	20	772	12	0,3	773	22
Ma21b0G0	0.11022	0.00262	4.87885	0.09618	0.32144	0.00470	0.7	1803	43	1799	35	1,797	26	0,1	1799	33
Ma21b051	0.07954	0.00360	2.26180	0.09458	0.20558	0.00354	0.4	1188	54	1200	50	1,206	21	0,4	1205	38

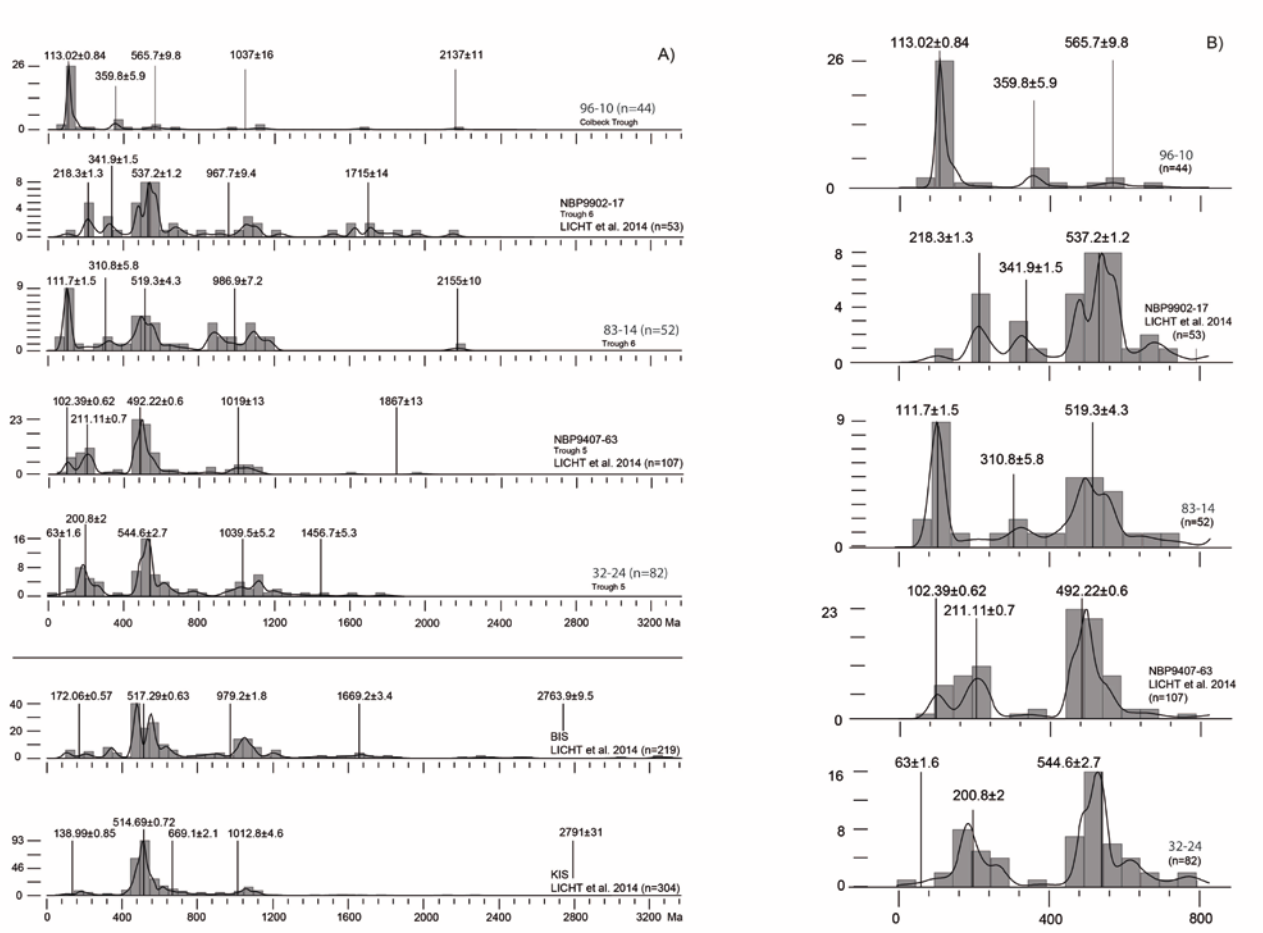

Figure 3.5- A) Kernel Density Estimates and histograms for the Zrn-UPb samples, realized with the DensityPlotter software (Vermeesch, 2012). Peaks automatically found by the DensityPlotter software. The results of Licht et al. (2014), regarding Ross Sea and Ice Streams samples are also displayed (BIS: Bindschadler Ice Stream; KIS: Kamb Ice Stream); B) Zoom of the 0-800 Ma interval of the Ross Sea samples plots (from this work and Licht et al., 2014).

3.5.5 Apatite fission track thermochronology

3.5.5.1 Analytical details

Apatite fission-track analysis was performed on grains acquired from 9 piston core samples. The latter are, located from east to west, 96-11, 96-16, 96-10, 32-27, 99-17, 83-14, 62-16, 32-24, 94-58. Sampling depths are listed in Table 3.1 and core sites are shown in Figure 2. Samples were analyzed at the Fission Track laboratory of the University of Padua. As for UPb analysis, samples were chosen from sand rich intervals of the cores and following the widest geographic distribution across the study area. Apatite grains were separated from 100 cc bulk samples after careful crushing using heavy liquids and magnetic separation techniques. Mounts of apatites in epoxy were ground and polished to expose planar surfaces within the grains and then etched with 5N HNO_3 at 20°C for 20 s to reveal spontaneous fission tracks. Samples then were irradiated with thermal neutrons in the reactor at the Radiation Center of Oregon State University with a nominal neutron fluence of 9^10^{15} n cm^2. The CN-5 dosimeter was used to measure neutron fluence. After irradiation, induced fission tracks in the low-U muscovite that covered apatite grain mounts and glass dosimeter were revealed by etching in 40% HF at 20°C for 40 min. Apatite FT dates (up to 40 grains per sample; analyst: Dr. B. Andreucci) were calculated using the external-detector and the zeta-calibration methods (Hurford and Green, 1983) with IUGS age standards (Durango and Fish Canyon apatites (Hurford,

1990)) and a value of 0.5 for the 4p/2p geometry correction factor. The observed grain-age distributions were decomposed into different component populations by using the binomial peak-fitting method (Brandon, 1996). This technique is based directly on the bimodal distribution that best represents counting statistics for FT dating. Individual fitted peaks have a mean age and standard error.

3.5.5.2 AFT Thermochronology results

Apatite Fission track results are reported in Table 3.4 and Figure 3.6; 40 to 100 grains were dated for each of nine cores, allowing a good decomposition into different populations. Where multiple samples from a single core were analyzed, no significant variability with depth was observed. Therefore, results obtained from the same core are presented and discussed together.

The easternmost samples from cores located in Sulzberger Bay yield Late Cretaceous to Early Eocene ages.

The Ross Sea samples yield multiple age populations. In order of abundance, these are: Cretaceous to Eocene (p3, p4, p5 in Table 3.4), Late Triassic-Jurassic (p6 in Table 3.4), and Oligocene (p2 in Table 3.4). Age populations represented by less than 3 crystals are reported in Table 3.4 (marked by an asterisk) and Figure 3.6, but are not considered significant for interpretation.

3.6 Discussion

3.6.1 Clasts provenance

Gravel-sized clasts found in LGM and post-LGM intervals from sampled piston cores should reflect the bedrock lithologies of West Antarctica, as suggested by many provenance studies and ice flow reconstructions (Licht et al., 2005; Farmer et al., 2006; Licht and Palmer, 2013; Licht et al., 2014).

The suite of clasts found in the eastern Ross Sea cores shows a predominant fraction composed by low grade metasediments. The only known low grade metamorphic unit in Marie Byrd Land is the Swanson Formation, a quartz-rich metaflysch sequence that is well exposed in the Swanson, Denfield, McKay, Clark and Allegheny Mountains in western Marie Byrd Land (Wade et al., 1977a, 1977b; 1978; Bradshaw et al., 1983). Moreover, correlative metasediments crop out in isolated nunataks, such as La Gorce peak, in Edward VII Peninsula (Wade et al., 1977c; Adams et al., 1995; Kleinschmidt and Petschick, 2003). Other greenschist facies metasediments crop out in Ruppert and Hobbs Coast (Pankhurst et al., 1998, Brand, 1979).

Fine to medium grained metasandstones and metagraywackes (i.e. Thin section 6, Fig. 3.3) found in marine cores are similar in texture, grain size and metamorphic grade (sub-green schist facies paragenesis) to those belonging to the Swanson Formation sequences (Bradshaw et al., 1983). Furthermore, some samples exhibit thermal metamorphism with spotted texture (i.e. thin section 62, Fig. 3.3), such as some bedrock portions of Swanson Formation rocks which underwent contact metamorphism due to pluton emplacement (Bradshaw et al., 1983; Adams et al., 1995; Kleinschmidt and Petschick, 2003).

White mica analysis carried out on micas defining the cleavage in metasedimentary clasts (Fig. 3.4c) show a variable composition, in most cases with a higher phengitic component (Si = 3.2-3.4 atoms per formula unit), compared to those in Bailey Ridge phyllite from PRR (Si < 3.1 a.p.f.u.) which is attributed to Swanson Formation. This difference could be due to different metamorphic conditions, namely higher pressure (4-8 Kbar or higher), in comparison to the low pressure regime suggested by the sample from PRR (c. 2 kbar following the method described in Massonne and Schreyer, 1984). Literature data clearly indicate that no

Sample	Depth	Grains	Spontaneous		Induced		$P(\chi^2)$	Dosimeter		Central Age	P1	P2	P3	P4	P5	P6
	(cm)	(n)	ρs	Ns	ρi	Ni		ρd	Nd	Ma ± (1σ)	Ma ± (1σ), %	Ma ± (1σ), %	Ma ± (1σ), %	Ma ± (1σ), %	Ma ± (1σ), %	Ma ± (1σ), %
96-11	40-43	40	11.20	2368	23.70	5005	0.3	8.79	2285	72.5 ± 6.3	-	-	-	65.6 ± 5.7, 71.8	92.9 ± 10.0, 28.2	-
96-16	2-6	40	10.80	1465	23.60	3200	0.0	8.74	2272	69.7 ± 6.4	-	-	54.5 ± 6, 40.8	81.8 ± 8, 59.2	-	-
96-10	9-14; 25-29; 188-190	138	5.82	3174	13.37	6985	0.1	9.86	2563	77.6 ± 2.5	-	36.2 ± 5.3, 12.9	-	73.5 ± 7.3, 48.8	93.0 ± 14.6, 21.2	142.8 ± 200, 3.5
32-27	55-60; 105-110	63	9.60	1266	22.15	2920	0.0	9.34	2429	72.9 ± 4.2	-	21.4 ± 4.7, 8.3	45.8 ± 7.5, 7.3	74.2 ± 7.1, 67.0	115.2 ± 22.0 17.4	-
99-17	134-139	35	9.90	978	15.70	1547	0.0	9.16	2382	108.6 ± 13.4	-	*26.6 ± 7.9, 7.5	-	68.9 ± 7.5, 29.5	-	156.4 ± 16.0, 62.9
83-14	81-86; 183-190; 231-236	91	9.58	1880	16.15	4798	1.6	9.83	2556	56.0 ± 3.0	-	26.9 ± 5.7, 7.5	45.0 ± 5.2, 37.7	74.5 ± 5.2, 42.3	96.0 ± 8.1, 9.5	*156.5 ± 2.9
62-16	111-117; 151-156	80	11.16	3045	16.66	4527	0.0	10.65	2769	111.4 ± 6.4	-	*29.6 ± 14.5, 2.3	-	77.9 ± 6.5, 45.4	129.1 ± 10.5,32.1	221.5 ± 16.6, 20.2
94-58	170-173	40	12.00	958	22.30	1781	0.0	8.95	2327	83.2 ± 9.2	-	-	44.7 ± 5.7, 26.9	-	92.7 ± 9.5,61.8	164.8 ± 28.4, 11.4
32-24	416-420	61	14.43	2280	25.93	2677	0.0	9.26	2408	82.5 ± 5.9	*5.8 ± 3.6, 3.2	35.4 ± 5.9, 13.9	-	74.5 ± 6.9, 47.3	113.0 ± 15.5,14.8	155.5 ± 16.8, 20.8

Table 3.4- AFT data: Central ages calculated using dosimeter glass CN5 and z-CN5 = 344.94±27.24. ρs: spontaneous track densities (105 cm2) measured in internal mineral surfaces; Ns: total number of spontaneous tracks; ri and rd: induced and dosimeter track densities (106 cm2) on external mica detectors (g = 0.5); Ni and Nd: total numbers of tracks; P(χ2): probability of obtaining c2-value for n degrees of freedom (where n = number of crystals-1); a probability >5% is indicative of an homogenous population. Samples with a probability < 5% have been analyzed with the binomial peak-fitting method to obtain the P1-P4 fitted peaks (P: age population). Peak values signed with * are represented by less than 3 crystals, and therefore they are considered non significant and not involved in discussion.

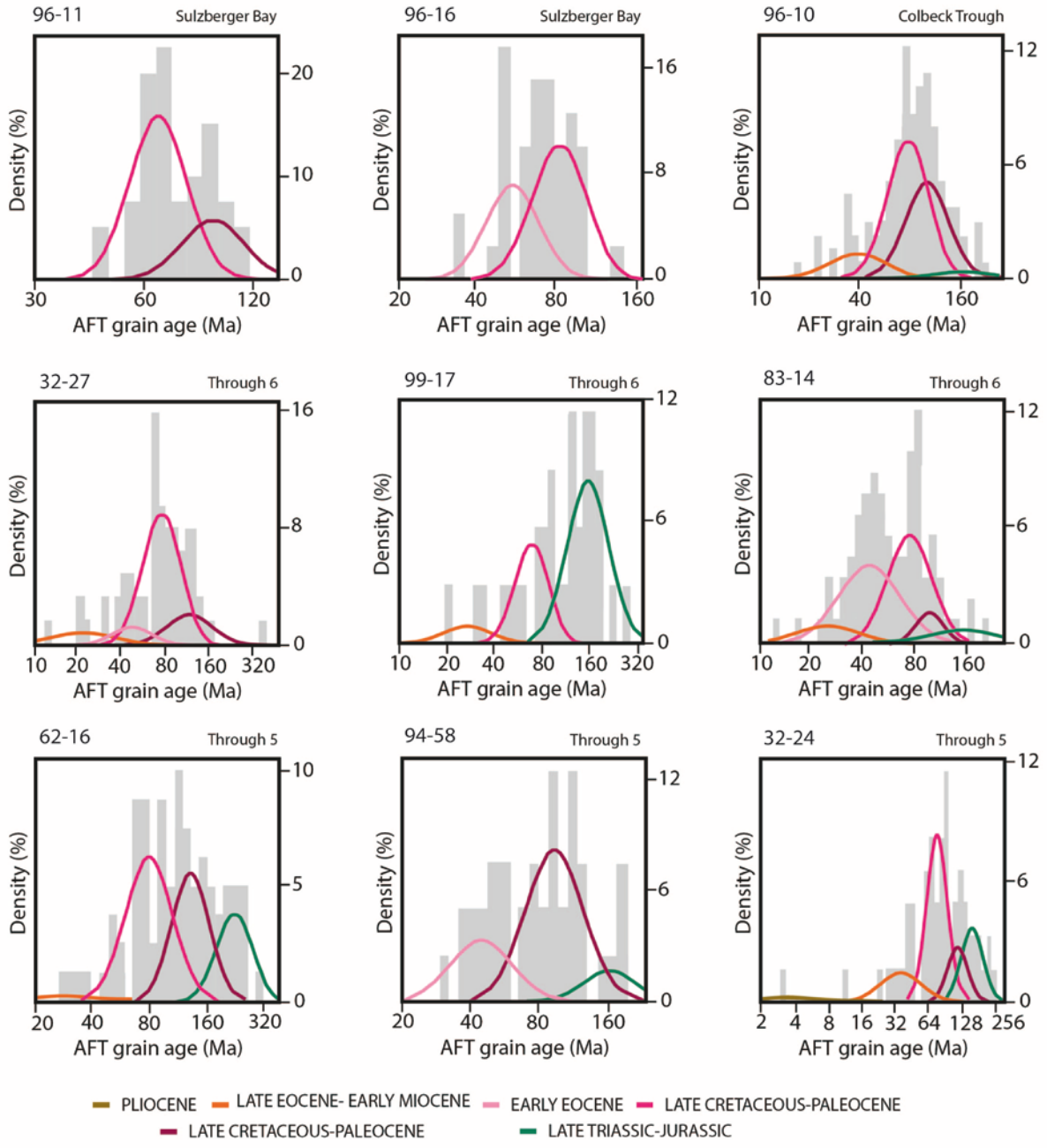

Figure 3.6- Histogram for AFT ages with best fit peaks, calculated with the Binomfit software (Brandon 1996)

other high pressure and low grade units are known in the region. However medium to high pressure conditions are recorded in the Fosdick migmatite-granite complex where a Devonian-Carboniferous event (~820–870 °C, 7.5–11.5 kbar) was superimposed by a Cretaceous high grade overprint at ~830–870 °C and ~6–7.5 kbar (Korhonen et al., 2010, 2012). Therefore, metasedimentary clasts found in the marine record could come from the erosion of rocks belonging to Swanson Formation, or a lithologically similar unit which experienced moderately high P low grade metamorphism, or to a lower grade correlative of the Fosdick complex, even if white mica is nearly absent from Fosdick and Alexandra migmatite complexes. An alternative source could be indicated in a lithologically similar unit that is younger than Swanson Formation (at least post-Permian) and that has been considered as the (meta)-sedimentary protolith of the metamorphic paragneiss cropping out in Alexandra Mountains, in Edward VII Peninsula (Pankhurst et al.,

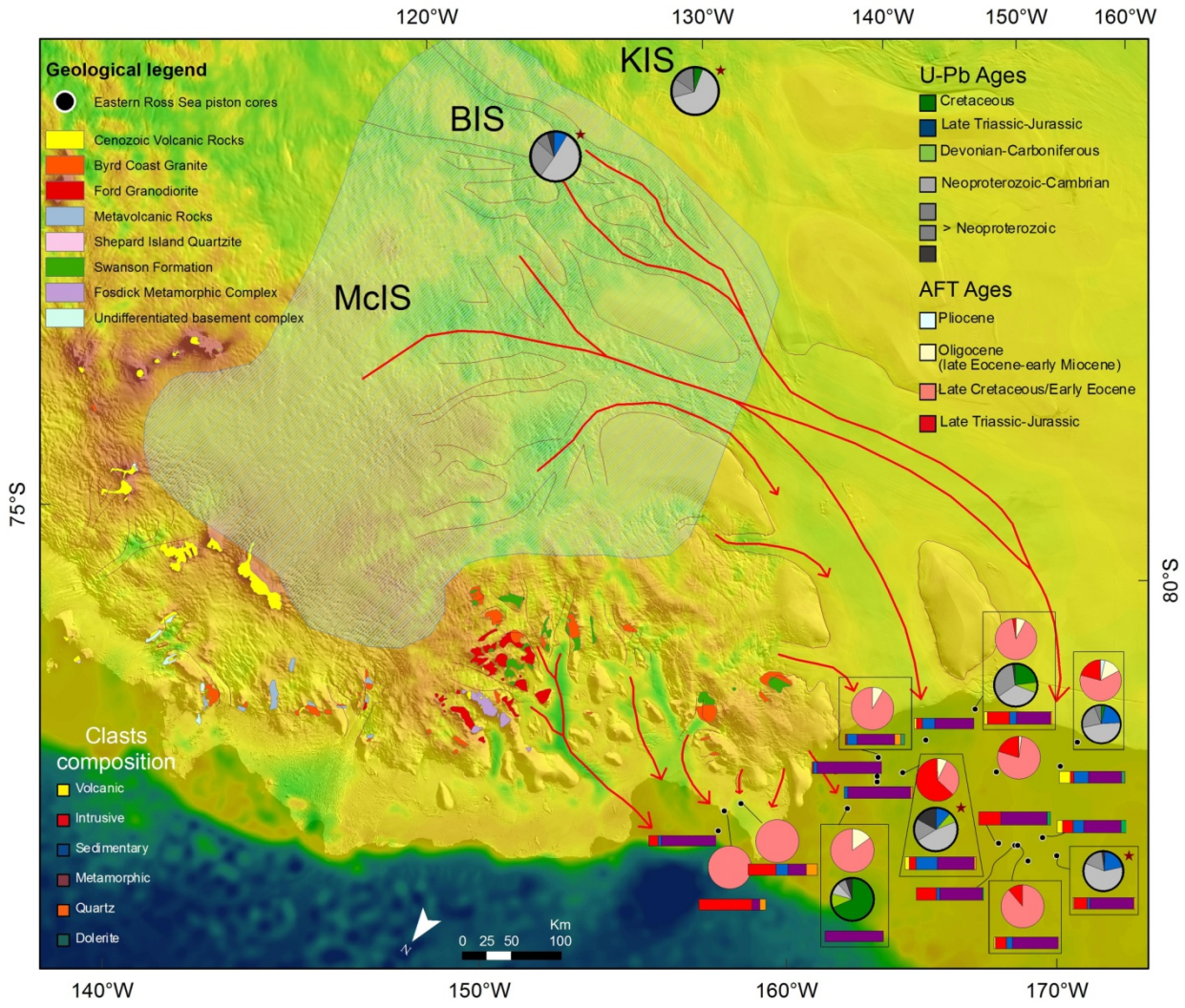

Figure 3.7- Bedmap of Marie Byrd Land region with geological units and AFT, Zrn-UPb and clast distribution data. Also ice flow paths reconstruction and LGM inferred catchment area are shown. Horizontal histograms show lithologies distribution, while pie charts evidence AFT and Zrn-UPb ages distributions. Samples marked with a red star are from Licht et al. 2014. McIs: MacAyeal Ice Stream; BIS: Bindschadler Ice Stream; KIS: Kamb Ice Stream. Geologic map from Wade et al. (1977a,b,c) and Wade et al. (1978).

1998). However the overall mineral data so far available from both clasts and bedrock samples from the Swanson Formation are still few and they do not allow a conclusive and robust statement to demonstrate this interpretation. Even available mineral chemistry data of Smith C.S. (1996) from Alexandra Mountains refer to higher grade rocks and to different minerals.

The petrographic features of the two groups of granitoids identified in detrital clasts are similar to those of the two granitic suites cropping out in Marie Byrd Land, the Devonian Ford Granodiorite and the Cretaceous Byrd Coast Granite. The black and white granodioritic to tonalitic biotite-hornblende variety (i.e. Thin section 15 in Fig. 3.3) is similar in texture, grain size and modal mineralogy to those exhibited by granodioritic to tonalitic Ford Granodiorite (Weaver et al., 1991, Yakymchuk et al., 2015). Chemical analysis of clinoamphiboles revealed similarities between Mg-hornblendes found in a biotite-hornblende tonalite from marine record and those of a Ford Granodiorite sample from the Phillips Mountains (Fig. 3.4a). Also biotites from these two samples show a similarity in composition (Fig. 3.4b). This calc-alkaline metaluminous to peraluminous I-type suite is widespread in the Ford Ranges and has its easternmost

outcrop in Ruppert Coast (Weaver et al., 1991; Pankhurst et al., 1998). On the contrary, the pinkish porphyritic monzogranite and leucogranite variety (i.e. Thin section 5 in Fig. 3.3) exhibits similar petrographic features with the alkaline suite of the Byrd Coast Granite. The latter is common in Edward VII Peninsula, the Ford Ranges and Ruppert Coast (Weaver et al., 1991, 1992 and 1994; Adams et al., 1995), with a predominantly leucogranite and syenogranite suites. Alkaline porphyritic varieties found in marine dataset could be associated to the Byrd Coast Granite too, as hypabyssal types of epizonal emplacement.

Sedimentary clasts found in piston cores (mainly quartz-arenite, graywackes and siltstones) could belong to rocks from Swanson Formation, even if they do not show any metamorphic overprint, or to a unit of sedimentary rocks in the sub-glacial environment, that is nowhere exposed. In the first case, this would mean the presence in West Antarctica of portions of the Swanson Formation that exhibit no metamorphic overprint. The second case is not directly verifiable, however, an airborne gravity model over Edward VII Peninsula and the Ford Ranges (Luyendyk et al., 2003) mapped some low-density sub-glacial units which could be made up of porphyritic varieties of Byrd Coast Granite, felsic volcanic rocks or sedimentary deposits. Because all of the exposed Swanson Formation in the Ford Ranges, together with its correlatives in northern Victoria Land and New Zealand are metamorphosed (Adams et al., 1995), it is difficult to imagine large areas of non-metamorphic Swanson Formation which could produce a significant marine detrital record. Therefore our favored interpretation is that detrital sedimentary clasts derive from a sub-glacial sedimentary unit that is so far undetected in the region. A possibility for the source rock could be portions of unmetamorphosed equivalent of the post-Permian unit in Edward VII Peninsula, considered the protolith of the Alexandra Mountains paragneisses (Pankhurst et al., 1998).

Volcanic rocks in Marie Byrd Land are well exposed as Cenozoic eruptive centres in the Flood Range, Hobbs Coast and Executive Committee Range (LeMasurier and Rex, 1989 and 1990; Panter et al., 1997 and 2000; Hart et al., 1997). These volcanoes are composed primarily by felsic alkaline lavas (phonolite, trachyte, and intermediate rocks) that comprise almost all the rocks exposed above ice level in most inland volcanoes as in Flood Range (LeMasurier et al., 2011). Pleistocene basaltic rocks were found also in the Fosdick Mountains (Gaffney and Siddoway, 2007). Volcanic clasts (i.e. Thin section 60), are very rare in the marine dataset: they show petrographic characteristics and felsic alkaline modal mineralogy which make them comparable to the Marie Byrd Land volcanic province. It is noteworthy that, although the bedrock geology testifies to the presence of many volcanic centres, volcanic detritus is rare in Eastern Ross Sea. This is in accordance with analysis carried out on detrital coarse sand from Eastern Ross Sea cores by Anderson et al. (1992), who identified specific petrographic provinces for Troughs 5 and 6 composed mainly by schists, granites, rounded quartz and minor amount of gneisses and diabase. Also data relating to sub-glacial till from Whillans Ice Stream in West Antarctica (Vogel et al., 2006) shows a lack of volcanic detritus, even if the catchment area of this ice stream could be related to the Transantarctic Mountains (Licht et al., 2014). One hypothesis which could explain the rarity of volcanic lithologies is that their presence in the marine record among gravel-sized clasts has been diluted by the long transport from known eruptive centres located in Flood Range and Executive Committee Range, or that the clasts are physically weathered. While other lithologies found in the marine record have their correlatives in bedrock geology close to the Marie Byrd Land coast, the volcanic clasts have their closest correlative outcrops in the Fosdick Mountains, requiring a very long transport (and stronger erosion) and a LGM ice flow path different from the modern draining system. The second hypothesis implies some unexposed volcanic sources beneath the Ice Sheet in the region east of the Ford Ranges; aerogeophysical surveys carried out over the WAIS (in particular the region of Ice Streams C and D, Behrendt et al., 1994; 1996; 2004) revealed a series of magnetic and topographic anomalies interpreted to be sub-glacial volcanic centres: some of them are supposed to be the remnants of residual topography after glacial removal by the WAIS. Also data from Ferraccioli et al. (2002)

and Luyendyk et al. (2003) suggest the presence of sub-ice volcanic centres in western Marie Byrd Land. These combined data suggest the presence of a sub-glacial source of the detrital clasts found in our dataset, rather than a source located farther east in MBL, even if the statistical rarity of clasts in marine record should imply volumetrically minor sources.

Dolerites and other mafic porphyritic varieties found in marine cores could be related to mafic plutonism throughout Marie Byrd Land during Cretaceous crustal extension, with emplacement of numerous dykes, sills and small plutons (Saito et al., 2013; Siddoway et al., 2005; Storey et al., 1999; Weaver et al., 1994). The rock types are widespread from Huppert-Hobbs Coast to Fosdick Mountains and Ford Ranges.

3.6.2 Data integration, with implications for tectonic and LGM ice-flows reconstructions

In the sample located in Colbeck Trough (96-10) and in Sulzberger Bay (96-11; 96-16) most of the AFT and Zrn-UPb dates are Cretaceous-Eocene, reflecting a local sedimentary provenance from exposed or concealed gneiss domes, or Byrd Coast Granites (or thermally overprinted Swanson Formation) as suggested by Adams et al. (1995). Clasts are predominantly composed of granitoid and metasedimentary lithologies, with an absence of volcanic detritus (Fig. 3.7). New AFT ages accord with the bedrock AFT ages of Adams et al. (1995) and Lisker and Olesch (1998) on rocks from Edward VII Peninsula. Similar AFT ages are reported for mylonitic gneisses dredged in Colbeck Trough, very close to Edward VII Peninsula (Siddoway et al., 2004b), and the Fosdick and Chester Mountains in the Ford Ranges (Richard et al., 1994); therefore, a mixing of local (Edward VII Peninsula) and distal (Ford Ranges) sources cannot be excluded for these cores, in particular for the core 96-11 which is located farther from the coast. Indirect information could account for such mixing: indeed, regional LGM ice-flows pattern from the Ford Ranges to the Sulzberger Bay is supported by the geomorphological study of Sugden et al. (2005). Sample 96-10 from Colbeck Trough shows an AFT Oligocene population, possibly a reflection of Oligocene AFT ages found in Ford Ranges (Lisker and Olesch, 1998), but since the position of this core suggests a direct ice draining from Edward VII Peninsula to Colbeck Trough, this implies an Oligocene local exhumation for this region.

Most of the sediments of troughs 5 and 6 (Fig. 7) yield Neoproterozoic-Cambrian Zrn-UPb age and Cretaceous AFT ages. Clasts consist mainly of metasedimentary lithologies followed by granitoids and sedimentary clasts (Fig. 3.7). This is compatible with a prevalent Swanson Formation source, associated with rocks affected by Cretaceous extensional tectonism following the Byrd Coast Granite emplacement. The most consistent Zrn-UPb Precambrian age is 987-1039 Ma; this age population appears to be quite common from both sides of the Ross Embayment, being present in detrital zircons from offshore samples located in the central and western Ross Sea (Licht et al., 2014; Licht and Palmer, 2013), and from Beacon Supergroup rocks in the central Transantarctic Mountains (Elliott and Fanning, 2008). However, since this age population is present also from Swanson Formation rocks (Pankhurst et al., 1998; Yakymchuk et al., 2015) and from BIS and KIS sub-glacial till samples (Licht et al., 2014, Fig. 3.7), direct attribution to a West Antarctic source for this age population appears to be likely for Trough 5 and 6 samples.

However, other minor populations of ages show the existence of exhumed bedrock having different crystallization-cooling paths.

- Cretaceous and Devonian-Carboniferous Zrn-UPb age populations (cores 96-10; 83-14; 32-24 and 94-63; 99-17; Kamb Ice Stream from Licht et al., 2014) can be associated to Byrd Coast Granite and Ford Granodiorite pluton emplacement or their related migmatites, respectively.

- A Late Triassic-Jurassic crystallization/metamorphism-cooling event is indicated by both Zrn-UPb and AFT dates (core 99-17 in trough 6 and all the samples in trough 5). The Zrn-UPb Triassic-Jurassic population was already been found from some offshore sites (Licht et al.,2014). A similar population of ages is documented in West Antarctica from Zrn-UPb data of Riley et al. (2016) in Thurston Island, where both Triassic and Jurassic magmatism occurred. The former is known also from Kohler Range in Walgreen Coast (eastern Marie Byrd Land, Pankhurst et al., 1998). The closest known Zrn-UPb ages, although slightly older than our age populations, have been found as minor peak population by Pankhurst et al. (1998) fom Alexandra Mountains paragneisses, in Edward VII Peninsula. However, as this population is absent or negligible in offshore samples located close to the Edward VII Peninsula and Roosevelt Island coasts, we suggest that it can be used as a proxy for the contribution of local vs. distal sedimentary provenance.

- An Oligocene AFT age population is present in most of the cores both in trough 5 and 6; this may correlate to an Oligocene-Pliocene cooling event documented in central Marie Byrd Land, that was related to the Oligocene-Pliocene volcanism and localized uplift (Hobbs Coast, Hart et al., 1997; LeMasurier and Rex, 1982). Spiegel et al. (2016) found an early Miocene AFT age population from Hobbs Coast glaciomarine sediment and they interpreted this age population as the result of an enhanced Neogene denudation, implying that uplift and relief formation in eastern Marie Byrd Land also started at about 20 Ma. Our samples record slightly an older age population, except for one sample (32-27 core) that has a similar age peak (P2 in Table 3.4). This similarity could imply that source rocks which experienced a ~ 20 Ma exhumation event and provided detritus to offshore sites in the eastern Ross Sea are located in a region involved in the uplift of Marie Byrd Land dome, supporting the hypothesis of Spiegel et al. (2016). However, a volcanic source for apatites yielding this age cannot be excluded, since volcanoes of similar age are present in the central Marie Byrd Land (LeMasurier and Rex, 1982).

Trough 6 core sediments are heterogeneous, likely due to mixed local (e.g. core 83-14, located close to Roosevelt Island coasts) and distal sedimentary provenance. This variability is also seen in the clast distribution record, with cores 96-09 and 96-08 characterized almost exclusively by metamorphic clasts, while the other cores in the center of the trough are composed also of granitoids and sedimentary clasts with negligible volcanic rocks. It is probable that the easternmost two cores of trough 6, proximal to Edward VII Peninsula coast, have been influenced by local ice masses flowing from this region. On the contrary, the core sediments of trough 5 yield more homogeneous Zrn-UPb and AFT age populations, suggesting a common provenance, from one or more Ice Streams draining Marie Byrd Land, and possibly yet more distal. This possibility supports the hypothesis of long transport paths, with a major erosion and desegregation of more unstable lithologies such as volcanic ones.

Comparing the Zrn-UPb results to those obtained by Licht et al. (2014) for the Bindschadler Ice Stream, it can be noticed that the Cretaceous, Carboniferous and Late Triassic-Jurassic populations are much more prevalent in the Ross Sea sediments (19-45% in the sediments with significant distal provenance) than in the Bindschadler Ice Stream (8.6%). This suggests that the major sedimentary flux into this sector of the Ross Sea at the LGM was from the MacAyeal Ice Stream with a minor contribution of the Bindschadler Ice Stream. So far, no geo and thermochronological data of the the MacAyeal Ice Stream are available, but from the present dataset and Licht et al. (2014) a complex catchment area is expected, well compatible with the Marie Byrd Land geology.

The data presented in this study and by Licht et al. (2014) imply that rocks formed or metamorphosed and cooled to low T (<ca. 100°C) in the Late Triassic-Jurassic are present in the MacAyeal and Bindschadler Ice Streams LGM catchment regions. Korhonen et al. (2010a) report few inherited zircon grains of both Triassic and Jurassic ages from Cretaceous granite in the Fosdick Mountains. So far such an event had been

documented in western Marie Byrd Land as inherited zircon grains from Alexandra Mountains paragneisses (Pankhurst et al., 1998).

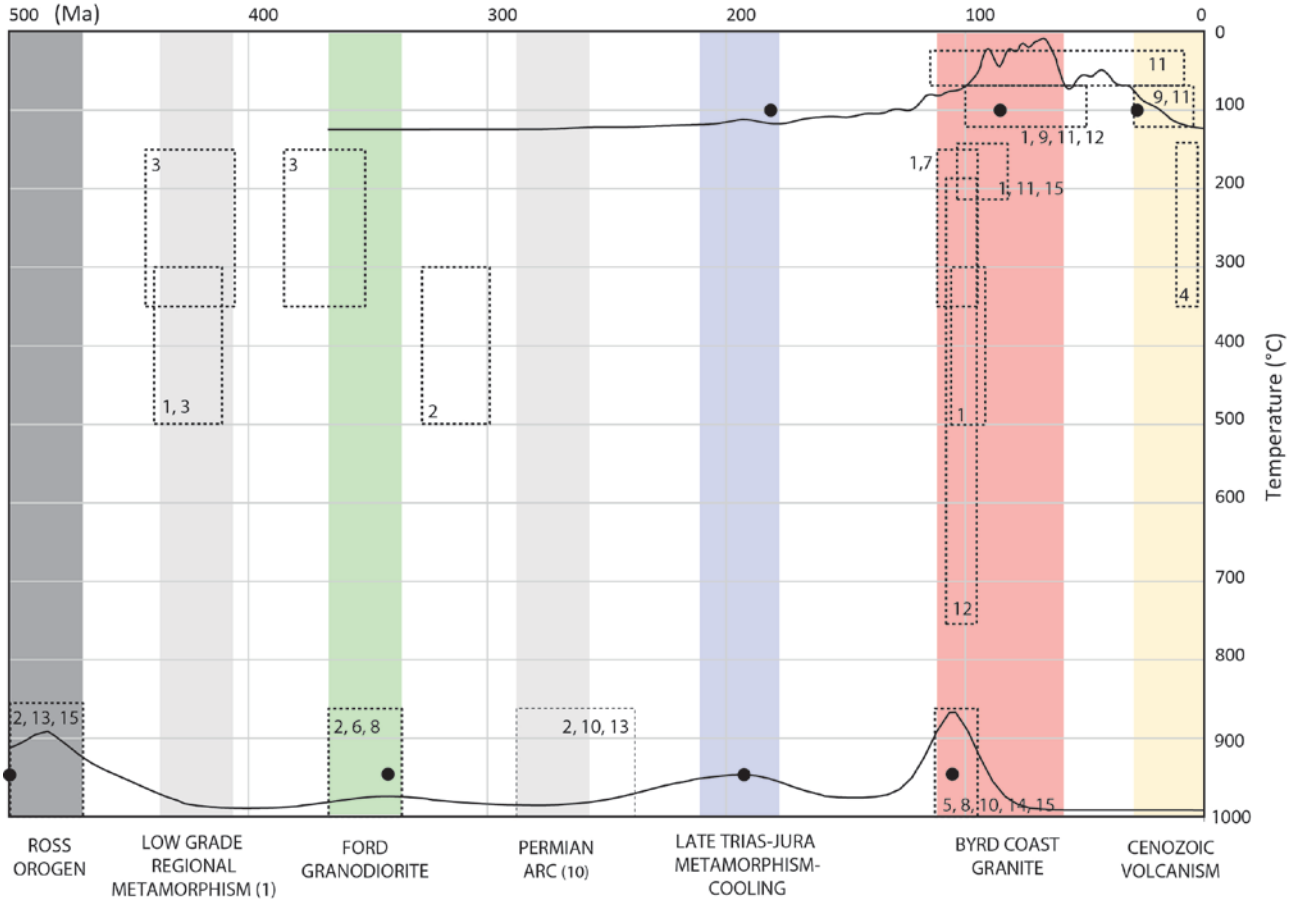

Figure 3.8- Summary of the geochronology and thermochronology of the Marie Byrd Land (dashed boxes, from literature), and of the Ross Sea sediments (black lines represent the Kernel Density Estimate curves of Zrn-UPb and AFT dates, black dots indicate the major population ages). 1-Adams et al. (1995); 2-Pankhurst et al. (1998); 3-Adams (1986); 4-Hart et al. (1997); 5-Saito et al. (2013); 6-Siddoway and Fanning (2009); 7-Siddoway et al. (2005); 8-Brown et al. (2016); 9-Lisker and Olesch (1998); 10-Mukasa and Dalziel (2000); 11-Spiegel et al. (2016); 12-Richard et al. (1994); 13-Yakymchuk et al. (2015); 14-McFadden et al. (2010); 15-Contreras et al. (2012); Vertical bands indicate the major geological events detected by geochronology and thermochronology (from literature and from present work).

The finding that most of the AFT dates are Cretaceous to Eocene suggest that a regional exhumation may have occurred at the time of the Byrd Coast granite emplacement and following this event in the source region. Heating preceding this exhumation episode may have reset AFT dates, with respect to previous cooling events (Fig. 3.8). However Late Triassic-Jurassic dates were not reset, implying that the portion of the catchment to which they belong was not affected by Cretaceous exhumation.

To conclude we infer a local provenance for samples located in the Sulzberger Bay and very close to the coastlines of Edward VII Peninsula and Roosevelt Island, a mixed local and distal provenance for samples located in trough 6, and mainly a distal provenance for samples located in trough 5. For both the troughs we hypothesize a possible sub-glacial unit that was eroded to provide for significant amount of sedimentary clasts.

Most of the distal sediments were discharged by the MacAyeal Ice Stream and the Bindschadler Ice Streams, the drainage area of the former being fully compatible with the Marie Byrd Land geology. However Late Triassic-Jurassic dates, already inferred by Licht et al. (2014), and with few evidences in the

Marie Byrd Land outcrops, were found to constitute a significant component of the Ross Sea sediments Zrn-UPb and AFT.

3.7 Conclusions

In this study, a multy-analytical provenance analysis involving three different techniques was carried out to LGM glaciomarine sediments located in the eastern Ross Sea and in Sulzberger Bay. The new detrital data inform about the WAIS dynamics and the features of the eroded area. The main conclusions are summarized as follows:

(1) Gravel-sized clasts petrographic analysis revealed a source area defined mainly by low grade metasedimentary units, namely Swanson Formation in western Marie Byrd Land and its correlatives in the region.

(2) Devonian-Carboniferous and Cretaceous Zrn-UPb age populations signify sources in the Ford Granodiorite and Byrd Coast Granite (or their related migmatites complexes) as the main sources for granitoid detritus, pointing out a source region compatible with western Marie Byrd Land geology.

(3) The rarity of both volcanic detritus and volcanic-related age populations suggests a volumetrically minor source located somewhere in a sub-glacial environment beneath WAIS, pyroclastic ejecta, or a distal source in volcanic ranges in central Marie Byrd Land. The latter requires a longer transport distance and major erosion. Unexposed sedimentary units are supposed to exist beneath WAIS in the LGM catchment areas, that could provide detrital clasts to the sedimentary record in the eastern Ross Sea.

(4) Significant detrital Zrn-UPb and AFT Triassic-Jurassic age populations, already documented in detrital studies of the region, suggests the presence of quite widespread rocks that either formed or metamorphosed at that time in the LGM catchment areas. These rocks are presently not exposed in western Marie Byrd Land, but rocks of similar ages are found in Thurston Island and Walgreen Coast (eastern Marie Byrd Land).

(5) The source area for the sediments is considered to be Edward VII Peninsula for the samples located in Sulzberger Bay and in Colbeck Trough, and the catchment areas of MacAyeal and to a lesser extent Bindschadler Ice Stream for samples located in trough 5 and 6. These draining patterns for the LGM is coherent with the composition and ages of detrital sediments, with the inland subglacial region of western Marie Byrd Land being the main source area.

(6) Detrital AFT ages found in eastern Ross Sea sediments inform about an Oligocene exhumation event occurred both in local source region (Edward VII Peninsula) and in distal source area. This event could be related to extensional tectonic setting (Siddoway, 2008) of this shoulder of the West Antarctic Rift System.

Acknowledgments

This work was funded by PNRA 2013/AZ2.08 project. All data used to support this study are present in the paper, in references, and in the Supporting Materials in form of tables. We thank the staff of the Marine Geology Antarctic Research Facility of Tallahassee, Florida (USA) for their support in the stage of core selection and logging and for providing the samples of this study. We also thank Dr Anne Grunow at the Polar Rock Repository in the Byrd Polar Research Centre, Ohio State University, for providing useful

samples of rocks from the study area. Mineral chemistry full data and Zrn-UPb data are available as supplementary materials.

Chapter IV.
Central and Western Ross Sea (Antarctica) LGM sediments: new data from petrography of gravel-sized clasts

4.1 Chapter Overview

This chapter focus on the gravel fraction of the glaciomarine sediments of Central and Western Ross Sea region. It is written as a portion of a journal paper that is in preparation. The structure of the paper will be completed with new AFT and ZrnUPb data from the region. At this step of the research, the chapter investigate the nature of gravel sized clasts recovered from LGM sediments distributed in Central and Western Ross Sea. It gives preliminary interpretation on the LGM paleo-ice flows able to provide this kind of detritus, on the basis of occurrence and distribution of detrital lithologies, comparison with outcrop geology of the region and existing LGM ice flows models provided by previous provenance studies.

4.1.1 Paper

Matteo Perotti[1], Benedetta Andreucci[2], Franco Talarico[1], Massimiliano Zattin[2], Antonio Langone[3]

[1] University of Siena, Department of Physical Sciences, Earth and Environment, Strada Laterina 8, 53100 Siena, Italy

[2] University of Padova, Department of Geosciences, Via Gradenigo 6, 35131 Padova, Italy

[3] Consiglio Nazionale della Ricerche–Istituto di Geoscienze e Georisorse, Unita` di Pavia, Via Ferrata 1, 27100, Pavia, Italy

4.2 Introduction

The Ross Sea drains almost one third of the ice discharged from Antarctica (Anderson, 1999), thus is a crucial area in understanding ice sheets dynamics over time. One of the most important aspect of this issue is to study the behavior of ice masses both from modern bass balance studies and from history of the Antarctic Ice Sheets in the past. Fronting this theme means also reconstruct the relative contribution of sectors of the Antarctic ice sheets that behave differently in terms of dynamics and climate control. In fact, while East Antarctic Ice Sheet (EAIS) is considered more stable since it is grounded on the continent, the marine-based West Antarctic Ice Sheet (WAIS) seems to be more susceptible and instable to ocean forcing. In this scenario, studies on the relative contribution of EAIS and WAIS in the Ross Sea during the LGM will help the construction of more reliable models able to describe also future behaviors of Antarctic Ice Sheet and its contribution to sea level rise (e.g. Pollard and DeConto, 2009; Deschamps et al., 2012).
Several studies modeled the reconstruction and the dynamics of EAIS and WAIS during the LGM in the Ross Sea region (Stuiver et al., 1981; Denton and Hughes, 2002; Huybrecths, 2002; Pollard and DeConto, 2009; Golledge et al., 2012, 2013). The first model proposed by Stuiver et al. (1981) account for a major role played by WAIS,

with a significant contribution of ice discharged by West Antarctic Ice Streams in the Central and Western Ross Sea. Instead, numerical models account for a major contribution of EAIS in the Central and Western Ross Sea (i.e. Denton and Hughes, 2002; Pollard and DeConto, 2009). Provenance analysis carried out on LGM tills by Licht et al. (2005), Farmer et al. (2006), Licht and Palmer (2013), Licht et al. (2014) have demonstrated that EAIS and WAIS ice have both a significant contribution in the LGM drainage pattern and that their flows converge in the Central Ross Sea at about 180° longitude. In particular, Licht and Palmer (2013) have evidenced the role of the Byrd Glacier in discharging ice in the Western and central-western Ross Sea. However, some numerical models seem to overestimate the contribution of EAIS outlet glacier discharge in the central Ross Sea (Golledge et al., 2012, 2013; Denton and Hughes, 2002), in comparison with sediment provenance data.
The aim of this work is to provide new data to refine the existing provenance models, applying an in-depth study of the gravel fraction from sediments in Central and Western Ross Sea, and to unravel the role of different outlet glacier of the Transantarctic Mountains to the LGM drainage pattern.

4.3 Physical and geological setting

4.3.1 Physical setting

The Ross Sea (RS) is bordered to the west by the Transantarctic Mountains along the Victoria Land coast, to the East by Marie Byrd Land in West Antarctica, to the south by the Ross Ice Shelf and to the north by the continental shelf break which deepens to the abyssal plain of the Pacific Ocean. The Ross Sea can be subdivided into three different regions: Western Ross Sea (WRS), Central Ross Sea (CRS) and Eastern Ross Sea (ERS).
The continental shelf has a slightly major gradient in the west than in the east (1.6° vs 0.6°, Hayes and Davey 1975). The RS continental shelf shows an accentuated counter-slope in the direction of the continent, associated with a considerable over-deepening. The sea bottom has an average depth of ~500 m below sea level, with minimum levels of ~250 m and maximum levels of ~1200 m (Hayes and Davey, 1975; Anderson, 1999; Shipp et al., 1999; Davey, 2004; Mosola and Anderson, 2006). Continental shelf over-deepening towards the continent side is caused by different processes: thermal subsidence of sediment-free margins, flexion caused by a large prograding sediment deposition on the platform edge, episodes of glacial erosion of the inner shelf (resulting in accumulation on the outer shelf) and isostatic depression of the continent due to the presence of the Antarctic Ice Sheet (Shipp et al., 1999; Davey, 1994; Anderson, 1999; Mosola and Anderson, 2006).
The bathymetry of RS is characterized by six north-east trending troughs which have similar dimensions to the Ice Streams currently feeding this region. The troughs are separated by banks in the Western Ross Sea (Mawson, Crary, Pennell and Ross Banks) and minor ridges in the Eastern Ross Sea (Mosola and Anderson, 2006); while banks in WRS have flat tops with average depth of 170-200 m below sea level, ridges in ERS have a more rounded profile and are located at a greater water depth, below 500 m (Mosola and Anderson, 2006).

4.3.2 Glaciological setting of the Ross Sea

The Antarctic Ice Sheet consists of two coalescing Ice Sheets called the East Antarctic Ice Sheet (EAIS) and the West Antarctic Ice Sheet (WAIS). EAIS is terrestrial-based, and it is steadily grounded on the continent above sea level. Its draining is slow and diverging towards the coastlines (Anderson et al., 2002). On the contrary, WAIS is marine-based, grounded below sea level and characterized by rapid flow and discharge in comparison

with EAIS (Anderson et al., 2014). The greatest discharge of WAIS is provided by fast-moving Ice Streams converging in the Ross Sea and forming the Ross Ice Shelf (RIS), which is constituted also by ice discharged by the EAIS through the outlet glaciers of the Transantarctic Mountains. Thus, RIS mainly represents the floating extension of six main Ice Streams, that are located along the Siple Coast (Hughes, 1977) and are considered the most dynamic features of the WAIS. Paleo-troughs recognized in the Ross Sea floor are considered the erosive signatures of the extended WAIS Ice Streams during past glacial cycles, and in particular the LGM (Mosola and Anderson, 2006). The present RIS grounding line is located approximately 700 ÷ 1200 km south of the RS continental shelf and has a sinuous path with wide gulfs corresponding to major troughs (Anderson et al., 2014, and reference therein).

4.3.3 Geological setting of the Central Ross Sea

The geology of the region around Central Ross Sea is mainly known from rock outcrops along the Transantarctic Mountains to the west (e.g. Bushnell and Craddock, 1970; Stump, 1995) and in Marie Byrd Land to the east (e.g. Wade et al., 1977a,b,c and Wade et al., 1978). The most extensive rock exposures are located along the Transantarctic Mountains that separate the EAIS and the WAIS (Fig. 4.1). The Transantarctic Mountains are composed of rock units spanning a period from Precambrian to Quaternary, and are composed essentially by seven main groups of rocks. The latter are, from the oldest to the youngest:

- Nimrod Group (Archean-Early Proterozoic), which is an heterogenous upper-amphibolite grade metamorphic complex composed of banded quartzo-feldspathic to mafic gneiss, schist, quartzite, marble, as well as granitic and gabbroic intrusive rocks, calc-silicate gneiss, relict eclogite and ultramafic pods (Goodge et al., 1993; Goodge and Fanning, 1999; Stump, 1995). The rocks of this group crop out mainly in the Miller and Geologists Ranges on the plateau side in the Central Transantarctic Mountains (Stump, 1995).

- Beardmore Group (upper Precambrian), a belt of lower greenschist grade rocks composed of graywackes, pelitic schists and hornfelses (Laird et al., 1971; Stump, 1995; Mirow et al., 2002; Goodge et al., 2002), cropping out in the central Transantarctic Mountains along the ice-shelf margin (Stump, 1995). The Beardmore Group included rocks known as the Cobham and Goldie formations in the central Transantarctic Mountains and the La Gorce, Duncan, and Party formations in the Queen Maud Mountains (Laird et al., 1971; Stump 1982, 1985). A revised stratigraphy of the Beardmore Group made by Goodge et al. (2002) led to differentiate two different sequences: an inboard, older assemblage (Neoproterozoic) comprising the Cobham and Goldie Formation “sensu strictu” and an outboard, volumetrically more important, younger assemblage (late Early Cambrian), which has been correlated temporally with the siliciclastic sequences of the Byrd Group (Starshot and Dick formations).

- Unconformably and tectonically overlying Beardmore Group along its western portion is the early-Cambrian Shackleton Limestone, cropping out northward to Byrd Glacier in the Central Transantarctic Mountains. This unit is unconformably overlain by clastic rocks sequences (Douglas Conglomerate and Dick and Starshot formations), which together with Shackleton Limestone define the Byrd Group (Stump, 1995; Bushnell and Craddock, 1970; Mirow et al., 2002). The Beardmore and Byrd Groups consist of two distinct tectonostratigraphic units of the Ross Supergroup. The portion of these packages of rocks

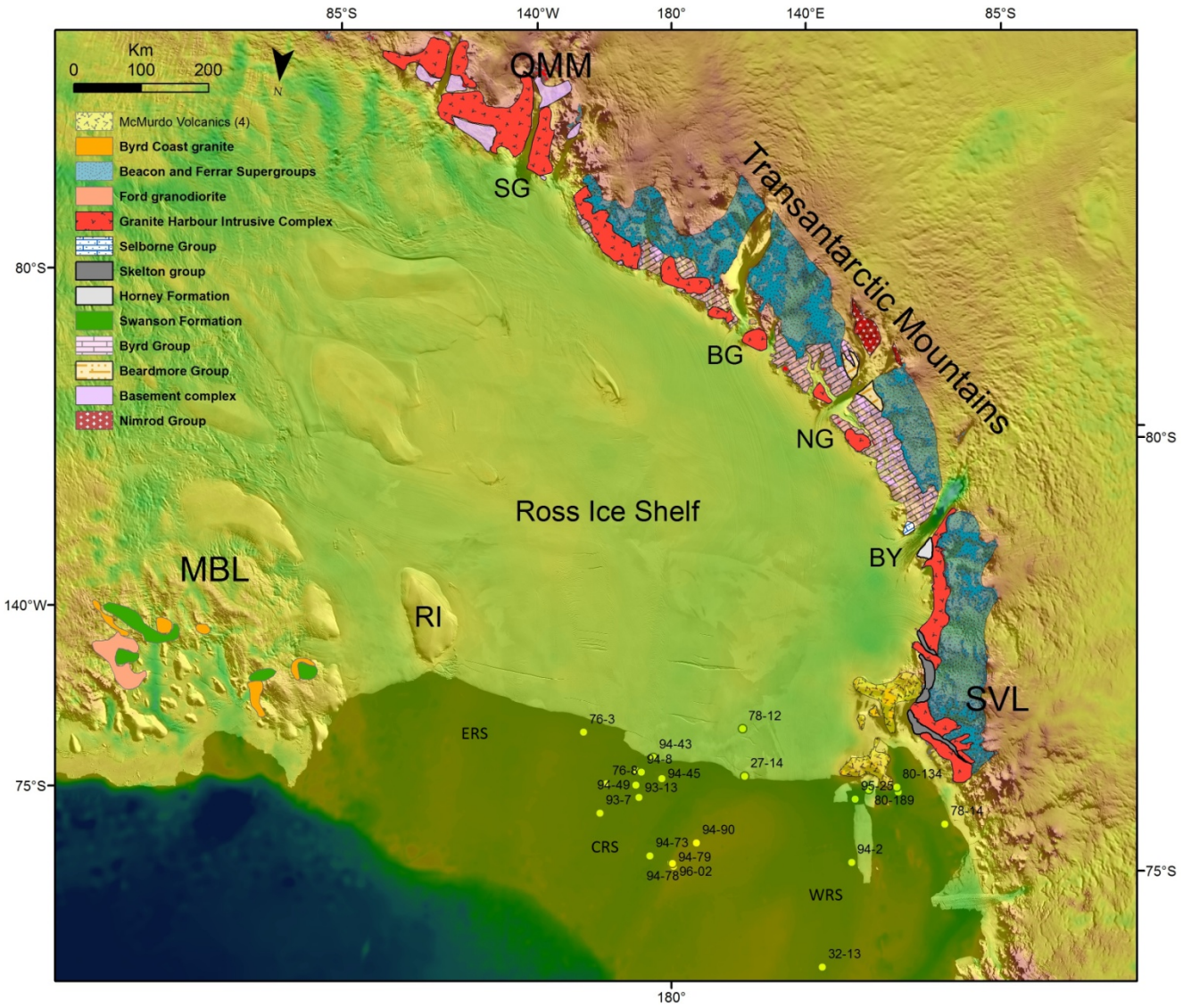

Figure 4.1. Bedmap overview of the Ross Sea region with sample site locations shown labeled as in Table 4.1 and geologic sketch map of the two sides of the Ross Sea Embayment. Basement rocks in the Queen Maud Mountains correspond to the outboard formations correlatives of the Byrd Group (Goodge et al., 2002) and associated Liv Group rocks (Stump 1985). Abbreviations are the following: BG: Beardmore Glacier; BY: Byrd Glacier; MBL: Marie Byrd Land; QMM: Queen Maud Mountains; RI: Roosevelt Island; ERS: Eastern Ross Sea; CRS: Central Ross Sea; WRS: Western Ross Sea; SVL: Southern Victoria Land. Geological maps are simplified from: Bushnell and Craddock (1970), Borg et al. (1989), Davis and Blakenship (2006), McGregor and Wade (1969), Carosi et al. (2007), Cox et al. (2012), Wade et al. (1977a, 1977b, 1977c, 1978).

located in central Transantarctic Mountains were referred as “inboard” and those located farther from the Antarctic craton (i.e. in the Queen Maud Mountains) were referred as “outboard” (Rowell et al., 1992). The younger stratigraphic sequences in the outboard localities in Queen Maud Mountains contain volcanic and volcanoclastic rocks interbedded with carbonates and siliciclastics rocks (Rowell and Rees, 1989). These sequences (Wyatt, Ackerman, Leverett, Taylor, Fairweather and Greenlee formations, cropping out in the Queen Maud Mountains) are collectively known as the Liv Group (Stump, 1985; Rowell and Rees,

1989; Rowell et al., 1997) and they are of Cambrian age, thus temporally correlatives of the Byrd Group sequences in the Central Transantarctic Mountains.

- Cambrian-Ordovician Granite Harbour Intrusive Complex series rocks are widespread in several plutons along the Transantarctic Mountains, cropping out from Ohio Range to the Southern Victoria Land (Stump, 1995). These include a variety of foliated to isotropic biotite ± hornblende granites, granodiorites to tonalites series, emplaced during the Ross Orogeny when the paleo-pacific plate subducted under East Antarctica. Subduction phase ended around 480-450 Ma (Stump, 1995).

- After Ross Orogeny, exhumation of granitic and basement rocks produced the erosion surface of the Kukri Peneplain (Barrett, 1991), an erosional unconformity that separates older rocks of East Antarctica with Beacon Supergroup (Devonian to Triassic), composed of sequences of quartz arenites, conglomerates, tillites, as well as fluvial sediments such sandstones, siltstones, shales and coal measures (Barrett, 1991). These were deposited in basins located between the East Antarctic Craton and a West Antarctic Permo-Triassic volcanic arc related to subduction of the proto-Pacific Ocean plate (Barrett, 1991; Elliot and Fanning, 2008). Beacon Supergroup is about 2.5-3.5 km thick and outcrops from Northern Victoria Land to the Ohio Range in southern sector of the TAM (Barrett, 1991).

- Intruding mainly Beacon Supergroup rocks, sills and plugs of the Triassic-Jurassic Ferrar Group rocks include tholeitic dolerite, basalts and volcanoclastic rocks. These rocks are related to a rifting stage occurred during the breakup of Gondwana and they are extended for 3500 km along the TAM, with variable thickness ranging from 1 m to hundreds of meters (Elliot and Fleming, 2008).

- McMurdo Volcanic Group (Tertiary to Quaternary) is characterized by alkaline volcanic rocks ranging in composition from basalts to rhyolites, forming several outcrops, from small cinder cones to large active volcanoes in a broad area comprising Southern Victoria Land and portions of Western Ross Sea (Kyle, 1990).

In the eastern side of Ross Sea, the best exposed rock units are located in Marie Byrd Land (MBL). Detailed geology of MBL has been described in the previous chapter (Chapter III, Perotti et al., 2017), and it will be briefly discussed here. The oldest unit cropping out in MBL is the Neoproterozoic-Cambrian Swanson Formation, a sequence of greenschist-sub-greenschists silicicastic rocks related to turbidite processes (Bradshaw et al., 1983; Adams, 1986; Pankhurst et al., 1998), cropping out mainly in the Ford Ranges in western MBL. This has been variably intruded during Devonian-Carboniferous and Cretaceous time by the I-type Ford Granodiorite suite and the A-type Byrd Coast Granite suite, respectively, with episodes of migmatization and high-grade metamorphic events, recorded for example in the Fosdick Mountains (Siddoway et al., 2004a). The emplacement of the youngest components of Byrd Coast Granite coincides with the onset of regional extension to transtention and the development of the West Antarctic Rift System (Siddoway, 2008). Pre-cenozoic rocks in MBL are marked by an erosive surface, the West Antarctic Erosion Surface (LeMasurier and Landis, 1996), while during the Cenozoic, the region was affected by intense alkaline volcanism and uplift of a volcano-tectonic dome. This activity started at about 34 Ma (Rocchi et al., 2006) followed by initial uplift of the dome around 28-30 Ma. Eighteen major shield volcanoes and many smaller centers are known from the

region, composed of felsic alkaline lavas, even if these felsic varieties are supposed to built up <10% of the total volcanic rocks in the province (LeMasurier et al., 2011).

4.4 Materials, Methods and Results

4.4.1 Sampling strategy

A total of 23 LGM and post-LGM piston cores collected by different scientific cruises across the Eastern Ross Sea was logged and sampled at the Marine Geology Antarctic Research Facility of Tallahassee, Florida. Distribution map and list of samples are shown in Fig. 4.1 and Table 4.1. The rationale of the choice of these piston cores is based on their geographic distribution, sediment recovery, and presence of clast rich glacial till sedimentary facies. Figure 4.1 shows geographic location of sites, which are distributed over the central Ross Sea in the Glomar Challenger Basin; in the Western Ross Sea portion, samples are located in the Central, Joides and Drigalski Basins. In figures 3, 4 and 5, stratigraphy and distribution of clasts along the entire length of each piston core, as well as classification of clast lithology, are shown. In some cases, detailed stratigraphic and chronological analysis were available in the literature, for examples the cores 80-133 and 80-189. These are located in western Ross Sea and were studied by McKay et al. (2008) and Licht et al. (1999) in order to provide constraints on the advance and retreat of the West Antarctic Ice Sheet in the Ross Sea embayment.
Logging was aimed to identify the distribution and the features of the gravel fraction (i.e. granule to cobble size clasts) along the entire length of each core. The size, shape and features of each clast >4mm was determined for each 10 cm interval of the working half split surface of the core. On the basis of distinctive macroscopic

Table 4.1. List of sample site locations. The same sites are shown labelled in other figures and elsewhere in the text. Clast log include counting, classification and selection of gravel-size clasts for detailed petrographic analysis. Abbreviation are: CRS: Central Ross Sea; WRS: Western Ross Sea.

Area	Cruise	Core	Label	Latitude	Longitude	Water depth (m)	Core length (cm)	Clast Log	N° Clasts	Sampled clasts
CRS	DF76	003-PC	76-3	-78.2	-174.183	558	671	x	49	7
CRS	DF76	008-PC	76-8	-77.533	-175.933	576	351	x	24	4
CRS	DF78	012-PC	78-12	-78.267	175.25	538	271	x	36	6
CRS	ELT27	014-PC	27-14	-77.627	175.377	720	394	x	99	4
CRS	NBP93-08	007-PC	93-7	-77.131	-175.671	388	262	x	47	9
CRS	NBP93-08	013-PC	93-13	-77.369	-177.987	676	217	x	44	9
CRS	NBP94-07	008-PC	94-8	-77.713	-178.083	544	292	x	12	10
CRS	NBP94-07	043-PC	94-43	-77.917	-178.822	725	241	x	35	10
CRS	NBP94-07	45-PC	94-45	-77.633	-179.391	661	172	x	13	5
CRS	NBP94-07	049-PC	94-49	-77.534	-177.775	670	316	x	40	8
CRS	NBP94-07	055-PC	94-55	-77.726	-177.798	676	312	x	66	6
CRS	NBP94-07	073-PC	94-73	-76.586	-178.758	644	135	x	10	7
CRS	NBP94-07	078-PC	94-78	-76.493	-179.963	375	270	x	53	8
CRS	NBP94-07	079-PC	94-79	-76.487	179.949	295	151	x	11	4
CRS	NBP94-07	090-PC	94-90	-76.76	178.535	298	359	x	115	9
CRS	NBP96-01	002-JPC	96-2	-76.452	179.881	373	419	x	112	15
WRS	DF78	014-PC	78-14	-76.5	164.0	424	334	x	98	22
WRS	DF80	133-PC	80-133	-77.083	166.167	897	258	x	9	3
WRS	DF80	134-PC	80-134	-77.15	166.183	869	260	x	26	3
WRS	DF80	189-PC	80-189	-77.2	167.883	907	193	x	34	5
WRS	ELT32	013-PC	32-13	-74.955	172.163	536	207	x	20	8
WRS	NBP94-01	002-PC	94-2	-76.284	169.704	679	174	x	37	2
WRS	NBP95-01	025-PC	95-25	-77.115	168.815	978	172	x	9	5

features, clasts were grouped into six major lithological groups (volcanic rocks; intrusive rocks; metamorphic rocks; sedimentary rocks; quartz; dolerite). Data acquisition also involved subdivision and counting of clasts occurrence in each group for each 10 cm interval of the cores. A summation of all clasts from different lithological groups was carried out for each core. Table 4.1 shows also number of logged clasts for each half split surface of cores. A total amount of 999 clasts were counted, measured and classified from the 23 cores and from these 169 representative clasts (granule to cobble sized) were sampled for detailed petrographic analysis.

4.4.2 Petrography

4.4.2.1 Analytical Details

A selection of 55 representative pebble sized clast thin sections was examined under a polarizer microscope in order to establish a detailed mineralogical and textural analysis for each sample. The identification of possible source rocks for pebbles was carried out thanks to a representative collection of rocks stored at the National Antarctic Museum of Siena (Italy) and at Polar Rock Repository at the Byrd Polar and Climate Research Center (Ohio State University).

4.4.2.2 Petrographic results

On the basis of detailed petrographic analysis, clasts recovered from the CRS and WRS piston cores can be grouped in the following 4 main lithological groups (Table 4.2 and Figure 4.2):

-Igneous plutonic rocks, including isotropic and foliated granodiorites to tonalites, isotropic gabbros and leucocratic syeno-granite.

- Igneous sub-volcanic and volcanic rocks, including dolerites, basalt, intermediate volcanic and rhyolite porphyries.

- Metamorphic rocks, including biotite ± white mica schists, biotite ± clinoamphibole schist, quartzites, metasandstones, marble, fine to medium grained calc-schists, biotite hornfels.

- Sedimentary rocks, including lithic arenite, sandstones, siltstones and limestones, and a variable amount of intraclasts.

Granodiorite to tonalite granitoid clasts are grey to pinkish inequigranular, sometimes porphyritic, fine to medium grained with hypidiomorphic texture. They include biotite ± green hornblende as mafic minerals and apatite, zircon and titanite as accessory phases. Sometimes (i.e. thin section 32), biotite is replaced by chlorite and epidote aggregates. In another case (thin section 24) epidote is associated with clinoamphibole. Quartz sometimes form granophyric interstitial texture with k-feldspar (thin section 32). In one case (thin section 30) the monzogranitic composition is characterized by a strong mylonitic foliation defined by granoblastic domains of elongated quartz. Leucocratic syeno-granite has an hypidiomorphic to allotriomorphic, equigranular medium grained texture with minor plagioclase, perthitic orthoclase and quartz; biotite is completely replaced by chlorite, and apatite, zircon and opaques minerals are the accessory phases. Mafic varieties include medium grained sub-ophitic gabbros, constituted by brownish clinopyroxene, plagioclase, opaque minerals and interstitial minor quartz with granophyric texture.

Table 4.2. List of analyzed thin sections, with petrographic features of each clasts and piston cores from which they were sampled. Piston cores are referred with site label name elsewhere in the text and in other figures. Mineral abbreviations according to Kretz (1983) except for opm=opaque minerals and wm=white mica. Other abbreviations: vfg=very fine grained; fg=fine grained; mg=medium grained; cg=coarse grained; Gr=groundmass.

Area	Thin section ID	Cruise	Core	Site Label	Top	Bottom	Lithology	Petro type	Pl (%)	Amp (%)	Bt (%)	Qtz (%)	Opm (%)	Kfs (%)	Cal (%)	Cpx (%)	Ol (%)	Grt (%)	Czo-Ep (%)	Ttn (%)	Ap (%)	Zrn (%)	Chl (%)	Wm (%)	Lithics (%)	Matrix (%)	Gr (%)	Glass (%)	Grain Size
CRS	24	DF76	03-PC	76-3	397	399	foliated hbl-tonalite	I	42	14	5	38	1						2	<1	<1		s	s					fg-mg
CRS	25	DF76	03-PC	76-3	595	599	bt-wm schist	M	3		12	75									<1	<1		9					fg
CRS	26	NBP 94-07	049-PC	94-49	13	14	cam-bt schist	M	2	20	7	66	<1		3				<1	1	<1	<1							fg
CRS	27	NBP 94-07	043-PC	94-43	184	185	bt-schist	M	2		25	71									<1			1					fg
CRS	28	NBP 94-07	078-PC	94-78	220	223	Dolerite	Isv	67				1			33													mg
CRS	29	NBP 94-07	078-PC	94-78	210	213	lith-arenite	S				50			12										29				mg-cg
CRS	30	NBP 94-07	090-PC	94-90	34	35	mylonitic monzogranite	M	30		4	40	<1	24					1				s						mg-cg
CRS	31	NBP 94-07	090-PC	94-90	112	113	bt-hbl granodiorite	I	35	9	6	45		5						<1	<1	<1	s						fg-mg
CRS	32	NBP 94-07	090-PC	94-90	165	167	bt-monzogranite	I	47			25	1	20					1		<1		7						mg
CRS	33	DF78	12-PC	78-12	83	85	microsparitic mudstone	S				<1	1		98														vfg
CRS	34	DF78	12-PC	78-12	71	79	leucocratic syeno-granite	I	10			49	<1	37					<1				3	<1					cg
CRS	35	DF78	12-PC	78-12	136	137	bt-wm-schist	M			10	84		2				<1			<1		3						fg
CRS	78	DF78	12-PC	78-12	85	87	rhyolite	Iv	6			9		2													83		mg
CRS	79	NBP 94-07	043-PC	94-43	93	97	metasandstone	M	1		3	92		1					1		<1	<1		1					fg-mg
CRS	80	NBP 94-07	043-PC	94-43	4	7	wm-quartzite	M				95	1								<1			3					fg
CRS	81	NBP 94-07	049-PC	94-49	107	108	sub-arkose	S	2		3	87	<1	5	1									<1	1				mg-cg
CRS	82	NBP 94-07	049-PC	94-49	275	276	bt-schist	M	1		12	86	<1								<1			<1					fg
CRS	83	NBP 94-07	055-PC	94-55	262	264	bt-wm schist	M	2		21	74									<1			2					fg
CRS	84	NBP 94-07	078-PC	94-78	220	221	Gabbro	I	62			<1	2			35													mg
CRS	85	NBP 94-07	090-PC	94-90	92	93	metasandstone	M	3	<1	19	66			2				8	1	<1	<1							fg
CRS	86	DF76	08-PC	76-8	86	89	foliated Bt-tonalite	I	35		18	40	<1	5							<1	<1							mg-cg
CRS	87	DF76	08-PC	76-8	30	35	Bt-Wm schist (altered)	M																					fg
CRS	88	NBP93-08	007-PC	93-7	20.5	21	Bt-cam-gneiss	M	25	15	12	45								1	<1	<1							mg
CRS	89	NBP93-08	007-PC	93-7	53	54	Phyllite	M			25	ND	<1											ND					fg-vfg
CRS	90	NBP93-08	007-PC	93-7	122	123	Bt-schist	M	3		18	77	<1							1	<1	<1							fg
CRS	91	NBP93-08	13-PC	93-13	51	52	limestone	S					2		98														fg
CRS	92	NBP93-08	13-PC	93-13	133	134	metasandstone	M	3		12	77	1		2						<1	<1		4					fg-mg
CRS	93	NBP93-08	13-PC	93-13	210	211	gabbro	I	55			3	2			38													
CRS	94	NBP93-08	13-PC	93-13	216	217	marble	M					1		99														mg
CRS	95	NBP96-01	JPC-02	96-2	130	135	metasandstone	M	2		8	84		1	2				<1		<1			2	1				fg-mg
CRS	96	NBP96-01	JPC-02	96-2	176	177	meta-siltstone	M	ND		55	ND	1											1					fg
CRS	97	NBP96-01	JPC-02	96-2	249	250	quartzite	M	2			94										<1	1	2					mg-cg
CRS	98	NBP 94-07	079-PC	94-79	78	79	bt-hornfels	M	2		38	57	1											2					fg-mg
CRS	99	NBP 94-07	073-PC	94-73	2	8	gneissic calc-schist	M																					
CRS	100	NBP 94-07	049-PC	94-49	307	309	metasandstone	M	1	3	45	47	1		2							<1							fg
CRS	101	NBP 94-07	008-PC	94-8	7	9	gabbro/dolerite	I	65			1	2			32													mg/cg
CRS	102	NBP 94-07	008-PC	94-8	116	119	cam phyllite	M		9	44	45	<1																fg
CRS	103	NBP 94-07	045-PC	94-45	30	31	bt-metasandstone	M	2		15	61													2	20			mg

Table 4.2. Continue from previous page.

Area	Thin section ID	Cruise	Core	Site Label	Top	Bottom	Lithology	Petro type	Pl (%)	Amp (%)	Bt (%)	Qtz (%)	Opm (%)	Kfs (%)	Cal (%)	Cpx (%)	Ol (%)	Grt (%)	Czo-Ep (%)	Ttn (%)	Ap (%)	Zrn (%)	Chl (%)	Wm (%)	Lithics (%)	Matrix (%)	Gr (%)	Glass (%)	Grain Size
CRS	104	NBP 94-07	045-PC	94-45	133	135	bt meta-sandstone	M	1		20	66	2		10						<1	<1							fg
CRS	106	NBP 94-07	090-PC	94-90	237	239	bt-schist	M	48		15	35									<1	<1		1					fg
CRS	107	NBP96-01	JPC-02	96-2	205	206	gabbro/dolerite	I	43			1	1			35													mg
WRS	36	DF80	189-PC	80-189	168	169	(meta) rhyolite	Iv	ND			15							<1			<1		<1	4		80		vfg-mg
WRS	37	DF80	189-PC	80-189	181	184	cam bt phyllite	M		8	30	ND			12														vfg
WRS	38	DF78	14-PC	78-14	125	128	bt-schist	M	1		25	54	2	7							<1	<1							fg
WRS	39	DF78	14-PC	78-14	145	151	meta-porphyry	Isv	10	ND		18							ND				ND				70		fg-mg
WRS	40	DF78	14-PC	78-14	290	294	Dolerite	Isv	41			1	2	1		55													mg-cg
WRS	41	NBP94-01	02-PC	94-2	117	121	bt-cam schist	M	3	8	15	66				5			3		<1	<1							fg
WRS	70	ELT32	13-PC	32-13	45	46	Dolerite	Isv	64			2	2			32													fg
WRS	71	ELT32	13-PC	32-13	112	115	intermediate volcanite	IV	25	4			2			4												65	fg-mg
WRS	72	DF80	133-PC	80-133	167	169	metasandstone	M			38	55			3							<1							fg
WRS	73	NBP 95-01	025-PC	95-25	73	80	Chl-schist	M	19			61	<1								<1	<1	15	2					fg-mg
WRS	74	DF80	134-PC	80-134	144	147	basalt	IV	29							8	3										60	<5	fg-mg
WRS	75	DF78	14-PC	78-14	152	153	impure sandstone	S	3			79									<1	<1	<1	<1	5	12			fg-mg
WRS	76	DF78	14-PC	78-14	216	217.5	siltstone	S				20															80		vfg
WRS	77	NBP94-01	02-PC	94-2	114	118	metasandstone	M	2		15	79	<1									<1		1	2				fg

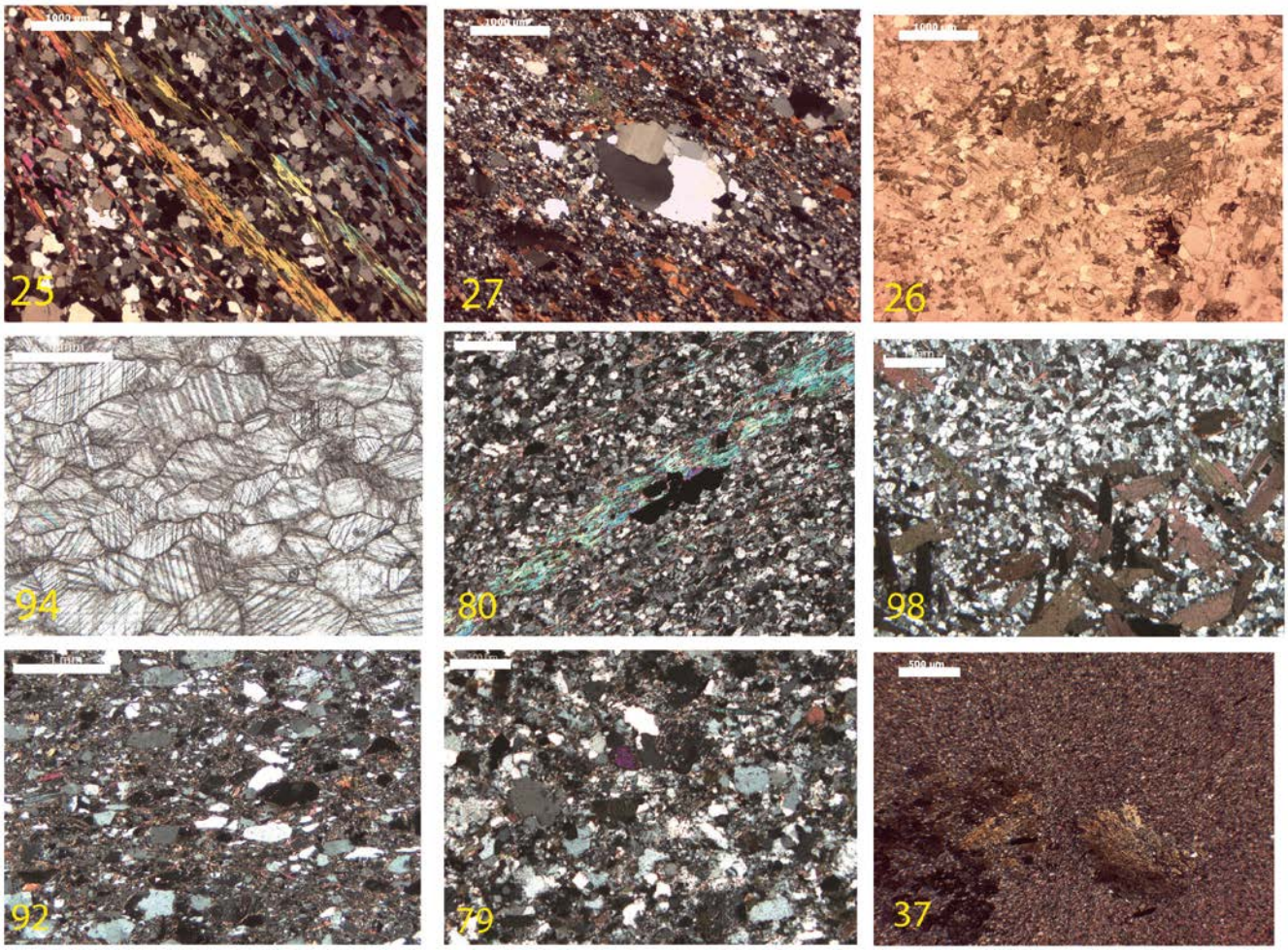

Figure 4.2. Photomicrographs of representative metamorphic clasts recovered from Central and Western Ross Sea analyzed clasts; thin section 25: biotite-white mica schist (XPL); thin section 27: biotite schist (XPL); thin section 26: biotite-actinolite schist (PPL); thin section 94: marble (PPL); thin section 80: white mica-bearing fine grained quartzite (XPL); thin section 98: biotite hornfels (XPL); thin section 92: medium grained foliated biotite meta-sandstone (XPL); thin section 79: medium grained isotropic epidote-biotite meta-sandstone (XPL); thin section 37: biotite-actinolite phillyte (XPL).

Sub-volcanic rocks include dolerites, characterized by a fine grained sub-ophitic texture defined by clinopyroxene and plagioclase, with minor opaque minerals. Sometimes quartz is present as minor interstitial phase. Other lithologies include granodioritic porphyry, with phenocrystals of quartz and plagioclase set in a quartz-feldspar fine grained groundmass (thin section 39). Volcanic rocks include two rhyolitic samples, characterized by medium grained phenocrystals of quartz and minor plagioclase set in a very fine grained quartz-feldspar groundmass. In one of these samples (thin section 36) groundmass is recrystallized with neoblastic tiny biotite. Moreover, one sample of basalt (thin section 74) shows an ipocrystalline vacuolar texture with microphenocrystals of augite, plagioclase and minor scheletric olivine set in a plagioclase-opaque minerals-clinopyroxene + glass groundmass. Instead, a sample of intermediate lava (thin section 71) shows an ipocrystalline texture with medium grained phenocrystals of zoned augite and brown amphibole, set in groundmass rich in plagioclase, clinopyroxene, minor sanidine and abundant glass.

Metamorphic rocks are generally characterized by fine to medium grained isotropic to granolepidoblastic textures and they show typical paragenesis suggesting a sedimentary (pelitic-psammitic) origin of the protoliths. They include biotite± white mica fine grained schists, in which foliation is defined by isorientation of tiny biotite idioblasts, alternating to granoblastic quartz-plagioclase domains; in some cases (e.g. thin section 82) foliation in not well developed. In one case (thin section 35), rare fine grained garnet porphyroblasts are associated to biotite and white mica foliation. In another case (thin section 26), biotite is associated with randomly oriented pale green clinoamphibole. A chlorite schist sample (thin section 73) is also present, with biotite lamellae almost completely replaced by chlorite idioblasts. Metasandstones include fine to medium/coarse grained, weakly to moderately foliated, rocks that preserve the original clastic texture, with quartz, feldspars and lithic grains, more or less enveloped by biotite tiny idioblasts to xenoblasts, which sometimes define a weak foliation. In weakly foliated varietes, also epidote xenoblasts are present. Sometimes, original textures are overprinted by sericite patches and randomly oriented white mica idioblasts (thin section 87). Quartzites have fine to coarse grained granoblastic textures, define by weakly foliated interlocking quartz grains, sometimes associated with tiny white mica layers and opaque minerals. In some cases (thin section 98), the original quartzite has been overprinted by randomly oriented biotite idioblasts caused by thermometamorphic recrystallization. Fine grained phyllites include a sample that has been thermal-overprinted with recrystallization of randomly oriented biotite idioblasts(thin section 89) and a sample defined by orientation of biotite, calcite and quartz, with peciloblastic medium grained pale green actinolite (thin section 37). A sample of medium grained marble is characterized by a polygonal weakly foliated texture of calcite and rare opaque minerals (thin section 94). Coarse grained varieties of metamorphic rocks include a quartz white mica-calcite paragneiss and a biotite-actinolite gneiss.

Sedimentary rocks are fine to coarse grained, poorly sorted, heterogranular siltstone to sandstones, with variable amount of matrix; in one case (thin section 29) cement is completely constituted by carbonate and matrix is absent, lithic grains are composed mainly by low grade metamorphic rocks, clastic lithics and limestones. Two samples of carbonate rocks have been examined: one sample (thin section 33) of very fine grained microsparitic mudstone, with stylolites and few areas of recrystallized calcite; and one sample (thin section 91) of recrystallized microsparitic limestone with a mosaic texture of fine grained calcite crystals. In addition to extrabasinal sedimentary clasts, a certain amount of intrabasinal clasts were found from the analyzed cores: these are polymictic fine to coarse grained matrix-rich non consolidated soft sediments incorporating lithics grains and quartz crystals; in some case they have microconglomerate grain size, in others they are silt-size. These sediments aggregates are variously called: till pebbles, till pellets, intraclasts, polymicts, even if the latter is preferable, since it gives any genetic connotation (van der Meer, 1993; Menzies et al., 2006).

4.4.3 Clasts distribution

CRS cores were divided spatially in two different groups: one with cores located in a proximal position in respect of the Ross Ice shelf line (7 cores, Figure 4.3), with some cores located directly below present day shelf (i.e. 78-12), and the other with cores located in a distal position, offshore towards the centre of the Glomar Challenger Basin (9 cores, Figure 4.4). The proximal cores have overall clasts assemblages dominated by sedimentary clasts (up to 95% in core 27-14), most of them being polymictic intrabasinal clasts. Metamorphic rock fragments are the other most represented lithology if we exclude polymictic intrabasinal clasts,

constituting up to 69% of the total assemblage in core 94-45. The most representative metamorphic clasts are fine to medium grained meta-sedimentary rocks, prevalently of low grade paragenesis. Granitoids are widespread in variable amount, ranging from 1% to 47% and constituting the second most represented lithology in 3 out of 7 cores. Volcanic rocks are minor and they do not exceed 3% in the analyzed cores. Taking in consideration all the proximal cores together as a single group, clast assemblage results to be made up of 55% of sedimentary clasts (mainly polymictic intrabasinal clasts), followed by metamorphic clasts (29%), granitoids (15%) and minor volcanic rocks (1%).

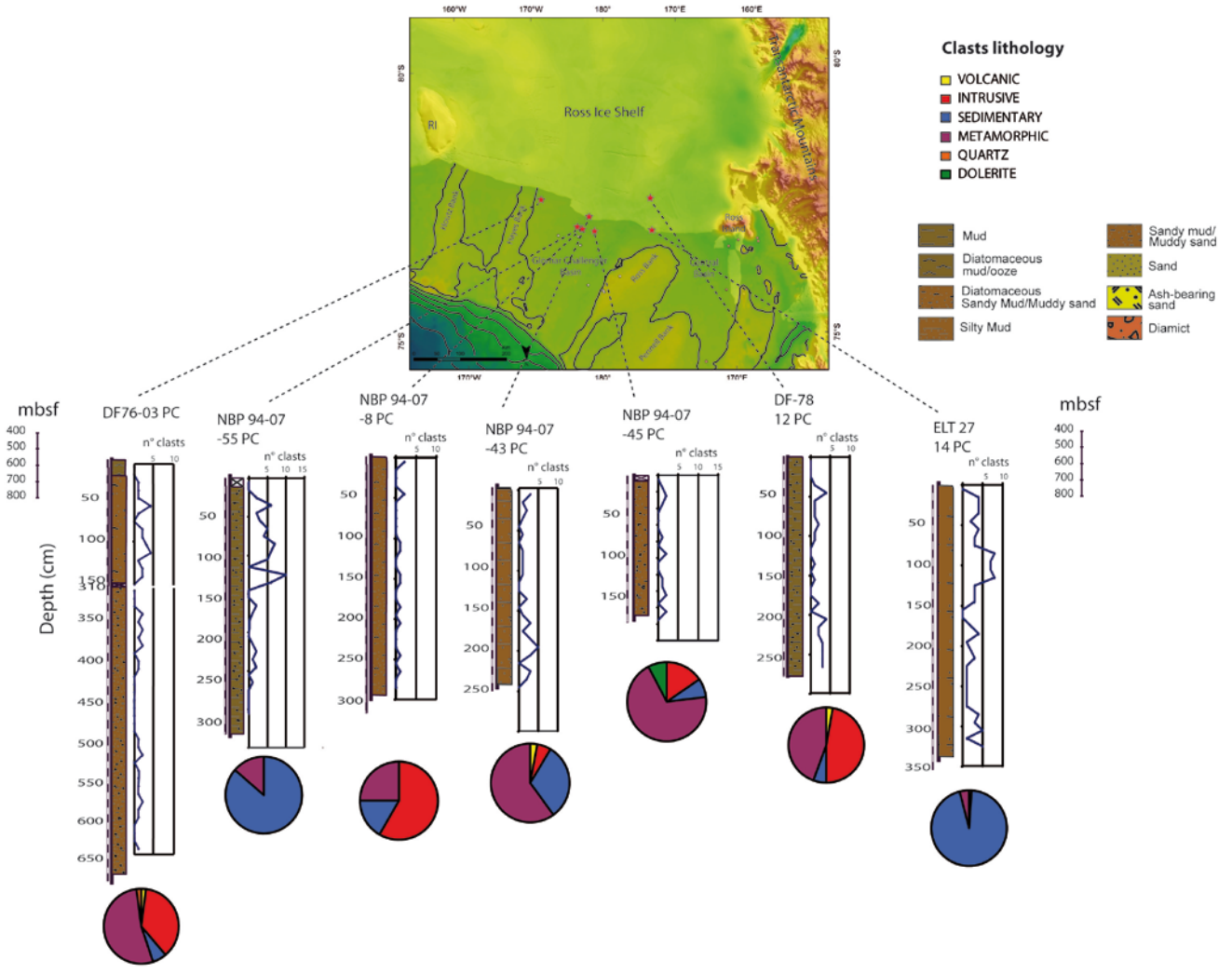

Figure 4.3. Distribution of proximal Central Ross Sea piston cores, with sediment descriptions and occurrence and lithology of gravel-size clasts along the depth of the cores. Vertical scales for sea floor depths and core depths are different. Mbsf: meters below sea floor. Sediment descriptions from Antarctic Marine Geology Research Facility reports, Florida State University.

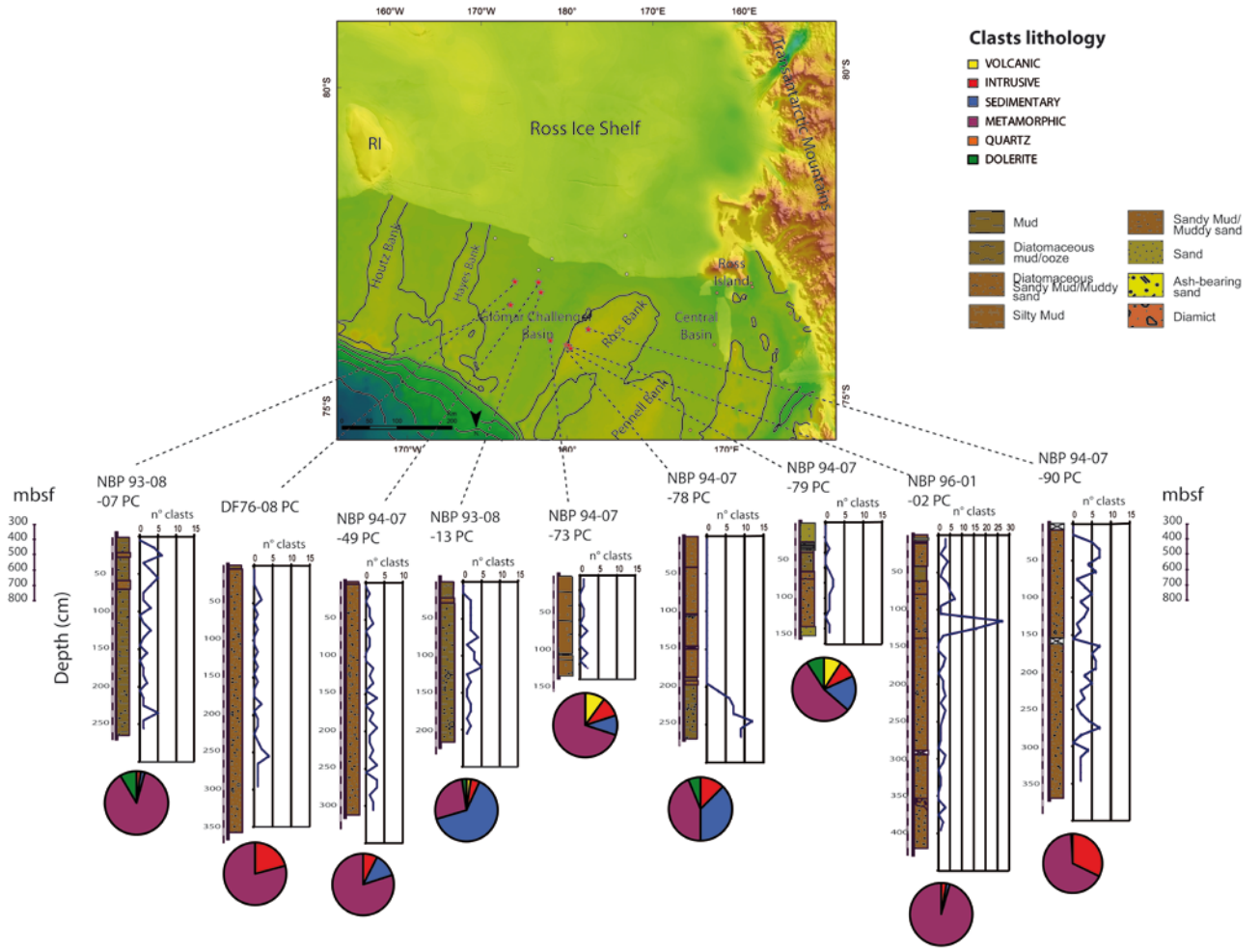

Figure 4.4 Distribution of distal Central Ross Sea piston cores, with sediment descriptions and occurrence and lithology of gravel-size clasts along the depth of the cores. Vertical scales for sea floor depths and core depths are different. Mbsf: meters below sea floor. Sediment descriptions from Antarctic Marine Geology Research Facility reports, Florida State University.

The distal CRS cores are prevalently constituted by metamorphic rock fragments, which are the most represented lithology in 8 out of 9 analyzed cores; only in one case (i.e. 93-13), sedimentary rocks prevail over metamorphic rock fragments, with 64% of the total assemblage. Granitoids are present in almost the same amount as in the proximal CRS group, ranging from 2% to 32% in the analyzed cores. The overall clast distribution of this group is characterized by 71% of metamorphic rock fragments, 14% of sedimentary clasts, 13% of granitoids, 2% of dolerites and 1% of volcanic rock fragments.

Western Ross Sea cores are characterized by a distinct, although variable, clast assemblage (figure 4.5). Indeed, in 3 out of 7 cores (i.e. 32-13; 80-133; 80-134), volcanic rock fragments compose the major fraction of clasts

assemblage, up to 88% of the total for the sample 80-134. The two volcanic clasts richest cores are located close to Ross

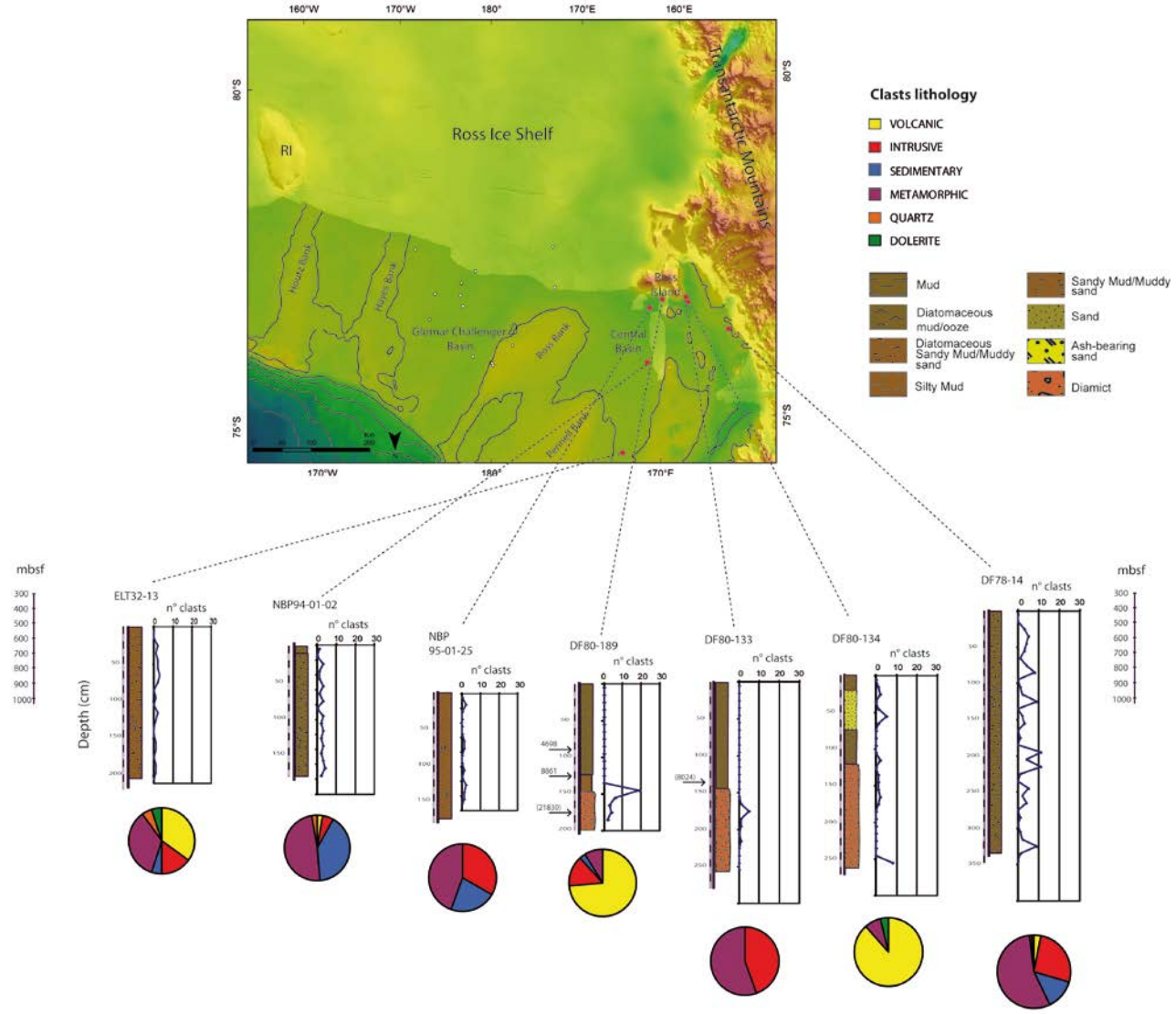

Figure 4.5. Distribution of Western Ross Sea piston cores, with sediment descriptions and occurrence and lithology of gravel-size clasts along the depth of the cores. Vertical scales for sea floor depths and core depths are different. Mbsf: meters below sea floor. Sediment descriptions from Antarctic Marine Geology Research Facility reports, Florida State University, except for DF80-189 and DF80-133 that are from McKay et al. (2008). In the latter also corrected and uncorrected (bracketed) ^{14}C age are shown (from McKay et al., 2008).

Island in McMurdo Sound, but core 32-13 has a volcanic percentage of 35% and it is located in the Joides Basin, nearly 200 km offshore from Ross Island. The second most represented lithology is the group of metamorphic rocks, composed of mainly low grade isotropic to slightly anisotropic fine to medium grained metasandstones, siltstones and quartzites. These group ranges from 35% to 56% of the total clast assemblage in the cores where volcanic clasts are not the major group (i.e. 80-133, 80-134). Granitoid lithic fragments are present in variable

amount and they ranges from 5% to 47%. Sedimentary clasts are in minor proportion, except in one core (i.e. 94-02) where they reach 41% of the total clast assemblage. Considering all the counted clasts together as a single group, WRS cores have an overall composition consisting of a major fraction of volcanic rock fragments (33%), and low-grade metamorphic rocks (32%), followed by granitoids (20%), and sedimentary rocks (13%).

Looking at the spatial distribution of analyzed cores and taking into account their positions, the following considerations could be made: the main differences in clast distribution between CRS and WRS cores is the amount of volcanic lithologies, which is consistent (33%) in the WRS and negligible (~1%) in the CRS. Granitoid rock fragments are slightly more abundant in the WRS (20%) than in the CRS (13%), while metamorphic rock fragments are more abundant in CRS cores than in WRS (54% vs 32%, respectively). Among the CRS cores, an ideal S-N profile highlights the main differences between the two groups, in a proximal and in a distal position. In particular a major occurrence of sedimentary clasts is present in cores that are proximal to the Ross Ice Shelf edge, in respect of those from distal positions (55% vs 14%, respectively); these are mainly intrabasinals polymictic clasts. Instead, a major occurrence of metamorphic lithics occurs among offshore cores, located towards the centre of the Glomar Challenger Basin (28% vs 71%, respectively), where granitoid lithics are present in the same amount in the two groups. Comparing this distribution with that occurring in ERS cores (described in Chapter III, Perotti et al. 2017), it is noteworthy that granitoid rocks are more abundant in ERS and WRS than in CRS, and that sedimentary rocks are more abundant than granitoids in CRS proximal cores (even if a great amount of sedimentary clasts are of intrabasinal origin). Instead, volcanic rocks fragments are minor or negligible in ERS and CRS, but they make up a consistent fraction in WRS, also from core located in an offshore position.

4.4.4 Mineral Chemistry

Mineral chemistry analyses were carried out on 8 representative clasts. These are hornblende-tonalite (thin section 24), three biotite-white mica schists (thin section 25, 35 and 83), biotite-amphibole schist (thin section 26), two metasandstones (thin section 92 and 95) from CRS cores and an intermediate alkaline basalt from WRS (thin section 71 from 32-13 core). They were chosen on the basis of the presence of unaltered minerals on their surfaces. Chemical analysis of the main mineral phases identified via petrographic microscope were carried out with an X-ray energy dispersive system EDAX DX4 attached to a Scansion Electron Microscope Philips XL30 at the Department of Physical Sciences, Earth and Environment of Siena (Italy). Thin sections have been polished and carbon coated before carrying out measurements. Analytical conditions were 20 kV of accelerating voltage, 25 μA of emission current, and a beam spot size of 0.2 Am. Natural minerals were used as standards. Fe^{3+} concentration in clinoamphiboles and clinopyroxenes was estimated by the equation of Droop (1987), assuming charge balance.

4.4.4.1 Mineral Chemistry Results

Clinoamphiboles, biotites, and white micas composition are shown in Figure 4.6. Clinoamphiboles were analyzed from three thin sections (24, 26, 71). All analyzed amphiboles are members of the calcic-amphibole group, as shown in Figure 6a (Leake et al., 1997). Clinoamphiboles in biotite amphibole schist (thin section 26) are magnesio-hornblende to actinolites in composition, with X_{Mg} of the cores varying from 0.63 to 0.77, and they are mostly slightly zoned, with a Mg-richer core and a Fe-richer rim. In biotite-amphibole tonalite (thin

section 24), amphiboles are mostly Mg-hornblendes to actinolitic hornblendes (X_{Mg} ranging from 0.51 to 0.64), in some cases having a strong zonation, with Fe-richer rim and Mg-richer core. In alkaline basalt (thin section 71) amphiboles phenocrystals belongs to the pargasite-edenite series (X_{Mg} ranging from 0.62 to 0.68), and they have Ti>0.50 atoms per formula unit, so they are all kaersutites, according to Leake et al. (1997) classification.

Biotite representative compositions are listed in Figure 6b. In most samples (e.g. Thin section 83), biotites have a narrow compositional range (X_{Fe} 0.46-0.48), and quite homogeneous composition. Biotites from thin section 35 exhibit in some cases strong zonation, with Fe enrichment and Mg depletion from core to rim. In general, all the analyzed biotites have X_{Fe} between 0.46 (thin section 83) and 0.64 (thin section 35), with variable amount of Al^{IV}. White mica representative compositions are listed in Figure 6c. White micas in petrographically similar metasandstone (thin sections 92 and 95), and biotite schist (thin section 83) and biotite-white mica ± garnet schist (thin section 35) are all muscovites; in certain cases they exhibit a wide range of composition, for example in thin section 92 and to a lesser extent in thin section 95 and 35, some single idioblasts have a more phengitic composition, evene if the majority of idioblasts have an average amount of Si per formula unit <6.3. Instead, another biotite-white mica schist (thin section 25) have an average composition fairly richer in Si per formula unit, ranging between 6.3 and 6.5.

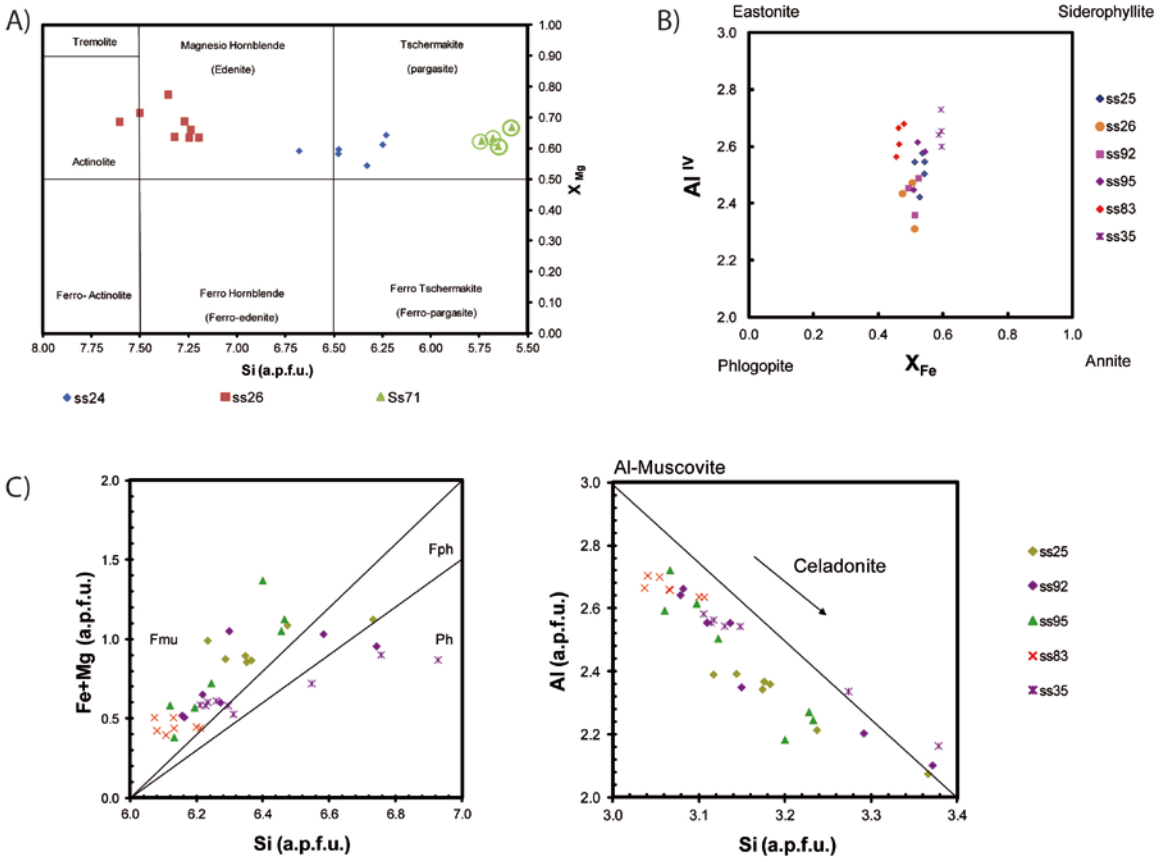

Figure 4.6. Representative chemical analysis of minerals from Western anc Central Ross Sea detrital clasts: (a) Ca-amphibole classification from Leake et al. (1997), in terms of X_{mg} versus Si (atoms per formula unit); circled points refer to amphiboles of the edenite-pargasite series ($Na+K_A \geq 0.50$ and Ti>0.50 atoms per formula unit, i.e. kaersutite field) (b) biotite composition in terms of Al^{IV} versus Fe/(Fe+Mg); (c) white mica composition in terms of Fe+Mg versus SI and Al versus Si (atoms per formula unit).

4.5 Discussion

4.5.1 Clasts source rocks

The collected petrographical data allow a preliminary identification of the most likely source rock units which are exposed in the Transantarctic Mountains area, in the east side of the Ross Sea embayment, and in its western portion, with a significantly minor outcrops extension , mainly located in Marie Byrd Land.

The major amount of analyzed clasts are low grade fine to medium grained metasedimentary rocks; this is testified by sub-greenschist/greenschist grade paragenesis, with occurrence of biotite ± chlorite ± actinolite ± (garnet) ± white mica in metapelitic and metapsammitic rocks and calcite ± epidote ± white mica assemblages in more Ca-rich rocks. In certain cases, foliation is not clearly developed and only a static recrystallization occurs, with biotite or actinolite porphyroblasts growth. These features are useful to identify potential source low-grade metamorphic units which also experienced a thermal overprinting caused by plutons emplacement. Table 4.3 show possible source units for each type of rocks identified in thin section, with a subdivision between east sources (i.e. Transantarctic Mountains) and west sources (West Antarctica-MBL).

Meta-sandstones/graywackes, meta-siltstones and phyllites (sometimes with spotted termo-metamorphic overprint) are present in (meta)sedimentary units in several areas in the Transantarctic Mountains; starting from Southern Victoria Land, rocks of regional metamorphism of low P-T conditions occur in the Skelton-Mulock glaciers area and Teall Island (Skinner, 1982; Cook and Craw, 2002) and they present in some cases similar features with those found in CRS and WRS piston cores. These units belong to the Skelton Group of Southern Victoria Land, that, south of the Royal Society Range, mainly consists of low-grade metapelitic rocks (Cook and Craw, 2002; Cox et al., 2012). Farther South, in the central Transantarctic Mountains, in the region around Nimrod Glacier, a sequence of thermally metamorphosed graywackes and argillite is part of the Goldie Formation of the Beardmore Group (Laird et al., 1971; Stump, 1985, 1995). This formation was successively revised and subdivided in an “inboard” Goldie formation, cropping out in a restricted area between the two sides of Nimrod Glacier, and a volumetrically more extensive “outboard” formation that has been considered correlative of the younger Starshot formation of the Byrd Group and assigned to it (Mirow et al., 2002; Goodge et al., 2002). These “outboard” sequences crop out along the Ross Ice Shelf side of the Shackleton Coast from Beardmore Glacier to the region south of Shackleton Glacier. Therefore, also silicoclastic sequences younger than Shackleton Limestone (i.e. Douglas Conglomerate, Starshot and Dick Formations), all belonging to the Byrd Group, could be considered possible source units for metasandstones. Douglas Conglomerate consists of coarse grained clastic successions (Mirow et al., 2002), while Starshot and Dick formations have an overall finer grained sequences defined by shales, sandstones and minor conglomerates. The regional metamorphism and the paragenesis of Byrd Group rocks (Shackleton Limestone and younger siliciclastic formations) are typical of a low P/T assemblage (Skinner, 1965) with the exception of the Mt Madison area (Selborne marble, Talarico et al., 2007, ; Stump et al., 2004). Other outboard sequences temporally correlatives with the Cambrian Byrd Group are located farther South, in the Queen Maud Mountains (Stump, 1985, 1995). In particular the La Gorce, Duncan and Party formations which include meta-graywackes, siltstones, quartzites and schists cropping out between the Scott and Reedy Glacier area and interpreted as deposits related to turbidity currents processes (Stump, 1982, 1985, 1995; Stump et al., 1981; Minshew, 1967).

As a result of their extensive occurrence in the Transantarctic Mountains at least three major regions (Skelton-Mulock Glaciers area; Nimrod-Beardmore Glaciers area and Queen Maud Mountains/Scott Glacier area) could provide detrital metasandstones and metagraywackes to Ross Sea embayment basins.

In contrast potential sources in West Antarctica are represented only by the Neoproterozoic-Cambrian Swanson Formation, a folded and cleaved low grade sequence of metaturbidites which crops out mainly in Ford Ranges in western Marie Byrd Land. This formation has been correlated chronologically with the Robertson Bay Group in Northern Victoria Land (Bradshaw et al., 1983; Adams et al., 2013; Pankhurst et al., 1998) and correlatives metasediments are sparse and are exposed in isolated nunataks in the region of Eastern Marie Byrd Land (Hobbs Coast and Ruppert Coast, Brand, 1979).

Quartzites and pelitic schists (biotite ± actinolite ± white mica schists) can have been sourced from the same low-grade siliciclastic units described above, but with some little differences. In Southern Victoria Land quartzites are a minor constituent of some units of the Skelton Group, in particular the Marshall Formation of Findlay et al. (1984), cropping out in the region between Blue and Koettlitz Glacier, where are interlayered with biotite schists and calc-silicates rocks. Also Salmon Marble and Hobbs Formation of Findlay et al. (1984), cropping out in the same region, are composed of interlayered sequences of marbles, micaschists, calc-silicates, hornfelses. However, these units are characterized by a low/medium to medium grade regional metamorphism (Findlay et al., 1984, Cox et al., 2012), so attribution of lower grade detrital clasts of marine dataset to these groups of rocks appears to be unlikely. Instead, in the region of Skelton Glacier, biotite-schists of greenschist facies are present (Cocks and Baronick units of Cook and Craw, 2002), but quartzites are a minor constituent. Farther south, among the Beardmore Group sequences, the older Cobham Formation is an interlayered succession of biotite hornfels quartzite, marbles and schists, with quartzites being the dominant lithology in the lower part of the studied section (Laird et al., 1971). The overlying Goldie Formation as well is dominated by a muddy quartzite altered in a quartz-sericite-biotite schist (Laird et al., 1971). In the same region of the Central Transantarctic Mountains, between Byrd and Shackleton Glacier, the Byrd Group crops out extensively: possible clastic units which could provide quartzitic and schistose detrital clasts are the Shackleton Limestone formation, that at its basal members is constituted by interbedded sandstones, shales and breccias; however, these members are minor constituents of the thicker calcareous sequence of this formation (Laird et al., 1971; Mirow et al., 2002). Instead, the most siliciclastic-rich sequences are the overlying Douglas, Dick and Starshot formations (Laird et al., 1971; Mirow et al., 2002). From the Queen Maud Mountains, the same outboard formations described for meta-sandstones contain considerable amount of interbedded quartzites and pelitic schists (La Gorce, Party, Duncan formations; Stump 1985), as well as rocks of the Liv Group (Greenlee, Taylor,

Table 4.3. List of possible source rock units cropping out in the Transantarctic Mountains and West Antarctica-Marie Byrd Land for clast lithologies found in WRS and CRS piston cores. Abbreviations: I=Igneous plutonic rocks; Iv= Igneous volcanic rocks; Isv=Igneous sub-volcanic rocks; M=metamorphic rocks; S=sedimentary rocks.

			Source rock units					
Examined clasts	**Clasts lithology**	**Petro type**	**West Antarctica (MBL)**	**Main Outcrops**	**References**	**Transantarctic Mountains**	**Main Outcrops**	**References**
3	bt ± hbl granodiorite to tonalite	I	Ford Granodiorite	Ford Ranges	Weaver et al. (1991); Pankhurst et al. (1998)	G.H.I.C. Queen Maud Wisconsin Range Batholith; G.H.I.C.Hope Granite; G.H.I.C. Blue Glacier Pluton; G.H.I.C. Bonney Pluton	Queen Maud Mts.; central TAM; Blue Gl. Area (SVL)	Stump (1995); Skinner (1983); Cox et al. (2012)
2	bt-monzogranite	I	Byrd Coast Granite	Ruppert-Hobbs Coast; Ford Ranges-Ed.VII Peninsula	Weaver et al. (1992); Mukasa and Dalziel 2000	G.H.I.C. Queen Maud Wisconsin Range Batholith; G.H.I.C. Hope Granite; G.H.I.C. Skelton Granodiorite; G.H.I.C. SVL (Dun, Catspaw, Bonney plutons)	Queen Maud Mts; central TAM; Skelton Gl. Area (SVL) Ferrar-Koettlitz Gl. Area	Stump (1995); Gunn and Warren (1962); Cox et al. (2012)
1	leucocratic syeno-granite	I	Byrd Coast Granite	Ruppert-Hobbs Coast; Ford Ranges-Ed.VII Peninsula	Weaver et al. (1992); Mukasa and Dalziel (2000)	G.H.I.C. Koettlitz Glacier Alkaline province; G.H.I.C. Mulock Granite	Glee Kempe Gl. Area (SVL); Mulock Glacier	Cook and Craw (2001); Cottle and Cooper (2006)
2	Gabbro (pl+cpx ± opx ±qtz)	I				Ferrar Group	central TAM; SVL	Elliott et al. (1995)
5	Dolerite	Isv	Mafic dykes	Ford Ranges	Storey et al. (1999); Siddoway et al. (2005); Saito et al. (2013)	Ferrar Group	central TAM; SVL	Elliott et al. (1995)
2	rhyolitic porphyry	Iv				Liv Group ; Skelton Group (meta-rhyolite)	Queen Maud Mountains; Skelton Gl. Area	Stump (1985, 1995); Rowell and Rees (1989); Skinner (1982)
4	Sedimentary rocks (lith-arenite; sub-arkose; siltstones)	S	Swanson Fm	Ford Ranges-Ed. VII Penisnula	Bradshaw et al. (1983)	Taylor Fm.; Beacon Supergroup; Byrd Group (siliciclastic fm); eocene erratics.	Queen Maud Mountains; central TAM; SVL	Barrett (1981); Collinson(1991); Mirow et al. (2002); Levy and Harwood (2000)
2	microsparitic mudstone	S				Taylor Fm; Shackleton Limestone (Byrd Group)	Queen Maud and Horlick Mts; Byrd-Nimrod Gl. Area	Stump (1985; 1995); Mirow et al. (2002)

Table 4.3. (Continue)

			Source rock units					
Examined clasts	**Clasts lithology**	**Petro type**	**West Antarctica (MBL)**	**Main Outcrops**	**References**	**Transantarctic Mountains**	**Main Outcrops**	**References**
10	bt ± chl ± wm schist	M	Basement Rocks	Hobbs Coast	Bradshaw et al. 1983; Pankhurst et al. (1998); Brand (1979)	LaGorce Formation; Party Fm.; Leverett Fm.; Argosy Fm. (Nimrod Group); Cobham Fm.; Goldie Fm. (Beardmore Group); Selborne Group (Contorsion Schist); Skelton Group; Hobbs Fm (Skelton Group)	Queen Maud-Horlick Mts; Nimrod Gl. area; Skelton Gl. Area	Laird et al. (1971); Stump (1995); Stump et al. (2004)
2	cam-bt schist	M	Basement Rocks	Hobbs Coast	Brand (1979)	Cocks Fm (Skelton Group); Hobbs Fm (Skelton Group)	Skelton Gl. Area; Miers-Garwood Valley area	Findlay et al (1984)
3	quartzite (±wm)	M	Swanson Fm	Ford Ranges-Ed. VII Penisnula	Bradshaw et al. (1983); Pankhurst et al. (1998); Brand (1979)	Taylor Fm.; Party Fm.; Argosy Fm.; Cobham Fm. (Beardmore Group); Base of Shackleton Limestone (Byrd Group); Anthill Limst (Skelton Group); Hobbs Fm (Skelton Group)	Queen Maud-Horlick Mts; central TAM, Skelton Gl. Area	Stump (1995); Laird et al. (1971); Cook and Craw (2002); Findlay et al. (1984)
10	Metasandstone	M	Swanson Fm	Ford Ranges-Ed. VII Penisnula	Bradshaw et al. (1983); Pankhurst et al. (1998)	LaGorce Fm.; Henson Marble; Goldie Fm. (Beardmore Group); Byrd Group (siliciclastic sequences); Skelton Group	Queen Maud-Horlick Mts; central TAM; Skelton Gl. Area	Stump (1985; 1995); Mirow et al. (2002)
1	Marble	M				Taylor Fm ; Fairweather Fm; Henson Marble; Leverett Fm (Queen Maud Mts); Worsley Fm (Nimrod Group); Cobham Fm. (Beardmore Group); Selbourne Group (Marble) (central TAM mt madison) Marshall Fm; Salmon Marble (Skelton Group)	Queen Maud-Horlick Mts; central TAM (Mt Madison); Skelton Gl. Area; SVL	Stump (1982, 1985, 1995); Stump et al. (2004); Laird et el. (1971)
3	bt ± act phyllite	M	Swanson Fm	Ford Ranges-Ed. VII Penisnula	Bradshaw et al. 1983; Pankhurst et al. (1998)	Ackerman Fm ; Greenlee Fm.; Taylor Fm (Queen Maud Mts); Goldie Fm. (Beardmore Group, central TAM); Byrd Group (siliciclastic fm.); Skelton Group (skelton Gl. Area)	Queen Maud-Horlick Mts; central TAM; Skelton Gl. Area; SVL	Stump (1985, 1995); Cook and Craw (2002); Mirow et al. (2002)

Table 4.3. (Continue)

			Source rock units					
Examined clasts	Clasts lithology	Petro type	West Antarctica (MBL)	Main Outcrops	References	Transantarctic Mountains	Main Outcrops	References
1	Bt-cam-gneiss	M				Party Fm.; Miller Fm; Argosy Fm. (Nimrod Group); Marshall Fm and Hobbs Fm. (Skelton Group)	Queen Maud-Horlick Mts; central TAM; Skelton Gl. Area; SVL	Laird et al. (1971); Stump (1982, 1985, 1995)
1	Gneissic calc-schist	M				Henson Marble; Party Fm.; Leverett Fm. (Horlick Mts); Cobham Fm. (Beardmore Group); Hobbs Fm. (Skelton Group)	Queen Maud-Horlick Mts; central TAM; Skelton Gl. Area; SVL	Laird et al. (1971); Stump (1982, 1985,1995); Findlay et al. (1984)
1	altered-porphyry	M				G.H.I.C.	Ferrar-Koettlitz Glacier Area	Cox et al. (2012)
2	Intermediate volcanite, Basalt	Iv	MBL volcanic province	Executive Commitee Range-Flood Range	LeMasurier (1990)	McMurdo Volcanic Group	Ross Island, Minna Bluff, Mount Morning; Mount Discovery	Kyle (1990)

Henson Marble Formations, Stump, 1985); moreover, also metaturbidite sequences of Swanson Formation in Marie Byrd Land could be a considered source rocks for these kind of detrital clasts (Bradshaw et al., 1983). Marbles are present in several regions of the Transantarctic Mountains: in Southern Victoria Land the Salmon Marble and Marshall Formations (in a lesser extent) of the Skelton Group, both cropping out in the region between Blue and Koettlitz Glacier, contain saccharoidal marble with rusty layers of pyrites, white mica and diopside, sometimes intercalated with biotite schists (Findlay et al. 1984). In the region of the Skelton glacier, the Skelton Group is also formed by a grey marble unit which crops out between Cocks and Baronick Glacier (Cook and Craw, 2002, the former Anthill Limestone of Gunn and Warren, 1962) and which is pervasively foliated. In the Central Transantarctic Mountains a unit of marbles crops out close to Cape Selborne in the southern side of Byrd Glacier, composed of bedded cream, grey and white scapolite marbles intercalated with biotite schists and hornblende hornfels, defined by Skinner (1964, 1965) the Selborne Marble. The revised stratigraphy of this unit made by Stump et al. (2004) include two units in the same Selborne Group, the Madison Marble and the Contorsion Schist. This is, however, an high grade unit, at least amphibolite-grade (Skinner, 1964; Stump et al., 2004, Talarico et al., 2007). Impure limestones and marbles are subordinately interbedded in the Cobham and Goldie Formation of the Beardmore Group (Laird et al., 1971; Mirow et al., 2002; Stump, 1995). In the region of the head of Nimrod Glacier, in the Miller and Geologists Ranges, the Nimrod Group provides evidence of the Archean and Paleoproterozoic basement, reactivated during Ross Orogeny (Goodge, 2007) and it is composed of upper amphibolites-lower granulite facies rocks; two formations, the Worsley and subordinately the Argosy formations, as they were described originally, contain calc-silicates and subordinate tremolite-bearing marbles (Stump, 1995). In the Queen Maud Mountains, marbles have been identified in outcrops of Taylor Formation, from the Shackleton Glacier region, Fairweather Formation from the Duncan Mountains (Liv Glacier area), and constitute the main lithology of the Henson Marble Formation, cropping out overlying the Fairweather Formation in the same area (Stump, 1985, 1995); Henson Marble is composed of thick portions of white, relatively pure marble, usually very coarsely crystalline (Stump, 1985). Instead, any marble-bearing units are known from outcrops located in West Antarctica, so possible source rocks of marble clast are likely located along the Transantarctic Mountains.

Limestone clasts found in marine dataset indicate a mainly calcareous source rock able to provide this kind of detritus: carbonate sequences from the Transantarctic Mountains are known from Shackleton Limestone formation of the Byrd Group, in the region between Byrd Glacier and the south side of Nimrod Glacier (Laird et al., 1971; Mirow et al., 2002). Calcareous members of this formation range from fine-grained limestone and quartzitic limestone to quartz dolomite, with traces of recrystallization and a fine saccaroidal texture (Skinner, 1965; Laird et al., 1971; Mirow et al., 2002). Other limestones occur in the uppermost portion of the Taylor Formation in the Shackleton Glacier area (Taylor Nunatak, Stump, 1985): these are prevalently micrites interlayered with chertlike rocks and volcanic rocks (Stump, 1985). Alternatively, a possible source area could be the same of calcareous sandstones and limestones belonging to the Eocene McMurdo Erratics that were reported as erratic boulders in Pleistocene glacial deposits of McMurdo Sound coast (Harwood and Levy, 2000; Levy and Harwood, 2000). Instead, in West Antarctica, some carbonate successions are present in Ellsworth-Thiel Mountains ridge (Storey and McDonald, 1987), as well as the Nelson Limestone in the Pensacola Mountains (Stump, 1995). Carbonate sequences are instead absent in all exposed rock units in Marie Byrd Land.

Granitoid rocks found in the marine dataset of CRS and WRS piston cores are prevalently biotite ± hornblende granodiorite to tonalite, but a sample of biotite monzogranite, a sample of syeno-granite and two samples of gabbros are also present. Granitic plutons are extensively cropping out in the Transantarctic Mountains, belonging to the Granite Harbour Intrusive Complex, as well as in Marie Byrd Land where two suites of granites are documented, the Ford Granodiorite and the Byrd Coast Granite. In marie Byrd Land, granodiorites and hornblende-tonalites are the main lithologic type of the Devonian-Carboniferous Ford Granodiorite, cropping out in the Ford Ranges (Weaver et al., 1991; Pankhurst et al., 1998), while syeno-granites are more common types in the cretaceous alkaline Byrd Coast Granite suite (Weaver et al., 1992), which crops out in Edward VII Peninsula, the Ford Ranges and in Ruppert and Hobbs Coast (Mukasa and Dalziel, 2000). Along the Transantarctic Mountains, starting with Southern Victoria Land, and considering the more extensive intrusions, the Bonney Pluton is the main hornblende-bearing granodioritic pluton (Smillie, 1992; Cox, 1993; Cox et al., 2012), cropping out extensively between the Ferrar and Koettlitz Glacier area. Tonalites are instead more represented in the Blue Glacier area, located north of Koettlitz Glacier (Skinner, 1983). Isotropic monzogranites and granodiorites are also constituents of the Skelton Granodiorite in the southern Skelton Glacier Area (Gunn and Warren, 1962). Farther south, in the region between Carlyon and Darwin Glacier, the Cooper Granodiorite is a pluton formed by biotite ± hornblende monzogranites to granodiorites (Simpson and Cooper, 2002), characterized by a strongly medium to coarse grained heterogranular texture. Syeno-granites are present in Southern Victoria Land as part of the Koettlitz Glacier Alkaline Suite of the Granite Harbour Intrusives Complex, which crops out mainly at the head of Koettlitz Glacier and comprises A-type granites, alkaline and sub-alkaline gabbros and nepheline-syenite (Read et al., 2002; Cox et al., 2012). However, other A-type plutonic intrusions crop out farther south, as far as in the region of the Darwin Glacier, where the Foggy Dog Granite and Mulock Granite have this kind of geochemical affinity (Simpson and Cooper, 2002; Cottle and Cooper, 2006a). South of Byrd Glacier discontinuity, granitoids are less extensive and metasedimentary units are dominant: the Hope Granite, a name originally used to describe a series of plutons cropping out between Nimrod and Beardmore Glacier, comprises quartz-monzonites and lesser granites (Gunn and Walcott, 1962; Laird et al., 1971; Stump, 1995), and they generally contain muscovite ± hornblende. Tonalites are reported from Bartrum Plateau in the area at the head of Nimrod Glacier (Laird et al., 1971; Stump, 1995). In the Queen Maud Mountains, Granite Harbour Intrusive Complex are mainly represented by the Queen Maud-Wisconsin Range Batholith, cropping out in a wide area between Shackleton Glacier and Ohio Range (Stump, 1995); the batholith is composed of a calc-alkaline suite of plutons ranging in composition from granite and quartz-monzonite to tonalite, diorite and hornblende gabbro, with medium to coarse grained, equigranular and porphyritic granodiorites-quartz monzonites, containing biotite and locally hornblende, being the most common rock types (Borg, 1983; Murtaugh, 1969). Gabbro-bearing units in Transantarctic Mountains are intrusions of the Koettlitz Glacier Alkaline Suite, with Glee Intrusives, Skelton Mafic Intrusives, Dromedary Mafic Complex and Panorama Pluton being all plutons cropping out in the region between Koettlitz and Skelton Glacier (Cox et al., 2012; Simpson and Aslund, 1996; Read et al., 2002). A gabbroic intrusion is present also in the region of Carlyon Glacier farther south (Cottle and Cooper 2006b). Moreover, gabbroic rocks are reported in the Central Tam (Holyoake Range, Laird, 1963) and in the Queen Maud Mountains, at Gabbro Hills (Stump, 1995). However, the typical mineralogy of these intrusions, that is plagioclase ± biotite, amphibole ± clinopyroxene ± minor alkali feldspar is not the same as detrital clasts found in CRS and ERS, which in texture (sub-ophitic to ophitic) and mineralogy (plagioclase + clinopyroxene + opaques minerals ± minor granophyric quartz) are more similar to Ferrar

Supergroup rocks, one of the most widespread rock types along the Transantarctic Mountains, emplaced as dykes in the basement complex and as extensive sills in the Beacon Supergroup sequences. Coarse grained varieties are most widespread in the centre of the sills, while dolerites and finer grained facies are typical of the sills margins (Gunn and Warren, 1962). However, these types of rocks are present also in Saunders-Ruppert-Hobbs Coast of central Marie Byrd Land in West Antarctica, in the form of mafic dykes and small intrusions, relating to the cretaceous rifting phase of the West Antarctic Rift System (Storey et al., 1999; Weaver et al., 1994; Saito et al., 2013); these mafic dykes are predominantly aphyric ophitic dolerites, in some cases containing augite as ferromagnesian phase ± biotite + plagioclase (Storey et al., 1999). Thus an absolute attribution of detrital gabbros and dolerites to Ferrar Group rocks is not unique, although likely, since mineralogically similar, although less extensive, rocks are present in West Antarctica.

Sedimentary clasts, comprising heterogranular, moderately sorted, matrix-rich sub-arkose, sandstones and siltstones, could derive from dismantling of Beacon Supergroup sequences, which are exposed in the inner Transantarctic Mountains. Usually, at least in the region of Southern Victoria Land, less mature lithologic types of Beacon Supergroup (arkoses, arkosic litharenite) are characteristic of the upper Victoria Group, while quartzarenites and sub-arkoses are more typical of the lower Taylor Group (Korsch, 1974; Bernet and Gaupp, 2005; Cornamusini and Talarico, 2016). In one case, a coarse sandstone clast (thin section 29) containing heterogeneous lithic fragments of different lithologies (plutonic, quartzites, low grade metamorphites and carbonates) could be considered as intrabasinal/intraformational clast, so its possible source cannot easily be determined, even if its lithic grains, in particular limestones, account for a source located in the Transantarctic Mountains. Petrographic characteristics of this clast, except for its lack of fossils, are similar to those of the McMurdo Erratics (coarse grained moderately sorted lithic arenite with calcite cement, Levy and Harwood, 2000; Landis, 1974), that are interpreted to be sourced in the Discovery Deep, a 1000 m deep trough located in front of the region of Byrd, Mulock and Skelton Glacier (Stilwell et al., 1997; Paulsen et al., 2011). West Antarctica possible sources for sedimentary clasts are not exposed in Marie Byrd Land, Ruppert and Hobbs Coast; however, sedimentary sequences are believed to exist beneath WAIS in the inner region of the Ford Ranges and Edward VII Pensinsula (Luyendyk et al., 2003); another alternative source rock could be considered unmetamorphosed equivalents of post-Permian units in Edward VII Pensinsula (Pankhurst et al., 1998).

Volcanic clasts are prevalently been found in WRS, thus in the closest region of Ross Sea to the McMurdo Volcanic Group outcrops, mainly located in the volcanic islands and peninsulas in McMurdo Sound (Ross, Black, White Islands, Minna Bluff). Basic and intermediate detrital lithotypes (e.g. thin section 71 and 74) could be confidently related to McMurdo Volcanic Group rocks. Mineral chemistry analyses carried out on thin section 71 revealed presence of brown kaersutite amphibole (Figure 6), that is typical of the intermediate lavas of the Erebus Volcanic Province (Kyle, 1990; LeMasurier and Thomson, 1990). Instead, felsic varieties such rhyolites (i.e. thin sections 78 and 36) are minor component in the Erebus Volcanic Province, forming only some flows at the base of Mount Morning-Mount Discovery volcanic complex (Martin et al., 2010; Wright-Grassham, 1987). Moreover, their mineralogy do not correspond with those of detrital clasts investigated from piston cores. Recrystallized meta-rhyolite with neoblastic biotite and white mica are reported from Skelton Glacier region (Mount Cocks and Northern Teall Island, Skinner, 1982; Cook and Craw, 2002), but also in this case detrital clasts do not have the same mineralogical assemblage and do not show any neoblastic recrystallization. Felsic rhyolitic porphyries are intercalated with metasedimentary rocks in the sequences of the Liv Group in the

Queen Maud Mountains, in particular in the Wyatt, Taylor and Leverett formations (Stump, 1985, 1995; Rowell and Rees, 1989). In West Antarctica, volcanoes located in Marie Byrd Land are rich of felsic varieties such as pantellerite and pantelleritic trachytes rocks, in particular in Ames and Flood Ranges (LeMasurier, 1990; LeMasurier et al., 2011), but their mineralogy is quite different from those of the detrital clasts.

4.5.2 Clast assemblages and ice flow implications

As described in the above paragraphs, the majority of clasts from CRS and WRS are low grade metasediments (meta-siltstones; meta-sandstones; quartzites; phyllites; pelitic schists); mineral paragenesis of most clasts and chemical analysis of white micas reveal a sub-greenschist/greenschist facies assemblage. These conditions are documented from both sides of the Ross Sea Embayment; in the Transantarctic Mountains, low P/T conditions are reported in three major areas: Skelton-Mulock Glaciers area (Cook and Craw, 2002), south side of Byrd Glacier-Beardmore Glaciers area, excluding the higher grade Selborne group (Goodge, 2007, Mirow et al., 2002, Stump et al., 2004) and Queen Maud Mountains (Shackleton-Scott Glacier area, Stump, 1985; Rowell and Rees, 1989). In West Antarctica, Swanson Formation in Marie Byrd Land records low P/T conditions as well (Bradshaw et al., 1983; Pankhurst et al., 1998). For these reasons, not only single lithologies but clasts assemblages from analyzed cores could be important in defining possible source regions. The following broad lithologic associations of clasts from single cores can be proposed:

Assemblage A: it comprises biotite ± hornblende granodiorite to tonalites, associated to mainly fine grained metamorphic rocks such as phyllites, meta-sandstones, biotite ± white mica schists, quartzites. In this assemblage granitoids are minor than metamorphic rocks, while sedimentary clasts are variable, but in some cases they are mainly intrabasinal polymicts in composition. Volcanic rocks are nearly absent.

Assemblage B: it comprises the same lithologies found in Assemblage A but with some diagnostic lithologies of a Transantarctic Mountains provenance, such as limestones and marbles, that are not present in any exposed unit in West Antarctica.

Assemblage C: it comprises biotite granodiorites associated with low grade metamorphic rocks such phyllites, pelitic schists and meta-sandstones, with a considerable amount of basalts and intermediate volcanic rocks, likely associated with McMurdo Volcanic Group volcanoes.

These assemblages are shown in Figure 4.7, with capital letters indicating their geographic distribution. The figure clearly shows that assemblage A is the most widespread and it is present both in CRS and WRS cores. Assemblage B is present in only 3 cores, 2 of them are located in CRS; this is an important evidence, since the position of these two cores could indicate, in the investigated core set, the easternmost influence of TAM-derived ice flows, with diagnostic lithologies that point out to the role of outlet glaciers drainage from the TAM rather than West Antarctic Ice Streams.

In this scenario, the easternmost core (i.e. 93-13) that shows a clast assemblage B is located in the eastern sector of CRS, about 40 km east of 180° longitude. Instead, assemblage C cores are all located in the Central Basin of WRS (Fig. 7), in one case in a distal position in respect of the volcanic islands of McMurdo Sound (i.e. core 32-13). Since these cores are rich in volcanic detritus derived from McMurdo Volcanic Group and their distribution is limited to the Central and Joides Basins, this somehow highlights geographic boundaries on the

distribution of volcanic-bearing flowing ice during LGM. These boundaries are constrained by ice flow reconstructions based on combined sediment provenance data and linear sub-glacial geomorphic features (Shipp et al., 1999; Licht and Palmer, 2013; Anderson et al., 2014). Distribution of volcanic clasts is coherent with a scenario of divergent south-north ice around Ross Bank, as documented by glacial lineations on the sea floor (Shipp et al., 1999): the portion of ice that flowed west of Ross Bank into the Central and Joides Basin must have carried out volcanic detritus after its passage around Ross Island, while the portion flowing east of Ross Bank did not eroded any volcanic source; this is indirectly evidenced by the cores located east of Ross Bank that lack McMurdo Volcanic Group detritus. These observations suggest that McMurdo Volcanic Group rocks have been eroded by grounded ice expanded from the TAM during LGM. This is not surprising, since previous petrological studies carried out on Holocene cores in McMurdo Sound area indicate clearly that glacimarine LGM sequence are dominated by McMurdo Volcanic Group sediments (Barrett et al., 2005; McKay et al., 2008).

In splitting clast assemblages, mafic lithologies such as gabbros and dolerites were not considered; this because they occur in association with all the three assemblages A, B and C. In previous provenance studies mafic components were considered diagnostic in revealing a TAM provenance, because they increased in glacial till detritus from East to West of the Ross Embayment (Licht et al., 2005). Since onshore TAM tills and offshore WRS tills contain a significant component of mafic minerals and lithic grains, possibly eroded from dismantling of Ferrar Group rocks, they were used as lithic tracers for erosion provided by TAM outlet glaciers such as Byrd and Nimrod Glaciers (Licht et al., 2005). In this dataset, gabbro and dolerites are minor lithologies and they do not exhibit a particular increase towards east Antarctic coastline. Their mineralogy can be related to a probable East Antarctic source (e.g. Ferrar Group rocks), but we prefer to not exclude a West Antarctic source, since similar mafic composition and textures are also shown by dykes along the Ford ranges in Marie Byrd Land (Storey et al., 1999; Weaver et al., 1994; Saito et al., 2013). Moreover some, although rare, mafic lithologies have been found also in Eastern Ross Sea LGM tills as described in Chapter III of this thesis (Perotti et al., 2017), so it is demonstrated that they are not lithologies cropping out uniquely along the TAM front, even if their extension in East Antarctica is much more relevant.

The overall data collected and the preliminary provenance inferences could be discussed considering LGM glaciological models and previous provenance studies in CRS and WRS tills. As a whole, clasts assemblage A indicates a possible source region defined by a low P/T meta-sedimentary terrane, locally intruded by plutons, which caused also local thermal metamorphism (biotite or actinolite hornfels). This geological setting is present in Marie Byrd Land, where Swanson Formation has been intruded by Ford Granodiorite during Devonian-Carboniferous time and by Byrd Coast Granite during Cretaceous time. However, this setting is present in different locations in the TAM front as well, for example in the Skelton-Mulock glacier area (Cook and Craw, 2002; Cottle and Cooper, 2006a), or in the Central TAM south of Byrd Glacier discontinuity, where silicoclastics sequences of the Byrd Group were intruded by Granite Harbour Intrusives (Stump, 1995; Goodge et al., 2002). Thus, assemblage A alone is not sufficient to discriminate a clear provenance from TAM front or from West Antarctica.

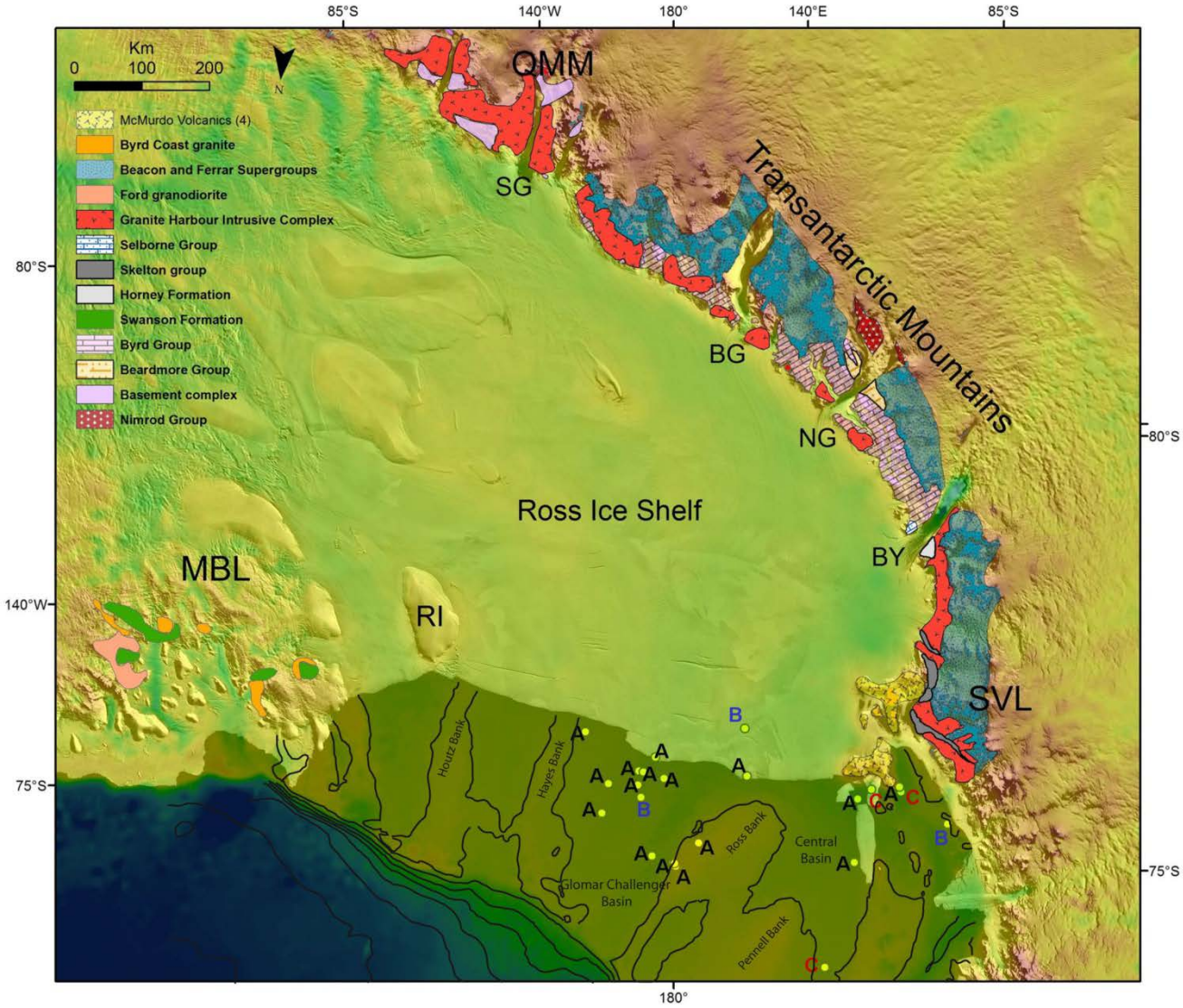

Figure 4.7. Clasts assemblage distribution in CRS and WRS. A,B and C are lithologic associations described in the text. Abbreviation as in Figure 4.1.

Nevertheless, the association with assemblage B in CRS could account for a mutual provenance from the same region in East Antarctica, that has to be considered not as a limited area but as an extensive region comprising outlet glaciers distributed for hundreds of kilometers along the TAM front. In this sense, one possible source region is represented by the Central TAM sector from the Byrd to the Beardmore Glacier. Previous provenance studies have demonstrated that ice fed by Byrd Glacier during the LGM has its easternmost extension over site 27-14 in CRS (Licht and Palmer, 2013), that is one of the same cores studied in this work. East of this site in CRS, geochronologic and petrographic data suggest a mixing process between ice fed by Byrd Glacier and that fed by Nimrod Glacier, the latter becoming more relevant to the east (Licht et al., 2005; Licht and Palmer, 2013; Farmer and Licht, 2016).

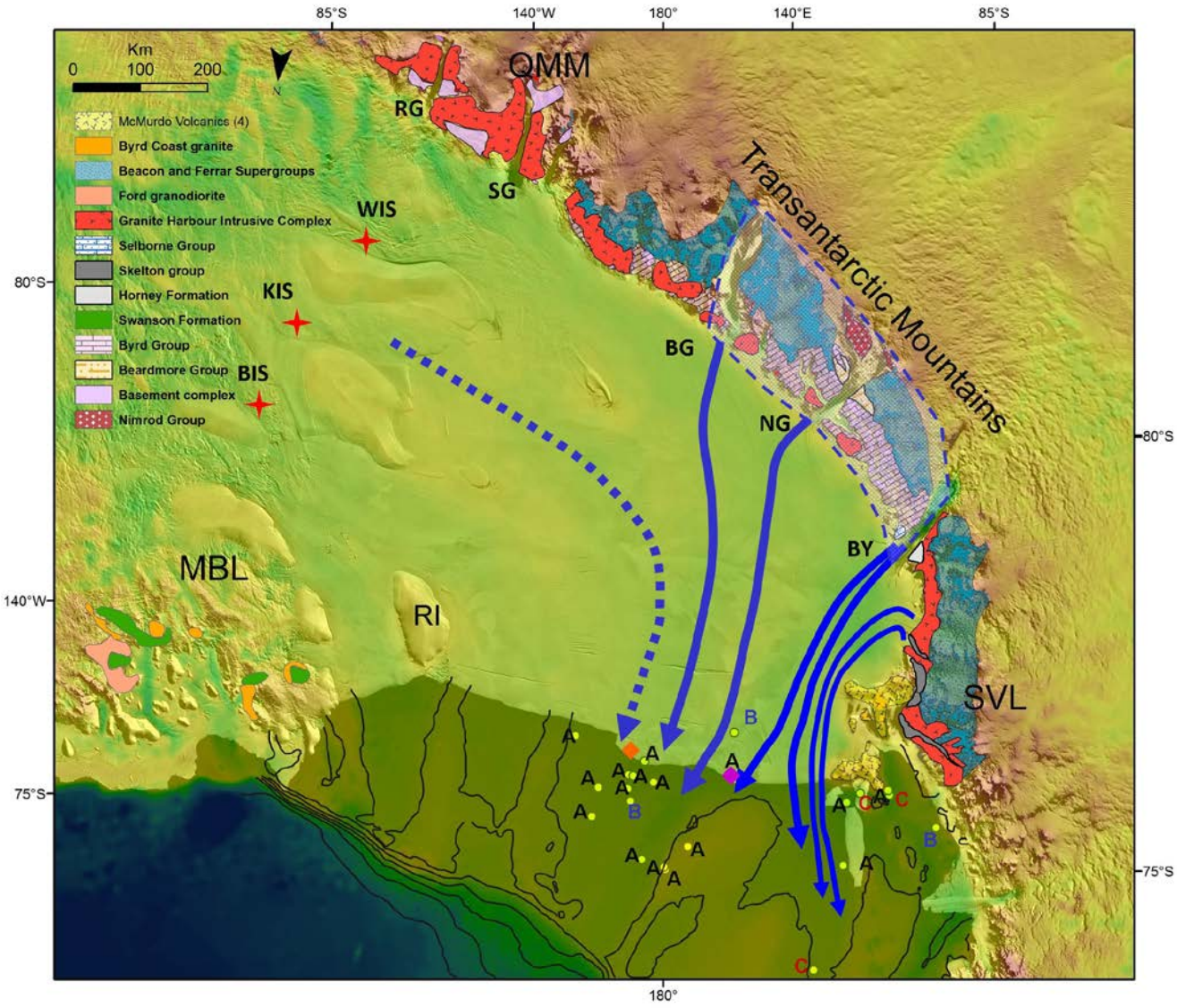

Figure 4.8. Possible LGM ice flow lines related to clast assemblages distribution in CRS and WRS. Possible source region for CRS core sites is highlighted with a dashed area. Also Ice Streams till sites from Licht et al. (2005) are shown. Purple diamond is ELT27-14 site, that is the easternmost site involved in expansion of Byrd Glacier ice during the LGM in the model of Licht and Palmer (2013). Orange diamond is the westernmost site that yielded a ZrnUPb population of age around 100 Ma, interpreted to be a diagnostic feature of West Antarctica provenance (Licht et al., 2014). Abbreviations: BG: Beardmore Glacier; BIS: Bindschadler Ice Stream; BY: Byrd Glacier; KIS: Kamb Ice Stream; MBL: Marie Byrd Land; NG: Nimrod Glacier; QMM: Queen Maud Mountains; RI: Roosevelt Island; RG: Reedy Glacier; SG: Scott Glacier; SVL: Southern Victoria Land; WIS: Whillans Ice Stream.

Moreover, East Antarctic outlet glaciers ice is constrained west of 94-39 site, which is located in the eastern portion of CRS. The latter shows a detrital U-Pb zircon age population of ~100 Ma (Licht et al., 2014), interpreted to be a typical West Antarctic age population (the age of intrusion of Byrd Coast Granite in Marie Byrd Land), present in some of the West Antarctic Ice Stream tills (BIS, Licht et al., 2014). Clast assemblage association A and B are located a little bit easternmost than site 94-39 of Licht et al. (2014), the easternmost

core site of assemblage B from this study being the 93-13 site. Assuming these two sites as reliable constraints of ice discharged from Byrd Glacier and from West Antarctic Ice Streams, distribution of association of assemblage A and B between them points out to a provenance area that involve at least the Nimrod and Beardmore Glaciers catchments. This is coherent with clasts dataset, with limestones and marbles that could be sourced from Byrd Group carbonate sequences (e.g. Shackleton Limestone), low grade metasediments sourced from the Beardmore Group formations or the outboard Byrd Group siliciclastic sequences, sedimentary extrabasinal clasts sourced from Beacon Supergroup rocks, and dolerites sourced from Ferrar Supergroup rocks. Absence of volcaniclastic and abundant silicic meta-porphyries associated to low grade sedimentary clasts suggests that Queen Maud Mountains terrane is a minor source area, since the majority of the basement rocks in QMM are interbedded volcanic and silicoclastics rocks of the Liv Group (Stump, 1985; Rowell and Rees, 1989). However, a contribution from outlet glaciers of QMM (e.g. Scott and Reedy Glaciers) to the LGM Central Ross Sea sediments could not be excluded a priori, since some rhyolitic porphyries could suggest a dismantling of silicic volcanic sequence such those occurring in the QMM. This hypothesis, although suggested for the eastern region of CRS by glaciological models of Golledge et al. (2012 and 2013), has not been so far confirmed by provenance analysis models (Licht et al., 2005; 2014) and still remains debatable.

It is noteworthy that clasts assemblages represent lithologies cropping out progressively from the downstream regions of main outlet glaciers (outboard formations) to the sequences farther inland at the head of the glaciers (Beacon and Ferrar rocks). This is in accordance with the geochronological findings of Licht and Palmer (2013) that Ross Sea tills are a mixture of Ross-Pan African age populations reflecting input from downstream glacier regions and also from glacier trunk areas, giving importance to erosion along single outlet glaciers profile.

Figure 4.8 shows possible configuration of LGM ice flows from Transantarctic Mountains taking into account data from previous provenance studies (Licht et al., 2005; Licht et al., 2014; Licht and Palmer, 2013), geomorphological evidences (Shipp et al., 1999) and available LGM glaciological models for the Ross Sea region (Denton and Hughes, 2002; Golledge et al., 2012 and 2013). This configuration evidences the major source area for CRS cores in the region between south side of Byrd Glacier to at least the Beardmore Glacier, highlighting the role of the latter and the Nimrod Glacier in discharging ice during glacial maximum. In WRS, clasts dataset reflects the importance of McMurdo Volcanic Group detritus associated to low grade metasediments: this points out to an important flux of ice discharged by Mulock and Skelton glaciers rather than Byrd Glacier, able to erode McMurdo Volcanic Rocks and to leave their detritus over distal positions in the Joides Basin (i.e. site 32-13). Metasediments found in WRS cores are petrographically similar to those found in ANDRILL sites and interpreted to be sourced in Skelton Mulock-Glacier region (Talarico et al., 2010; Sandroni and Talarico, 2011). Moreover, any clast association has been found in analyzed cores revealing higher pressure conditions and medium/high grade metamorphic regime, which is localized in Britannia Range, between Darwin and Byrd Glacier (Carosi et al., 2007). However, since it has been demonstrated that ice discharged by Darwin and Byrd Glaciers has an important draining role in WRS during glacial maxima (Talarico and Sandroni, 2011, Licht and Palmer, 2013, McKay et al., 2016), it is possible that WRS analyzed cores reflect a mixed contribution from both Skelton-Mulock glacier area and Darwin-Byrd Glacier region, since some holocene sites ~60 km east of Ross Island have yielded detrital clasts from Darwin and Byrd Glacier region (McKay et al., 2016). The model of Talarico et al. (2010), in which eroded source areas for the Plio-Pleistocene period in AND-1B drillcore have been identified in the Skelton-Mulock Glacier area for glacial maxima (related to diamictite sequences) is

consistent also for LGM data from this study. Diamictite intervals of Mid-Late Pleistocene age in AND-1B show high amount of Skelton-Mulock Glacier derived clasts supplied from basement and Ferrar-Beacon supergroup rocks. Changes in paleogeography occurred after emergence of volcanic centres in the region may have determined a splitting of ice sourced from Skelton-Mulock area during LGM time; one portion of volcanic-rich ice may have crossed Ross Island and deposited IRD farther north, while other flows may have entered in McMurdo Sound northwestern of Minna Bluff over AND-1B site.

4.6 Conclusions

A provenance study has been carried out on LGM and post-LGM glacimarine sediments in the Central and Western Ross Sea area. Petrological investigations on the gravel sized clasts from 23 piston core yielded at least three major clasts assemblages: the most widespread assemblage is composed mainly of intrusive rocks and low grade metasedimentary rocks, with minor sedimentary units. This assemblage could account for a source area located both from the Transantarctic Mountains and from West Antarctica (Marie Byrd Land area). The second clast assemblage contains rocks exclusively located along the central Transantarctic Mountains such as marbles and limestones and its distribution in the central portion of the Glomar Challenger Basin suggests a contribution of ice during the LGM from the region located south of the Byrd Glacier, with a significant contribution of the Nimrod and Beardmore Glacier. The third clast assemblage contains volcanic detritus belonging to the McMurdo Volcanic Group rocks and its distribution is limited to the Western Ross Sea sector, in association with low grade metasedimentary rocks. This implies that an important role of ice drainage in WRS has been played during LGM by the Skelton and Mulock Glaciers, which may have carried out detrital low-grade clasts of the Skelton Group and successively may have eroded islands and peninsulas of the McMurdo Sound coast. However, in WRS a mixed contribution of Skelton-Mulock and Byrd-Darwin Glaciers is more likely, with ice discharged from the latter being constrained east of Ross Island towards the Ross Bank and in the western-central Ross Sea.

Chapter V.
Provenance of Ross Sea Drift in McMurdo Sound (Antarctica) and implications for LGM glacial transport: new evidences from petrographic data

5.1 Chapter Overview

This chapter shows a provenance study carried out on late Quaternary glacial unconsolidated samples belonging to the Ross Sea Drift and cropping out in McMurdo Sound coast. A petrographic approach has been applied to the glacial erratic clasts constituting the sediments in order to reveal provenance of different lithologies. The chapter is a paper that is in preparation and has the body of a journal paper.

5.2 Paper

Matteo Perotti[1], Luca Zurli[1], Sonia Sandroni[2], Gianluca Cornamusini[1,3] and Franco Talarico[1]

[1] University of Siena, Department of Physical Sciences, Earth and Environment, Strada Laterina 8, 53100 Siena, Italy

[2] National Museum of Antarctica, University of Siena, Italy

[3] Centre of Geotechnologies, University of Siena, San Giovanni Valdarno, Italy

5.3 Abstract

Provenance of Quaternary to LGM Ross Sea Drift deposits from McMurdo Sound region has been investigated by means of petrographic techniques. A total amount of 19 bulk till samples from four different areas was analyzed for three different granulometric fraction: pebble to cobble, granule and coarse to very coarse sand grain size. Deposits were classified following the lithological composition of clasts and occurrence of different petrographic groups was evaluated for each sample. Clasts composition predominantly reflect source rocks cropping out in the region between Mackay and Koettlitz Glacier, with McMurdo Volcanic Group rocks being the most represented lithologies in the Royal Society Range (RSR) foothills, while Granite Harbour Intrusive Complex rocks are more widespread in Taylor and Wright Valleys. Lithological distribution of collected samples supports a distal provenance due to a grounded Ross Ice Sheet in Taylor Valley, while specific distribution of volcanic lithologies in RSR foothills accounts for a northward ice flow from Koettlitz Glacier catchment, thus supporting previous glaciological models of an expanded lobe during LGM. In addition, Late Quaternary Trilogy Drift composition from Wright Valley accounts for a local provenance, thus allowing the hypothesis of a thickened Wilson Piedmont Glacier rather than a grounded Ross Ice Sheet during past ice advances.

5.4.Introduction

The Antarctic Ice Sheet is a fundamental feature to study ice dynamics and climate influence, as it contains the majority of fresh water reservoir on the Earth. Understanding its behavior and its dynamics during past glacial cycles is crucial to study global sea level issues. A key area is represented by the Ross Sea Embayment, as it drains about one third of ice masses both from West and East Antarctica. During the Last Glacial Maximum (LGM), the Ross Sea was occupied by an advancing grounded ice sheet. Its extension and timing of expansion and retreat has been deeply studied and constrained with several marine and terrestrial geological and geophysical investigations (Anderson et al., 2014 and reference therein). The Ross Sea Ice Sheet was fed in part by fast-moving Ice Streams located in West Antarctica, and in part by the contribution of outlet glaciers along the Transantarctic Mountains front (Licht et al., 2005; Hall et al., 2013). After it retreated, it left glacial deposits in the form of sheet drifts and moraines along the glaciated coasts of the Ross Embayment. These deposits have been used to study maximum ice extension and thickness during the LGM, and they also have been used to produce numerical models for the reconstruction of the LGM Antarctic Ice Sheet and its drainage pattern (Golledge et al., 2012, 2013; Anderson et al., 2014).

In this sense, a primary region is represented by McMurdo Sound, where the geological evidences of the last advance of a grounded Ross Sea Ice Sheet are testified by the presence of extensive glacial sediments along the coast and in the flanks of the Transantarctic Mountains, called the Ross Sea Drift (Stuiver et al., 1981; Denton and Marchant, 2000; Denton and Hughes, 2000; Hall and Denton, 2000; Cox et al., 2012; Hall et al., 2013). The geomorphology, chronology and erratic distributions of these glacial sediments have been extensively investigated (Denton and Hughes, 2000, Denton and Marchant, 2000; Hall and Denton, 2005; Hall et al., 2013; Anderson et al., 2014). However, ice flows reconstruction in McMurdo Sound during the LGM is a question that is still debatable, since different models have been proposed so far (Stuiver et al., 1981, Denton and Hughes, 2000; Wilson, 2000; Greenwood et al., 2012; Anderson et al., 2017).

In this paper, we applied a petrographic approach in studying LGM glacial sediments. Petrographic analysis has been widely used in Antarctica as a provenance tool, both from medium sand sized detrital sediments and from gravel-sized clasts analysis. Point counting methods have been used to discriminate provenance of LGM sediments in the Ross Embayment (Licht et al., 2005), while gravel sized clasts analysis has been successfully used to identify glacially eroded source areas and to reconstruct ice drainage pattern during past glacial cycles (Talarico et al., 2010). In this work, different granulometric fractions composing the Ross Sea Drift collected in different regions from McMurdo Sound coast have been studied in order to establish their lithological and mineralogical composition. Petrographic analysis of the sampled clasts allowed us to discriminate different lithologic distributions among the analyzed samples and to identify eroded source areas in the region, thus providing new data on the existing reconstructions of LGM ice flow drainage pattern in McMurdo Sound.

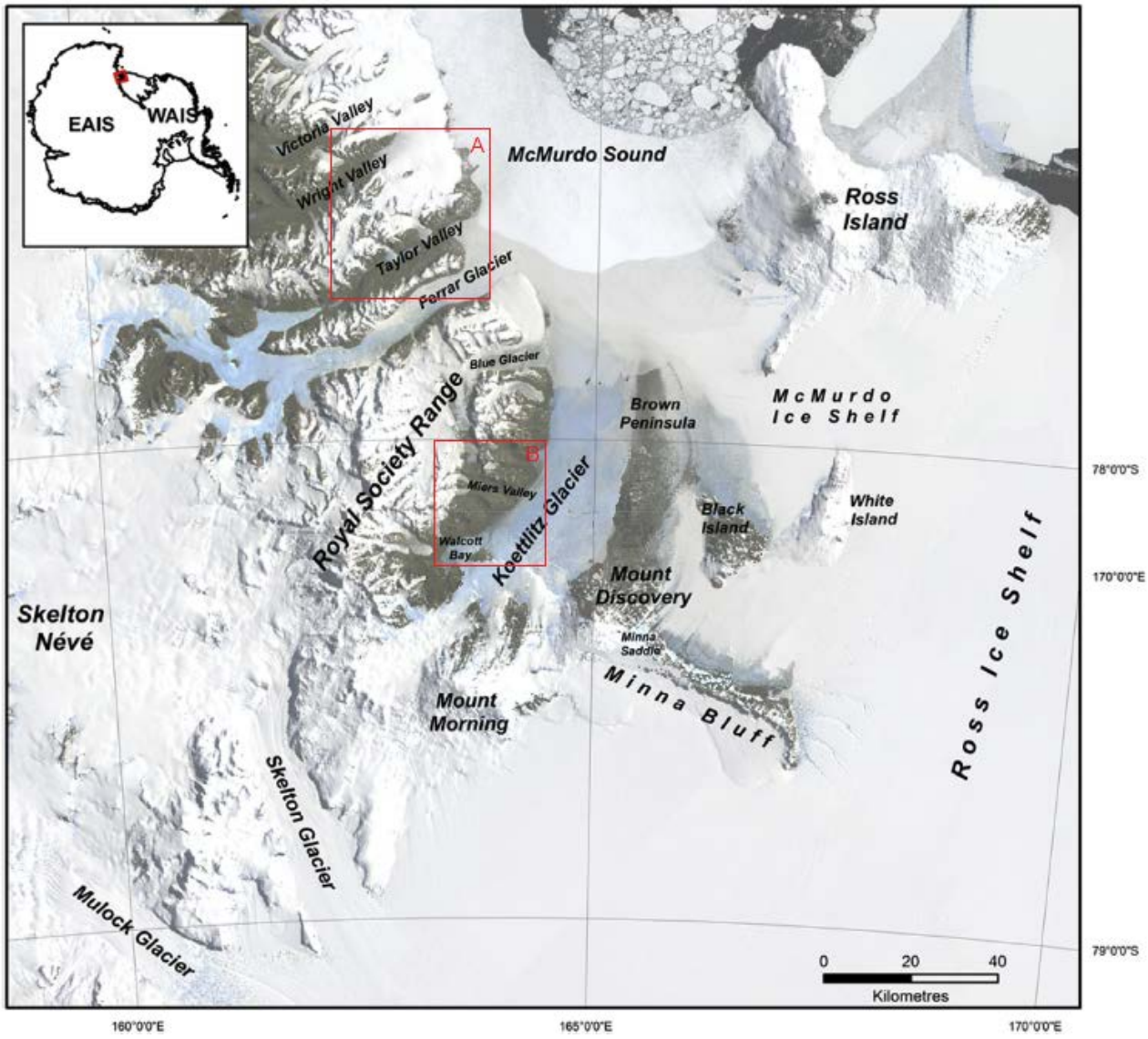

Figure 5.1. Overview of the southern Victoria Land in Antarctica. The red boxes refer to the sampling areas (the same are enlarged in figure 2 and 3. A: Wright and Taylor Valley; B: foothills of the Royal Society Range. Modified after Anderson et al. (2017).

5.5 Geological setting

5.5.1 Geology of the study area

The investigated area of this study extends between Wright Valley to the north of McMurdo Sound and Royal Society Range foothills to the south. This region is extensively characterized by Cenozoic volcanic centres (Mount Morning-Mount Discovery complex to the south, Brown Peninsula, Minna Bluff, Black Island and White Island to the east, Ross Island to the north, Figure 5.1). These features influenced the development of McMurdo Ice Shelf that is an extension of the Ross Ice Shelf, and during past glacial cycles, constrained the behavior of a grounded Ross Ice Sheet in the region (e.g. Denton and Hughes, 2000; Naish et al., 2009; McKay et al., 2012).

Volcanic centres belong to the alkalic Erebus Volcanic Province of the more extended McMurdo Volcanic Group (Kyle, 1990), and their activity is divided into an earlier phase (18.7- to 11.4 Ma,

Martin et al., 2010) of mainly trachytic rocks, and a more voluminous second phase (last 10 Ma), mainly characterized by basanitic to phonolitic rocks.

The western side of McMurdo Sound is topographically dominated by the South Victoria Land (SVL) sector of the Transantarctic Mountains. Basement rocks of the SVL include the cambro-ordovician granitoids of the Granite Harbour Intrusive Complex (Gunn and Warren, 1962; Smillie, 1992; Cox et al., 2012). These are heterogeneous undeformed and foliated plutons cropping out extensively in the Dry Valleys area (Allibone et al. 1993a; Cox et al., 2012), including biotite±hornblende granites, granodiorites, tonalites, quartz monzo-diorites and diorites. The most extended pluton of the Dry Valleys area is the Bonney Pluton, a northwest trending foliated pluton which extends for a length of 53 km from the Ferrar Glacier to the Olympus Range (Allibone et al., 1993a; Cox et al., 2012). Minor lamprophyric, felsic and mafic plugs and dykes also constitute multiple intrusions in the Granite Harbour Intrusive Complex (Allibone et al., 1993a,b; Cox et al., 2012). The latter intruded a Late-Proterozoic-Cambrian metamorphic basement composed of upper-amphibolite to upper greenschist facies rocks of the Skelton Group, in the past referred as the Koettlitz Group (Findlay et al., 1984; Cook and Craw, 2001; Cox et al., 2012). In general, regional metamorphism of the Skelton Group is of low P/high T conditions (Allibone, 1992). The main lithologies belonging to the Skelton Group exposed in the region north of the Koettlitz Glacier are pure and impure marbles, calc-silicates rocks, paragneisses, amphibolites and amphibolitic schists (Findlay et al., 1984), comprising three different formations (Marshall Formation, Salmon Marble Formation and Hobbs Formation). Biotite± hornblende orthogneisses are intercalated with metasediments of the Skelton Group and are interpreted as the deformed precursor of the younger plutons (Cox and Allibone, 1991). To the southwest of Mount Discovery volcanic centre, Skelton Group rocks in the Skelton and Mulock Glacier area include mainly lower greenschist to lower amphibolite facies metasediments, consisting of metalimestones, marbles, quartzites, metaconglomerates and metasandstones (Skinner, 1982; Cook and Craw, 2002; Cook, 2007). Moreover, some minor alkaline quartz-syenites and granites crop out in the same region, in particular in Teall Island and in the Mulock Glacier area (Cottle and Cooper, 2006; Carosi et al., 2007).

Emplacement of plutons of the Granite Harbour Intrusive Complex was followed by an uplift and erosion stage, with the development of a regional erosion surface (Kukri Peneplain) and the deposition during Devonian to Triassic time of sub-horizontal strata of sandstones, conglomerates, siltstones and minor coal measures of the Beacon Supergroup (Harrington, 1965; Barrett, 1981), which is subdivided into a lower quartzose unit (Taylor Group) and an upper carbonaceous unit (Victoria Group). Beacon Supergroup rocks are restricted to inland exposures at about 25-40 km from the coastline of McMurdo Sound (Cox et al., 2012). During Jurassic time, both basement rocks and Beacon Supergroup units were involved in the emplacement of dolerite sills and dykes of the Ferrar Supergroup and its extrusive component, the Kirkpatrick Basalt, in response of the initiation of the West Antarctic Rift (Kyle et al., 1981).

5.5.2 Late Quaternary geomorphological setting and ice-flows reconstruction

Southern McMurdo Sound region was interested during the Late Quaternary by more than one episodes of flowing grounded ice (the Ross Sea Ice Sheet), mainly supplied by outlet glaciers of the Transantarctic Mountains. This ice flowed over the volcanic islands and peninsulas of the region and penetrated into the Dry Valleys (Stuiver et al., 1981; Denton and Hughes, 2000; Denton and Marchant, 2000; Hall and Denton, 2000). Once retreated, this expanded Ice Sheet left glacial sediments in the form of moraines and drift sheets all along the flanks of the South Victoria Land mountains, valleys and foothills fronting McMurdo Sound. These deposits are generally known as the Ross Sea Drift (Denton and Marchant, 2000; Hall and Denton, 2000; Cox et al., 2012). In their geological map of Southern Victoria Land, Cox et al. (2012) mapped distinct deposits of the Ross Sea Drift, the youngest is named Ross Sea I Drift and is dated between 26 and 6 ka (Cox et al., 2012; Anderson et al., 2017). The distribution of erratics belonging to Ross Sea I Drift and the morphology of moraines were adopted by Stuiver et al. (1981), Denton and Marchant, (2000) and Denton and Hughes (2000) to reconstruct LGM surface elevation of the Ross Sea Ice Sheet and paleo-ice flows in the region (Figure 5.2a). However, ice-flow lines reconstruction during the Last Glacial Maximum is a question that is still debatable. Stuiver et al. (1981) and Denton and Hughes (2000) argued that part of LGM grounded ice of the Ross Sea Ice Sheet flowed westward and southwestward in the direction of the Victoria Land coast, bypassing Ross Island. This grounded ice dammed the mouth of the Dry Valleys across the McMurdo Sound coast flowing from the northern tip of Ross Island southward to Miers Valley in the Royal Society Range foothills. Meantime, other southern ice flowlines reached McMurdo Sound crossing the region between Minna Bluff and Ross Island. The geologic basis for this model are mainly the moraines slope across the Sound and the presence of anorthoclase-phyric phonolite erratics on the flanks of the Royal Society Range and in the Dry Valleys (Denton and Marchant, 2000): since the only known outcrop of anorthoclase-phyric phonolite (in the past referred as kenyte, Cox et al., 2012) is in the western coast of Ross Island, only a southward direction of ice flow could transport this type of rock in the sites where they have been recovered.

Two alternative hypothesis for LGM ice flows reconstruction have been proposed by indipendent types of methodologies: the first was proposed by Greenwood et al. (2012) and was based on multibeam bathymetric data of the seafloor of McMurdo Sound. Based on the presence of glacial lineations and grounding zone wedges, these authors proposed an initial ice flow northward between Brown Peninsula and Black Island, and subsequently a shift from northward to westward, around Ross Island towards Victoria Land coast (Figure 5.2c). The second reconstruction, proposed by Wilson (2000), comprises three grounded glacial lobes in southern McMurdo Sound and it has been suggested on the basis of geomorphological evidences and erratics distribution. In this reconstruction, a Koettlitz Glacier lobe flowed northward and coalesced with a Minna Bluff northwest lobe and northward Ross Ice Shelf lobe that covered White Island and flowed north of Black Island. Recently, an implemented interpretation of this reconstruction, based on new chronology and sediment provenance data, led to a two-stage scenario for LGM and post-LGM setting (Anderson et al., 2017): the first stage occurred prior the Last Glacial Termination, that is interpreted by Hall et al. (2015) to be occurred between 18.7 and 12.2 ka (Figure 5.2b).

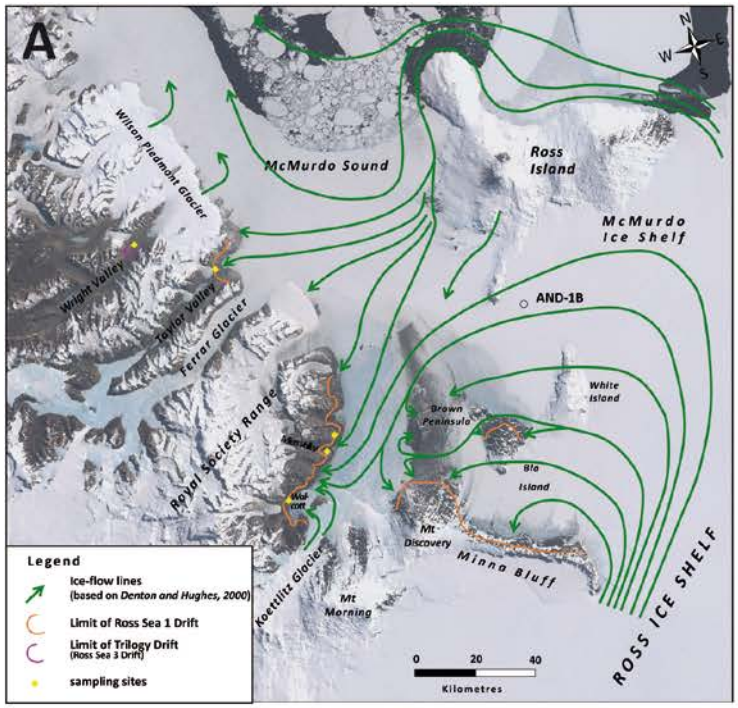

Figure 5.2. LGM ice-flows reconstruction in the region of McMurdo Sound, based on geomorphological, chronological, geophysical and erratics provenance data. Also sampling sites locations from this study are shown, together with extension of Ross Sea Drift deposits as described in Cox et al. (2012). A) Model from Denton and Hughes (2000), based on moraine slope and distribution of anorthoclase-phyric erratics across the region. B) Two stages model of Anderson et al. (2017), based on chronology, glacial mapping and erratics provenance. C) two stages model of Greenwood et al. (2012), based on geophysical reconstruction of geomorphic features on the seafloor of McMurdo Sound.

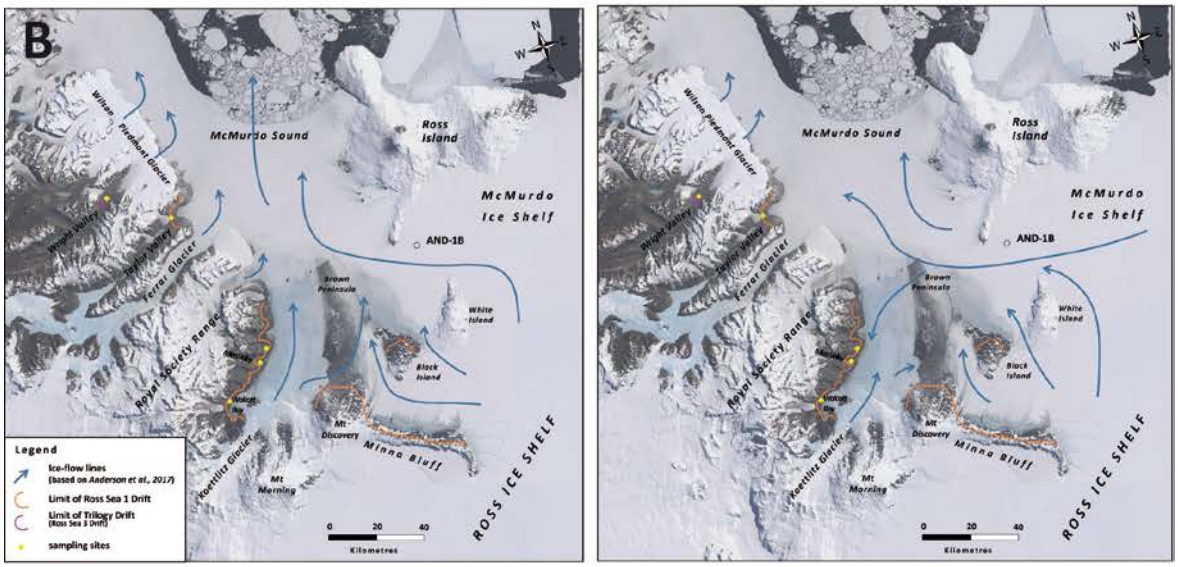

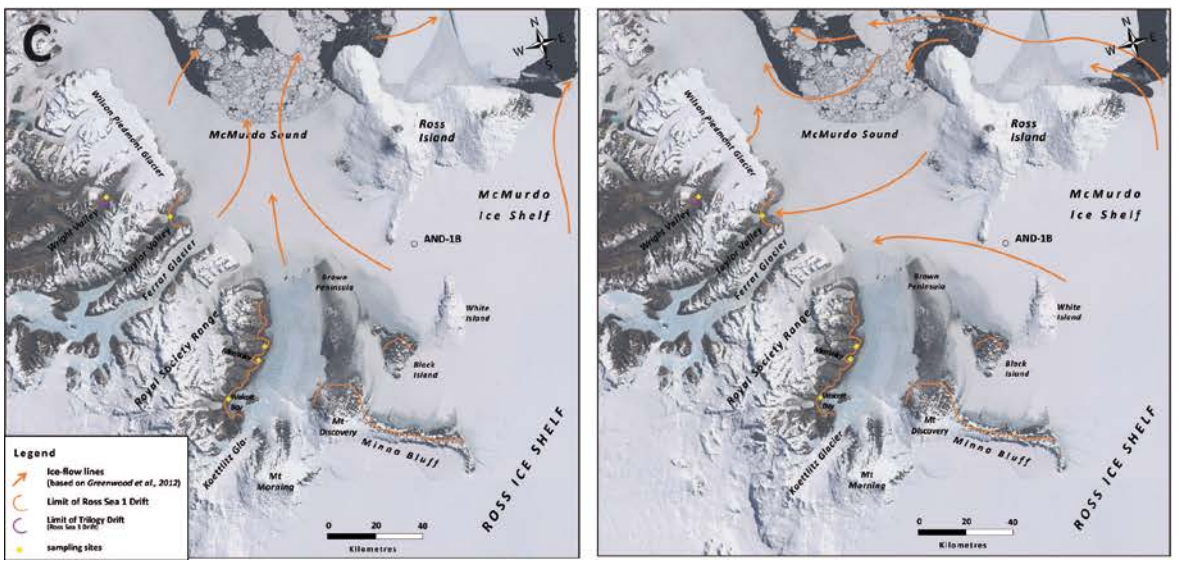

Table 5.1. List of analyzed samples. Abbreviations follow the legend of geologic map from Cox et al. (2012): ur3-Ross Sea 3 Drift; ur1-Ross Sea 1 Drift; uk1-Ross Sea 1 Drift lacustrine facies. Ages are from Denton and Marchant (2000) and Hall and Denton (2005). Samples are shown labelled elsewhere in the text.

Area	Sample	Label	Latitude	Longitude	Deposit	Age
Lower Wright Valley	20-01-2015 P1	20-P1	-77.441	162.534	ur3 (Trilogy)	early-middle Quaternary
Lower Wright Valley	20-01-2015 P2	20-P2	-77.441	162.534	ur3 (Trilogy)	early-middle Quaternary
Lower Wright Valley	20-01-2015 P3	20-P3	-77.441	162.536	ur3 (Trilogy)	early-middle Quaternary
Lower Wright Valley	20-01-2015 P4	20-P4	-77.441	162.536	ur3 (Trilogy)	early-middle Quaternary
Lower Taylor Valley	20-01-2015 P10A	20-P10A	-77.562	163.400	ur1	LGM
Lower Taylor Valley	22-01-2015 P14	22-P14	-77.564	163.425	ur1	LGM
Lower Taylor Valley	22-01-2015 P15	22-P15	-77.564	163.425	ur1	LGM
Lower Taylor Valley	22-01-2015 P16	22-P16	-77.564	163.425	ur1	LGM
Lower Taylor Valley	23-01-2015 P1	23-P1	-77.589	163.371	uk1	LGM
Lower Taylor Valley	23-01-2015 P2	23-P2	-77.589	163.371	uk1	LGM
Lower Taylor Valley	23-01-2015 P3	23-P3	-77.589	163.361	uk1	LGM
Lower Taylor Valley	23-01-2015 P4	23-P4	-77.589	163.361	uk1	LGM
Lower Taylor Valley	23-01-2015 P5	23-P5	-77.589	163.361	uk1	LGM
Lower Taylor Valley	23-01-2015 P6	23-P6	-77.589	163.361	uk1	LGM
Marshall Valley	21-01-2015 P19	21-P19	-78.067	164.315	ur1	LGM
Marshall Valley	21-01-2015 P21	21-P21	-78.067	164.315	ur1	LGM
Miers Valley	21-01-2015 P16	21-P16	-78.111	164.124	ur1	LGM
Walcott Bay (Howchin Glacier)	21-01-2015 P14	21-P14	-78.216	163.492	ur1	LGM
Walcott Bay (Howchin Glacier)	21-01-2015 P15A	21-P15A	-78.216	163.492	ur1	LGM

This stage reflects the reconstruction of Wilson (2000), with mainly a northward and northwest flow fed by Ross Sea grounded ice and an expanded Koettlitz Glacier ice. The second stage, occurring between ~18.7 ka and the major retreat of grounded ice in the Sound (~10-11 Ka), is characterized by the reduction of the Koettlitz Glacier lobe that led to the intrusion of westward and northward ice fed by the Ross Sea Ice Sheet into McMurdo Sound (Anderson et al., 2017).

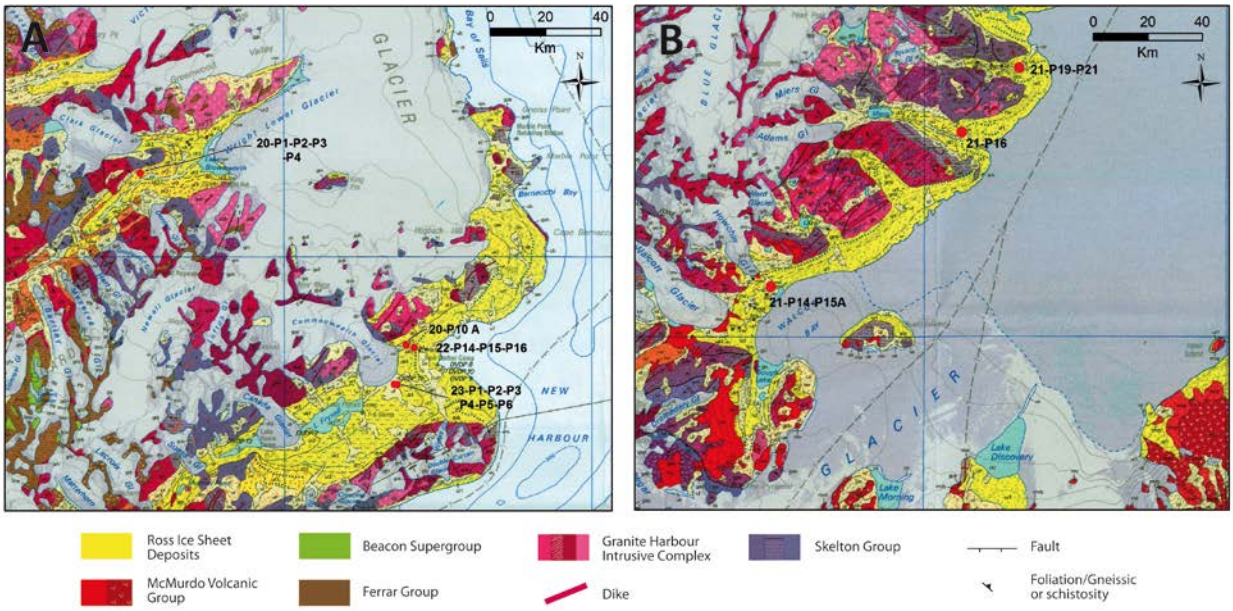

Figure 5.3. Geological map of the areas from the two boxes (A and B) shown in Figure 5.1, with sampling sites location and simplified legend. Maps from Cox et al. (2012).

5.6 Materials and Methods

A total amount of 19 samples was collected in the Dry Valleys region in a coastal area comprised between the Wright Valley and the foothills located in front of the Royal Society Range (Figures 5.3 and Table 5.1). As a whole, four main sampling area can be identified: Wright Valley, Taylor Valley, Royal Society Range foothills (Marshall and Miers Valleys), Howchin Glacier/Walcott Bay (Figure 5.3). In each sampling site at least one surficial and one 15-20 cm depth bulk till sample was taken. Target samples are bulk loose till sediments of the Ross Sea Drift. Specifically, samples from Taylor, Miers, Marshall Valleys and Walcott Bay deposits were taken from the continuous drift sheet that covers the eastern slopes and coastal valleys south from Marble Point, occurring also as extensive deposits on Brown Peninsula, Black Island, Minna Bluff and on Ross and White Islands (Stuiver et al., 1981). This is called Ross Sea 1 Drift (Ur1) in the geologic map of Cox et al. (2012), and it is composed of unweathered to slightly weathered loose till, waterlaid diamicton, glaciolacustrine silt, stratified sand, with interbedded silt, sand and gravel (Stuiver et al., 1981; Hall et al., 2000; Cox et al., 2012). Locally, Ross Sea 1 Drift is defined by lacustrine facies (Uk 1, Cox et al., 2012). Chronology of this deposit that testifies a grounded ice sheet in McMurdo Sound is described in Denton and Marchant (2000): the last grounding event occurred in the region at circa 27 ka, with the permanence of the ice sheet during the LGM and the lowering during mid-to late Holocene. Instead, samples from Wright Valley were taken from an older deposit, specifically the Trilogy Drift, that is a sandy diamicton with stained and ventifacted clasts, defined by 1-3 m high moraines mainly located in the north side wall of the Wright Valley (Hall and Denton, 2005; Figure 5.4). An age of early-middle Quaternary has been proposed for this deposit, on the basis of stratigraphic position in respect of the overlying Brownworth Drift, which has been dated with ^{14}C at more than 49000 years BP (data from an overlying lacustrian algal deposit, Hall and Denton,

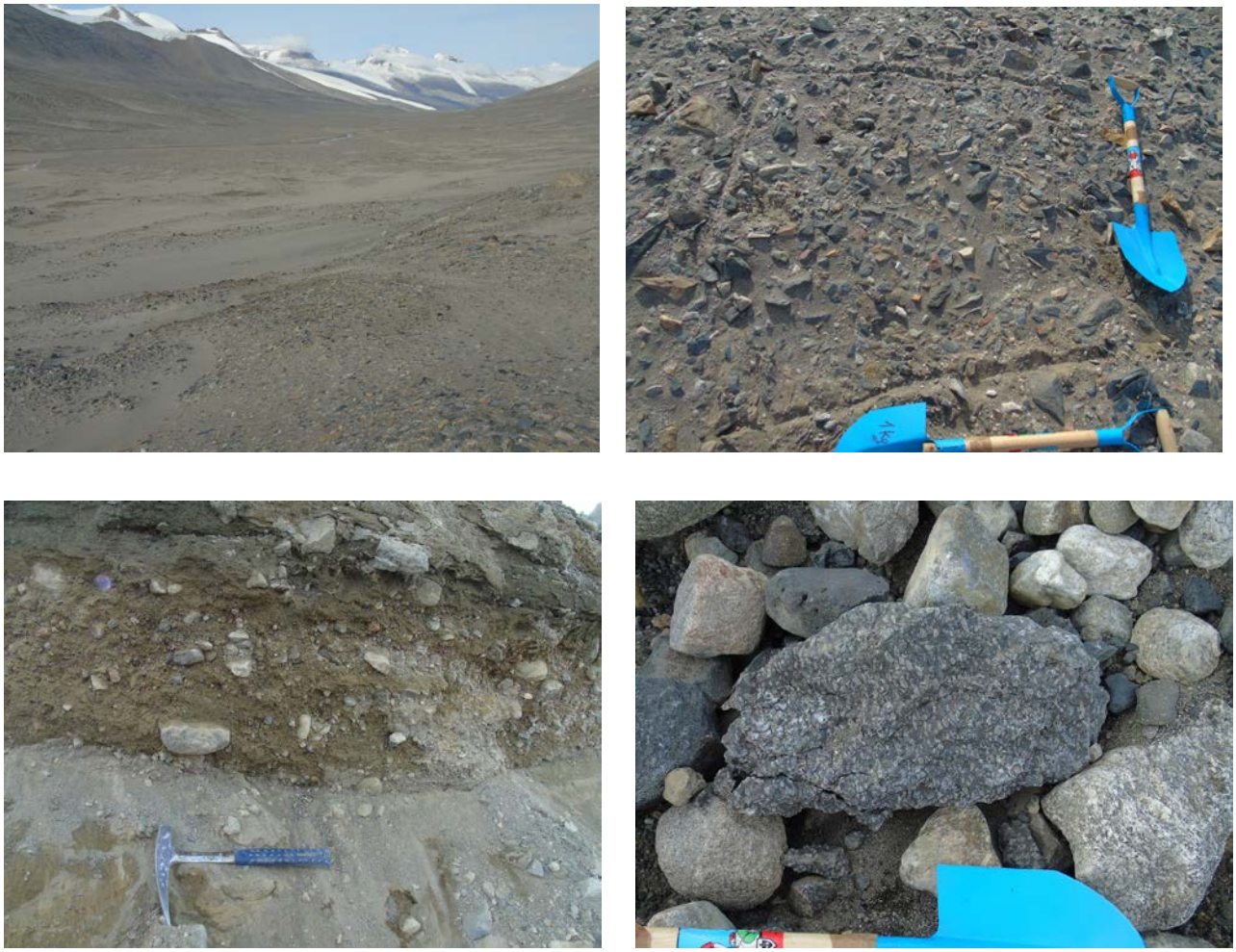

Figure 5.4. a) Lateral moraines of the Trilogy Drift on the north wall of the lower Wright Valley. B) detail of the sampled surface with scattered clasts of different lithologies. c) Diamicton facies of Ross Sea 1 Drift from Marshall Valley incised stream. d) Cobbles of granitoids and plagioclase-phyric intermediate volcanites from the same site. Hammer is about 30 cm long, while shovel is 1 meter long.

2005). This drift belongs to the Ross Sea 3 Drift deposit in the geologic map of Cox et al. (2012). Table 5.1 shows the exact locations of samples.

Bulk till samples were dried and sieved in order to obtain different granulometric fraction for each sample. For specific petrographic analysis the fraction >4 mm was analyzed macroscopically and some thin sections were made for representative pebble to cobble-sized clasts. Broad lithological groups were made for macroscopic analysis, and each clast was classified and counted for each sample. Moreover the granulometric fractions between 4 to 2 mm (granule-sized) and 2mm-425 µm (very coarse to coarse sand-sized) were impregnated with epoxy and made into thin sections following the standard preparation, taking care about putting as much grains as possible in the thin section plane.

For the granulometric fraction 4-2 mm, microscopic petrographic analysis was aimed to identify the main lithological features of single lithic grains and to quantify them by counting each lithic fragments for each thin section. Volcanic lithic fragments were classified on the basis of the mineral assemblages recognised in thin section, following the classifications adopted by Pompilio et al. (2007) and Panter et al. (2008) for clasts recovered in Andrill cores (AND1B and AND2A,

Table 5.2. Classification used for lithic fragments identification in 2mm-425 µm samples petrographic analysis. The same classification was used by Licht et al. (2005).

	Petrographic features
Sedimentary	
Silt/sand	distinct sand and/or silt size grains ± finer matrix minerals
Mudstone	Contain silt and clay sized particles difficult to examine exact composition
Claystone	No discernable grain boundaries
Intrusive igneous fragments	Large crystals with interlocking boundaries
Felsic	qtz+k-spar±pla, bt, hbl, ms
Intermediate	qtz+>50% pl+minor K-spar±hbl, bt, cpx
Mafic	>50% pl + orto/clinopx ±olv, iron oxide
Extrusive igneous fragments	±larger crystals with matrix of smaller elongate angular crystals
Basalt±andesite±ryolite	fine grained matrix±zoned and/or polysyntetic twinned pl±volcanic glass±abundant opm± cpx
Metamorphic lithics	
Quartzite	intergrowth of quartz crystals
Marble	twinned calcite
Schist	grains exhibit fabric

respectively). Thus volcanic lithologies were grouped in three different composition: i) basaltic (occurrence of phenocrysts of clinopyroxenes (Mg-rich), olivine and plagioclase); ii) intermediate (phenocrysts of plagioclase ± kaersutitic amphiboles ± clinopyroxene); iii) felsic (phenocrysts of K-feldspar ± kaersutite ± sodic clinopyroxene (aegirine-augite)).

Instead for the 2mm-425 µm thin sections the Indiana Point Counting (Suttner, 1974; Suttner et al., 1981) was carried out. With this method, at least 300 counts for each sample were made, identifying both single minerals and lithic fragments petrography. The lithic fragments classification used for point counts was the same described by Licht et al. (2005) for bulk till sediments analysis and it is shown in Table 5.2. Note that not every sample reached 300 counts because of the limited number of grains present in some thin sections. (see Table 5.4).

Chemical analysis of some mineral phases identified throughout petrographic microscope were carried out with an X-ray energy dispersive system EDAX DX4 attached to a Scansion Electron Microscope Philips XL30 at the Department of Physical Sciences, Earth and Environment of Siena (Italy). Selected thin sections have been polished and carbon coated before carrying out measurements. Analytical conditions were 20 kV of accelerating voltage, 25 µA of emission current, and a beam spot size of 0.2 Am. Natural minerals were used as standards. Fe^{3+} concentration in clinoamphiboles and clinopyroxenes was estimated by the equation of Droop (1987), assuming charge balance.

5.7 Results

5.7.1 Wright Valley

Samples collected in Wright Valley are 20-P1, 20-P2, 20-P3 and 20-P4. Compositionally, these 4 samples yielded a quite homogeneous lithological distribution. Macroscopic analysis carried out for the gravel size fraction is shown in Table 5.3. The samples from Wright Valley exhibit a predominant clasts composition defined by granitoids, variably distributed from medium to fine grained, isotropic to foliated biotite-leucogranite to monzogranite, to intermediate compositions (granodiorite to quartz-diorite). Some rock fragments exhibit a porphyritic texture with coarse grained k-feldspar phenocrysts. A discrete amount of fine grained isotropic mafic intrusives rocks is also present (microdiorite, dolerite, gabbro). Minor role is played by schistose rock fragments and basaltic volcanic rocks. Microscopically, rock fragments distribution of the granulometric fraction 4mm-2mm is shown in figure 5.5. Samples from Wright Valley exhibit a whole composition dominated by felsic and intermediate granitoids, isotropic or foliated, characterized by biotite or biotite-hornblende monzogranite to quartz-diorite in composition (modal mineralogy was only semiquantitatively determined because of the too small size of lithic clasts). Lithic association is completed by minor occurrence of dolerite, mafic intrusives rocks, such as diorite, gabbro, and a series of metamorphic rock clasts (mainly ca-silicates, amphibolites and orthogneisses). Dolerites exhibit fine grained isotropic intergranular to sub-ophitic texture, while diorites show an hypidiomorphic biotite-clinoamphibole-plagioclase texture. Metamorphic rocks are generally foliated heterogranular fine to medium grained biotite ± clinoamphibole schists and gneisses with granolepidoblastic texture, while granofels lithic fragments commonly exhibit fine grained plagioclase-quartz-clinopyroxene±clinoamphibole granoblastic texture. Very rare volcanic lithic fragments are present.

Point counting analysis yielded results summarized in table 5.4 and ternary diagrams in figure 5.6. In the latter it is evident from Quartz-Feldspar-Lithics (QFL) diagram that lithic fragments are the main constituents of the 2mm-425 μm fraction samples, with minor quartz and feldspars; comparing Wright Valley samples with those from other sampled areas in the QFL diagram (Figure 5.6a), the former have a slight increase in quartz and feldspars than the latter. Anyway, the greatest difference is shown in L_m-L_{g+m}-L_v diagram (Fig. 5.6b), with Wright valley samples yielding a larger proportion of granitoid and metamorphic lithic fragments and a minor proportion of volcanic lithic fragments, in comparison with other samples. This difference is also clear in the 4-2 mm fraction analysis (Fig. 5.5).

Furthermore, taking in consideration only single minerals grain counts (Table 5.4), Wright Valley samples are mainly characterized by a combination of quartz, pyroxenes and feldspars, with minor amounts of opaques minerals and amphiboles (up to 2% of the total counts).

5.7.2 Taylor Valley

Some of the samples from Taylor Valley (23-P1; 23-P2; 23-P3; 23-P4; 23-P5; 23-P6) were taken from tills at the bottom of the valley, southeast of the Commonwealth Glacier, from the glaciolacustrine facies of the Ross Sea 1 Drift (Figure 5.4); while some others (22-P14; 22-P15; 22-

P16; 20-P10A) were sampled from the section incised by the Commonwealth Stream east of the same glacier. Macroscopically, these samples have a quite homogeneous gravel-sized clasts composition; the only exception is sample 20-01-15 P10A, which yielded an anomalously high proportion of volcano-clastic sand-sized lithic fragments (about 70% of the total). The other samples show a lithological composition defined mainly by felsic granitoids (medium to fine grained, isotropic to slightly foliated pink to brownish leuco-granites to monzogranites), intermediate granitoids (fine to medium grained variably foliated granodiorite to quartz-diorite), foliated biotite-orthogneisses and a variable amount of aphanitic, sometimes vescicular, basaltic clasts (from 4% to ~25% of the total amount). Moreover, a variable amount of dolerite was found, ranging in percentage from ~1% to 16% of the total, with the only exception of the volcanoclastic lithics-dominated sample. A minor amount of olocrystalline very fine grained texture microdiorite was also present, up to ~10% of the total in one sample, and below 10% in the other samples. Other lithologies are represented in negligible amount from these samples.
Figure 5 shows the lithic fragments distribution for the 4mm-2mm granulometric fraction from Taylor Valley samples. With the only exception of sample 20-01-10 P10A, the other samples show a major granitoid (both felsic and biotite-hornblende intermediate composition) occurrence, together with a variably rich percentage of mafic rocks (dolerite, fine grained gabbro, biotite-hornblende diorite) and metamorphic lithologies (prevalently biotite-orthogneisses with minor amount of ca-silicates, amphibolites and marbles). Moreover each samples has a consistent component of volcanic lithic fragments, composed mainly by porphyritic microcrystalline to vitrophyric basalt with ubiquitous clinopyroxene micro-phenocrysts and widespread olivine micro-phenocrysts; isotropic ipocrystalline textures are common but also pylotaxitic and trachytic textures are frequent. Groundmasses are characterized by the presence of plagioclase, clinopyroxenes and opaques minerals. In some cases (e.g. some clasts from samples 23-P5 and 23-P6) also kaersutitic brown amphibole was recognized as micro-phenocrysts, set in a groundmass of plagioclase, opaque minerals and sometimes blackish to brownish glass.

5.7.3 Marshall and Miers Valley

Samples from Marshall Valley (21-P19; 21-P21) were taken from the main section incised by the stream along the central axis of the valley. They consist of loose till diamicton facies of the Ross Sea 1 Drift of Cox et al. (2012). Among the cobble and boulder sized clasts of the drift, foliated granitoids, aphiric basalts and plagioclase-phyric intermediate volcanites were recognized in the field (Fig. 5.3). Miers Valley sample (21-P16) was taken from a basalt-rich outcrop of evaporitic glaciolacustrine facies along the section of the main stream of the valley.
Macroscopically, gravel and cobble sized composition of these samples define a major role played by volcanic lithic fragments, in one case constituting up to ~80% (sample 21-P16, Table 5.3); granitoids are the second most representative lithologies with predominant isotropic to variably foliated felsic varieties (e.g samples 21-P19 and 21-P21). Metamorphic rocks are in minor occurrence, with few bt-schists and orthogneisses, while sedimentary rocks are completely absent (Table 5.3).

Table 5.3. Lithological composition of clasts from >4 mm granulometric fraction. Values are in percentage related to the total number of recovered clasts. Classification based on macroscopic appearance.

AREA	Sample ID	Medium to fine grained isotropic to slightly foliated leucogranite	Medium to fine grained, isotropic to slighlty foliated monzogranite to monzonite	Micro-granitoid	Intermediate granitoid (medium to fine grained granodiorite to qtz-diorite)	Dolerite/ microgabbro	Micro-diorite	Foliated granitoid/ Orthogneiss	Schist	Basalt	Basic or intermediate porphyry and lamprophyre	Quartzite	Sandstone	Silt	Loose sediments	Volcano-clastics	ND	TOT
Wright Valley	20-P1	7.9	24.9	6.6	28.7	4.4	17.7	0.0	7.3	0.0	2.5	0.0	0.0	0.0	0.0	0.0	0.0	317
	20-P2	31.6	19.6	0.0	5.6	3.2	4.8	17.2	14.4	0.0	1.2	0.0	0.0	0.0	0.0	0.0	2.4	250
	20_P3	23.3	21.4	0.0	19.8	7.3	19.8	2.7	0.0	5.0	0.8	0.0	0.0	0.0	0.0	0.0	0.0	262
	20-P4	17.2	17.2	0.0	27.6	0.0	17.2	0.0	6.9	10.3	3.4	0.0	0.0	0.0	0.0	0.0	0.0	29
Taylor Valley	20-P10A	7.3	3.0	0.0	4.3	0.0	4.6	0.3	0.0	4.6	0.0	0.0	0.3	3.6	0.3	69.9	1.7	302
	22-P14	13.3	29.1	3.9	15.1	9.5	4.9	1.4	0.0	20.7	0.4	0.0	0.0	0.0	0.0	1.8	0.0	285
	22-P15	30.4	12.0	0.0	10.5	13.6	11.0	0.5	0.0	20.4	0.0	0.0	0.0	1.0	0.0	0.0	0.5	191
	22-P16	24.7	23.5	0.0	12.7	13.9	5.4	0.6	0.0	18.1	0.0	1.2	0.0	0.0	0.0	0.0	0.0	166
	23-P1	16.7	11.3	3.0	16.1	12.1	2.0	7.7	0.0	24.8	3.0	0.0	0.0	0.0	0.0	1.4	2.0	504
	23-P2	36.5	4.7	1.2	14.1	11.8	10.6	1.2	0.0	12.9	7.1	0.0	0.0	0.0	0.0	0.0	0.0	85
	23-P3	13.9	5.2	1.7	11.3	13.9	0.0	0.9	0.0	16.5	1.7	0.0	0.0	0.0	0.0	0.0	34.8	115
	23-P4	32.0	6.7	8.0	8.0	13.3	8.0	0.0	0.0	20.0	4.0	0.0	0.0	0.0	0.0	0.0	0.0	75
	23-P5	19.2	26.0	1.4	13.7	1.4	0.0	0.0	0.0	17.8	2.7	0.0	0.0	0.0	0.0	6.8	11.0	73
	23-P6	7.9	13.5	0.0	20.2	16.9	3.4	18.0	1.1	15.7	2.2	0.0	0.0	0.0	0.0	0.0	1.1	89
Marshall Valley	21-P19	18.5	23.1	0.0	6.8	4.0	4.0	2.2	0.0	32.0	0.6	0.0	0.0	0.0	0.0	0.3	5.8	325
	21-P21	15.8	11.1	7.1	5.1	2.0	0.0	2.8	0.0	53.8	0.4	0.0	0.0	0.0	0.0	0.0	1.6	253
Miers Valley	21-P16	3.8	0.0	0.0	0.0	0.0	0.0	0.0	1.9	90.6	0.0	0.0	0.0	0.0	0.0	0.0	0.0	53
Walcott Bay	21-P14	12.5	18.7	4.5	5.3	0.0	4.6	1.0	1.5	46.2	0.2	0.0	0.0	0.0	0.0	0.0	4.8	582
	21-P15A	0.0	23.3	1.9	0.0	0.0	0.0	0.0	0.6	58.5	0.0	0.0	0.0	0.0	0.0	2.5	13.2	159

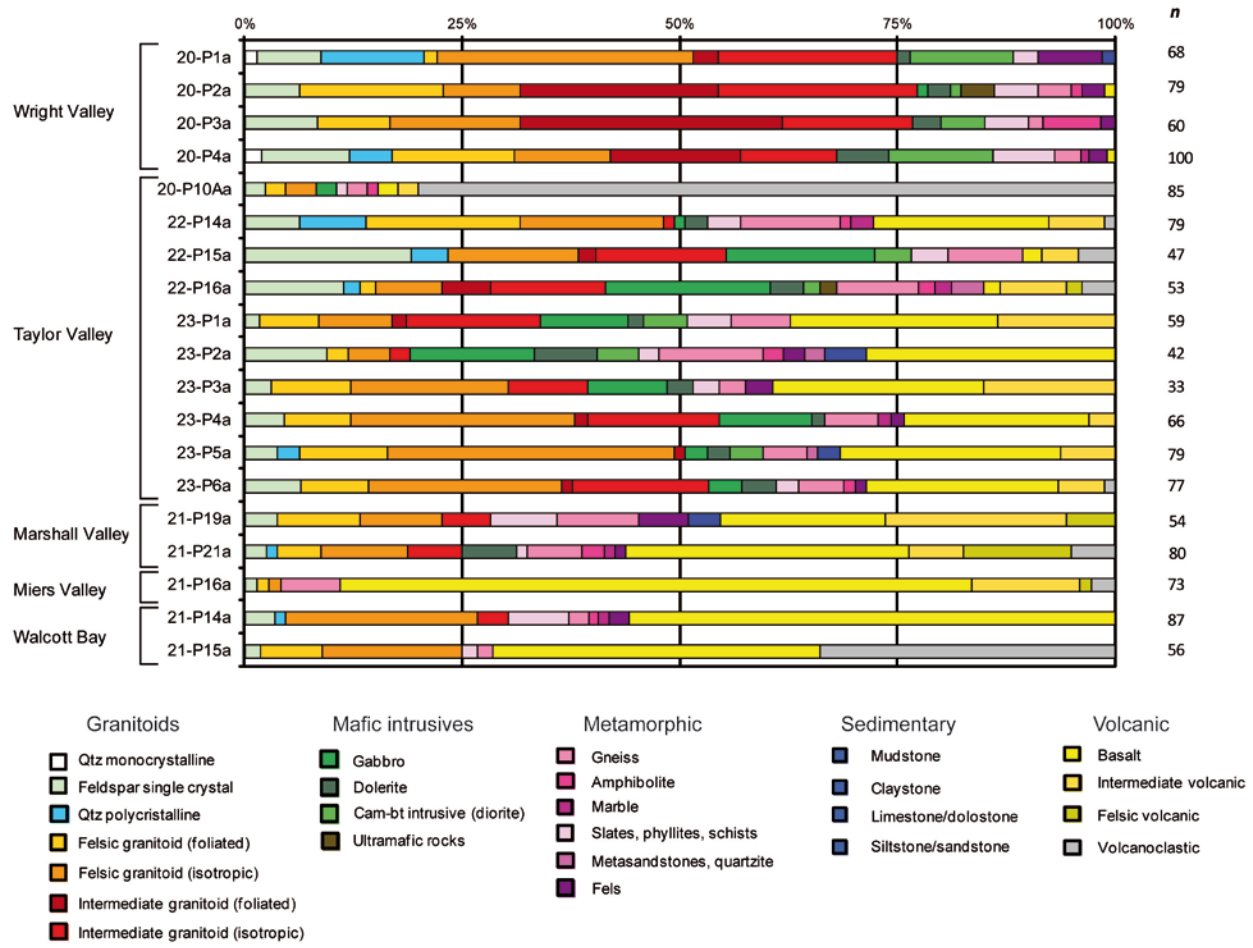

Figure 5.5. Relative distribution of lithologies in 4mm-2mm fraction petrographic analysis. n: total number of analyzed clasts.

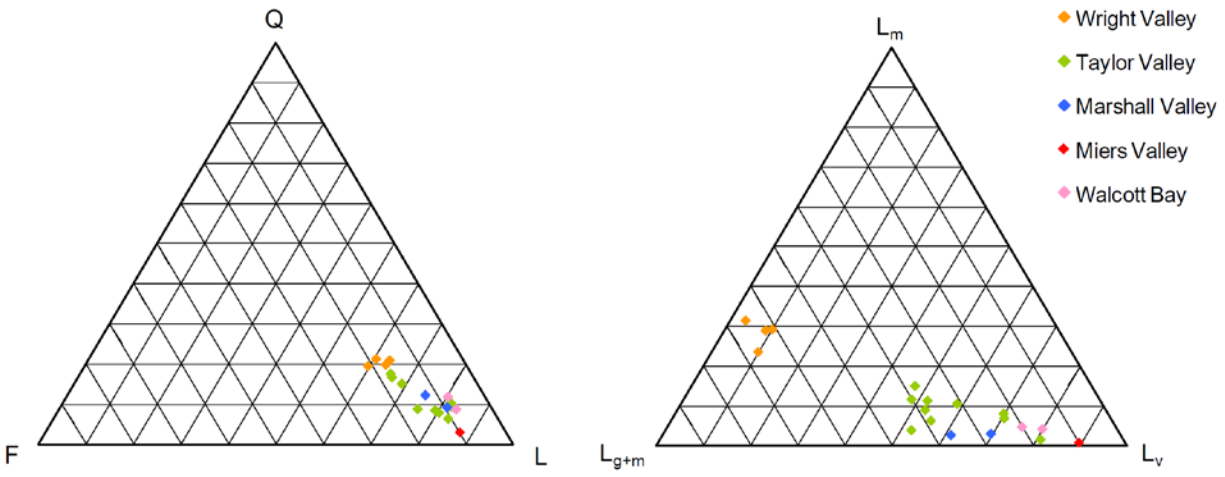

Figure 5.6. QFL diagram and L_m-L_{g+m}-L_v diagram for 2mm-425 µm point counting petrographic analysis. Lm= mafic intrusive lithic fragments; Lg+m= granitoids and metamorphic lithic fragments; Lv= volcanic lithic fragments. Data are normalized to 100.

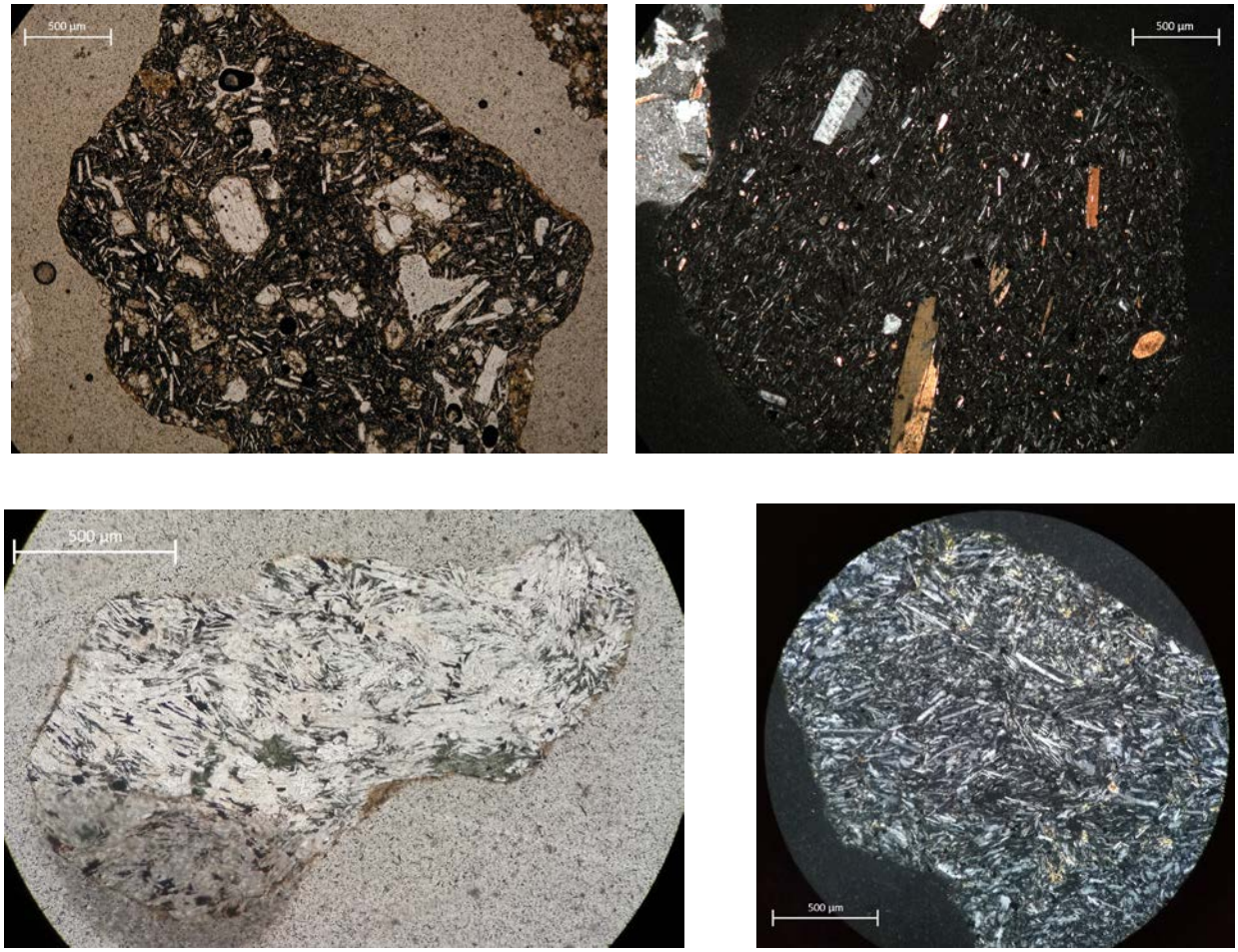

Figure 5.7. Representative photomicrographs of volcanic clasts recovered in Ross Sea Drift samples. A) microporphyritic clinopyroxene-olivine ipocrystalline basaltic clasts (PPL, Walcott Bay sample); B) microporphyritic sanidine-plagioclase-brown amphibole intermediate clast (XPL, Marshall Valley sample) C) olocrystalline trachytic feldspars-green clinopyroxenes felsic clast (PPL, Marshall Valley sample); D) same lithology as C (XPL, Marshall Valley sample).

Lithic fragments petrographic analysis of the 4-2 mm granulometric fraction yielded the results showed in Figure 5. Volcanic lithic fragments are the most represented, with a prevalence of fine grained microporphyritic ipocrystalline to olocrystalline basaltic rocks. Colourless to light brown clinopyroxene is the most widespread phenocryst species, often associated to microporphyritic olivine. Groundmasses are prevalently ipocrystalline with plagioclases, opaque minerals and clinopyroxenes associated to a brownish to yellowish glass. In these samples, also a variable percentage of felsic volcanic rocks is present, in particular in samples from Marshall Valley: these clasts show a olocrystalline trachytic texture with aligned laths of plagioclase and alkaline-feldspar associated to intergranular green clinopyroxenes, opaque minerals and in some cases brown kaersutitic amphiboles. Hypidiomorphic isotropic to slightly foliated granitoid rock fragments are present in a lesser extent. Metamorphic lithic fragments are prevalently fine grained clinopyroxene-quartz-plagioclase ± amphiboles granofels with granoblastic texture, granolepidoblastic biotite schists and gneisses and rare marbles. In one case (21-P19 from Marshall Valley) two clasts of medium grained sandstone were recognized.

Table 5.4. Point counting data from 425 µm-2 mm petrographic analysis. Mineral abbreviations: Qtz=Quartz; Px=Pyroxene; Kfs=K-feldspar; Pl=Plagioclase; Cam=amphibole; Cal=Calcite; Olv=Olivine; Wm=white mica; Bt=Biotite; Chl=Chlorite; Crd=Cordierite; Grt=Garnet; Opm=opaque mineral. Other abbreviations: Silt/Sand=Siltstone/Sandstone; Mudst=mudstone; Lmst=limestone; Pyrocl.=pyroclastic; Extr.=extrusive; Interm.=intermediate; Metam.=metamorphic. Data are shown in percentage on the basis of total counts *n*.

		Single minerals														Lithic fragments										
Area	ID	Qtz	Px	Kfs	Pl	Cam	Cal	Olv	Iron Ore	Wm	Bt	Chl	Crd	Grt	Opm	Other/ Altered	Silt/ Sand	Mudst	Clayst	Lmst	Pyrocl.	Extr.	Mafic	Interm.	Felsic	Metam	*n*
Wright Valley	20-01-15 P1b	15.3	19.3	5.3	7.7	2.3	0.0	0.7	0.0	0.0	0.0	0.3	0.0	0.0	0.7	0.3	0.3	0.0	0.0	0.0	0.0	4.7	14.0	10.3	10.3	8.3	300
Wright Valley	20-01-15 P2b	15.6	19.4	7.3	9.2	1.0	0.0	0.3	0.0	0.0	0.0	0.0	0.0	0.0	0.0	1.3	0.6	0.3	0.0	0.0	0.0	3.8	13.1	10.5	8.9	8.6	314
Wright Valley	20-01-15 P3b	15.6	27.0	5.2	8.1	0.0	0.0	0.0	0.0	0.0	0.0	0.0	0.0	0.0	0.0	0.7	0.0	0.0	0.0	0.0	0.0	1.3	13.7	12.1	10.1	6.2	307
Wright Valley	20-01-15 P4b	16.4	19.3	4.6	7.5	1.3	0.0	0.0	0.0	0.0	0.3	0.7	0.0	0.0	0.7	2.6	2.3	0.0	0.0	0.0	0.0	4.3	10.5	11.8	9.5	8.2	305
Taylor Valley	20-01-15 P10Ab	9.8	5.7	1.9	5.7	0.0	0.3	0.6	0.0	0.0	0.0	0.3	0.0	0.0	0.0	0.6	0.0	0.0	0.0	0.0	22.4	38.2	1.3	1.9	9.5	1.9	317
Taylor Valley	22-01-15 P14b	14.3	10.5	3.5	11.1	0.3	0.6	3.2	0.0	0.0	0.0	0.0	0.0	0.0	0.6	1.3	0.0	0.0	0.0	0.3	1.0	28.9	3.5	6.0	9.5	5.4	315
Taylor Valley	22-01-15 P15b	13.9	6.8	4.2	10.3	0.0	0.0	1.3	0.0	0.0	0.3	0.0	0.0	0.0	1.0	4.8	0.3	0.0	0.0	0.0	3.5	30.0	6.1	10.0	5.2	2.6	310
Taylor Valley	22-01-15 P16b	8.0	6.7	6.7	7.3	0.3	0.0	2.5	0.0	0.0	0.0	0.0	0.0	0.0	1.6	4.8	0.0	0.0	0.0	0.0	0.3	29.6	7.3	11.8	6.7	6.4	314
Taylor Valley	23-01-15 P1b	7.7	6.8	4.2	6.8	0.0	0.0	1.9	0.0	0.0	0.0	0.0	0.0	0.0	1.6	2.6	1.0	0.6	0.0	0.0	0.0	46.5	5.5	4.5	5.5	4.8	310
Taylor Valley	23-01-15 P2b	9.6	4.8	2.6	4.8	0.0	0.0	1.0	0.0	0.0	0.0	0.3	0.0	0.0	1.0	1.3	0.3	0.6	0.0	0.0	0.0	38.6	6.8	5.5	14.8	8.0	311
Taylor Valley	23-01-15 P3b	9.0	4.7	1.2	6.7	0.0	0.0	0.8	0.0	0.0	0.0	0.0	0.0	0.0	0.4	2.7	1.6	0.4	0.0	0.0	0.0	51.0	5.1	3.1	8.6	4.7	255
Taylor Valley	23-01-15 P4b	5.9	6.6	3.3	6.2	0.0	0.3	1.6	0.0	0.0	0.0	0.3	0.0	0.0	1.0	2.6	0.3	0.3	0.0	0.0	0.0	33.8	10.8	7.2	11.8	7.9	305
Taylor Valley	23-01-15 P5b	7.3	6.3	3.0	7.6	0.7	0.0	0.7	0.0	0.0	0.0	0.0	0.0	0.0	2.0	3.6	2.0	0.0	0.0	0.3	0.0	34.4	7.6	4.6	14.2	5.6	302
Taylor Valley	23-01-15 P6b	17.0	2.0	7.2	9.2	0.0	1.0	0.0	0.0	0.0	0.0	0.0	0.3	0.0	0.7	4.6	0.7	0.3	0.0	0.3	0.0	29.5	2.3	5.9	10.2	8.9	305
Marshall Valley	21-01-15 P19b	8.4	7.4	2.9	5.5	0.3	0.6	1.0	0.0	0.0	0.0	0.0	0.0	0.0	1.3	1.0	0.3	0.0	0.0	0.0	2.9	46.6	2.3	2.3	9.3	8.0	311
Marshall Valley	21-01-15 P21b	11.3	2.7	3.4	7.9	0.3	1.2	2.7	0.0	0.0	0.0	0.0	0.0	0.0	2.1	2.4	0.3	0.3	0.0	0.3	0.0	39.6	1.8	4.3	11.9	7.3	328
Miers Valley	21-01-15 P16b	2.9	2.9	3.2	6.1	0.0	0.3	0.3	0.0	0.0	0.0	0.0	0.0	0.0	0.0	1.6	0.0	0.0	0.0	0.0	3.2	70.6	0.6	1.0	2.6	4.5	309
Walcott Bay	21-01-15 P14b	10.0	8.2	4.7	1.9	0.0	1.3	6.0	0.0	0.0	0.0	0.0	0.0	0.0	0.9	1.6	0.6	0.0	0.0	0.6	0.0	48.3	3.1	1.6	6.3	5.0	319
Walcott Bay	21-01-15 P15Ab	7.3	16.1	3.9	2.4	0.5	0.0	1.0	0.0	0.0	0.0	0.0	0.0	0.0	0.0	1.5	0.0	0.0	0.0	0.0	18.5	35.1	2.9	0.0	6.3	4.4	205

Also with point counting analysis of finer granulometric fraction (2mm-425µm) the results show a prevalent volcanic lithic fragments composition, with Miers Valley sample composed almost exclusively by volcanic clasts (Fig. 6).

5.7.4 Walcott Bay

Two clast-rich loose diamicton samples were taken from Walcott Bay area, along the Howchin Glacier stream (21-P14; 21-P15). Diamicton belongs to Ross Sea 1 Drift of Cox et al. (2012). Macroscopically, gravel and cobble sized clast are composed prevalently of basaltic rocks, up to 50% of the total, followed by felsic leucocratic granitic rocks and intermediate granodioritic to qtz-dioritic variably foliated rocks (Table 3).

Microscopic analysis carried out on the 4-2 mm granulometric fraction yielded a lithologic distribution defined mainly by basaltic lithic fragments; these are characterized by a micro-porphyritic ipocrystalline to vitrophyric texture, with micro-phenocrysts of clinopyroxene and olivine set in a groundmass composed of plagioclases, clinopyroxenes, opaque minerals and, when present, a black -brownish to yellowish glass. Volcanic lithic fragments were classified exclusively as basic volcanics. Sample 21-P15A shows also a relative amount of volcanoclastic lithic fragments (Figure 5). Isotropic felsic granitoids are in minor amount, together with metamorphic lithic fragments composed mainly by bt±cam schists, gneisses, and minor cpx- granofels and marbles.

Walcott Bay 2mm-425µm petrographic analysis are shown in figure 6. The two samples are composed mainly of volcanic lithic grains, and their position in the L_m-L_{g+m}-L_v diagram is very close to L_v vertex, as do the one from Miers Valley.

5.7.5 Mineral chemistry

Chemical analysis were carried out on seven thin sections: these are 21-P14d from Walcott Bay area, 21-P19b, 21-P21b, 21-P21d from Marshall Valley, 21-P16c from Miers Valley, 22-P15b from Taylor Valley and 20-P1b from Wright Valley. For each thin sections, several analytical spots were carried out on specific mineral phases belonging both to volcanic and basement (i.e. granitoids and metamorphic lithics) clasts. In the case of pyroxenes, also single mineral grains were analyzed throughout thin sections. Analyzed minerals include pyroxenes, feldspars and clinoamphiboles.

Pyroxenes representative composition are shown in Table 5.5. Pyroxenes have been found as micro-porphyritic brownish to purplish crystals as far as groundmass phases in most volcanic clasts, of basic and intermediate composition; moreover, mafic lithic fragments (e.g. dolerites and gabbros) contain clinopyroxenes and orthopyroxenes. Finally, also some metamorphic lithic clasts such as granofels contain colourless clinopyroxenes. Figure 5.8a shows composition of analyzed pyroxenes in the quadrilateral diagram from Morimoto et al. (1988).

Clinopyroxenes from volcanic clasts range from diopside to titaniferous augite composition: in some cases they are zoned, with enrichment of Mg and depletion of Fe from cores to rims. In some others they are homogeneous in composition. There are no significant difference in composition of volcanic clinopyroxenes between samples taken from different areas.

Table 5.5. Representative chemical composition of pyroxenes from Ross Sea Drift clasts. Mp: micro-porphyritic phases from volcanic lithics. Opx: orthopyroxene. En=Mg/ (Fe^{3+} +Mg + Fe^{2+} + Ca); Fs=(Fe^{3+} +Fe^{2+})/ (Fe^{3+} + Mg +Fe^{2+} + Ca); Wo=Ca /(Fe^{3+} + Mg +Fe^{2+} + Ca).

	Walcott Bay	Marshall Valley							Taylor Valley		Wright Valley
Oxides (Wt%)	21-P14d	21-P19						21-P21	22-P15		20-P1
	clast7	clast8		clast6		clast3		clast12	clast2		
	mp	mp				mp		opx			opx
		core	rim	core	rim	core	rim		core	rim	
SiO_2	46.21	45.99	47.23	52.84	53.26	45.45	46.39	55.94	50.07	49.84	55.52
TiO_2	3.50	3.25	3.29	0.00	0.15	3.07	3.56	0.14	0.72	0.58	0.12
Al_2O_3	8.97	9.19	6.95	1.24	1.10	8.53	7.24	1.60	1.55	1.57	1.57
Cr_2O_3	0.56	0.11	0.00	0.00	0.17	0.12	0.00	0.22	0.00	0.00	0.24
Fe_2O_3	0.00	0.00	0.00	0.00	0.00	0.00	0.00	0.00	0.00	0.00	0.00
FeO	5.55	7.58	7.07	10.35	10.42	7.86	6.73	10.28	26.56	25.96	10.95
MnO	0.32	0.26	0.21	0.27	0.43	0.31	0.00	0.28	0.73	0.62	0.25
MgO	13.07	11.16	13.13	11.58	11.61	12.00	13.32	28.59	8.25	7.24	28.24
CaO	20.70	21.50	21.35	23.16	22.16	21.13	21.74	2.54	11.56	13.19	2.29
Na_2O	1.00	0.89	0.78	0.52	0.51	1.47	1.02	0.33	0.41	0.81	0.77
Total	99.88	99.93	100.01	99.96	99.81	99.94	100.00	99.92	99.85	99.81	99.95
Structural formulae on the basis of 6 oxygens											
Si	1.71	1.71	1.75	1.99	2.01	1.68	1.71	1.98	1.99	1.98	1.96
Ti	0.10	0.09	0.09	0.00	0.00	0.09	0.10	0.00	0.02	0.02	0.00
Al	0.39	0.40	0.30	0.06	0.05	0.37	0.31	0.07	0.07	0.07	0.07
Cr	0.02	0.00	0.00	0.00	0.01	0.00	0.00	0.01	0.00	0.00	0.01
Fe^{3+}	0.06	0.05	0.07	0.01	0.00	0.20	0.14	0.00	0.00	0.00	0.05
Fe^{2+}	0.11	0.19	0.15	0.32	0.33	0.05	0.07	0.30	0.88	0.86	0.28
Mn	0.01	0.01	0.01	0.01	0.01	0.01	0.00	0.01	0.02	0.02	0.01
Mg	0.72	0.62	0.73	0.65	0.65	0.66	0.73	1.51	0.49	0.43	1.49
Ca	0.82	0.86	0.85	0.93	0.90	0.84	0.86	0.10	0.49	0.56	0.09
Na	0.07	0.06	0.06	0.04	0.04	0.11	0.07	0.02	0.03	0.06	0.05
Total	4.00	4.00	4.00	4.00	4.00	4.00	4.00	4.00	4.00	4.00	4.00
Wo	47.90	50.06	47.30	48.91	47.71	48.06	47.75	5.05	26.41	30.30	4.57
En	42.08	36.16	40.47	34.03	34.78	37.98	40.71	79.02	26.23	23.14	78.38
Fs	10.02	13.78	12.23	17.06	17.51	13.96	11.54	15.94	47.36	46.55	17.05

Clinopyroxenes from basement metamorphic clasts are mainly diopsidic. Orthopyroxenes of enstatitic composition have been found from intrusive lithics fragments (gabbro and dolerite) in samples from Taylor, Wright and Marshall Valleys (Fig. 5.8a). Clinopyroxenes from Taylor Valley show a general Fe enrichment in comparison with other areas.

Feldpsars representative composition are listed in Table 6, the same are plotted in Figure 5.8b in a ternary diagram. Plagioclases from volcanic lithic fragments are mainly bytownitic to labradoritic, ranging from An84 to An45. Instead, some volcanic lithic fragments of felsic mineralogy yielded mainly alkaline-feldspar of anorthoclase composition (figure 5.8b). The latter have been identified only in Marshall Valley samples. Feldspars from other metamorphic and intrusive lithologies yielded a main andesine-oligoclase composition, with few samples being bytownitic in composition.

Clino-amphiboles representative chemical analysis are shown in Table 5.7. Amphiboles were analyzed in samples taken from Marshall, Taylor and Wright Valley. All analyzed amphiboles are members of the calcic amphibole group (Leake et al., 1997, Figure 5.9). Amphiboles from Wright Valley sample are mainly ferro-hornblende and magnesio-hornblende, in some cases they exhibit strong zonation (X_{Mg} varying from 0.47 to 0.55 from core to rim), while in some other weak zonation (X_{Mg} from 0.38 to 0.30 from core to rim). Amphiboles from Taylor Valley vary from ferro-edenitic hornblende to ferro-pargasite (with weak zonation, X_{Mg} from 0.44 to 0.46 from core to rim). Instead amphiboles from Marshall Valley sample yielded both a ferro-edenitic hornblende composition and a magnesio-hornblende composition, with two crystals from volcanic lithic fragments that are kaersutite ($Ca_B \geq 1.50$; $(Na+K)_A \geq 0.50$ and Ti>0.50 a.p.f.u., Figure 5.9).

Table 5.6. Representative composition of feldspars from Ross Sea Drift clasts. Mp: micro-porphyritic phases within volcanic lithics; g: groundmass phases within volcanic lithics.

	Walcott Bay	Marshall Valley					Taylor Valley	Wright Valley
Oxides (Wt%)	21-P14d	21-P19				21-P21d	22-P15	20-P1
	clast3	clast9	clast15		clast5	clast5	clast2	clast7
	g		mp		g			
			core	rim				
SiO_2	50.69	63.73	49.86	49.24	45.29	65.99	56.39	59.83
TiO_2	0.38	0.29	0.14	0.16	0.22	0.36	0.00	0.25
Al_2O_3	29.92	22.19	31.31	31.43	33.44	19.05	26.77	25.01
Cr_2O_3	0.22	0.22	0.11	0.05	0.07	0.04	0.00	0.09
Fe_2O_3	0.00	0.00	0.00	0.00	0.00	0.00	0.00	0.00
FeO	0.74	0.21	0.70	0.62	0.77	0.26	0.93	0.32
MnO	0.22	0.14	0.09	0.05	0.18	0.06	0.21	0.00
MgO	0.80	0.00	0.00	0.89	0.88	0.66	0.00	0.00
CaO	13.09	4.16	14.92	14.24	17.20	0.74	11.29	7.10
BaO	0.00	0.00	0.00	0.00	0.00	0.00	0.00	0.00
Na_2O	3.70	8.63	2.61	3.13	1.75	7.49	3.99	6.92
K_2O	0.25	0.42	0.27	0.19	0.18	5.35	0.42	0.48
Total	100.01	99.99	100.01	100.00	99.98	100.00	100.00	100.00
Structural formulae on the basis of 8 oxygens								
Si	2.31	2.84	2.29	2.24	2.08	2.94	2.58	2.68
Ti	0.01	0.01	0.00	0.01	0.01	0.01	0.00	0.01
Al	1.60	1.16	1.69	1.69	1.81	1.00	1.44	1.32
Cr	0.01	0.01	0.00	0.00	0.00	0.00	0.00	0.00
Fe^{3+}	0.00	0.00	0.00	0.00	0.00	0.00	0.00	0.00
Fe^{2+}	0.03	0.01	0.03	0.02	0.03	0.01	0.04	0.01
Mn	0.01	0.01	0.00	0.00	0.01	0.00	0.01	0.00
Mg	0.05	0.00	0.00	0.06	0.06	0.04	0.00	0.00
Ca	0.64	0.20	0.73	0.69	0.84	0.04	0.55	0.34
Ba	0.00	0.00	0.00	0.00	0.00	0.00	0.00	0.00
Na	0.33	0.75	0.23	0.28	0.16	0.65	0.35	0.60
K	0.01	0.02	0.02	0.01	0.01	0.30	0.02	0.03
Total	5.00	5.00	5.00	5.00	5.00	5.00	5.00	5.00
An	65.18	20.52	74.73	70.74	83.57	3.58	59.39	35.16
Al	33.34	77.02	23.66	28.14	15.39	65.59	37.98	62.01
Or	1.48	2.47	1.61	1.12	1.04	30.83	2.63	2.83

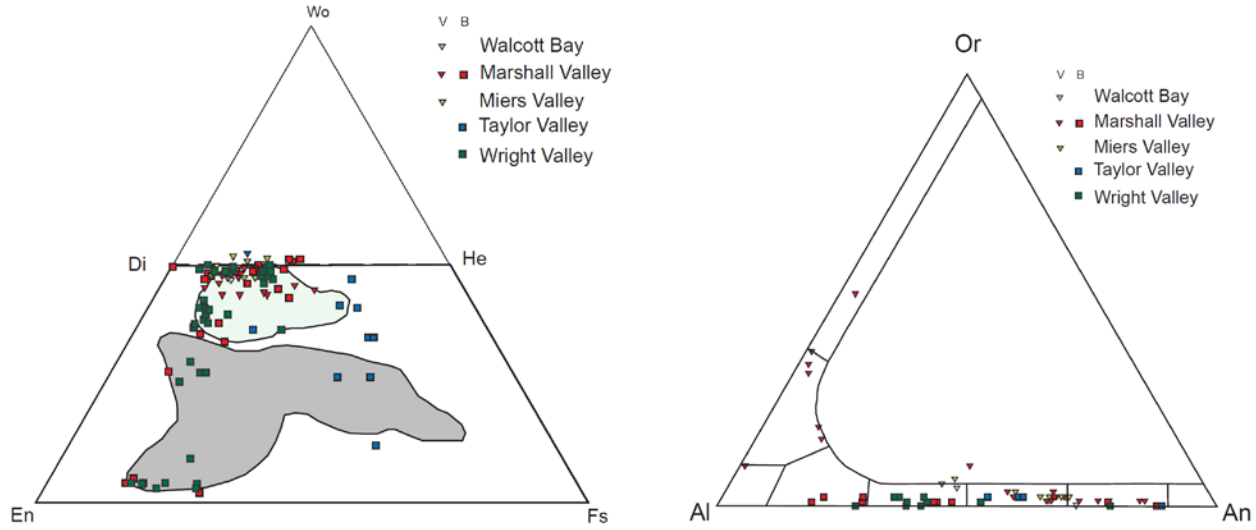

Figure 5.8. A) pyroxenes diagram of analyzed clasts from Ross Sea Drift. Coloured fields show pyroxenes chemical composition of the Erebus Volcanic Province (after Gamble et al., 1986, light blue) and from the Ferrar Province (after Haban and Elliot, 1985, grey). B) feldspar ternary diagram of analyzed clasts. Abbreviations: V= volcanic lithic fragments; B= metamorphic and intrusive lithic fragments.

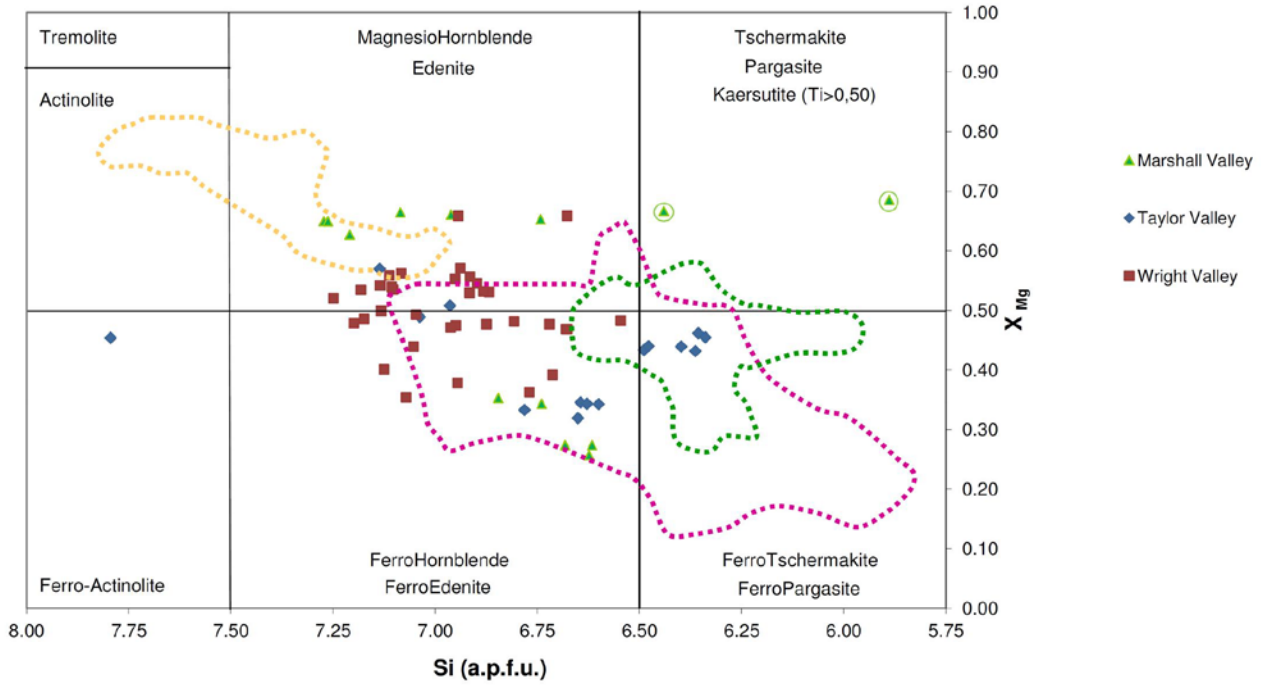

Figure 5.9. Calcic-amphiboles classification (Leake et al., 1997) for Ross Sea Drift clasts. Coloured fields are amphibole compositions from known bedrock sources (Talarico et al., 2011, 2013): yellow=Skelton-Mulock glacier area; purple=Southern Victoria Land granitoids; green: Britannia Range area. Circled spots are kaersutite amphiboles ($(Na+K)_A \geq 0.50$ and Ti>0.50 a.p.f.u.).

Olivine from analyzed clasts are mainly forsteritic, with a composition ranging from Fo_{88} to Fo_{70}; only in few cases (clasts from Taylor Valley samples), olivine has a composition of Fo_{60} to Fo_{57}.

5.8 Discussion

5.8.1 Clasts provenance

Recovered clasts that compose the Ross Sea 1 Drift and the Trilogy Drift along the southern coast of McMurdo Sound and in Wright and Taylor Valleys are composed mainly by rocks sourced from the intrusive basement complex and volcanic rocks supplied by the several volcanic centers of the region. However, a more detailed discussion about the specific provenance of lithologies composing the drifts needs to be evaluated.

Table 5.7. Representative clinoamphiboles composition of clasts from Ross Sea Drift. X_{Mg}=Mg/(Fe+Mg).

	Marshall Valley					Wright Valley				Taylor Valley		
Oxides (Wt%)	21-P19					20-P1				22-P15		22-P16c
	Clast9		Clast11bis	Clast11		Clast8		Clast1		Clast1		
	cam2		cam1	cam1		cam1		cam1		cam2		cam5
	core	rim		core	rim	core	rim	core	rim	core	rim	
SiO_2	42.94	43.74	39.83	49.69	50.47	46.50	47.29	44.93	45.48	42.31	42.57	43.11
TiO_2	2.33	2.17	6.62	1.60	1.14	1.43	1.25	1.74	1.21	1.75	1.61	2.27
Al_2O_3	8.92	8.47	13.20	7.26	6.35	9.09	8.15	8.77	8.92	12.05	12.37	9.16
FeO	24.11	24.54	10.24	13.30	12.05	17.74	17.18	20.67	20.97	19.54	19.18	23.06
MnO	0.68	0.73	0.38	0.35	0.38	0.53	0.60	0.60	0.60	0.53	0.39	0.57
MgO	5.10	4.70	12.53	12.57	14.42	8.99	10.34	7.05	7.28	7.62	7.95	6.15
CaO	10.92	10.86	11.42	11.96	11.44	11.41	11.15	10.66	10.47	11.63	11.20	10.14
Na_2O	1.70	1.47	2.93	0.93	1.29	1.27	1.23	2.34	2.21	1.08	1.57	2.27
K_2O	1.31	1.18	1.17	0.52	0.53	1.13	0.79	1.27	1.03	1.53	1.47	1.41
Cr_2O_3	0.12	0.19	0.18	0.14	0.16	0.00	0.21	0.05	0.00	0.00	0.00	0.00
Total	98.12	98.02	98.50	98.32	98.22	98.09	98.18	98.08	98.16	98.02	98.31	98.12
Structural formulae on the basis of 23 oxygens												
Si	6.68	6.81	5.89	7.21	7.23	6.95	6.98	6.88	6.89	6.40	6.39	6.63
Al^{IV}	1.32	1.19	2.11	0.79	0.77	1.05	1.02	1.12	1.11	1.60	1.61	1.37
Al^{VI}	0.32	0.36	0.19	0.45	0.31	0.55	0.39	0.46	0.48	0.54	0.58	0.29
Ti	0.27	0.25	0.74	0.17	0.12	0.16	0.14	0.20	0.14	0.20	0.18	0.26
Fe^{3+}	0.00	0.00	0.00	0.00	0.19	0.00	0.26	0.00	0.10	0.28	0.32	0.27
Fe^{2+}	3.14	3.20	1.27	1.61	1.25	2.22	1.86	2.65	2.55	2.19	2.09	2.70
Mn	0.09	0.10	0.05	0.04	0.05	0.07	0.07	0.08	0.08	0.07	0.05	0.07
Mg	1.18	1.09	2.76	2.72	3.08	2.00	2.27	1.61	1.65	1.72	1.78	1.41
Cr	0.01	0.02	0.02	0.02	0.02	0.00	0.02	0.01	0.00	0.00	0.00	0.00
Ca	1.82	1.81	1.81	1.86	1.76	1.83	1.76	1.75	1.70	1.88	1.80	1.67
Na	0.51	0.44	0.84	0.26	0.36	0.37	0.35	0.70	0.65	0.32	0.46	0.68
K	0.26	0.23	0.22	0.10	0.10	0.22	0.15	0.25	0.20	0.30	0.28	0.28
Total	15.61	15.51	15.89	15.23	15.23	15.41	15.29	15.70	15.55	15.49	15.54	15.62
X_{Mg}	0.27	0.25	0.69	0.63	0.71	0.47	0.55	0.38	0.39	0.44	0.46	0.34

The source of isotropic and foliated intermediate granitoids can be confidently assigned to the several plutons of the Granite Harbour Intrusive Complex that crop out in the region from the Wright Valley to the Koettlitz Glacier; modal mineralogy was impossible to achieve for the small dimensions of lithic grains, so it is possible that also lithics classified as felsic granitoids (quartz-feldspathic composition with minor mafic minerals, following the classification shown in table 5.2) could belong to a generic granitic/granodioritic composition. In particular, one possible source for felsic granitoids recovered in Wright Valley could be the Brownworth Pluton, a coarse grained alkali-feldspar megacryst granite cropping out in the eastern valley (Allibone et al., 1993a). Similarly, the isotropic biotite-leucogranite Catspaw Pluton crops out in eastern Taylor Valley (Allibone et al., 1993a; Cox et al., 2012), and could be considered as one possible source rock for felsic granitoid lithic fragments recovered in eastern Taylor Valley. Alternatively, biotite leucomonzogranite forms porphyritic varieties of cross-cutting dykes of the Bonney and Hedley plutons in the region of the Ferrar Glacier (Smillie, 1992). Biotite-hornblende isotropic and foliated intermediate granitoids (in the sense described in table 5.2) could be associated to the Bonney Pluton, which is the most extensive pluton of the region, cropping out from Wright Valley to Koettlitz Glacier area (Cox et al., 2012). However, since this pluton crops out west of the sampling sites in Wright and Taylor Valleys and in Royal Society Range foothills, a Ross Sea provenance of the drift would exclude it as the main source of biotite-hornblende granitoids, unless its occurrence is considered the results of a recycling process of already eroded material. Thus, the likely sources of the biotite-hornblende granitoid rock fragments could again be identified in the smaller Brownworth and Catspaw Plutons, that contain both biotite and hornblende (Allibone et al., 1993a; Forsyth et al., 2002). Also chemical composition of amphiboles from Wright and Taylor Valley samples matches very well the Southern Victoria Land intrusives field, with also some

amphiboles from Taylor Valley which exhibit a Fe-tschermakitic composition, resembling those obtained by Talarico et al. 2011 for bedrock samples in Britannia Range area (figure 5.9).
Metamorphic clasts recovered from sampling sites could be related to the generic Skelton Group rocks (previously referred as the Koettlitz Group, Cox et al., 2012). Indeed, amphibolites, biotite-actinolite schists, clinopyroxenes-actinolite granofels are common lithologies among the Marshall Formation (Miers-Garwood Valleys) and the Hobbs Formation (Victoria Valley- Koettlitz glacier area) of Findlay et al. (1984), as far as marbles from the Salmon Marble Formation. All these formations could be generally grouped in the Skelton Group (Cox et al., 2012). Biotite orthogneisses are intercalated with the Skelton Group rocks in many outcrops, including Garwood Valley and Wilson Piedmont Glacier areas (Cox et al., 2012). In few cases, amphiboles from samples located in Marshall Valley match the composition of amphiboles of the Skelton-Mulock glacier area (Figure 5.9, Talarico et al., 2011).
Mafic intrusive lithic fragments could be related to gabbros and dolerites of the Ferrar Supergroup, cropping out as dykes in the basement complex and sills within Beacon Supergroup sequences and along the Kukri Peneplain surface (Gunn and Warren, 1962, Cox et al., 2012). Gabbros are typical of the centre of the sills, whereas dolerites are widespread in the sill margins (Gunn and Warren, 1962). Mineral chemistry analysis supports a provenance from Ferrar Supergroup rocks, with some samples yielding orthopyroxenes comparable with composition reported by Haban and Elliot (1985) for the Ferrar Dolerite (fig. 8a). Gabbros are present also in the upper Koettlitz Glacier within the Dromedary Mafic Complex (Simpson and Aslund, 1996; Cox et al., 2012) and intruding Skelton Group rocks close to Panorama Glacier (Panorama Pluton, Mellish et al., 2002). In particular the Dromedary Mafic Complex is characterized by orthopyroxene-bearing lithologies such as norites and pyroxenites ($X_{ENST\ 0.75\text{-}0.78}$, Simpson and Aslund, 1996) so occurrence of detrital orthopyroxenes grains could not be considered exclusive of Ferrar Group source.
Volcanic clasts are related to the McMurdo Volcanic Group, Erebus Volcanic Province, cropping out extensively on Ross, White and Black Islands and in the Mount Morning-Mount Discovery area (Kyle, 1990). Minor and scattered Pliocene-Pleistocene basanite scoria cones are present also in the eastern Wright Valley, between the Bartley and Goodspeed Glacier and in Taylor Valley, around Taylor Glacier snout and Lake Bonney and in the Kukri Hills (Wright and Kyle, 1990a; Cox et al., 2012). Also in the foothills of the Royal Society Range, over 50 basanite vents and scoria cones are present, mainly of Pleistocene ages (Wright and Kyle, 1990b; Cox et al., 2012). Petrography and mineralogy of analyzed clasts reflect a composition related to basic lithologies, such as basanites/tephrites; in some cases they exhibit a mineralogy suggesting an intermediate composition (mainly feldspar phenocrystals and kaersutitic amphiboles), up to a felsic mineralogy with flow-aligned K-feldspar and green clinopyroxenes, that reflect a felsic source rock such as trachytes (Fig. 6). Chemical composition of clinopyroxenes of volcanic clasts (diopside to titaniferous augites) corresponds to those obtained by Gamble et al. (1986) for the Erebus Volcanic Province rocks. Olivine chemical compositions (Mg-rich olivine) found in clasts from the analyzed samples correspond in most cases to a basic-ultrabasic type source rock, according to data from Kyle et al. (1992) for the Mount Erebus lavas and from Wright-Grassham (1987) for the Mount Morning area. According to the same authors, Fe-richer olivine (Fo_{60}), found only in few

Taylor Valley lithic grains, correspond to a more differentiate source rock of intermediate composition (tephriphonolite to phonolite type).

5.8.2 Implications for Ice-flow pattern

Clasts distribution of Ross Sea 1 Drift and Trilogy Drift revealed by this study shows a clear differences between the composition found in Taylor and Wright Valleys samples and those found in samples from Royal Society Range foothills (Marshall and Miers Valley and Walcott Bay). In particular the main difference regards the eastern Wright Valley (Figure 5.5 and Tables 5.3 and 5.4), where the analyzed samples substantially lack of volcanic lithologies of McMurdo Volcanic Group, being characterized only by basement rocks such as granitoids, mafic intrusives and metamorphic rocks. Samples from the Taylor Valley area and foothills of Royal Society Range all contain volcanic lithic fragments, transported by grounded ice that eroded McMurdo Volcanic Group outcrops, thus suggesting a seaward Ross Ice Sheet provenance. This possibility is plausible if the small vents and scoria cones scattered in the flanks and bottom of western Taylor Valley are excluded as source rocks.

A deepening discussion of petrographic data obtained in this study is necessary to explain the differences between Ross Sea Drift 1 and Trilogy Drift compositions. The latter, located in eastern Wright Valley, is a deposit older than LGM (early to mid-Quaternary age based on its weathering, Hall and Denton 2005), thus relating to previous glacial advance than those occurred in LGM. Clast composition of Trilogy Drift from Hall and Denton (2005), as well as this study data, reveals a minor percentage of McMurdo Volcanic Group basalts (figures 5.5 and 5.6, Tables 5.3 and 5.4). This opens two possible interpretations for the origin of this drift, already considered by Hall and Denton (2005): a) intrusion of grounded ice directly from Ross Sea, carrying volcanic lithics derived from erosion of known volcanic outcrops in the region; b) local advance of the Wilson Piedmont Glacier inland towards the site of deposition of the drift, carrying local lithologies and few volcanic clasts that lie beneath the glacier in small cones and vents. This second interpretation is more consistent with our results. Indeed, our petrogaphic data reveal a distribution of clasts for Wright Valley samples that is compatible with local lithologies cropping out in eastern Wright Valley (granitoids and metamorphic rocks of the Skelton Group); also dolerites of the Ferrar Group, that are present in samples from this study (and also from Hall and Denton, 2005), could not be considered as far-travelled erratics, since some sills of dolerite crop out in eastern Wright Valley, north of Brownworth Lake (Cox et al., 2012), thus allowing the possibility of a local Ferrar dolerite source. Moreover, looking at samples from Taylor Valley, in which a grounded ice incursion during LGM is well documented (Denton and Marchant, 2000; Hall et al., 2000), McMurdo volcanic group lithics make up a consistent percentage of total clast assemblage (5-25% for >4 mm granulometric fraction, ~20-25% for 2-4 mm granulometric fraction, ~30-50% for 2mm-425µm granulometric fraction). Volcanic clasts composition in Taylor Valley samples is quite variable, with a majority of basic lithologies, followed by intermediate compositions and rare felsic rocks, suggesting a source area defined by different volcanic lithologies. Assuming a Ross Sea grounded ice incursion during mid-Quaternary in Wright Valley, one would expect a similar percentage of McMurdo volcanic lithics for the assemblage found in Trilogy Drift, given the proximity between Taylor and Wright

Valleys. Instead, occurrence of basaltic clasts found in the four Wright Valley samples is documented by significantly lower amounts than those of all other samples of our dataset (5-10% for >4mm fraction, less than 5% for 2-4 mm fraction, 1-4% for the 2mm-425µm fraction, Figure 5). These low percentages are consistent with a scenario of few volcanic cones widespread between Lake Brownworth and the Bay of Sails rather than an extended volcanic centre such as the islands of McMurdo Sound, which could provide much more volcanic detritus. If this hypothesis is valid, then the main transport for Trilogy Drift would be consistent with a phase of thickening and advance of the Wilson Piedmont Glacier, as happened in the LGM, during which grounded Ross Sea ice did not extend to the eastern Wright Valley (Hall and Denton, 2005). However, this hypothesis is in contrast with the magnitude of thickening required for the Wilson Piedmont Glacier alone to extend so much in the interior of Wright Valley (Hall and Denton, 2005), so the question remains contentious.

The second point to underline is the difference in composition between Taylor Valley samples and the samples from Royal Society Range foothills; the latter have a bigger percentage of McMurdo Volcanic Group rocks (up to 90% in 2-4 mm fraction of one sample from Miers Valley), that in a certain sense dilutes the occurrence of other lithologies. This could be caused by the geographic position of the Royal Society Range foothills, closer to the main volcanic centres of Minna Bluff, Brown Peninsula, Mount Morning and Mount Discovery than Taylor Valley. However, some specific differences between samples from these two areas exist. In particular, volcanic clasts distribution is noteworthy. In a strict petrographic sense, without a precise available bulk chemical composition of volcanic clasts, and considering the context of the Erebus Volcanic Province rocks (Kyle 1990), basic lithologies can be identified as including in “basanite-tephrite” type rocks, intermediate lithologies can be identified as including in “phono-tephrite to phonolite” type rocks and felsic lithologies in “phonolitic-trachytic” type rocks. In particular, volcanic clasts of samples from Marshall and Miers Valley are in some cases of felsic composition, revealing a mineralogy typical of trachytoids rocks (anorthoclase to sanidine k-feldspar ± green clinopyroxene ± opaque minerals, Fig. 5.7), while volcanic clasts from Taylor Valley and Walcott Bay samples are almost exclusively of basaltic or intermediate composition. The most widespread volcanic rock types in the McMurdo Sound are basanitic to phonotephritic lavas (Kyle, 1990; Cox et al., 2012), while felsic rocks of trachytic mineralogy are less widespread and mainly concentrated in the southern portion of McMurdo Sound: the west side of Brown Peninsula (Kyle et al., 1979), some lavas from Black Island (Cole and Ewart, 1968) and the Phase I lavas from the Mount Morning volcanic complex (Martin et al., 2010; Wright-Grassham, 1987). Given this distribution across McMurdo Sound, it is possible that felsic trachytoid clasts found in samples from Marshall and Miers Valley could derive from erosion of some southern volcanic centers. For instance, Mount Morning volcano had an important mildly alkaline magmatism phase occurred between 18.7 and 11.4 Ma and rocks of felsic composition (mainly trachytes and rhyolites) are believed to be much more voluminous beneath present day ice that covers the area (Martin et al., 2010). To deposit trachytoid rocks from a southern volcanic centre to the latitude of Marshall and Miers Valley, a northward ice flow is necessary. If so, this hypothesis would imply an extended Koettlitz glacier lobe at the time of deposition of the Ross Sea 1 Drift, at least to Marshall Valley latitude,

confirming the initial statement of Wilson (2000) of a three-ice lobes setting in McMurdo Sound at LGM. Additionally,

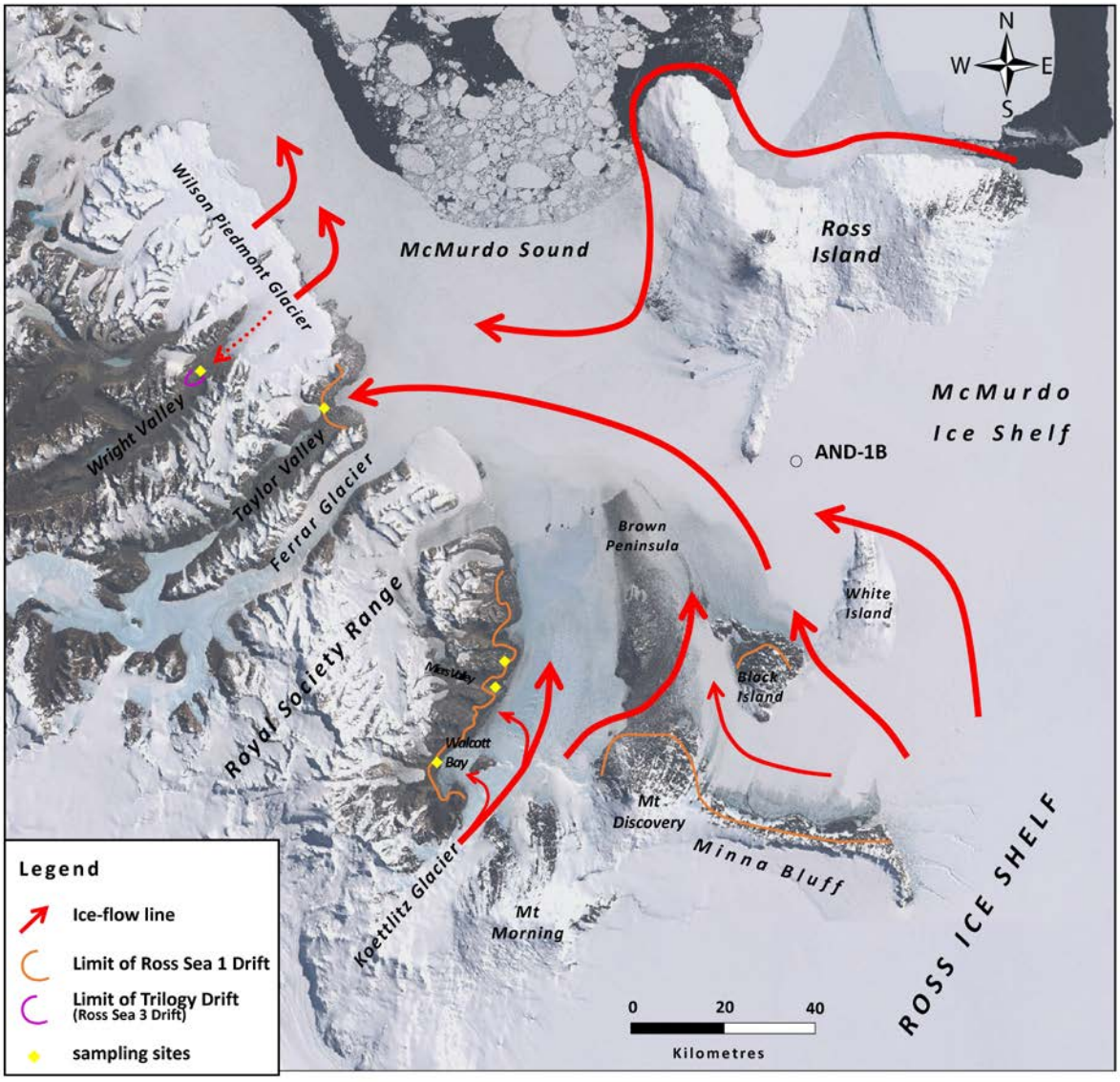

Figure 5.9. Ice-flow reconstruction in McMurdo Sound during LGM, based on the results of Wilson (2000), Anderson et al. (2017) and petrographic data from this study. Yellow points are location of sampling sites. Orange lines show the limit of Ross Sea 1 Drift (Denton and Marchant, 2000, Cox et al., 2012), while purple line marks the limit of Trilogy Drift in Wright Valley (Hall and Denton, 2005). Also location of AND1B is shown.

rarity of dolerites and gabbros from the southern samples of our dataset (Marshall Valley, Miers Valley, Walcott Bay areas) suggest an eroded area with minor outcrops of Ferrar Group rocks, such as the catchment area of the Koettlitz Glacier, in which only the Dromedary Mafic Complex and the Panorama Pluton could provide mafic intrusive rocks. Moreover, these rocks are petrographically distinct from those of Ferrar Group (Simpson and Aslund, 1996; Mellish et al., 2002). On the contrary, Taylor Valley samples, as well as drifts on Black and White Island, Minna Bluff and the eastern sides of Brown Peninsula contain dolerite erratics (Denton and Marchant, 2000), suggesting a different ice flow that carried Ferrar Group clasts (as well as sandstones of

Beacon Supergroup and Eocene erratics, Talarico et al., 2013) from regions located further south along the Transantarctic Mountains. In addition, ferro-tschermakitic amphiboles of some analyzed clasts from Taylor Valley are similar in composition to those found by Talarico et al. (2011) for basement lithologies located in the Britannia Range area, in the region between Mulock and Byrd Glaciers. This would imply for Taylor Valley a LGM grounded ice sheet able to provide detritus initially eroded from southern regions, as already demonstrated for past glacial cycles in AND1B drillcore (Talarico et al., 2012).

Thus, ice-flow reconstruction based on petrographic data supports a scenario characterized by a local provenance (i.e. Koettlitz Glacier) for samples of the Royal Society Range foothills, and a distal provenance from a westward ice flow in Taylor Valley. This scenario is shown in Figure 5.9. The hypothesis of a westward ice-flow intrusion in Miers Valley area, occurred during a later stage after Koettlitz Glacier retreat (Greenwood et al., 2012; Anderson et al., 2017, figure 5.2), that would explain also the presence of anorthoclase-phyric phonolite erratics in these drifts, is not in contrast with our data. Indeed, it is possible that the drifts we sampled from Royal Society Range foothills refer to the early phase of expansion of the Koettlitz Glacier lobe, that afterwards retired and led to the westward advance of a Ross Ice Sheet lobe, as demonstrated by Anderson et al. (2017). Composition of samples from Miers and Marshall Valleys could effectively be coherent also with west-south-west ice flow lines not involving Koettlitz Glacier expansion but considering detritus carried out from the south over Minna Bluff and Brown Peninsula. Indeed volcanic felsic lithologies are present also in the eastward side of Mount Morning complex, at Mason Spur (Martin et al., 2010), so occurrence of these rocks in Miers and Marshall Valleys can be alternatively ascribed to a northward Koettlitz Glacier ice flow, or a south-westward Ross Ice Sheet expansion. The only doubt on this second hypothesis would be scarcity of dolerite clasts in these samples comparing with those from Taylor Valley; according to Marshall and Miers Valleys petrographic data, the catchment of Koettlitz Glacier appears to be more likely, with absence of far-travelled erratics such dolerites or sandstones, that are widespread on the east side of Brown Peninsula, suggesting that ice during LGM did not flow over Brown Saddle into the Walcott Bay (Anderson et al. 2017). Recent LGM ice-flows reconstruction (Anderson et al., 2017) and also the results of this work are partially in contrast with the early McMurdo Sound models of Stuiver (1981) and Denton and Hughes (2000). The main debatable question is the occurrence of anorthoclase-phyric phonolite in the coastal drift of Royal Society Range foothills, the only known outcrop of this rock is in the western coast of Ross Island. However, the presence of anorthoclase-phyric phonolite erratics at Black Island (Anderson et al., 2017) and clasts from Quaternary sequences of AND1B drillcore, associated with detrital clasts belonging to rocks located in the Skelton and Mulock Glaciers area (McKay et al., 2012, Talarico et al., 2012), suggests a grounded ice sheet flowed from the south into McMurdo Sound during past glacial periods. This aspect suggests a possible other source rather than western Ross Island for this kind of rock, so far undetected in the region. Alternatively, a multicycle erosive process may have occurred, with initial erosion of phonolites, transport south of Ross Island, and successive glacial transport into the western portion of McMurdo Sound (i.e. Royal Society Range foothills).

5.9 Conclusions

- Provenance of Ross Sea Drift deposits (of mid-Quaternary to LGM age) from Wright Valley, Taylor Valley and Royal Society Range foothills was studied applying a petrographic approach. Deposits were classified following the lithological composition of cobble, gravel, and sand sized granulometric fractions.

- Composition of clasts predominantly show source rocks which crop out in the region between Mackay and Koettlitz glacier, with volcanic lithics fragments of McMurdo Volcanic Group being the most represented lithology in Royal Society Range samples, while granitoid rocks of the Granite Harbour Intrusive Complex are the most abundant in Taylor and Wright Valley samples. Metamorphic rocks of the Skelton Group and mafic intrusive rocks (Ferrar Group) are in minor abundance, while sedimentary rocks (such as Beacon Supergroup sandstones) are almost absent.

- Lithological composition of Ross Sea Drift I supports a glacial transport from a grounded ice sheet from Ross Sea in Taylor Valley and RSR foothills during LGM. Instead, Trilogy Drift from Wright Valley (mid-Quaternary age) reflect local sources, possibly due to a thickening of Wilson Piedmont Glacier that reduced transport of high quantities of volcanic lithic clasts from volcanic centres across McMurdo Sound. This support the speculative hypothesis of small volcanic vents and cones distributed underneath Wilson Piedmont Glacier, which could provide few volcanic rocks to the site of deposition of the drift.

- An expanded lobe of Koettlitz glacier during LGM, is consistent with clasts composition of Ross Sea I Drift in the coast facing Royal Society Range. This lobe advanced northward at least to Marshall Valley latitude, carrying trachytoids volcanic lithic fragments possibly sourced from Mount Morning area. This scenario has already been supported by previous geomorphological and chronological studies and accounts for a local input of flowing ice at least in an early stage during LGM. Instead, Taylor Valley samples composition reflect a distal west-northwestward ice flow from an expanded Ross Ice Sheet, able to transport detritus from southern regions.

Chapter VI.
Conclusions

In this work, a provenance study primarily based on a petrographic approach has been carried out in two different geographic and geologic setting, involving both LGM offshore and onshore samples. The first case involves gravel-sized samples from glaciomarine cores distributed across Ross Sea embayment, the second case comprises unconsolidated sediments transported by a grounded ice sheet in the coast of McMurdo Sound (Ross Sea Drift).

Offshore samples from Eastern Ross Sea have been coupled with ZrnUPb and AFT data and yielded results consistent with a West Antarctica source area. This region could be identified mainly in the catchments of McAyeal and Bindschadler Ice Streams, since both clasts petrology and ZrnUPb and AFT ages suggest an inland portion of Marie Byrd Land as the most likely eroded area. In particular petrologic data suggest a prevalently low grade unit to be eroded during LGM, in association with two kind of intrusive granitoid rocks. These units have been identified in the Swanson Formation, Ford Granodiorite and Byrd Coast Granite, respectively, cropping out in western Marie Byrd Land. It is noteworthy that the collected data are coherent with previous geochronological detrital studies carried out in the region, pointing out to a ZrnUPb Cretaceous signal as a major proxy for West Antarctica provenance. Moreover, a significant detrital Zrn-UPb and AFT Triassic-Jurassic age population, already documented in detrital studies of the region, suggests the presence of quite widespread rocks that either formed or metamorphosed at that time in the LGM catchment areas.

In the Central and Western Ross Sea petrologic investigations revealed mainly three clasts assemblages, two of them including specific Transantarctic Mountains lithologies (i.e. McMurdo Volcanic Group volcanic clasts and carbonates of the Byrd and/or Beardmore Group). The distribution of the latter are concentrated in Western Ross Sea and in the central part of the Glomar Challenger Basin (Central Ross Sea), respectively. This occurrence, in association with data from previous provenance studies and from geomorphic features on the sea floor, suggest an LGM drainage pattern in which the Western Ross Sea was filled by ice mainly sourced from the Skelton-Mulock Glacier area and in part from the Byrd Glacier. Instead, the Glomar Challenger Basin was filled by ice prevalently discharged from an area south of the Byrd Glacier, where low-grade metasedimentary units in association with carbonate sequences, Beacon and Ferrar Supergroups crop out extensively. One point to stress is that this hypothesis should be verified in the future by coupling petrological data with new geo- and thermo-chronologic data and by comparing them to those present from onshore record. This would create a more consistent offshore database, since existing data from literature have a too broad spatial resolution, with only some scattered samples in the CRS which is the key area where the two Ice Sheet are coalescing.

Onshore data from McMurdo Sound Coast revealed a LGM drainage reconstruction which is coherent with new geomorphologic and chronologic data on moraines and unconsolidated sediments of the Ross Sea Drift: an expanded lobe of the Koettlitz Glacier accounts for a local sedimentary input on the Royal Society Range foothills, at least to Marshall Valley latitude and at least in an early stage of LGM, while grounded ice supplied by the Ross Sea Ice Sheet transported glacial erratics in the mouth of Taylor Valley and coalesced with ice from the Koettlitz Glacier.

References

Ackert, R., et al., 1999. Measurement of past ice sheet elevations in interior West Antarctica. Science 286, 276-280.

Ackert, R., Mukhopadhyay, S., Parizek, B., Borns Jr., H.W., 2007. Ice elevation near the West Antarctic Ice Sheet divide during the last glaciation. Geophys. Res. Lett. 34, L21506.

Ackert, R., Mukhopadhyay, S., Pollard, D., DeConto, R.M., Putnam, A.E., Borns, H.W., 2011. West Antarctic Ice Sheet elevations in the Ohio Range: geologic constraints and ice sheet modeling prior to the last highstand. Earth Planet. Sci. Lett. 307, 83-93.

Adams, C.J., 1986. Geochronological studies of the Swanson Formation of Marie Byrd Land, West Antarctica, and correlation with northern Victoria Land, East Antarctica, and South Island, New Zealand. N. Z. J. Geol. Geophys. 29, 345–358.

Adams, C.J., Mortimer, N., Campbell, H.J., and Griffin, W.L., 2013. The mid-Cretaceous transition from basement to cover within sedimentary rocks in eastern New Zealand; evidence from detrital zircon age patterns: Geol. Mag., v. 150, p. 455–478.

Adams, C.J., Seward, D., Weaver, S.D., 1995. Geochronology of Cretaceous granites and metasedimentary basement on Edward VII Peninsula, Marie Byrd Land, West Antarctica. Antarct. Sci. 7, 265–276.

Alley, R.B., Blankenship, D.D., Bentley, C.R., Rooney, S.T., 1986. Deformation of till beneath ice stream B, West Antarctica. Nature 322, 57-59.

Allibone, A.H., 1992. Low pressure/high temperature metamorphism of Koettlitz Group schists, Taylor Valley and upper Ferrar Glacier area, South Victoria Land, Antarctica. N. Z. J. Geol. Geophys. 35, 115–127.

Allibone, A.H., Cox, S.C., Graham, I.J., Smellie, R.W., Johnstone, R.D., Ellery, S.G., Palmer, K., 1993a. Granitoids of the Dry Valleys area, southern Victoria Land, Antarctica: Plutons, field relationships, and isotopic dating. N. Z. J. Geol. Geophys. 36, 281–297.

Allibone, A.H., Cox, S.C., Smillie, R.W., 1993b. Granitoids of the Dry Valleys area, southern Victoria Land: Geochemistry and evolution along the early Paleozoic Antarctic Craton margin. N. Z. J. Geol. Geophys. 36, 299–316.

Anderson, J.B., Kurtz, D.D., Domack, E.W., Balshaw, K.M., 1980. Antarctic glacial marine sediments. J. Geol. 88, 399-414.

Anderson, J.B., Brake, C.F., Myers, N.C., 1983. Sedimentation in the Ross Sea, Antarctica. Mar. Geol. 57, 295-333.

Anderson, J. B., 1999. Antarctic Marine Geology. Cambridge University Press, 1999. Book, pp. 289.

Anderson, J., Shipp, S., Bartek, L., Reid, D.E., 1992. Evidence for a grounded ice sheet on the Ross Sea continental shelf during the late Pleistocene and preliminary paleodrainage reconstruction. Am. Geophys. Union Antarct. Res. Ser. 57, 39—62.

Anderson, J.B., Shipp, S.S., Lowe, A.L., Wellner, J.S., Mosola, A.B., 2002. The Antarctic ice sheet during the last glacial maximum and its subsequent retreat history: a review. Quat. Sci. Rev. 21, 49-70.

Anderson, J.B., Conway, H., Bart, P.J., Witus, A.E., Greenwood, S.L., McKay, R.M., Hall, B.L., Ackert, R.P., Licht, K., Jakobsson, M., Stone, J.O., 2014. Ross Sea paleo-ice sheet drainage and deglacial history during and since the LGM. Quat. Sci. Rev. 100, 31–54.

Anderson, J.T.H., Wilson, G.S., Fink, D., Lilly, K., Levy, R.H., Townsend, D., 2017. Reconciling marine and terrestrial evidence for post LGM ice sheet retreat in southern McMurdo Sound, Antarctica. Quat. Sci. Rev. 157, 1–13.

Andreucci, B., 2013. Thermochronology of the Polish and Ukrainian Carpathians, PHD thesis, University of Padua, Italy.

Balshaw, K. M., 1981. Antarctic glacial chronology reflected in the Oligocene through Pliocene sedimentary section in the Ross Sea. Rice University, Houston, Texas. Ph.D. Dissertation, 140 pp.

Barker, P.F., Camerlenghi, A., 2002. In: Barker, P.F., Camerlenghi, A., Acton, G.D., Ramsay, A.T.S. (Eds.), Glacial history of the Antarctic Peninsula from Pacific Margin Sediments. Proceedings of the Ocean Drilling Program, Scientific Results. vol. 178.

Baroni, C., Hall, B.L., 2004. A new Holocene relative sea-level curve for Terra Nova Bay, Victoria Land, Antarctica. J. Quat. Sci. 19, 377-396.

Baroni, C., Orombelli, G., 1991. Holocene raised beaches at Terra Nova Bay, Victoria Land, Antarctica. Quat. Res. 36, 157-177.

Barrett P.J., 1981. History of the Ross Sea region during the deposition of the Beacon Supergroup 400 - 180 million years ago. J. R. Soc. N. Z. 11, 447–458.

Barrett P.J., 1991. The Devonian to Triassic Beacon Supergroup of the Transantarctic Mountains and correlatives in other parts of Antarctica. In: Tingey J. (Eds.), The Geology of Antarctica, Oxford University Press, New York, pp. 120-152.

Bart, P.J., Cone, A.N., 2012. Early stall of West Antarctic Ice Sheet advance on the eastern Ross Sea middle shelf followed by retreat at 27,500 14C yr BP. Palaeogeogr. Palaeoclimatol. Palaeoecol 335-336, 52-60.

Bart, P.J., Owolana, B., 2012. On the duration of West Antarctic ice sheet grounding events in Ross Sea during the quaternary. Quat. Sci. Rev. 47, 101–115.

Behrendt, J. C., D. D. Blankenship, C. A. Finn, R. E. Bell, R. E. Sweeney, S. M. Hodge, and J. M. Brozena. 1994. Casertz aeromagnetic data reveal Late Cenozoic flood basalts (?) in the West Antarctic Rift System. Geology 22:527-530.

Behrendt, J. C., R. Saltus, D. Damaske, A. McCafferty, C. A. Finn, D. Blankenship, and R. E. Bell. 1996. Patterns of late Cenozoic volcanic and tectonic activity in the West Antarctic rift system revealed by aeromagnetic surveys. Tectonics 15:660-676.

Behrendt, J. C., D. D. Blankenship, D. L. Morse, and R. E. Bell (2004). Shallow source aeromagnetic anomalies observed over the West Antarctic Ice Sheet compared with coincident bed topography from radar ice sounding: New evidence for glacial ‘‘removal’’ of subglacially erupted Late Cenozoic rift related volcanic edifices, Global Planet. Change, 42, 177– 193.

Bernet, M., Gaupp, R., 2005. Diagenetic history of Triassic sandstone from the Beacon Supergroup in central Victoria Land, Antarctica. N. Z. J. Geol. Geophys. 48, 447–458.

Bockheim, J., Wilson, S.C., Denton, G.H., Andersen, B.G., Stuiver, M., 1989. Late Quaternary ice-surface fluctuations of Hatherton Glacier, Transantarctic Mountains. Quat. Sci. Rev. 31, 229-254.

Borg, S.G., 1983. Petrology and geochemistry of the Queen Maud Batholith, central Transantarctic Mountains, with implications for the Ross Orogeny, in Proceedings of the International Symposium on Antarctic Earth Sciences, R.L. Oliver, P.R.. James, and J.B. Jago, eds., Australian Academy of Science, Series B. no. 4, p. 165-169.

Borg, S.G., DePaolo, D.J., Wendlandt, E.D., Drake, T.G., 1989. Studies of granites and metamorphic rocks, Byrd Glacier area. Antarctic Journal of the United States 24, 19–21.

Bradshaw, J. D., Andrews, P. B., & Field, B. D., 1983. Swanson Formation and related rocks of Marie Byrd Land and a comparison with the Robertson Bay Group of northern Victoria Land. Antarct. Earth Sci., 1982, 274-279.

Brand, J.F., 1979. Low Grade Metamorphic Rocks of the Ruppert and Hobbs Coasts of Marie Byrd Land, Antarctica. M.Sc. Thesis Texas Tech University, 49 pp.

Brandon, M. T., 1996. Probability density plot for fission-track grain-age samples. Radiat. Meas., 26(5), 663-676.

Brandon, M.T., 2002. Decomposition of mixed grain-age distributions using BINOMFIT. On Track. 24, 13–18.

Bromley, G.R., Hall, B.L., Stone, J.O., Conway, H., Todd, C., 2010. Late Cenozoic deposits at Reedy Glacier, Transantarctic Mountains: implications for former thickness of the West Antarctic Ice Sheet. Quat. Sci. Rev. 29, 384-398.

Bromley, G.R., Hall, B.L., Stone, J.O., Conway, H., Todd, C., 2012. Late Cenozoic deposits at Scott Glacier, Transantarctic Mountains: implications for former thickness of the West Antarctic Ice Sheet. Quat. Sci. Rev. 50, 1-13.

Brown, C. R., Yakymchuk, C., Brown, M., Fanning, C. M., Korhonen, F. J., Piccoli, P. M., & Siddoway, C. S., 2016. From Source to Sink: Petrogenesis of Cretaceous Anatectic Granites from the Fosdick Migmatite–Granite Complex, West Antarctica. J. Petrol., 57(7), 1241-1278.

Bushnell, V.C., Craddock, C. (Eds.), 1970. Antarctic Map Folio Series. American Geographical Society, New York Map 64–29.

Cape Roberts Science Team, 1998a. Quaternary strata in CRP-1, Cape Roberts Project, Antarctica. Terra Antartica 5, 31–62.

Cape Roberts Science Team, 1998b. Miocene strata in CRP-1, Cape Roberts Project, Antarctica. Terra Antartica 5, 63–124.

Carosi, R., Giacomini, F., Talarico, F., Stump, E., 2007. Geology of the Byrd Glacier Discontinuity (Ross Orogen): New survey data from the Britannia Range, Antarctica. In: Cooper, A.K., Raymond, C.R., et

al. (Eds), Antarctica: A Keystone in a Changing World — Online Proceedings of the 10th ISAES, USGS Open-File Report 2007-1047, Short Research Paper 030, 6 pp.

Clayton-Greene, J., Hendy, C., Hogg, A., 1988. Chronology of a Wisconsin age proglacial lake in the Miers Valley, Antarctica. N. Z. J. Geol. Geophys. 31, 353-361.

Clark, P.U., Dyke, A.S., Shakum, J.D., Carlson, A.E., Clark, J., Wohlfarth, B., Mitrovica, J.X., Hostetler, S.W., McCabe, A.M., 2009. The Last Glacial Maximum. Science 325 (5941), 710-714.

Cole, J.W., Ewart, A., 1968, Contribution to the geology of Black Island, Brown Peninsula, and Cape Bird areas, McMurdo Sound, Antarctica. New Zealand Journal of Geology and Geophysics 1: 793-828.

Contreras, A., Siddoway, C.S., Reiners, P. and Gehrels, G., 2012. New insights on the timing and extent of Cretaceous exhumation in the West Antarctic rift system, from U-Pb and (U-Th)/He zircon analysis.- Geological Society of America Abstracts with Program, 43 (5): 100, paper No. 32-2.

Conway, H., Hall, B.L., Denton, G.H., Gades, A.M., Waddington, E.D., 1999. Past and future grounding-line retreat of the West Antarctic Ice Sheet. Science 286, 280-283.

Cook, Y. a., 2007. Precambrian rift-related magmatism and sedimentation, south Victoria Land, Antarctica. Antarct. Sci. 19, 471–484.

Cook, Y.A., Craw, D., 2002. Neoproterozoic structural slices in the Ross Orogen, Skelton Glacier area, South Victoria Land, Antarctica. N. Z. J. Geol. Geophys. 45, 133–143.

Cook, Y.A., Craw, D., 2001. Amalgamation of disparate crustal fragments in the Walcott Bay-Foster Glacier area, South Victoria Land, Antarctica. N. Z. J. Geol. Geophys. 44, 403–416.

Cornamusini, G., and Talarico F., 2016. Miocene Antarctic ice dynamics in the Ross Embayment (Western Ross Sea, Antarctica): Insights from provenance analyses of sedimentary clasts in the AND-2A drill core, Global and Planetary Change 146, 38–52.

Cottle, J.M., Cooper, A.F., 2006a. Geology, geochemistry, and geochronology of an A-type granite in the Mulock Glacier area, southern Victoria Land, Antarctica. New Zealand Journal of Geology and Geophysics 49, 191–202.

Cottle, J., Cooper, A., 2006b. The Fontaine Pluton: An early Ross Orogeny calc-alkaline gabbro from southern Victoria Land, Antarctica. New Zealand Journal of Geology & Geophysics, Vol. 49: 177–189.

Cox, S.C., Allibone, A.H., 1991. Petrogenesis of orthogneisses in the Dry Valleys region, South Victoria Land. Antarct. Sci. 3.

Cox, S.C., 1993. Inter-related plutonism and deformation in South Victoria Land. Antarctica, Geological Magazine 130, 1–14.

Cox, S.C., Turnbull, I.M., Isaac, M.J., Townsend, D.B., Smith Lyttle, B., 2012. Geology of Southern Victoria Land, Antarctica (compilers). Institute of Geological & Nuclear Sciences, 1:25,000 geological map 22. 135 p. þ 1 folded map. Lower Hutt, New Zealand. GNS Science.

Cunningham, W.L., Leventer, A., Andrews, J.T., Jennings, A.E., Licht, K.J., 1999. Late Pleistocene-Holocene marine conditions in the Ross Sea, Antarctica: evidence from the diatom record. Holocene 9, 129-139.

Davey, F. J., 1981. Geophysical studies in the Ross Sea region. J. of the Royal Soc. N. Z., vol. 11, n. 4, pp 465-479, ff. 7.

Davey, F. J., 1994. Bathymetry and gravity of the Ross Sea, Antarctica. Terra Antarctica, vol. 1, n. 2, pp 357-358.

Davey, F. J., 2004. Ross Sea Bathymetry 1:2.000.000, version 1.0. Institute of Geological & Nuclear Sciences geophysical map 16. Institute of Geological & Nuclear Sciences Limited Lower Hutt, New Zealand.

Davey F. J., Bennett D. J. & Houtz R. E., 1982. Sedimentary basins of the Ross Sea, Antarctica. N. Z. J. Geol. Geophys., vol. 25, pp. 245-255.

Davis, M.B., and Blankenship D., 2006, Geology of the Scott-Reedy Glaciers Area, Southern Transantarctic Mountains, Antarctica, GSA Map Series MCH093F, The Geological Society of America, Boulder, CO.

Denton, G.H., Bockheim, J., Wilson, S., Stuiver, M., 1989. Late Wisconsin and early Holocene glacial history, inner Ross Embayment, Antarctica. Quat. Res. 31, 151-182.

Denton, G.H., Marchant, D., 2000. The geologic basis for a reconstruction of a grounded ice sheet in McMurdo Sound, Antarctica, at the last glacial maximum. Geogr. Ann. 82A, 167-212.

Denton, G.H., Hughes, T., 2000. Reconstruction of the Ross ice drainage system, Antarctica, at the last glacial maximum. Geogr. Ann. 82A, 143-166.

Deschamps, P., Durand, N., Bard, E., Hamelin, B., Camoin, G., Thaomas, A.L., Henderson, G.M., Okuno, J., Yokoyama, Y., 2012. Ice-sheet collapse and sea-level rise at the Bølling warming 14,600 years ago. Nature 483, 559-564.

Dickinson, W.R., 1970. Interpreting detrital modes of graywacke and arkose. Journal of Sedimentary Petrology 40, 695–707.

Di Venere, V.J., Kent, D.V., and Dalziel, I.W.D., 1994. Mid-Cretaceous paleomagnetic results from Marie Byrd Land, West Antarctica; a test of post–100 Ma relative motion between East and West Antarctica: Journal of Geophysical Research, v. 99, p. 15,115–15,139.

Dochat, T.M., Marchant, D., Denton, G.H., 2000. Glacial geology of Cape Bird, Ross Island, Antarctica. Geogr. Ann. 82A, 237-247.

Domack, E., Jacobson, E., Shipp, S., Anderson, J., 1999. Late Pleistocene-Holocene retreat of the West Antarctic Ice Sheet in the Ross Sea: part 2-sedimentologic and stratigraphic signature. Geol. Soc. Am. Bull. 111, 1517-1536.

Donelick, R.A., O'Sullivan, P.B., Ketcham, R.A., 2005. Apatite Fission-Track Analysis, in Reiners, P.W., Ehlers, T.A. (Eds.). Low Temperature Thermochronology: Techniques, Interpretations, and Applications. Rev. Min. Geochem. 58, 49-94.

Droop, G.T.R., 1987. A general equation for estimating Fe3+ concentrations in ferromagnesian silicates and oxides from microprobe analyses, using stoichiometric criteria. Mineral. Mag. 51, 431–435.

Elliot, D.H., Fanning, C.M., 2008. Detrital zircons from upper Permian and lower Triassic Victoria Group sandstones, Shackleton Glacier region, Antarctica: evidence for multiple sources along the Gondwana plate margin. Gondwana Research 13, 259–274.

Elliot, D. H., and T. H. Fleming, 2008. Physical volcanology and geological relationships of the Jurassic Ferrar Large Igneous Province, Antarctica,J. Volcanol. Geotherm. Res., 172, 20–37.

Elsner, M., Schöner, R., Gerdes, A., & Gaupp, R., 2013. Reconstruction of the early Mesozoic plate margin of Gondwana by U–Pb ages of detrital zircons from northern Victoria Land, Antarctica. Geol. Soc. London Special Pub., 383(1), 211-232.

Farmer, G.L., Licht, K., Swope, R.J., Andrews, J.T., 2006. Isotopic constraints on the provenance of fine-grained sediment in LGM tills from the Ross Embayment, Antarctica. Earth Planet. Sci. Lett. 249, 90-107.

Farmer, G.L., Licht, K., 2016. Generation and fate of glacial sediments in the central Transantarctic Mountains based on radiogenic isotopes and implications for reconstructing past ice dynamics. Quat. Sci. Rev. 150, 98-109.

Ferraccioli, F., Bozzo, E., Damaske, D., 2002. Aeromagnetic signatures over western Marie Byrd Land provide insight into magmatic arc basement, mafic magmatism and structure of the Eastern Ross Sea Rift flank. Tectonophysics 347, 139–165. doi: 10.1016/S0040-1951(01)00242-6

Findlay, R.H., Craw, D., Skinner, D.N.B., 1984. Lithostratigraphy and structure of the Koettlitz Group, McMurdo Sound, Antarctica. N. Z. J. Geol. Geophys. 27, 513–536.

Fleischer, R.L., Price, P.B., Walker, R.M., 1975. Nuclear Tracks in Solids. Univ. Calif. Press, Berkeley, pp. 605.

Forsyth, P.J., Mortimer, N., Turnbull, I.M., 2002. Plutonic rocks from the Cape Roberts hinterland: Wilson Piedmont Glacier, southern Victoria Land, Antarctica. Terra Antartica 9, 57–72.

Gaffney, Amy M. and Siddoway C.S., 2007. Heterogeneous sources for Pleistocene lavas of Marie Byrd Land, Antarctica: new data from the SW Pacific diffuse alkaline magmatic province (extended abstract). In: Cooper, A. and Raymond, C., Antarctica: A Keystone in a Changing World. Proceedings and Conference Abstracts, U.S. Geological Survey, USGS OFR-2007-1047-ea063. 4 pages.

Galbraith, R.F., Green, P.F., 1990. Estimating the component ages in a finite mixture. Nucl. Tracks Radiation Meas. 17, 197–206.

Galbraith, R.F., Laslett, G.M, 1993. Statistical models for mixed fission track ages. Nucl. Tracks. 5, 3–14.

Gamble J.A., Barrett P.J., Adams C.J., 1986. Basaltic clasts from Unit 8. In: Barrett PJ (eds) Antarctic Cenozoic History from the MSSTS-1 Drillhole, McMurdo Sound. DSIR Bull 237:145–152.

Gasquet, D., Bertrand, J. M., Paquette, J. L., Lehmann, J., Ratzov, G., Guedes, R. D. A., ... & Nomade, S., 2010. Miocene to Messinian deformation and hydrothermal activity in a pre-Alpine basement massif of the French western Alps: new U-Th-Pb and argon ages from the Lauzière massif. B. Soc. Géol. Fr., 181(3), 227-241.

Gazzi, P., 1966. Le arenarie del flysch sopracretaceo dell'Appennino modenese; correlazioni con il flysch di Monghidoro. Mineralogica et Petrographica Acta 12, 69–97.

Gehrels, G.,2010. U-Th-Pb analytical methods for Zircon. Arizona LaserChron Center, University of Arizona.

Gehrels, G., 2011. Detrital zircon U–Pb geochronology: Current methods and new opportunities. In: Busby C and Azor A (eds.) Tectonics of sedimentary Basins: Recent Advances, pp. 45–62. Hoboken, NJ: Wiley.

Golledge, N.R., Fogwill, C.J., Mackintosh, A.N., Buckley, K.M., 2012. Dynamics of the Last Glacial Maximum Antarctic ice-sheet and its response to ocean forcing. Proc. Nat. Acad. Sci. U. S. A. 109, 16052-16056.

Golledge, N.R., Levy, R.H., McKay, R.M., Fogwill, C.J., White, D.A., Graham, A.G.C., Smith, J.A., Hillenbrand, C.-D., Licht, K.J., Denton, G.H., Ackert, J., Robert, P., Maas, S.M., Hall, B.L., 2013. Glaciology and geological signature of the last glacial maximum Antarctic ice sheet. Quat. Sci. Rev. 78, 225-247.

Goodge, J.W., Fanning, C.M., 1999. 2.5 billion years of punctuated Earth history as recorded in a single rock. Geology 27 (11), 1007–1010.

Goodge, J.W., Walker, N.W., and Hansen, V.L., 1993. Neoproterozoic–Cambrian basement-involved orogenesis within the Antarctic margin of Gondwana: Geology, v. 21, p. 7–40.

Goodge, J.W., Myrow, P.M., Williams, I.S., and Bowring, S., 2002. Age and provenance of the Beardmore Group, Antarctica: Constraints on Rodinia supercontinent breakup: Journal of Geology, v. 110, no. 4, p. 393–406.

Greenwood, S.L., Gyllencreutz, R., Jakobsson, M., Anderson, J.B., 2012. Ice flow switching and East/West Antarctic Ice Sheet roles in glaciation of the western Ross Sea. Geol. Soc. Am. Bull.

Gunn, B.M., Warren, G., 1962. Geology of Victoria Land between the Mawson and Mulock Glaciers, Antarctica. New Zealand Geological Survey Bulletin 71, 1–157.

Gunn, B. M.; Walcott, R. I. 1962. The geology of the Mt Markham region, Ross Dependency, Antarctica. N.z. Journal of Geology and Geophysics 5 (3): 407-26.

Haban M.A., Elliot D.H. (1985) Mineral chemistry of the Kirkpatrick basalt, northern Victoria Land. Antarct J Unit States 19:30–31

Hall, B.L., Denton, G.H., 2000a. Radiocarbon chronology of Ross Sea drift, eastern Taylor Valley, Antarctica: evidence for a grounded ice sheet in the Ross Sea at the last glacial maximum. Geogr. Ann. 82A, 305-336.

Hall, B.L., Denton, G.H., 2000b. Extent and chronology of the Ross Sea ice sheet and the Wilson Piedmont Glacier along the Scott Coast at and since the last glacial maximum. Geogr. Ann. 82A, 275-303.

Hall, B.L., Denton, G.H., Hendy, C.H., 2000. Evidence from Taylor Valley for a grounded ice sheet in the Ross Sea, Antarctica. Geogr. Ann. Ser. Phys. Geogr. 82, 275–303.

Hall, B.L., Denton, G.H., Baroni, C., 2004. Holocene relative sea-level history of the Southern Victoria Land Coast, Antarctica. Glob. Planet. Chang. 42, 241-263.

Hall, B.L., Denton, G.H., 2005. Surficial geology and geomorphology of eastern and central Wright Valley, Antarctica. Geomorphology 64, 25–65.

Hall, B.L., Denton, G.H., Stone, J.O., Conway, H., 2013. History of the grounded ice sheet in the Ross Sea sector of Antarctica during the Last Glacial Maximum and the Last Termination. In: Geological Society of London, Special Publication, vol. 381.

Hall, B.L., Denton, G.H., Heath, S.L., Jackson, M.S., Koffman, T.N., 2015. Accumulation and marine forcing of ice dynamics in the western Ross Sea during the last deglaciation. Nat. Geosci. 8 (8), 625-628.

Harrington, H.J., 1965. Geology and morphology of Antarctica. Biogeography and ecology in Antarctica. Monographiae Biologicae 15, 1–71.

Hart, S. R., Blusztajn, J., LeMasurier, W. E., & Rex, D. C., 1997. Hobbs Coast Cenozoic volcanism: implications for the West Antarctic rift system. Chem. Geol., 139(1), 223-248. doi: 10.1016/S0009-2541(97)00037-5

Harwood DM, Levy RH 2000. Introduction and overview. In: Stilwell JD, Feldmann RM eds. Paleobiology and Paleo-environments of Eocene Fossiliferous Erratics, McMurdo Sound, East Antarctica. American Geophysical Union, Antarctic Research Series 76. Pp. 118.

Hayes D. E. & Davey F. J. – 1975 - A geophysical study of the Ross Sea, Antarctica. In: Hayes D. E. and Frakes L. (Eds.), Initial reports of the Deep Sea Drilling Project, Vol., 28. Washington D. C., U. S. Government Printing Office, pp. 887-907.

Hiess, J., Condon, D. J., McLean, N., & Noble, S. R., 2012. 238U/235U systematics in terrestrial uranium-bearing minerals. Science, 335(6076), 1610-1614.

Horn, I., Rudnick, R. L., & McDonough, W. F., 2000. Precise elemental and isotope ratio determination by simultaneous solution nebulization and laser ablation-ICP-MS: application to U–Pb geochronology. Chem. Geol., 164(3), 281-301.

Horstwood, M. S., Foster, G. L., Parrish, R. R., Noble, S. R., & Nowell, G. M., 2003. Common-Pb corrected in situ U–Pb accessory mineral geochronology by LA-MC-ICP-MS. J. Anal. Atom. Spectrom., 18(8), 837-846.

Hughes, T., 1973. Is the West Antarctic Ice Sheet disintegrating? J. Geophys. Res. 78, 7884-7910.

Hurford, A. J., 1990. Standardization of fission track dating calibration: recommendation by the Fission Track Working Group of the IUGS Subcommission on Geochronology. Chem. Geol.: Isotope Geoscience Section, 80(2), 171-178.

Hurford, A. J., & Green, P. F., 1983. The zeta age calibration of fission-track dating. Chem. Geol., 41, 285-317.

Huybrechts, P., 2002. Sea-level changes at the LGM from ice-dynamic reconstructions of the Greenland and Antarctic ice sheets during the glacial cycles. Quaternary Science Reviews 21, 203-231.

Ireland, T.R., Floettmann, T., Fanning, C.M., Gibson, G.M., and Preiss, W.V., 1998. Development of the early Paleozoic Pacific margin of Gondwana from detrital zircon ages across the Delamerian orogen: Geology, v. 26, p. 243–246.

Ivany, L.C., Van Simaeys, S., Domack, E.W., Samson, S.D., 2006. Evidence for an earliest Oligocene ice sheet on the Antarctic Peninsula. Geology 34, 377–380.

Jackson, S. E., Pearson, N. J., Griffin, W. L., & Belousova, E. A., 2004. The application of laser ablation-inductively coupled plasma-mass spectrometry to in situ U–Pb zircon geochronology. Chem. Geol., 211(1), 47-69.

Kellogg, T.B., Truesdale, R.S., Osterman, L.E., 1979. Late Quaternary extent of the West Antarctic Ice Sheet: new evidence from the Ross Sea cores. Geology 7, 249-253.

Ketchum, J. W., Jackson, S. E., Culshaw, N. G., & Barr, S. M., 2001. Depositional and tectonic setting of the Paleoproterozoic Lower Aillik Group, Makkovik Province, Canada: evolution of a passive margin-foredeep sequence based on petrochemistry and U–Pb (TIMS and LAM-ICP-MS) geochronology. Precambrian Res., 105(2), 331-356.

Kleinschmidt and Petschick 2003, Regional metamorphism of the Swanson Formation, western Marie Byrd Land, Antarctica.- Geol. Jb. B95:11-33, Hannover.

Kretz, R., 1983. Symbols for rock forming minerals. Am. Mineral. 68, 277–279.

Korhonen, F.J., Saito, S., Brown, M., Siddoway, C.S., and Day, J.M.D., 2010a. Multiple generations of granite in the Fosdick Mountains, Marie Byrd Land, West Antarctica; implications for polyphase intracrustal differentiation in a continental margin setting: J. Petrol., v. 51, p. 627–670.

Korhonen, F.J., Saito, S., Brown, M., and Siddoway, C.S., 2010b. Modeling multiple melt loss events in the evolution of an active continental margin: Lithos, v. 116, p. 230–248, doi: 10 .1016 /j .lithos .2009 .09 .004 .

Korhonen, F.J., Brown, M., Grove, M., Siddoway, C.S., Baxter, E.F., and Inglis, J.D., 2012. Separating metamorphic events in the Fosdick migmatite-granite complex, West Antarctica: J. Metamorph. Geol., v. 30, p. 165–192.

Korsch, R.J., 1974. Petrographic comparison of the Taylor and Victoria Groups (Devonian to Triassic) in South Victoria Land, Antarctica. N. Z. J. Geol. Geophys. 17 (3), 523–541.

Kyle, P.R., Adams, J., Rankin, P.C., 1979, Geology and petrology of the McMurdo Volcanic Group at Rainbow Ridge, Brown Peninsula, Antarctica. Geological Society of America Bulletin, 90:676-688.

Kyle, P.R., Elliot, D.H., Sutter, J.F., 1981. Jurassic Ferrar Supergroup tholeiites from the Transantarctic Mountains, Antarctica, and their relationship to the initial fragmentation of Gondwana. In: Cresswell, M.M., Vella, P. (Eds.), Gondwana Five. Fifth International Gondwana Symposium, pp. 283–287.

Kyle PR, 1990, McMurdo Volcanic Group, western Ross embayment. Introduction. In: Le Masurier WE, Thomson JW (eds) Volcanoes of the Antarctic plate and Southern Oceans. AGU Antarctic Research Series, vol 48, pp 19–25.

Kyle, P.R., 1990, Erebus Volcanic Province: Summary. In: LeMasurier, W.E., Thomson J.W. eds.. Volcanoes of the Antarctic Plate and Southern Oceans. Antarctic Research Series, 48, Washington DC, American Geophysical Union, pp. 81-88.

Kyle, P.R., Moore, J.A., Thirlwall, M.F., 1992. Petrologic evolution of anorthoclase phonolite lavas at Mount Erebus, Ross Island, Antarctica. J. Petrol. 33, 849–875.

Laird, M.G., 1963. Geomorphology and stratigraphy of the Nimrod Glacier–Beaumont Bay region, southern Victoria Land, Antarctica. New Zealand Journal of Geology and Geophysics 6, 465–484.

Laird, M.G., Mansergh, G.D., and Chappell, J.M.A., 1971. Geology of the central Nimrod Glacier area, Antarctica: New Zealand Journal of Geology and Geophysics, v. 14, p. 427–468.

Langone, A., Caggianelli, A., Festa, V., & Prosser, G., 2014. Time constraints on the building of the Serre Batholith: consequences for the thermal evolution of the Hercynian continental crust exposed in Calabria (southern Italy). J. Geol., 122(2), 183-199.

Leake, B.E., Woolley, A.R., Arps, C.E.S., Birch, W.D., Gilbert, M.C., Grice, J.D., Hawthorne, F.C.,Kato, F.C., Kisch, H.J., Krichovichev, V.G., Linthout, K., Lair, J., Mandarino, J.A., Maresch, W.V., Nickel, E.H., Rock, N.M.S., Schumacher, J.C., Smith, D.C., Stephenson, N.C.M.N., Ungaretti,L.,Whittaker,E.J.W.,Youzhi,G.,1997. Nomenclature of amphiboles: report of the subcommittee on amphiboles of the International Mineralogical Association, commission on new minerals and mineral names. Am. Mineral. 82, 1019–1037.

LeMasurier, W. E., & Rex, D. C., 1982. Volcanic record of Cenozoic glacial history in Marie Byrd Land and western Ellsworth Land: Revised chronology and evaluation of tectonic factors. Antarct. geosci., 89, 725-734.

LeMasurier, W. E., and D. C. Rex, 1989. Evolution of linear volcanic ranges in Marie Byrd Land, West Antarctica, J. Geophys. Res., 94, 7223–7236.

LeMasurier, W. E., and D. C. Rex, 1990. Late Cenozoic volcanism on the Antarctic Plate: An overview, in Volcanoes of the Antarctic Plate and Southern Oceans, Antarct. Res. Ser., vol. 48, edited by W. E. LeMasurier and J. W. Thompson, pp. 1–17, Am. Geophys. Union, Washington, D. C.

LeMasurier WE, Thomson JW (eds), 1990. Volcanoes of the Antarctic Plate and Southern Oceans, Antarctic Research Series, vol 48, pp 488.

LeMasurier WE, 1990, Marie Byrd Land. Introduction. In: Le Masurier WE, Thomson JW (eds) Volcanoes of the Antarctic plate and Southern Oceans. AGU Antarctic Research Series, vol 48, pp 19–25.

LeMasurier, W.E., Choi, S.H., Kawachi, Y., Mukasa, S.B., Rogers, N.W., 2011. Evolution of pantellerite-trachyte-phonolite volcanoes by fractional crystallization of basanite magma in a continental rift setting, Marie Byrd Land, Antarctica. Contrib. Mineral. Petrol. 162, 1175–1199.

Levy RH, Harwood DM 2000. Sedimentary lithofacies and depositional environments of the McMurdo Sound erratics. In: Stilwell JD, Feldmann RM eds. Paleobiology and Paleoenvironments of Eocene fossiliferous Erratics, McMurdo Sound, East Antarctica. American Geophysical Union, Antarctic Research Series 76. Pp. 39-61.

Licht, K., Jennings, A.E., Andrews, J.T., Williams, K., 1996. Chronology of late Wisconsin ice retreat from the western Ross Sea, Antarctica. Geology 24, 223-226.

Licht K. J., Fastook J. – 1998 – Constraining a numerical ice sheet model with geologic data over one ice sheet advance/retreat cycle in the Ross Sea. Chapman Conference on the West Antarctic Ice Sheet, University of Main, pp. 25-26.

Licht, K., Dunbar, N., Andrews, J.T., Jennings, A.E., 1999. Distinguishing subglacial till and glacial marine diamictons in the western Ross Sea, Antarctica: implications for a last glacial maximum grounding line. Geol. Soc. Am. Bull. 111, 91-103.

Licht, K., Andrews, J.T., 2002. A 14C record of late Pleistocene ice advance and retreat in the central Ross Sea, Antarctica. Arct. Alp. Res. 34, 324e333.

Licht, K.J., Lederer, J.R., Swope, R.J., 2005. Provenance of LGM glacial till (sand fraction) across the Ross Embayment, Antarctica. Quat. Sci. Rev. 24, 1499-1520.

Licht, K., Lederer, J., Farmer, G.L., Swope, R.J., Andrews, J.T., 2006. Petrographic and isotopic composition of Late Quaternary Ross Embayment till. Terra Antarct Rep. 12, 35-42.

Licht, K., Palmer, E.F., 2013. Glacial erosion and transport by Byrd Glacier, Antarctica during the Last Glacial Maximum. Quat. Sci. Rev. 62, 32-48.

Licht, K. J., A. J. Hennessy, and B. M. Welke, 2014. The U-Pb detrital zircon signature of West Antarctic ice stream tills in the Ross embayment, with implications for Last Glacial Maximum ice flow reconstructions, Antarct. Sci., 26, 687–697.

Lisker, F., & Olesch, M., 1998. Cooling and denudation history of western Marie Byrd Land, Antarctica, based on apatite fission-tracks. In Advances in Fission-Track Geochronology (pp. 225-240). Springer Netherlands.

Ludwig, K. R., 2003. User's manual for Isoplot 3.00: a geochronological toolkit for Microsoft Excel (No. 4). Kenneth R. Ludwig.

Luyendyk, B.P., Wilson, D.S., Siddoway, C.S., 2003. Eastern margin of the Ross Sea Rift in western Marie Byrd Land, Antarctica: Crustal structure and tectonic development. Geochem. Geophys. Geosystems 4, n/a-n/a. doi:10.1029/2002GC000462

Martin, A.P., Cooper, A.F., Dunlap, W.J., 2010. Geochronology of Mount Morning, Antarctica: two-phase evolution of a long-lived trachyte-basanite-phonolite eruptive center. Bull. Volcanol. 72, 357–371.

Massonne, H-J.; Schreyer, W. 1987. Phengite geobarometry based on the limiting assemblage with K-feldspar, phlogopite, and quartz. Contrib. Mineral. Petr. 96: 212-224.

McFadden, R.R., Siddoway, C.S., Teyssier, C., & Fanning, C.M., 2010a. Cretaceous oblique extensional deformation and magma accumulation in the Fosdick Mountains migmatite-cored gneiss dome, West Antarctica. Tectonics 29.

McFadden, R.R., Teyssier, C., Siddoway, C.S.,Whitney, D.L., & Fanning, C.M., 2010b. Oblique dilation, melt transfer, and gneiss dome emplacement. Geology 38, 375–378.

McGregor, V.R., Wade, F.A., 1969, Geology of the Western Queen Maud Mountains. American Geographical Society. Antarctic Map Folio Series (folio 12, plate 15).

McKay, R.M., Dunbar, G.B., Naish, T.R., Barrett, P.J., Carter, L., Harper, M., 2008. Retreat history of the Ross Ice Sheet (Shelf) since the Last Glacial Maximum from deep-basin sediment cores around Ross Island. Palaeogeogr. Palaeoclimatol. Palaeoecol. 260, 245-261.

McKay, R., Naish, T., Powell, R., Barrett, P., Scherer, R., Talarico, F., Kyle, P., Monien, D., Kuhn, G., Jackolski, C., Williams, T., 2012. Pleistocene variability of antarctic ice sheet extent in the Ross embayment. Quat. Sci. Rev. 34, 93-112.

McKay, R.M., Golledge, N.R., Maas, S., Naish, T., Levy, R., Dunbar, G., and Kuhn, G., 2016. Antarctic marine ice-sheet retreat in the Ross Sea during the early Holocene. *Geology*, 44(1): 7-10.

Mellish SD, Cooper AF, Walker NW 2002. The Panorama Pluton: a composite gabbro-monzodiorite, early Ross Orogeny intrusion in southern Victoria Land, Antarctica. In: Gamble JA, Skinner DNB, Henrys S ed. Antarctica at the close of a millennium. The Royal Society of New Zealand Bulletin 35: 129-141.

Mercer, J.H., 1968. Antarctic Ice and Sangamon Sea Level. In: International Association of Scientific Hydrology Symposia, vol. 79, pp. 217-225.

Menzies, J., van der Meer, J.J.M., Rose, J., 2006. Till e as a glacial "tectomict", its internal architecture, and the development of a "typing" method for till differentiation. Geomorphology 75, 172-200.

Minshew, V. H. 1967, Geology of the Scott Glacier and Wisconsin Range areas, central Transantarctic Mountains, Antarctica. Unpublished doctoral dissertation, Ohio State University.

Mosola, A.B., Anderson, J.B., 2006. Expansion and rapid retreat of the West Antarctic Ice Sheet in Eastern Ross Sea: possible consequence of over-extended ice streams? Quat. Sci. Rev. 25, 2177-2196.

Morimoto N. & Subcommittee Members, 1988. Nomenclature of pyroxenes. Mineral. Mag., 52, 535-550.

Mukasa, S.B., Dalziel, I.W.D., 2000. Marie Byrd Land, West Antarctica: Evolution of Gondwana's Pacific margin constrained by zircon U-Pb geochronology and feldspar common-Pb isotopic compositions. Geol. Soc. Am. Bull. 112, 611–627.

Murtaugh, J.G., 1969, Geology of the Wisconsin Range Batholith, Transantarctic Mountains, New Zealand Journal of Geology and Geophysics, v. 12, no. 2&3, p. 526-551.

Myrow, P. M.; Pope, M. C.; Goodge, J. W.; Fischer, W.; Palmer, A. R. 2002, Depositional history of pre-Devonian strata and timing of Ross orogenic tectonism in the central Transantarctic Mountains, Antarctica. Geological Society of America Bulletin 114: 1070-1088.

Naish, T., Powell, R., Levy, R., Wilson, G., Scherer, R., Talarico, F., Krissek, L., Niessen, F., Pompilio, M., Wilson, T., Carter, L., DeConto, R., Huybers, P., McKay, R., Pollard, D., Ross, J., Winter, D., Barrett, P., Browne, G., Cody, R., Cowan, E., Crampton, J., Dunbar, G., Dunbar, N., Florindo, F., Gebhardt, C., Graham, I., Hannah, M., Hansaraj, D., Harwood, D., Helling, D., Henrys, S., Hinnov, L., Kuhn, G.,

Kyle, P., Läufer, A., Maffioli, P., Magens, D., Mandernack, K., McIntosh, W., Millan, C., Morin, R., Ohneiser, C., Paulsen, T., Persico, D., Raine, I., Reed, J., Riesselman, C., Sagnotti, L., Schmitt, D., Sjunneskog, C., Strong, P., Taviani, M., Vogel, S., Wilch, T., Williams, T., 2009. Obliquity-paced Pliocene West Antarctic ice sheet oscillations. Nature 458, 322–328.

Orombelli, G., Baroni, C., Denton, G.H., 1990. Late Cenozoic glacial history of the Terra Nova Bay region, Northern Victoria Land, Antarctica. Geogr. Fis. Din. Quat. 13, 139-163.

Pankhurst, R. J., Weaver, S. D., Bradshaw, J. D., Storey, B. C., & Ireland, T. R., 1998. Geochronology and geochemistry of pre-Jurassic superterranes in Marie Byrd Land, Antarctica. J. Geophys. Res.- Sol. Ea., 103(B2), 2529-2547.

Panter, K.S., Hart, S.R., Kyle, P., Blusztanjn, J., Wilch, T., 2000. Geochemistry of Late Cenozoic basalts from the Crary Mountains: characterization of mantle sources in Marie Byrd Land, Antarctica. Chem. Geol. 165, 215–241.

Panter, K.S., Kyle, P.R., Smellie, J.L., 1997. Petrogenesis of a phonolite–trachyte succession at Mount Sidley, Marie Byrd Land, Antarctica. J. Petrol. 38, 1225–1253.

Panter, K.S., Talarico, F., Bassett, K., Del Carlo, P., Field, B., Frank, T., Hoffmann, S., Kuhn, G., Reichelt, L., Sandroni, S., Taviani, M., Bracciali, L., Cornamusini, G., von Eynatten, H., Rocchi, S., the ANDRILL-SMS Science Team, 2008. Petrologic and Geochemical Composition of the AND-2A Core, ANDRILL Southern McMurdo Sound Project, Antarctica. Terra Antartica 15, 147–192.

Paquette, J. L., & Tiepolo, M., 2007. High resolution (5 µm) U–Th–Pb isotope dating of monazite with excimer laser ablation (ELA)-ICPMS. Chem. Geol., 240(3), 222-237.

Parizek, B.R., Alley, R.B., 2004. Ice thickness and isostatic imbalances in the Ross Embayment, West Antarctica: model results. Glob. Planet. Chang. 42, 265-278.

Parizek, B.R., Alley, R.B., Hulbe, C.L., 2003. Subglacial thermal balance permits ongoing grounding line retreat along the Siple Coast of West Antarctica. Ann. Glaciol. 36, 251-256.

Paulsen, T., Encarnacion, E., Valencia, V.A., Roti Roti, J.M., Rasoazanamaranay, C., 2011. Detrital U-Pb zircon analysis of an Eocene McMurdo Erratic sandstone, McMurdo Sound, Antarctica. N. Z. J. Geol. Geophys. 54, 353–360.

Perotti, M., B. Andreucci, F. Talarico, M. Zattin, and A. Langone (2017), Multianalytical provenance analysis of Eastern Ross Sea LGM till sediments (Antarctica): Petrography,geochronology, andthermochronology detrital data,Geochem. Geophys. Geosyst., 18.

Pollard, D., DeConto, R.M., 2009. Modelling West Antarctic ice sheet growth and collapse through the past five million years. Nature 458, 329–332.

Pompilio, M., Dunbar, N., Gebhardt, A.C., Helling, D., Kuhn, G., Kyle, P., McKay, R., Talarico, F., Tulaczyk, S., Vogel, S., Wilch, T., 2007. Petrology and geochemistry of AND-1B Core, ANDRILL McMurdo Ice Shelf Project, Antarctica. Terra Antartica 14, 255-288.

Price, P.B., Walker, R.M., 1963. Fossil tracks of charged particles in mica and the age of minerals. J. Geophys. Res. 68, 4847-4862.

Read, S.E., Cooper, A.F., Walker, N.W., 2002. Geochemistry and U-Pb geochronology of the Neoproterozoic-Cambrian Koettlitz Glacier Alkaline Province, Royal Society Range, Transantarctic Mountains Antarctica. In: Gamble, J.A., Skinner, D.N.B., Henrys, S. (Eds.), Antarctica at the close of a millennium. The Royal Society of New Zealand Bulletin 35, Wellington, New Zealand, pp. 143–151.

Reiners, P.W., Brandon, M.T., 2006, Using Thermochronology to Understand Orogenic Erosion, Annu. Rev. Earth Pl. Sc., 34, 419-466.

Richard, S.M., Smith, C.H., Kimbrough, D.L., Fitzgerald, P.G., Luyendyk, B.P., McWilliams, M.O., 1994. Cooling history of the northern Ford Ranges, Marie Byrd Land, West Antarctica. Tectonics 13 (4), 837–857.

Riley, T.R., Flowerdew, M.J., Pankhurst, R.J., Leat, P.T., Millar, I.L., Fanning, C.M. and Whitehouse, M.J. 2016. A revised geochronology of Thurston Island, West Antarctica, and correlations along the proto-Pacific margin of Gondwana.- Antarctic Science.

Rocchi, S., LeMasurier,W., Di Vicenzo, G., 2006. Oligocene to Holocene erosion and glacial history in Marie Byrd Land,West Antarctica, inferred from exhumation of the Dorrel rock intrusive complex and from volcano morphologies. Geol. Soc. Am. Bull. 118,991–1005.

Rowell, A.J., Rees, M.N., and Evans, K.R., 1992, Evidence of major Middle Cambrian deformation in the Ross orogen, Antarctica: Geology, v. 20, p. 31–34.

Rowell, A.J., and Rees, M.N., 1989, Early Paleozoic history of the upper Beardmore Glacier area: Implications for a major Antarctic structural boundary within the Transantarctic Mountains: Antarctic Science, v. 1, p. 249–260.

Rowell, A.J., Gonzalez, D.A., McKenna, L.W., Evans, K.R., Stump, E., and Van Schmus, W.R., 1997, Lower Paleozoic rocks in the Queen Maud Mountains: Revised ages and significance, in Ricci, C.A., ed., The Antarctic Region: Geological Evolution and Processes: Siena, Italy, Terra Antarctica Publication, p. 201–207.

Saito, S., Brown, M., Korhonen, F.J., McFadden, R.R., Siddoway, C.S., 2013. Petrogenesis of Cretaceous mafic intrusive rocks, Fosdick Mountains, West Antarctica: Melting of the sub-continental arc mantle along the Gondwana margin. Gondwana Res. 23, 1567–1580.

Shipp, S., Anderson, J., Domack, E., 1999. Late Pleistocene-Holocene retreat of the West Antarctic Ice Sheet system in the Ross Sea: part 1-geophysical results. Geol. Soc. Am. Bull. 111, 1486-1516.

Siddoway, C., 2008. Tectonics of the West Antarctic rift system: new light on the history and dynamics of distributed intracontinental extension. In: Cooper, A.K.,Barrett, P.J., Stagg, H., Storey, B., Stump, E., Wise, W., 10th ISAES editorial team (Eds.),Antarctica: A Keystone in a Changing World, Proceedings of the 10th International Symposium on Antarctic Earth Sciences. The National Academies Press,Washington, DC, pp. 91–114.

Siddoway, C.S., Richard, S.M., Fanning, C.M., and Luyendyk,B.P., 2004a, Origin and emplacement of a Middle Cretaceous gneiss dome, Fosdick Mountains, West Antarctica, in Whitney, D.L., Teyssier, C., and Siddoway, C.S., eds., Gneiss Domes in Orogeny: Geological Society of America Special Paper 380, p. 267–294.

Siddoway, C.S., Baldwin, S.L., Fitzgerald, P.G., Fanning, C.M., & Luyendyk, B.P., 2004b. Ross Sea mylonites and the timing of intracontinental extensionwithin theWest Antarctic rift system. Geology 32, 57–60.

Siddoway, C.S., Fanning, C.M., 2009. Paleozoic tectonism on the East Gondwana margin: Evidence from SHRIMP U–Pb zircon geochronology of a migmatite–granite complex in West Antarctica. Tectonophysics 477, 262–277.

Siddoway, C. S., L. C. III Sass, and R. P. Esser, 2005. Kinematic history of the Marie Byrd Land terrane, West Antarctica: Direct evidence from Cretaceous mafic dykes, in Terrane Processes at the Margin of Gondwana, edited A. Vaughan, P. Leat, and R. J. Pankhurst, pp. 417–438, Geol. Soc. London, Special Pub. 246.

Simpson, G., Aslund, T., 1996. Diorite and gabbro of the Dromedary mafic complex, south Victoria Land, Antarctica. New Zealand Journal of Geology and Geophysics 39, pp. 403–414.

Simpson, A.L., Cooper, A.F., 2002. Geochemistry of the Darwin Glacier region granitoids, southern Victoria Land. Antarctic Science 14, pp. 425–426.

Skinner, D.N.B. 1964, A summary of the geology of the region between Byrd and Starshot glaciers, south Victoria Land. in ADIE, R.J., ed. Antarctic geology. Amsterdam: North-Holland Publishing Co., 284-292.

Skinner, D. N. B. 1965: Petrographic criteria of the rock units between the Byrd and Starshot glaciers, South Victoria Land, Antarctica. New Zealand Journal of Geology and Geophysics 8: 292-303.

Skinner, D.N.B., 1982. Stratigraphy and structure of lower grade metasediments of Skelton Group, McMurdo Sound — does Teall greywacke really exist? In: Craddock, C. (Ed.), Antarctic Geoscience. University of Wisconsin Press, Madison, pp. 555–563.

Skinner, N .B. 1983. The granites and two orogenies of Southern Victoria Land, Antarctica. In OLIVER,. L., JAMES, P.R. & JAGO, J.B., eds. Antarctic earth science. Canberra: Australian Academy of Science & Cambridge: Cambridge University Press, 160-163.

Smillie, R.W., 1992. Suite subdivision and petrological evolution of granitoids from the Taylor Valley and Ferrar Glacier region, south Victoria Land.Antarctic Science 4, 71–87.

Smith, C.H., 1996. Migmatites of the Alexandra Mountains, West Antarctica: Pressure-temperature conditions of formation and regional context: Geologisches Jahrbuch, v. B52, p. 169–178.

Spiegel, C., Lindow, J., Kamp, P. J. J., Gohl, K., 2016. Tectonomorphic evolution of Marie Byrd Land – Implications for Cenozoic rifting activity and onset of West Antarctic glaciation, Global Planet. Change, 145, 98-115.

Steiger, R. H.; Jäger, E.; 1977. Subcommission on geochronology: convention on the use of decay constants in geo- and cosmochronology: Earth and Planetary Science Letters, 36: 359-362.

Stilwell, J.D., Levy, R.H., Feldmann, R.M., Harwood, D.M., 1997. On the rare occurrence of Eocene Callianassid Decapods (Arthropoda) preserved in their burrows, Mount Discovery, East Antarctica. J. Paleontol. 71 (2), 284–287.

Stone, J.O., et al., 2003. Holocene deglaciation of Marie Byrd Land, West Antarctica. Science 299, 99-102.

Storey, B. C., P. T. Leat, S. D. Weaver, J. D. Pankhurst, and S. Kelley, 1999. Mantle plumes and Antarctic-New Zealand rifting: Evidence from mid-Cretaceous mafic dykes, J. Geol. Soc., 156, 659–671.

Storti, F., Balestrieri, M.L., Balsamo, F., Rossetti, F., 2008. Structural and thermochronological constraints to the evolution of the West Antarctic Rift System in central Victoria Land. Tectonics 27, TC4012.

Sugden, D. E., Balco G. A., Cowdery S. G., Stone, J. O. and Sass L. C., 2005. Selective glacial erosion and weathering zones in the coastal mountains of Marie Byrd Land, Antarctica.- Geomorphology 67: 317-334.

Stuiver, M., Denton, G.H., Hughes, T., Fastook, J., 1981. History of the Marine Ice Sheet in West Antarctica during the last glaciation. In: Denton, G., Hughes, T. (Eds.), The Last Great Ice Sheets. Wiley Interscience, New York, pp. 319-436.

Stump, E., 1982, The Ross Supergroup in the Queen Maud Mountains, in Craddock, C., ed., Antarctic geoscience: Madison, University of Wisconsin Press, p. 565–569.

Stump, E., 1985. Stratigraphy of the Ross Supergroup, central Transantarctic Mountains. Antarctic Research Series 36, 225–274.

Stump, E., 1995, The Ross orogen of the Transantarctic Mountains: Cambridge, UK, Cambridge University Press, 284 p.

Stump, E., Gootee, B.F., Talarico, F., Van Schmus, W.R., Brand, P.K., Foland, K.A., Fanning, C.M., 2004. Correlation of Byrd and Selbourne Groups, with implications for the Byrd Glacier discontinuity, central Transantarctic Mountains. New Zealand Journal of Geology and Geophysics 47, 157–171.

Suttner, L.J., 1974. Sedimentary petrographic provinces: an evaluation. In: Ross, C.A. (Ed.), Paleogeographic Provinces and Provinciality. SEPM Special Publication, Vol. 21, pp. 75–84.

Suttner, L.J., Basu, A., Mack, G.H., 1981. Climate and the origin of quartz arenites. Journalof Sedimentary Petrology 51, 1235–1246.

Tagami, T., O'Sullivan, P.B., 2005. Fundamentals of fission-track thermochronology. Rev. Mineral. Geochem. 58,19-47.

Talarico, F.M., Stump, E., Gootee, B.F., Foland, K.A., Palmeri, R., van Schmus, W.R., Brand, P.K., and Ricci, C.A., 2007, First evidence of "Barrovian"-type metamorphic regime in the Ross orogen of Byrd Glacier area, Central Transantarctic Mountains: Antarctic Science, v. 19, p. 451–470.

Talarico, F.M., Sandroni, S., 2009. Provenance signatures of the Antarctic Ice Sheets in the Ross Embayment during the Late Miocene to Early Pliocene: The ANDRILL AND-1B core record. Glob. Planet. Change 69, 103–123.

Talarico, F. M., and S. Sandroni (2011), Early Miocene basement clasts in ANDRILL AND-2A core and their implications for paleoenvironmental changes in the McMurdo Sound region (western Ross Sea, Antarctica), Global Planet. Change, 78, 23–35.

Talarico, F.M., Pace, D., Sandroni, S., 2011. Amphibole-bearing metamorphic clasts in ANDRILL AND-2A core: A provenance tool to unravel the Miocene glacial history in the Ross Embayment (western Ross Sea, Antarctica). Geosphere GES00653–1.

Talarico, F.M., McKay, R.M., Powell, R.D., Sandroni, S., Naish, T., 2012. Late Cenozoic oscillations of Antarctic ice sheets revealed by provenance of basement clasts and grain detrital modes in ANDRILL core AND-1B. Glob. Planet. Change 96-97, 23-40.

Talarico, F.M., Pace, D., Levy, R.H., 2013. Provenance of basement erratics in Quaternary coastal moraines, southern McMurdo Sound, and implications for the source of Eocene sedimentary rocks. Antarct. Sci. 25, 681–695.

The RAISED Consortium, Michael J. Bentley, Colm Ó Cofaigh, John B. Anderson, Howard Conway, Bethan Davies, Alastair G.C. Graham, Claus-Dieter Hillenbrand, Dominic A. Hodgson, Stewart S.R. Jamieson, Robert D. Larter, Andrew Mackintosh, James A. Smith, Elie Verleyen, Robert P. Ackert, Philip J. Bart, Sonja Berg, Daniel Brunstein, Miquel Canals, Eric A. Colhoun, Xavier Crosta, et al. 2014. A community-based geological reconstruction of Antarctic Ice Sheet deglaciation since the Last Glacial Maximum, Quaternary Science Reviews, v. 100, pp 1-9.

Tiepolo, M., 2003. In situ Pb geochronology of zircon with laser ablation–inductively coupled plasma–sector field mass spectrometry. Chem. Geol., 199(1), 159-177.

Tokuhashi S., Agyingi C. M. & Nishimura A. - 1996 - Areal and vertical variation of heavy mineral composition of the surface sediments, Ross Sea, Antarctica. Proc. NIRP Symposium Antarctic Geoscience n. 9, pp. 127-140.

Tulaczyk S., Kamb B., Scherer R. P. & Engelhardt H. F. – 1998 - Sedimentary processes at the base of a West Antarctic ice stream: constraints from textural and compositional properties of subglacial debris. Journal of Sedimentary Research, vol. 68, no. 3, pp. 487-496.

Tulloch, A.J., Ramezani, J., Kimbrough, D.L., Faure, K., and Allibone, A.H., 2009. U-Pb geochronology of mid-Paleozoic plutonism in western New Zealand; implications for S-type granite generation and growth of the east Gondwana margin: Geological Society of America Bulletin, v. 121, p. 1236–1261.

van der Meer, J.J.M., 1993. Microscopic Evidence of Subglacial Deformation. Quaternary Science Reviews 12, 553-587.

Van Achterbergh, E., Ryan, C. G., Jackson, S. E., & Griffin, W. L., 2001. Data reduction software for LA-ICP-MS. Laser-Ablation-ICPMS in the earth sciences—principles and applications. Miner. Assoc. Can. (short course series), 29, 239-243.

Vermeesch, P., 2012. On the visualisation of detrital age distributions. Chem. Geol., 312, 190-194.

Vogel, S. W., S. Tulaczyk, S. Carter, P. Renne, B. Turrin, and A. Grunow (2006), Geologic constraints on the existence, distribution of West Antarctic subglacial volcanism, Geophys. Res. Lett., 33, L23501.

Wade, F. A., C. A. Cathey, and J. B. Oldham, 1977a. Reconnaissance geologic map of the Guest Peninsula quadrangle, Marie Byrd Land, Antarctica, Map A-7, U. S. Antarc. Res. Program, Reston, Va.

Wade, F. A., C. A. Cathey, and J. B. Oldham, 1977b. Reconnaissance geologic map of the Boyd Glacier quadrangle, Marie Byrd Land, Antarctica, Map A-6., U. S. Antarc. Res. Program, Reston, Va.

Wade, F. A., C. A. Cathey, and J. B. Oldham, 1977c. Reconnaissance geologic map of the Alexandra Mountains quadrangle, Marie Byrd Land, Antarctica, Map A-5, U. S. Antarc. Res. Program Reston, Va.

Wade, F. A., C. A. Cathey, and J. B. Oldham, 1978. Reconnaissance geologic map of the Gutenko Nunataks quadrangle, Marie Byrd Land, Antarctica, Map A-11, U. S. Antarc. Res. Program, Reston, Va.

Weaver, S. D., J. D. Bradshaw, and C. J. Adams, 1991. Granitoids of the Ford Ranges, Marie Byrd Land, Antarctica, in Geological Evolution of Antarctica, edited by M. R. A. Thompson et al., pp. 345 – 351, Cambridge Univ. Press, Cambridge, Mass.

Weaver, S.D., Adams, C.J., Pankhurst, R.J., & Gibson, I.L., 1992. Granites of Edward VII Peninsula, Marie Byrd Land: anorogenic magmatism related to Antarctic-New Zealand rifting. In: Brown, E., Chappell, B.W. (Eds.), Proceedings of the Second Hutton Symposium on the Origin of Granites and Related Rocks. Transactions of the Royal Society Edinburgh - Earth Sciences, pp. 281–290.

Weaver, S. D., Storey, B. C., Pankhurst, R. J., Mukasa, S. B., DiVenere, V. J., & Bradshaw, J. D., 1994. Antarctica-New Zealand rifting and Marie Byrd Land lithospheric magmatism linked to ridge subduction and mantle plume activity. Geology, 22(9), 811-814.

Wheterill, G. W.; 1956. Discordant uranium-lead ages: Transactions of the American Geophysical Union, 37: 320-326.

Wilson, G.S., 2000. Glacial geology and origin of fossiliferous-erratic-bearing moraines, southern McMurdo Sound, Antarctica - an alternative ice sheet hypothesis. In: Stilwell, J.D., Feldmann, R.M. (Eds.), Paleobiology and Paleoenvrionments of Eocene Rocks, McMurdo Sound, East Antarctica. American Geophysical Union, Washington, D. C., pp. 19-37

Wright, A.C., Kyle, P.R., 1990a, A.25, Taylor and Wright Valleys. In: LeMasurier, W.E., Thomson J.W. eds.. Volcanoes of the Antarctic Plate and Southern Oceans. Antarctic Research Series, 48, Washington DC, American Geophysical Union, pp. 131-133.

Wright, A.C., Kyle, P.R., 1990b, A.24, Royal Society Range. In: LeMasurier, W.E., Thomson J.W. eds.. Volcanoes of the Antarctic Plate and Southern Oceans. Antarctic Research Series, 48, Washington DC, American Geophysical Union, pp. 134-135.

Wright-Grassham AC (1987) Volcanic geology, mineralogy, and petrogenesis of the Discovery Volcanic Subprovince, Southern Victoria Land, Antarctica. PhD thesis, New Mexico Institute of Mining and Technology, Socorro.

Yakymchuk, C., Brown, C.R., Brown, M., Siddoway, C.S., Fanning, C.M., Korhonen, F.J., 2015. Paleozoic evolution of western Marie Byrd Land, Antarctica. Geol. Soc. Am. Bull. 127, 1464–1484.

APPENDIX A: Thin section petrographic descriptions

The following section show petrographic descriptions of pebbles and cobbles found in the sampled piston core discussed in this thesis (Chapters III and IV). These descriptions are associated with two micrographs taken in plane polarized light and/or in crossed polarized light. Nomenclature follows the names used elsewhere in the text and in the related tables. Thin section ID is a progressive number from 1 to 107 that follows simply the order of thin sections manufacturing. Each ID is followed in brackets by the specification of sampling sites, i.e. Name of cruise-Piston core number-Progressive number of logged Pebbles- Sampling depth (Top and Bottom) expressed in centimeters below sea floor.

Thin section 1 (NBP-96-01-Piston core 11-Pebble 3-Top: 261; Bottom:262)

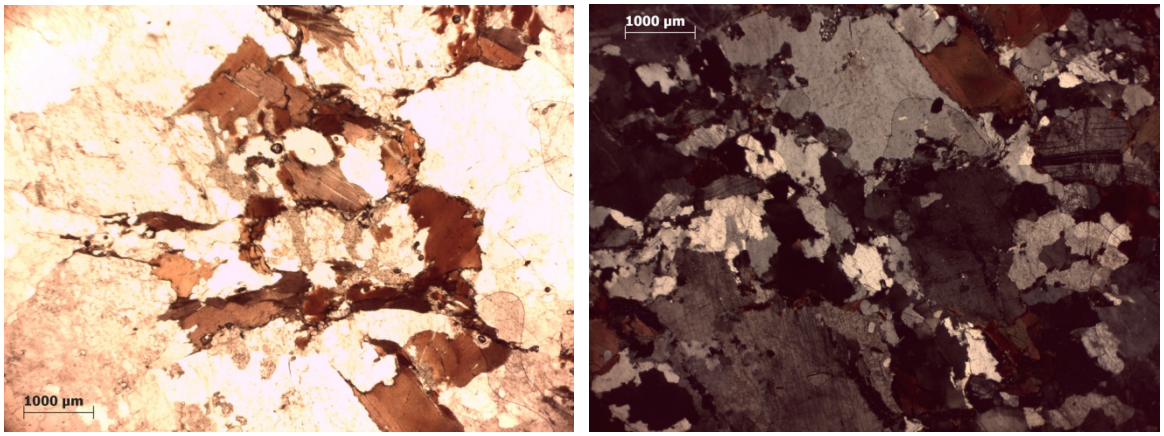

The rock has a slightly etero-granular medium grained igneous hypidiomorphic texture defined by slightly porphyritic plagioclase and minor k-feldspar associated with euedral to anhedral biotite flakes, sometimes replaced by secondary chlorite. Quartz is interstitial and exhibits prevalently an ondulouse extinction with sutured grain boundaries. Accessory minerals are opaques, apatite, zircon. The rock is a biotite-granodiorite.

Thin section 3 (NBP-96-01-Piston core 11-Pebble 6-Top: 295; Bottom:297)

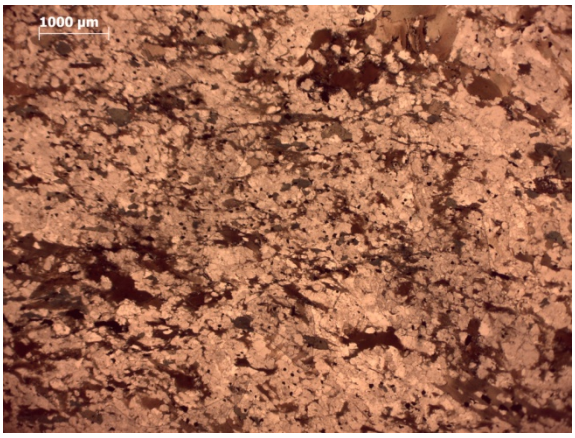

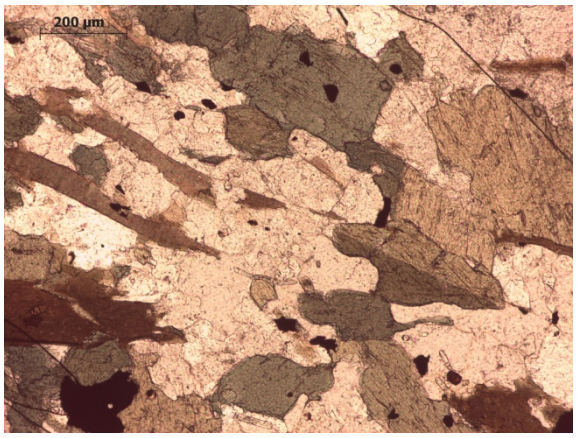

The rock has an equigranular to slightly etero-granular fine to medium grained, slightly lepido-nematoblastic texture defined by sub-idioblasts of biotite and green amphibole which define a weak foliation. Biotite often shows chloritization. Granoblastic domains are composed of fine grained xenoblasts of interstitial quartz and plagioclase that sometimes are enveloped by biotite flakes. Accessory minerals are opaques, apatite, zircon and rare epidote. The rock is a biotite-amphibole schist.

Thin section 4 (NBP-96-01-Piston core 11-Pebble 7-Top: 310; Bottom:312)

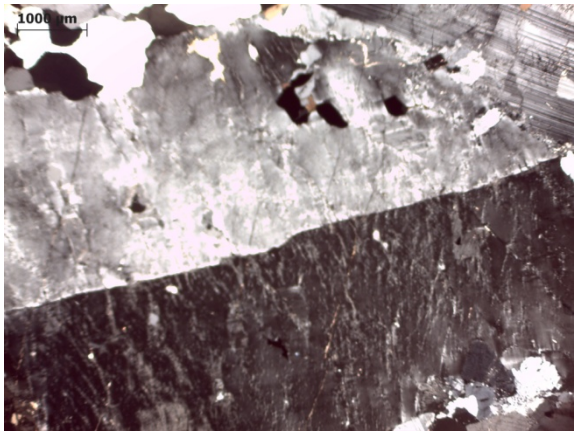

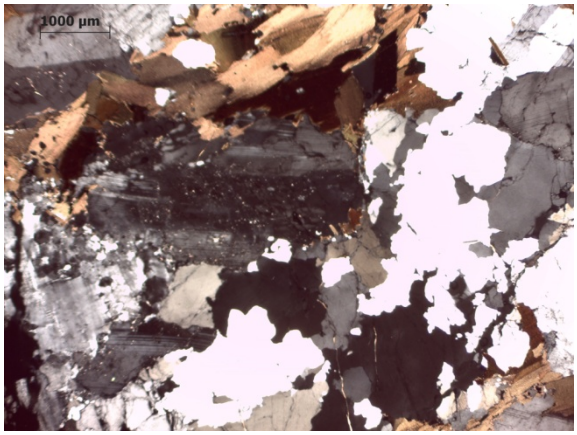

The rock has an etero-granular medium to coarse grained igneous porphyritic, hypidiomorphic and slightly foliated texture defined by orientation of perthitic orthoclase and minor plagioclase phenocrystals associated with brown biotite. Quartz is interstitial and shows ondulouse extinction. Accessory minerals are opaques, apatite and zircon. The rock is a biotite monzogranite.

Thin section 5 (NBP-96-01-Piston core 14-Pebble 7-Top: 43; Bottom:44)

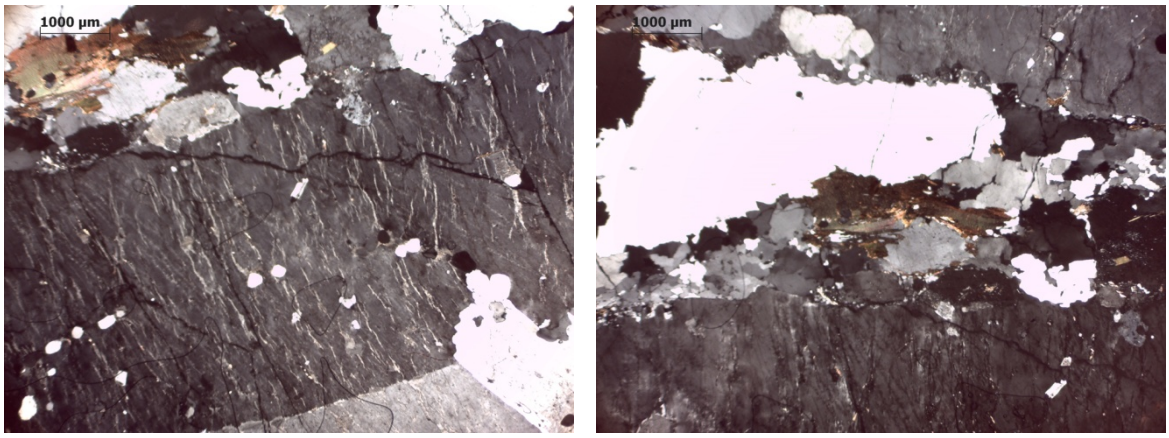

The rock has an etero-granular medium to coarse grained porphyritic, hypidiomorphic, slightly foliated igneous texture, defined by orientation of perthitic orthoclase phenocrystals (poikilitic with quartz and plagioclase), interstitial anhedral quartz with ondulouse extinction and brown biotite. Plagioclase is a minor phase. Accessory minerals include apatite, zircon and opaques. The rock is a biotite alkaline feldspar granite.

Thin section 6 (NBP-96-01-Piston core 14-Pebble 3-Top: 84; Bottom:85)

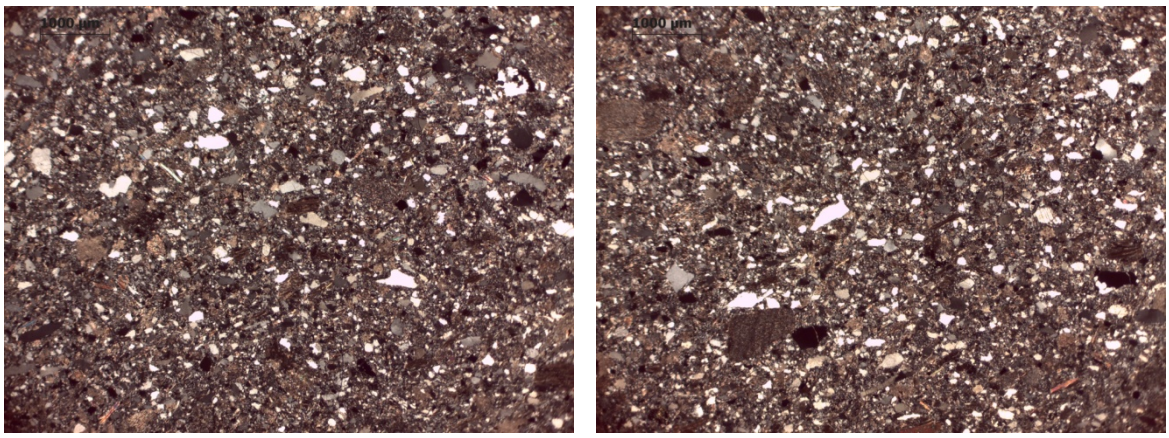

The rock shows an etero-granular fine to medium grained clastic texture defined by poorly sorted sub-angular to sub-rounded quartz (polycrystalline and monocrystalline, 80%), feldspars (2%) and lithic grains (18%), mainly of phylladic and sedimentary composition. Fine grained matrix constitutes up to 12% of the rock total volume; phyllosilicates cement and calcite patches are sparse. The rock is classified as a lithic arenite.

Thin section 7 (NBP-96-01-Piston core 16-Pebble 4-Top: 62; Bottom:65)

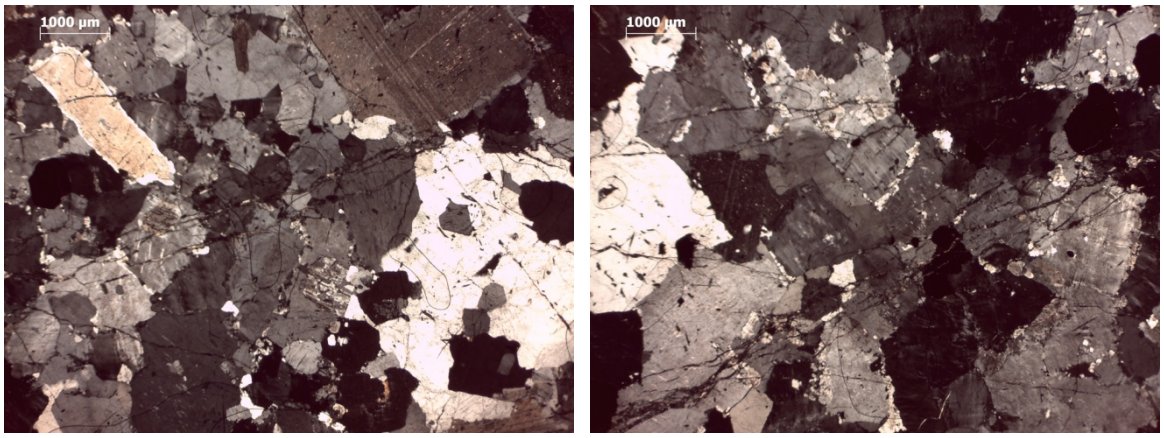

The rock has an equigranular to eterogranular medium grained, allotriomorphic to slightly hypidiomorphic igneous texture, defined by the association of perthitic orthoclase, plagioclase (sometimes altered in sericite aggregates), interstitial anhedral quartz and minor biotite. Accessory minerals include apatite and opaque minerals. The rock is classified as lucocratic biotite-bearing syeno-granite.

Thin section 8 (NBP-96-01-Piston core 16-Pebble 5-Top: 62; Bottom:65)

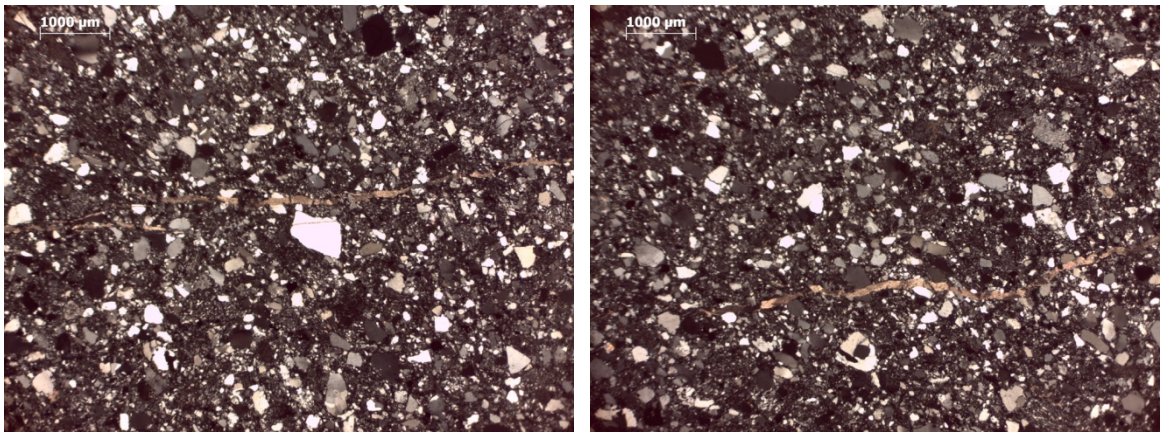

The rock has an etero-granular medium grained clastic texture defined by poorly sorted sub-angular to sub-rounded quartz (90%), feldspar (2%) and lithic grains (8%) of mainly sedimentary composition; grains are set in a very fine grained quartzo-feldspathic matrix that constitutes up to 16% of the total rock volume. Some thin veins are filled with carbonates. The rock is classified as a graywacke.

Thin section 9 (ELT 32-Piston core 27-Pebble 14-Top: 117; Bottom:118)

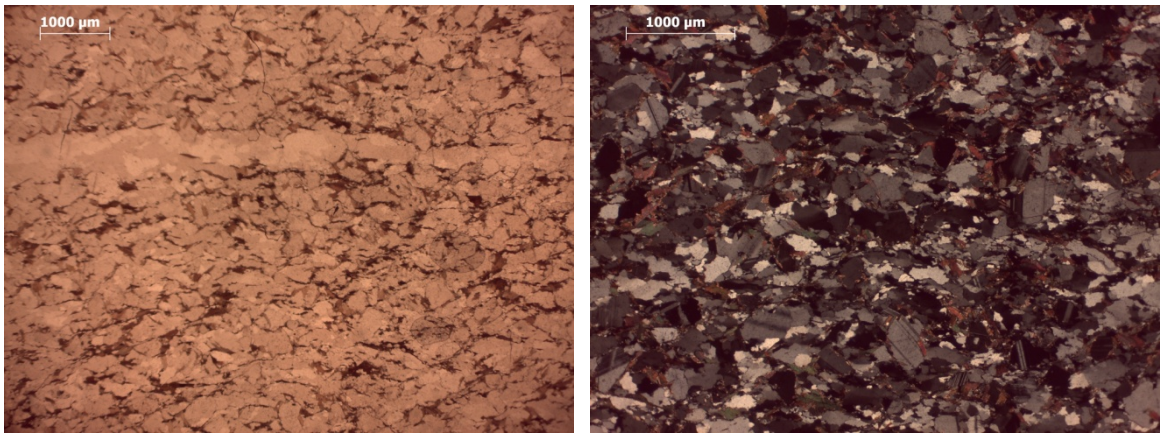

The rock has a mainly equigranular, fine grained, granolepidoblastic texture defined by a weak orientation of biotite idioblasts associated with polycrystalline quartz and plagioclase sub-idioblasts domains. Quartz has ondulouse extinction and often exhibits interlocking grain boundaries. Accessory minerals include apatite and zircon. The rock is classified as a biotite-plagioclase schist.

Thin section 10 (NBP-96-01-Piston core 08-Pebble 1-Top: 99; Bottom:100)

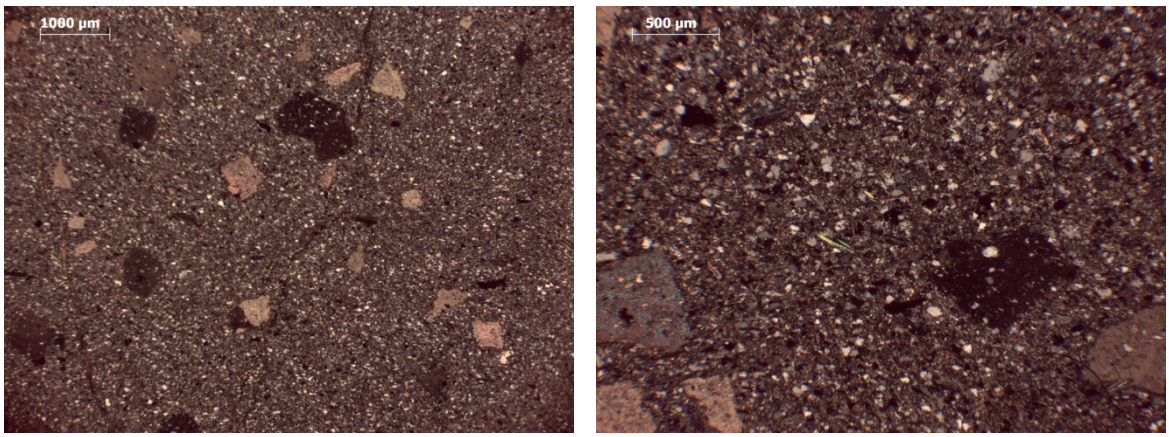

The rock has an equigranular fine grained clastic texture constituted by detrital grains made up of quartz (95%), feldspars (2%) and lithics (<1%), set in a very fine grained quartz and phyllosilicate-rich matrix ; detrital white micas and opaque minerals are also present in a lesser amount. Some larger grains of poikiloblastic calcite define a spotted texture. The rock is classified as a meta-siltstone.

Thin section 11 (NBP-96-01-Piston core 08-Pebble 2-Top: 111; Bottom:112)

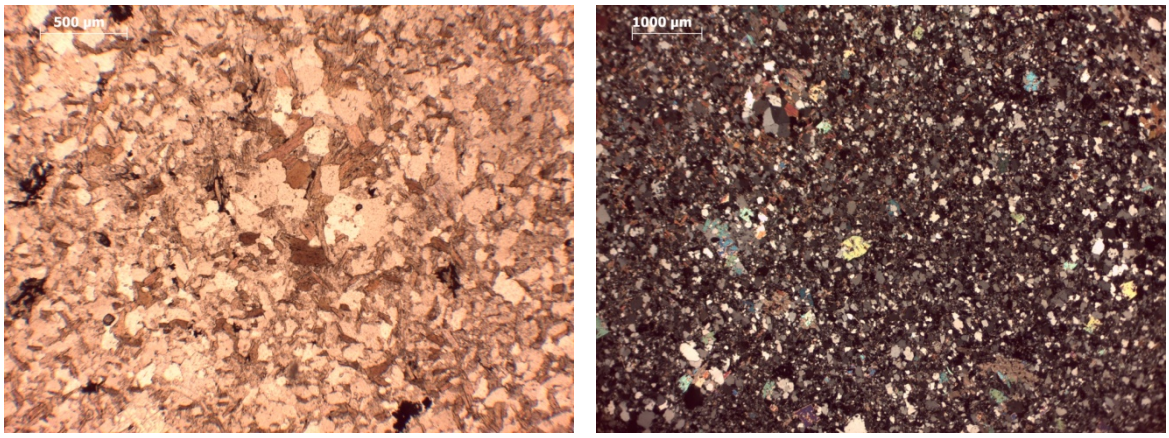

The rock has an equigranular, fine to medium sand-sized clastic texture, defined by detrital quartz grains (97%), feldspars (1%) and rare lithics. Randomly oriented biotite-chlorite lamellae and white mica neoblastic and in some cases poikiloblastic aggregates define a spotted texture. Accessory minerals include opaques, apatite and zircon. The rock is classified as a meta-sandstone (hornfels).

Thin section 12 (NBP-99-02-Piston core 17-Pebble 3-Top: 16; Bottom:19)

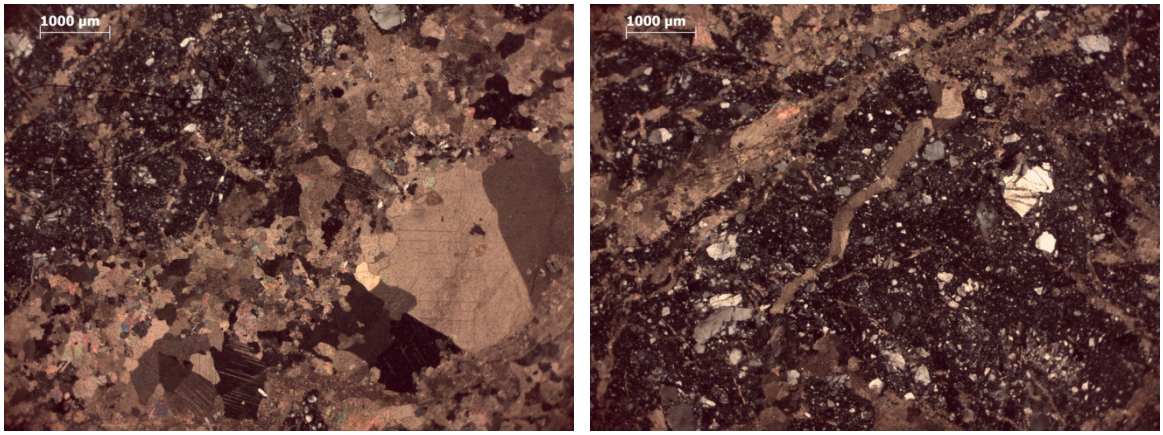

The rock has an eterogranular fine to medium sand-sized clastic texture, defined mainly by sub-angular to angular quartz grains set in a very fine grained argillaceous black matrix, and appears to be very disturbed by fractures and veins filled with carbonates, which cover the largest area of the thin section. The rock is classified as a fine grained breccia, with post-depositional fracturing.

Thin section 13 (NBP-99-02-Piston core 17-Pebble 1-Top: 1; Bottom:3)

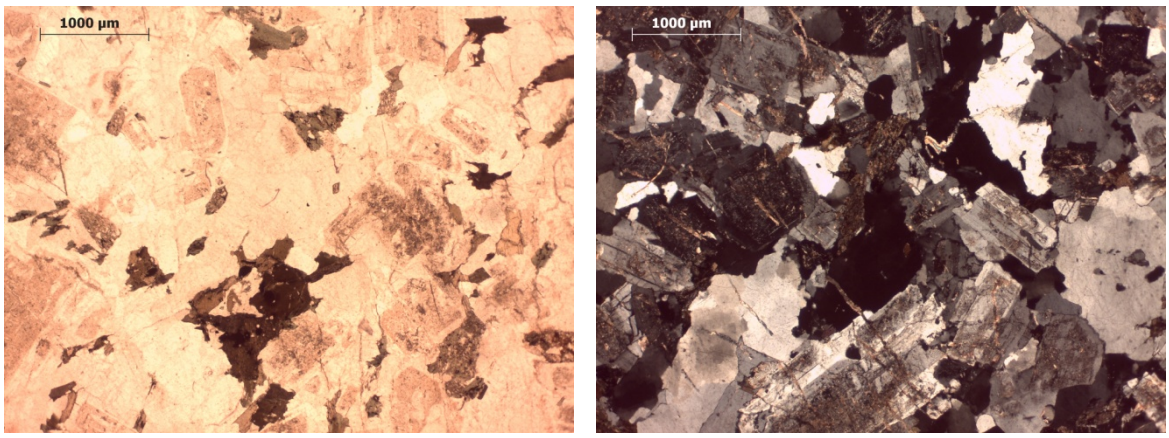

The rock has a slightly eterogranular, medium grained, igneous hypidiomorphic texture defined by the association of sub-euhedral plagioclase (often altered in sericite aggregates), minor alkaline feldspar, anhedral quartz (with ondulouse extinction and interlocking grain boundaries) and brown biotite lamellae, often replaced by chlorite. Accessory minerals include opaques, apatite and zircon. The rock is classified as a biotite tonalite.

Thin section 15 (DF83-Piston core 14-Pebble 16-Top: 241; Bottom:245)

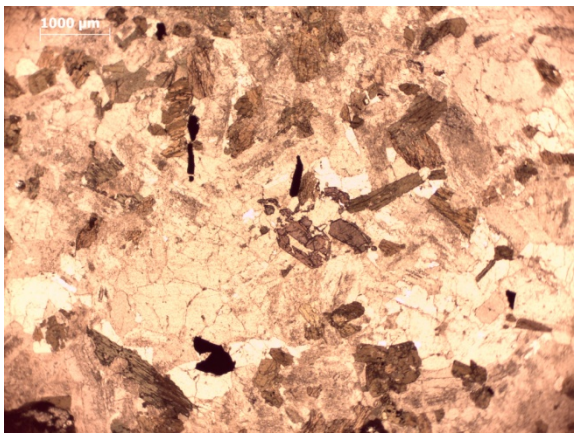

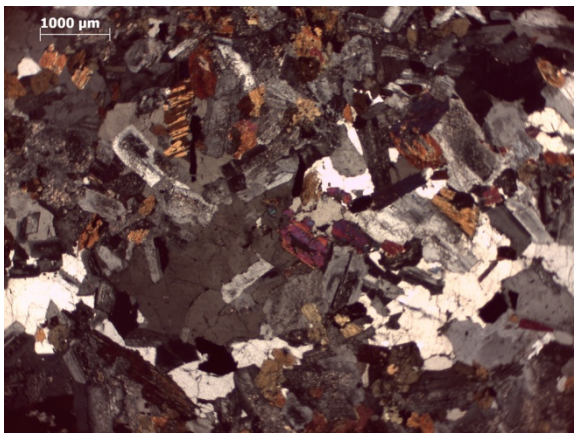

The rock has a mainly equigranular, medium grained, igneous hypidiomorphic texture defined by the association of sub-euhedral plagioclase (often altered in sericite aggregates), interstitial anhedral quartz with ondulouse extinction and minor alkaline feldspar. Mafic minerals are represented by light brown altered amphibole and biotite lamellae, often replaced by chlorite. Accessory minerals include titanite, opaques, apatite and zircon. The rock is quite altered and is classified as a biotite-hornblende tonalite.

Thin section 16 (DF83-Piston core 14-Pebble 17-Top: 252; Bottom:256)

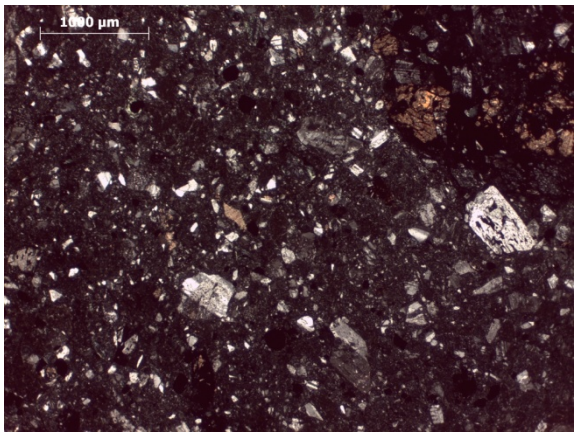

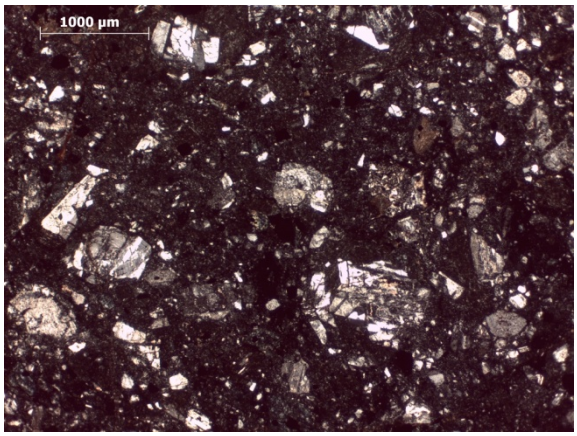

The rock has an eterogranular, porphyritic igneous texture defined by euhedral medium grained plagioclase phenocrystals and completely altered clinopyroxenes phenocrystals set in a very fine grained microcrystalline quartzo-feldspathic groundmass which is difficult to examine under standard microscope magnifiers. Some fine grained calcite pseudomorphs are sparse in the groundmass. The rock is globally very altered, and is classified as a meta-clynopyroxene porphyry.

Thin section 17 (NBP94-07-Piston core 57-Pebble 2-Top: 15; Bottom:16)

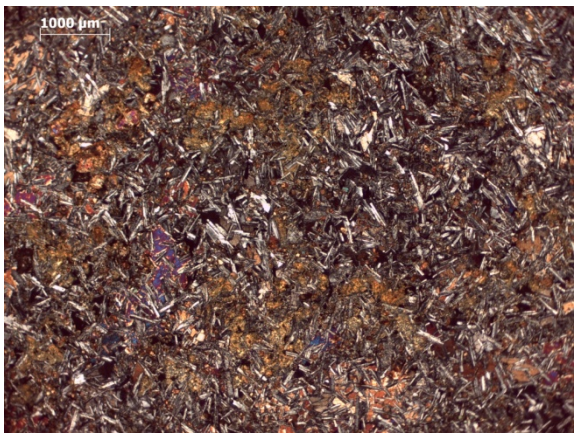

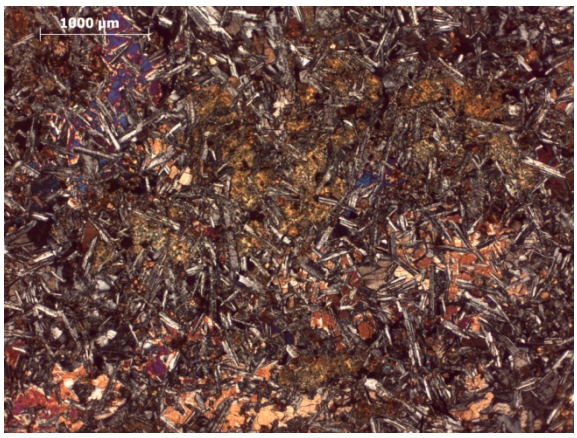

The rock has an eterogranular, fine to medium grained, igneous sub-ophitic texture defined by the association of brownish clinopyroxenes, opaque minerals and fine grained plagioclase laths that are sometimes partially included in larger sized clinopyroxenes. Interstitial rare olivine crystals are present, although they are completely altered in calcite. Some chlorite aggregates are also present as secondary alteration on clinopyroxenes. The rock is classified as fine grained dolerite.

Thin section 18 (NBP94-07-Piston core 57-Pebble 3-Top: 36; Bottom:37)

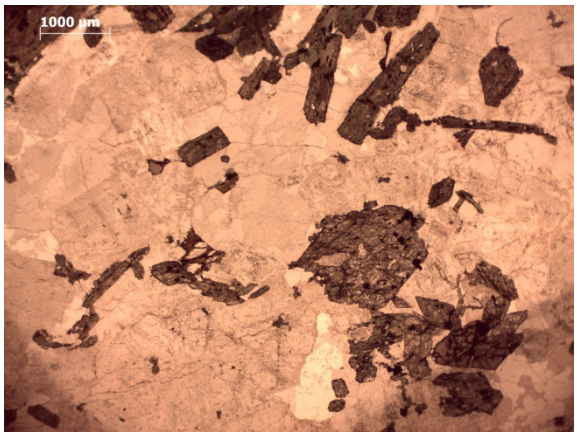

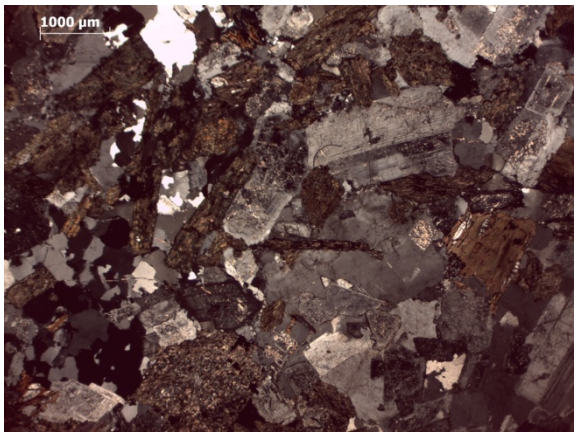

The rock has a medium grained, slightly eterogranular, hypidiomorphic igneous texture, defined by slightly oriented sub-euhedral plagioclase crystals (often altered in sericite aggregates), interstitial anhedral quartz grains and minor alkaline feldspar. Mafic minerals are represented by brown sub-euhedral very altered amphibole and biotite lamellae, almost completely replaced by chlorite. Accessory minerals include titanite, apatite , zircon and opaques. Some thin carbonate veins are present. Overall, the rock is quite altered, and it is classified as a biotite-hornblende tonalite.

Thin section 19 (NBP94-07-Piston core 58-Pebble 2-Top: 113; Bottom:117)

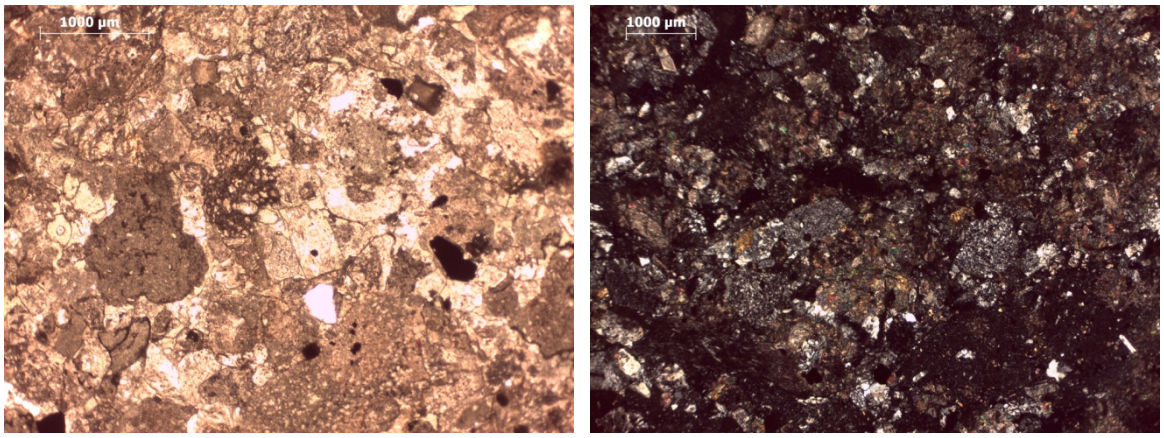

The rock has an eterogranular, medium to coarse grained, clastic texture defined by, where discernable, lithic fragments, mainly of volcanic composition; some feldspar phenocrysals are also present, set in a fine grained altered matrix. The rock is strongly altered by chlorite and epidote aggregates, that overprint the original texture, both among clasts and matrix. The rock is classified as a meta-volcanoclastite.

Thin section 20 (NBP94-07-Piston core 63-Pebble 3-Top: 213; Bottom:214)

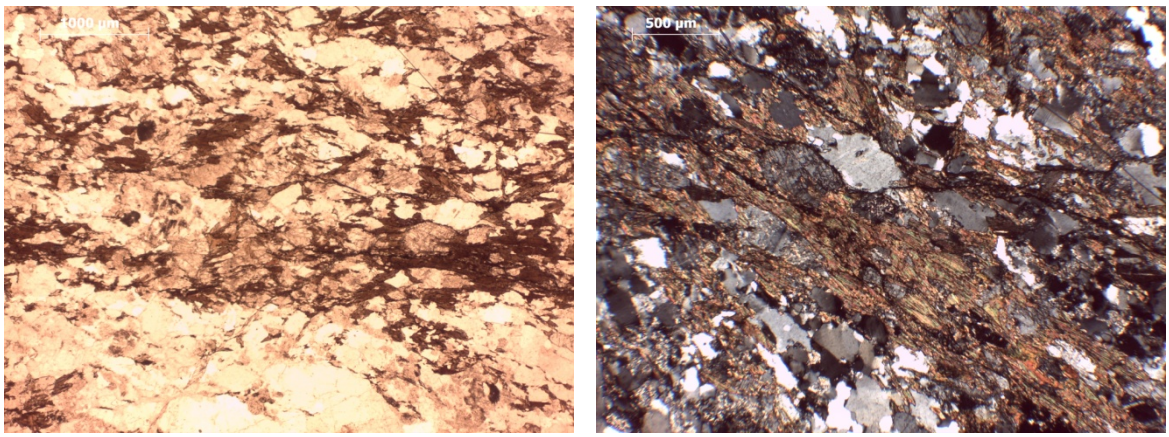

The rock has a fine to medium grained grano-lepido-nematoblastic texture, with foliation defined by idioblasts of brown biotite lamellae and peciloblastic brown actinolitic amphibole. Granoblastic domains are defined by quartz (ondulouse extinction) and plagioclase blasts association. Accessory minerals include apatite, zircon and titanite. The rock is classified as a biotite-actinolite schist.

Thin section 21 (NBP99-02-Piston core 04-Pebble 1-Top: 8; Bottom:9)

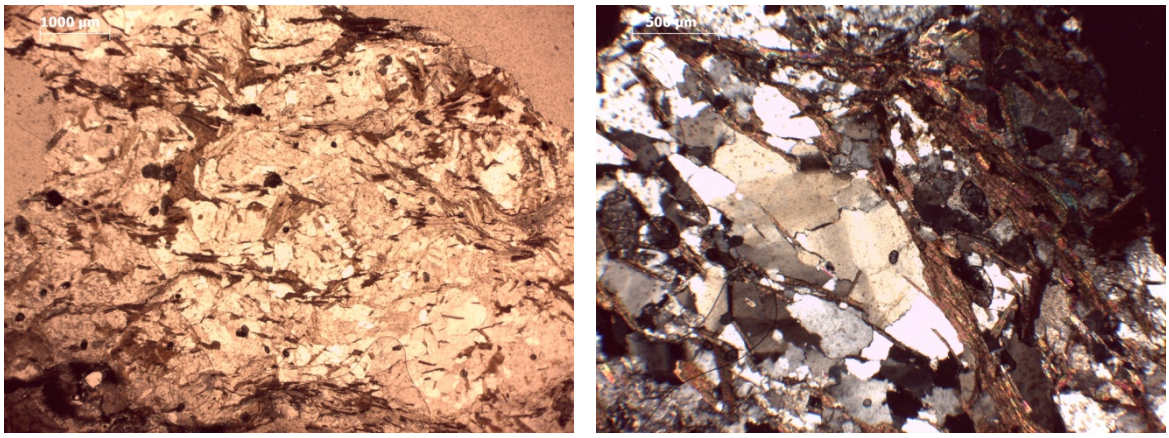

The rock has a slightly crenulated fine to medium grained lepidoblastic texture defined by the orientation of brown biotite and white mica sub-idioblasts; granoblastic domains are defined by quartz and plagioclase xenoblasts. Accessory minerals include apatite and tourmaline. The rock is classified as a gneissic biotite-white mica schist.

Thin section 22 (NBP99-02-Piston core 04-Pebble 6-Top: 34; Bottom:35)

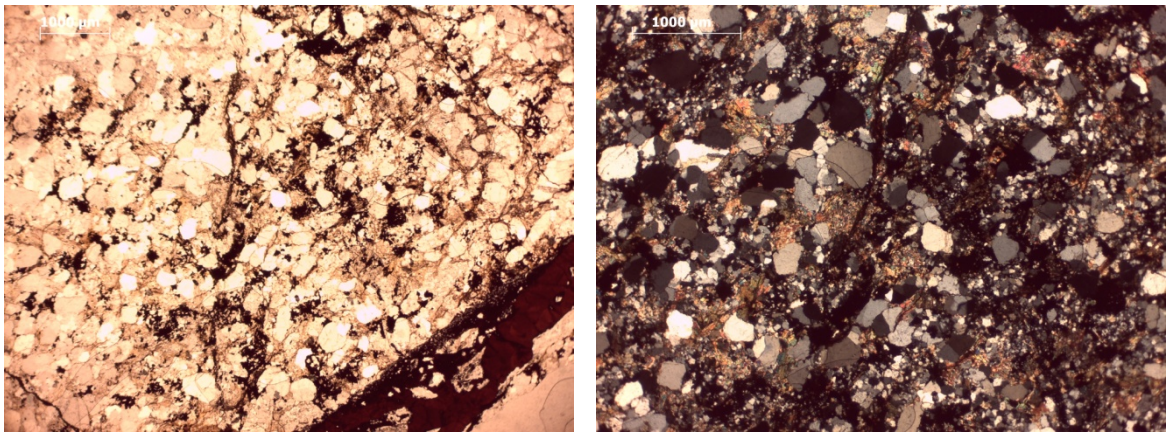

The rock has an heterogranular fine to medium metaclastic texture defined by grains of quartz and feldspars which in place show a granoblastic texture with interlocking and stretched grain boundaries. Sericite patches envelope clastic grains and in place show acicular habit. The rock is characterized by cataclastic and brecciated fine grained bands associated to widespread hematite and opaque minerals plagues. Chlorite and epidote are present as secondary alteration phases. The rock is classified as a metasandstone.

Thin section 23 (NBP99-02-Piston core 04-Pebble 12-Top: 92; Bottom:93)

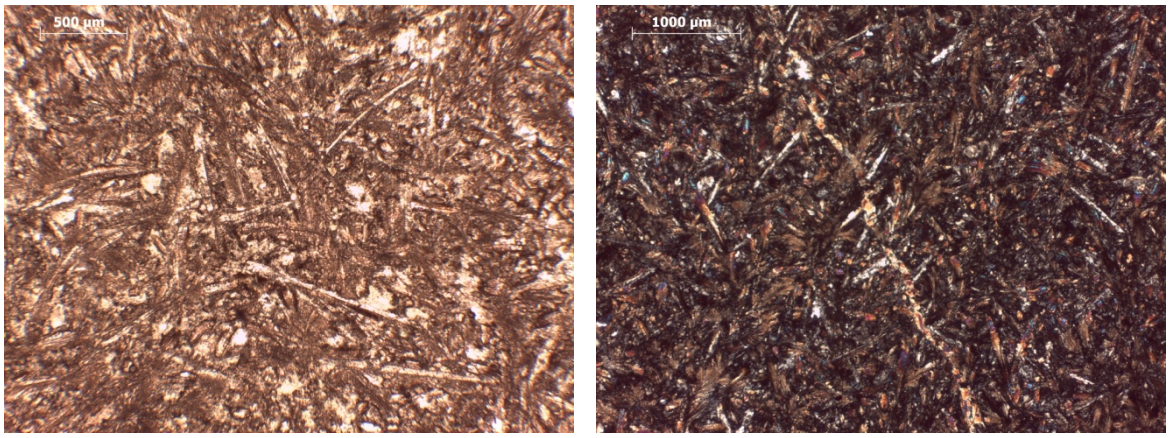

The rock has an equigranular, fine grained, in places slightly spherulitic, olocrystalline igneous texture. It is defined by elongated radial crystals of altered brown clinopyroxenes and interstitial plagioclase, opaque minerals and rare quartz set in a very fine grained matrix. Sometimes clynopyroxenes are chloritized. The rock is classified as a dolerite.

Thin section 24 (DF76-Piston core 03-Pebble 5-Top: 397; Bottom:399)

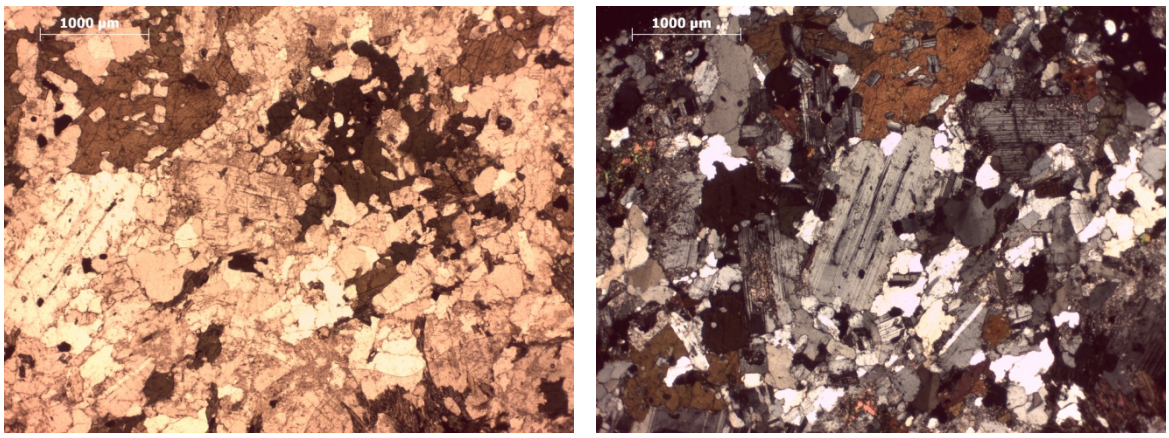

The rock has an inequigranular, fine to medium grained, hypidiomorphic, slightly porphyritic igneous texture. Plagioclase is slightly porphyritic, medium grained, while interstices are filled with fine grained anhedral quartz and minor ortochlase. Mafic phases are represented by slightly oriented brownish to greenish amphiboles, sometimes pecilitic with fine grained plagioclase laths, and altered biotite flakes. Epidote sometimes alters amphibole crystals. The rock is classified as a tonalite.

Thin section 25 (DF76-Piston core 03-Pebble 6-Top: 595; Bottom:599)

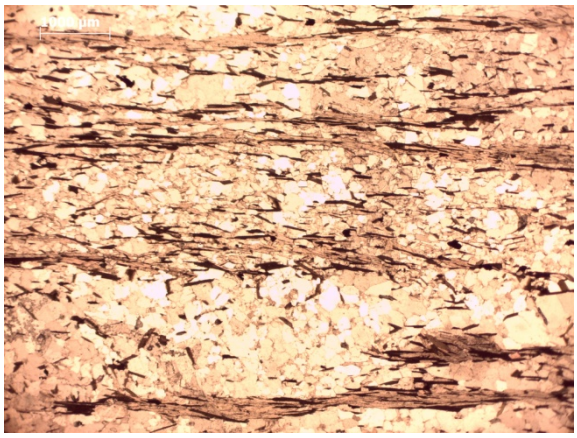

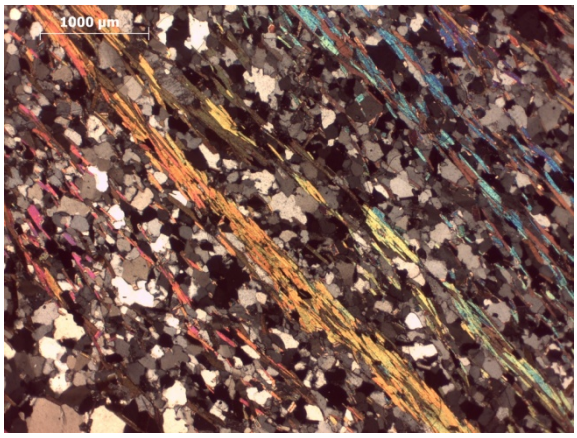

The rock has a fine grained, grano-lepidoblastic texture, with well developed and spaced foliation defined by orientation of biotite and white mica idioblasts and granoblastic domains defined by poligonal anhedral quartz and rare altered plagioclase. In places biotite is replaced by chlorite flakes. Apatite and zircon are present as accessory phases. The rock is classified as a biotite-white mica schist.

Thin section 26 (NBP94-07-Piston core 49-Pebble 1-Top: 13; Bottom:14)

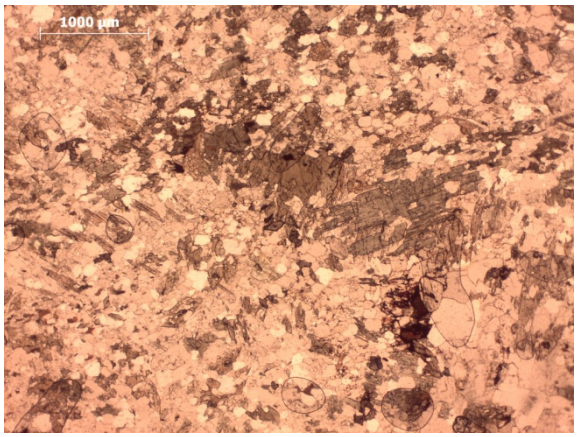

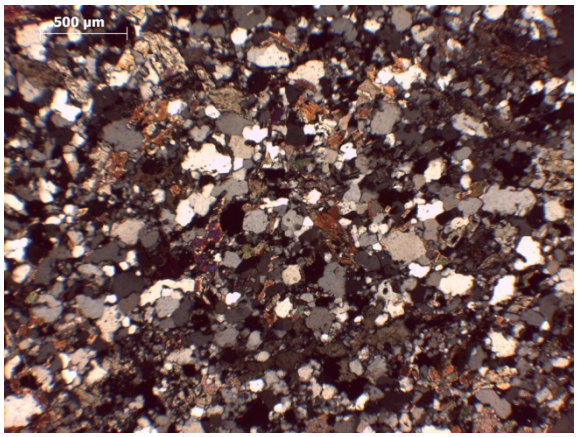

The rock has an heterogranular fine grained granoblastic texture defined by quartz grains domains , associated with rare plagioclase grains and calcite patches. Biotite xenoblasts define a weak foliation and are sometimes replaced by chlorite. Moreover randomly oriented pale green amphibole xenoblasts to idioblasts are scattered in the thin section. Titanite is present as accessory mineral. The rock is classified as a biotite-actinolite schistose metasandstone.

Thin section 27 (NBP94-07-Piston core 43-Pebble 1-Top: 184; Bottom:185)

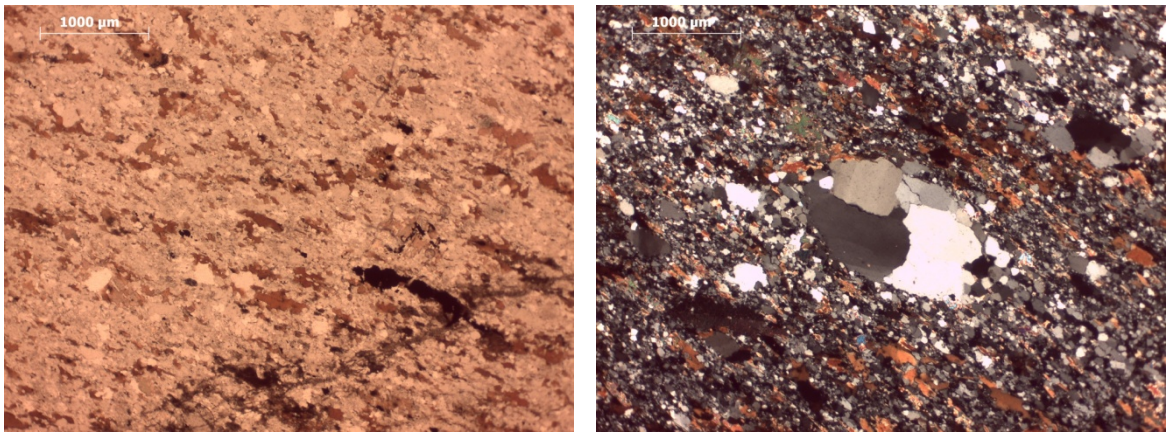

The rock has a slightly heterogranular fine to medium grained grano-lepidoblastic texture. Orientation of brown biotite xenoblasts to idioblasts, in some cases associated to opaque minerals, define a developed foliation. Granoblastic domains are constituted by heterogranular quartz xenoblasts and rare plagioclase. In places there are rare wollastonite and calcite patches. Accessory minerals are zircon, apatite and titanite. The rock is classified as a biotite schist.

Thin section 28 (NBP94-07-Piston core 78-Pebble 6-Top: 220; Bottom:223)

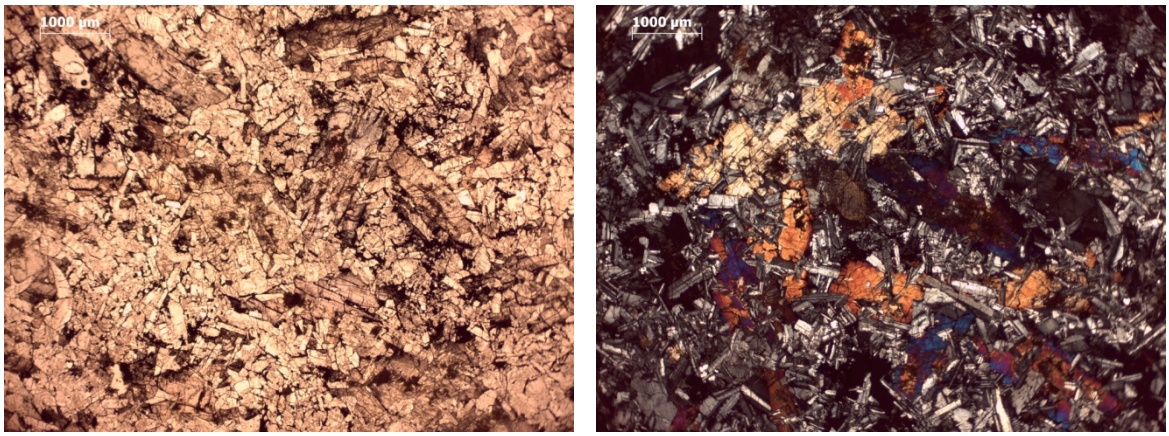

The rock has a medium to coarse grained igneous sub-ophitic texture defined by brownish coarse grained anhedral clinopyroxenes which are partially pecilitic with finer grained euhedral to subeuhedral plagioclase crystals. Interstices between the two main minerals are filled with anhedral opaque minerals. The rock is classified as a coarse grained dolerite.

Thin section 29 (NBP94-07-Piston core 78-Pebble 5D-Top: 210; Bottom:213)

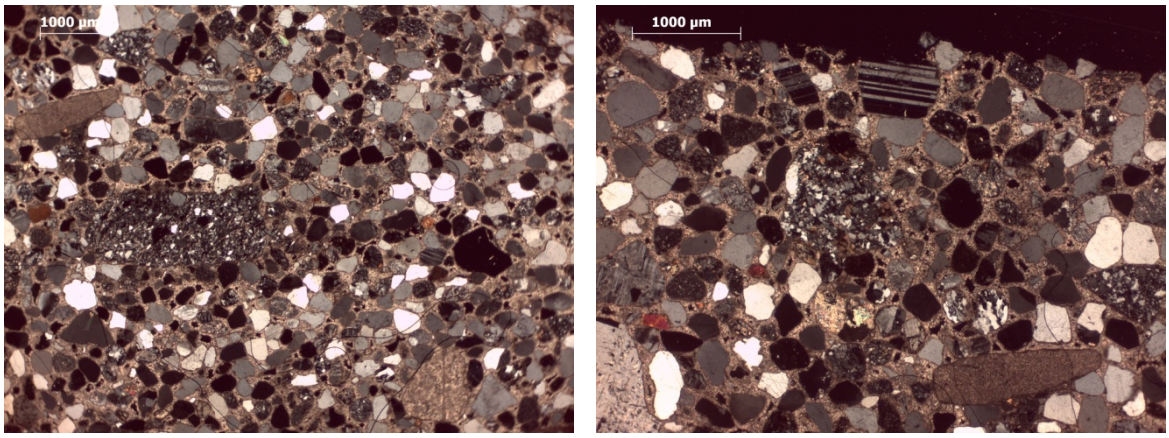

The rock has a clastic texture with medium to very coarse sand grains; grains are sub-angular to rounded, heterogranular and weakly sorted. Cement is almost exclusively of carbonate composition and matrix is absent. Lithic grains make up the 30% of the total grains and they are of different composition: sedimentary lithics, granitoids, policrystalline quartz, low-grade metamorphites, limestones and rare vulcanics. The rock is classified as a lithic arenite.

Thin section 30 (NBP94-07-Piston core 90-Pebble 2-Top: 34; Bottom:35)

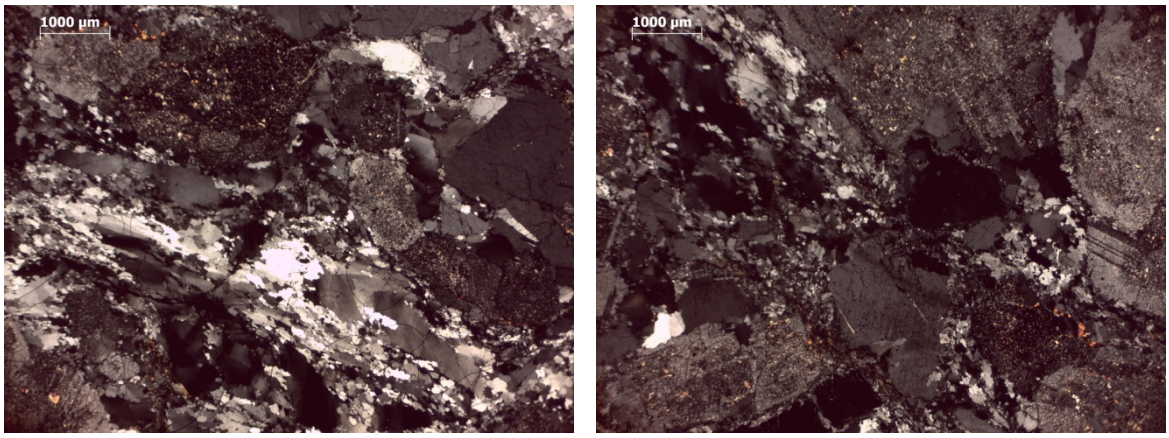

The rock has an heterogranular coarse grained allotriomorphic texture. Policrystalline granoblastic quartz domains with interlobate grain boundaries define a mylonitic foliation and are alternated with porphyritic anhedral to subeuhedral plagioclase and microcline. Chlorite and rare epidote blasts are associated to the main foliation. The composition is monzogranitic. The rock is classified as a foliated monzogranite.

Thin section 31 (NBP94-07-Piston core 90-Pebble 5-Top: 112; Bottom:113)

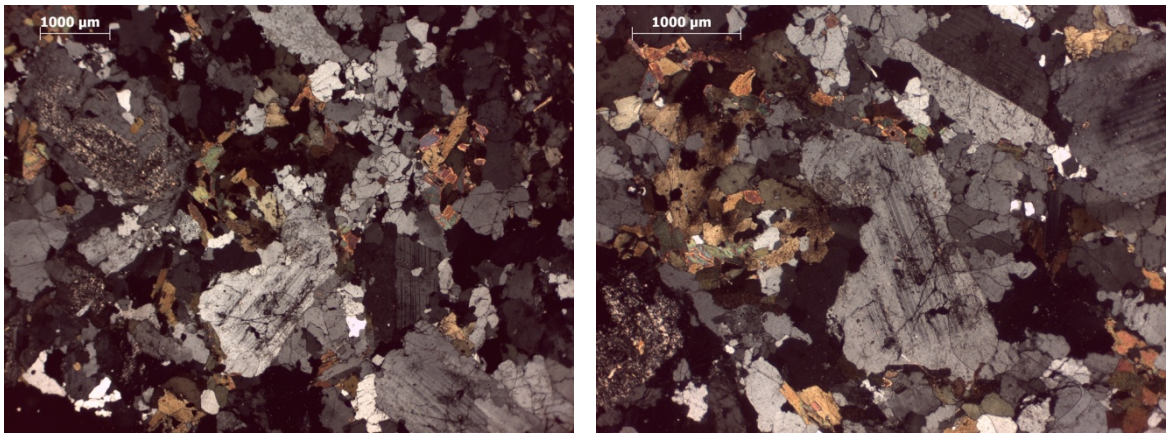

The rock has a slightly heteroquigranular, porphyritic , fine to medium grained, hypidiomorphic texture. It is defined by slightly porphyritic subeuhedral to euhedral plagioclase crystals, sometimes sericitized, associated with anhedral quartz and minor alkaline feldspar. Mafic minerals are biotite, sometimes replaced by chlorite, and brownish hornblende. Apatite, zircon, titanite and opaque minerals are accessory minerals. The rock is classified as a biotite-hornblende tonalite.

Thin section 32 (NBP94-07-Piston core 90-Pebble 1-Top: 165; Bottom:167)

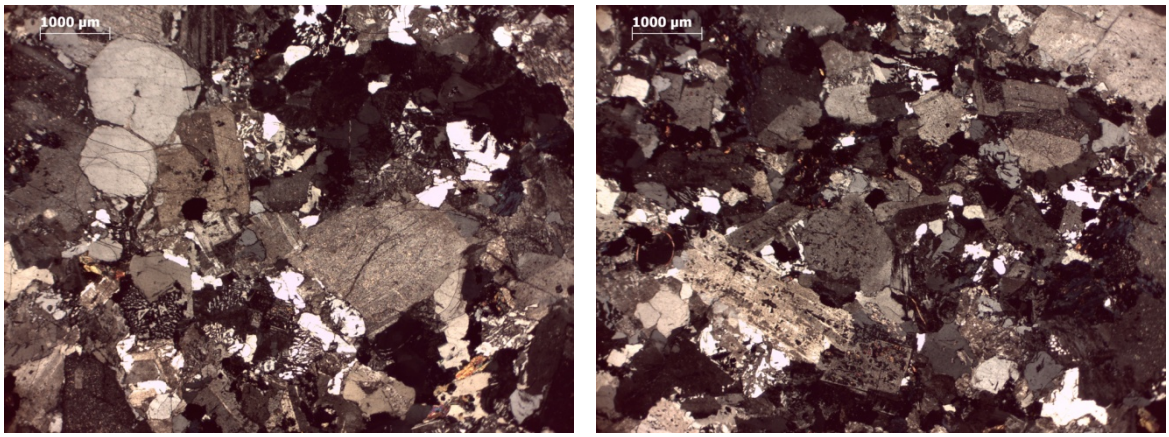

The rock has a slightly porphyritic heterogranular, medium grained, hypidiomorphic texture. Plagioclase is slightly porphyritic, anhedral to subeuhedral and strongly sericitized. Quartz is interstitial and forms granophyric intergrowths with alkaline feldspars; mafic mineral is biotite, completely replaced by aggregates of chlorite and epidotes. In general the rock is strongly altered. The rock is classified as a biotite monzogranite.

Thin section 33 (DF78-Piston core 12-Pebble 2-Top: 83; Bottom:85)

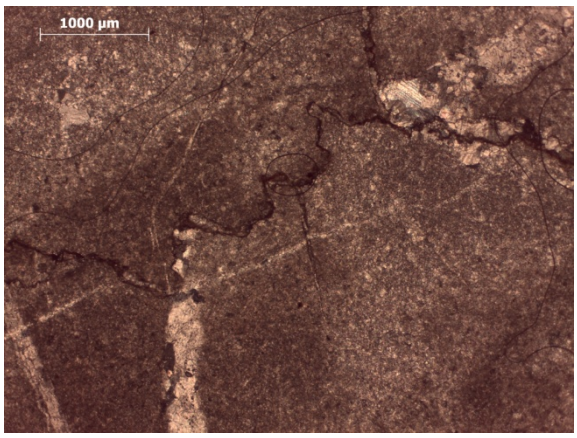

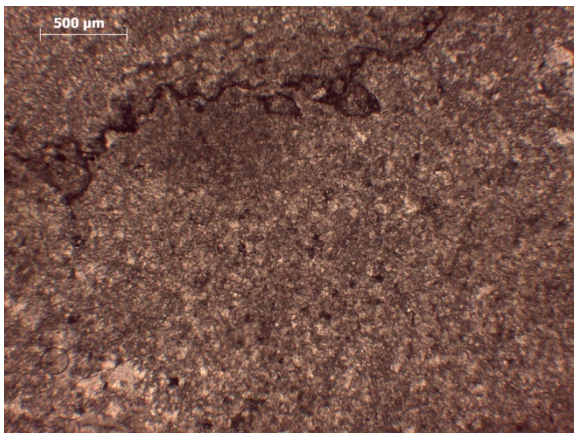

The rock has a slightly heterogranular mud –supported sedimentary texture. It is composed almost exclusively by fine grained microsparitic calcite, with lack of allochems components; in places there are some recrystallized domains with scattered neomorphic calcite crystals. Rare opaque rich stylolites and sparitic carbonate veins are present. The rock is classified as a microscparitic mudstone.

Thin section 34 (DF78-Piston core 12-Pebble 3-Top: 71; Bottom:79)

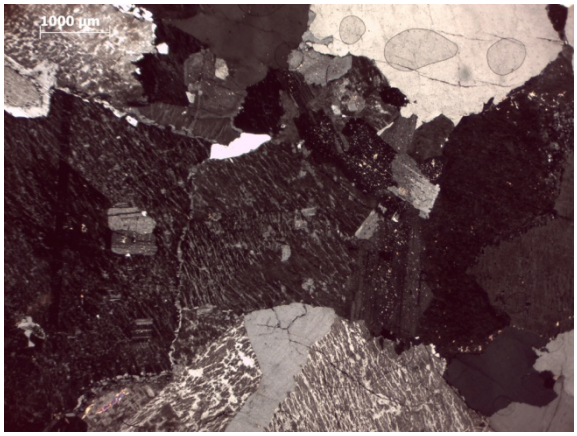

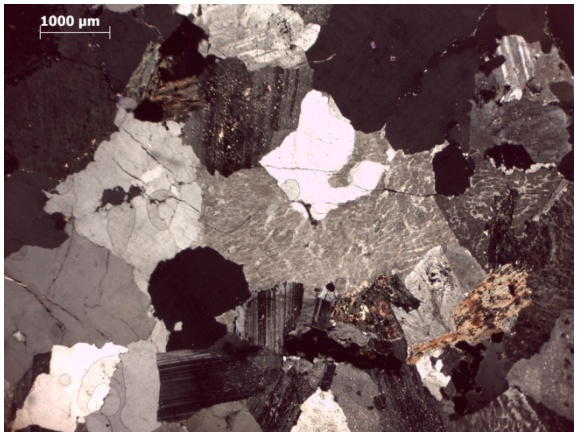

The rock has an equigranular to heterogranular, medium to coarse grained, hypidiomorphic to allotriomorphic, igneous texture. It is composed of anhedral to subeuhedral perthitic orthoclase, sometimes pecilitic with plagioclase, medium grained anhedral quartz and minor plagioclase. Mafic minerals are represented by rare biotite which is completely replaced by chlorite. Accessory phases are opaque minerals, epidote and zircon. The rock is classified as a leucocratic syeno-granite.

Thin section 35 (DF78-Piston core 12-Pebble 5-Top: 136; Bottom:137)

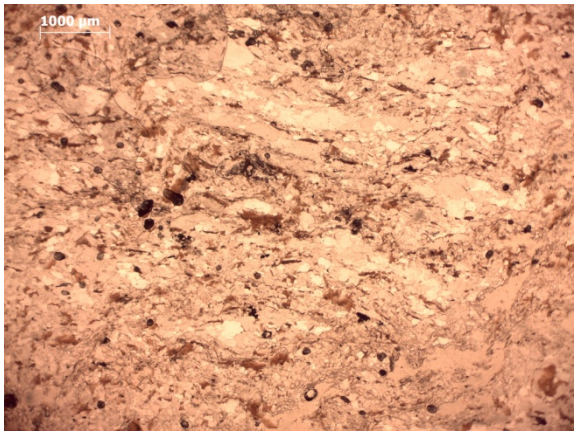

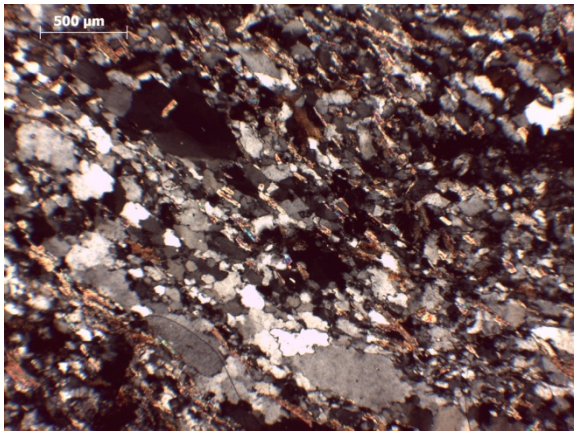

The rock has a fine grained, slightly crenulated, lepidoblastic texture. Foliation is defined by orientation of tiny biotite and rare white mica idioblasts, interlayered with granoblastic domains composed of quartz and feldspars. In places some rare fine grained garnet porphryoblasts are present. Accessory minerals are apatite, zircon, tourmaline and opaque minerals. The rock is classified as a biotite schist.

Thin section 36 (DF80-Piston core 189-Pebble 2-Top: 168; Bottom:169)

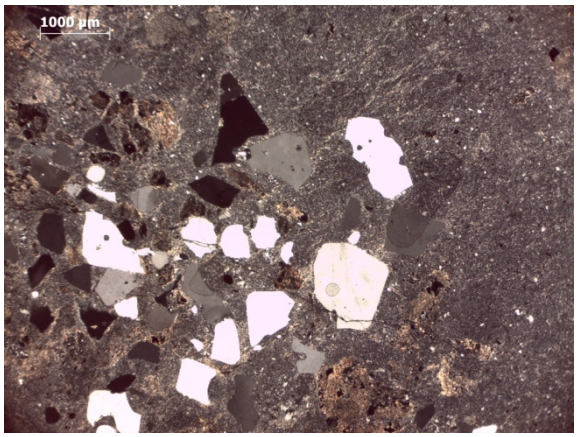

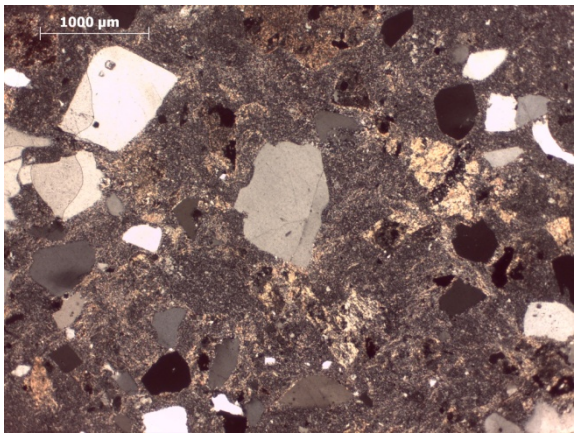

The rock has an heterogranular porphyrytic texture with medium grained phenocrystals of embayed quartz set in a very fine groundmass composed of feldspars and quartz. Some very altered xenolithics grains (quartzite + volcanic lithics?) are concentrated in a phenocrysts rich band, together with altered plagioclase. The rock is classified as an acidic porphyry.

Thin section 37 (DF80-Piston core 189-Pebble 5-Top: 181; Bottom:184)

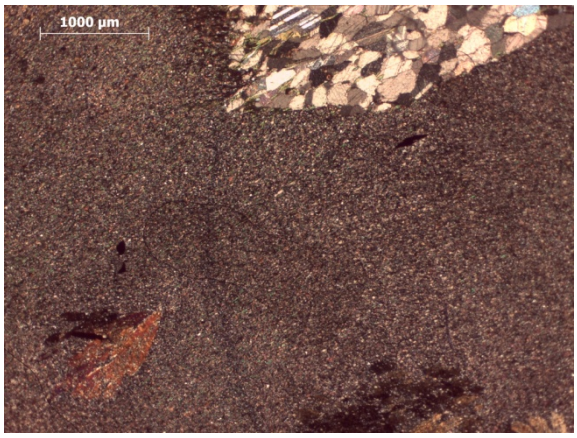

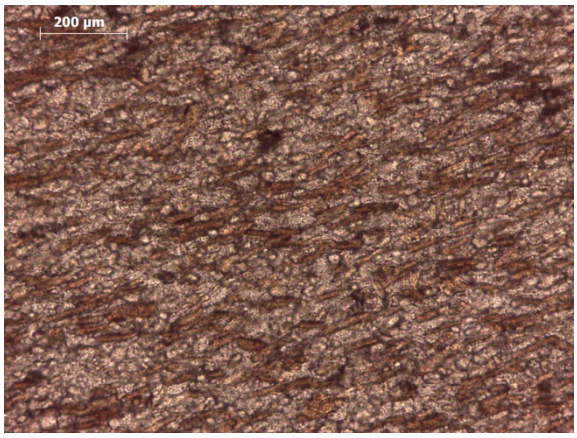

The rock has a very fine grained lepidoblastic texture. The foliation is defined by tiny biotite lamellae orientation, associated with quartz and calcite grains. Sometimes are present plagues filled by sparry calcite and rare quartz. A medium grained, randomly oriented, peciloblastic green actinolite amphibole is present. Epidote and opaque minerals are accessory phases. The rock is classified as a filladic calc-schist.

Thin section 38 (DF78-Piston core 14-Pebble 12-Top: 125; Bottom:128)

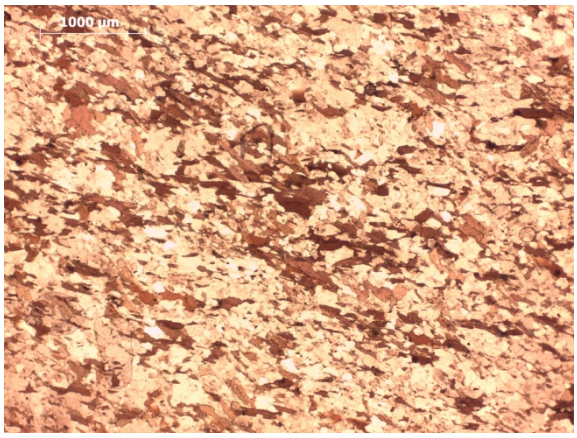

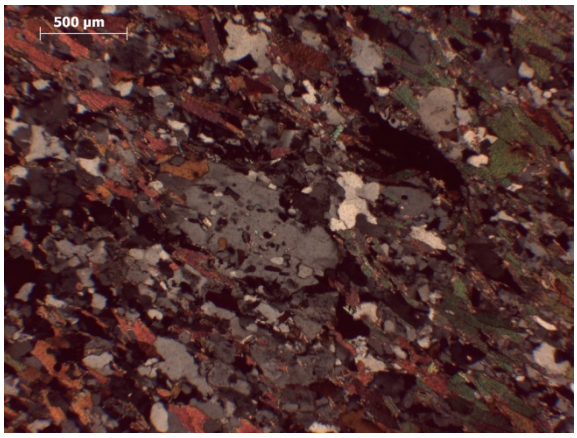

The rock has a fine grained lepidoblastic texture. Foliation is defined by orientation of biotite idioblasts to xenoblasts, alternated with granoblastic domains defined by quartz and peciloblastic k-feldspar which include tiny biotite lamellae and quartz inclusions. Plagioclase is rare and very altered in sericite. Accessory minerals include zircon, apatite, tourmaline and opaque minerals. The rock is classified as a biotite-schist.

Thin section 39 (DF78-Piston core 14-Pebble 14-Top: 145; Bottom:151)

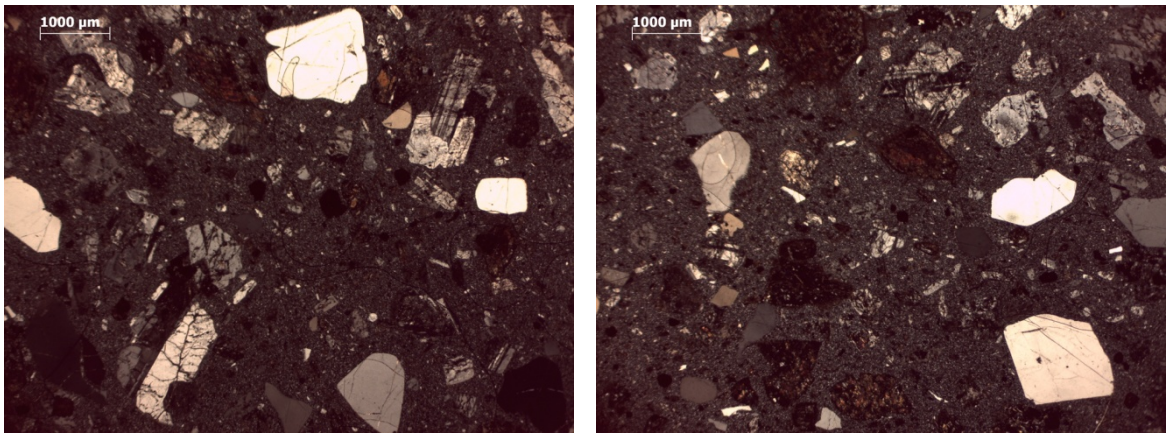

The rock is divided into two portion: one portion is rich of medium grained xenoclastic lithics, very altered, with lithic clasts such chert-like rocks and volcanic lithics set in chlorite and epidote matrix, with unknown mafic minerals replaced by green amphiboles overgrowths; the other portion is porphyritic, heterogranular with medium grained phenocrystals of quartz, plagioclase and completely altered (epidote and chlorite) femic minerals fenocrysts, set in fine quartz and plagioclase fine groundmass. The rock is classified as a meta-porphyry.

Thin section 40 (DF78-Piston core 14-Pebble 11-Top: 290; Bottom:294)

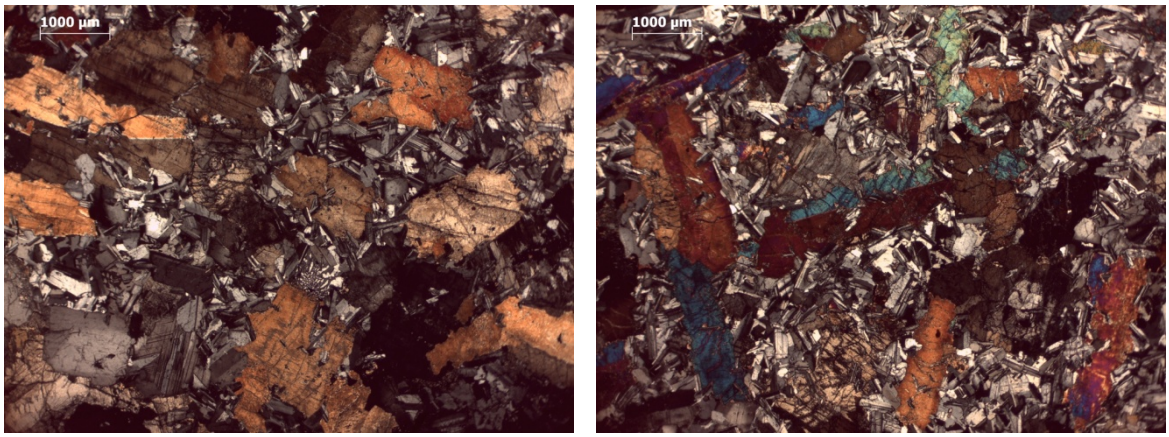

The rock has a sub-ophitic medium to coarse grained igneous texture. It is composed of coarse grained anhedral to sub-euhedral brown augitic clinopyroxenes, partially ophitic with medium grained plagioclase laths. Ortopyroxene is present, although rare. Quartz forms interstitial myrmechitic textures with rare k-feldspar. Accessory minerals are opaque minerals, biotite, epidote and chlorite as secondary alteration phases. The rock is classified as a coarse grained dolerite.

Thin section 41 (NBP94-Piston core 01-Pebble 4-Top: 117; Bottom:121)

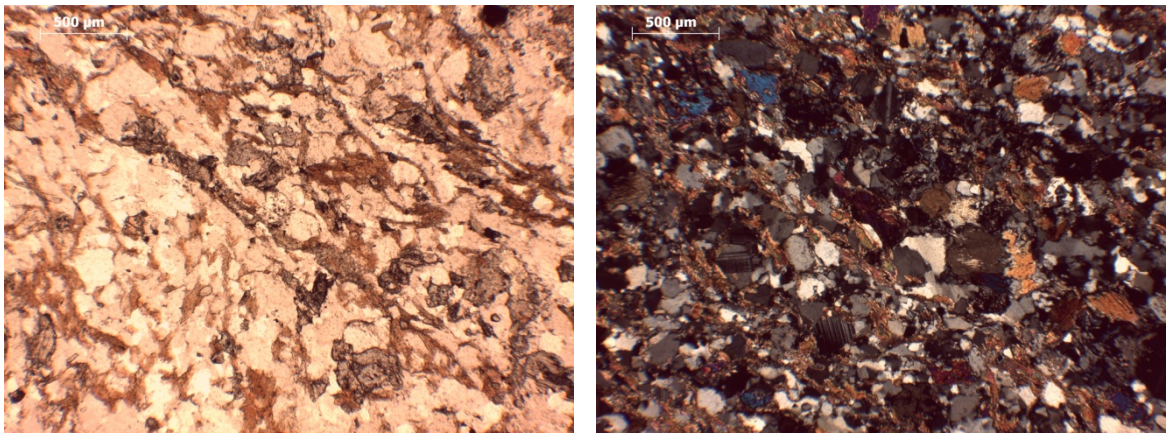

The rock has a fine grained slightly grano-lepidoblastic texture. Foliation is defined by a weak orientation of xenoblastic brown biotite lamellae, associated with rare clinopyroxene and clinoamphibole. Lepidoblastic domains are alternated with granoblastic domains composed of quartz and plagioclase, with rare clinozoisitic epidote xenoblasts. Apatite, zircon and tourmaline are accessory minerals. The rock is classified as a botite-(amphibole)-schist.

Thin section 42 (ELT32-Piston core 27-Pebble 6-Top: 49; Bottom:52)

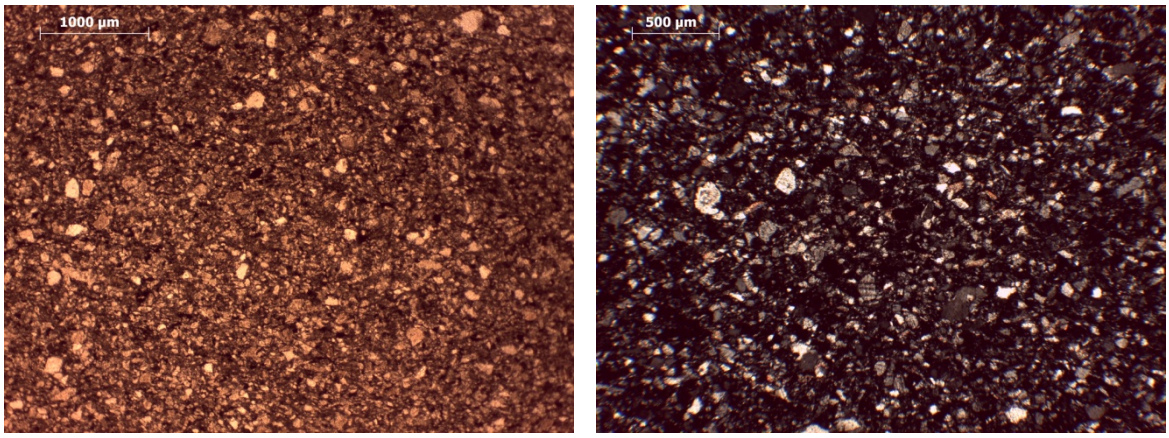

The rock has an heterogranular, poorly sorted, very fine to fine grained clastic texture. Fine grained brownish matrix constitutes up to 10% of the rocks, while among grains quartz make up 95%, feldspars 3% and lithics 1% of the total amount. Calcite and sericite patches are common in the matrix. The rock is classified as an impure arenite.

Thin section 43 (ELT32-Piston core 27-Pebble 9-Top: 68; Bottom:72)

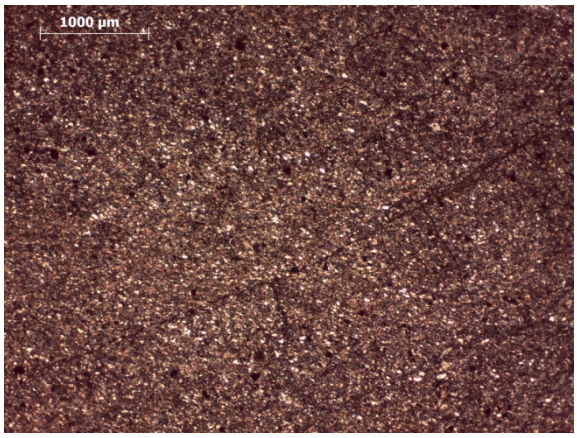

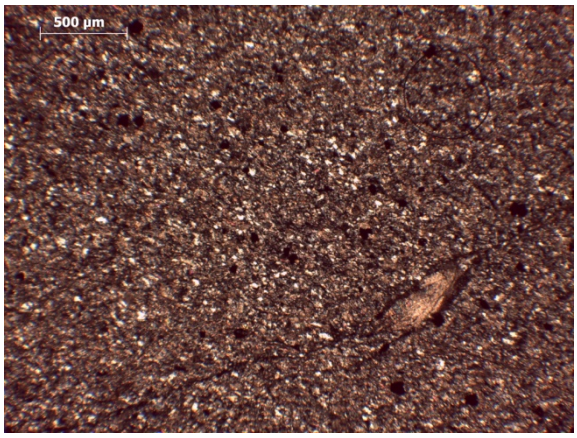

The rock has an equigranular very fine grained slightly foliated clastic texture. Foliation is defined by orientation of tiny white mica and chlorite lamellae, alternated with very fine grained quartz and calcite grains. Tourmaline and opaque minerals are accessory minerals. The rock is classified as a meta-siltstone.

Thin section 44 (ELT32-Piston core 27-Pebble 17-Top: 135; Bottom:138)

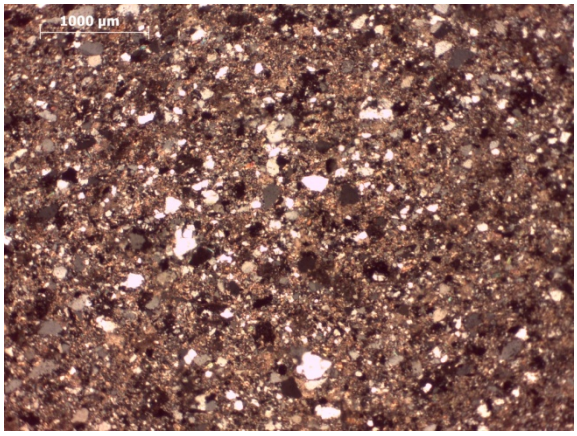

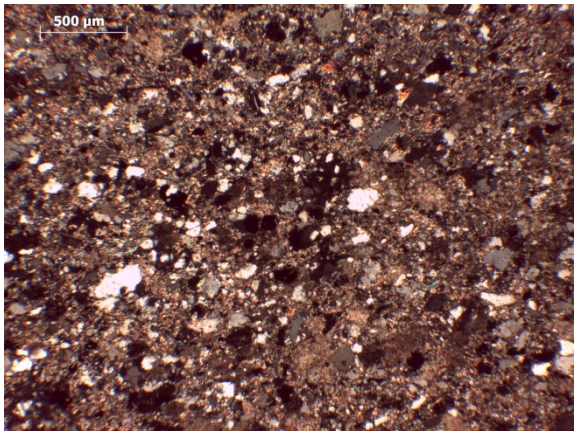

The rock has an heterogranular, poorly sorted, fine to medium sand sized clastic texture. Intergranular spaces are filled with calcite and sericite patches and fine grained matrix make up the 12% of the total thin section. Grains are sub-rounded to sub-angular and are made up by quartz(95)-feldspars (2)- and lithics (2). The rock is classified as a greywacke.

Thin section 45 (NBP99-02-Piston core 17-Pebble 11-Top: 77; Bottom:82)

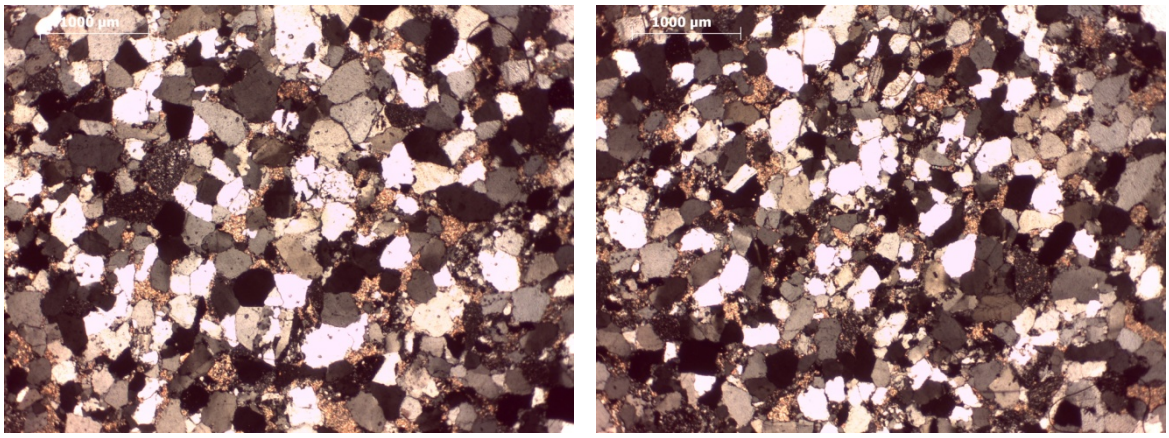

The rock has an equigranular, moderately sorted, medium to coarse grained sand clastic texture. Elements are composed of sub-angular to sub-rounded quartz (96), lithic grains (3) made up by sedimentary chert and low grade metamorphic lithics; cement is made up by siliceous overgrowth around grains. Calcite and sericite are common phases in intergranular spaces. The rock is classified as a quartz-arenite.

Thin section 46 (NBP99-02-Piston core 17-Pebble 15-Top: 176; Bottom:180)

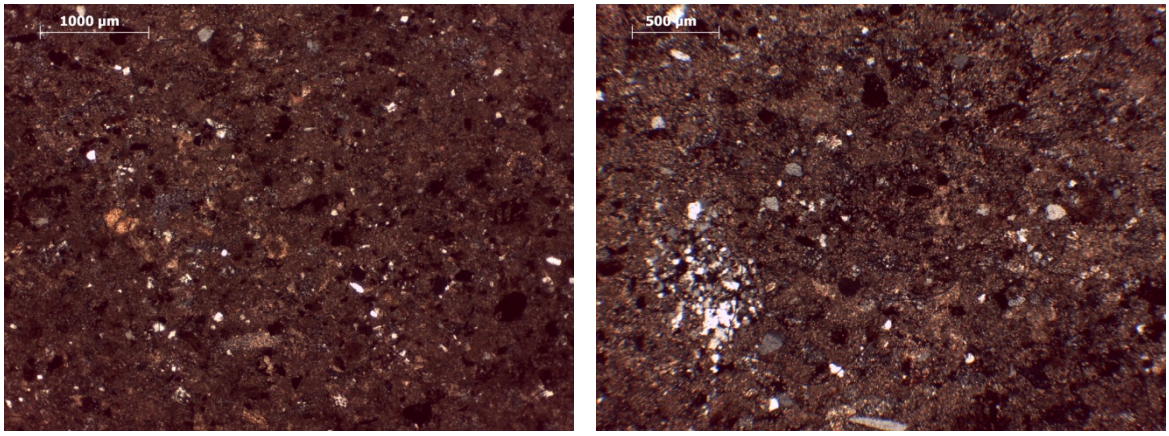

The rock has fine grained clastic texture. The grade of alteration is high and the rocks appears totally overprinted by a very fine grained matrix of oxides-hydroxides layer. Grains are difficult to identify, and there is prevailing quartz and minor lithic grains (sedimentary composition). The rock is classified as an altered greywacke.

Thin section 47 (ELT32-Piston core 26-Pebble 8-Top: 140; Bottom:146)

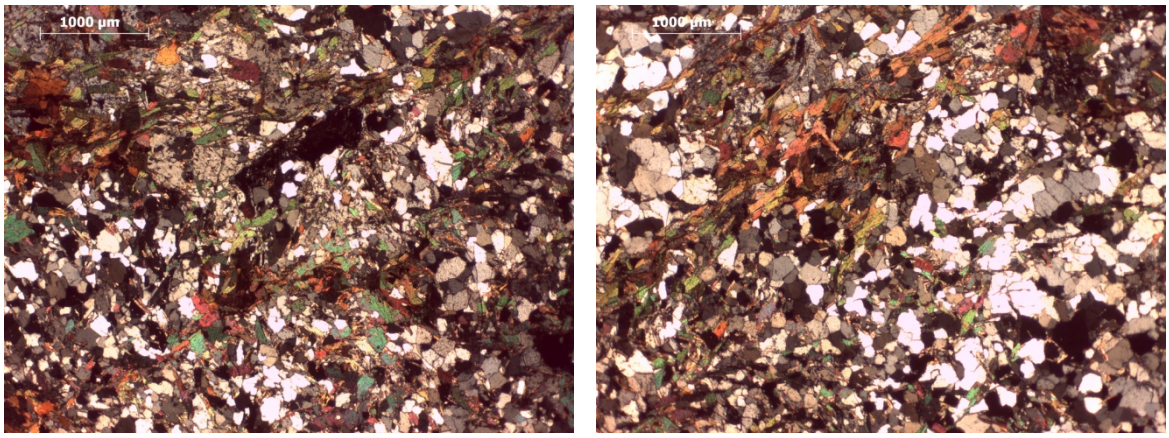

The rock has an heterogranular medium grained grano-lepidoblastic texture. Foliation is defined by xenoblastic to idioblastic biotite lamellae which envelope k-feldspar porphyroblast. Rare white mica is associated to biotite foliation. Granoblastic domains are composed of anhedral quartz and minor plagioclase. Accessory minerals are zircon, apatite and opaque minerals. The rock is classified as a biotite gneiss.

Thin section 48 (ELT32-Piston core 26-Pebble 13-Top: 237; Bottom:238)

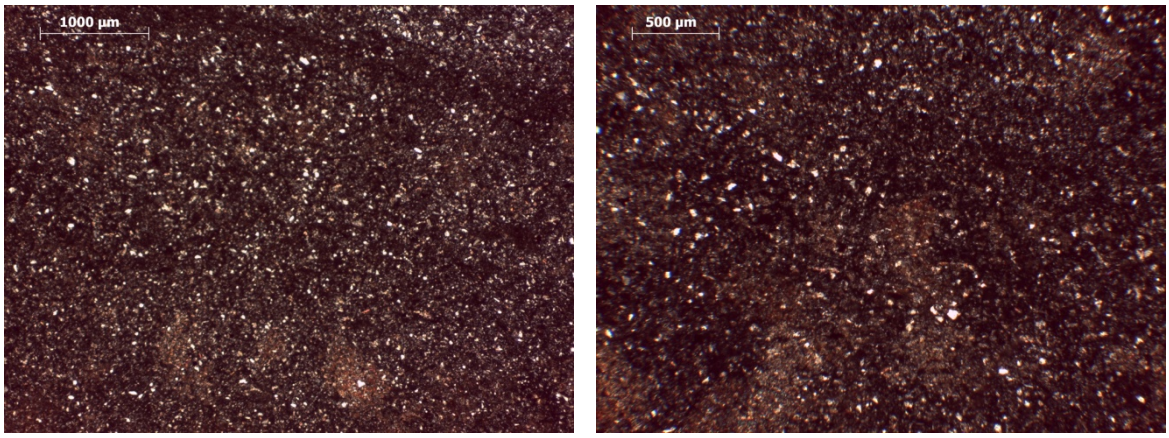

The rock has a very fine grained clastic texture and it is difficult to recognize with standard magnifiers. In places there is a thin lamination of coarser sediment, which is composed of quartz grains and abundant dark argillaceous matrix. Fe-oxides and mica aggregates poikilitic patches define a spotted texture. The rock is classified as a siltstone.

Thin section 49 (DF83-Piston core 14-Pebble 14-Top: 208; Bottom:210)

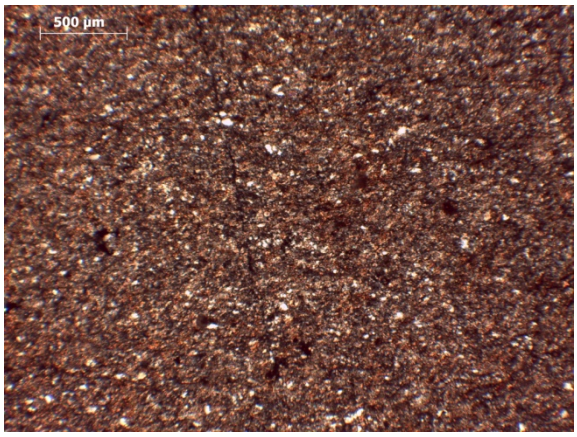

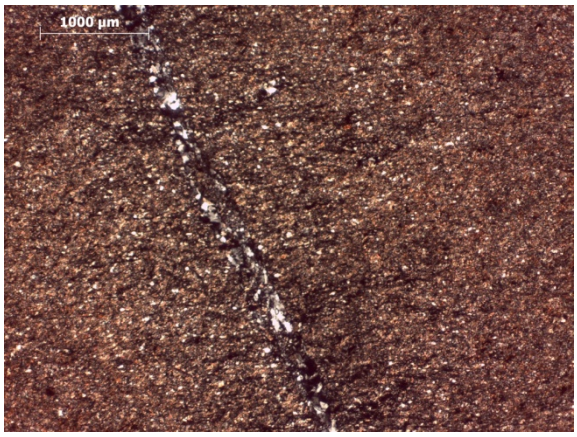

The rock has a very fine grained lepidoblastic foliated texture. Foliation is defined by orientation of tiny idioblasts of biotite and white mica; however, foliation is not pervasive, since a pre-existing clastic texture is still recognizable. Clasts are formed by quartz grains, calcite and rare plagioclase. Opaque minerals are present as accessory minerals. Quartz veins are present. The rock is classified as a phyllite.

Thin section 50 (DF83-Piston core 14-Pebble 2-Top: 31; Bottom:33)

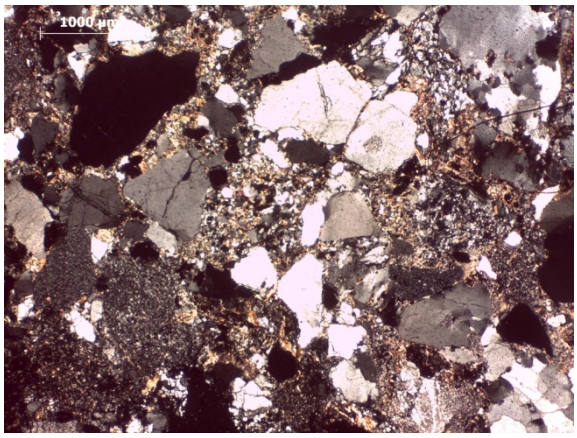

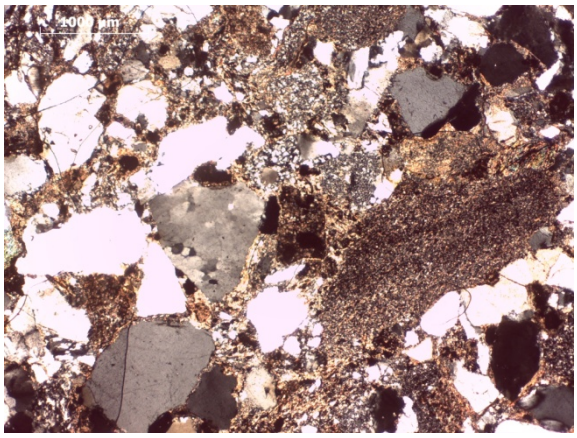

The rock has an heterogranular, poorly sorted, medium to coarse grained clastic texture. Grains are sub-angular to sub-rounded and are composed of quartz grains, often with ondulouse extinction, and lithic grains (mainly polycristalline quartz + phyllites + siltstones). Intergranular pores are filled with calcite, sericite and opaque minerals. The rock is classified as a sub-litharenite.

Thin section 51 (DF83-Piston core 14-Pebble 18-Top: 269; Bottom:273)

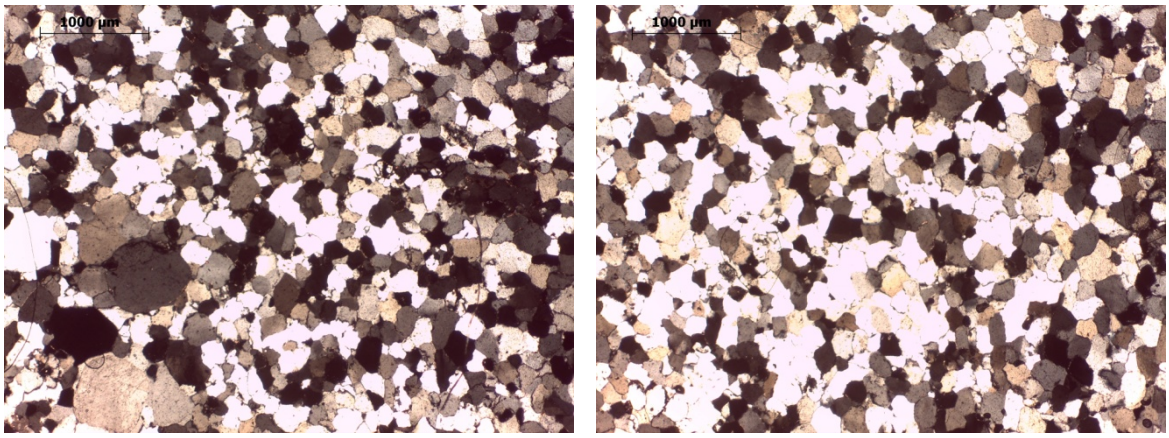

The rock has a slightly heterogranular, moderately sorted, fine to medium grained clastic texture. Grains are constituted by almost exclusively quartz grains, with interlocking intergranular boundaries and recrystallized siliceous overgrowth cement; accessory minerals are rare opaque minerals and white mica flakes dispersed in intergranular pores. The rock is classified as a qtz-arenite.

Thin section 52 (NBP94-07-Piston core 58-Pebble 1-Top: 55; Bottom:57)

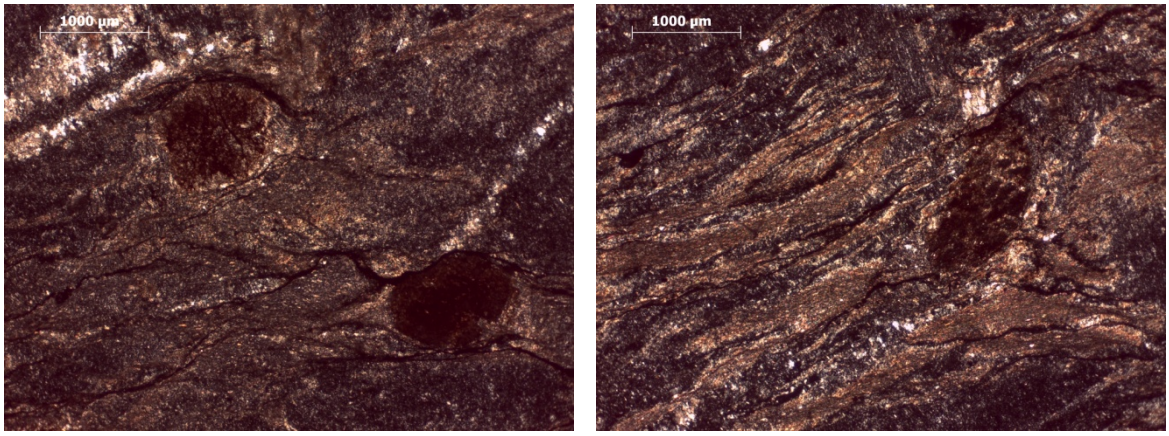

The rock has a very fine grained slaty cleavage texture. Cleavage is defined by mutual orientation of tiny mica quartz and opaque minerals banding. Medium grained fe-oxides porphyroblasts are enveloped by cleavage. The rock is classified as a slate.

Thin section 53 (NBP94-07-Piston core 58-Pebble 3-Top: 121; Bottom:125)

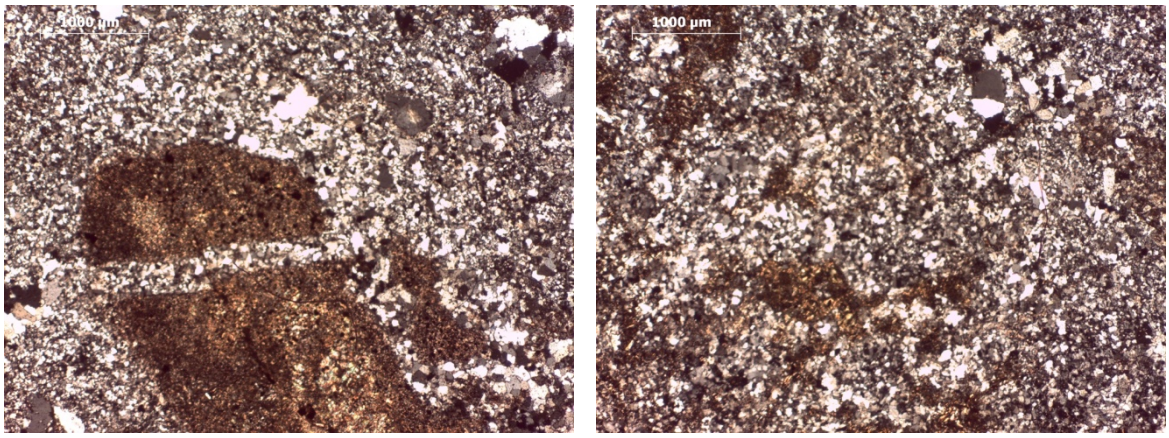

The rock has an heterogranular fine to medium grained granoblastic texture. Some altered lithic grains (sericite and chlorite) are present, as well as medium grained plagioclase porphyroblasts. Granoblastic texture is defined mainly by fine grained polygonal quartz. Opaque minerals are present as accessory phases. The rock is classified as a quartzite.

Thin section 54 (NBP94-07-Piston core 63-Pebble 4-Top: 222; Bottom:223)

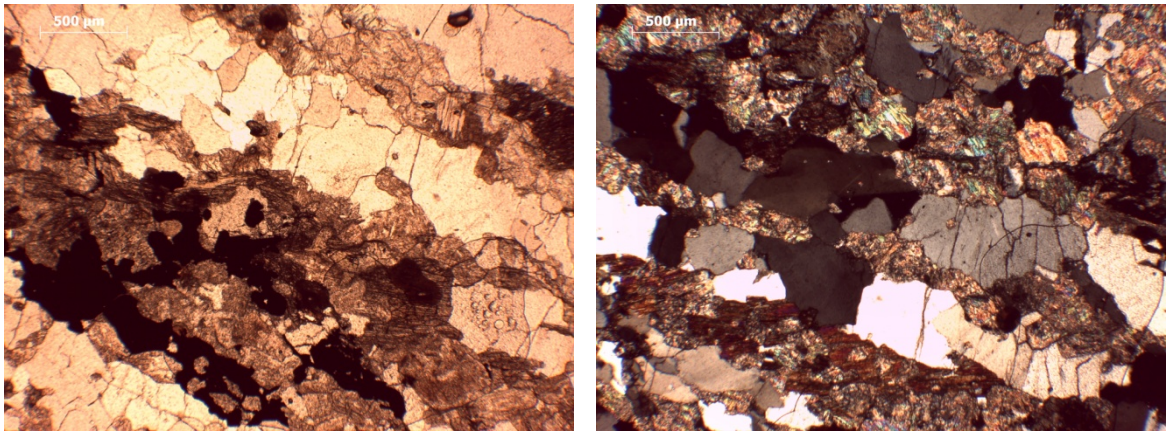

The rock is characterized by a moderately altered gneissic layering defined by granoblastic medium grained quartz domains; plagioclase is completely altered in sericite. Granoblastic domains are alternated with nematoblastic layers defined by altered hornblende clinoamphiboles iso-orientation, associated with biotite and rare garnet. Apatite, titanite, k-felsdpar, and secondary calcite are accessory minerals. The rock is classified as a biotite-hornblende gneiss.

Thin section 55 (NBP94-07-Piston core 63-Pebble 1-Top: 11; Bottom:14)

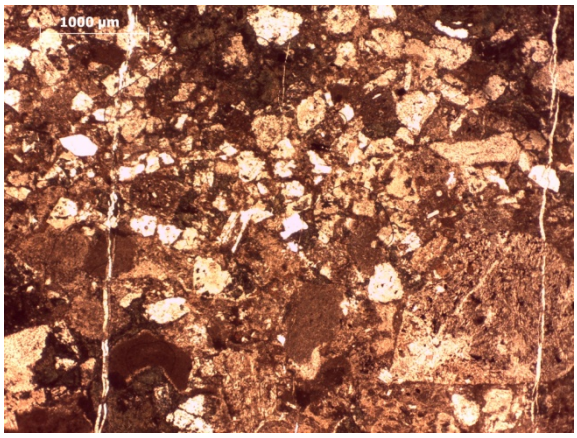

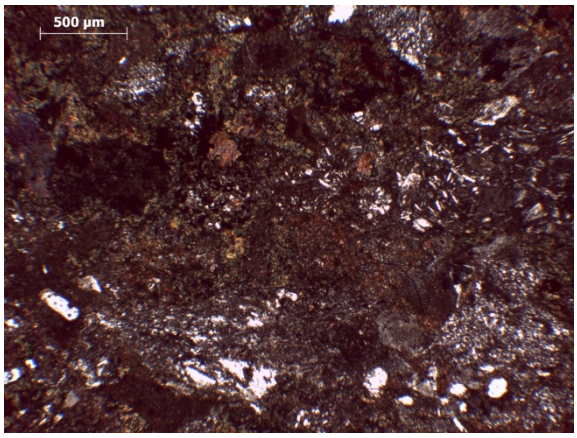

The rock has a medium to coarse grained, unsorted, clastic texture. Clasts are composed of embayed quartz grains, porphyritic plagioclase and volcanic lithic fragments with pylotaxitic texture. The majority of lithic grains are completely altered. Matrix is composed of a fine grained mixture of chlorite and amphibole which envelope the majority of grains. The rock is classified as a meta-vulcanoclastite.

Thin section 56 (NBP94-07-Piston core 56-Pebble 6-Top: 140; Bottom:142)

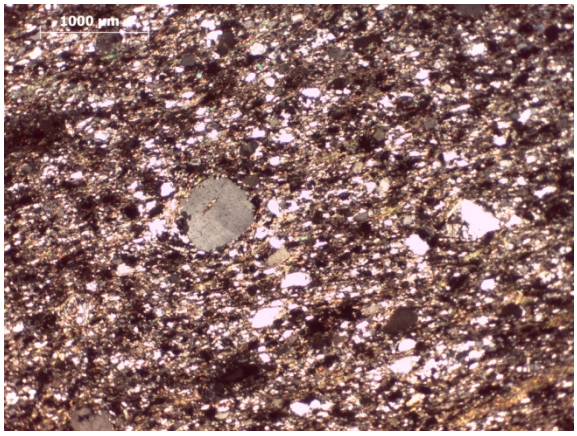

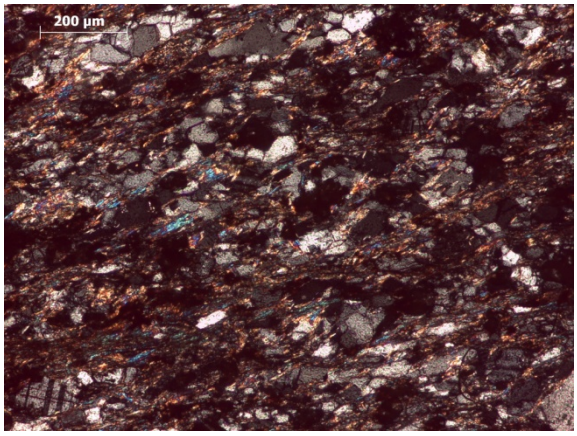

The rock has a fine to medium grained lepidoblastic texture. Clastic nature of the rock is still maintained. Foliation is defined by oriented xenoblasts to idioblasts of white mica, chlorite and opaque minerals which envelope porphyroclastic quartz and rare plagioclase. The rock is classified as a metasandstone.

Thin section 57 (NBP94-07-Piston core 56-Pebble 4-Top: 216; Bottom:217)

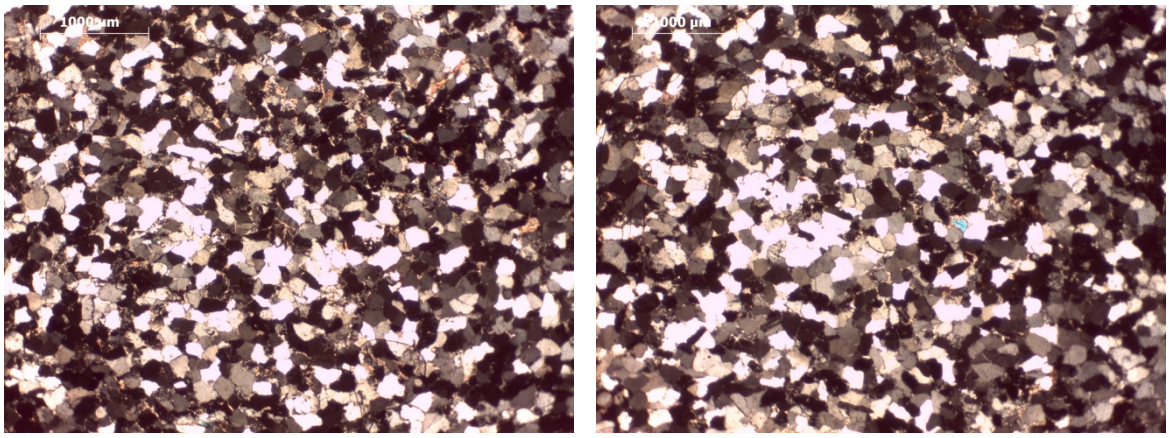

The rock has a fine to medium grained sand equigranular, well sorted, clastic texture. Clasts are sub-angular to sub-rounded and include quartz (97), feldspars (2) and lithic grains (<1); cement is quartzose. Rare white mica detrital flakes and opaque minerals as accessory phases. The rock is classified as a quartz-arenite.

Thin section 58 (NBP94-07-Piston core 56-Pebble 5-Top: 234; Bottom:235)

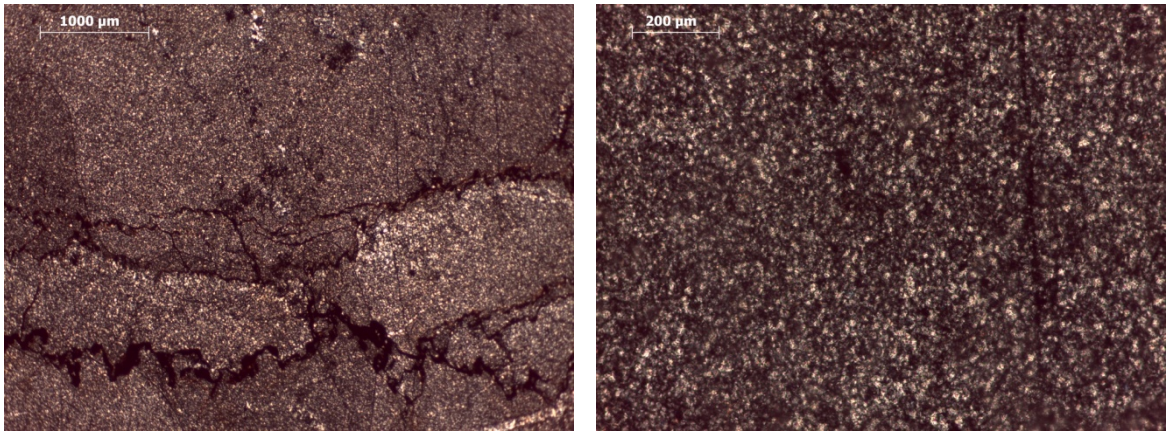

The rock has a very fine grained clastic texture, single minerals are difficult to identify with standard magnifiers. The greatest portion of the rock is composed of a very fine grained quartzose and opaque minerals matrix. Some parallel stylolites host concentration of opaques banding and fe-oxides material. The rock is classified as quartzose (meta)-siltstone.

Thin section 59 (NBP94-07-Piston core 56-Pebble 6-Top: 305; Bottom:308)

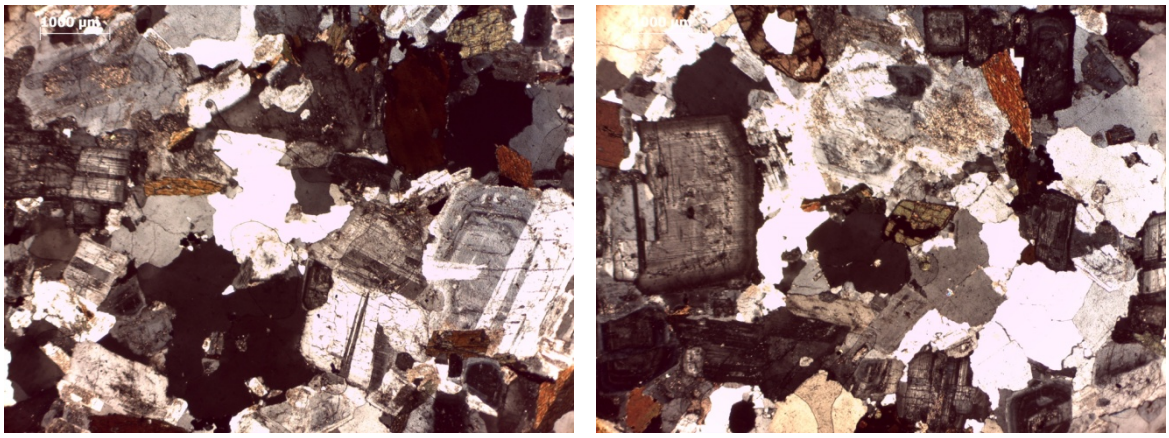

The rock has an heterogranular, medium to coarse grained, isotropic, hypidiomorphic igneous texture. It is composed of sub-euhedral to euhedral zoned and twinned plagioclase, sometimes altered in sericite, medium grained anhedral quartz and minor k-feldspar. Mafic minerals are constituted by brown biotite and greenish-brownish hornblende. Accessory minerals are zircon, apatite, opaque minerals and titanite. The rock is classified as a biotite-hornblende tonalite.

Thin section 60 (NBP94-07-Piston core 65-Pebble 5-Top: 31; Bottom:34)

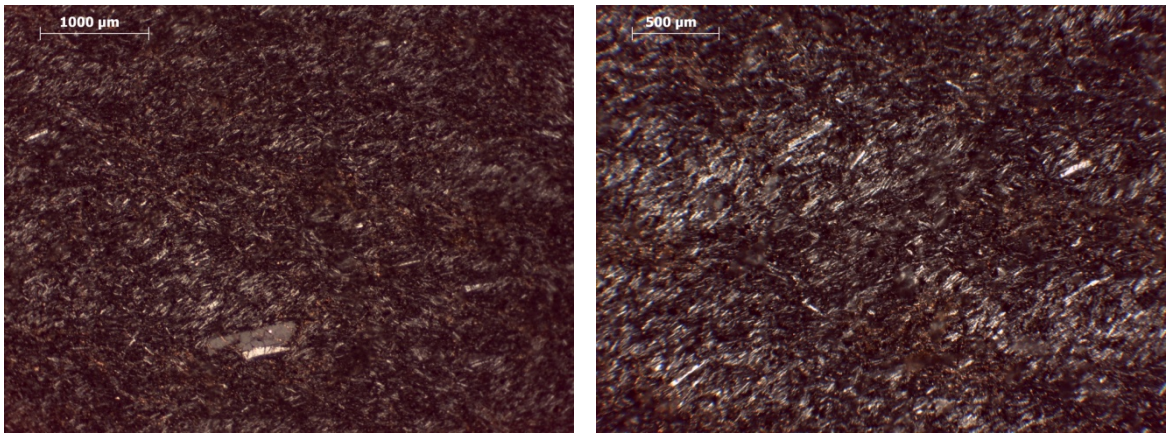

The rock has an olocrystalline fine grained trachytic igneous texture. Texture is defined by orientation of fine grained laths of k-feldspar and plagioclase. Porphyritic index is low, since rare sanidine phenocrystals are present. Groundmass is composed also of interganular opaque minerals and clinopyroxenes. The rock is classified as a trachyte.

Thin section 61 (NBP94-07-Piston core 65-Pebble 4-Top: 16; Bottom:18)

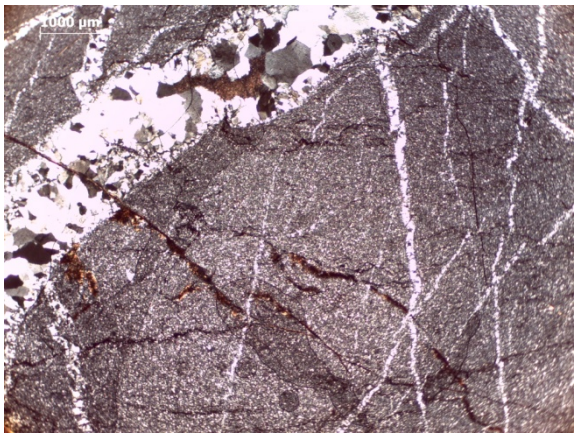

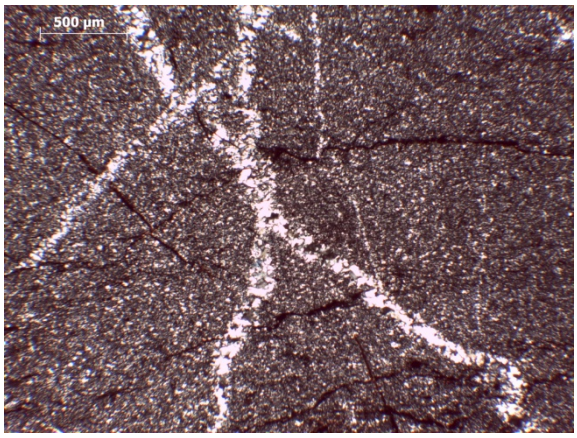

The rock has a very fine grained clastic texture. Clasts are difficult to discern by standard magnifiers; prevalently quartz grains are recognized set in a fine grained dark phyllosilicates matrix, with some rare white micas. The rock is crossed by millimeter sized quartz veins and sometimes opaque minerals and fe-oxides dark banding. The rock is classified as a quartz siltstone.

Thin section 62 (NBP96-01-Piston core 09-Pebble 1-Top: 5; Bottom:6)

The rock has a fine to medium grained grano-lepidoblastic texture with superimposition of a spotted texture. Pre-existing foliation is defined by lepidoblastic domains of idioblastic to xenoblastic biotite lamellae, alternated with granoblastic domains of quartz and rare plagioclase. Some spots of randomly oriented biotite and white mica idioblasts overprint the original texture. Zircon, opaque minerals and apatite are present as accessory minerals. The rock is classified as a biotite-white mica hornfels.

Thin section 63 (NBP96-01-Piston core 09-Pebble 5-Top: 122; Bottom:124)

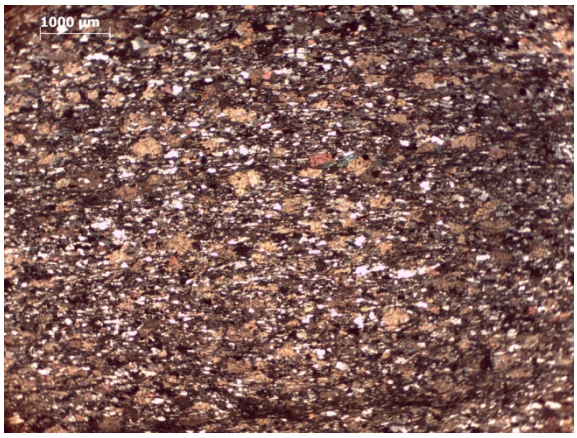

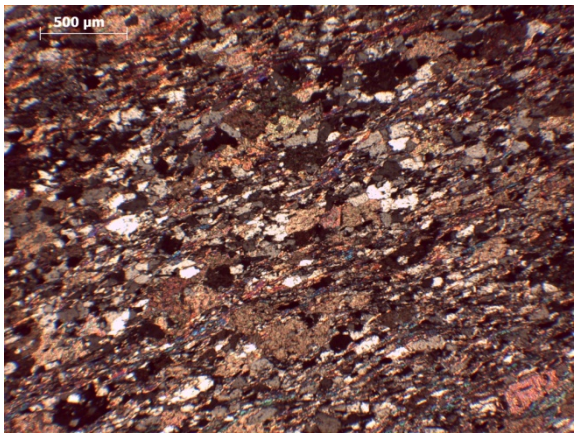

The rock has a fine grained lepidoblastic texture. Foliation is defined by sub-idioblastic to idioblast white mica lamellae orientation, alterned to granoblastic domains of intergranular quartz, calcite and plagioclase blasts. Opaque minerals are present as accessory minerals. The rock is classified as a calc-schist.

Thin section 64 (NBP96-01-Piston core 09-Pebble 1-Top: 145; Bottom:150)

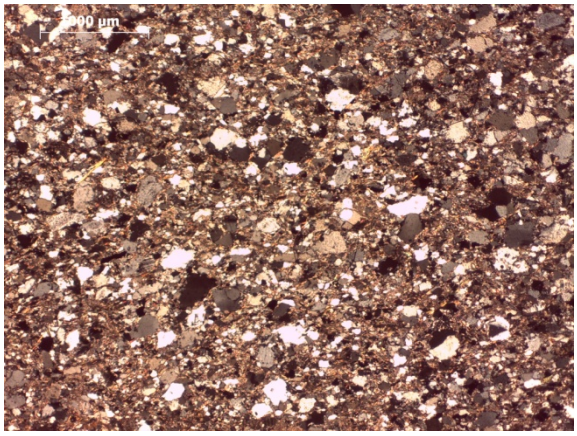

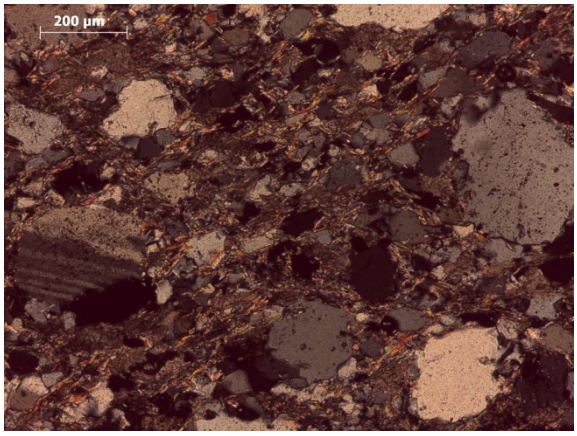

The rock has an heterogranular, poorly sorted, fine to medium sand clastic texture; clasts are sub-angular to sub-rounded and are composed of quartz(95), feldspars (2) and lithic grains (2). Matrix make up the 12% of the total rock area and is altered in calcite patches and intergranular sericite. Slightly oriented white mica lamellae are common. Accessory minerals are zircon, opaque minerals and epidote. The rock is classified as a medium grained (meta)sandstone.

Thin section 65 (NBP94-07-Piston core 58-Pebble 5-Top: 225; Bottom:226)

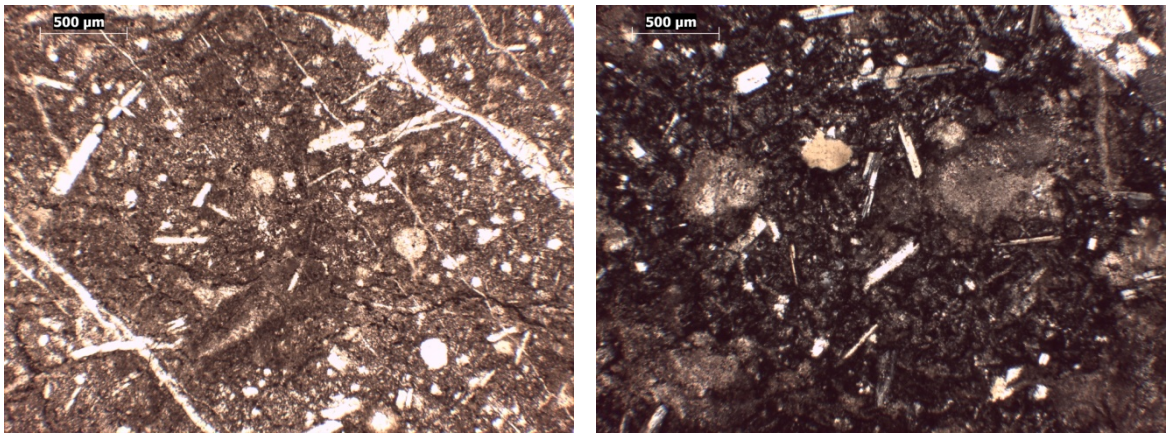

The rock has fine grained porphyritic cryptocrystalline texture. Overall the rock is very altered. Fine grained plagioclase phenocrystals are set in a cryptocrystalline quartz and plagioclase groundmass. Original voids are filled with quartz and sometimes carbonate crystals. Mafic minerals are completely altered in carbonate pseudomorphs. Thin carbonate veins are common. The rock is classified as a mafic vulcanite but its grade of alteration is too high to establish a confident petrographic name.

Thin section 66 (DF83-Piston core 14-Pebble 7-Top: 90; Bottom:94)

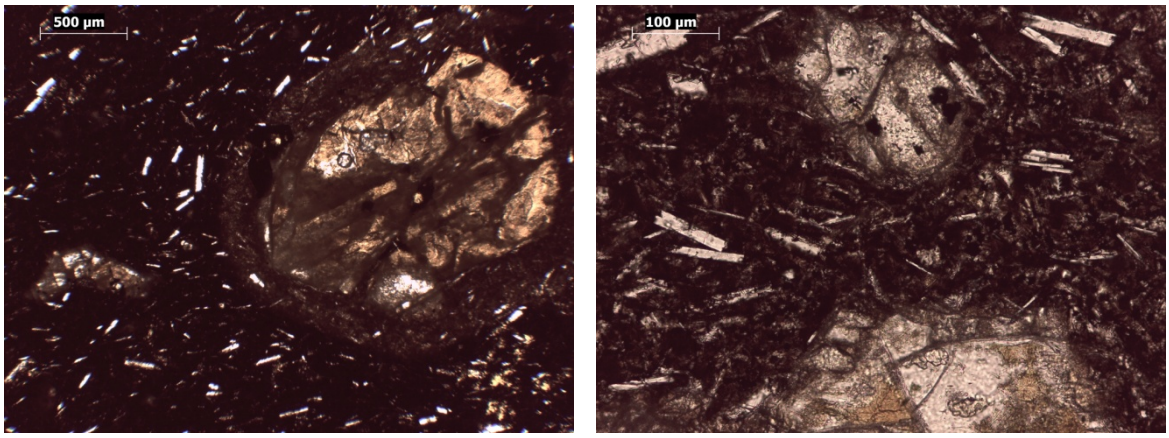

The rock has fine grained ipocrystalline porphyritic texture. Phenocrystals of olivine completely altered in pseudomorphic carbonates are set in a fine grained ipocrystalline groundmass with slightly oriented plagioclase microliths, opaque minerals, rare clinopyroxenes and dark glass. The rock is quite altered and is classified as basalt.

Thin section 67 (ELT32-Piston core 27-Pebble 5-Top: 34; Bottom:36)

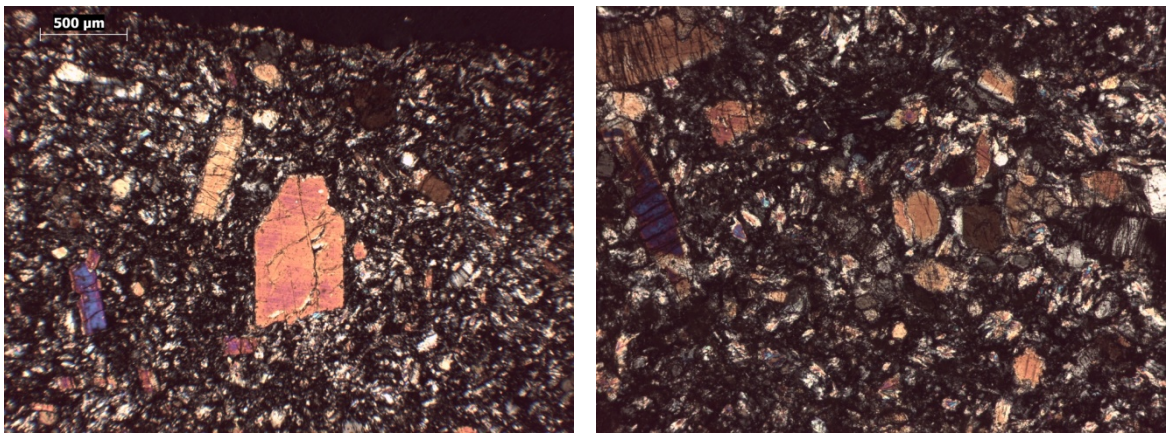

The rock has a fine grained porphyritic olocrystalline igneous texture. Phenocrystals are brownish clinopyroxenes, sometimes zoned and twinned, and rare amphiboles. Groundmass is microcrystalline and is composed of spherulitic chlorite and sericite aggregates, associated to intergranular plagioclases, clinopyroxenes and opaque minerals. The rock is quite altered and it is classified as a mafic porphyry.

Thin section 68 (NBP94-07-Piston core 65-Pebble 3-Top: 17; Bottom:20)

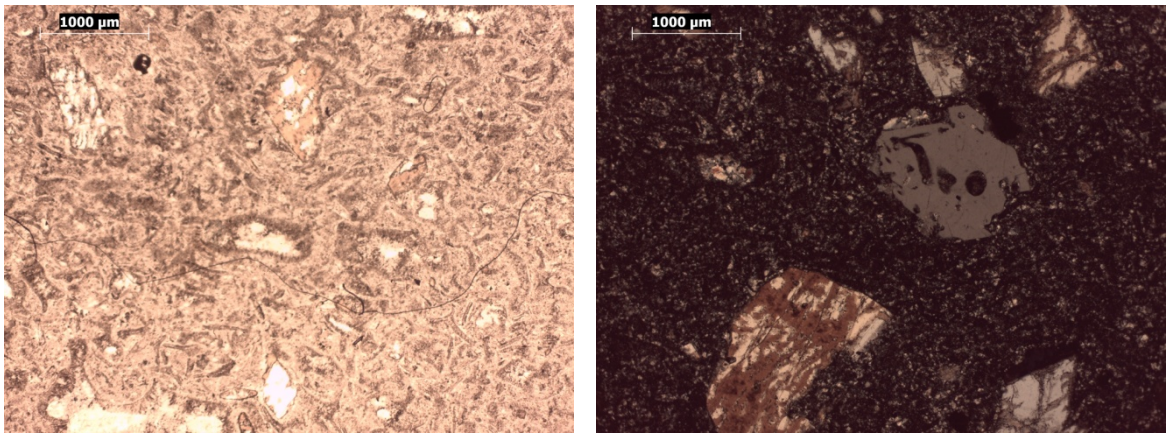

The rock has a porphyritic fluidal to eutassitic texture. Phenocrystals are medium grained embayed quartz and altered k-feldspars set in a microcrystalline groundmass with some glass shards, very fined grained quartz and feldspars aggregates and opaque minerals. The rock is classified as rhyolitic vulcanite.

Thin section 69 (NBP94-07-Piston core 63-Pebble 5-Top: 227; Bottom:228)

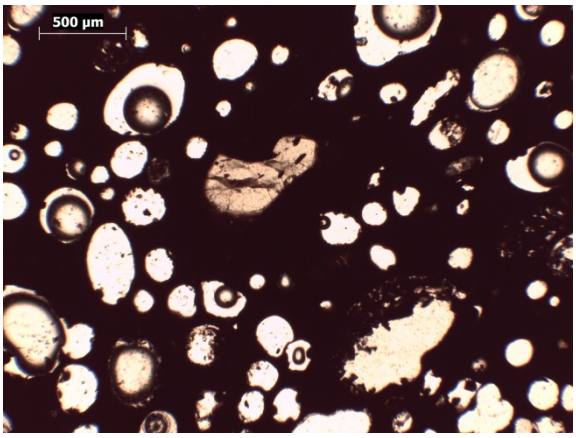

The rock has an oloialine vescicular texture. Vesciculae are rounded to elongated, groundmass is composed of dark glass and extremely rare plagioclase microliths and olivine microphenocrystals. The rock is classified as basaltic scoria.

Thin section 70 (ELT32-Piston core 13-Pebble 3-Top: 45; Bottom:46)

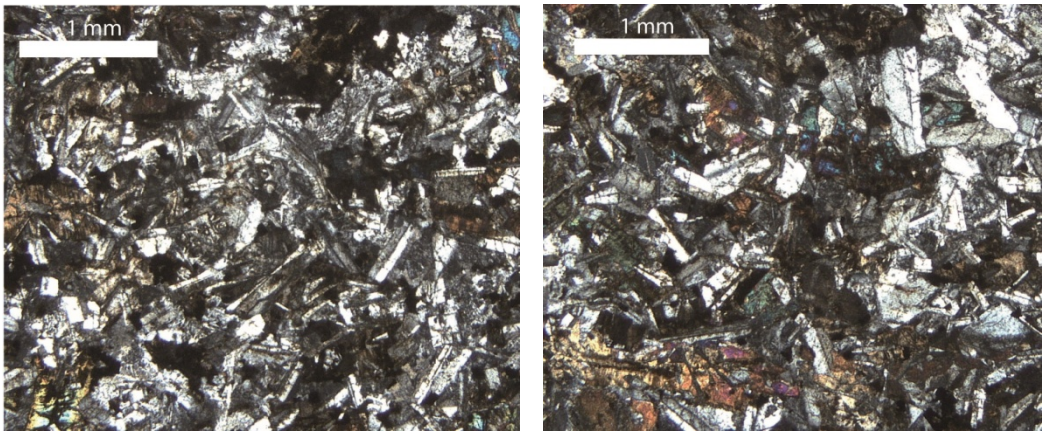

The rock has a fine to medium grained intergranular to sub-ophitic igneous texture. Texture is defined by fine to medium grained brownish clinopyroxene (sometimes altered with fe-oxides coronas and chloritic rims), orthopyroxene, sub-ophitic with euhedral to subeuhedral plagioclase; quartz is a minor component, interstitial and myrmekitic with rare k-feldspar. Accessory minerals are opaques minerals. The rock is classified as a dolerite.

Thin section 71 (ELT32-Piston core 13-Pebble 4-Top: 112; Bottom:113)

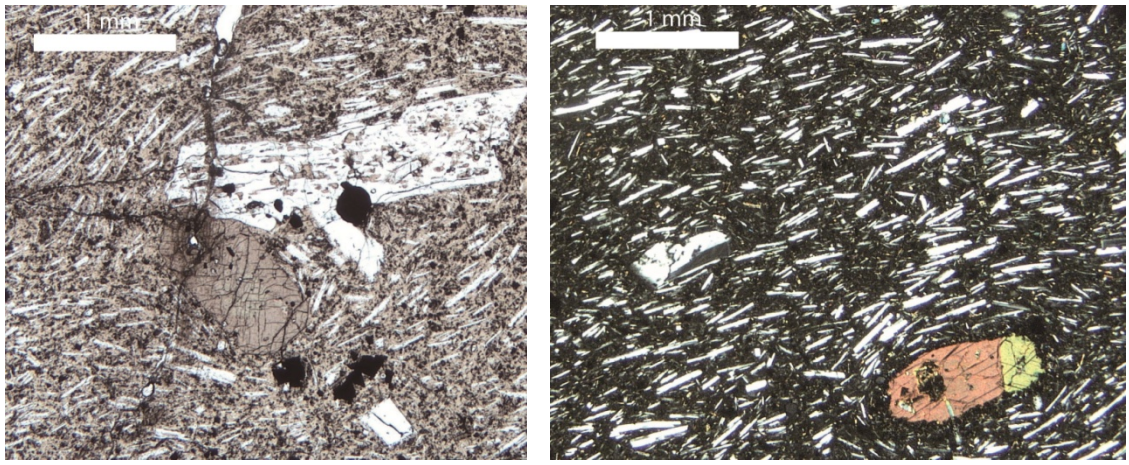

The rock has an ipocrystalline trachytic texture. Medium grained phenocrystals of plagioclase (sometimes poikilitic with glass fragments, apatite and clinopyroxene), brownish and zones augitic clinopyroxene , brown amphibole, opaque minerals are settled in a fine grained matrix defined by oriented plagioclase, opaque minerals, rare sanidine, clinopyroxene and abundant brownish glass. Accessory minerals include apatite. The rock is classified as an alkaline basalt.

Thin section 72 (DF80-Piston core 133-Pebble 1-Top: 167; Bottom:169)

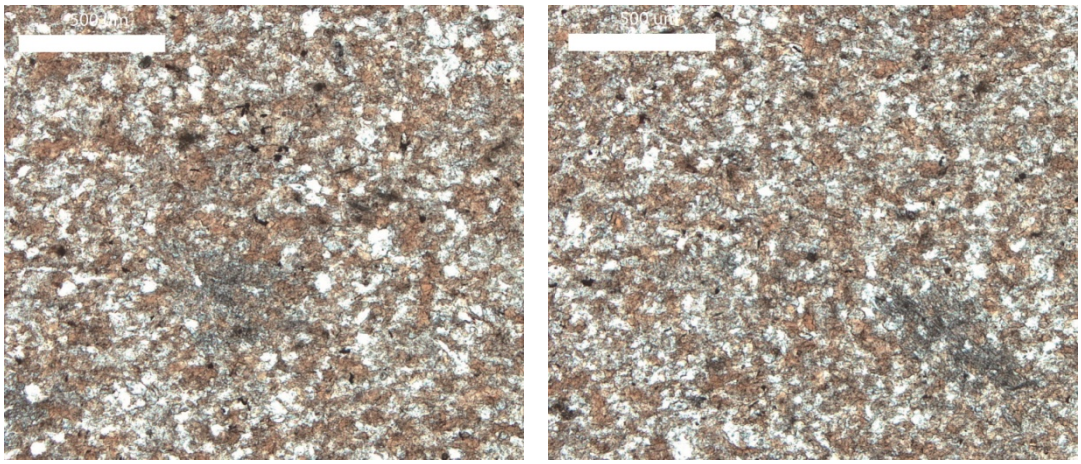

The rock has very fine grained clastic texture. Clasts are mainly quartz grains enveloped by randomly oriented biotite xenoblasts and calcite patches. Biotite sometimes shows a very weak orientation. Very dispersed and rare white mica aggregates. The rock is classified as biotite meta-sandstone.

Thin section 73 (NBP95-01-Piston core 25-Pebble 5-Top: 73; Bottom:80)

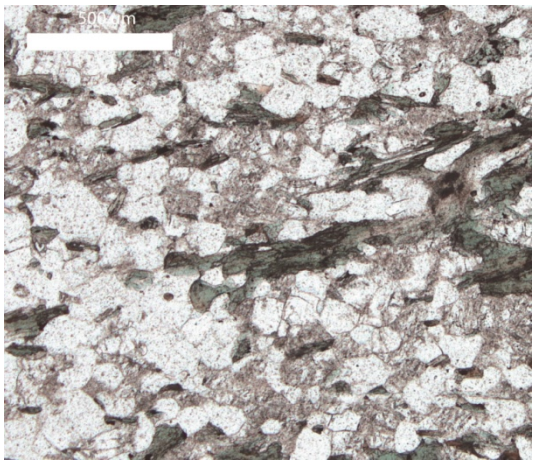

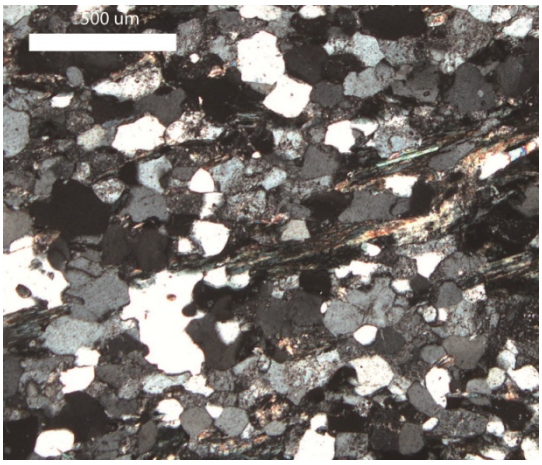

The rock has a fine to medium grained grano-lepidoblastic texture. Foliation is defined by oriented chlorite xenoblasts, sometimes associated with rare white mica xenoblasts which are instead randomly oriented. Granoblastic domains are composed of intergranular quartz and completely altered plagioclase. Sometimes is evident the chlorite replacement of the preexisting biotite crystals. Accessory minerals are zircon, apatite and opaque minerals.

Thin section 74 (DF80-Piston core 134-Pebble 3-Top: 144; Bottom:147)

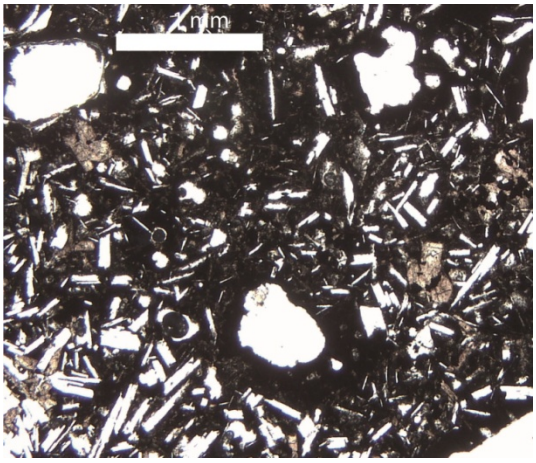

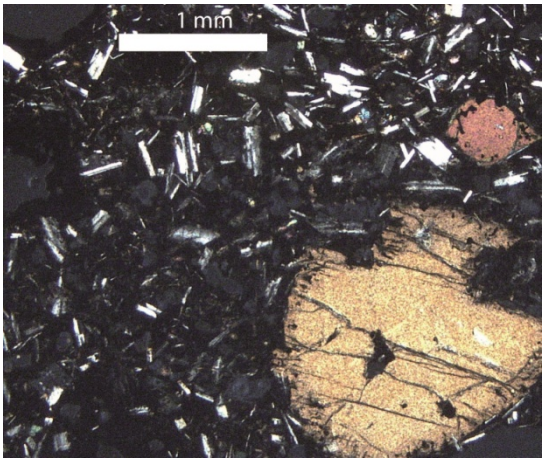

The rock has an ipocrystalline porphyritic vacuolar texture. Rare medium grained phenocrystals of brown augite (sometimes strongly zoned), microphenocrystals of plagioclase, and rare olivine (sometimes with scheletric habitus) aresettled in a fine grained ipocrystalline groundmass composed of plagiocalse, clinopyroxene, scheletric olivine, opaque minerals , and glass (<5%). The rock is classified as a basalt.

Thin section 75 (DF78-Piston core 14-Pebble 15-Top: 152; Bottom:153)

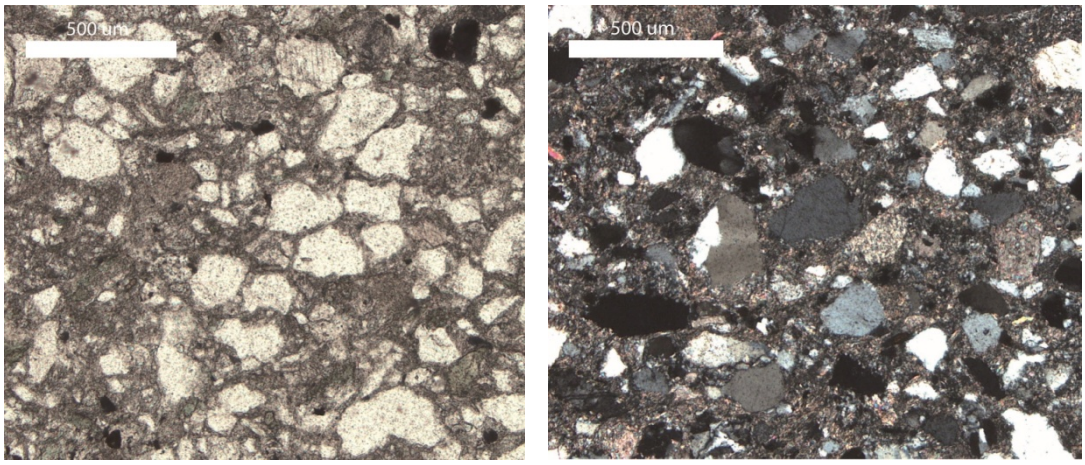

The rock has a poorly sorted, heterogranular, fine to medium sand size grained clastic texture. Clasts are angular to sub-angular and are composed of quartz grains(92), lithics (5) and feldspars (3), settled in abundant matrix (10) composed of biotite, chlorite, calcite and argillaceous material. Zircon, apatite and white mica are present as accessory minerals. The rock is classified as an impure sandstone.

Thin section 76 (DF78-Piston core 14-Pebble 5-Top: 216; Bottom:217.5)

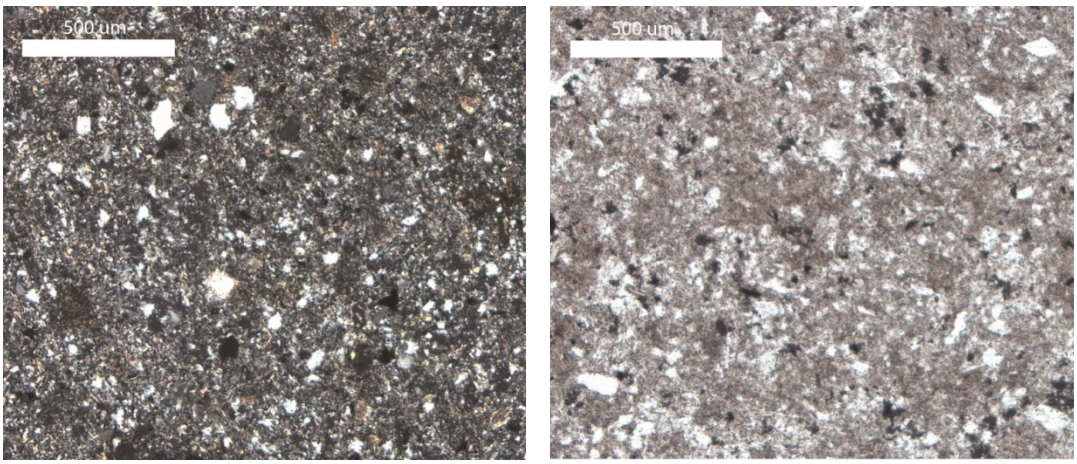

The rock has a silt to very fine sand sized grained clastic texture. Clasts, where recognizable, are composed of quartz grains and rare plagioclase, settled within a finer matrix composed of biotite, white mica and other phyllosilicates, associated to opaque minerals plagues. Zircon and apatite are present as accessory minerals. The rock is classified as a coarse grained siltstone.

Thin section 77 (NBP94-01-Piston core 02-Pebble 3-Top: 114; Bottom:118)

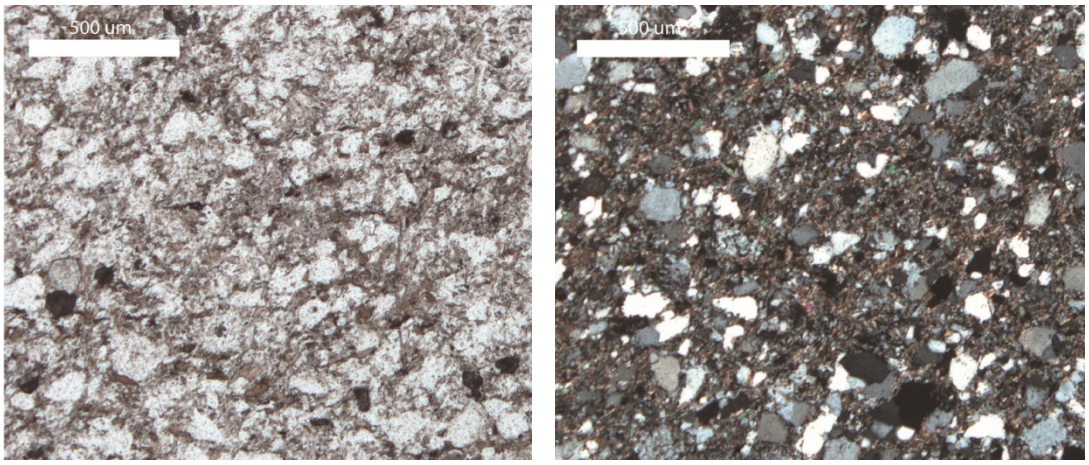

The rock has am heterogranular poorly sorted, fine grain sized clastic texture. Clasts are composed of sub-angular to sub-rounded quartz, plagioclase and lithic grains enveloped by tiny biotite idioblasts to xenoblasts which define a weak foliation; associated to the main foliation there rare white mica idioblast; zircon and opaque minerals are present as accessory minerals. The rock is classified as a meta-sandstone.

Thin section 78 (DF78-Piston core 12-Pebble 4-Top: 85; Bottom:87)

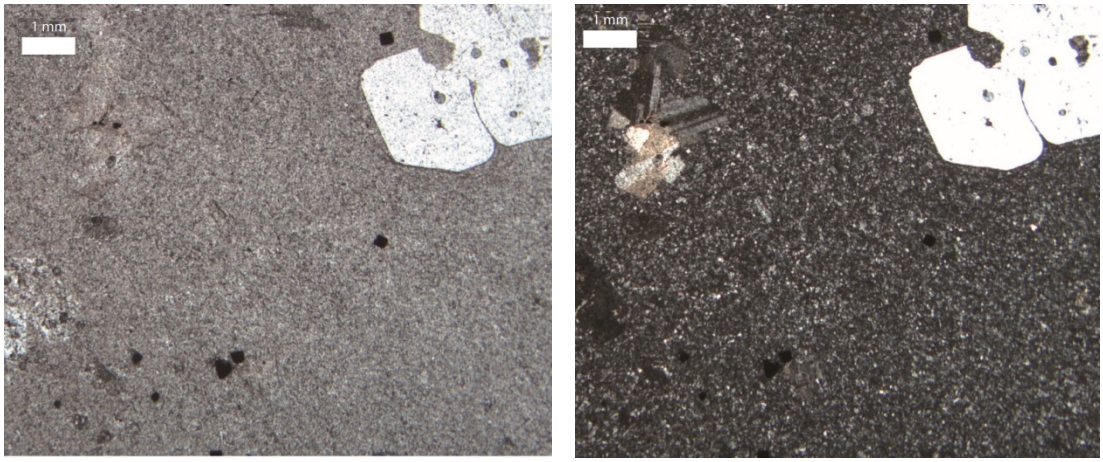

The rock has a fine grained olocrystalline porphyritic (in places glomeroporphyritic, with medium to coarse grained phenocrystals) texture. Phenocrystals are composed of embayed quartz, glomeroporphyritic plagioclase and rare sanidine, set in a fine very fine grained groundmass of quartz-feldspathic composition and opaque minerals. Sometimes are present carbonate alteration on feldspars. The rock is classified as a rhyolitic porphyry.

Thin section 79 (NBP94-07-Piston core 43-Pebble 7-Top: 93; Bottom:97)

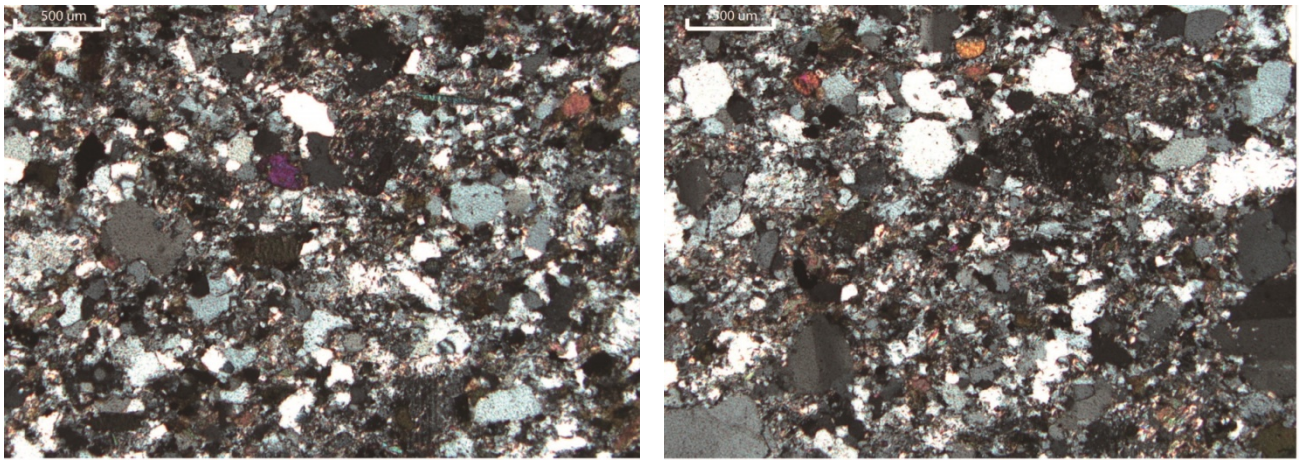

The rock has an heterogranular fine to medium sand sized grained clastic texture. A weak foliation is defined by oriented dark green biotite sub-idioblasts, which envelope to quartz-plagioclase clastic grains; rare chert lithics are present, which sometimes develop a granoblastic texture. Very fine grained white mica crystals sometimes envelope quartz and feldspar grains. Anhedral epidote crystals also present. Zircon and apatite are present as accessory phases. The rock is classified as a meta-sandstone.

Thin section 80 (NBP94-07-Piston core 43-Pebble 1-Top: 4; Bottom:7)

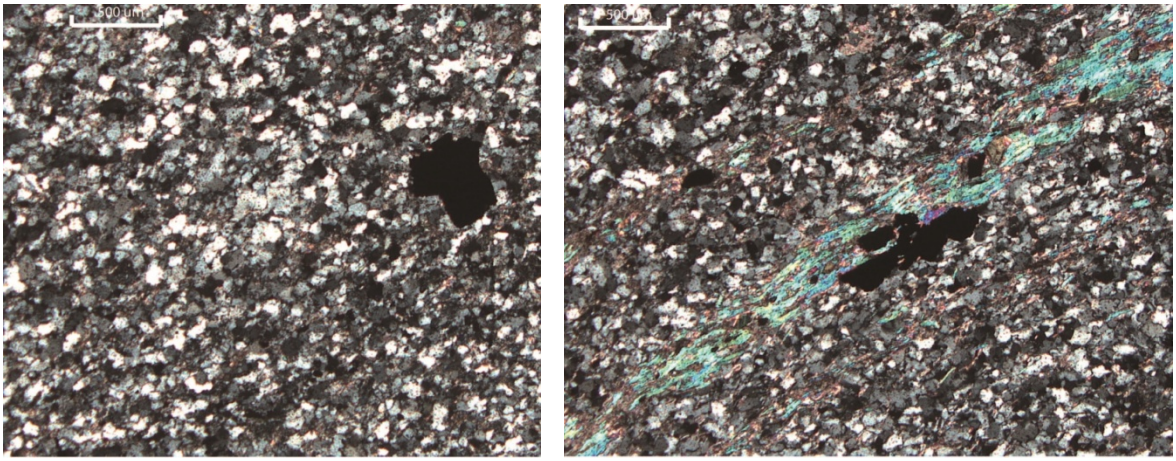

The rock has a fine grained granoblastic texture. The texture is defined by quartz xenoblasts which are slightly oriented; in places there are some white mica, opaque minerals, tourmaline and rare biotite lepidoblastic layering which define a foliation. Opaque minerals are also widespread in granoblastic area, as far as tiny isolated white mica lamellae. The rock is classified as a white mica bearing quartzite.

Thin section 81 (NBP94-07-Piston core 49-Pebble 5-Top: 107; Bottom:108)

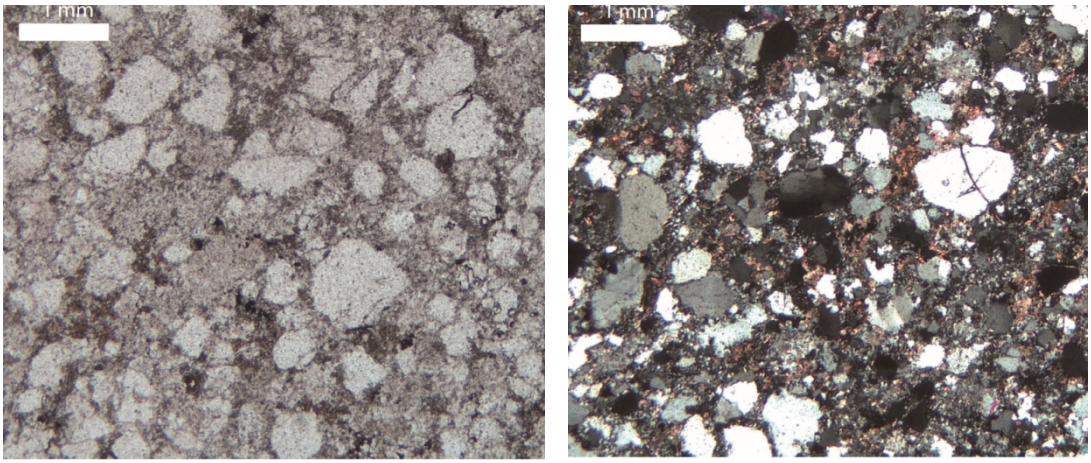

The rock has a medium to coarse grained, heterogranular, poorly sorted, clastic texture. Clasts are composed of angular to sub-rounded polycristalline and monocrystalline quartz grains. Feldspar grains appear very altered by sericitization, and volumetrically consist of 5% of grains. Rare chert lithics grains. Interstitial biotite, calcite, and rare white mica aggregates define matrix together with fine grained quartz grains filling interstices. Accessory phases are zircon, apatite and opaque minerals. The rock is classified as an arkosic arenite.

Thin section 82 (NBP94-07-Piston core 49-Pebble 4-Top: 275; Bottom:276)

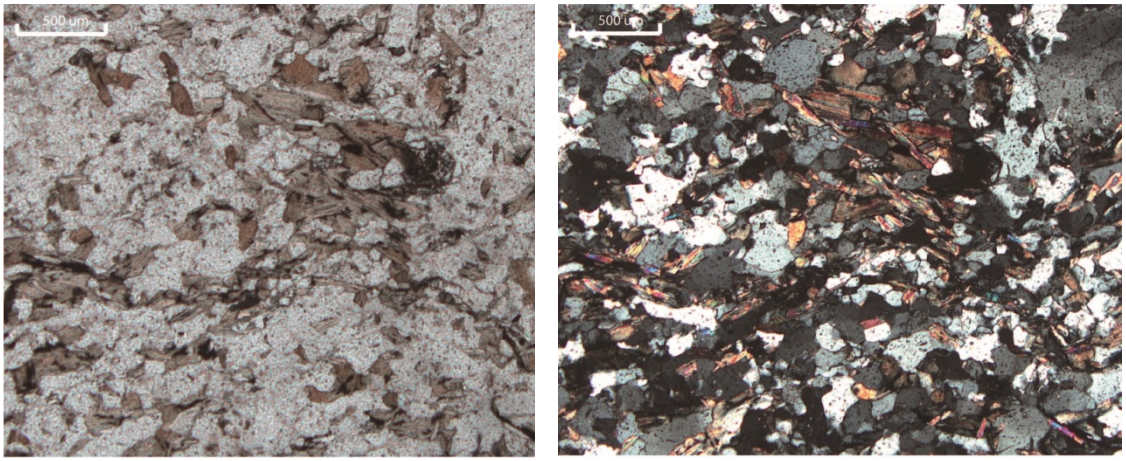

The rock has a fine grained grano-lepidoblastic texture defined by heterogranular interlobate quartz xenoblasts associated with rare plagioclase; some granoblastic portions have coarser grain size. Biotite xenoblasts to idioblasts lamellae define a discontinous foliation; rare white mica lamellae are present but are not associated to the main foliation; accessory minerals are apatite and zircon. The rock is classified as a biotite schist.

Thin section 83 (NBP94-07-Piston core 55-Pebble 2-Top: 262; Bottom:264)

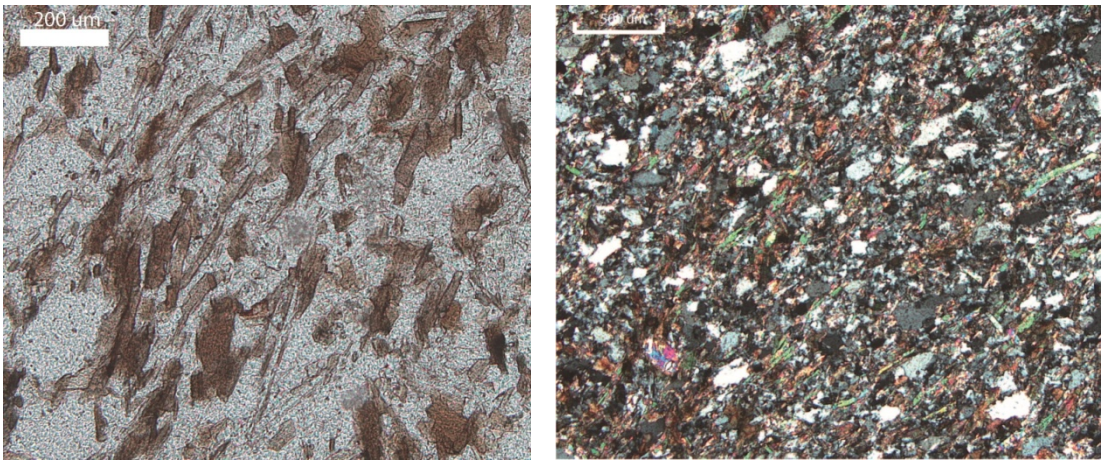

The rock has a fine grained lepidoblastic texture defined by orientation of biotite xenoblasts to idioblasts and white mica lamellae; Granoblastic domains are formed by elongated quartz and rare plagioclase filling the space between cleavage layering. Accessory minerals are tourmaline and apatite. The rock is classified as a biotite-white mica schist.

Thin section 84 (NBP94-07-Piston core 78-Pebble 7-Top: 220; Bottom:221)

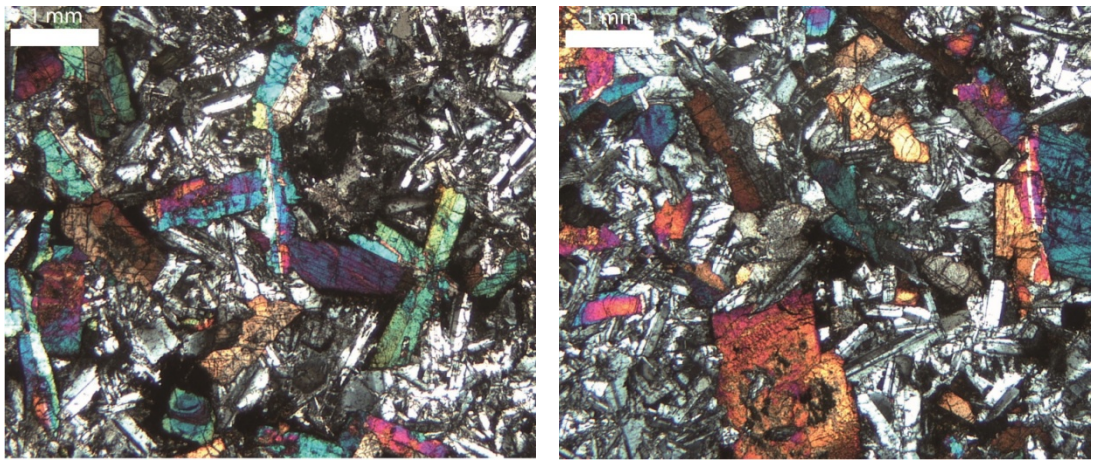

The rock has an intergranular to sub-ophitic medium to coarse grained igneous texture. The texture is defined by clinopyroxene (light brown, twinned and sometimes zoned), plagioclase (twinned and sometimes zoned), opaque minerals and with minor interstitial quartz. The rock is classified as a doleritic gabbro.

Thin section 85 (NBP94-07-Piston core 90-Pebble 3-Top: 92; Bottom:93)

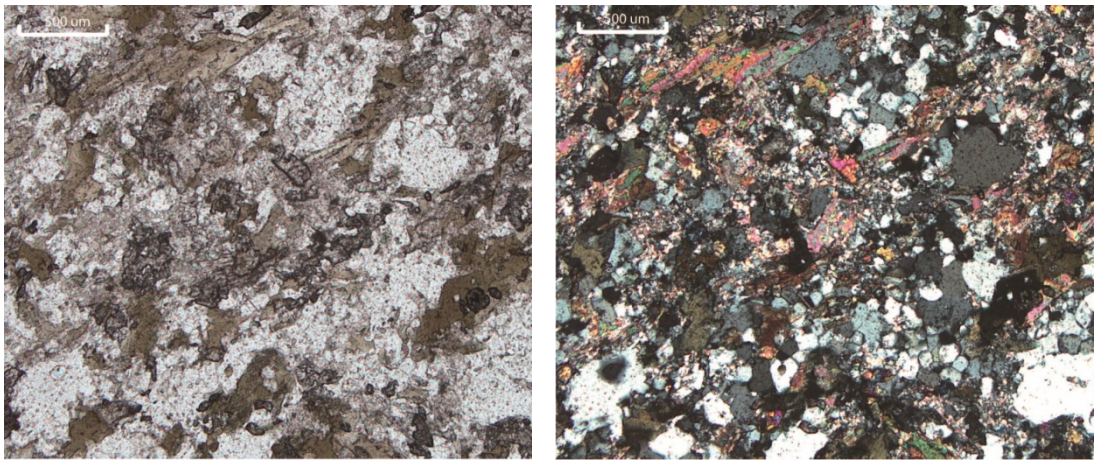

The rock has a fine grained grano-lepidoblastic texture with a preserved clastic appearance. The texture is defined by pale green biotite idioblasts to xenobasts and sparse epidote xenoblasts, set in a matrix of monocrystalline and polycristalline heterogranular quartz grains, rare plagioclase and calcite grains. Biotite sometimes is replaced by chlorite. Rare green amphibole xenoblasts are sparse. Opaque minerals are present as accessory minerals. The rock is classified as a meta-sandstone.

Thin section 86 (DF76-Piston core 08-Pebble 2-Top: 86; Bottom:89)

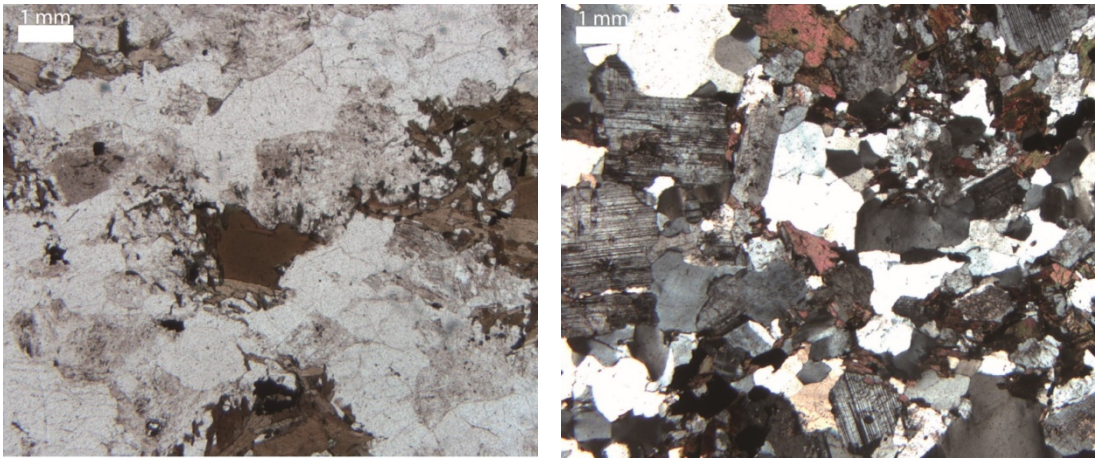

The rock has a medium to coarse grained heterogranular, hypidiomorphic, slightly foliated igneous texture. It is composed of slightly porphyritic plagioclase, interstitial anhedral quartz with undulose extinction and rare microcline; mafic minerals are composed of brown biotite which define a weak foliation. Accessory minerals are zircon , apatite and opaque minerals. The rock is classified as a foliated biotite granodiorite/tonalite.

Thin section 87 (DF76-Piston core 08-Pebble 1-Top: 30; Bottom:35)

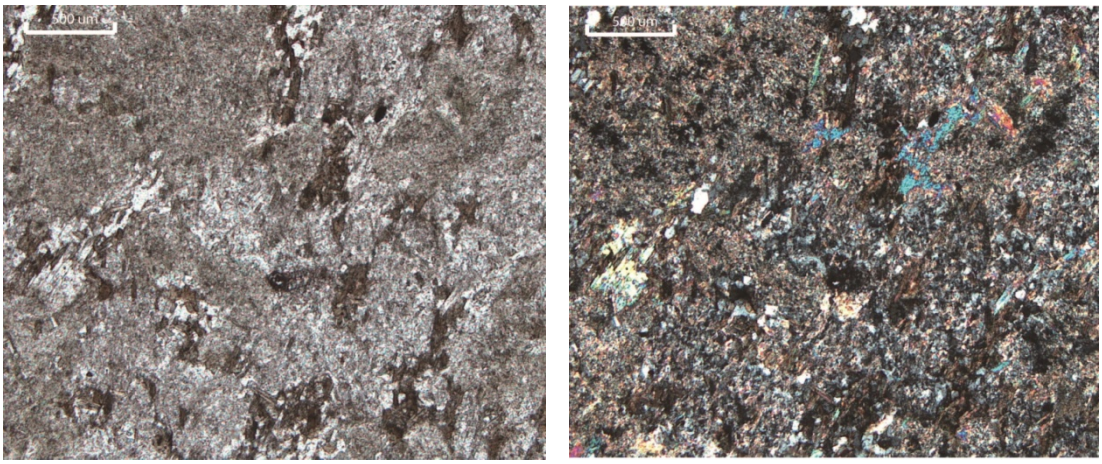

The rock has very fine grained grano-lepidoblastic texture defined by tiny biotite xenoblasts to idioblasts. Coarser grained randomly oriented white mica idioblasts are superimposed on the original texture. The majority of the rock is completely altered by sericite and chlorite aggregates. Smaller portion of qtz small grains are recognizable, sometimes poikilitic with biotite inclusions. The rock has the characteristics of a biotite schist which has been hornfelsed with a thermo-metamorphic overprint, but overall it is too altered to precisely classify it.

Thin section 88 (NBP93-08-Piston core 07-Pebble 2-Top: 20.5; Bottom:21)

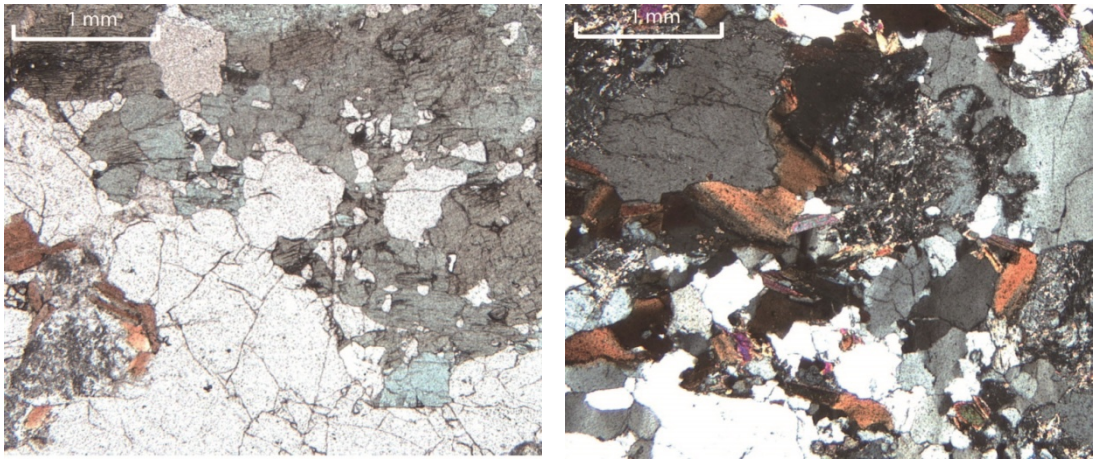

The rock has a medium to coarse grained heterogranular, hypidiomorphic, foliated texture with granoblastic domains. Plagioclase crystals are very altered in sericite aggregates, quartz is medium grained, with interlobate grain boundaries and with undulose extinction. Mafic minerals are represented by brown biotite and medium grained pale green amphibole. Accessory minerals are opaque minerals and zircon. The rock is classified as a biotite-amphibole gneiss.

Thin section 89 (NBP93-08-Piston core 07-Pebble 3-Top: 53; Bottom: 54)

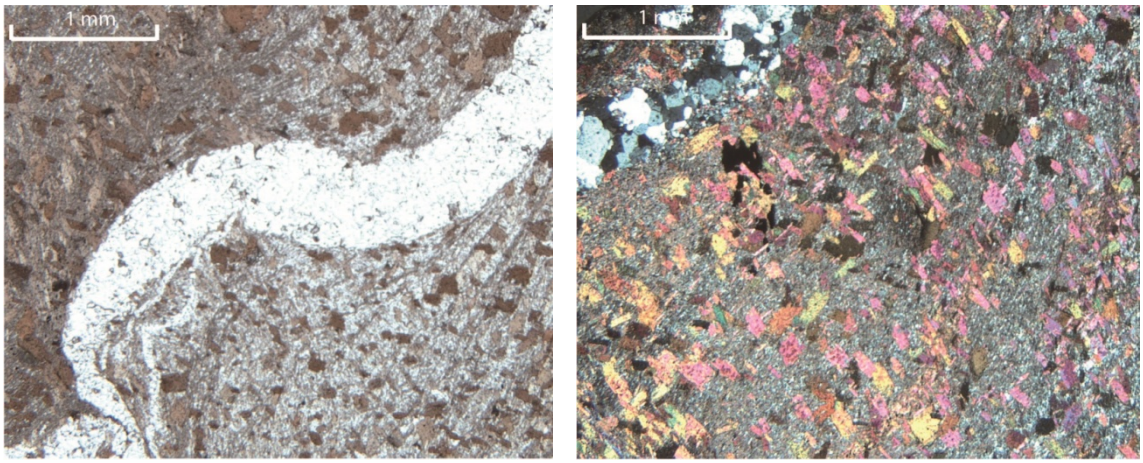

The rock has at least two generations of foliations: a very fine grained lepidoblastic texture (s1) defined by tiny biotite and white mica lamellae and quartz grains, which represent the original phylladic foliation; the latter is oveprinted by coarser grained brown biotite idioblasts to xenoblasts which define a second generation of cleavage (perpendicular to the previous one) and in places define a crenulation cleavage. Quartz veins parallel to S1 are similarly micro-folded. Opaque minerals and apatite are present as accessory minerals. The rock is classified as a phyllite.

Thin section 90 (NBP93-08-Piston core 07-Pebble 8-Top: 122; Bottom: 123)

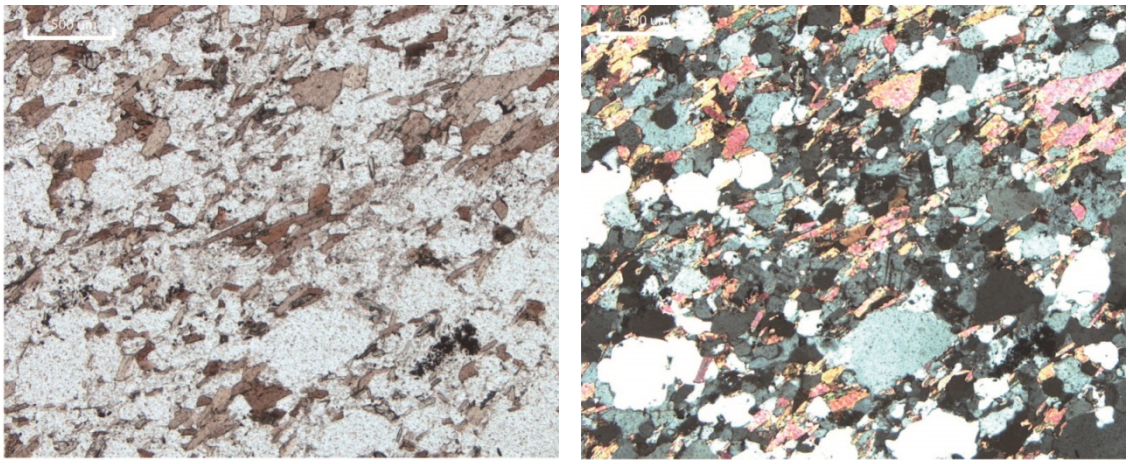

The rock has a fine grained heterogranular grano-lepidoblastic texture. The texture is defined by orientation of biotite idioblasts to xenoblasts and differently elongated qtz (with undulose extinction) associated with rare plagioclase domains. Quartz is heterogranular and sometimes is recrystallized in coarser size crystals. Plagioclase is altered by sericite and sometimes poikilitic with quartz grains. Accessory phases are titanite, apatite, zircon and tourmaline. The rock is classified as a biotite schist.

Thin section 91 (NBP93-08-Piston core 13-Pebble 4-Top: 51; Bottom: 52)

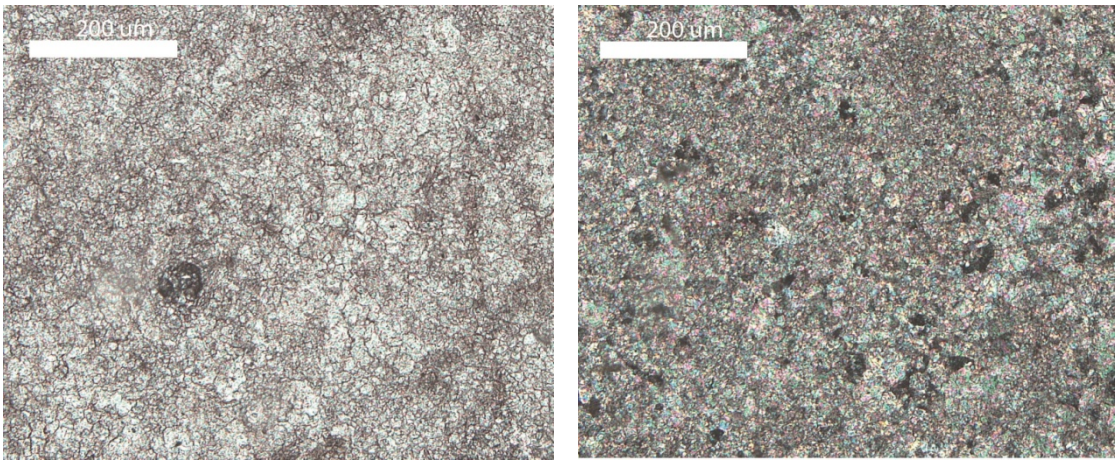

The rock has a fine grained mud-supported texture defined by a mosaic of microsparitic and micritic calcite crystals. In places calcite exhibits a recrystallization in sparitic-size grains (more than 100 micron size). Some rare internal pores are present. Opaque minerals are extremely rare. The rock is classified as a microsparitic limestone.

Thin section 92 (NBP93-08-Piston core 13-Pebble 5-Top: 133; Bottom: 134)

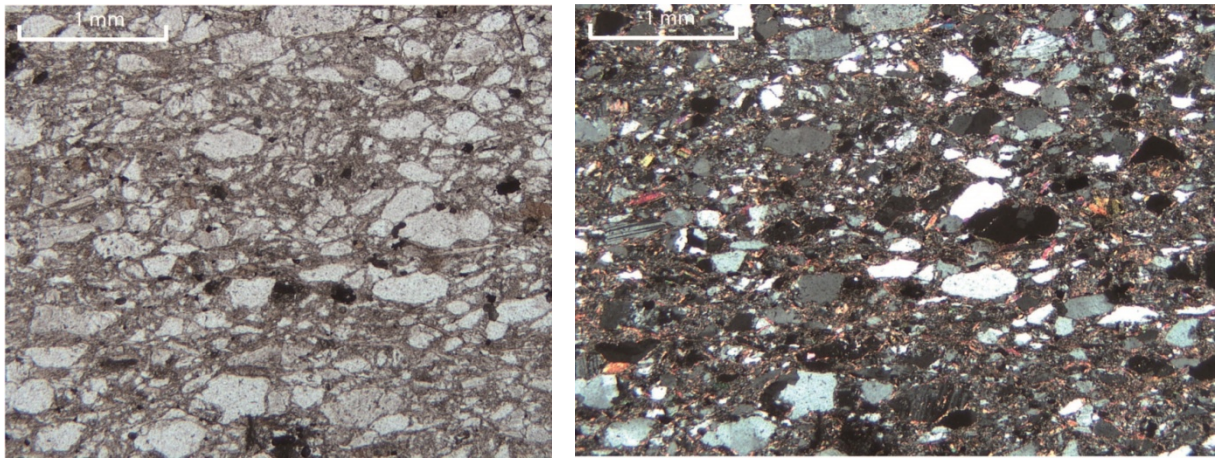

The rock has a fine to medium grained foliated clastic texture. Clasts are composed of elongated sub-angular quartz and plagioclase grains, with rare lithics, which are enveloped by a fine grained foliated matrix composed of biotite and white mica. Widespread in the matrix there are carbonate patches. The rock is classified as a biotite meta-sandstone.

Thin section 93 (NBP93-08-Piston core 13-Pebble 7-Top: 210; Bottom: 211)

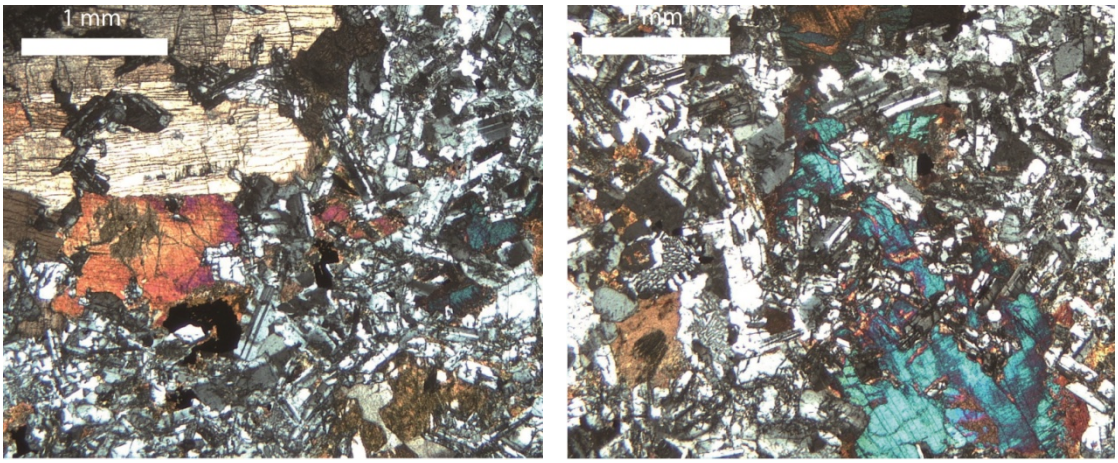

The rock has a medium grained intergranular to sub-ophitic igneous texture. It is composed of light brownish clinopyroxene (twinned, sometimes zoned, slightly altered with oxides rims), sub-ophitic with plagioclase (twinned), opaque minerals and interstitial minor quartz, in granophyric texture with rare k-feldspar. The rock is classified as a doleritic gabbro.

Thin section 94 (NBP93-08-Piston core 13-Pebble 9-Top: 216; Bottom: 217)

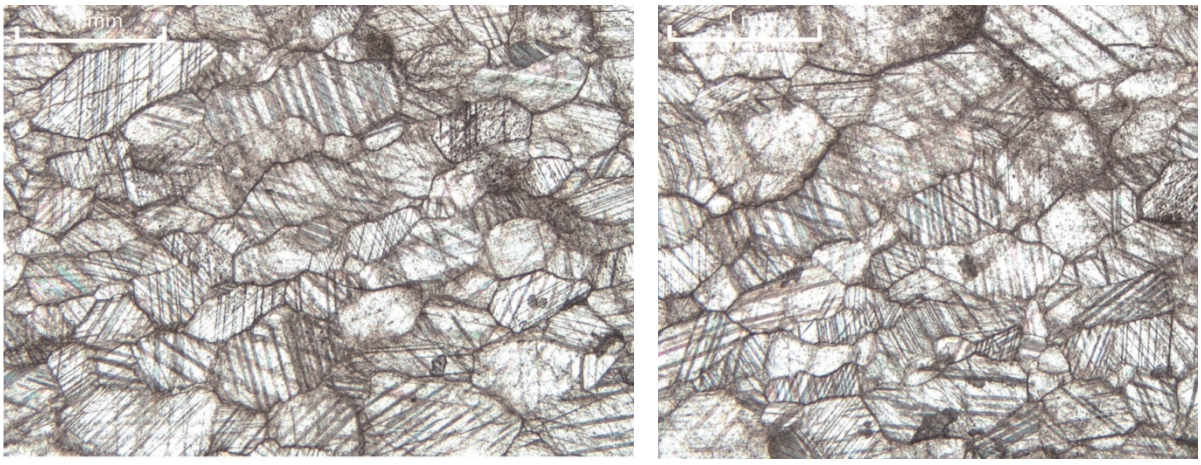

The rock has a medium grained saccaroid texture. The texture is defined by a monomineralic mosaic of sparitic calcite which in places is twinned and elongated. Rare opaque minerals plagues are present. The rock is classified as a marble.

Thin section 95 (NBP96-01-Piston core 02-Pebble 5-Top: 130; Bottom: 135)

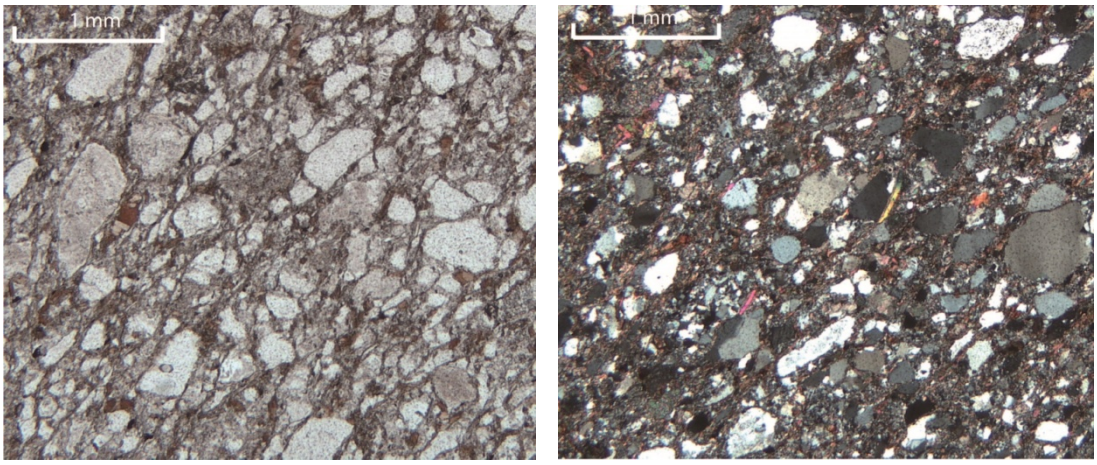

The rock has a fine to medium grained foliated clastic texture. The texture is defined by quartz (monocrystalline, undulose extinction, polycrystalline, elongated clasts), plagioclase, lithics (mainly chert and sedimentary types), enveloped by a slight foliation defined by biotite and white mica lamellae orientation; Calcite patches are sometimes present in the original matrix. Accessory minerals are epidote, apatite, zircon.

Thin section 96 (NBP96-01-Piston core 02-Pebble 2-Top: 176; Bottom: 177)

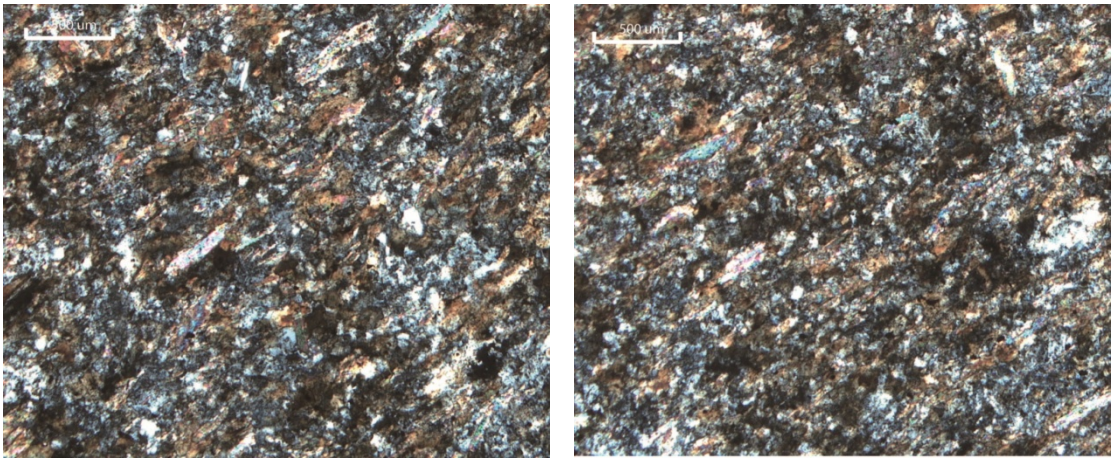

The rock has a fine grained lepidoblastic texture. Slightly oriented biotite xenoblastic lamellae and rare white mica define a weakly developed foliation, which overprint a original quartz-plagioclase-lithic siltitic clastic assemblage. Overall the rock is altered by a sericite patch. The rock is classified as a meta-siltite.

Thin section 97 (NBP96-01-Piston core 02-Pebble 5-Top: 249; Bottom: 250)

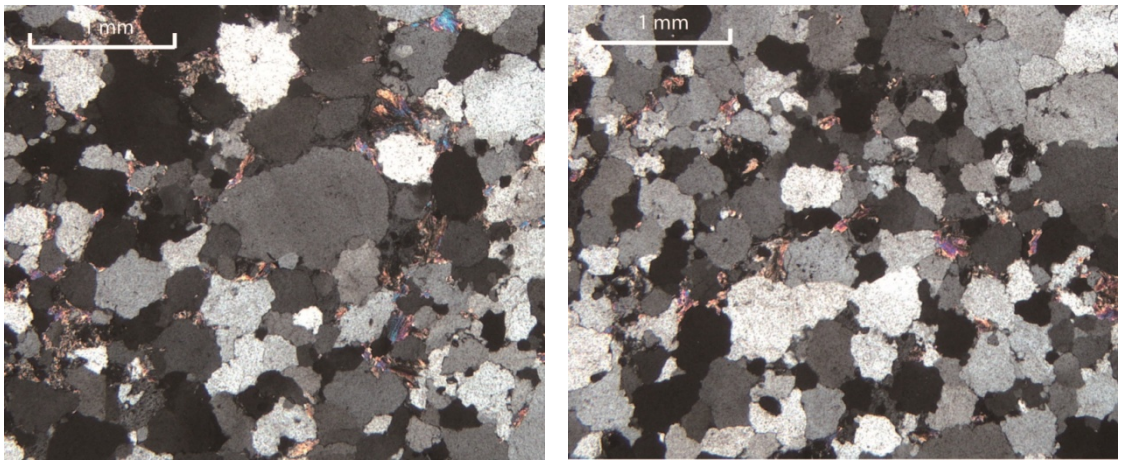

The rock has a medium to coarse sand isotropic heterogranular clastic texture. It is composed almost exclusively of quartz grains (undulose extinction, interlobate grain boundaries), rare interstitial k-feldspar, widespread interstitial white mica and chlorite aggregates which sometimes replace original feldspar grains. Opaque minerals and zircon are accessory minerals. The rock is classified as a quartzite.

Thin section 98 (NBP94-07-Piston core 79-Pebble 4-Top: 78; Bottom: 79)

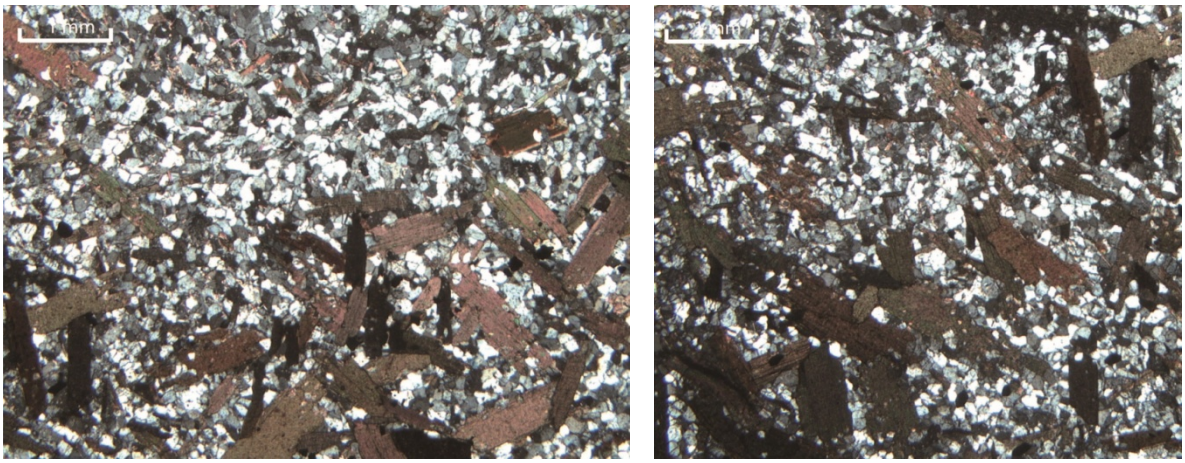

The rock has a fine to medium grained decussate texture. The texture is defined by biotite medium to coarse grained brown idioblasts (sometimes poikilitic with quartz) settled in a fine grained granoblastic domain composed of quartz and rare plagioclase. Rare randomly oriented tiny white mica lamellae are in association with quartzo-feldspathic domain. Accessory minerals are zircon and opaque minerals. The rock is classified as a biotite-hornfels.

Thin section 99 (NBP94-07-Piston core 73-Pebble 1-Top: 2; Bottom: 8)

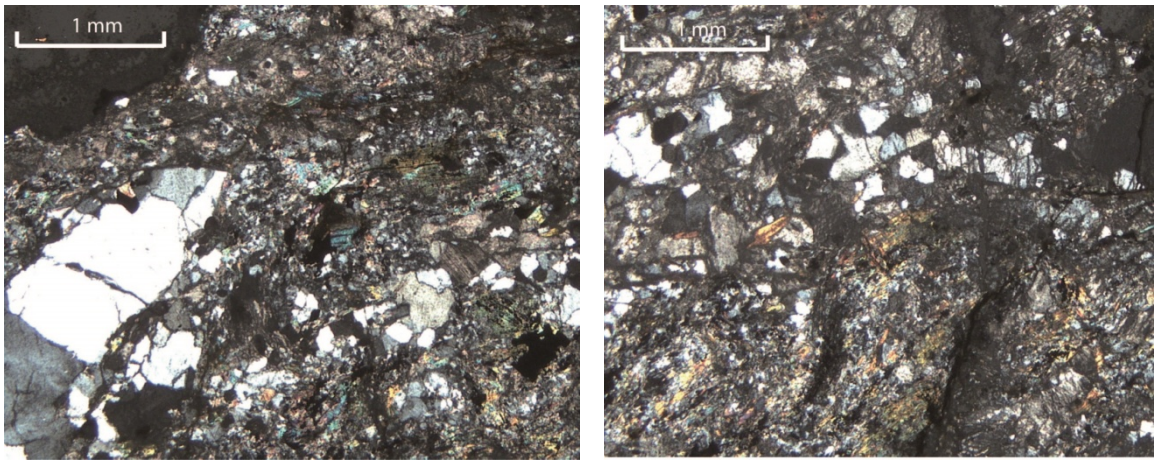

The rock is divided into two different domains: one very fine grained phylladic quartz-calcite-phyllosilicates domain; this portion is very altered and minerals are difficult to distinguish. The other portion is a medium grained gneissic domain defined by granoblastic calcite-quartz-opaque minerals altered to lepidoblastic layering defined by white mica idioblasts to xenoblasts. In places minerals are broken and reduced in finer grain sizes. The rock is classified as a gneissic calc-schist but its grade of alteration do not allow a precise classification.

Thin section 100 (NBP94-07-Piston core 49-Pebble 5-Top: 307; Bottom: 309)

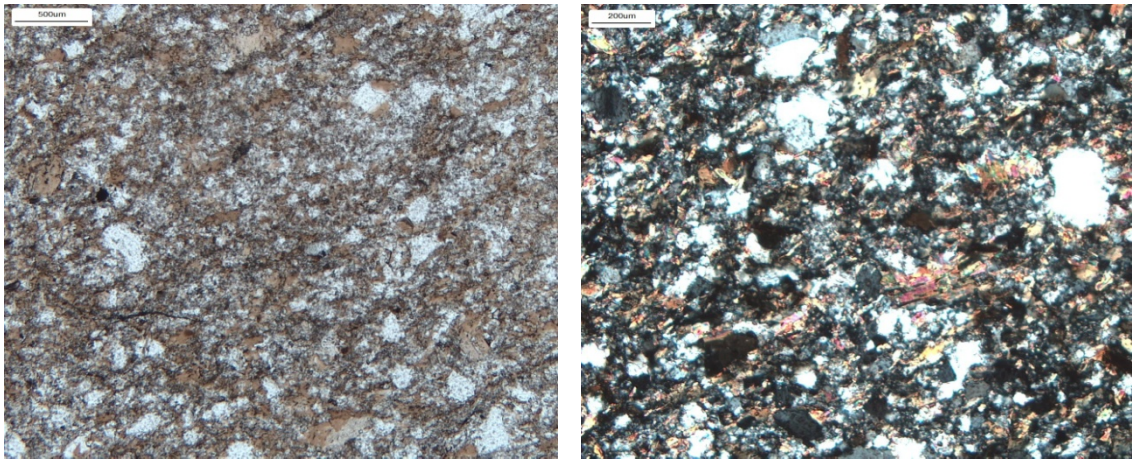

The rock has a fine grained grano-lepidoblastic texture. Foliation is not well developed and it is defined by biotite xenoblasts to randomly oriented idioblasts that envelope heterogranular clasts of quartz and rare altered plagioclase. A thin layer of nematoblastic pale green pleochroic amphibole associated with calcite is present. Accessory minerals are zircon, apatite, tourmaline and opaque minerals. The rocks is classified as a metasandstone.

Thin section 101 (NBP94-07-Piston core 08-Pebble 2-Top: 7; Bottom: 9)

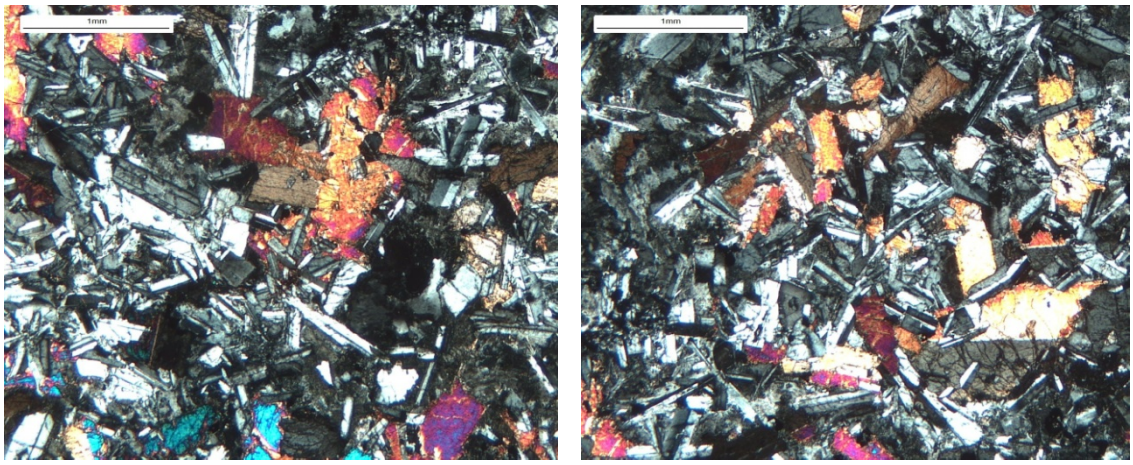

The rock has medium to coarse grained sub-ophitic igneous texture. Texture is defined byintergranular and sub-ophitic clinopyroxene, plagioclase, opaque minerals and rare ortopyroxene. Quartz is interstitial and shows a granophyric texture with rare k-feldspar. Plagioclase is slighlty altered in chlorite aggregates. The rock is classified as a doleritic grabbro.

Thin section 102 (NBP94-07-Piston core 08-Pebble 6-Top: 116; Bottom: 119)

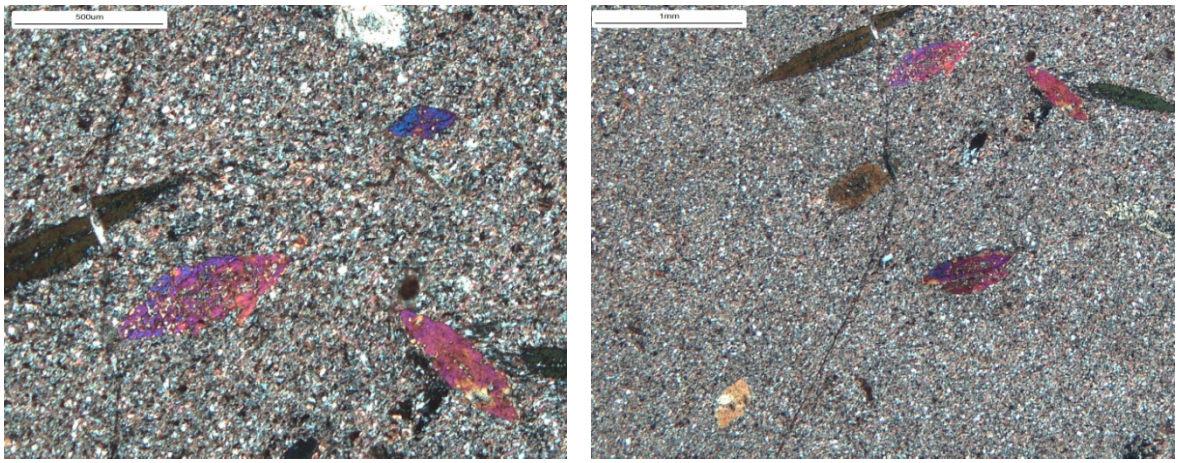

The rock has a fine grained grano-lepidoblastic texture which is defined by tiny biotite idioblasts lamellae ingerlayered with fine grained quartz. Sometimes quartzose domains are slightly coarser grained. Foliation is slightly crenulated. Original foliation is overprinted by randomly oriented fine to medium grained actinolite porphyroblasts, which in places are also poikiloblastic with biotite and quartz. Opaque minerals are present as accessory minerals. The rock is classified as phyllite.

Thin section 103 (NBP94-07-Piston core 45-Pebble 1-Top: 30; Bottom: 31)

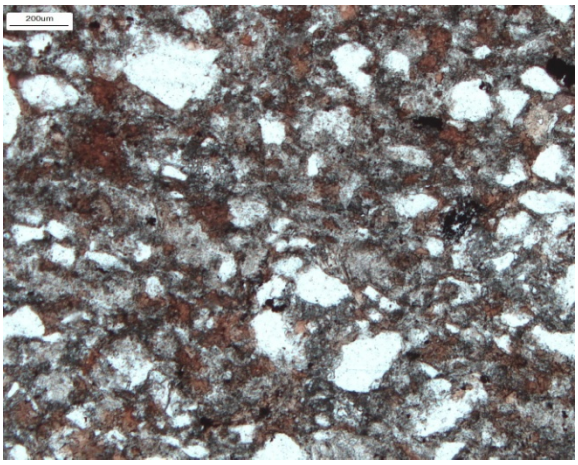

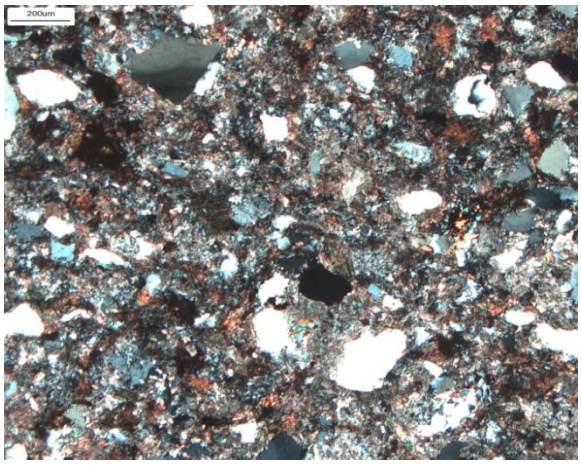

The rock has a medium to coarse sand, poorly sorted, clastic texture. Clasts are sub-angular to sub-rounded quartz, completely altered feldspars, lithics (mainly polycrystalline qtz), settled in a patchy matrix of calcite, sericite and neoblastic biotite that define a weak foliation. Opaque minerals, apatite, zircon and tourmaline are present as accessory minerals. The rock is classified as a meta-graywacke.

Thin section 104 (NBP94-07-Piston core 45-Pebble 4-Top: 133; Bottom: 135)

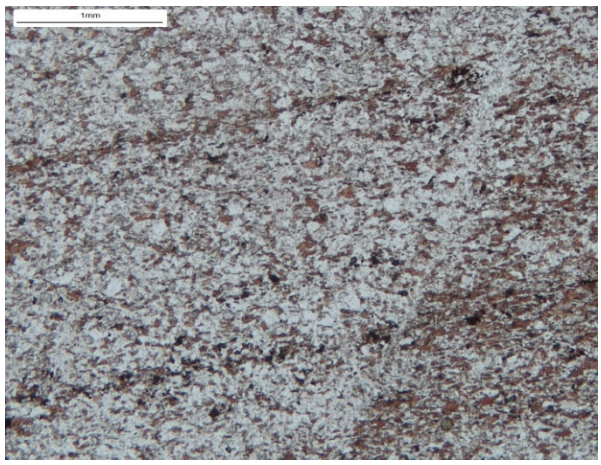

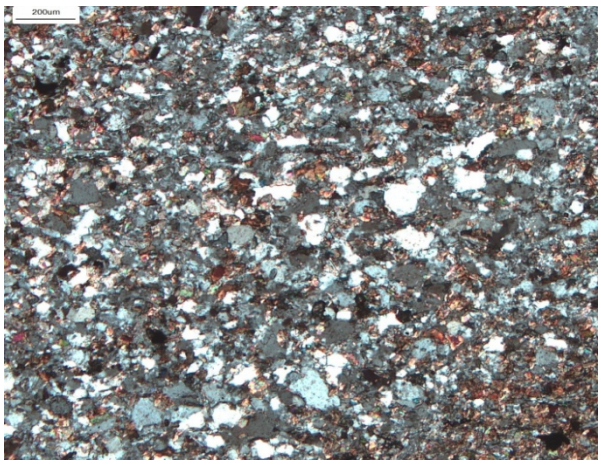

The rock has a fine grained lepidoblastic texture defined by interlayered tiny biotite idioblasts that define a foliation and quartz,calcite and rare plagioclase granoblastic layerings. Microfaults are present along some fractures filled with carbonates. Opaque materials form rare thin layers. Zircon , apatite and tourmaline are present as accessory minerals. The rock is classified as biotite meta-sandstone.

Thin section 105 (NBP94-07-Piston core 79-Pebble 5-Top: 86; Bottom: 87)

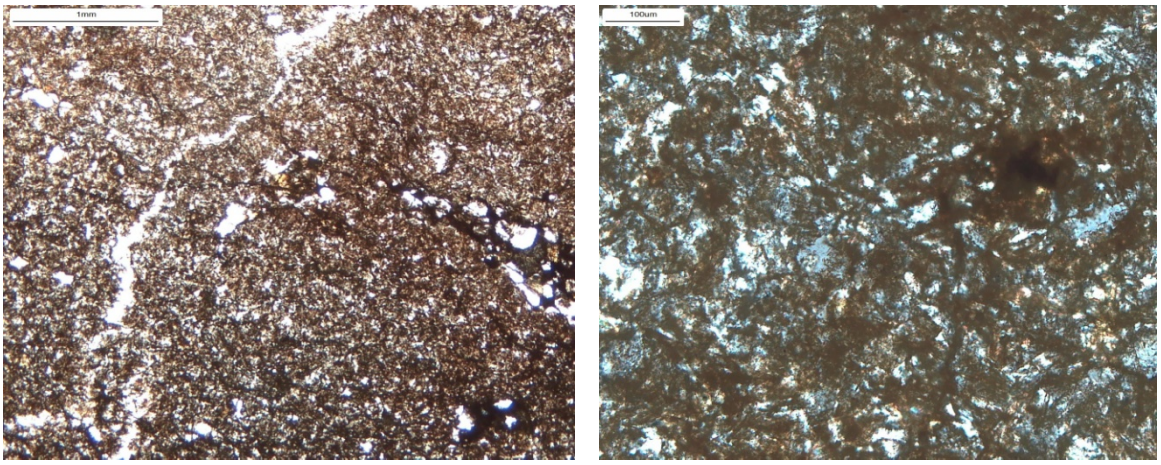

The rock is completely altered. Some fine grained quartz clasts are grouped together set in a felted matrix composed by fe-oxides, sericite and widespread relict texture reminding pylotaxitic and/or granophyric textures. The rock is not determined since its grade of alteration is too high.

Thin section 106 (NBP94-07-Piston core 90-Pebble 6-Top: 237; Bottom: 239)

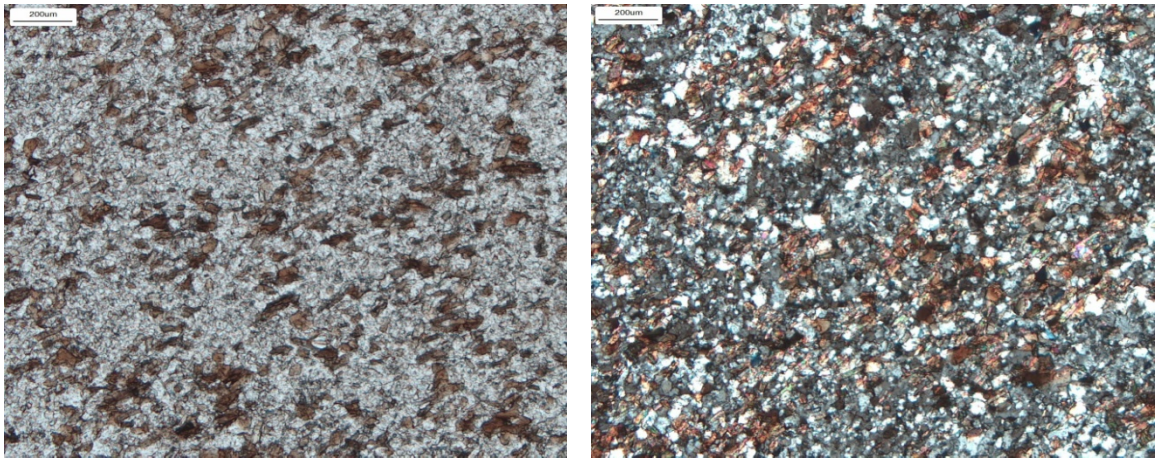

The rock has a fine grained lepidoblastic texture. The texture is defined by biotite idioblasts to sub-idioblasts which define a weak foliation, alterned with granoblastic domains defined by poikiloblastic plagioclase that include quartz xenoblasts. Rare white mica idioblast are randomly oriented and scattered throughout the thin section. Accessory minerals are zircon and apatite. The rock is classified as a biotite schist.

Thin section 107 (NBP96-01-Piston core 2-Pebble 3-Top: 205; Bottom: 206)

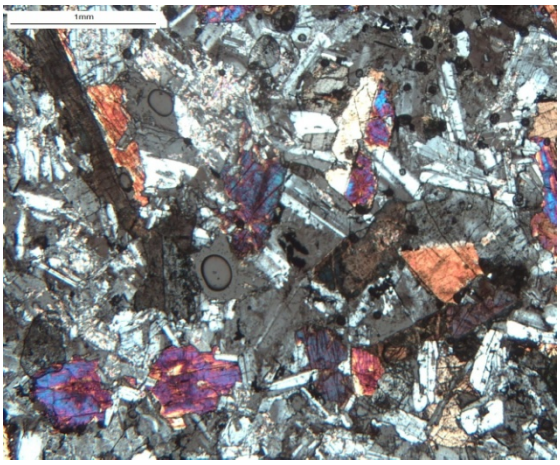
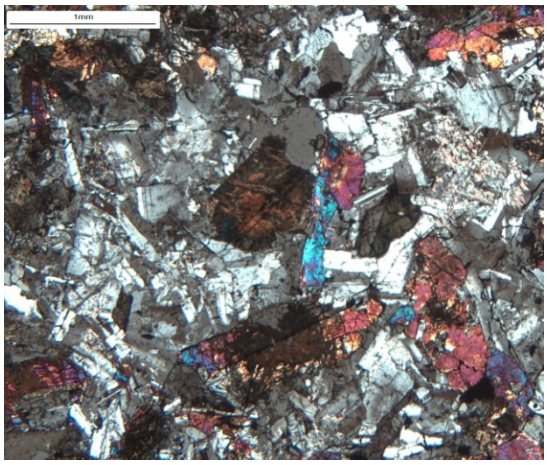

The rock has a medium to coarse grained sub-ophitic igneous texture. The texture is formed by intergranular brownish clinopyroxene, plagioclase and opaque minerals; quartz is interstitial and has a granophyric texture with rare k-feldspar. Clinopyroxene is sometimes altered in greeenish chloritic aggregates. The rock is classified as a doleritic gabbro.

APPENDIX B: mineral chemistry

This appendix includes the tables reporting all mineral chemistry data, discussed in this thesis. Mineral chemistry analysis was carried out on 10 representative clasts from Chapter III, 8 representative clasts from Chapter IV and minerals and lithic grains mounted on polished thin sections from Chapter V. An X-ray energy dispersive system EDAX DX4 attached to a Scansion Electron Microscope Philips XL30 at the Department of Physical Sciences, Earth and Environment of Siena (Italy) was used. The tables are organized with the list of major oxides and atoms per formula units on the left and the values for each analyzed mineral on the right, for each thin section. Where possible, core and rim of each minerals were analyzed. Abbreviations are the following: bt: biotite; hbl: hornblende; cam: clinoamphibole; cpx: clinopyroxene.

The first section (APPENDIX B1) is related to Chapter III: Each table refers to different analyzed minerals (e.g. S1 for white micas, S2 for biotites, S3 for amphiboles, S4 for pyroxenes). Each table has been subdivided in a),b),c) etc. sub-tables, referring to the different examined thin sections. Data are discussed in the Chapter III in the section Mineral Chemistry.

The second section (APPENDIX B2) refers to Chapter IV: it is organized with the list of tables of each analyzed mineral (i.e. biotite, amphibole, white mica). Data are discussed and presented within Chapter IV.

The third section (APPENDIX B3) refers to Chapter V: it is organized with the list of tables of each analyzed mineral (i.e. biotite, pyroxene, plagioclase, amphibole, olivine). Data are discussed and presented within Chapter IV.

APPENDIX B1-Chemical Analysis from Chapter III.

Oxide (Wt%) -----	Thin section 11 (Metasandstone)																			
	White mica1		White mica2		White mica3		White mica4		White mica5		White mica6		White mica7		White mica8		White mica9		White mica10	
	core	rim	core	rim	core	rim	core	rim	core	rim	core	rim	core	rim	core	rim	core	rim	core	Rim
SiO_2	47,56	47,97	47,67	48,14	48,50	47,70	47,81	47,63	47,56	54,10	47,37	46,91	48,02	56,21	47,51	47,87	47,31	49,26	47,82	46,89
TiO_2	1,06	0,83	1,14	0,83	0,65	0,80	1,73	0,76	0,67	0,63	0,97	0,74	1,26	0,96	1,09	0,75	0,82	0,58	0,71	0,59
Al_2O_3	31,45	31,98	31,00	31,04	30,84	31,21	30,16	30,06	31,28	26,27	29,83	30,56	29,32	22,74	31,31	30,92	30,67	29,86	30,83	29,45
FeO	2,45	2,19	2,46	2,63	2,70	2,63	1,97	2,39	2,27	2,17	2,14	2,34	2,31	2,52	2,09	2,30	2,76	4,78	2,48	3,29
MnO	0,07	0,13	0,18	0,13	0,00	0,20	0,00	0,13	0,08	0,15	0,11	0,15	0,13	0,23	0,00	0,14	0,06	0,13	0,10	0,10
MgO	1,66	1,52	1,95	2,02	1,89	1,98	1,58	2,55	2,34	1,65	2,17	2,41	2,51	2,13	1,55	1,83	2,15	2,02	1,94	3,68
CaO	0,18	0,20	0,30	0,18	0,06	0,23	0,26	0,19	0,13	0,15	0,20	0,14	0,17	0,25	0,17	0,18	0,19	0,37	0,13	0,18
Na_2O	0,27	0,35	0,27	0,18	0,30	0,34	0,13	0,59	0,58	0,10	0,47	0,53	0,44	0,37	0,29	0,18	0,18	0,33	0,25	0,95
K_2O	10,65	10,78	11,24	11,01	11,18	10,79	11,24	10,60	10,72	9,73	11,29	10,44	10,53	8,61	10,78	10,69	11,17	7,67	11,02	9,68
Total	95,40	95,98	96,43	96,21	96,12	95,98	94,97	95,06	95,64	95,02	94,56	94,32	94,78	94,26	94,79	95,01	95,43	95,10	95,44	94,95
Formula																				
Si	6,374	6,383	6,367	6,415	6,465	6,378	6,448	6,429	6,363	7,151	6,435	6,373	6,485	7,465	6,396	6,442	6,380	6,572	6,429	6,354
Al^{IV}	1,626	1,617	1,633	1,585	1,535	1,622	1,552	1,571	1,637	0,849	1,565	1,627	1,515	0,535	1,604	1,558	1,620	1,428	1,571	1,646
Al^{VI}	3,343	3,397	3,246	3,288	3,308	3,296	3,243	3,211	3,296	3,243	3,212	3,265	3,153	3,024	3,363	3,345	3,255	3,266	3,312	3,058
Ti	0,107	0,083	0,114	0,083	0,066	0,080	0,175	0,077	0,067	0,062	0,100	0,075	0,128	0,096	0,110	0,076	0,083	0,058	0,071	0,060
Fe^{2+}	0,275	0,243	0,275	0,293	0,301	0,294	0,222	0,269	0,254	0,239	0,243	0,266	0,261	0,280	0,236	0,259	0,311	0,534	0,279	0,372
Mn	0,008	0,015	0,021	0,015	0,000	0,023	0,000	0,015	0,009	0,017	0,013	0,017	0,015	0,025	0,000	0,016	0,007	0,015	0,011	0,012
Mg	0,332	0,301	0,388	0,401	0,376	0,394	0,317	0,513	0,467	0,326	0,441	0,487	0,506	0,422	0,312	0,368	0,432	0,401	0,388	0,744
Ca	0,026	0,029	0,043	0,026	0,008	0,033	0,037	0,027	0,019	0,022	0,029	0,021	0,025	0,036	0,025	0,026	0,028	0,053	0,019	0,026
Na	0,069	0,089	0,070	0,047	0,077	0,087	0,035	0,154	0,151	0,024	0,125	0,139	0,114	0,095	0,077	0,047	0,047	0,086	0,065	0,249
K	1,820	1,829	1,915	1,871	1,901	1,840	1,935	1,825	1,830	1,640	1,957	1,809	1,814	1,458	1,851	1,835	1,922	1,306	1,890	1,673
Total	13,979	13,987	14,072	14,024	14,037	14,047	13,964	14,092	14,093	13,573	14,118	14,080	14,017	13,436	13,974	13,972	14,084	13,719	14,036	14,195

Table S1. a) SEM-EDS mineral chemistry analysis of white micas. Thin section 11.

Oxide (Wt%) -----	Thin section 21 (Bt-wm gneissic schist)																			
	White mica1		White mica2		White mica3		White mica4		White mica5		White mica6		White mica7		White mica8		White mica9		White mica10	
	core	rim	core	rim	core	rim	core	rim	core	rim	core	rim	core	rim	core	rim	core	rim	core	rim
SiO_2	46,93	47,19	47,96	47,89	48,26	48,32	48,10	46,46	47,48	47,93	50,36	47,03	49,76	47,50	47,16	54,02	47,56	47,48	46,69	54,89
TiO_2	0,70	0,76	0,65	0,71	0,60	1,16	0,47	0,88	0,71	0,72	0,65	0,67	0,54	0,98	0,58	0,62	0,93	0,93	0,73	0,59
Al_2O_3	30,77	31,21	31,29	31,06	30,79	31,52	32,27	31,92	31,34	32,21	27,36	31,51	29,18	31,28	31,52	27,55	32,06	29,67	31,89	27,40
FeO	2,15	2,08	2,25	2,49	2,49	2,30	2,32	2,21	2,17	2,05	2,68	2,33	2,44	2,12	2,36	1,99	2,29	4,83	2,42	1,99
MnO	0,13	0,05	0,00	0,10	0,06	0,19	0,15	0,12	0,11	0,24	0,20	0,10	0,15	0,22	0,17	0,08	0,21	0,19	0,07	0,00
MgO	2,17	2,04	1,20	1,29	1,38	1,28	1,29	1,91	1,78	1,09	2,35	2,09	2,71	2,29	2,11	1,45	1,23	1,56	1,65	1,48
CaO	0,14	0,11	0,20	0,20	0,27	0,10	0,10	0,29	0,11	0,16	0,36	0,16	0,11	0,30	0,21	0,16	0,17	0,26	0,29	0,15
Na_2O	0,81	0,87	0,28	0,21	0,30	0,19	0,18	0,91	0,58	0,24	0,18	0,85	0,85	1,00	0,86	0,43	0,13	0,24	0,52	0,43
K_2O	10,72	10,35	11,06	11,05	11,15	10,63	10,84	10,62	10,35	10,42	10,72	10,55	10,28	10,08	10,79	9,24	10,67	10,42	11,18	8,96
Total	94,54	94,75	94,88	95,07	95,34	95,76	95,74	95,32	94,78	95,20	95,01	95,43	96,03	95,93	95,76	95,55	95,33	95,84	95,63	95,89
Formula																				
Si	6,364	6,366	6,457	6,451	6,485	6,436	6,408	6,254	6,397	6,411	6,782	6,323	6,610	6,339	6,322	7,072	6,371	6,428	6,289	7,134
Al^{IV}	1,636	1,634	1,543	1,549	1,515	1,564	1,592	1,746	1,603	1,589	1,218	1,677	1,390	1,661	1,678	0,928	1,629	1,572	1,711	0,866
Al^{VI}	3,282	3,328	3,422	3,382	3,361	3,384	3,475	3,319	3,374	3,488	3,124	3,315	3,178	3,258	3,301	3,322	3,432	3,163	3,351	3,330
Ti	0,071	0,077	0,065	0,072	0,061	0,116	0,047	0,089	0,072	0,073	0,065	0,068	0,054	0,098	0,059	0,061	0,094	0,095	0,074	0,058
Fe^{2+}	0,243	0,235	0,253	0,281	0,280	0,256	0,258	0,249	0,245	0,229	0,302	0,262	0,271	0,237	0,264	0,218	0,256	0,547	0,273	0,217
Mn	0,015	0,005	0,000	0,011	0,007	0,022	0,017	0,014	0,013	0,027	0,023	0,011	0,017	0,025	0,020	0,008	0,024	0,022	0,008	0,000
Mg	0,440	0,410	0,240	0,260	0,277	0,255	0,257	0,383	0,358	0,218	0,471	0,419	0,536	0,456	0,421	0,283	0,246	0,315	0,332	0,286
Ca	0,021	0,016	0,029	0,029	0,038	0,014	0,014	0,041	0,016	0,023	0,052	0,023	0,015	0,043	0,030	0,023	0,025	0,038	0,041	0,021
Na	0,214	0,228	0,072	0,055	0,077	0,049	0,047	0,236	0,151	0,062	0,047	0,221	0,220	0,258	0,224	0,109	0,035	0,063	0,135	0,109
K	1,854	1,780	1,900	1,898	1,910	1,806	1,842	1,823	1,779	1,779	1,841	1,810	1,743	1,716	1,845	1,543	1,823	1,799	1,921	1,485
Total	14,140	14,080	13,981	13,988	14,010	13,902	13,956	14,154	14,007	13,898	13,926	14,129	14,034	14,090	14,164	13,568	13,933	14,041	14,134	13,506

Table S1. b) SEM-EDS mineral chemistry analysis of white micas. Thin section 21.

Oxide (Wt%)	Thin section 63 (Calc-schist)													
-----	White mica1		White mica2		White mica3		White mica4		White mica5		White mica6		White mica7	
	core	rim	core	rim	core	rim	core	rim	core	rim	core	rim	core	rim
SiO_2	48,55	47,69	48,06	48,80	48,41	48,43	47,21	47,82	47,34	49,01	48,59	48,85	47,42	49,91
TiO_2	0,88	0,57	0,78	0,72	0,42	0,81	0,64	0,74	0,62	0,60	0,67	0,80	0,88	0,80
Al_2O_3	31,74	33,01	32,17	32,22	32,03	31,34	32,55	31,89	31,91	31,43	31,60	29,93	31,57	29,40
FeO	1,81	1,72	1,94	1,75	1,85	1,74	1,93	2,06	1,98	1,81	2,14	1,84	1,94	2,64
MnO	0,00	0,14	0,23	0,12	0,05	0,07	0,10	0,20	0,31	0,00	0,15	0,24	0,20	0,13
MgO	1,86	1,31	1,11	1,19	1,22	1,30	1,63	0,82	1,79	1,97	1,37	2,29	1,79	1,85
CaO	0,24	0,19	0,27	0,28	0,13	0,11	0,10	0,25	0,16	0,09	0,20	0,24	0,45	0,21
Na_2O	0,74	0,54	0,35	0,42	0,41	0,31	1,03	0,35	0,58	0,65	0,33	0,98	0,72	0,24
K_2O	10,12	10,54	10,68	10,15	10,39	10,69	10,12	11,38	11,00	10,45	10,46	9,68	10,50	10,52
Total	96,03	95,83	95,65	95,82	94,95	94,83	95,43	95,79	95,84	96,02	95,64	94,95	95,72	95,83
Formula														
Si	6,425	6,338	6,405	6,461	6,468	6,490	6,310	6,411	6,336	6,482	6,470	6,540	6,349	6,645
Al^{IV}	1,575	1,662	1,595	1,539	1,532	1,510	1,690	1,589	1,664	1,518	1,530	1,460	1,651	1,355
Al^{VI}	3,374	3,508	3,457	3,489	3,512	3,440	3,437	3,449	3,369	3,381	3,429	3,262	3,331	3,259
Ti	0,088	0,057	0,079	0,072	0,042	0,081	0,064	0,074	0,063	0,060	0,067	0,080	0,089	0,080
Fe^{2+}	0,200	0,191	0,216	0,194	0,207	0,194	0,215	0,231	0,222	0,201	0,239	0,206	0,218	0,293
Mn	0,000	0,016	0,026	0,014	0,005	0,008	0,012	0,023	0,035	0,000	0,017	0,027	0,023	0,015
Mg	0,368	0,260	0,220	0,235	0,244	0,260	0,325	0,165	0,358	0,388	0,272	0,457	0,357	0,367
Ca	0,034	0,027	0,038	0,039	0,019	0,016	0,014	0,036	0,023	0,012	0,029	0,034	0,065	0,030
Na	0,190	0,138	0,091	0,108	0,106	0,081	0,267	0,092	0,152	0,167	0,084	0,254	0,186	0,062
K	1,708	1,787	1,816	1,714	1,771	1,827	1,725	1,946	1,878	1,763	1,777	1,652	1,793	1,787
Total	13,962	13,983	13,944	13,864	13,906	13,908	14,058	14,015	14,100	13,973	13,914	13,972	14,061	13,893

Table S1. c) SEM-EDS mineral chemistry analysis of white micas. Thin section 63.

Oxide (Wt%) -----	Thin section 56 (Wm-metasandstone)																			
	White mica1		White mica2		White mica3		White mica4		White mica5		White mica6		White mica7		White mica8		White mica9		White mica10	
	core	rim	core	rim	core	rim	core	rim	core	rim	core	rim	core	rim	core	rim	core	rim	core	rim
SiO_2	49,96	48,72	51,42	48,46	51,20	49,49	49,81	48,07	48,03	48,91	48,12	48,65	48,84	45,75	50,06	49,70	49,30	47,79	48,87	48,15
TiO_2	0,83	0,89	1,06	0,87	0,55	0,70	0,90	0,35	0,37	0,83	0,89	0,20	0,82	0,99	0,96	0,65	0,74	0,66	0,48	0,93
Al_2O_3	28,45	29,02	27,00	31,40	27,40	26,34	29,51	32,58	32,85	30,37	29,13	32,20	29,48	27,73	29,12	28,16	29,58	30,66	31,89	27,86
FeO	2,82	2,57	2,53	1,49	4,50	7,15	2,69	1,75	1,28	2,28	2,56	2,55	2,77	7,61	2,55	2,24	2,81	2,04	1,50	3,46
MnO	0,10	0,06	0,32	0,18	0,25	0,11	0,13	0,12	0,11	0,12	0,18	0,05	0,21	0,19	0,16	0,09	0,12	0,08	0,16	0,14
MgO	2,20	2,72	1,42	1,52	2,26	2,43	1,92	0,88	1,92	2,41	2,90	0,88	2,03	2,11	2,17	3,36	1,92	2,56	1,78	1,76
CaO	0,16	0,18	0,49	0,18	0,19	0,24	0,08	0,62	0,11	0,18	0,16	0,25	0,12	0,38	0,17	0,16	0,21	0,04	0,13	0,19
Na_2O	0,10	0,49	1,77	0,96	0,15	0,24	0,22	0,29	0,87	0,49	0,79	1,00	0,33	0,25	0,14	0,89	0,13	0,74	0,46	0,13
K_2O	10,62	10,41	9,61	9,73	8,12	8,46	9,90	10,46	10,00	10,09	10,35	9,26	10,35	10,14	10,71	9,54	10,16	10,78	9,78	12,58
Total	95,43	95,07	96,01	94,98	94,76	95,21	95,34	95,12	95,62	95,82	95,32	95,13	95,17	95,54	96,05	94,87	95,10	95,45	95,25	95,37
Formula																				
Si	6,692	6,550	6,855	6,472	6,846	6,714	6,643	6,419	6,364	6,502	6,486	6,481	6,568	6,338	6,646	6,657	6,608	6,411	6,488	6,582
Al^{IV}	1,308	1,450	1,145	1,528	1,154	1,286	1,357	1,581	1,636	1,498	1,514	1,519	1,432	1,662	1,354	1,343	1,392	1,589	1,512	1,418
Al^{VI}	3,183	3,147	3,096	3,414	3,164	2,925	3,281	3,545	3,492	3,261	3,113	3,536	3,240	2,865	3,202	3,102	3,279	3,258	3,478	3,070
Ti	0,084	0,090	0,106	0,088	0,055	0,071	0,090	0,035	0,037	0,083	0,090	0,020	0,083	0,104	0,096	0,066	0,075	0,066	0,048	0,095
Fe^{2+}	0,316	0,289	0,283	0,167	0,503	0,811	0,300	0,195	0,142	0,254	0,289	0,284	0,311	0,882	0,284	0,251	0,314	0,229	0,167	0,396
Mn	0,012	0,006	0,036	0,020	0,028	0,013	0,015	0,014	0,012	0,014	0,021	0,005	0,024	0,022	0,018	0,011	0,014	0,009	0,018	0,017
Mg	0,440	0,545	0,282	0,303	0,450	0,491	0,381	0,176	0,380	0,479	0,582	0,176	0,406	0,436	0,430	0,671	0,384	0,512	0,353	0,360
Ca	0,023	0,026	0,070	0,026	0,027	0,035	0,011	0,088	0,015	0,026	0,023	0,035	0,018	0,057	0,025	0,023	0,030	0,005	0,019	0,028
Na	0,027	0,129	0,457	0,248	0,039	0,063	0,057	0,074	0,224	0,126	0,207	0,258	0,087	0,067	0,037	0,232	0,035	0,194	0,118	0,035
K	1,815	1,785	1,634	1,657	1,385	1,465	1,684	1,782	1,690	1,711	1,780	1,573	1,776	1,791	1,814	1,631	1,736	1,844	1,657	2,193
Total	13,900	14,018	13,964	13,922	13,652	13,873	13,818	13,911	13,992	13,954	14,104	13,887	13,945	14,224	13,905	13,985	13,867	14,117	13,856	14,193

Table S1. d) SEM-EDS mineral chemistry analysis of white micas. Thin section 56.

Oxide (Wt%) -----	Thin section 62 (Bt-wm hornfels)															
	White mica1		White mica2		White mica3		White mica4		White mica5		White mica6		White mica7		White mica8	
	core	rim	core	rim	core	rim	core	rim	core	rim	core	rim	core	rim	core	rim
SiO_2	47,18	45,48	46,78	46,08	46,01	46,27	46,10	47,18	46,75	47,33	47,23	47,10	46,25	46,75	47,68	47,86
TiO_2	0,39	0,61	0,32	0,55	0,45	0,58	1,01	0,75	0,57	1,30	1,38	0,95	0,62	0,45	0,49	0,77
Al_2O_3	34,01	33,85	35,34	35,25	34,11	33,31	32,82	33,56	32,45	30,70	32,38	32,55	33,04	33,24	32,63	31,77
FeO	1,40	1,44	1,14	0,90	1,37	1,56	1,36	1,64	1,68	2,10	1,49	1,78	1,83	1,33	1,50	1,76
MnO	0,12	0,22	0,09	0,22	0,00	0,17	0,12	0,10	0,20	0,22	0,19	0,20	0,18	0,07	0,14	0,08
MgO	0,70	1,58	0,58	0,46	1,30	1,43	1,65	0,91	1,74	2,24	0,91	2,09	1,86	1,60	1,11	1,47
CaO	0,10	0,15	0,15	0,00	0,14	0,34	0,23	0,16	0,16	0,00	0,09	0,13	0,25	0,11	0,24	0,00
Na_2O	0,33	0,88	0,37	0,28	0,77	0,64	0,92	0,22	0,65	0,78	0,20	1,09	0,86	0,58	0,34	0,26
K_2O	11,08	10,81	11,26	11,34	10,78	10,69	10,89	10,98	10,92	10,29	10,81	9,96	10,35	11,21	10,94	11,15
Total	95,43	95,14	96,10	95,21	94,93	95,16	95,25	95,62	95,21	95,14	94,85	96,03	95,41	95,35	95,26	95,17
Formula																
Si	6,295	6,124	6,196	6,166	6,178	6,219	6,202	6,290	6,285	6,369	6,346	6,261	6,204	6,259	6,382	6,416
Al^{IV}	1,705	1,876	1,804	1,834	1,822	1,781	1,798	1,710	1,715	1,631	1,654	1,739	1,796	1,741	1,618	1,584
Al^{VI}	3,643	3,497	3,712	3,724	3,575	3,496	3,406	3,564	3,425	3,238	3,475	3,361	3,428	3,503	3,530	3,434
Ti	0,039	0,062	0,032	0,056	0,045	0,059	0,102	0,075	0,058	0,132	0,139	0,095	0,063	0,045	0,049	0,078
Fe^{2+}	0,157	0,162	0,127	0,101	0,153	0,175	0,153	0,183	0,188	0,237	0,167	0,197	0,205	0,149	0,167	0,197
Mn	0,014	0,025	0,010	0,025	0,000	0,020	0,014	0,011	0,023	0,025	0,022	0,023	0,021	0,008	0,016	0,009
Mg	0,139	0,317	0,114	0,091	0,260	0,286	0,330	0,181	0,349	0,449	0,182	0,415	0,372	0,320	0,221	0,293
Ca	0,015	0,022	0,022	0,000	0,020	0,049	0,033	0,023	0,023	0,000	0,012	0,019	0,036	0,016	0,034	0,000
Na	0,086	0,231	0,096	0,072	0,200	0,166	0,241	0,057	0,169	0,204	0,052	0,280	0,223	0,151	0,089	0,067
K	1,886	1,857	1,903	1,935	1,847	1,832	1,868	1,867	1,873	1,767	1,854	1,688	1,771	1,915	1,867	1,907
Total	13,978	14,172	14,014	14,003	14,102	14,083	14,148	13,960	14,108	14,050	13,903	14,078	14,119	14,107	13,973	13,984

Table S1. e) SEM-EDS mineral chemistry analysis of white micas. Thin section 62.

Oxide (Wt%) -----	PRR34239 (Phyllite-Swanson Formation)																			
	White mica1		White mica2		White mica3		White mica4		White mica5		White mica6		White mica7		White mica8		White mica9		White mica10	
	core	rim	core	rim	core	rim	core	rim	core	rim	core	rim	core	rim	core	rim	core	rim	core	rim
SiO_2	46,04	46,00	45,28	46,85	46,44	46,79	45,48	46,78	47,05	46,71	46,10	46,84	46,57	43,88	46,37	47,15	47,12	42,79	45,96	46,71
TiO_2	1,44	1,20	1,10	0,98	1,83	1,08	1,11	1,16	1,29	0,86	1,45	1,01	1,35	1,27	1,32	1,10	1,57	2,08	1,76	1,20
Al_2O_3	34,69	34,61	35,11	34,98	34,71	34,64	34,85	35,01	34,71	34,31	34,80	35,00	34,98	33,02	34,90	35,58	34,36	33,40	34,24	34,87
FeO	0,82	0,92	0,85	0,88	0,97	0,92	0,92	0,81	0,96	1,12	0,82	0,69	0,85	4,30	1,02	1,36	0,86	1,95	0,85	1,00
MnO	0,12	0,07	0,10	0,12	0,09	0,08	0,14	0,07	0,19	0,17	0,09	0,07	0,00	0,27	0,24	0,18	0,09	0,35	0,22	0,24
MgO	1,36	1,29	1,26	0,62	0,51	1,47	1,39	1,55	0,49	1,38	1,35	1,36	0,43	2,66	0,52	0,57	0,46	0,60	0,56	0,36
CaO	0,05	0,06	0,13	0,19	0,14	0,09	0,04	0,15	0,20	0,11	0,12	0,13	0,19	0,25	0,08	0,27	0,06	0,43	0,24	0,23
Na_2O	1,46	1,35	1,30	0,71	0,76	1,37	1,35	1,58	0,56	1,56	1,35	1,49	0,66	0,95	0,70	0,59	0,70	0,22	0,93	0,71
K_2O	9,72	9,28	9,92	9,63	10,24	9,56	9,65	8,19	9,99	9,06	9,66	9,08	10,38	8,98	9,74	8,49	9,90	13,40	10,06	9,79
Total	95,78	94,76	95,12	95,10	95,78	96,01	94,97	95,43	95,64	95,32	95,87	95,67	95,42	95,72	95,09	95,43	95,12	95,68	94,97	95,32
Formula																				
Si	6,100	6,133	6,049	6,216	6,153	6,164	6,075	6,156	6,227	6,194	6,100	6,167	6,179	5,931	6,174	6,202	6,250	5,891	6,151	6,205
Al^{IV}	1,900	1,867	1,951	1,784	1,847	1,836	1,925	1,844	1,773	1,806	1,900	1,833	1,821	2,069	1,826	1,798	1,750	2,109	1,849	1,795
Al^{VI}	3,516	3,570	3,577	3,685	3,573	3,542	3,561	3,587	3,641	3,555	3,525	3,596	3,647	3,192	3,650	3,716	3,620	3,310	3,551	3,663
Ti	0,143	0,121	0,111	0,098	0,182	0,108	0,112	0,115	0,129	0,086	0,144	0,100	0,135	0,129	0,132	0,109	0,157	0,215	0,177	0,120
Fe^{2+}	0,091	0,102	0,095	0,098	0,107	0,102	0,103	0,089	0,106	0,124	0,091	0,076	0,094	0,486	0,113	0,150	0,095	0,225	0,095	0,111
Mn	0,014	0,007	0,011	0,014	0,010	0,009	0,016	0,007	0,021	0,019	0,010	0,007	0,000	0,031	0,027	0,020	0,010	0,041	0,025	0,027
Mg	0,269	0,256	0,250	0,122	0,100	0,289	0,276	0,303	0,096	0,273	0,267	0,267	0,085	0,536	0,104	0,112	0,090	0,124	0,112	0,072
Ca	0,007	0,008	0,019	0,027	0,020	0,012	0,005	0,022	0,028	0,016	0,018	0,019	0,027	0,036	0,011	0,038	0,008	0,064	0,034	0,033
Na	0,374	0,348	0,338	0,183	0,194	0,351	0,349	0,404	0,145	0,402	0,347	0,381	0,169	0,248	0,182	0,151	0,181	0,059	0,241	0,182
K	1,643	1,578	1,691	1,631	1,730	1,607	1,644	1,375	1,687	1,532	1,631	1,525	1,757	1,548	1,654	1,425	1,675	2,352	1,717	1,659
Total	14,057	13,991	14,090	13,859	13,917	14,018	14,067	13,902	13,853	14,007	14,032	13,971	13,915	14,207	13,873	13,721	13,836	14,390	13,952	13,866

Table S1. f) SEM-EDS mineral chemistry analysis of white micas. Thin section PRR34239

Oxide (Wt%)	Thin section 20 (Bt-Act Schist)										Thin section 54 (Hbl gneiss)			
-----	bt1		bt2		bt3		bt4		bt5		bt1		bt2	
	core	rim	core	rim	core	rim	core	rim	core	rim	core	rim	core	rim
SiO_2	37,13	36,87	36,95	38,21	38,28	37,98	38,37	38,58	37,55	37,29	38,28	36,89	37,12	35,33
TiO_2	4,46	3,95	3,30	2,21	4,11	3,77	3,38	3,05	3,44	3,10	3,87	2,92	2,70	2,02
Al_2O_3	16,35	17,35	17,78	16,66	16,05	16,00	15,59	16,02	16,78	16,24	15,97	18,23	16,61	17,72
FeO	18,75	19,38	18,63	18,16	17,26	17,62	17,40	17,10	17,60	19,31	15,91	17,89	15,56	19,11
MnO	0,47	0,43	0,43	0,42	0,23	0,42	0,54	0,38	0,26	0,29	0,35	0,24	0,34	0,44
MgO	11,70	12,48	12,71	11,19	10,67	10,60	10,83	11,47	11,24	11,73	14,05	16,15	16,84	17,79
CaO	0,47	2,16	0,50	0,24	0,18	0,87	0,18	0,00	0,24	0,17	0,26	1,55	0,17	0,26
Na_2O	0,47	0,37	0,28	0,15	0,41	0,32	0,24	0,48	0,66	0,51	0,35	0,86	0,74	0,73
K_2O	6,54	3,26	5,88	9,21	9,42	8,71	9,78	9,34	8,69	7,74	7,28	1,61	6,09	2,95
Total	96,53	96,35	96,65	96,57	96,61	96,49	96,45	96,71	96,61	96,57	96,47	96,39	96,44	96,54
Formula														
Si	5,50	5,40	5,43	5,69	5,68	5,66	5,73	5,73	5,58	5,56	5,60	5,30	5,41	5,16
Al^{IV}	2,50	2,60	2,57	2,31	2,32	2,34	2,27	2,27	2,42	2,44	2,40	2,70	2,59	2,84
Al^{VI}	0,35	0,39	0,51	0,62	0,49	0,47	0,48	0,53	0,52	0,42	0,35	0,38	0,27	0,20
Ti	0,50	0,43	0,36	0,25	0,46	0,42	0,38	0,34	0,38	0,35	0,43	0,32	0,30	0,22
Fe^{2+}	2,32	2,37	2,29	2,26	2,14	2,20	2,17	2,12	2,19	2,41	1,95	2,15	1,90	2,33
Mn	0,06	0,05	0,05	0,05	0,03	0,05	0,07	0,05	0,03	0,04	0,04	0,03	0,04	0,05
Mg	2,58	2,72	2,78	2,49	2,36	2,36	2,41	2,54	2,49	2,61	3,06	3,46	3,66	3,87
Ca	0,08	0,34	0,08	0,04	0,03	0,14	0,03	0,00	0,04	0,03	0,04	0,24	0,03	0,04
Na	0,14	0,10	0,08	0,04	0,12	0,09	0,07	0,14	0,19	0,15	0,10	0,24	0,21	0,21
K	1,24	0,61	1,10	1,75	1,78	1,66	1,86	1,77	1,65	1,47	1,36	0,29	1,13	0,55
TOTAL	15,26	15,03	15,26	15,50	15,41	15,39	15,48	15,49	15,49	15,47	15,33	15,11	15,53	15,48
X_{Fe}	0,47	0,47	0,45	0,48	0,48	0,48	0,47	0,46	0,47	0,48	0,39	0,38	0,34	0,38

Table S2. a) SEM-EDS mineral chemistry analysis of biotites. Thin sections 20 and 54.

Oxide (Wt%)	Thin section 21(bt-wm gneissic schist)									
-----	bt1		bt2		bt3		bt4		bt5	
	core	rim	core	rim	core	rim	core	rim	core	rim
SiO_2	38,03	37,59	37,69	37,89	36,55	38,05	37,98	38,24	37,53	37,88
TiO_2	2,57	2,29	2,58	2,64	2,77	2,41	2,52	2,26	2,98	3,25
Al_2O_3	17,39	17,60	18,26	17,72	17,71	18,23	18,30	18,62	17,21	17,32
FeO	18,51	18,41	17,67	17,92	18,78	19,68	17,67	17,53	18,64	17,98
MnO	0,34	0,45	0,25	0,42	0,68	0,55	0,44	0,42	0,48	0,45
MgO	9,81	10,05	9,62	9,48	9,17	9,08	9,76	9,70	9,57	9,34
CaO	0,20	0,10	0,17	0,11	0,20	0,17	0,17	0,13	0,12	0,22
Na_2O	0,29	0,48	0,71	0,39	0,68	0,66	0,42	0,25	0,23	0,26
K_2O	9,36	9,63	9,49	9,77	9,70	7,64	9,18	9,26	9,62	9,58
Total	96,50	96,62	96,44	96,39	96,47	96,70	96,61	96,56	96,49	96,42
Formula										
Si	5,67	5,62	5,61	5,66	5,52	5,65	5,64	5,66	5,63	5,66
Al^{IV}	2,33	2,38	2,39	2,34	2,48	2,35	2,36	2,34	2,37	2,34
Al^{VI}	0,73	0,72	0,81	0,78	0,68	0,84	0,84	0,91	0,67	0,71
Ti	0,29	0,26	0,29	0,30	0,31	0,27	0,28	0,25	0,34	0,37
Fe^{2+}	2,31	2,30	2,20	2,24	2,37	2,44	2,19	2,17	2,34	2,25
Mn	0,04	0,06	0,03	0,05	0,09	0,07	0,06	0,05	0,06	0,06
Mg	2,18	2,24	2,13	2,11	2,07	2,01	2,16	2,14	2,14	2,08
Ca	0,03	0,02	0,03	0,02	0,03	0,03	0,03	0,02	0,02	0,04
Na	0,08	0,14	0,21	0,11	0,20	0,19	0,12	0,07	0,07	0,08
K	1,78	1,84	1,80	1,86	1,87	1,45	1,74	1,75	1,84	1,83
TOTAL	15,44	15,56	15,50	15,47	15,62	15,30	15,41	15,37	15,47	15,40
X_{Fe}	0,51	0,51	0,51	0,51	0,53	0,55	0,50	0,50	0,52	0,52

Table S2. b) SEM-EDS mineral chemistry analysis of biotites. Thin section 21.

Oxide (Wt%)	Thin section 62 (bt-wm hornfels)											
-----	bt1		bt2		bt3		bt4		bt5		bt6	
	core	rim	core	rim	core	rim	core	rim	core	rim	core	rim
SiO_2	37,71	45,85	36,97	37,94	37,53	35,93	36,59	36,51	36,40	35,97	36,23	37,55
TiO_2	1,79	1,35	2,32	1,58	2,07	1,83	2,54	2,14	2,10	1,97	2,04	1,85
Al_2O_3	19,45	18,37	19,15	20,05	19,74	19,75	19,68	20,36	19,39	19,80	19,11	18,86
FeO	16,74	13,13	17,43	15,88	16,84	17,90	17,33	17,03	17,28	19,10	18,43	17,80
MnO	0,17	0,21	0,49	0,43	0,14	0,41	0,40	0,33	0,36	0,45	0,50	0,25
MgO	10,48	7,04	10,07	11,10	9,96	10,33	9,40	9,89	9,69	8,87	9,43	9,63
CaO	0,25	0,22	0,08	0,19	0,22	0,10	0,24	0,12	0,20	0,15	0,14	0,06
Na_2O	0,39	1,04	0,38	0,55	0,33	0,73	0,76	0,41	0,40	0,12	0,15	0,12
K_2O	9,73	9,40	9,46	8,52	9,53	9,41	9,40	9,58	9,66	10,03	10,14	10,34
Total	96,72	96,67	96,54	96,42	96,47	96,51	96,36	96,44	95,67	96,54	96,41	96,46
Formula												
Si	5,56		5,50	5,56	5,55	5,38	5,45	5,42	5,48	5,41	5,46	5,60
Al^{IV}	2,44		2,50	2,44	2,45	2,62	2,55	2,58	2,52	2,59	2,54	2,40
Al^{VI}	0,95		0,87	1,03	0,99	0,86	0,91	0,99	0,92	0,93	0,85	0,92
Ti	0,20		0,26	0,17	0,23	0,21	0,29	0,24	0,24	0,22	0,23	0,21
Fe^{2+}	2,07		2,17	1,95	2,08	2,24	2,16	2,12	2,17	2,40	2,32	2,22
Mn	0,02		0,06	0,05	0,02	0,05	0,05	0,04	0,05	0,06	0,06	0,03
Mg	2,31		2,23	2,43	2,20	2,30	2,09	2,19	2,17	1,99	2,12	2,14
Ca	0,04		0,01	0,03	0,04	0,02	0,04	0,02	0,03	0,02	0,02	0,01
Na	0,11		0,11	0,16	0,09	0,21	0,22	0,12	0,12	0,03	0,05	0,03
K	1,83		1,80	1,59	1,80	1,80	1,79	1,81	1,85	1,93	1,95	1,97
TOTAL	15,52		15,51	15,41	15,44	15,68	15,54	15,52	15,55	15,59	15,61	15,53
X_{Fe}	0,47		0,49	0,45	0,49	0,49	0,51	0,49	0,50	0,55	0,52	0,51

Table S2. c) SEM-EDS mineral chemistry analysis of biotites. Thin section 62.

Oxide (Wt%)	Thin section 47 (bt-gneiss)											
-----	bt1		bt2		bt3		bt4		bt5		bt6	
	core	rim	core	rim	core	rim	core	rim	core	rim	core	rim
SiO_2	39,09	38,67	38,55	38,52	38,57	38,71	38,40	37,93	38,18	37,93	38,40	38,55
TiO_2	1,44	1,30	0,91	1,35	1,78	1,54	1,30	1,33	2,38	3,27	2,18	2,09
Al_2O_3	18,82	19,59	19,77	18,89	18,93	19,39	19,25	19,40	18,38	18,05	18,35	18,65
FeO	14,98	14,49	13,55	14,36	14,90	14,53	15,01	14,23	14,55	15,90	14,58	14,80
MnO	0,10	0,13	0,14	0,30	0,35	0,21	0,26	0,24	0,31	0,12	0,27	0,14
MgO	11,93	12,12	13,15	12,57	12,20	12,24	12,42	12,76	12,37	11,01	12,02	12,32
CaO	0,11	0,17	0,15	0,23	0,19	0,20	0,20	0,32	0,25	0,26	0,22	0,08
Na_2O	0,21	0,19	0,86	0,70	0,41	0,20	0,39	0,80	0,38	0,13	0,76	0,43
K_2O	9,79	9,62	9,14	9,42	9,25	9,39	9,32	9,15	9,53	10,05	9,57	9,42
Total	96,65	96,41	96,43	96,57	96,63	96,61	96,66	96,42	96,39	96,70	96,51	96,53
Formula												
Si	5,71	5,64	5,61	5,63	5,63	5,64	5,61	5,55	5,60	5,59	5,63	5,63
Al^{IV}	2,29	2,36	2,39	2,37	2,37	2,36	2,39	2,45	2,40	2,41	2,37	2,37
Al^{VI}	0,95	1,01	0,99	0,89	0,89	0,97	0,92	0,90	0,78	0,72	0,81	0,84
Ti	0,16	0,14	0,10	0,15	0,20	0,17	0,14	0,15	0,26	0,36	0,24	0,23
Fe^{2+}	1,83	1,77	1,65	1,76	1,82	1,77	1,83	1,74	1,78	1,96	1,79	1,81
Mn	0,01	0,02	0,02	0,04	0,04	0,03	0,03	0,03	0,04	0,01	0,03	0,02
Mg	2,60	2,64	2,85	2,74	2,66	2,66	2,71	2,78	2,70	2,42	2,63	2,68
Ca	0,02	0,03	0,02	0,04	0,03	0,03	0,03	0,05	0,04	0,04	0,03	0,01
Na	0,06	0,05	0,24	0,20	0,11	0,06	0,11	0,23	0,11	0,04	0,22	0,12
K	1,82	1,79	1,70	1,76	1,72	1,75	1,74	1,71	1,78	1,89	1,79	1,76
TOTAL	15,45	15,45	15,57	15,57	15,47	15,43	15,51	15,59	15,49	15,44	15,54	15,47
X_{Fe}	0,41	0,40	0,37	0,39	0,41	0,40	0,40	0,38	0,40	0,45	0,41	0,40

Table S2. d) SEM-EDS mineral chemistry analysis of biotites. Thin section 47.

Oxide (Wt%)	Thin section 59 (bt-hbl tonalite)											
-----	bt1		bt2		bt3		bt4		bt5		bt6	
	core	rim	core	rim	core	rim	core	rim	core	rim	core	rim
SiO_2	38,77	38,51	38,49	38,74	38,59	39,94	39,44	39,30	38,87	38,59	38,25	39,00
TiO_2	4,59	4,21	4,03	3,90	3,99	3,93	3,72	4,36	4,69	4,18	4,61	4,30
Al_2O_3	13,96	13,96	13,69	14,22	13,62	13,87	13,89	13,49	13,44	13,82	13,63	14,31
FeO	14,86	14,64	15,24	14,58	15,53	15,40	14,84	14,33	15,23	15,15	15,33	14,58
MnO	0,39	0,50	0,47	0,59	0,46	0,55	0,41	0,67	0,54	0,61	0,65	0,33
MgO	14,24	14,20	13,98	14,64	13,79	13,41	14,06	13,67	13,59	14,00	13,74	13,94
CaO	0,08	0,20	0,15	0,18	0,08	0,29	0,23	0,27	0,17	0,19	0,23	0,06
Na_2O	0,43	0,62	0,84	0,41	0,78	0,34	0,41	0,54	0,39	0,46	0,39	0,87
K_2O	9,35	9,40	9,65	9,16	9,60	8,68	9,38	9,53	9,32	9,32	9,59	9,17
Total	96,65	96,45	96,72	96,63	96,55	96,51	96,43	96,38	96,39	96,47	96,58	96,53
Formula												
Si	5,70	5,70	5,71	5,70	5,73	5,87	5,81	5,81	5,76	5,72	5,68	5,73
Al^{IV}	2,30	2,30	2,29	2,30	2,27	2,13	2,19	2,19	2,24	2,28	2,32	2,27
Al^{VI}	0,12	0,13	0,10	0,17	0,11	0,27	0,22	0,16	0,10	0,13	0,07	0,21
Ti	0,51	0,47	0,45	0,43	0,45	0,43	0,41	0,48	0,52	0,47	0,51	0,47
Fe^{2+}	1,83	1,81	1,89	1,79	1,93	1,89	1,83	1,77	1,89	1,88	1,90	1,79
Mn	0,05	0,06	0,06	0,07	0,06	0,07	0,05	0,08	0,07	0,08	0,08	0,04
Mg	3,12	3,13	3,09	3,21	3,05	2,94	3,09	3,01	3,00	3,09	3,04	3,05
Ca	0,01	0,03	0,02	0,03	0,01	0,05	0,04	0,04	0,03	0,03	0,04	0,01
Na	0,12	0,18	0,24	0,12	0,23	0,10	0,12	0,15	0,11	0,13	0,11	0,25
K	1,75	1,77	1,83	1,72	1,82	1,63	1,76	1,80	1,76	1,76	1,82	1,72
TOTAL	15,52	15,59	15,68	15,55	15,65	15,36	15,51	15,51	15,48	15,56	15,58	15,54
X_{Fe}	0,37	0,37	0,38	0,36	0,39	0,39	0,37	0,37	0,39	0,38	0,38	0,37

Table S2. e) SEM-EDS mineral chemistry analysis of biotites. Thin section 59.

Oxide (Wt%)	PRR34239 (Phyllite-Swanson Formation)													
-----	bt1		bt2		bt3		bt4		bt5		bt6		bt7	
	core	rim	core	rim	core	rim	core	rim	core	rim	core	rim	core	rim
SiO_2	37,34	37,67	36,77	37,88	36,48	36,75	37,28	36,24	37,15	38,95	36,74	36,01	36,31	36,66
TiO_2	2,80	2,06	2,77	2,38	3,12	2,73	3,09	2,92	2,57	2,45	3,17	3,73	2,86	2,73
Al_2O_3	19,79	19,35	19,69	19,50	19,45	19,84	19,28	19,23	20,67	21,31	20,15	20,22	19,69	19,69
FeO	16,55	16,78	16,45	16,65	17,22	16,92	17,07	17,78	15,34	13,33	16,01	16,18	16,24	16,79
MnO	0,36	0,36	0,35	0,27	0,37	0,30	0,35	0,36	0,37	0,25	0,44	0,40	0,41	0,27
MgO	9,84	11,04	10,45	9,75	10,04	10,37	9,71	10,15	10,75	11,14	10,00	9,61	10,98	10,54
CaO	0,08	0,15	0,14	0,13	0,17	0,09	0,08	0,19	0,15	0,05	0,19	0,15	0,14	0,18
Na_2O	0,26	0,34	0,59	0,27	0,31	0,33	0,22	0,31	0,55	0,60	0,69	0,92	0,89	0,52
K_2O	9,32	8,78	8,92	9,29	8,89	8,91	9,07	9,01	8,50	8,13	8,66	9,16	8,85	8,71
Total	96,43	96,56	96,23	96,32	96,15	96,36	96,21	96,38	96,12	96,28	96,24	96,52	96,48	96,30
Formula														
Si	5,51	5,54	5,45	5,60	5,43	5,44	5,53	5,41	5,45	5,60	5,43	5,34	5,37	5,43
Al^{IV}	2,49	2,46	2,55	2,40	2,57	2,56	2,47	2,59	2,55	2,40	2,57	2,66	2,63	2,57
Al^{VI}	0,96	0,90	0,88	1,00	0,84	0,90	0,89	0,79	1,02	1,21	0,93	0,87	0,81	0,87
Ti	0,31	0,23	0,31	0,26	0,35	0,30	0,34	0,33	0,28	0,26	0,35	0,42	0,32	0,30
Fe^{2+}	2,04	2,06	2,04	2,06	2,14	2,09	2,12	2,22	1,88	1,60	1,98	2,00	2,01	2,08
Mn	0,04	0,04	0,04	0,03	0,05	0,04	0,04	0,05	0,05	0,03	0,06	0,05	0,05	0,03
Mg	2,17	2,42	2,31	2,15	2,23	2,29	2,15	2,26	2,35	2,39	2,20	2,12	2,42	2,33
Ca	0,01	0,02	0,02	0,02	0,03	0,01	0,01	0,03	0,02	0,01	0,03	0,02	0,02	0,03
Na	0,07	0,10	0,17	0,08	0,09	0,09	0,06	0,09	0,16	0,17	0,20	0,26	0,25	0,15
K	1,76	1,65	1,69	1,75	1,69	1,68	1,72	1,72	1,59	1,49	1,63	1,73	1,67	1,65
TOTAL	15,37	15,42	15,45	15,35	15,41	15,41	15,33	15,48	15,35	15,16	15,38	15,48	15,55	15,44
X_{Fe}	0,49	0,46	0,47	0,49	0,49	0,48	0,50	0,50	0,44	0,40	0,47	0,49	0,45	0,47

Table S2. f) SEM-EDS mineral chemistry analysis of biotites. Thin section PRR34239.

Oxide (Wt%)	PRR33877 (Ford Granodiorite)													
-----	bt1		bt2		bt3		bt4		bt5		bt6		bt7	
	core	rim	core	rim	core	rim	core	rim	core	rim	core	rim	core	rim
SiO_2	38,54	36,92	37,80	37,96	37,68	37,67	37,37	37,67	37,89	37,69	37,70	37,63	37,83	37,65
TiO_2	4,12	3,17	4,28	3,85	4,59	4,22	4,61	2,85	4,86	4,70	4,26	4,05	4,73	4,51
Al_2O_3	13,22	14,93	14,17	14,48	13,29	13,71	13,80	14,89	12,92	13,00	13,60	13,78	13,62	14,16
FeO	18,93	19,26	17,84	18,42	19,26	18,49	17,64	18,33	18,85	18,14	18,82	18,93	17,78	17,93
MnO	0,25	0,41	0,23	0,39	0,33	0,28	0,37	0,24	0,36	0,38	0,38	0,23	0,35	0,44
MgO	11,41	13,12	12,03	11,97	11,21	11,73	11,77	11,64	11,10	11,85	11,24	11,15	11,75	11,52
CaO	0,09	0,22	0,10	0,14	0,12	0,11	0,11	0,13	0,00	0,20	0,18	0,16	0,17	0,23
Na_2O	0,13	0,26	0,27	0,20	0,17	0,32	0,70	0,29	0,20	0,21	0,32	0,43	0,52	0,41
K_2O	9,77	7,96	9,54	8,71	9,68	9,42	9,47	9,94	10,01	9,84	9,73	9,82	9,40	9,26
Total	96,45	96,37	96,31	96,25	96,37	96,18	96,03	96,10	96,26	96,16	96,29	96,32	96,22	96,25
Formula														
Si	5,80	5,54	5,67	5,69	5,70	5,69	5,65	5,69	5,74	5,71	5,71	5,70	5,69	5,67
Al^{IV}	2,20	2,46	2,33	2,31	2,30	2,31	2,35	2,31	2,26	2,29	2,29	2,30	2,31	2,33
Al^{VI}	0,15	0,18	0,18	0,25	0,08	0,14	0,11	0,34	0,05	0,03	0,13	0,16	0,11	0,18
Ti	0,47	0,36	0,48	0,43	0,52	0,48	0,52	0,32	0,55	0,54	0,48	0,46	0,54	0,51
Fe^{2+}	2,38	2,42	2,24	2,31	2,44	2,34	2,23	2,32	2,39	2,30	2,38	2,40	2,24	2,26
Mn	0,03	0,05	0,03	0,05	0,04	0,04	0,05	0,03	0,05	0,05	0,05	0,03	0,04	0,06
Mg	2,56	2,93	2,69	2,68	2,53	2,64	2,65	2,62	2,51	2,67	2,54	2,52	2,64	2,58
Ca	0,01	0,04	0,02	0,02	0,02	0,02	0,02	0,02	0,00	0,03	0,03	0,03	0,03	0,04
Na	0,04	0,08	0,08	0,06	0,05	0,09	0,21	0,08	0,06	0,06	0,09	0,13	0,15	0,12
K	1,88	1,52	1,83	1,67	1,87	1,82	1,83	1,92	1,94	1,90	1,88	1,90	1,80	1,78
TOTAL	15,52	15,58	15,54	15,46	15,55	15,56	15,61	15,66	15,55	15,58	15,58	15,62	15,54	15,52
X_{Fe}	0,48	0,45	0,45	0,46	0,49	0,47	0,46	0,47	0,49	0,46	0,48	0,49	0,46	0,47

Table S2. g) SEM-EDS mineral chemistry analysis of biotites. Thin section 62.

Oxides (Wt%) -----	Thin section 20 (Bt-Act Schist)																			
	cam1		cam2		cam3		cam4		cam5		cam6		cam7		cam8		cam9		cam10	
	core	rim	core	rim	core	rim	core	rim	core	rim	core	rim	core	rim	core	rim	core	rim	core	rim
SiO_2	52,82	51,26	50,50	49,59	52,52	52,60	54,61	54,36	51,45	53,20	53,81	54,97	51,46	52,44	53,90	50,55	51,18	53,68	51,87	48,10
TiO_2	0,44	0,25	0,24	0,24	0,42	0,47	0,35	0,09	0,30	0,25	0,00	0,28	0,60	0,51	0,24	0,60	0,74	0,09	0,60	0,39
Al_2O_3	4,40	6,37	6,28	6,17	4,66	3,49	2,19	2,47	5,86	3,85	3,63	1,08	5,58	4,77	3,35	6,25	6,02	3,97	4,93	8,16
FeO	13,89	13,12	12,93	12,70	13,85	14,19	12,78	14,07	14,31	13,86	14,77	12,82	13,98	14,20	13,43	14,83	13,81	13,08	13,95	13,07
MnO	0,41	0,61	0,60	0,59	0,63	0,59	0,54	0,52	0,57	0,55	0,54	0,71	0,56	0,37	0,53	0,50	0,64	0,43	0,67	0,51
MgO	13,56	13,84	13,63	13,39	13,39	14,08	15,17	13,84	12,67	13,76	14,82	14,97	12,92	13,25	14,65	13,26	12,91	14,05	13,61	13,15
CaO	12,09	11,33	11,16	10,96	11,34	11,57	11,74	12,19	11,95	12,03	10,09	11,83	11,84	11,81	11,49	10,74	11,53	11,98	11,40	13,24
Na_2O	0,55	1,17	1,15	1,13	0,95	0,59	0,77	0,33	0,77	0,55	0,58	0,72	0,79	0,46	0,87	1,12	0,63	0,66	0,65	1,28
K_2O	0,25	0,34	0,34	0,33	0,18	0,25	0,08	0,20	0,39	0,28	0,18	0,22	0,47	0,37	0,00	0,40	0,39	0,26	0,36	0,54
Cr_2O_3	0,12	0,06	0,06	0,06	0,21	0,11	0,17	0,05	0,09	0,09	0,08	0,28	0,00	0,15	0,00	0,11	0,23	0,10	0,25	0,00
Total	98,54	98,37	98,51	98,21	98,14	97,94	98,42	98,12	98,38	98,41	98,50	97,89	98,19	98,34	98,44	98,36	98,05	98,27	98,29	98,45
Formula																				
Si	7,58	7,32	7,32	7,32	7,55	7,56	7,78	7,84	7,44	7,64	7,52	7,93	7,44	7,54	7,65	7,22	7,38	7,70	7,44	7,03
Al tot	0,75	1,07	1,07	1,07	0,79	0,59	0,37	0,42	1,00	0,65	0,60	0,18	0,95	0,81	0,56	1,05	1,02	0,67	0,83	1,41
Al^{IV}	0,42	0,68	0,68	0,68	0,45	0,44	0,22	0,16	0,56	0,36	0,48	0,07	0,56	0,46	0,35	0,78	0,62	0,30	0,56	0,97
Al^{VI}	0,33	0,39	0,39	0,39	0,34	0,15	0,15	0,26	0,44	0,29	0,12	0,11	0,39	0,35	0,21	0,28	0,40	0,37	0,27	0,43
Ti	0,05	0,03	0,03	0,03	0,05	0,05	0,04	0,01	0,03	0,03	0,00	0,03	0,07	0,06	0,03	0,06	0,08	0,01	0,06	0,04
Fe tot	1,67	1,57	1,57	1,57	1,67	1,71	1,52	1,70	1,73	1,66	1,73	1,55	1,69	1,71	1,59	1,77	1,66	1,57	1,67	1,60
Fe^{3+}	0,03	0,37	0,37	0,37	0,15	0,37	0,12	0,00	0,04	0,07	1,12	0,00	0,06	0,11	0,35	0,66	0,17	0,00	0,33	0,00
Fe^{2+}	1,64	1,20	1,20	1,20	1,52	1,33	1,40	1,70	1,69	1,59	0,61	1,55	1,63	1,60	1,25	1,11	1,49	1,57	1,34	1,60
Mn	0,05	0,07	0,07	0,07	0,08	0,07	0,07	0,06	0,07	0,07	0,06	0,09	0,07	0,05	0,06	0,06	0,08	0,05	0,08	0,06
Mg	2,90	2,94	2,94	2,94	2,87	3,02	3,22	2,98	2,73	2,95	3,09	3,22	2,79	2,84	3,10	2,83	2,78	3,00	2,91	2,86
Cr	0,01	0,01	0,01	0,01	0,02	0,01	0,02	0,01	0,01	0,01	0,01	0,03	0,00	0,02	0,00	0,01	0,03	0,01	0,03	0,00
Ca	1,86	1,73	1,73	1,73	1,75	1,78	1,79	1,88	1,85	1,85	1,51	1,83	1,83	1,82	1,75	1,64	1,78	1,84	1,75	2,07
Na	0,15	0,32	0,32	0,32	0,27	0,16	0,21	0,09	0,22	0,15	0,16	0,20	0,22	0,13	0,24	0,31	0,18	0,18	0,18	0,36
K	0,05	0,06	0,06	0,06	0,03	0,05	0,01	0,04	0,07	0,05	0,03	0,04	0,09	0,07	0,00	0,07	0,07	0,05	0,07	0,10
Total	15,07	15,13	15,13	15,13	15,07	15,00	15,04	15,02	15,15	15,07	14,71	15,10	15,14	15,03	14,99	15,04	15,05	15,08	15,03	15,54
X_{Mg}	0,64	0,71	0,71	0,71	0,65	0,69	0,70	0,64	0,62	0,65	0,84	0,68	0,63	0,64	0,71	0,72	0,65	0,66	0,68	0,64

Table S3. a) SEM-EDS mineral chemistry analysis of amphiboles. Thin section 20.

Oxides (Wt%) -----	Thin section 54 (Hbl gneiss)																			
	cam1		cam2		cam3		cam4		cam5		cam6		cam7		cam8		cam9		cam10	
	core	rim	core	rim	core	rim	core	rim	core	rim	core	rim	core	rim	core	rim	core	rim	core	rim
SiO_2	49,73	51,24	52,16	52,67	49,53	56,35	49,53	51,70	49,87	52,12	51,61	52,17	48,83	48,94	48,87	50,92	51,04	50,32	49,53	49,80
TiO_2	1,53	1,23	0,66	0,45	1,45	0,00	1,51	1,15	1,40	0,72	1,13	0,89	1,87	1,74	1,69	1,27	1,57	1,32	1,57	1,74
Al_2O_3	7,53	6,46	6,04	4,63	8,22	2,87	8,54	6,33	8,42	5,96	6,11	6,57	8,82	9,21	9,16	6,75	7,38	7,18	8,44	7,18
FeO	12,15	11,79	11,03	10,45	11,88	10,01	11,00	11,19	12,05	11,43	10,70	11,05	11,75	11,80	12,06	11,34	11,57	11,63	11,36	11,74
MnO	0,82	0,84	0,67	0,61	0,64	0,52	0,87	0,81	0,38	0,57	0,69	0,60	0,47	0,58	0,67	0,80	0,52	0,83	0,50	0,81
MgO	13,21	13,83	14,97	15,35	13,65	16,92	14,10	14,31	13,46	14,69	15,57	14,82	13,53	13,25	13,33	14,55	13,78	14,18	14,19	13,72
CaO	11,60	11,34	11,32	12,55	11,16	11,33	10,68	11,73	11,33	11,89	11,12	11,22	11,34	11,27	10,83	10,95	11,31	10,92	10,78	11,20
Na_2O	0,93	0,61	0,84	0,93	0,81	0,53	1,35	0,47	0,89	0,54	0,98	0,69	1,07	0,80	0,96	0,90	0,47	0,80	1,21	1,16
K_2O	0,72	0,55	0,38	0,19	0,63	0,00	0,56	0,49	0,61	0,33	0,41	0,28	0,77	0,71	0,64	0,45	0,61	0,73	0,52	0,69
Cr_2O_3	0,20	0,10	0,00	0,04	0,05	0,00	0,18	0,12	0,00	0,08	0,18	0,06	0,08	0,00	0,00	0,24	0,04	0,21	0,00	0,24
Total	98,42	97,97	98,06	97,87	98,03	98,52	98,32	98,31	98,41	98,35	98,49	98,34	98,53	98,30	98,21	98,17	98,31	98,11	98,09	98,26
Formula																				
Si	7,16	7,32	7,38	7,56	7,07	7,81	7,02	7,35	7,10	7,39	7,26	7,34	6,97	6,98	6,95	7,22	7,24	7,16	7,02	7,15
Al tot	1,28	1,09	1,01	0,78	1,38	0,47	1,43	1,06	1,41	1,00	1,01	1,09	1,48	1,55	1,54	1,13	1,24	1,20	1,41	1,22
Al^{IV}	0,84	0,68	0,62	0,44	0,93	0,19	0,98	0,65	0,90	0,61	0,74	0,66	1,03	1,02	1,05	0,78	0,76	0,84	0,98	0,85
Al^{VI}	0,44	0,41	0,39	0,34	0,45	0,28	0,45	0,41	0,51	0,39	0,27	0,43	0,46	0,52	0,48	0,35	0,48	0,37	0,43	0,37
Ti	0,17	0,13	0,07	0,05	0,16	0,00	0,16	0,12	0,15	0,08	0,12	0,09	0,20	0,19	0,18	0,14	0,17	0,14	0,17	0,19
Fe tot	1,46	1,41	1,31	1,25	1,42	1,16	1,30	1,33	1,43	1,36	1,26	1,30	1,40	1,41	1,43	1,34	1,37	1,38	1,35	1,41
Fe^{3+}	0,04	0,23	0,36	0,00	0,41	0,40	0,43	0,15	0,28	0,21	0,47	0,41	0,23	0,34	0,53	0,42	0,25	0,44	0,52	0,13
Fe^{2+}	1,43	1,18	0,94	1,25	1,01	0,76	0,88	1,18	1,16	1,15	0,78	0,89	1,17	1,07	0,90	0,92	1,13	0,95	0,83	1,28
Mn	0,10	0,10	0,08	0,07	0,08	0,06	0,10	0,10	0,05	0,07	0,08	0,07	0,06	0,07	0,08	0,10	0,06	0,10	0,06	0,10
Mg	2,83	2,95	3,16	3,28	2,90	3,50	2,98	3,03	2,86	3,11	3,27	3,11	2,88	2,82	2,82	3,08	2,92	3,01	3,00	2,94
Cr	0,02	0,01	0,00	0,00	0,01	0,00	0,02	0,01	0,00	0,01	0,02	0,01	0,01	0,00	0,00	0,03	0,00	0,02	0,00	0,03
Ca	1,79	1,74	1,72	1,93	1,70	1,68	1,62	1,79	1,73	1,81	1,68	1,69	1,74	1,72	1,65	1,66	1,72	1,67	1,64	1,72
Na	0,26	0,17	0,23	0,26	0,23	0,14	0,37	0,13	0,24	0,15	0,27	0,19	0,30	0,22	0,27	0,25	0,13	0,22	0,33	0,32
K	0,13	0,10	0,07	0,03	0,11	0,00	0,10	0,09	0,11	0,06	0,07	0,05	0,14	0,13	0,12	0,08	0,11	0,13	0,09	0,13
Total	15,20	15,01	15,02	15,23	15,05	14,83	15,11	15,02	15,08	15,03	15,04	14,93	15,18	15,07	15,03	15,02	14,96	15,04	15,06	15,20
X_{Mg}	0,67	0,71	0,77	0,72	0,74	0,82	0,77	0,72	0,71	0,73	0,81	0,78	0,71	0,73	0,76	0,77	0,72	0,76	0,78	0,70

Table S3. b) SEM-EDS mineral chemistry analysis of amphiboles. Thin section 54.

Oxides (Wt%)	Thin section 59 (bt-hbl tonalite)																			
-----	cam1		cam2		cam3		cam4		cam5		cam6		cam7		cam8		cam9		cam10	
	core	rim	core	rim	core	rim	core	rim	core	rim	core	rim	core	rim	core	rim	core	rim	core	rim
SiO_2	48,90	49,57	50,07	48,93	50,42	48,20	49,79	49,67	50,22	49,96	50,70	50,79	49,86	51,95	49,53	52,97	50,44	49,56	50,80	50,08
TiO_2	1,21	0,74	0,74	1,07	1,02	1,00	0,95	1,02	1,02	1,10	0,81	0,81	1,33	0,71	1,16	0,42	1,25	1,25	0,85	0,93
Al_2O_3	6,34	6,45	6,19	6,50	6,45	5,10	6,33	6,14	5,96	6,06	7,20	5,47	6,12	5,29	6,17	4,19	5,95	6,13	6,24	5,58
FeO	12,27	12,33	11,64	12,35	12,10	15,23	11,98	12,62	13,20	12,94	11,37	11,38	13,04	10,80	11,88	9,99	12,02	12,10	11,60	12,86
MnO	0,54	0,38	0,52	0,63	0,68	0,77	0,62	0,61	0,55	0,67	0,55	0,57	0,58	0,44	0,80	0,65	0,75	0,79	0,55	0,74
MgO	14,68	15,10	15,22	14,86	14,47	12,81	14,85	14,09	13,71	14,13	14,43	15,72	14,13	16,11	14,72	16,79	14,80	15,03	14,91	14,22
CaO	11,55	11,37	11,33	11,33	11,10	13,66	11,38	11,63	11,56	11,55	10,72	11,42	11,63	11,10	11,27	11,53	11,14	11,30	11,91	11,76
Na_2O	2,02	1,76	1,88	1,70	0,99	0,68	1,89	1,62	1,01	1,26	1,64	1,53	0,97	1,46	1,48	1,29	1,12	1,37	1,03	1,24
K_2O	0,55	0,61	0,49	0,48	0,74	0,73	0,60	0,65	0,70	0,60	0,63	0,51	0,57	0,39	0,68	0,38	0,55	0,49	0,56	0,59
Cr_2O_3	0,09	0,00	0,00	0,18	0,18	0,19	0,00	0,09	0,06	0,06	0,14	0,00	0,04	0,00	0,24	0,19	0,21	0,13	0,00	0,11
Total	98,13	98,32	98,09	98,01	98,14	98,36	98,39	98,15	97,99	98,32	98,19	98,20	98,27	98,24	97,95	98,42	98,21	98,14	98,47	98,12
Formula																				
Si	7,07	7,09	7,17	7,04	7,20	7,17	7,14	7,19	7,26	7,19	7,22	7,23	7,16	7,33	7,14	7,47	7,19	7,09	7,24	7,24
Al tot	1,08	1,09	1,04	1,10	1,09	0,89	1,07	1,05	1,01	1,03	1,21	0,92	1,04	0,88	1,05	0,70	1,00	1,03	1,05	0,95
Al^{IV}	0,93	0,91	0,83	0,96	0,80	0,83	0,86	0,81	0,74	0,81	0,78	0,77	0,84	0,67	0,86	0,53	0,81	0,91	0,76	0,76
Al^{VI}	0,15	0,18	0,21	0,14	0,28	0,06	0,21	0,24	0,27	0,21	0,43	0,15	0,20	0,21	0,18	0,17	0,20	0,12	0,29	0,19
Ti	0,13	0,08	0,08	0,12	0,11	0,11	0,10	0,11	0,11	0,12	0,09	0,09	0,14	0,08	0,13	0,04	0,13	0,13	0,09	0,10
Fe tot	1,48	1,47	1,39	1,49	1,44	1,89	1,44	1,53	1,60	1,56	1,35	1,36	1,57	1,27	1,43	1,18	1,43	1,45	1,38	1,55
Fe^{3+}	0,23	0,49	0,37	0,48	0,43	0,00	0,31	0,13	0,23	0,32	0,29	0,44	0,39	0,48	0,33	0,30	0,46	0,55	0,26	0,23
Fe^{2+}	1,25	0,99	1,02	1,00	1,01	1,89	1,13	1,40	1,36	1,24	1,06	0,91	1,17	0,79	1,10	0,88	0,97	0,90	1,13	1,32
Mn	0,07	0,05	0,06	0,08	0,08	0,10	0,08	0,07	0,07	0,08	0,07	0,07	0,07	0,05	0,10	0,08	0,09	0,10	0,07	0,09
Mg	3,17	3,22	3,25	3,19	3,08	2,84	3,17	3,04	2,95	3,03	3,06	3,34	3,02	3,39	3,16	3,53	3,15	3,20	3,17	3,06
Cr	0,01	0,00	0,00	0,02	0,02	0,02	0,00	0,01	0,01	0,01	0,02	0,00	0,00	0,00	0,03	0,02	0,02	0,01	0,00	0,01
Ca	1,79	1,74	1,74	1,75	1,70	2,18	1,75	1,80	1,79	1,78	1,64	1,74	1,79	1,68	1,74	1,74	1,70	1,73	1,82	1,82
Na	0,57	0,49	0,52	0,47	0,27	0,20	0,53	0,45	0,28	0,35	0,45	0,42	0,27	0,40	0,41	0,35	0,31	0,38	0,29	0,35
K	0,10	0,11	0,09	0,09	0,13	0,14	0,11	0,12	0,13	0,11	0,11	0,09	0,10	0,07	0,12	0,07	0,10	0,09	0,10	0,11
Total	15,47	15,34	15,35	15,33	15,13	15,53	15,38	15,39	15,21	15,25	15,22	15,26	15,17	15,15	15,31	15,19	15,13	15,22	15,21	15,29
X_{Mg}	0,72	0,77	0,76	0,76	0,75	0,60	0,74	0,68	0,68	0,71	0,74	0,79	0,72	0,81	0,74	0,80	0,76	0,78	0,74	0,70

Table S3. c) SEM-EDS mineral chemistry analysis of amphiboles. Thin section 59.

Oxides (Wt%)	Thin section 3 (Bt-Hbl-Schist)											
-----	cam1	cam2	cam3	cam4	cam5	cam6	cam7	cam8	cam9	cam10	cam11	cam12
	core	core	core	core	core	core	core	core	core	core	core	core
SiO_2	44,99	45,01	45,48	47,13	45,71	44,14	44,04	44,64	46,52	43,63	45,42	43,60
TiO_2	1,19	1,11	0,97	0,74	0,54	0,79	1,17	1,16	0,90	0,72	1,06	0,37
Al_2O_3	10,48	11,00	10,97	10,43	11,50	11,83	10,48	10,44	10,70	12,18	11,43	12,61
FeO	18,72	17,67	17,82	17,90	18,27	19,20	20,15	18,93	17,80	18,46	16,89	20,47
MnO	0,53	0,67	0,57	0,52	0,40	0,54	0,63	0,71	0,59	0,72	0,65	0,49
MgO	9,00	9,45	9,65	9,46	8,77	8,13	8,42	8,52	9,02	8,55	9,84	7,28
CaO	11,23	10,73	11,00	10,71	11,70	11,71	11,48	11,38	11,09	11,48	10,67	11,69
Na_2O	0,91	1,58	1,36	0,89	0,88	1,18	0,82	1,15	1,03	1,49	1,64	1,22
K_2O	0,60	0,68	0,63	0,64	0,61	0,56	0,66	0,78	0,76	0,75	0,72	0,73
Cr_2O_3	0,15	0,14	0,00	0,00	0,00	0,22	0,26	0,26	0,08	0,22	0,05	0,19
Total	97,78	98,05	98,45	98,41	98,38	98,31	98,09	97,98	98,48	98,21	98,37	98,66
Formula												
Si	6,67	6,63	6,65	6,85	6,73	6,57	6,57	6,67	6,82	6,50	6,63	6,50
Al tot	1,83	1,91	1,89	1,79	1,99	2,08	1,84	1,84	1,85	2,14	1,97	2,22
Al^{IV}	1,33	1,37	1,35	1,15	1,27	1,43	1,43	1,33	1,18	1,50	1,37	1,50
Al^{VI}	0,50	0,54	0,54	0,63	0,72	0,65	0,41	0,51	0,67	0,63	0,60	0,72
Ti	0,13	0,12	0,11	0,08	0,06	0,09	0,13	0,13	0,10	0,08	0,12	0,04
Fe tot	2,32	2,18	2,18	2,17	2,25	2,39	2,51	2,37	2,18	2,30	2,06	2,55
Fe^{3+}	0,58	0,57	0,65	0,66	0,38	0,34	0,64	0,33	0,36	0,40	0,58	0,39
Fe^{2+}	1,73	1,61	1,53	1,52	1,86	2,05	1,87	2,03	1,82	1,90	1,48	2,16
Mn	0,07	0,08	0,07	0,06	0,05	0,07	0,08	0,09	0,07	0,09	0,08	0,06
Mg	1,99	2,08	2,10	2,05	1,92	1,80	1,87	1,90	1,97	1,90	2,14	1,62
Cr	0,02	0,02	0,00	0,00	0,00	0,03	0,03	0,03	0,01	0,03	0,01	0,02
Ca	1,78	1,69	1,72	1,67	1,84	1,87	1,83	1,82	1,74	1,83	1,67	1,87
Na	0,26	0,45	0,39	0,25	0,25	0,34	0,24	0,33	0,29	0,43	0,47	0,35
K	0,11	0,13	0,12	0,12	0,11	0,11	0,12	0,15	0,14	0,14	0,13	0,14
Total	15,17	15,29	15,23	15,03	15,21	15,34	15,23	15,34	15,19	15,43	15,27	15,38
X_{Mg}	0,53	0,56	0,58	0,57	0,51	0,47	0,50	0,48	0,52	0,50	0,59	0,43

Table S3. d) SEM-EDS mineral chemistry analysis of amphiboles. Thin section 3.

Oxides (Wt%)	PRR33877 (Ford Granodiorite)																			
-----	cam1		cam2		cam3		cam4		cam5		cam6		cam7		cam8		cam9		cam10	
	core	rim	core	rim	core	rim	core	rim	core	rim	core	rim	core	rim	core	rim	core	rim	core	rim
SiO_2	48,34	49,76	51,30	53,27	54,30	50,40	46,99	49,60	47,69	51,15	52,58	51,61	50,89	49,37	50,42	50,06	50,69	50,05	50,90	48,40
TiO_2	1,39	1,08	0,38	0,31	0,35	1,02	1,81	1,35	1,71	0,88	0,20	0,45	0,74	1,10	1,21	0,90	0,89	0,79	1,00	1,30
Al_2O_3	6,63	5,47	4,61	2,32	2,35	5,13	7,33	5,71	7,49	5,76	4,02	4,83	4,59	5,65	5,15	5,78	5,62	6,09	5,27	6,57
FeO	14,99	14,93	13,49	16,75	11,74	14,95	14,36	14,19	14,69	13,97	13,47	13,57	14,59	15,37	14,41	14,70	13,79	13,77	13,83	14,56
MnO	0,51	0,64	0,46	0,44	0,59	0,37	0,61	0,59	0,38	0,50	0,37	0,62	0,49	0,61	0,54	0,53	0,47	0,39	0,45	0,54
MgO	12,33	12,81	14,45	11,94	15,70	12,65	12,87	13,06	12,21	13,28	14,20	14,06	13,56	12,59	13,12	12,51	13,66	13,46	13,79	13,24
CaO	11,73	11,63	11,80	11,98	11,59	12,24	11,09	11,20	11,33	11,61	12,14	11,47	10,99	11,66	11,49	12,03	11,38	11,75	11,52	11,36
Na_2O	1,31	1,25	1,24	0,61	0,78	0,74	2,02	1,25	1,79	0,71	0,80	1,26	1,42	1,13	1,04	0,95	1,40	1,50	0,77	1,75
K_2O	0,68	0,67	0,25	0,28	0,26	0,60	0,73	0,63	0,74	0,57	0,29	0,38	0,45	0,48	0,50	0,63	0,51	0,55	0,51	0,63
Cr_2O_3	0,20	0,13	0,09	0,12	0,48	0,06	0,17	0,22	0,00	0,00	0,11	0,13	0,15	0,10	0,10	0,05	0,00	0,05	0,24	0,04
Total	98,12	98,35	98,07	98,02	98,13	98,17	97,98	97,79	98,01	98,43	98,17	98,38	97,88	98,04	97,98	98,12	98,41	98,39	98,26	98,37
Formula																				
Si	7,10	7,26	7,39	7,83	7,75	7,37	6,89	7,23	7,00	7,35	7,58	7,42	7,38	7,21	7,33	7,32	7,30	7,25	7,32	7,03
Al tot	1,15	0,94	0,78	0,40	0,39	0,88	1,27	0,98	1,29	0,97	0,68	0,82	0,78	0,97	0,88	1,00	0,95	1,04	0,89	1,13
Al^{IV}	0,90	0,74	0,61	0,17	0,25	0,63	1,11	0,77	1,00	0,65	0,42	0,58	0,62	0,79	0,67	0,68	0,70	0,75	0,68	0,97
Al^{VI}	0,24	0,20	0,17	0,23	0,15	0,25	0,15	0,21	0,29	0,32	0,26	0,23	0,16	0,18	0,21	0,31	0,25	0,29	0,22	0,16
Ti	0,15	0,12	0,04	0,03	0,04	0,11	0,20	0,15	0,19	0,09	0,02	0,05	0,08	0,12	0,13	0,10	0,10	0,09	0,11	0,14
Fe tot	1,84	1,82	1,63	2,06	1,40	1,83	1,76	1,73	1,80	1,68	1,62	1,63	1,77	1,88	1,75	1,80	1,66	1,67	1,66	1,77
Fe^{3+}	0,10	0,15	0,29	0,00	0,05	0,00	0,31	0,22	0,13	0,26	0,06	0,26	0,35	0,27	0,20	0,00	0,26	0,10	0,31	0,37
Fe^{2+}	1,74	1,67	1,34	2,06	1,35	1,83	1,45	1,51	1,68	1,42	1,57	1,37	1,41	1,61	1,55	1,80	1,40	1,57	1,36	1,40
Mn	0,06	0,08	0,06	0,05	0,07	0,05	0,08	0,07	0,05	0,06	0,05	0,08	0,06	0,08	0,07	0,07	0,06	0,05	0,06	0,07
Mg	2,70	2,78	3,10	2,62	3,34	2,76	2,81	2,84	2,67	2,84	3,05	3,01	2,93	2,74	2,84	2,73	2,93	2,91	2,96	2,87
Cr	0,02	0,01	0,01	0,01	0,05	0,01	0,02	0,03	0,00	0,00	0,01	0,01	0,02	0,01	0,01	0,01	0,00	0,01	0,03	0,00
Ca	1,84	1,82	1,82	1,89	1,77	1,92	1,74	1,75	1,78	1,79	1,87	1,77	1,71	1,82	1,79	1,88	1,76	1,82	1,78	1,77
Na	0,37	0,35	0,35	0,17	0,21	0,21	0,57	0,35	0,51	0,20	0,22	0,35	0,40	0,32	0,29	0,27	0,39	0,42	0,21	0,49
K	0,13	0,12	0,05	0,05	0,05	0,11	0,14	0,12	0,14	0,10	0,05	0,07	0,08	0,09	0,09	0,12	0,09	0,10	0,09	0,12
Total	15,37	15,31	15,22	15,13	15,09	15,25	15,47	15,24	15,43	15,09	15,16	15,20	15,21	15,24	15,19	15,28	15,24	15,35	15,11	15,38
X_{Mg}	0,61	0,62	0,70	0,56	0,71	0,60	0,66	0,65	0,61	0,67	0,66	0,69	0,67	0,63	0,65	0,60	0,68	0,65	0,69	0,67

Table S3. e) SEM-EDS mineral chemistry analysis of amphiboles. Thin section PRR33877.

Oxides (Wt%)	Thin section 17 (Dolerite)																			
	cpx1		cpx2		cpx3		cpx4		cpx5		cpx6		cpx7		cpx8		cpx9		cpx10	
-----	core	rim	core	rim	core	rim	core	rim	core	rim	core	rim	core	rim	core	rim	core	rim	core	rim
SiO_2	52,23	51,27	49,85	50,28	51,99	50,94	50,08	50,75	50,75	50,58	50,97	49,66	50,48	48,77	50,33	50,45	50,67	50,12	51,51	51,26
TiO_2	1,35	1,97	2,11	1,93	1,11	1,42	2,22	1,81	2,02	2,13	1,63	2,41	2,01	3,28	1,79	1,92	2,09	2,48	1,28	2,02
Al_2O_3	2,42	3,87	5,18	4,37	3,47	4,35	5,16	4,18	4,00	4,17	2,33	3,56	4,17	4,18	4,75	4,21	3,31	4,14	2,22	3,60
Cr_2O_3	0,30	0,12	0,51	0,18	0,23	0,23	0,53	0,15	0,14	0,35	0,38	0,26	0,22	0,29	0,38	0,33	0,10	0,00	0,42	0,15
FeO	7,07	7,59	5,98	6,73	6,74	6,61	6,41	6,83	7,75	7,46	8,54	9,36	6,98	9,36	6,48	6,60	8,33	8,60	7,52	8,22
MnO	0,50	0,26	0,15	0,16	0,10	0,09	0,38	0,36	0,39	0,36	0,52	0,57	0,36	0,48	0,35	0,35	0,14	0,24	0,37	0,30
MgO	15,51	14,36	14,18	14,79	16,23	14,82	14,83	14,85	13,81	14,44	13,61	12,98	14,64	12,61	14,58	14,66	13,91	13,01	14,16	13,68
CaO	19,59	19,73	20,83	20,32	19,13	20,75	19,68	20,33	20,09	19,66	21,20	20,40	19,99	19,60	20,33	20,81	20,67	20,36	21,85	20,24
Na_2O	0,98	0,74	1,04	1,06	0,98	0,71	0,63	0,55	1,04	0,77	0,83	0,81	1,16	1,31	1,00	0,65	0,60	1,05	0,48	0,54
K_2O	0,05	0,10	0,17	0,18	0,00	0,08	0,07	0,19	0,00	0,09	0,00	0,00	0,00	0,11	0,00	0,00	0,19	0,00	0,18	0,00
Total	100,00	100,00	100,00	100,00	100,00	100,00	100,00	100,00	100,00	100,00	100,00	100,00	100,00	100,00	100,00	100,00	100,00	100,00	100,00	100,00
Formula																				
Si	1,92	1,90	1,83	1,85	1,90	1,87	1,85	1,87	1,88	1,87	1,90	1,86	1,86	1,82	1,85	1,86	1,88	1,86	1,91	1,91
Ti	0,04	0,05	0,06	0,05	0,03	0,04	0,06	0,05	0,06	0,06	0,05	0,07	0,06	0,09	0,05	0,05	0,06	0,07	0,04	0,06
Al^{IV}	0,04	0,05	0,11	0,10	0,07	0,09	0,09	0,08	0,06	0,07	0,06	0,08	0,09	0,09	0,10	0,08	0,06	0,07	0,05	0,03
Al^{VI}	0,06	0,12	0,12	0,09	0,08	0,10	0,13	0,10	0,11	0,11	0,05	0,08	0,09	0,10	0,11	0,10	0,09	0,12	0,05	0,12
Fe^{3+}	0,04	0,00	0,06	0,09	0,05	0,03	0,00	0,02	0,03	0,01	0,06	0,04	0,07	0,08	0,05	0,02	0,02	0,03	0,04	0,00
Cr^{3+}	0,01	0,00	0,01	0,01	0,01	0,01	0,02	0,00	0,00	0,01	0,01	0,01	0,01	0,01	0,01	0,01	0,00	0,00	0,01	0,00
Fe^{2+}	0,18	0,23	0,12	0,12	0,16	0,17	0,20	0,19	0,21	0,22	0,21	0,25	0,15	0,21	0,15	0,18	0,24	0,24	0,20	0,26
Mn	0,02	0,01	0,00	0,00	0,00	0,00	0,01	0,01	0,01	0,01	0,02	0,02	0,01	0,02	0,01	0,01	0,00	0,01	0,01	0,01
Mg	0,85	0,79	0,78	0,81	0,88	0,81	0,82	0,82	0,76	0,80	0,76	0,72	0,80	0,70	0,80	0,81	0,77	0,72	0,78	0,76
Ca	0,77	0,78	0,82	0,80	0,75	0,82	0,78	0,80	0,80	0,78	0,85	0,82	0,79	0,78	0,80	0,82	0,82	0,81	0,87	0,81
Na	0,07	0,05	0,07	0,08	0,07	0,05	0,05	0,04	0,07	0,06	0,06	0,06	0,08	0,09	0,07	0,05	0,04	0,08	0,03	0,04
K	0,00	0,00	0,01	0,01	0,00	0,00	0,00	0,01	0,00	0,00	0,00	0,00	0,00	0,01	0,00	0,00	0,01	0,00	0,01	0,00
Total	4,00	4,00	3,99	3,99	4,00	4,00	4,00	3,99	4,00	4,00	4,00	4,00	4,00	3,99	4,00	4,00	3,99	4,00	3,99	4,00

Table S4. SEM-EDS mineral chemistry analysis of clinopyroxenes. Thin section 17.

APPENDIX B2: SEM-EDS chemical analysis of Amphibole (Chapter IV)

Oxides (Wt%)	Thin section 24											
--------	anf1		anf2		anf3		anf4		anf5		anf6	
	core	rim	core	rim	core	rim	core	rim	core	rim	core	rim
SiO_2	43.57	43.42	43.50	41.69	42.02	42.26	45.23	43.63	42.20	42.53	42.31	42.18
TiO_2	1.72	1.66	2.16	1.43	1.18	2.05	1.26	1.48	0.73	1.55	1.59	1.60
Al_2O_3	9.19	9.41	8.74	11.92	10.72	9.83	8.80	10.51	11.14	10.38	10.23	10.63
FeO	19.22	19.81	18.04	20.13	20.90	19.91	18.08	18.33	20.45	19.55	20.68	20.99
MnO	0.61	0.64	1.11	0.79	0.50	0.58	0.67	0.28	0.43	0.66	0.45	0.32
MgO	10.14	9.87	10.62	8.15	9.35	9.79	10.56	10.16	9.83	9.39	9.14	8.66
CaO	10.84	11.02	11.05	10.58	10.44	10.32	11.33	10.50	10.73	11.43	11.13	10.61
Na_2O	1.50	1.28	1.33	1.30	1.49	1.68	1.15	1.66	1.56	1.28	1.42	1.17
K_2O	1.46	1.03	1.45	1.96	1.43	1.30	1.16	1.49	1.23	1.41	1.48	1.64
Cr_2O_3	0.29	0.26	0.52	0.27	0.11	0.22	0.17	0.08	0.09	0.23	0.08	0.08
Total	98.54	98.37	98.51	98.21	98.14	97.94	98.42	98.12	98.38	98.41	98.50	97.89
	Structural formulae on the basis of 23 oxygens											
Si	6.48	6.45	6.48	6.27	6.25	6.31	6.68	6.46	6.23	6.37	6.33	6.33
Al^{IV}	1.52	1.55	1.52	1.73	1.75	1.69	1.32	1.54	1.77	1.63	1.67	1.67
Al^{VI}	0.09	0.09	0.01	0.38	0.13	0.03	0.22	0.29	0.17	0.20	0.14	0.21
Ti	0.19	0.19	0.24	0.16	0.13	0.23	0.14	0.16	0.08	0.17	0.18	0.18
Fe^{3+}	0.78	0.93	0.65	0.77	1.29	1.09	0.63	0.81	1.32	0.70	0.88	1.01
Fe^{2+}	1.61	1.52	1.59	1.76	1.31	1.39	1.61	1.46	1.20	1.75	1.71	1.62
Mn	0.08	0.08	0.14	0.10	0.06	0.07	0.08	0.03	0.05	0.08	0.06	0.04
Mg	2.25	2.18	2.36	1.83	2.07	2.18	2.33	2.24	2.16	2.10	2.04	1.94
Ca	1.73	1.75	1.76	1.70	1.66	1.65	1.79	1.66	1.70	1.83	1.79	1.71
Na	0.43	0.37	0.38	0.38	0.43	0.49	0.33	0.48	0.45	0.37	0.41	0.34
K	0.28	0.19	0.27	0.38	0.27	0.25	0.22	0.28	0.23	0.27	0.28	0.31
Total	15.44	15.31	15.42	15.46	15.37	15.38	15.34	15.42	15.38	15.47	15.48	15.36
X_{Mg}	0.58	0.59	0.60	0.51	0.61	0.61	0.59	0.61	0.64	0.55	0.54	0.54

Oxides (Wt%)	Thin section 26															
--------	anf1		anf2		anf3		anf4		anf5		anf6		anf7		anf8	
	core	rim	core	rim	core	rim	core	rim	core	rim	core	rim	core	rim	core	rim
SiO_2	53.24	51.06	50.68	52.58	49.90	50.13	50.27	47.37	50.63	48.85	52.32	52.32	51.80	50.03	49.74	47.86
TiO_2	0.00	0.56	0.29	0.28	0.50	0.47	0.42	0.57	0.32	0.52	0.31	0.41	0.45	0.61	0.52	0.58
Al_2O_3	3.65	4.37	5.90	3.47	5.75	5.57	6.30	9.05	5.83	7.17	2.78	3.17	4.11	6.17	6.58	8.31
FeO	14.82	15.33	15.27	13.91	15.85	15.77	15.38	16.29	14.95	15.55	14.96	15.42	14.25	16.28	15.51	15.43
MnO	0.55	0.71	0.55	0.37	0.63	0.87	0.33	0.53	0.44	0.60	0.44	0.68	0.52	0.65	0.48	0.77
MgO	13.80	13.31	13.07	14.70	12.50	12.46	12.81	11.58	12.90	11.84	14.71	13.42	14.87	11.59	12.43	11.62
CaO	11.17	11.32	11.26	11.37	11.73	11.70	11.79	11.10	12.15	11.79	11.95	11.36	11.23	11.28	11.38	11.32
Na_2O	0.86	0.94	0.89	0.93	0.58	0.65	0.53	0.88	0.50	0.89	0.59	0.79	0.74	0.72	1.15	1.20
K_2O	0.23	0.44	0.49	0.19	0.64	0.44	0.49	0.66	0.59	0.63	0.32	0.29	0.24	0.65	0.51	0.87
Cr_2O_3	0.14	0.26	0.09	0.09	0.31	0.22	0.13	0.22	0.13	0.25	0.06	0.19	0.17	0.16	0.23	0.23
Total	98.45	98.32	98.50	97.89	98.39	98.28	98.45	98.23	98.43	98.08	98.43	98.08	98.39	98.16	98.56	98.19
	Structural formulae on the basis of 23 oxygens															
Si	7.61	7.38	7.27	7.53	7.25	7.28	7.24	6.86	7.33	7.15	7.50	7.57	7.36	7.29	7.20	6.99
Al^{IV}	0.39	0.62	0.73	0.47	0.75	0.72	0.76	1.14	0.67	0.85	0.50	0.43	0.64	0.71	0.80	1.01
Al^{VI}	0.22	0.13	0.27	0.12	0.23	0.23	0.31	0.40	0.32	0.38	-0.03	0.11	0.05	0.35	0.32	0.42
Ti	0.00	0.06	0.03	0.03	0.05	0.05	0.05	0.06	0.03	0.06	0.03	0.05	0.05	0.07	0.06	0.06
Fe^{3+}	0.42	0.43	0.56	0.47	0.37	0.41	0.43	0.73	0.23	0.20	0.54	0.37	0.77	0.32	0.34	0.33
Fe^{2+}	1.35	1.43	1.27	1.20	1.56	1.51	1.42	1.24	1.58	1.70	1.25	1.50	0.92	1.66	1.54	1.56
Mn	0.07	0.09	0.07	0.04	0.08	0.11	0.04	0.06	0.05	0.07	0.05	0.08	0.06	0.08	0.06	0.10
Mg	2.94	2.87	2.80	3.14	2.71	2.70	2.75	2.50	2.78	2.58	3.15	2.90	3.15	2.52	2.68	2.53
Ca	1.71	1.75	1.73	1.75	1.83	1.82	1.82	1.72	1.88	1.85	1.84	1.76	1.71	1.76	1.76	1.77
Na	0.24	0.26	0.25	0.26	0.16	0.18	0.15	0.25	0.14	0.25	0.16	0.22	0.20	0.20	0.32	0.34
K	0.04	0.08	0.09	0.04	0.12	0.08	0.09	0.12	0.11	0.12	0.06	0.05	0.04	0.12	0.09	0.16
Total	14.99	15.10	15.07	15.04	15.11	15.08	15.06	15.09	15.13	15.22	15.06	15.04	14.96	15.09	15.18	15.27
X_{Mg}	0.69	0.67	0.69	0.72	0.63	0.64	0.66	0.67	0.64	0.60	0.71	0.66	0.77	0.60	0.64	0.62

Oxides (Wt%)	Thin section 71							
--------	anf1		anf2		anf3		anf4	
	core	rim	core	rim	core	rim	core	rim
SiO_2	38.59	38.50	37.70	38.14	37.99	38.23	37.73	37.83
TiO_2	6.84	6.72	7.39	6.90	6.92	6.85	6.92	6.97
Al_2O_3	12.93	12.99	13.78	13.64	12.67	12.83	13.15	13.51
FeO	13.41	13.38	11.74	11.44	13.44	13.19	13.92	13.69
MnO	0.11	0.14	0.20	0.15	0.33	0.18	0.25	0.27
MgO	11.47	11.45	12.24	12.49	11.56	11.85	11.02	11.29
CaO	11.30	11.32	11.37	11.34	11.20	11.08	11.23	10.94
Na_2O	2.55	2.78	2.74	2.75	2.79	2.81	2.76	2.89
K_2O	1.28	1.08	1.19	1.28	1.20	1.16	1.06	1.06
Cr_2O_3	0.00	0.00	0.10	0.00	0.07	0.00	0.10	0.06
Total	98.48	98.37	98.44	98.12	98.18	98.17	98.12	98.51
	Structural formulae on the basis of 23 oxygens							
Si	5.74	5.74	5.59	5.65	5.68	5.69	5.66	5.62
Al^{IV}	2.26	2.26	2.41	2.35	2.32	2.31	2.34	2.38
Al^{VI}	0.01	0.02	-0.01	0.03	-0.08	-0.06	-0.02	-0.01
Ti	0.77	0.75	0.82	0.77	0.78	0.77	0.78	0.78
Fe^{3+}	0.14	0.11	0.12	0.14	0.18	0.27	0.15	0.30
Fe^{2+}	1.53	1.56	1.34	1.28	1.50	1.37	1.59	1.40
Mn	0.01	0.02	0.03	0.02	0.04	0.02	0.03	0.03
Mg	2.54	2.54	2.70	2.76	2.58	2.63	2.46	2.50
Ca	1.80	1.81	1.80	1.80	1.80	1.77	1.80	1.74
Na	0.74	0.80	0.79	0.79	0.81	0.81	0.80	0.83
K	0.24	0.21	0.23	0.24	0.23	0.22	0.20	0.20
Total	15.78	15.82	15.82	15.83	15.84	15.80	15.81	15.77
X_{Mg}	0.62	0.62	0.67	0.68	0.63	0.66	0.61	0.64

APPENDIX B2: SEM-EDS chemical analysis of biotite (Chapter IV)

Sample	thin section 25										thin section 26		
-----	bt1		bt2		bt3		bt4		bt5		bt1	bt2	bt3
Oxide (Wt%)	core (corr)	rim (corr)	core (corr)	rim (corr)	core (corr)	rim (corr)	core (corr)	rim (corr)	core (corr)	rim (corr)	core (corr)	core(corr)	core (corr)
SiO_2	35.40	35.92	36.02	36.06	35.93	35.35	36.64	36.57	35.49	37.84	37.53	36.34	36.76
TiO_2	2.94	2.68	2.54	2.58	2.42	2.92	2.87	3.13	2.93	2.68	2.17	2.06	2.36
Al_2O_3	15.91	16.13	16.02	16.24	16.72	16.21	15.81	15.68	15.70	15.37	15.11	15.67	15.70
FeO	21.20	21.19	21.25	20.98	20.14	20.85	19.87	20.91	21.10	21.02	20.28	20.32	18.69
MnO	0.56	0.50	0.25	0.59	0.25	0.54	0.36	0.66	0.75	0.58	0.42	0.35	0.44
MgO	10.29	9.97	10.07	10.36	10.75	10.36	9.98	9.43	9.96	9.08	10.85	11.18	11.61
CaO	0.00	0.06	0.27	0.00	0.00	0.13	0.18	0.25	0.22	0.27	0.11	0.35	0.42
Na_2O	1.01	0.45	0.69	0.66	0.81	0.84	0.74	0.67	0.56	0.46	0.50	0.95	0.61
K_2O	9.04	9.45	9.53	8.93	9.43	9.01	9.90	9.07	9.61	9.03	9.42	9.28	9.69
Total	96.53	96.35	96.65	96.57	96.61	96.49	96.45	96.71	96.61	96.57	96.63	96.67	96.58
Formula													
Si	5.42	5.49	5.49	5.49	5.45	5.41	5.58	5.57	5.45	5.74	5.69	5.53	5.56
Al^{IV}	2.58	2.51	2.51	2.51	2.55	2.59	2.42	2.43	2.55	2.26	2.31	2.47	2.44
Al^{VI}	0.29	0.40	0.38	0.40	0.44	0.33	0.41	0.39	0.30	0.49	0.39	0.34	0.36
Ti	0.34	0.31	0.29	0.29	0.28	0.34	0.33	0.36	0.34	0.31	0.25	0.24	0.27
Fe^{2+}	2.72	2.71	2.71	2.67	2.56	2.67	2.53	2.66	2.71	2.67	2.57	2.58	2.36
Mn	0.07	0.06	0.03	0.08	0.03	0.07	0.05	0.09	0.10	0.07	0.05	0.04	0.06
Mg	2.35	2.27	2.29	2.35	2.43	2.36	2.26	2.14	2.28	2.05	2.45	2.53	2.62
Ca	0.00	0.01	0.04	0.00	0.00	0.02	0.03	0.04	0.04	0.04	0.02	0.06	0.07
Na	0.30	0.13	0.20	0.19	0.24	0.25	0.22	0.20	0.17	0.14	0.15	0.28	0.18
K	1.77	1.84	1.86	1.73	1.83	1.76	1.92	1.76	1.88	1.75	1.82	1.80	1.87
TOTAL	15.84	15.74	15.80	15.72	15.81	15.80	15.75	15.64	15.81	15.52	15.70	15.87	15.79
X_{Fe}	0.54	0.54	0.54	0.53	0.51	0.53	0.53	0.55	0.54	0.56	0.51	0.50	0.47

Sample	thin section 92			thin section 95					thin section 83					
-----	bt1	bt2	bt3	bt1	bt2		bt3		bt1		bt2		bt3	
Oxide (Wt%)	core (corr)	core(corr)	core (corr)	core (corr)	core (corr)	rim (corr)	core (corr)	rim (corr)	core (corr)	rim (corr)	core (corr)	rim (corr)	core (corr)	rim (corr)
SiO_2	36.75	36.19	37.27	36.81	35.39	36.65	35.32	36.07	36.27	35.62	35.85	35.30	35.22	35.33
TiO_2	2.08	2.07	2.03	2.16	2.27	2.18	2.37	2.23	2.32	2.34	2.57	2.45	2.87	2.72
Al_2O_3	16.65	16.30	15.98	17.00	17.17	17.16	16.44	16.95	17.50	18.60	17.68	18.24	17.98	17.89
FeO	19.60	20.87	20.20	19.72	20.77	19.65	21.36	21.32	17.67	17.75	18.01	18.29	18.42	18.08
MnO	0.45	0.37	0.33	0.47	0.31	0.29	0.21	0.10	0.30	0.19	0.18	0.17	0.24	0.24
MgO	11.29	10.62	10.75	10.66	10.69	10.50	10.03	10.13	11.86	11.82	11.67	11.36	11.24	11.63
CaO	0.13	0.25	0.09	0.19	0.12	0.25	0.20	0.15	0.15	0.18	0.15	0.14	0.15	0.09
Na_2O	0.35	0.67	0.43	0.45	0.69	0.47	0.70	0.38	0.68	0.37	0.43	0.45	0.34	0.66
K_2O	8.87	8.87	9.15	8.72	8.91	9.09	9.84	9.38	9.92	9.78	9.88	9.91	9.86	9.68
Total	96.47	96.39	96.44	96.50	96.44	96.39	96.47	96.70	96.72	96.67	96.54	96.42	96.47	96.51
Formula														
Si	5.55	5.51	5.64	5.55	5.38	5.53	5.42	5.47	5.44	5.33	5.39	5.33	5.32	5.33
Al^{IV}	2.45	2.49	2.36	2.45	2.62	2.47	2.58	2.53	2.56	2.67	2.61	2.67	2.68	2.67
Al^{VI}	0.51	0.44	0.49	0.57	0.46	0.58	0.39	0.50	0.52	0.61	0.52	0.57	0.52	0.50
Ti	0.24	0.24	0.23	0.24	0.26	0.25	0.27	0.25	0.26	0.26	0.29	0.28	0.33	0.31
Fe^{2+}	2.47	2.66	2.56	2.49	2.64	2.48	2.74	2.70	2.21	2.22	2.26	2.31	2.33	2.28
Mn	0.06	0.05	0.04	0.06	0.04	0.04	0.03	0.01	0.04	0.02	0.02	0.02	0.03	0.03
Mg	2.54	2.41	2.43	2.40	2.43	2.36	2.29	2.29	2.65	2.64	2.62	2.56	2.53	2.61
Ca	0.02	0.04	0.02	0.03	0.02	0.04	0.03	0.02	0.02	0.03	0.02	0.02	0.02	0.02
Na	0.10	0.20	0.13	0.13	0.20	0.14	0.21	0.11	0.20	0.11	0.13	0.13	0.10	0.19
K	1.71	1.72	1.77	1.68	1.73	1.75	1.93	1.82	1.90	1.87	1.90	1.91	1.90	1.86
TOTAL	15.64	15.75	15.65	15.60	15.78	15.64	15.89	15.72	15.81	15.75	15.76	15.79	15.75	15.80
X_{Fe}	0.49	0.52	0.51	0.51	0.52	0.51	0.54	0.54	0.46	0.46	0.46	0.47	0.48	0.47

Sample	thin section 83		thin section 35							
-----	bt4		bt1		bt2		bt3		bt4	
Oxide (Wt%)	core (corr)	rim (corr)	core (corr)	rim (corr)	core (corr)	rim (corr)	core (corr)	rim (corr)	core (corr)	rim (corr)
SiO_2	35.26	35.71	35.04	34.16	34.72	35.63	35.04	34.30	34.15	35.60
TiO_2	2.35	2.40	2.79	2.48	2.61	2.39	2.80	2.67	2.65	2.63
Al_2O_3	17.63	18.39	17.71	16.51	17.61	17.84	16.71	17.17	17.46	17.38
FeO	18.18	17.62	21.98	24.56	22.53	21.86	22.90	23.76	22.92	21.56
MnO	0.25	0.21	0.29	0.39	0.39	0.32	0.37	0.39	0.37	0.35
MgO	11.86	11.89	8.70	7.87	8.61	8.45	8.72	8.15	8.81	8.83
CaO	0.22	0.07	0.14	0.16	0.04	0.16	0.12	0.00	0.18	0.18
Na_2O	0.62	0.40	0.67	0.47	0.41	0.29	0.38	0.36	0.70	0.44
K_2O	9.87	9.72	9.27	9.75	9.34	9.54	9.37	9.70	9.35	9.29
Total	96.36	96.44	96.65	96.41	96.43	96.57	96.63	96.61	96.66	96.42
Formula										
Si	5.33	5.35	5.36	5.34	5.34	5.44	5.40	5.32	5.27	5.44
Al^{IV}	2.67	2.65	2.64	2.66	2.66	2.56	2.60	2.68	2.73	2.56
Al^{VI}	0.48	0.60	0.55	0.38	0.54	0.65	0.43	0.46	0.44	0.57
Ti	0.27	0.27	0.32	0.29	0.30	0.27	0.32	0.31	0.31	0.30
Fe^{2+}	2.30	2.21	2.81	3.21	2.90	2.79	2.95	3.08	2.96	2.76
Mn	0.03	0.03	0.04	0.05	0.05	0.04	0.05	0.05	0.05	0.04
Mg	2.67	2.66	1.98	1.84	1.98	1.92	2.00	1.88	2.03	2.01
Ca	0.04	0.01	0.02	0.03	0.01	0.03	0.02	0.00	0.03	0.03
Na	0.18	0.12	0.20	0.14	0.12	0.09	0.11	0.11	0.21	0.13
K	1.90	1.86	1.81	1.95	1.83	1.86	1.84	1.92	1.84	1.81
TOTAL	15.87	15.74	15.73	15.89	15.73	15.65	15.74	15.82	15.86	15.66
X_{Fe}	0.46	0.45	0.59	0.64	0.59	0.59	0.60	0.62	0.59	0.58

APPENDIX B2: SEM-EDS chemical analysis of white mica (Chapter IV)

Sample	Thin section 25													
	White mica1		White mica2		White mica3		White mica4		White mica5		White mica6		White mica7	
Oxide (Wt%)	core (corr)	rim (corr)	core (corr)	rim (corr)	core (corr)	rim (corr)	core (corr)	rim (corr)	core (corr)	rim (corr)	core (corr)	rim (corr)	core (corr)	rim (corr)
SiO_2	47.23	54.00	46.49	47.90	49.85	47.10	45.20	45.01	46.55	46.66	46.26	46.13	46.33	45.97
TiO_2	1.00	1.14	1.24	1.25	0.71	1.20	1.41	1.69	1.30	1.37	1.52	1.02	1.22	1.43
Al_2O_3	27.43	25.26	30.04	29.56	26.09	30.15	29.43	29.92	29.18	29.07	29.28	29.48	29.17	28.92
FeO	4.90	3.98	4.28	3.88	4.63	4.25	4.99	4.46	4.42	4.36	4.46	4.65	4.40	4.59
MnO	0.35	0.32	0.22	0.18	0.35	0.22	0.13	0.30	0.29	0.23	0.00	0.18	0.20	0.00
MgO	2.58	1.75	1.95	2.07	2.99	1.57	2.03	1.69	1.93	1.60	1.68	1.57	1.77	1.68
CaO	0.24	0.00	0.28	0.23	0.14	0.17	0.00	0.19	0.21	0.31	0.24	0.19	0.14	0.09
Na_2O	0.90	0.88	1.03	1.03	0.54	0.72	0.95	0.97	0.91	1.02	0.69	0.56	0.58	0.68
K_2O	10.52	8.56	10.66	9.87	10.57	10.47	10.63	10.53	10.66	10.20	10.22	10.44	10.85	10.75
Total	95.39	95.99	96.42	96.20	96.12	95.98	94.97	95.06	95.64	95.02	94.56	94.32	94.78	94.26
Formula														
Si	6.47	7.12	6.29	6.43	6.73	6.36	6.23	6.20	6.35	6.38	6.35	6.35	6.36	6.35
Al^{IV}	1.53	0.88	1.71	1.57	1.27	1.64	1.77	1.80	1.65	1.62	1.65	1.65	1.64	1.65
Al^{VI}	2.90	3.04	3.07	3.10	2.88	3.16	3.01	3.05	3.03	3.07	3.09	3.14	3.09	3.07
Ti	0.10	0.11	0.13	0.13	0.07	0.12	0.15	0.18	0.13	0.14	0.16	0.11	0.13	0.15
Fe(ii)	0.56	0.44	0.48	0.43	0.52	0.48	0.57	0.51	0.50	0.50	0.51	0.54	0.51	0.53
Mn	0.04	0.04	0.03	0.02	0.04	0.03	0.02	0.04	0.03	0.03	0.00	0.02	0.02	0.00
Mg	0.53	0.34	0.39	0.41	0.60	0.32	0.42	0.35	0.39	0.33	0.34	0.32	0.36	0.35
Ca	0.03	0.00	0.04	0.03	0.02	0.02	0.00	0.03	0.03	0.05	0.04	0.03	0.02	0.01
Na	0.24	0.22	0.27	0.27	0.14	0.19	0.25	0.26	0.24	0.27	0.18	0.15	0.15	0.18
K	1.84	1.44	1.84	1.69	1.82	1.80	1.87	1.85	1.85	1.78	1.79	1.84	1.90	1.89
Cl	0.00	0.00	0.00	0.00	0.00	0.00	0.00	0.00	0.00	0.00	0.00	0.00	0.00	0.00
F	0.00	0.00	0.00	0.00	0.00	0.00	0.00	0.00	0.00	0.00	0.00	0.00	0.00	0.00
TOTAL	14.25	13.64	14.25	14.09	14.10	14.12	14.29	14.26	14.22	14.16	14.11	14.14	14.18	14.18

Sample	Thin section 92													
	White mica1		White mica2		White mica3		White mica4		White mica5		White mica6		White mica7	
Oxide (Wt%)	core (corr)	rim (corr)	core (corr)	rim (corr)	core (corr)	rim (corr)	core (corr)	rim (corr)	core (corr)	rim (corr)	core (corr)	rim (corr)	core (corr)	rim (corr)
SiO_2	45.41	45.45	46.07	46.85	49.86	48.81	46.10	49.20	45.69	47.81	45.86	46.47	48.93	46.22
TiO_2	1.01	1.10	0.81	0.46	0.96	1.02	0.71	0.98	0.76	1.13	1.15	1.04	0.68	0.77
Al_2O_3	33.09	32.95	31.85	31.39	26.40	26.67	33.82	27.06	28.95	29.16	32.00	31.58	27.81	30.67
FeO	2.17	2.08	3.57	3.25	3.06	3.26	2.13	3.08	4.17	2.86	2.86	2.75	3.52	4.38
MnO	0.28	0.09	0.34	0.21	0.28	0.38	0.00	0.46	0.38	0.28	0.27	0.26	0.23	0.20
MgO	1.36	1.39	0.96	1.29	3.03	3.44	1.37	3.13	2.78	2.36	1.63	1.37	3.18	1.62
CaO	0.13	0.14	0.07	0.20	0.19	0.29	0.12	0.00	0.28	0.23	0.09	0.28	0.00	0.31
Na_2O	0.97	0.90	0.60	0.86	0.49	0.70	0.94	0.89	0.90	0.65	0.56	0.88	0.76	0.65
K_2O	9.86	10.47	10.31	10.45	10.81	10.70	10.49	10.25	10.65	10.48	10.33	10.56	10.82	10.88
Total	94.54	94.75	94.88	95.07	95.34	95.76	95.74	95.32	94.78	95.20	95.01	95.43	96.03	95.93
Formula														
Si	6.16	6.16	6.27	6.35	6.74	6.62	6.16	6.65	6.30	6.47	6.22	6.28	6.58	6.28
Al^{IV}	1.84	1.84	1.73	1.65	1.26	1.38	1.84	1.35	1.70	1.53	1.78	1.72	1.42	1.72
Al^{VI}	3.44	3.42	3.38	3.36	2.95	2.88	3.49	2.96	3.00	3.12	3.33	3.31	2.99	3.19
Ti	0.10	0.11	0.08	0.05	0.10	0.10	0.07	0.10	0.08	0.11	0.12	0.11	0.07	0.08
Fe(ii)	0.25	0.24	0.41	0.37	0.35	0.37	0.24	0.35	0.48	0.32	0.32	0.31	0.40	0.50
Mn	0.03	0.01	0.04	0.02	0.03	0.04	0.00	0.05	0.04	0.03	0.03	0.03	0.03	0.02
Mg	0.27	0.28	0.20	0.26	0.61	0.70	0.27	0.63	0.57	0.48	0.33	0.28	0.64	0.33
Ca	0.02	0.02	0.01	0.03	0.03	0.04	0.02	0.00	0.04	0.03	0.01	0.04	0.00	0.04
Na	0.26	0.24	0.16	0.23	0.13	0.18	0.24	0.23	0.24	0.17	0.15	0.23	0.20	0.17
K	1.70	1.81	1.79	1.81	1.86	1.85	1.79	1.77	1.87	1.81	1.79	1.82	1.86	1.89
Cl	0.00	0.00	0.00	0.00	0.00	0.00	0.00	0.00	0.00	0.00	0.00	0.00	0.00	0.00
F	0.00	0.00	0.00	0.00	0.00	0.00	0.00	0.00	0.00	0.00	0.00	0.00	0.00	0.00
TOTAL	14.08	14.12	14.07	14.12	14.06	14.17	14.12	14.09	14.33	14.08	14.08	14.12	14.17	14.22

Sample	Thin section 95													
	White mica1		White mica2		White mica3		White mica4		White mica5		White mica6		White mica7	
Oxide (Wt%)	core (corr)	rim (corr)	core (corr)	rim (corr)	core (corr)	rim (corr)	core (corr)	rim (corr)	core (corr)	rim (corr)	core (corr)	rim (corr)	core (corr)	rim (corr)
SiO_2	45.58	46.51	45.80	46.77	46.43	46.90	47.64	50.88	46.12	46.14	47.20	46.49	46.23	46.13
TiO_2	1.52	1.17	0.45	0.22	1.30	1.04	0.84	0.77	0.78	0.82	0.59	0.72	0.90	1.20
Al_2O_3	32.79	34.46	34.50	34.03	26.90	27.56	28.47	28.80	33.06	32.88	27.85	28.00	31.48	31.50
FeO	2.24	1.24	1.60	1.64	5.79	4.81	3.46	2.32	2.79	2.82	5.78	5.71	2.97	2.69
MnO	0.45	0.11	0.47	0.16	0.00	0.00	0.29	0.26	0.11	0.10	0.08	0.15	0.11	0.18
MgO	1.67	1.11	1.02	1.39	3.42	3.23	3.27	2.04	1.29	1.52	2.28	2.28	1.93	2.09
CaO	0.26	0.18	0.26	0.00	0.05	0.11	0.21	0.18	0.00	0.04	0.07	0.07	0.05	0.21
Na_2O	0.88	0.68	1.00	1.00	0.82	0.79	0.77	0.62	0.59	0.96	0.75	0.93	0.98	0.86
K_2O	10.33	10.36	10.27	10.61	10.16	10.33	10.25	9.70	11.02	10.60	11.05	10.45	10.94	10.87
Total	96.03	95.83	95.65	95.82	94.95	94.83	95.43	95.79	95.84	96.02	95.64	94.95	95.72	95.83
Formula														
Si	6.12	6.17	6.13	6.22	6.40	6.43	6.45	6.74	6.19	6.19	6.46	6.41	6.24	6.22
Al^{IV}	1.88	1.83	1.87	1.78	1.60	1.57	1.55	1.26	1.81	1.81	1.54	1.59	1.76	1.78
Al^{VI}	3.31	3.55	3.58	3.56	2.77	2.89	3.00	3.24	3.43	3.38	2.96	2.96	3.25	3.22
Ti	0.15	0.12	0.05	0.02	0.13	0.11	0.09	0.08	0.08	0.08	0.06	0.07	0.09	0.12
Fe(ii)	0.25	0.14	0.18	0.18	0.67	0.55	0.39	0.26	0.31	0.32	0.66	0.66	0.34	0.30
Mn	0.05	0.01	0.05	0.02	0.00	0.00	0.03	0.03	0.01	0.01	0.01	0.02	0.01	0.02
Mg	0.33	0.22	0.20	0.28	0.70	0.66	0.66	0.40	0.26	0.30	0.47	0.47	0.39	0.42
Ca	0.04	0.03	0.04	0.00	0.01	0.02	0.03	0.03	0.00	0.01	0.01	0.01	0.01	0.03
Na	0.23	0.17	0.26	0.26	0.22	0.21	0.20	0.16	0.15	0.25	0.20	0.25	0.26	0.22
K	1.77	1.75	1.75	1.80	1.79	1.81	1.77	1.64	1.89	1.81	1.93	1.84	1.89	1.87
Cl	0.00	0.00	0.00	0.00	0.00	0.00	0.00	0.00	0.00	0.00	0.00	0.00	0.00	0.00
F	0.00	0.00	0.00	0.00	0.00	0.00	0.00	0.00	0.00	0.00	0.00	0.00	0.00	0.00
TOTAL	14.13	13.99	14.11	14.12	14.29	14.24	14.17	13.83	14.13	14.16	14.29	14.28	14.23	14.21

Sample	Thin section 83											
	White mica1		White mica2	White mica3	White mica4		White mica5		White mica6		White mica7	
Oxide (Wt%)	core (corr)	rim (corr)	core (corr)	core (corr)	core (corr)	rim (corr)	core (corr)	rim (corr)	core (corr)	rim (corr)	core (corr)	rim (corr)
SiO_2	45.60	45.78	45.91	45.35	45.20	47.42	45.28	45.90	46.35	46.29	46.10	46.26
TiO_2	1.17	0.81	1.25	0.91	0.96	1.14	1.24	1.02	0.90	1.11	0.90	0.84
Al_2O_3	34.22	33.61	33.79	33.42	34.13	31.08	33.73	33.47	33.39	32.42	33.29	33.14
FeO	1.48	1.28	1.39	1.44	1.34	1.74	1.40	1.37	1.33	2.03	1.45	1.40
MnO	0.17	0.06	0.15	0.00	0.00	0.20	0.11	0.09	0.13	0.08	0.12	0.17
MgO	1.16	1.53	1.44	1.71	1.37	1.68	1.76	1.73	1.47	2.14	1.43	1.69
CaO	0.28	0.16	0.12	0.04	0.18	0.32	0.15	0.18	0.00	0.19	0.24	0.09
Na_2O	0.72	0.86	0.59	0.97	1.16	1.71	0.92	0.81	0.53	0.64	0.65	1.17
K_2O	10.49	10.79	11.23	10.81	10.81	9.79	11.06	11.19	11.21	10.23	10.79	10.64
Total	95.43	95.07	96.01	94.76	95.34	95.12	95.62	95.82	95.32	95.13	95.17	95.54
Formula												
Si	6.11	6.16	6.13	6.13	6.08	6.37	6.07	6.14	6.21	6.22	6.20	6.20
Al^{IV}	1.89	1.84	1.87	1.87	1.92	1.63	1.93	1.86	1.79	1.78	1.80	1.80
Al^{VI}	3.51	3.49	3.45	3.45	3.49	3.28	3.40	3.42	3.48	3.35	3.47	3.43
Ti	0.12	0.08	0.13	0.09	0.10	0.12	0.13	0.10	0.09	0.11	0.09	0.08
Fe(ii)	0.17	0.14	0.15	0.16	0.15	0.20	0.16	0.15	0.15	0.23	0.16	0.16
Mn	0.02	0.01	0.02	0.00	0.00	0.02	0.01	0.01	0.02	0.01	0.01	0.02
Mg	0.23	0.31	0.29	0.35	0.27	0.34	0.35	0.35	0.29	0.43	0.29	0.34
Ca	0.04	0.02	0.02	0.01	0.03	0.05	0.02	0.03	0.00	0.03	0.03	0.01
Na	0.19	0.23	0.15	0.25	0.30	0.44	0.24	0.21	0.14	0.17	0.17	0.30
K	1.79	1.85	1.91	1.86	1.85	1.68	1.89	1.91	1.92	1.75	1.85	1.82
Cl	0.00	0.00	0.00	0.00	0.00	0.00	0.00	0.00	0.00	0.00	0.00	0.00
F	0.00	0.00	0.00	0.00	0.00	0.00	0.00	0.00	0.00	0.00	0.00	0.00
TOTAL	14.06	14.13	14.12	14.18	14.20	14.12	14.20	14.18	14.09	14.07	14.08	14.16

Sample	Thin section 35																	
	White mica1		White mica2		White mica3		White mica4		White mica5		White mica6		White mica7		White mica8		White mica9	
Oxide (Wt%)	core (corr)	rim (corr)	core (corr)	rim (corr)	core (corr)	rim (corr)	core (corr)	rim (corr)	core (corr)	rim (corr)	core (corr)	rim (corr)	core (corr)	rim (corr)	core (corr)	rim (corr)	core (corr)	rim (corr)
SiO_2	46.19	46.26	47.09	46.27	46.29	46.00	48.67	47.27	50.42	45.89	45.99	46.05	51.95	50.20	46.31	49.15	47.18	45.35
TiO_2	0.93	0.81	0.76	1.00	0.76	1.03	0.58	0.77	0.34	1.09	0.86	0.97	0.42	0.48	0.79	0.82	0.78	0.83
Al_2O_3	32.17	32.98	32.30	32.51	31.94	33.19	29.50	33.29	27.42	32.59	32.47	33.22	26.27	27.77	32.33	28.39	32.38	32.66
FeO	2.11	1.83	2.33	1.92	1.95	1.70	2.19	1.40	2.39	1.94	1.83	1.88	2.30	2.29	1.85	2.26	2.04	1.87
MnO	0.26	0.10	0.17	0.19	0.18	0.18	0.14	0.00	0.00	0.23	0.15	0.23	0.17	0.10	0.12	0.10	0.18	0.13
MgO	1.72	1.79	1.62	1.78	1.95	1.71	2.38	1.41	3.18	1.52	1.89	1.71	3.09	3.25	1.98	2.82	1.51	1.68
CaO	0.25	0.14	0.13	0.13	0.13	0.12	0.08	0.20	0.22	0.17	0.20	0.15	0.25	0.10	0.10	0.20	0.09	0.05
Na_2O	0.99	1.01	0.58	1.04	0.95	0.95	0.64	0.74	0.87	0.73	0.92	1.02	0.46	0.95	0.98	0.49	0.59	0.83
K_2O	10.61	10.14	10.90	10.16	10.63	10.15	11.02	10.52	10.29	10.80	10.46	10.68	10.43	10.12	10.72	10.89	10.88	11.36
Total	95.43	95.14	96.10	95.21	94.93	95.16	95.25	95.62	95.21	95.14	94.85	96.03	95.41	95.35	95.26	95.17	95.78	94.76
Formula																		
Si	6.23	6.21	6.29	6.22	6.26	6.18	6.55	6.28	6.76	6.20	6.21	6.16	6.93	6.71	6.23	6.61	6.31	6.16
Al^{IV}	1.77	1.79	1.71	1.78	1.74	1.82	1.45	1.72	1.24	1.80	1.79	1.84	1.07	1.29	1.77	1.39	1.69	1.84
Al^{VI}	3.34	3.42	3.38	3.38	3.35	3.43	3.22	3.50	3.08	3.38	3.38	3.39	3.05	3.09	3.36	3.11	3.41	3.39
Ti	0.09	0.08	0.08	0.10	0.08	0.10	0.06	0.08	0.03	0.11	0.09	0.10	0.04	0.05	0.08	0.08	0.08	0.09
Fe(ii)	0.24	0.21	0.26	0.22	0.22	0.19	0.25	0.16	0.27	0.22	0.21	0.21	0.26	0.26	0.21	0.25	0.23	0.21
Mn	0.03	0.01	0.02	0.02	0.02	0.02	0.02	0.00	0.00	0.03	0.02	0.03	0.02	0.01	0.01	0.01	0.02	0.02
Mg	0.35	0.36	0.32	0.36	0.39	0.34	0.48	0.28	0.64	0.31	0.38	0.34	0.61	0.65	0.40	0.57	0.30	0.34
Ca	0.04	0.02	0.02	0.02	0.02	0.02	0.01	0.03	0.03	0.02	0.03	0.02	0.04	0.01	0.01	0.03	0.01	0.01
Na	0.26	0.26	0.15	0.27	0.25	0.25	0.17	0.19	0.23	0.19	0.24	0.26	0.12	0.25	0.26	0.13	0.15	0.22
K	1.82	1.74	1.86	1.74	1.83	1.74	1.89	1.78	1.76	1.86	1.80	1.82	1.77	1.73	1.84	1.87	1.86	1.97
Cl	0.00	0.00	0.00	0.00	0.00	0.00	0.00	0.00	0.00	0.00	0.00	0.00	0.00	0.00	0.00	0.00	0.00	0.00
F	0.00	0.00	0.00	0.00	0.00	0.00	0.00	0.00	0.00	0.00	0.00	0.00	0.00	0.00	0.00	0.00	0.00	0.00
TOTAL	14.16	14.10	14.09	14.10	14.16	14.09	14.09	14.02	14.04	14.12	14.14	14.17	13.91	14.04	14.17	14.05	14.06	14.24

APPENDIX B3: SEM-EDS analysis of Amphiboles (Chapter V)

Area	Marshall Valley												
Sample	21-01-15 P21b							21-01-15 P19b					
Clast N°	clast 2		clast 16	clast 11		clast 3		Clast9					
	2.1	2.2	16.1	11.1	11.2	3.1	3.2	amp1		amp2		amp3	
Oxides (Wt%)	core	core	core	core	core	core	core	core	rim	core	rim	core	rim
SiO_2	44.66	43.76	44.66	39.83	42.07	46.52	48.24	42.46	42.19	42.94	43.74	42.57	42.74
TiO_2	1.51	1.63	1.51	6.62	5.00	1.90	1.33	2.31	1.90	2.33	2.17	2.36	2.44
Al_2O_3	8.31	9.00	8.31	13.20	11.92	9.81	8.66	10.38	10.43	8.92	8.47	9.16	9.08
FeO	22.14	22.13	22.14	10.24	9.87	14.32	14.07	23.50	23.20	24.11	24.54	24.25	24.15
MnO	0.71	0.75	0.71	0.38	0.30	0.40	0.22	0.52	0.51	0.68	0.73	0.69	0.32
MgO	6.78	6.49	6.78	12.53	11.09	11.99	12.54	4.57	5.28	5.10	4.70	5.13	5.14
CaO	11.08	11.22	11.08	11.42	14.05	10.65	10.74	10.92	10.54	10.92	10.86	10.87	10.77
Na_2O	1.70	1.95	1.70	2.93	2.91	1.86	1.75	1.86	2.29	1.70	1.47	2.05	2.23
K_2O	1.42	1.46	1.42	1.17	1.08	0.77	0.85	1.62	1.52	1.31	1.18	1.22	1.37
Cr_2O_3	0.19	0.11	0.19	0.18	0.23	0.28	0.11	0.09	0.00	0.12	0.19	0.16	0.06
Total	98.50	98.50	98.50	98.50	98.50	98.50	98.50	98.21	97.87	98.12	98.02	98.45	98.31
Si	6.85	6.74	6.85	5.89	6.44	6.74	6.96	6.62	6.56	6.68	6.81	6.62	6.66
Al^{IV}	1.15	1.26	1.15	2.11	1.56	1.26	1.04	1.38	1.44	1.32	1.19	1.38	1.34
Al^{VI}	0.35	0.37	0.35	0.19	0.59	0.42	0.43	0.53	0.47	0.32	0.36	0.29	0.33
Ti	0.17	0.19	0.17	0.74	0.58	0.21	0.14	0.27	0.22	0.27	0.25	0.28	0.29
Fe^{3+}	0.00	0.00	0.00	0.00	0.00	0.36	0.31	0.00	0.02	0.00	0.00	0.00	0.00
Fe^{2+}	2.84	2.85	2.84	1.27	1.26	1.38	1.39	3.07	2.99	3.14	3.20	3.15	3.15
Mn	0.09	0.10	0.09	0.05	0.04	0.05	0.03	0.07	0.07	0.09	0.10	0.09	0.04
Mg	1.55	1.49	1.55	2.76	2.53	2.59	2.70	1.06	1.22	1.18	1.09	1.19	1.19
Cr	0.02	0.01	0.02	0.02	0.03	0.03	0.01	0.01	0.00	0.01	0.02	0.02	0.01
Ca	1.82	1.85	1.82	1.81	2.30	1.65	1.66	1.83	1.76	1.82	1.81	1.81	1.80
Na	0.51	0.58	0.51	0.84	0.86	0.52	0.49	0.56	0.69	0.51	0.44	0.62	0.67
K	0.28	0.29	0.28	0.22	0.21	0.14	0.16	0.32	0.30	0.26	0.23	0.24	0.27
Total	15.63	15.73	15.63	15.89	16.41	15.35	15.32	15.72	15.75	15.61	15.51	15.69	15.75
X_{Mg}	0.35	0.34	0.35	0.69	0.67	0.65	0.66	0.26	0.29	0.27	0.25	0.27	0.28

Area	Marshall Valley								Taylor Valley							
Sample	21-01-15 P19b								22-01-15-P15b							
Clast N°	Clast11								CLAST 1							
	amp1		amp2		amp3		amp4		amp1		amp2		amp3		amp4	
Oxides (Wt%)	core	rim	core	rim	core	rim	core	rim	core (corr)	rim(corr)	core (corr)	rim(corr)	core (corr)	rim(corr)	core (corr)	rim(corr)
SiO_2	49.69	50.47	50.43	49.90	50.41	50.02	48.91	49.89	43.12	43.27	42.31	42.57	42.16	42.70	42.08	43.82
TiO_2	1.60	1.14	1.11	1.33	1.25	1.32	1.23	1.44	1.37	1.31	1.75	1.61	1.92	1.51	1.63	1.43
Al_2O_3	7.26	6.35	7.25	7.02	7.12	6.96	7.39	6.89	12.54	12.19	12.05	12.37	12.36	12.38	12.14	11.57
FeO	13.30	12.05	12.71	13.07	12.80	12.83	13.47	13.19	18.75	19.08	19.54	19.18	18.62	18.74	20.01	18.48
MnO	0.35	0.38	0.22	0.33	0.28	0.48	0.34	0.31	0.45	0.47	0.53	0.39	0.54	0.56	0.30	0.25
MgO	12.57	14.42	13.10	13.31	13.11	13.31	13.18	13.14	7.64	7.43	7.62	7.95	8.07	8.03	7.62	7.95
CaO	11.96	11.44	11.60	11.33	11.58	11.61	11.45	11.42	11.47	11.61	11.63	11.20	11.13	11.14	11.53	12.04
Na_2O	0.93	1.29	0.98	1.37	0.98	1.01	1.50	0.85	1.36	1.15	1.08	1.57	1.82	1.55	1.38	1.20
K_2O	0.52	0.53	0.59	0.47	0.57	0.65	0.70	0.62	1.41	1.31	1.53	1.47	1.53	1.46	1.70	1.19
Cr_2O_3	0.14	0.16	0.00	0.00	0.05	0.14	0.00	0.11	0.00	0.00	0.00	0.00	0.00	0.00	0.00	0.00
Total	98.32	98.22	97.98	98.13	98.16	98.34	98.18	97.87	98.12	97.85	98.02	98.31	98.16	98.08	98.38	97.94
Si	7.21	7.23	7.27	7.19	7.26	7.21	7.09	7.21	6.49	6.54	6.40	6.39	6.36	6.41	6.36	6.62
Al^{IV}	0.79	0.77	0.73	0.81	0.74	0.79	0.91	0.79	1.51	1.46	1.60	1.61	1.64	1.59	1.64	1.38
Al^{VI}	0.45	0.31	0.50	0.38	0.47	0.39	0.35	0.38	0.71	0.71	0.54	0.58	0.55	0.61	0.53	0.68
Ti	0.17	0.12	0.12	0.14	0.14	0.14	0.13	0.16	0.16	0.15	0.20	0.18	0.22	0.17	0.19	0.16
Fe^{3+}	0.00	0.19	0.02	0.17	0.02	0.08	0.20	0.17	0.12	0.11	0.28	0.32	0.23	0.32	0.27	0.00
Fe^{2+}	1.61	1.25	1.52	1.41	1.52	1.47	1.44	1.42	2.24	2.30	2.19	2.09	2.11	2.03	2.26	2.33
Mn	0.04	0.05	0.03	0.04	0.03	0.06	0.04	0.04	0.06	0.06	0.07	0.05	0.07	0.07	0.04	0.03
Mg	2.72	3.08	2.82	2.86	2.82	2.86	2.85	2.83	1.71	1.67	1.72	1.78	1.81	1.80	1.72	1.79
Cr	0.02	0.02	0.00	0.00	0.01	0.02	0.00	0.01	0.00	0.00	0.00	0.00	0.00	0.00	0.00	0.00
Ca	1.86	1.76	1.79	1.75	1.79	1.79	1.78	1.77	1.85	1.88	1.88	1.80	1.80	1.79	1.87	1.95
Na	0.26	0.36	0.27	0.38	0.27	0.28	0.42	0.24	0.40	0.34	0.32	0.46	0.53	0.45	0.40	0.35
K	0.10	0.10	0.11	0.09	0.10	0.12	0.13	0.11	0.27	0.25	0.30	0.28	0.29	0.28	0.33	0.23
Total	15.23	15.23	15.17	15.22	15.17	15.21	15.33	15.13	15.52	15.47	15.49	15.54	15.62	15.52	15.60	15.53
X_{Mg}	0.63	0.71	0.65	0.67	0.65	0.66	0.66	0.67	0.43	0.42	0.44	0.46	0.46	0.47	0.43	0.43

Area	Taylor Valley												
Sample	22-01-15-P15b				23-01-15 P2c			22-01-15 P16c					
Clast N°	CLAST 1												
	amp5		amp6		amp1	amp2	amp3	amp1	amp2	amp3	amp4	amp5	amp6
Oxides (Wt%)	core (corr)	rim(corr)	core (corr)	rim(corr)	core	core	core	core	core	core	core	core	core
SiO_2	42.95	42.95	42.11	42.70	48.56	47.33	46.85	43.25	43.21	44.12	52.19	43.11	42.92
TiO_2	1.51	0.95	1.71	1.58	1.15	1.77	1.82	2.71	2.73	2.36	0.18	2.27	2.69
Al_2O_3	12.01	13.03	12.36	11.84	7.06	7.81	7.95	8.90	8.62	8.15	3.65	9.16	9.26
FeO	19.14	18.55	19.77	19.77	16.27	17.97	17.49	23.75	22.91	23.43	19.54	23.06	22.70
MnO	0.49	0.47	0.35	0.53	0.58	0.56	0.56	0.58	0.77	0.38	0.57	0.57	0.51
MgO	7.74	8.10	7.76	7.37	11.15	9.43	9.91	5.64	6.25	6.15	9.12	6.15	6.22
CaO	11.52	11.40	11.38	11.62	11.00	11.25	11.16	10.01	10.19	10.29	11.67	10.14	10.02
Na_2O	1.41	1.50	1.37	1.23	1.61	1.28	1.43	1.85	2.01	1.86	0.70	2.27	2.46
K_2O	1.21	1.18	1.41	1.48	0.63	0.82	0.95	1.28	1.37	1.44	0.46	1.41	1.43
Cr_2O_3	0.00	0.00	0.00	0.00	0.16	0.00	0.23	0.17	0.15	0.00	0.07	0.00	0.00
Total	97.98	98.14	98.23	98.12	98.16	98.21	98.35	98.13	98.20	98.17	98.16	98.12	98.22
Si	6.48	6.42	6.34	6.47	7.14	7.04	6.96	6.65	6.64	6.78	7.79	6.63	6.60
Al^{IV}	1.52	1.58	1.66	1.53	0.86	0.96	1.04	1.35	1.36	1.22	0.21	1.37	1.40
Al^{VI}	0.61	0.71	0.53	0.58	0.36	0.41	0.36	0.26	0.21	0.26	0.44	0.29	0.28
Ti	0.17	0.11	0.19	0.18	0.13	0.20	0.20	0.31	0.32	0.27	0.02	0.26	0.31
Fe^{3+}	0.20	0.35	0.40	0.17	0.16	0.05	0.05	0.30	0.24	0.19	0.00	0.27	0.19
Fe^{2+}	2.21	1.97	2.09	2.33	1.84	2.18	2.13	2.76	2.71	2.82	2.44	2.70	2.73
Mn	0.06	0.06	0.05	0.07	0.07	0.07	0.07	0.08	0.10	0.05	0.07	0.07	0.07
Mg	1.74	1.80	1.74	1.66	2.44	2.09	2.20	1.29	1.43	1.41	2.03	1.41	1.43
Cr	0.00	0.00	0.00	0.00	0.02	0.00	0.03	0.02	0.02	0.00	0.01	0.00	0.00
Ca	1.86	1.83	1.84	1.89	1.73	1.79	1.78	1.65	1.68	1.69	1.87	1.67	1.65
Na	0.41	0.43	0.40	0.36	0.46	0.37	0.41	0.55	0.60	0.55	0.20	0.68	0.73
K	0.23	0.22	0.27	0.29	0.12	0.16	0.18	0.25	0.27	0.28	0.09	0.28	0.28
Total	15.51	15.49	15.51	15.53	15.33	15.32	15.40	15.47	15.57	15.53	15.17	15.62	15.66
X_{Mg}	0.44	0.48	0.45	0.42	0.57	0.49	0.51	0.32	0.35	0.33	0.45	0.34	0.34

Area	Wright Valley																	
Sample	20-01-15 P1b																	
Clast N°	Clast 8						S-c	Clast5									Clast5	
	amp1		amp2		amp3		amp1	amp1		amp2	amp3		amp4		amp5		amp6	
Oxides (Wt%)	core	rim	core	rim	core	rim	core (corr)	core	rim	core	core	rim	core	rim	core	rim	core	rim
SiO_2	46.72	46.94	46.50	47.29	45.34	48.84	44.05	47.48	46.50	46.44	44.48	45.44	44.12	46.45	46.02	49.93	46.68	47.42
TiO_2	1.44	1.38	1.43	1.25	1.41	0.42	2.09	1.39	1.22	1.34	2.11	1.60	1.84	0.91	1.59	0.00	1.51	0.75
Al_2O_3	9.00	8.09	9.09	8.15	9.29	6.97	9.89	8.11	8.65	8.24	10.37	9.32	9.70	9.12	8.28	6.25	8.66	8.94
FeO	16.96	18.01	17.74	17.18	18.05	17.72	20.06	18.20	19.46	18.50	19.62	18.44	19.19	18.92	19.03	18.40	18.45	18.00
MnO	0.47	0.62	0.53	0.60	0.41	0.59	0.52	0.41	0.33	0.33	0.42	0.57	0.57	0.36	0.51	0.43	0.55	0.44
MgO	9.95	9.17	8.99	10.34	9.26	10.28	7.25	9.34	7.95	9.26	7.38	8.86	8.34	8.82	9.19	9.77	9.04	9.17
CaO	10.96	11.86	11.41	11.15	11.30	11.68	11.25	11.23	12.21	11.53	11.49	11.09	11.37	11.62	11.34	12.02	11.40	11.28
Na_2O	1.43	1.00	1.27	1.23	1.78	0.77	1.47	1.18	0.80	1.54	1.08	1.42	1.57	1.13	1.33	0.71	0.97	1.22
K_2O	1.07	0.99	1.13	0.79	1.08	0.65	1.56	0.71	1.11	0.85	1.15	0.92	1.12	0.83	0.81	0.47	0.92	0.88
Cr_2O_3	0.11	0.18	0.00	0.21	0.08	0.10	0.00	0.00	0.00	0.04	0.00	0.23	0.29	0.00	0.16	0.00	0.15	0.06
Total	98.10	98.23	98.09	98.18	97.98	98.04	98.14	98.05	98.22	98.08	98.09	97.86	98.13	98.19	98.27	97.95	98.34	98.13
Si	6.92	7.03	6.95	6.98	6.81	7.21	6.71	7.05	7.03	6.96	6.72	6.81	6.68	6.93	6.87	7.41	6.94	7.04
Al^{IV}	1.08	0.97	1.05	1.02	1.19	0.79	1.29	0.95	0.97	1.04	1.28	1.19	1.32	1.07	1.13	0.59	1.06	0.96
Al^{VI}	0.49	0.46	0.55	0.39	0.45	0.43	0.49	0.47	0.57	0.42	0.57	0.46	0.41	0.53	0.33	0.50	0.46	0.60
Ti	0.16	0.15	0.16	0.14	0.16	0.05	0.24	0.16	0.14	0.15	0.24	0.18	0.21	0.10	0.18	0.00	0.17	0.08
Fe^{3+}	0.15	0.00	0.00	0.26	0.04	0.19	0.00	0.13	0.00	0.00	0.00	0.14	0.03	0.14	0.21	0.00	0.11	0.07
Fe^{2+}	1.95	2.26	2.22	1.86	2.23	2.00	2.56	2.13	2.46	2.32	2.48	2.17	2.40	2.22	2.17	2.28	2.18	2.16
Mn	0.06	0.08	0.07	0.07	0.05	0.07	0.07	0.05	0.04	0.04	0.05	0.07	0.07	0.05	0.06	0.05	0.07	0.06
Mg	2.20	2.05	2.00	2.27	2.07	2.26	1.65	2.07	1.79	2.07	1.66	1.98	1.88	1.96	2.05	2.16	2.00	2.03
Cr	0.01	0.02	0.00	0.02	0.01	0.01	0.00	0.00	0.00	0.00	0.00	0.03	0.04	0.00	0.02	0.00	0.02	0.01
Ca	1.74	1.90	1.83	1.76	1.82	1.85	1.84	1.79	1.98	1.85	1.86	1.78	1.84	1.86	1.81	1.91	1.82	1.79
Na	0.41	0.29	0.37	0.35	0.52	0.22	0.43	0.34	0.23	0.45	0.32	0.41	0.46	0.33	0.38	0.20	0.28	0.35
K	0.20	0.19	0.22	0.15	0.21	0.12	0.30	0.13	0.21	0.16	0.22	0.18	0.22	0.16	0.15	0.09	0.18	0.17
Total	15.36	15.40	15.41	15.29	15.55	15.20	15.57	15.26	15.42	15.47	15.40	15.40	15.56	15.34	15.37	15.20	15.29	15.32
X_{Mg}	0.53	0.48	0.47	0.55	0.48	0.53	0.39	0.49	0.42	0.47	0.40	0.48	0.44	0.47	0.49	0.49	0.48	0.48

Area	Wright Valley																	
Sample	20-01-15 P1b																	
Clast N°	Clast16				Clast3						Clast4				Clast4			
	amp1		amp2		amp1		amp2		amp3	amp4	amp1		amp2		amp3	amp4	amp5	
Oxides (Wt%)	core	rim	core	rim	core	rim	core	rim	core	core	core	rim	core	rim	core	core	core	rim
SiO_2	43.90	44.42	43.87	44.08	48.46	49.75	47.69	49.20	48.41	48.65	47.93	49.08	45.42	47.35	46.96	48.20	46.40	48.91
TiO_2	1.83	1.81	1.65	1.97	1.17	0.74	1.44	1.11	1.26	1.17	1.43	1.06	1.81	1.28	1.52	1.24	1.71	1.00
Al_2O_3	9.74	9.10	9.44	8.90	8.04	6.95	8.27	7.29	7.55	6.99	8.15	7.93	10.04	9.22	8.90	7.90	9.17	6.77
FeO	22.60	22.96	22.92	22.84	15.64	15.74	16.16	16.01	16.34	16.59	16.00	14.77	16.93	15.95	15.50	15.40	16.43	15.63
MnO	0.59	0.78	0.69	0.85	0.52	0.31	0.37	0.43	0.40	0.50	0.32	0.34	0.40	0.21	0.60	0.42	0.41	0.41
MgO	6.22	5.69	6.32	6.03	10.78	11.26	10.43	10.63	10.37	10.59	10.63	11.71	9.47	10.45	10.88	11.09	10.22	11.26
CaO	10.51	10.86	10.59	10.66	11.30	11.82	11.33	11.81	12.10	11.89	11.84	11.88	11.64	11.80	11.59	11.85	11.60	11.95
Na_2O	1.77	1.14	1.74	1.40	0.99	0.90	1.40	0.86	0.76	0.91	0.96	0.88	1.20	1.11	1.57	1.23	0.90	1.19
K_2O	1.14	1.29	1.06	1.18	0.76	0.54	0.78	0.70	0.74	0.60	0.79	0.69	1.18	0.90	0.68	0.73	1.03	0.63
Cr_2O_3	0.00	0.22	0.00	0.13	0.20	0.00	0.11	0.11	0.12	0.14	0.07	0.00	0.14	0.00	0.10	0.05	0.11	0.31
Total	98.30	98.25	98.28	98.02	97.85	98.01	97.98	98.13	98.06	98.05	98.12	98.34	98.21	98.26	98.31	98.09	97.99	98.05
Si	6.68	6.81	6.68	6.75	7.13	7.29	7.05	7.25	7.17	7.20	7.07	7.14	6.77	6.97	6.91	7.10	6.87	7.24
Al^{IV}	1.32	1.19	1.32	1.25	0.87	0.71	0.95	0.75	0.83	0.80	0.93	0.86	1.23	1.03	1.09	0.90	1.13	0.76
Al^{VI}	0.43	0.45	0.37	0.36	0.52	0.49	0.49	0.52	0.49	0.42	0.49	0.50	0.53	0.57	0.46	0.48	0.47	0.42
Ti	0.21	0.21	0.19	0.23	0.13	0.08	0.16	0.12	0.14	0.13	0.16	0.12	0.20	0.14	0.17	0.14	0.19	0.11
Fe^{3+}	0.30	0.09	0.40	0.24	0.04	0.00	0.00	0.00	0.00	0.00	0.00	0.04	0.00	0.00	0.02	0.00	0.11	0.00
Fe^{2+}	2.57	2.85	2.52	2.69	1.88	1.93	2.00	1.97	2.02	2.05	1.97	1.76	2.11	1.96	1.89	1.90	1.92	1.93
Mn	0.08	0.10	0.09	0.11	0.06	0.04	0.05	0.05	0.05	0.06	0.04	0.04	0.05	0.03	0.07	0.05	0.05	0.05
Mg	1.41	1.30	1.43	1.38	2.36	2.46	2.30	2.33	2.29	2.34	2.34	2.54	2.10	2.29	2.39	2.44	2.26	2.48
Cr	0.00	0.03	0.00	0.02	0.02	0.00	0.01	0.01	0.01	0.02	0.01	0.00	0.02	0.00	0.01	0.01	0.01	0.04
Ca	1.71	1.78	1.73	1.75	1.78	1.86	1.79	1.86	1.92	1.89	1.87	1.85	1.86	1.86	1.83	1.87	1.84	1.90
Na	0.52	0.34	0.51	0.42	0.28	0.26	0.40	0.25	0.22	0.26	0.28	0.25	0.35	0.32	0.45	0.35	0.26	0.34
K	0.22	0.25	0.21	0.23	0.14	0.10	0.15	0.13	0.14	0.11	0.15	0.13	0.22	0.17	0.13	0.14	0.19	0.12
Total	15.46	15.40	15.45	15.41	15.23	15.21	15.36	15.25	15.29	15.28	15.30	15.23	15.44	15.35	15.42	15.36	15.31	15.39
X_{Mg}	0.35	0.31	0.36	0.34	0.56	0.56	0.54	0.54	0.53	0.53	0.54	0.59	0.50	0.54	0.56	0.56	0.54	0.56

Area	Wright Valley										
Sample	20-01-15 P1b										
Clast N°	Clast1		Clast2								
	amp1		amp1		amp2		amp3		amp4	amp5	
Oxides (Wt%)	core	rim	core	rim	core	rim	core	rim	core	core	rim
SiO_2	44.93	45.48	48.24	48.84	48.42	47.66	48.12	51.03	48.02	48.38	50.39
TiO_2	1.74	1.21	1.21	0.99	1.30	1.45	1.18	0.68	1.04	1.35	0.73
Al_2O_3	8.77	8.92	7.17	6.90	7.08	7.71	7.40	5.38	8.78	7.20	6.14
FeO	20.67	20.97	16.16	16.14	16.29	16.69	16.97	15.23	16.50	16.00	15.68
MnO	0.60	0.60	0.66	0.57	0.63	0.64	0.36	0.52	0.37	0.48	0.46
MgO	7.05	7.28	10.88	11.01	10.98	10.87	10.56	12.28	9.98	11.29	11.60
CaO	10.66	10.47	11.72	11.81	11.63	11.16	11.77	11.58	11.30	11.31	11.68
Na_2O	2.34	2.21	1.09	0.85	1.08	1.10	0.98	0.99	1.26	1.46	0.88
K_2O	1.27	1.03	0.67	0.58	0.55	0.70	0.61	0.42	0.70	0.72	0.49
Cr_2O_3	0.05	0.00	0.33	0.21	0.22	0.23	0.08	0.04	0.00	0.07	0.13
Total	98.08	98.16	98.12	97.89	98.18	98.21	98.01	98.15	97.95	98.25	98.17
Si	6.88	6.89	7.13	7.21	7.13	7.00	7.11	7.42	7.08	7.11	7.36
Al^{IV}	1.12	1.11	0.87	0.79	0.87	1.00	0.89	0.58	0.92	0.89	0.64
Al^{VI}	0.46	0.48	0.38	0.41	0.36	0.33	0.40	0.35	0.61	0.35	0.42
Ti	0.20	0.14	0.13	0.11	0.14	0.16	0.13	0.07	0.12	0.15	0.08
Fe^{3+}	0.00	0.10	0.00	0.01	0.06	0.32	0.07	0.10	0.01	0.11	0.01
Fe^{2+}	2.65	2.55	2.00	1.98	1.95	1.73	2.02	1.75	2.02	1.86	1.90
Mn	0.08	0.08	0.08	0.07	0.08	0.08	0.05	0.06	0.05	0.06	0.06
Mg	1.61	1.65	2.40	2.42	2.41	2.38	2.33	2.66	2.19	2.47	2.53
Cr	0.01	0.00	0.04	0.02	0.03	0.03	0.01	0.00	0.00	0.01	0.01
Ca	1.75	1.70	1.86	1.87	1.84	1.76	1.86	1.81	1.79	1.78	1.83
Na	0.70	0.65	0.31	0.24	0.31	0.31	0.28	0.28	0.36	0.42	0.25
K	0.25	0.20	0.13	0.11	0.10	0.13	0.11	0.08	0.13	0.13	0.09
Total	15.70	15.55	15.33	15.24	15.27	15.23	15.27	15.17	15.28	15.34	15.19
X_{Mg}	0.38	0.39	0.55	0.55	0.55	0.58	0.53	0.60	0.52	0.57	0.57

Area	Wright Valley													
Sample	20-01-15 P1b													
Clast N°	Clast15						Clast10						Clast14	
	amp1		amp1		amp2		amp3		amp4		amp5		amp1	
Oxides (Wt%)	core	rim	core	rim	core	rim	core	rim	core	rim	core	rim	core	rim
SiO_2	46.51	45.91	45.98	46.52	46.61	46.15	48.62	49.70	49.67	49.65	47.11	48.09	42.94	43.85
TiO_2	0.93	1.13	1.53	1.74	1.45	1.37	1.08	0.83	1.11	0.89	1.40	1.03	1.59	1.77
Al_2O_3	8.48	8.85	9.54	10.09	9.10	9.53	7.41	6.95	6.11	6.48	8.57	8.40	10.45	10.19
FeO	18.89	18.94	17.43	16.62	16.00	16.18	15.93	15.70	15.60	15.80	15.98	15.93	20.17	21.18
MnO	0.39	0.77	0.24	0.27	0.30	0.44	0.43	0.38	0.49	0.33	0.43	0.40	0.74	0.65
MgO	9.21	8.82	9.07	9.20	10.14	10.12	10.84	11.14	12.01	11.44	10.92	10.87	7.60	6.62
CaO	11.29	11.15	12.20	11.65	11.74	11.78	12.01	12.06	11.83	12.31	11.71	11.88	10.99	11.16
Na_2O	1.46	1.35	0.97	1.02	1.35	1.25	0.89	0.72	0.81	0.67	1.13	0.88	2.07	1.36
K_2O	1.08	1.16	1.18	1.10	0.99	1.07	0.72	0.68	0.59	0.73	0.98	0.66	1.49	1.48
Cr_2O_3	0.00	0.18	0.00	0.00	0.16	0.08	0.08	0.00	0.05	0.00	0.13	0.08	0.16	0.00
Total	98.24	98.26	98.12	98.21	97.84	97.98	98.01	98.16	98.26	98.32	98.36	98.21	98.21	98.25
Si	6.94	6.87	6.90	6.91	6.95	6.86	7.18	7.29	7.25	7.29	6.94	7.05	6.55	6.68
Al^{IV}	1.06	1.13	1.10	1.09	1.05	1.14	0.82	0.71	0.75	0.71	1.06	0.95	1.45	1.32
Al^{VI}	0.44	0.43	0.58	0.67	0.55	0.53	0.47	0.50	0.30	0.41	0.43	0.51	0.42	0.51
Ti	0.10	0.13	0.17	0.19	0.16	0.15	0.12	0.09	0.12	0.10	0.15	0.11	0.18	0.20
Fe^{3+}	0.17	0.19	0.00	0.00	0.00	0.00	0.00	0.00	0.15	0.00	0.08	0.08	0.12	0.07
Fe^{2+}	2.19	2.19	2.19	2.06	2.00	2.01	1.97	1.93	1.75	1.94	1.89	1.88	2.46	2.63
Mn	0.05	0.10	0.03	0.03	0.04	0.06	0.05	0.05	0.06	0.04	0.05	0.05	0.10	0.08
Mg	2.05	1.97	2.03	2.04	2.25	2.24	2.39	2.44	2.61	2.51	2.40	2.38	1.73	1.50
Cr	0.00	0.02	0.00	0.00	0.02	0.01	0.01	0.00	0.01	0.00	0.01	0.01	0.02	0.00
Ca	1.81	1.79	1.96	1.85	1.88	1.88	1.90	1.90	1.85	1.94	1.85	1.87	1.80	1.82
Na	0.42	0.39	0.28	0.29	0.39	0.36	0.26	0.20	0.23	0.19	0.32	0.25	0.61	0.40
K	0.21	0.22	0.23	0.21	0.19	0.20	0.13	0.13	0.11	0.14	0.18	0.12	0.29	0.29
Total	15.44	15.42	15.47	15.36	15.47	15.45	15.30	15.23	15.19	15.26	15.37	15.25	15.72	15.51
X_{Mg}	0.48	0.47	0.48	0.50	0.53	0.53	0.55	0.56	0.60	0.56	0.56	0.56	0.41	0.36

Area	Wright Valley				
Sample	20-01-15 P3c				
Clast N°					
	amp1	anf2 corr	anf3 corr	anf4 corr	anf5 corr
Oxides (Wt%)	core	core	core	core	core
SiO_2	49.60	51.64	56.56	44.63	54.83
TiO_2	1.44	0.84	0.21	2.35	0.62
Al_2O_3	8.21	5.43	1.52	11.86	3.41
FeO	12.04	11.17	9.10	13.39	9.02
MnO	0.25	0.50	0.42	0.50	0.44
MgO	13.25	14.91	18.08	11.51	16.82
CaO	11.60	11.95	11.76	11.54	11.63
Na_2O	1.12	1.07	0.31	1.59	0.91
K_2O	0.62	0.50	0.09	0.76	0.19
Cr_2O_3	0.11	0.23	0.19	0.10	0.38
Total	98.25	98.25	98.25	98.25	98.25
Si	7.13	7.40	7.87	6.51	7.72
Al^{IV}	0.87	0.60	0.13	1.49	0.28
Al^{VI}	0.52	0.32	0.12	0.55	0.29
Ti	0.16	0.09	0.02	0.26	0.07
Fe^{3+}	0.00	0.00	0.30	0.20	0.00
Fe^{2+}	1.45	1.34	0.76	1.43	1.06
Mn	0.03	0.06	0.05	0.06	0.05
Mg	2.84	3.19	3.75	2.50	3.53
Cr	0.01	0.03	0.02	0.01	0.04
Ca	1.79	1.84	1.75	1.80	1.76
Na	0.31	0.30	0.08	0.45	0.25
K	0.11	0.09	0.02	0.14	0.03
Total	15.23	15.25	14.87	15.41	15.08
X_{Mg}	0.66	0.70	0.83	0.64	0.77

APPENDIX B3: SEM-EDS analysis of Olivines (Chapter V)

Area	Walcott Bay								Marshall Valley			
Sample	**21-01-15 P14d**								**21-01-15 P19b**			
Clast °N	clast7		clast2		clast3	clast18			Clast15			
	ol1	ol2	ol1	ol2	olf	ol1	ol2	ol3	ol1		ol2 (g)	
									core	rim	core	rim
SiO_2	39.36	39.05	38.72	39.78	39.03	23.46	39.23	39.7	39.15	39.81	38.99	38.96
TiO_2	0.21	0.24	0.33	0.28	0.22	0.57	0.24	0.42	0.09	0.19	0.2	0.27
Al_2O_3	0.38	0.61	0.64	0.56	0.25	5.64	0.76	0.48	0.54	0.22	0.99	0.49
Cr_2O_3	0.09	0.19	0.25	0.24	0.11	0.25	0.07	0.3	0.06	0	0	0.07
Fe_2O_3	0	0	0	0	0	0	0	0				
FeO	17.86	15	12.34	9.72	16.8	64.93	16.39	10.97	17.98	18.16	21.72	21.7
MnO	0.36	0.36	0.49	0.33	0.42	0.7	0.39	0.53	0.31	0.39	0.49	0.63
MgO	40.82	43.13	45.86	47.8	42.4	1.95	41.58	46.52	40.75	40.51	36.26	36.64
CaO	0.37	0.48	0.42	0.51	0.33	2.46	0.34	0.41	0.39	0.42	0.72	0.7
Total	99.45	99.06	99.05	99.22	99.56	99.96	99	99.33	99.27	99.7	99.37	99.46
end member	%	%	%	%	%	%	%	%	%	%	%	%
Te	0.4	0.4	0.5	0.3	0.5	1.0	0.4	0.6	0.3	0.4	0.6	0.7
Fo	79.6	82.8	85.9	88.8	81.1	4.8	81.1	87.3	79.4	79.1	73.6	73.8
Fa	19.5	16.2	13.0	10.1	18.0	89.8	17.9	11.6	19.7	19.9	24.7	24.5
Ca-Ol	0.5	0.7	0.6	0.7	0.5	4.4	0.5	0.6	0.5	0.6	1.1	1.0

Area	Marshall Valley											
Sample	**21-01-15 P19b**											
Clast °N	Clast8		Clast7		Clast4							
	ol1(mp)		ol1 (mp)		ol1 (mp)		ol 2(mp)		ol 3(mp)		ol 4(mp)	
	core	rim	core	rim	core	rim	core	rim	core	rim	core	rim
SiO_2	39.97	40.14	40.5	39.74	39.88	39.41	39.64	40.38	41.24	39.68	39.59	41.1
TiO_2	0.15	0.18	0	0.11	0.19	0.23	0.13	0	0.07	0.38	0.09	0.39
Al_2O_3	0.78	0.86	0.92	0.39	0.61	0.39	0.42	0.71	0.57	0.93	0.68	2.4
Cr_2O_3	0.11	0	0.06	0.13	0.14	0.17	0.17	0	0.04	0.16	0.06	0
Fe_2O_3												
FeO	13.32	15.34	11.72	15.27	12.21	16.61	15.78	16.26	7.11	18.4	15.1	16.78
MnO	0.37	0.33	0.32	0.35	0.31	0.41	0.4	0.25	0.14	0.6	0.34	0.29
MgO	44.05	41.59	45.2	43.31	45.34	41.89	42.8	41.08	49.7	38.69	42.86	36.97
CaO	0.34	0.52	0.28	0.31	0.42	0.42	0.17	0.41	0.17	0.54	0.34	0.94
Total	99.09	98.96	99	99.61	99.1	99.53	99.51	99.09	99.04	99.38	99.06	98.87
end member	%	%	%	%	%	%	%	%	%	%	%	%
Te	0.4	0.4	0.3	0.4	0.3	0.5	0.4	0.3	0.1	0.7	0.4	0.3
Fo	84.7	81.9	86.7	82.8	86.1	81.0	82.3	81.1	92.2	77.8	82.8	78.3
Fa	14.4	17.0	12.6	16.4	13.0	18.0	17.0	18.0	7.4	20.8	16.4	19.9
Ca-Ol	0.5	0.7	0.4	0.4	0.6	0.6	0.2	0.6	0.2	0.8	0.5	1.4

Area							Marshall Valley						
Sample	**21-01-15 P19b**						**21-01-15 P21b**		**21-01-15 P21d**				
Clast °N	Clast5				Clast3		Clast 8	Clast 7	Clast 11		Clast 8	Clast 13	
	ol1 (g)		ol2 (g)		ol1 (mp)		ol1	ol1	ol1	ol2	ol3	ol1	ol2
	core	rim	core	rim	core	rim							
SiO_2	38.08	38.35	38.92	38.16	39.01	39.23	39.49	39.94	39.95	40.06	39.52	39.27	39.5
TiO_2	0.5	0.17	0.4	0.38	0.06	0.08	0.17	0.07	0.13	0.19	0.07	0.2	0.19
Al_2O_3	0.22	0.3	0.45	0.38	0.37	0.61	0.78	0.27	0.43	0.42	0.59	0.53	0.6
Cr_2O_3	0.22	0.11	0.07	0.09	0.14	0.07	0.09	0.07	0.14	0.07	0	0.15	0.09
Fe_2O_3													
FeO	23.1	24.61	24.3	24.56	17.77	17.6	14.17	14.86	10.45	10.37	17.11	13.65	16.4
MnO	0.78	0.64	0.64	0.75	0.43	0.35	0.36	0.42	0.32	0.31	0.28	0.46	0.4
MgO	35.99	34.59	34.01	34.56	41.13	40.69	43.81	43.44	47.49	47.47	41.34	44.37	41.6
CaO	0.64	0.68	0.6	0.71	0.5	0.5	0.3	0.42	0.22	0.34	0.26	0.45	0.37
Total	99.53	99.45	99.39	99.59	99.41	99.13	100	100	99.13	99.23	99.17	99.08	99.15
end member	%	%	%	%	%	%	%	%	%	%	%	%	%
Te	0.9	0.7	0.8	0.9	0.5	0.4	0.4	0.5	0.3	0.3	0.3	0.5	0.4
Fo	72.2	70.2	70.2	70.1	79.6	79.6	84.0	83.0	88.4	88.4	80.6	84.3	81.1
Fa	26.0	28.0	28.1	28.0	19.3	19.3	15.2	15.9	10.9	10.8	18.7	14.6	17.9
Ca-Ol	0.9	1.0	0.9	1.0	0.7	0.7	0.4	0.6	0.3	0.5	0.4	0.6	0.5

Area	Miers Valley								Taylor Valley									
Sample	21-01-15 P16c								22-01-15-P15b									
Clast °N	Clast 8			Clast 10	Clast 14	Clast 6	Clast 1	Clast 5	Clast3						Clast6			
	ol1	ol2	ol3	ol3	ol1	ol1	ol2	ol1	ol1		ol2		ol3		ol1		ol2	
									core	rim	core	rim	core	rim	core	rim	core	rim
SiO_2	39.92	39.7	39.73	39.35	39.49	39.1	38.13	40.27	38.91	40.03	39.72	38.55	40.01	39.39	37.1	37.57	36.01	37.62
TiO_2	0.16	0.17	0.42	0.32	0.13	0.23	0	0.36	0.46	0.21	0.14	0.38	0.15	0.32	0.18	0.2	0.43	0.23
Al_2O_3	0.64	0.61	0.39	0.42	0.62	0.59	0.3	0.25	0.67	0.84	0.72	0.74	0.51	0.46	0.52	0.38	0.62	0.55
Cr_2O_3	0.08	0.13	0.26	0.23	0.33	0.15	0.15	0.05										
Fe_2O_3																		
FeO	12.88	13.49	13.45	12.09	9.82	14.68	26.35	10.58	14.7	12.64	13.79	17.05	12.39	15.03	32.46	31.52	31.88	30.51
MnO	0.29	0.35	0.54	0.28	0.46	0.44	1.16	0.33	0.52	0.2	0.3	0.38	0.18	0.52	1.6	1.6	1.53	1.68
MgO	44.76	44.37	44.1	46.34	48.05	43.37	32.84	47.38	43.61	44.63	44.11	41.7	45.77	43.13	26.95	27.77	27.26	28.14
CaO	0.39	0.25	0.53	0.39	0.31	0.5	0.43	0.36	0.35	0.34	0.28	0.36	0.19	0.37	0.65	0.59	1.31	0.63
Total	99.12	99.07	99.42	99.42	99.21	99.06	99.36	99.58	99.22	98.89	99.06	99.16	99.2	99.22	99.46	99.63	99.04	99.36
end member	%	%	%	%	%	%	%	%	%	%	%	%	%	%	%	%	%	%
Te	0.3	0.4	0.6	0.3	0.5	0.5	1.4	0.3	0.6	0.2	0.3	0.4	0.2	0.6	2.0	1.9	1.9	2.0
Fo	85.4	84.8	84.3	86.5	88.9	83.1	67.6	88.1	83.2	85.7	84.5	80.6	86.4	82.7	57.9	59.4	58.1	60.3
Fa	13.8	14.5	14.4	12.7	10.2	15.8	30.4	11.0	15.7	13.6	14.8	18.5	13.1	16.2	39.1	37.8	38.1	36.7
Ca-Ol	0.5	0.3	0.7	0.5	0.4	0.7	0.6	0.5	0.5	0.5	0.4	0.5	0.3	0.5	1.0	0.9	2.0	1.0

APPENDIX B3: SEM-EDS analysis of Pyroxenes(Chapter V)

Area	Howchin glacier-Walcott Bay					Marshall Valley							
Sample	21-01-15 P14d					21-01-15 P19b							
Clast N°	Clast 7	Clast3			Clast18	Clast12			Clast13				
	7-2a	3a	3b	3e	18e	cpx1		cpx2	cpx1	cpx2	cpx3	cpx4	cpx5
Oxides (Wt%)						core	rim	core					
SiO_2	46.21	46.44	47.15	44.78	45.31	54.94	57.44	55.9	53.5	52.38	53.05	52.51	52.78
TiO_2	3.5	2.75	3.04	5.47	3.76	0.74	0.09	0.37	0	0.12	0	0.19	0.19
Al_2O_3	8.97	9.8	8.59	7.84	9.51	4.39	1.7	4.09	1.13	1.26	0.9	1.17	0.94
Cr_2O_3	0.56	0.09	0.17	0.2	0.24	0.22	0	0	0	0.16	0	0.19	0.11
Fe_2O_3	0	0	0	0	0	0	0	0	0	0	0	0	0
FeO	5.55	6.53	6.8	7.35	6.31	6.15	6.51	5.96	10.9	12.32	13.48	12.5	12.4
MnO	0.32	0.14	0.36	0.37	0.2	0.3	0	0.09	0.14	0.27	0.22	0.3	0.31
MgO	13.07	12.93	12.85	11.78	12.5	19.85	20.53	19.83	11.04	10.04	8.71	9.51	9.63
CaO	20.7	20	19.93	20.83	20.95	12.41	12.76	12.29	22.46	22.63	23.17	23.02	23.2
Na_2O	1	1.24	0.98	1.29	1.08	0.69	0.84	1.08	0.82	0.77	0.38	0.43	0.44
Total	99.88	99.92	99.87	99.91	99.86	99.69	99.87	99.61	99.99	99.95	99.91	99.82	100
Si	1.71	1.71	1.74	1.71	1.71	1.99	2.07	2.02	2.02	1.99	2.04	2.01	2.01
Ti	0.10	0.08	0.08	0.16	0.11	0.02	0.00	0.01	0.00	0.00	0.00	0.01	0.01
Al	0.39	0.42	0.37	0.35	0.42	0.19	0.07	0.17	0.05	0.06	0.04	0.05	0.04
Cr	0.02	0.00	0.00	0.01	0.01	0.01	0.00	0.00	0.00	0.00	0.00	0.01	0.00
Fe^{3+}	0.06	0.09	0.03	0.00	0.00	0.00	0.00	0.00	0.00	0.01	0.00	0.00	0.00
Fe^{2+}	0.11	0.11	0.18	0.23	0.20	0.19	0.20	0.18	0.34	0.38	0.43	0.40	0.40
Mn	0.01	0.00	0.01	0.01	0.01	0.01	0.00	0.00	0.00	0.01	0.01	0.01	0.01
Mg	0.72	0.71	0.71	0.67	0.70	1.07	1.10	1.07	0.62	0.57	0.50	0.54	0.55
Ca	0.82	0.79	0.79	0.85	0.85	0.48	0.49	0.48	0.91	0.92	0.95	0.94	0.95
Na	0.07	0.09	0.07	0.00	0.00	0.05	0.06	0.08	0.06	0.06	0.03	0.03	0.03
Total	4.00	4.00	4.00	4.00	4.00	4.00	4.00	4.00	4.00	4.00	4.00	4.00	4.00
end member*	%	%	%	%	%	%	%	%	%	%	%	%	%
Wo	47.90	46.42	46.22	48.49	48.42	27.68	27.50	27.60	48.48	48.97	50.58	50.03	50.13
En	42.08	41.75	41.47	38.16	40.20	61.61	61.55	61.96	33.16	30.23	26.45	28.76	28.95
Fs	10.02	11.83	12.31	13.36	11.38	10.71	10.95	10.45	18.36	20.81	22.97	21.21	20.91

Area	Marshall Valley																
Sample	21-01-15 P19b																
Clast N°	Clast8		Clast7	Clast 6								Clast 4		Clast 5			
	cpx1(mp)		cpx1 (mp)	cpx1		cpx2		cpx3		cpx4		cpx1 (mp)		cpx1 (mp)		cpx2 (mp)	
Oxides (Wt%)	core	rim		core	rim	core	rim	core	rim	core	rim	core	rim	core	rim	core	rim
SiO_2	45.99	47.23	49.3	52.84	53.26	53.05	52.72	53.25	52.19	53.66	52.42	49.47	46.52	49.34	46.99	45.71	49.1
TiO_2	3.25	3.29	1.61	0	0.15	0.27	0.19	0	0.23	0	0.15	1.84	3.6	1.89	3.94	3.44	2.94
Al_2O_3	9.19	6.95	7.81	1.24	1.1	1.01	1.17	0.85	1.34	0.89	1.41	4.79	7.66	4.95	6.46	8.21	4.19
Cr_2O_3	0.11	0	0.63	0	0.17	0.19	0.18	0.12	0.12	0.2	0.24	0.04	0.04	0.05	0	0	0.13
Fe_2O_3	0	0	0	0	0	0	0	0	0	0	0	0	0	0	0	0	0
FeO	7.58	7.07	4.99	10.35	10.42	9.51	11.17	10.29	11.1	9.89	10.89	6.48	6.78	6.82	7.28	7.08	7.65
MnO	0.26	0.21	0.19	0.27	0.43	0.56	0.57	0.49	0.62	0.55	0.59	0.12	0.09	0.2	0.12	0.19	0.41
MgO	11.16	13.13	14.91	11.58	11.61	11.75	11.23	11.94	11.06	11.89	10.89	14.86	12.93	13.82	12.65	12.69	13.17
CaO	21.5	21.35	19.87	23.16	22.16	23.01	22.24	22.49	22.67	22.28	22.52	21.33	21.68	22.1	21.8	22.03	21.76
Na_2O	0.89	0.78	0.69	0.52	0.51	0.52	0.53	0.48	0.5	0.65	0.85	1.03	0.7	0.75	0.73	0.64	0.6
Total	99.93	100.01	100	99.96	99.81	99.87	100	99.91	99.83	100.01	99.96	99.96	100	99.92	99.97	99.99	99.95
Si	1.71	1.75	1.80	1.99	2.01	2.00	1.99	2.01	1.98	2.02	1.98	1.81	1.72	1.82	1.75	1.70	1.83
Ti	0.09	0.09	0.04	0.00	0.00	0.01	0.01	0.00	0.01	0.00	0.00	0.05	0.10	0.05	0.11	0.10	0.08
Al	0.40	0.30	0.34	0.06	0.05	0.04	0.05	0.04	0.06	0.04	0.06	0.21	0.33	0.22	0.28	0.36	0.18
Cr	0.00	0.00	0.02	0.00	0.01	0.01	0.01	0.00	0.00	0.01	0.01	0.00	0.00	0.00	0.00	0.00	0.00
Fe^{3+}	0.05	0.07	0.00	0.01	0.00	0.00	0.00	0.00	0.01	0.00	0.03	0.13	0.06	0.09	0.05	0.10	0.03
Fe^{2+}	0.19	0.15	0.15	0.32	0.33	0.30	0.35	0.32	0.35	0.31	0.32	0.06	0.15	0.13	0.18	0.12	0.21
Mn	0.01	0.01	0.01	0.01	0.01	0.02	0.02	0.02	0.02	0.02	0.02	0.00	0.00	0.01	0.00	0.01	0.01
Mg	0.62	0.73	0.81	0.65	0.65	0.66	0.63	0.67	0.62	0.67	0.61	0.81	0.71	0.76	0.70	0.70	0.73
Ca	0.86	0.85	0.78	0.93	0.90	0.93	0.90	0.91	0.92	0.90	0.91	0.84	0.86	0.88	0.87	0.88	0.87
Na	0.06	0.06	0.05	0.04	0.04	0.04	0.04	0.04	0.04	0.05	0.06	0.07	0.05	0.05	0.05	0.05	0.04
Total	4.00	4.00	4.00	4.00	4.00	4.00	4.00	4.00	4.00	4.00	4.00	4.00	4.00	4.00	4.00	4.00	4.00
end member*	%	%	%	%	%	%	%	%	%	%	%	%	%	%	%	%	%
Wo	50.06	47.30	44.64	48.91	47.71	49.19	47.74	47.71	48.52	47.87	48.77	45.32	48.22	47.37	48.35	48.72	47.25
En	36.16	40.47	46.61	34.03	34.78	34.95	33.54	35.25	32.94	35.54	32.82	43.93	40.01	41.22	39.04	39.05	39.79
Fs	13.78	12.23	8.75	17.06	17.51	15.87	18.72	17.04	18.54	16.59	18.41	10.75	11.77	11.41	12.60	12.22	12.97

Area	Marshall Valley																			
Sample	21-01-15 P19b																			
Clast N°	Clast 3						Clast 1			Clast 2					Clast 10				Clast 16 (s-c)	
	cpx1 (mp)		cpx2 (mp)		cpx3 (mp)		cpx1	cpx2	cpx3	opx1	cpx2	opx3	opx4	cpx5	cpx1	cpx2	cpx3	cpx4		
Oxides (Wt%)	core	rim	core	rim	core	rim													core	rim
SiO_2	45.45	46.39	49.17	43.83	46.38	43.75	53.9	54.31	53.71	56.19	53.41	53.97	54.04	52.64	53.19	52.93	53.58	53.78	50.61	50.89
TiO_2	3.07	3.56	2.07	4.67	3.75	5.44	0.09	0.09	0.1	0.27	0.49	0.3	0.42	0.26	0	0.19	0	0	1.43	0.96
Al_2O_3	8.53	7.24	5.96	9.5	6.88	9.83	1.35	1.29	1.38	1.59	1.88	1.47	1.24	1.99	0.91	1.34	0.85	1.12	5.11	4.61
Cr_2O_3	0.12	0	0.21	0.26	0.1	0	0.11	0.09	0.08	0.26	0.23	0.18	0.13	0.25	0.2	0.17	0.05	0	0.23	0.83
Fe_2O_3	0	0	0	0	0	0	0	0	0	0	0	0	0	0	0	0	0	0	0	0
FeO	7.86	6.73	5.25	6.61	6.98	6.81	4.86	5.16	4.97	9.33	9.13	17.55	17.14	10.51	10.1	9.17	9.55	9.47	4.43	3.94
MnO	0.31	0	0	0.11	0.16	0	0.3	0.37	0.43	0.32	0.23	0.47	0.49	0.3	0.27	0.34	0.12	0.09	0.26	0.29
MgO	12	13.32	14.33	11.92	13.42	11.34	15.31	15.42	15.61	29.33	16.4	23.88	24.13	16.88	12.08	12.36	12.27	12.36	15.44	15.87
CaO	21.13	21.74	22.28	22.24	21.47	22.09	23.16	22.8	22.86	2.33	17.61	1.4	1.8	16.25	22.85	22.79	23.34	22.75	21.77	21.84
Na_2O	1.47	1.02	0.64	0.69	0.75	0.69	0.8	0.43	0.76	0.29	0.5	0.77	0.46	0.84	0.34	0.72	0.2	0.42	0.72	0.77
Total	99.94	100	99.91	99.83	99.89	99.95	99.88	99.96	99.9	99.91	99.88	99.99	99.85	99.92	99.94	100.01	99.96	99.99	100	100
Si	1.68	1.71	1.81	1.63	1.72	1.64	1.98	2.00	1.97	1.98	1.97	1.97	1.97	1.94	2.00	1.98	2.01	2.02	1.85	1.85
Ti	0.09	0.10	0.06	0.13	0.10	0.15	0.00	0.00	0.00	0.01	0.01	0.01	0.01	0.01	0.00	0.01	0.00	0.00	0.04	0.03
Al	0.37	0.31	0.26	0.42	0.30	0.43	0.06	0.06	0.06	0.07	0.08	0.06	0.05	0.09	0.04	0.06	0.04	0.05	0.22	0.20
Cr	0.00	0.00	0.01	0.01	0.00	0.00	0.00	0.00	0.00	0.01	0.01	0.01	0.00	0.01	0.01	0.01	0.00	0.00	0.01	0.02
Fe^{3+}	0.20	0.14	0.05	0.10	0.10	0.04	0.04	0.00	0.05	0.00	0.00	0.04	0.00	0.08	0.00	0.02	0.00	0.00	0.05	0.07
Fe^{2+}	0.05	0.07	0.11	0.11	0.12	0.17	0.11	0.16	0.10	0.28	0.28	0.50	0.52	0.25	0.32	0.27	0.30	0.30	0.09	0.05
Mn	0.01	0.00	0.00	0.00	0.01	0.00	0.01	0.01	0.01	0.01	0.01	0.01	0.02	0.01	0.01	0.01	0.00	0.00	0.01	0.01
Mg	0.66	0.73	0.79	0.66	0.74	0.63	0.84	0.84	0.85	1.54	0.90	1.30	1.31	0.93	0.68	0.69	0.69	0.69	0.84	0.86
Ca	0.84	0.86	0.88	0.89	0.85	0.88	0.91	0.90	0.90	0.09	0.70	0.05	0.07	0.64	0.92	0.91	0.94	0.91	0.85	0.85
Na	0.11	0.07	0.05	0.05	0.05	0.05	0.06	0.03	0.05	0.02	0.04	0.05	0.03	0.06	0.02	0.05	0.01	0.03	0.05	0.05
Total	4.00	4.00	4.00	4.00	4.00	4.00	4.00	4.00	4.00	4.00	4.00	4.00	4.00	4.00	4.00	4.00	4.00	4.00	4.00	4.00
end member*	%	%	%	%	%	%	%	%	%	%	%	%	%	%	%	%	%	%	%	%
Wo	48.06	47.75	48.10	50.56	47.09	51.15	47.99	47.22	47.17	4.62	37.03	2.90	3.69	33.90	48.06	48.34	48.76	48.06	46.61	46.47
En	37.98	40.71	43.05	37.71	40.96	36.54	44.14	44.44	44.82	80.94	47.98	68.76	68.87	48.99	35.35	36.48	35.67	36.33	45.99	46.99
Fs	13.96	11.54	8.85	11.73	11.95	12.31	7.86	8.34	8.01	14.44	14.99	28.35	27.44	17.11	16.58	15.18	15.57	15.61	7.40	6.54

Area	Marshall Valley																			
Sample	21-01-15 P21b									21-01-15 P21d										
Clast N°	Clast 15	Clast 5		Clast 4	Clast 6	Clast 10	Clast 12		Clast 11	Clast 11	Clast 6		Clast 5		Clast 7		Clast 8	Clast 10	Clast 13	
	px1	px1	px2	px1	px1	px1	px1	px2	px3	px3	px1	px5	px1	px5	px2	px7	px1	px1	px4	
Oxides (Wt%)																				
SiO_2	54.66	52.34	51.36	54.09	53.32	52.06	55.94	55.03	52.18	48.72	46.33	47.37	52.01	51.81	53.07	52.82	47.67	52.02	45.28	
TiO_2	0.09	0.24	0.48	0.06	0.11	1.63	0.14	0.22	1.47	2.59	3.1	2.62	0.87	0.83	0.74	0.56	2.28	0.86	4.6	
Al_2O_3	1.29	2.04	2.78	2.31	1.19	4.32	1.6	1.68	3.98	5.68	8	7.27	1.21	1.55	1.72	1.74	8.74	2.94	8.44	
Cr_2O_3	0.26	0	0.14	0	0.15	0	0.22	0.24	0.09	0.2	0.16	0.26	0.15	0.1	0.06	0.21	0	0	0.13	
Fe_2O_3	0	0	0	0	0	0	0	0	0	0	0	0	0	0	0	0	0	0	0	
FeO	0.59	12.78	13.99	7.84	7.5	8.27	10.28	10.97	7.13	5.94	6.83	5	13.74	15.59	11.43	11.19	7.49	8.85	7.46	
MnO	0.45	0.48	0.54	0.19	0.42	0.51	0.28	0.4	0.2	0.3	0.26	0.22	1.11	1.35	1.02	0.94	0.24	0.54	0.4	
MgO	17.93	10.84	10.63	18.07	13.5	11.77	28.59	28.1	14.65	14.14	13.3	13.37	9.76	8.36	11.56	11.84	12.37	13.77	11.96	
CaO	23.99	20.46	19.13	17.04	22.86	19.39	2.54	2.47	19.79	21.56	20.85	21.52	20.18	18.89	19.42	19.59	20.01	19.69	20.4	
Na_2O	0.75	0.6	0.55	0.39	0.84	1.74	0.33	0.72	0.51	0.79	1.04	1.09	0.78	1.47	0.91	1.06	1.01	1.13	1.24	
Total	100	100	100	100	100	100	100	100	100	99.92	99.87	98.72	99.81	99.95	99.93	99.95	99.81	99.8	99.91	
Si	1.96	1.99	1.96	1.98	1.98	1.94	1.98	1.95	1.93	1.80	1.71	1.76	1.99	1.99	2.00	1.99	1.77	1.93	1.69	
Ti	0.00	0.01	0.01	0.00	0.00	0.05	0.00	0.01	0.04	0.07	0.09	0.07	0.03	0.02	0.02	0.02	0.06	0.02	0.13	
Al	0.06	0.09	0.13	0.10	0.05	0.19	0.07	0.07	0.17	0.25	0.35	0.32	0.05	0.07	0.08	0.08	0.38	0.13	0.37	
Cr	0.01	0.00	0.00	0.00	0.00	0.00	0.01	0.01	0.00	0.01	0.00	0.01	0.00	0.00	0.00	0.01	0.00	0.00	0.00	
Fe^{3+}	0.02	0.00	0.00	0.00	0.04	0.00	0.00	0.06	0.00	0.07	0.13	0.08	0.00	0.01	0.00	0.00	0.03	0.04	0.09	
Fe^{2+}	0.00	0.41	0.45	0.24	0.19	0.26	0.30	0.27	0.22	0.12	0.08	0.07	0.44	0.50	0.36	0.35	0.20	0.23	0.15	
Mn	0.01	0.02	0.02	0.01	0.01	0.02	0.01	0.01	0.01	0.01	0.01	0.01	0.04	0.04	0.03	0.03	0.01	0.02	0.01	
Mg	0.96	0.61	0.61	0.98	0.75	0.65	1.51	1.49	0.81	0.78	0.73	0.74	0.56	0.48	0.65	0.66	0.68	0.76	0.66	
Ca	0.92	0.83	0.78	0.67	0.91	0.77	0.10	0.09	0.78	0.85	0.82	0.86	0.83	0.78	0.79	0.79	0.79	0.78	0.81	
Na	0.00	0.04	0.04	0.03	0.06	0.13	0.02	0.05	0.04	0.06	0.07	0.08	0.06	0.11	0.07	0.08	0.07	0.08	0.09	
Total	4.00	4.00	4.00	4.00	4.00	4.00	4.00	4.00	4.00	4.00	4.00	4.00	4.00	4.00	4.00	4.00	4.00	4.00	4.00	
end member*	%	%	%	%	%	%	%	%	%	%	%	%	%	%	%	%	%	%	%	
Wo	49.02	44.95	42.66	35.28	48.13	45.92	5.05	4.93	43.27	47.00	46.66	48.88	45.36	44.25	43.71	43.73	46.46	43.03	47.59	
En	50.98	33.14	32.98	52.05	39.55	38.79	79.02	77.99	44.57	42.89	41.41	42.25	30.53	27.25	36.21	36.77	39.96	41.87	38.82	
Fs	0.00	21.92	24.35	12.67	12.32	15.29	15.94	17.08	12.17	10.11	11.93	8.86	24.11	28.50	20.08	19.50	13.57	15.10	13.58	

Area	Miers Valley									Taylor valley									
Sample	21-01-15 P16c									22-01-15-P15b									
Clast N°	Clast 7			Clast 10		Clast 14	Clast 6	Clast 1	Clast 5	Clast 2								Clast4	
	Px1	Px2	Px4	Px1	Px2	Px1	Px1	Px1	Px1	cpx1		cpx2		cpx3		cpx4		cpx1	
Oxides (Wt%)										core	rim	core	rim	core	rim	core	rim	core	rim
SiO_2	46.32	43.96	47.16	49.71	47.51	48.3	41.94	49.77	43.3	50.07	49.84	50.63	51.31	50.7	48.93	50.52	49.84	46.49	43.51
TiO_2	3.64	4.65	3.8	1.92	3.07	3.16	5.69	2.58	5.17	0.72	0.58	0.62	0.61	0.56	0.57	0.6	0.76	2.54	5.43
Al_2O_3	8.8	9.94	6.32	8.2	9.22	6.04	10.81	5.59	10.75	1.55	1.57	1.51	1.33	1.17	1.25	1.13	1.25	8.89	10.12
Cr_2O_3	0.16	0	0.25	0.45	0.39	0.11	0.16	0.2	0.24										
Fe_2O_3	0	0	0	0	0	0	0	0	0	0	0	0	0	0	0	0	0	0	0
FeO	8.93	8.96	9.01	4.62	4.75	6.68	7.52	7.95	5.73	26.56	25.96	23.96	21.3	21.55	24.93	30.98	27.23	7.12	6.82
MnO	0.47	0.46	0.77	0.07	0	0.3	0.14	0.52	0.12	0.73	0.62	0.63	0.64	0.44	1.04	0.79	0.81	0.33	0.19
MgO	9.61	9.98	11.37	13.79	12.99	13.61	11.05	11.97	11.83	8.25	7.24	10.46	7.26	7.01	4.51	10.1	6.95	11.28	11.01
CaO	21.01	20.59	20.09	20.38	21.18	20.99	21.39	20.25	21.81	11.56	13.19	11.75	16.39	18.17	18.17	5.55	12.79	22.68	21.74
Na_2O	0.92	1.32	0.96	0.87	0.9	0.8	1.1	1.06	0.92	0.41	0.81	0.36	0.92	0.4	0.48	0.27	0.37	0.67	1.19
Total	99.86	99.86	99.73	100.01	100.01	99.99	99.8	99.89	99.87	99.85	99.81	99.92	99.76	100	99.88	99.94	100	100	100.01
Si	1.75	1.65	1.78	1.82	1.75	1.79	1.57	1.86	1.61	1.99	1.98	2.01	2.01	2.00	1.96	2.01	1.99	1.73	1.62
Ti	0.10	0.13	0.11	0.05	0.08	0.09	0.16	0.07	0.14	0.02	0.02	0.02	0.02	0.02	0.02	0.02	0.02	0.07	0.15
Al	0.39	0.44	0.28	0.35	0.40	0.26	0.48	0.25	0.47	0.07	0.07	0.06	0.06	0.05	0.06	0.05	0.06	0.39	0.44
Cr	0.00	0.00	0.01	0.01	0.01	0.00	0.00	0.01	0.01	0.00	0.00	0.00	0.00	0.00	0.00	0.00	0.00	0.00	0.00
Fe^{3+}	0.00	0.09	0.01	0.00	0.00	0.04	0.14	0.00	0.08	0.00	0.00	0.00	0.00	0.00	0.02	0.00	0.00	0.06	0.10
Fe^{2+}	0.28	0.19	0.27	0.14	0.15	0.17	0.09	0.25	0.09	0.88	0.86	0.70	0.70	0.71	0.82	1.03	0.91	0.16	0.12
Mn	0.02	0.01	0.02	0.00	0.00	0.01	0.00	0.02	0.00	0.02	0.02	0.02	0.02	0.01	0.04	0.03	0.03	0.01	0.01
Mg	0.54	0.56	0.64	0.75	0.71	0.75	0.62	0.67	0.65	0.49	0.43	0.43	0.43	0.41	0.27	0.60	0.41	0.63	0.61
Ca	0.85	0.83	0.81	0.80	0.83	0.83	0.86	0.81	0.87	0.49	0.56	0.69	0.69	0.77	0.78	0.24	0.55	0.90	0.87
Na	0.07	0.10	0.07	0.06	0.06	0.06	0.08	0.08	0.07	0.03	0.06	0.07	0.07	0.03	0.04	0.02	0.03	0.05	0.09
Total	4.00	4.00	4.00	4.00	4.00	4.00	4.00	4.00	4.00	4.00	4.00	4.00	4.00	4.00	4.00	4.00	4.00	4.00	4.00
end member*	%	%	%	%	%	%	%	%	%	%	%	%	%	%	%	%	%	%	%
Wo	50.81	49.65	46.78	47.20	49.30	46.50	50.17	46.97	51.03	26.41	30.30	26.11	38.01	40.61	41.39	12.68	29.26	51.62	51.29
En	32.34	33.48	36.84	44.44	42.07	41.95	36.06	38.63	38.51	26.23	23.14	32.34	23.43	21.80	14.29	32.10	22.12	35.73	36.15
Fs	16.86	16.86	16.38	8.35	8.63	11.55	13.77	14.39	10.46	47.36	46.55	41.55	38.56	37.59	44.32	55.23	48.62	12.65	12.56

Area	Taylor Valley									Wright valley												
Sample	22-01-15-P15b									20-01-15-P1b												
Clast N°	Clast5									Clast7			Single crystal									
	cpx1		cpx2	cpx3		cpx4		cpx5		cpx1	cpx2	cpx3	cpx1	cpx2	cpx3	cpx4	cpx5	cpx6	cpx7	cpx8	cpx9	
Oxides (Wt%)	core	rim	core	core	rim	core	rim	core	rim	core	core	core										
SiO_2	52.23	50.01	51.99	50.59	50.34	50.3	50.31	50.54	50.6	53.05	52.77	52.65	53.55	53.48	55.52	53.4	53.9	55.41	53.98	53.3	54.35	
TiO_2	0.44	0.5	0	0.64	0.64	0.86	0.59	0.54	0.73	0	0	0.37	0.28	0.54	0.12	0.45	0.33	0.41	0.45	0.21	0.25	
Al_2O_3	1.91	2.72	1.21	1.81	1.96	1.54	1.57	1.43	1.55	1	1.19	1.29	1.91	2.25	1.57	2.01	2.18	1.4	1.92	2.09	1.1	
Cr_2O_3										0	0	0.29	0.17	0.19	0.24	0.38	0.22	0.31	0.23	0.09	0	
Fe_2O_3	0	0	0	0	0	0	0	0	0	0	0	0	0	0	0	0	0	0	0	0	0	
FeO	13.25	16.53	18.68	19.44	22.13	23.95	21.41	24.53	25.39	11.55	10.97	11.12	10.04	6.55	10.95	6.31	8.74	13.56	10.57	6.96	17.4	
MnO	0.34	0.6	0.82	0.72	0.66	0.67	0.66	0.63	0.77	0.69	0.57	0.63	0.38	0.24	0.25	0.35	0.31	0.45	0.31	0.35	0.35	
MgO	14.32	11.84	6.2	7.72	7.42	7.06	6	6.65	6.71	11.16	11.5	11.69	19.62	18.21	28.24	16.89	21.31	25.68	18.83	17.68	24	
CaO	17.11	16.82	20.15	18.53	15.95	15.2	18.62	15.12	13.68	21.67	22.06	21.1	13.2	17.56	2.29	19.62	12.34	2.27	12.84	18.44	2.03	
Na_2O	0.4	0.76	0.74	0.4	0.76	0.42	0.78	0.49	0.45	0.88	0.8	0.73	0.71	0.8	0.77	0.43	0.68	0.42	0.8	0.77	0.39	
Total	100	99.78	99.79	99.85	99.86	100	99.94	99.93	99.88	100	99.86	99.87	99.86	99.82	99.95	99.84	100.01	99.91	99.93	99.89	99.87	
Si	1.96	1.90	2.04	1.98	1.98	1.99	1.98	2.01	2.02	2.00	1.99	1.99	1.95	1.95	1.96	1.96	1.95	2.00	1.98	1.94	1.99	
Ti	0.01	0.01	0.00	0.02	0.02	0.03	0.02	0.02	0.02	0.00	0.00	0.01	0.01	0.01	0.00	0.01	0.01	0.01	0.01	0.01	0.01	
Al	0.08	0.12	0.06	0.08	0.09	0.07	0.07	0.07	0.07	0.04	0.05	0.06	0.08	0.10	0.07	0.09	0.09	0.06	0.08	0.09	0.05	
Cr	0.00	0.00	0.00	0.00	0.00	0.00	0.00	0.00	0.00	0.00	0.00	0.01	0.00	0.01	0.01	0.01	0.01	0.01	0.01	0.00	0.00	
Fe^{3+}	0.00	0.10	0.00	0.00	0.00	0.00	0.00	0.00	0.00	0.02	0.03	0.00	0.04	0.03	0.05	0.00	0.04	0.00	0.00	0.06	0.00	
Fe^{2+}	0.41	0.43	0.61	0.64	0.73	0.79	0.71	0.81	0.85	0.35	0.32	0.35	0.27	0.17	0.28	0.19	0.23	0.41	0.32	0.15	0.53	
Mn	0.01	0.02	0.03	0.02	0.02	0.02	0.02	0.02	0.03	0.02	0.02	0.02	0.01	0.01	0.01	0.01	0.01	0.01	0.01	0.01	0.01	
Mg	0.80	0.67	0.36	0.45	0.43	0.42	0.35	0.39	0.40	0.63	0.65	0.66	1.07	0.99	1.49	0.92	1.15	1.38	1.03	0.96	1.31	
Ca	0.69	0.69	0.85	0.78	0.67	0.65	0.79	0.64	0.58	0.88	0.89	0.85	0.52	0.68	0.09	0.77	0.48	0.09	0.50	0.72	0.08	
Na	0.03	0.06	0.06	0.03	0.06	0.03	0.06	0.04	0.03	0.06	0.06	0.05	0.05	0.06	0.05	0.03	0.05	0.03	0.06	0.05	0.03	
Total	4.00	4.00	4.00	4.00	4.00	4.00	4.00	4.00	4.00	4.00	4.00	4.00	4.00	4.00	4.00	4.00	4.00	4.00	4.00	4.00	4.00	
end member*	%	%	%	%	%	%	%	%	%	%	%	%	%	%	%	%	%	%	%	%	%	
Wo	36.11	36.41	46.47	41.69	36.63	34.77	42.63	34.74	31.94	46.89	47.32	45.82	27.31	36.58	4.57	40.84	25.28	4.67	27.15	38.04	4.14	
En	42.06	35.66	19.90	24.17	23.71	22.47	19.11	21.26	21.80	33.60	34.32	35.32	56.48	52.78	78.38	48.91	60.74	73.54	55.40	50.75	68.14	
Fs	21.83	27.93	33.63	34.14	39.67	42.76	38.26	44.00	46.27	19.51	18.37	18.85	16.21	10.65	17.05	10.25	13.98	21.78	17.45	11.21	27.71	

Area	Wright Valley																	
Sample	20-01-15-P1b																	
Clast N°	Single crystal														Clast6			
	cpx10	cpx11	cpx12	cpx13	cpx14	cpx15	cpx16	cpx17	cpx18	cpx19	cpx20	cpx21	cpx22	cpx23	px1	px2	px3	px4
Oxides (Wt%)																		
SiO_2	53.87	55.28	56.16	53.23	54.56	53.82	52.69	53.03	55.56	52.43	55.29	53.31	53.93	53.93	53.14	52.66	53.13	52.67
TiO_2	0.37	0.19	0.25	0.4	0.36	0.57	1.01	0.34	0.23	0.62	0.18	0.4	0.09	0.42	0	0.56	0.23	0.24
Al_2O_3	1.93	1.52	1.3	2.12	2.06	1.86	1.87	2.61	2.09	1.33	1.09	2.14	1.89	1.14	1.16	1.53	0.57	1.42
Cr_2O_3	0.21	0.3	0.25	0.31	0.31	0.24	0.32	0.32	0.22	0.11	0.12	0.19	0.13	0.22	0.07	0.24	0.2	0.12
Fe_2O_3	0	0	0	0	0	0	0	0	0	0	0	0	0	0	0	0	0	0
FeO	7.03	12.99	11.13	7.07	5.57	7.65	9.09	6.11	9.82	15.51	16.82	6.58	8.6	15	10.45	10.13	10.54	10.24
MnO	0.4	0.51	0.34	0.41	0.3	0.42	0.48	0.27	0.33	0.5	0.54	0.37	0.46	0.56	0.51	0.71	0.64	0.43
MgO	17.02	26.98	28.09	16.58	16.5	16.94	15.44	16.86	28.66	12.52	23.62	18.2	19.7	23.42	11.33	11.63	11.3	11.62
CaO	18.87	1.85	2.01	19.31	19.84	18.04	18.38	19.55	2.32	16.62	1.88	17.95	14.36	4.92	22.56	21.61	23.06	22.4
Na_2O	0.3	0.37	0.41	0.42	0.47	0.41	0.56	0.85	0.74	0.24	0.33	0.72	0.79	0.29	0.73	0.87	0.23	0.8
Total	100	99.99	99.94	99.85	99.97	99.95	99.84	99.94	99.97	99.88	99.87	99.86	99.95	99.9	99.95	99.94	99.9	99.94
Si	1.98	1.98	2.00	1.96	2.00	1.98	1.96	1.93	1.96	2.00	2.03	1.94	1.96	1.97	2.00	1.98	2.01	1.98
Ti	0.01	0.01	0.01	0.01	0.01	0.02	0.03	0.01	0.01	0.02	0.00	0.01	0.00	0.01	0.00	0.02	0.01	0.01
Al	0.08	0.06	0.05	0.09	0.09	0.08	0.08	0.11	0.09	0.06	0.05	0.09	0.08	0.05	0.05	0.07	0.03	0.06
Cr	0.01	0.01	0.01	0.01	0.01	0.01	0.01	0.01	0.01	0.00	0.00	0.01	0.00	0.01	0.00	0.01	0.01	0.00
Fe^{3+}	0.00	0.00	0.00	0.00	0.00	0.00	0.00	0.05	0.03	0.00	0.00	0.05	0.05	0.00	0.00	0.00	0.00	0.02
Fe^{2+}	0.22	0.39	0.33	0.22	0.17	0.24	0.28	0.13	0.26	0.49	0.52	0.15	0.21	0.46	0.33	0.32	0.33	0.30
Mn	0.01	0.02	0.01	0.01	0.01	0.01	0.02	0.01	0.01	0.02	0.02	0.01	0.01	0.02	0.02	0.02	0.02	0.01
Mg	0.93	1.44	1.49	0.91	0.90	0.93	0.85	0.92	1.51	0.71	1.29	0.99	1.07	1.28	0.64	0.65	0.64	0.65
Ca	0.74	0.07	0.08	0.76	0.78	0.71	0.73	0.76	0.09	0.68	0.07	0.70	0.56	0.19	0.91	0.87	0.94	0.90
Na	0.02	0.03	0.03	0.03	0.03	0.03	0.04	0.06	0.05	0.02	0.02	0.05	0.06	0.02	0.05	0.06	0.02	0.06
Total	4.00	4.00	4.00	4.00	4.00	4.00	4.00	4.00	4.00	4.00	4.00	4.00	4.00	4.00	4.00	4.00	4.00	4.00
end member*	%	%	%	%	%	%	%	%	%	%	%	%	%	%	%	%	%	%
Wo	39.28	3.74	4.04	40.31	42.08	37.91	39.14	40.92	4.65	36.02	3.93	37.08	29.62	10.00	48.54	47.29	49.05	48.11
En	49.30	75.79	78.51	48.16	48.70	49.54	45.75	49.10	79.97	37.75	68.65	52.31	56.54	66.21	33.92	35.41	33.45	34.72
Fs	11.42	20.47	17.45	11.52	9.22	12.55	15.11	9.98	15.37	26.23	27.42	10.61	13.85	23.79	17.55	17.30	17.50	17.17

Area	Wright Valley										
Sample	20-01-15-P1b										
Clast N°	Clast9				Clast13			Clast17			
	px1	px2	px3	px4	px1	px2	px3	cpx1	cpx2	cpx3	cpx4
Oxides (Wt%)											
SiO_2	53.54	53.98	53.39	53.76	54.25	54.51	53.93	53.43	52.31	53.15	52.43
TiO_2	0.17	0	0	0	0	0.14	0	0.13	0.25	0	0.11
Al_2O_3	1.04	0.97	1.07	1.17	0.74	0.71	0.91	0.96	1.09	0.83	1.4
Cr_2O_3	0.16	0	0.1	0.04	0.16	0.04	0.06	0.15	0.17	0.17	0.15
Fe_2O_3	0	0	0	0	0	0	0	0	0	0	0
FeO	6.97	7.31	7.13	6.32	3.75	4.1	5.49	10.57	10.79	10.69	10.77
MnO	0.42	0.17	0.31	0.31	0.29	0.19	0.27	0.8	0.74	0.64	0.94
MgO	14.15	13.4	13.51	14.28	16.09	15.51	15.13	11.19	11.04	10.91	11.1
CaO	23	23.39	23.62	23.13	24.22	24.31	23.44	22.26	22.67	22.97	22.17
Na_2O	0.41	0.77	0.76	0.85	0.44	0.36	0.77	0.35	0.77	0.55	0.91
Total	99.86	99.99	99.89	99.86	99.94	99.87	100	99.84	99.83	99.91	99.98
Si	1.99	2.00	1.98	1.98	1.98	2.00	1.98	2.03	1.98	2.01	1.98
Ti	0.00	0.00	0.00	0.00	0.00	0.00	0.00	0.00	0.01	0.00	0.00
Al	0.05	0.04	0.05	0.05	0.03	0.03	0.04	0.04	0.05	0.04	0.06
Cr	0.00	0.00	0.00	0.00	0.00	0.00	0.00	0.00	0.01	0.01	0.00
Fe^{3+}	0.00	0.01	0.05	0.04	0.03	0.00	0.06	0.00	0.03	0.00	0.04
Fe^{2+}	0.22	0.22	0.18	0.15	0.09	0.13	0.11	0.34	0.31	0.34	0.30
Mn	0.01	0.01	0.01	0.01	0.01	0.01	0.01	0.03	0.02	0.02	0.03
Mg	0.78	0.74	0.75	0.79	0.88	0.85	0.83	0.63	0.62	0.62	0.62
Ca	0.91	0.93	0.94	0.91	0.95	0.96	0.92	0.90	0.92	0.93	0.90
Na	0.03	0.06	0.05	0.06	0.03	0.03	0.05	0.03	0.06	0.04	0.07
Total	4.00	4.00	4.00	4.00	4.00	4.00	4.00	4.00	4.00	4.00	4.00
end member*	%	%	%	%	%	%	%	%	%	%	%
Wo	47.79	48.99	49.23	48.26	48.90	49.52	48.06	48.31	48.80	49.40	48.17
En	40.91	39.05	39.18	41.45	45.20	43.96	43.16	33.79	33.07	32.65	33.56
Fs	11.30	11.95	11.60	10.29	5.91	6.52	8.79	17.90	18.13	17.95	18.27

APPENDIX B3: SEM-EDS analysis of Plagioclase(Chapter V)

Area	Walcott bay				Marshall Valley									
Sample	21-01-15 P14d				21-01-15 P19b									
Clast N°	clast 7	clast 2	clast 3	clast 18	clast9		clast11		clast15					
	c	a	c	d	pl1	pl2	pl1	pl2	pl1 (mp)		pl2 (mp)		pl3 (mp)	
Oxides (Wt%)									core	rim	core	rim	core	rim
SiO_2	50.02	56.95	50.69	49.57	63.73	62.64	56.18	56.63	49.86	49.24	50.5	50.78	49.6	51.74
TiO_2	0.59	0.82	0.38	0.4	0.29	0.18	0.08	0.15	0.14	0.16	0.4	0.28	0.08	0.23
Al_2O_3	29.64	23.28	29.92	31.14	22.19	22.87	27.06	26.58	31.31	31.43	30.46	30.4	31.73	29.19
Cr_2O_3	0.24	0.19	0.22	0.24	0.22	0.05	0.13	0.2	0.11	0.05	0.13	0.14	0.04	0.14
Fe_2O_3	0	0	0	0	0	0	0	0	0	0	0	0	0	0
FeO	1.11	2.18	0.74	0.66	0.21	0.1	0.26	0.26	0.7	0.62	0.82	1.02	0.58	1.05
MnO	0.26	0.15	0.22	0.24	0.14	0	0.16	0.13	0.09	0.05	0.3	0	0	0.12
MgO	0.86	1.75	0.8	0.66	0	0.7	0.76	0.79	0	0.89	0	0	0	0.83
CaO	13.66	8.73	13.09	14.03	4.16	3.95	8.9	8.75	14.92	14.24	14.22	14.19	15.35	12.37
BaO	0	0	0	0	0	0	0	0	0	0	0	0	0	0
Na_2O	3.26	5.17	3.7	3.03	8.63	9.15	6.25	6.2	2.61	3.13	2.98	2.93	2.37	3.95
K_2O	0.36	0.78	0.25	0.04	0.42	0.35	0.21	0.32	0.27	0.19	0.18	0.25	0.24	0.38
Total	100	100	100	100	100	100	100	100	100	100	100	100	100	100
Si	2.29	2.59	2.31	2.26	2.84	2.76	2.52	2.54	2.29	2.24	2.32	2.33	2.28	2.35
Ti	0.02	0.03	0.01	0.01	0.01	0.01	0.00	0.01	0.00	0.01	0.01	0.01	0.00	0.01
Al	1.60	1.25	1.60	1.68	1.16	1.19	1.43	1.40	1.69	1.69	1.65	1.64	1.72	1.56
Cr	0.01	0.01	0.01	0.01	0.01	0.00	0.00	0.01	0.00	0.00	0.00	0.01	0.00	0.01
Fe^{3+}	0.00	0.00	0.00	0.00	0.00	0.00	0.00	0.00	0.00	0.00	0.00	0.00	0.00	0.00
Fe^{2+}	0.04	0.08	0.03	0.03	0.01	0.00	0.01	0.01	0.03	0.02	0.03	0.04	0.02	0.04
Mn	0.01	0.01	0.01	0.01	0.01	0.00	0.01	0.00	0.00	0.00	0.01	0.00	0.00	0.00
Mg	0.06	0.12	0.05	0.04	0.00	0.05	0.05	0.05	0.00	0.06	0.00	0.00	0.00	0.06
Ca	0.67	0.42	0.64	0.69	0.20	0.19	0.43	0.42	0.73	0.69	0.70	0.70	0.75	0.60
Ba	0.00	0.00	0.00	0.00	0.00	0.00	0.00	0.00	0.00	0.00	0.00	0.00	0.00	0.00
Na	0.29	0.46	0.33	0.27	0.75	0.78	0.54	0.54	0.23	0.28	0.27	0.26	0.21	0.35
K	0.02	0.05	0.01	0.00	0.02	0.02	0.01	0.02	0.02	0.01	0.01	0.01	0.01	0.02
Total														
	mole %	mole %	mole %	mole %	mole %	mole %	mole %	mole %	mole %	mole %	mole %	mole %	mole %	mole %
An	68.3	45.9	65.2	71.7	20.5	18.9	43.5	43.0	74.7	70.7	71.7	71.7	77.0	61.9
Ab	29.5	49.2	33.3	28.0	77.0	79.1	55.3	55.1	23.7	28.1	27.2	26.8	21.5	35.8
Or	2.1	4.9	1.5	0.2	2.5	2.0	1.2	1.9	1.6	1.1	1.1	1.5	1.4	2.3

Area	Marshall Valley														
Sample	21-01-15 P19b														
Clast N°	clast8		clast7		clast6		Clast4		Clast5		Clast 3		Clast1	Clast2	
	pl1(g)		pl1 (g)	pl2 (g)	pl1	pl2	pl1	pl2	pl1 (g)	pl2 (g)	pl1 (g)	pl2	pl1	pl1	pl2
Oxides (Wt%)	core	rim													
SiO_2	52.05	51.61	54.25	51.14	62.33	61.56	49.53	50.22	45.29	47.16	50.12	51.68	55.29	47.54	47.63
TiO_2	0.4	0.48	0.26	0.38	0.09	0	0.23	0.21	0.22	0.15	0.4	0.33	0	0	0.15
Al_2O_3	29.26	29.43	28.29	30.41	23.54	23.83	30.71	30.3	33.44	32.77	30.22	29.66	27.56	32.74	32.17
Cr_2O_3	0.14	0.19	0.15	0.16	0.11	0.15	0	0	0.07	0.12	0.15	0.13	0	0.12	0.1
Fe_2O_3	0	0	0	0	0	0	0	0	0	0	0	0	0	0	0
FeO	1.01	1.09	0.69	0.72	0.11	0.29	0.78	0.64	0.77	0.95	0.73	0.84	0.09	0.59	0.51
MnO	0.09	0.23	0.16	0.14	0.06	0.19	0	0	0.18	0.11	0.05	0.21	0.14	0.07	0.05
MgO	0.12	0.13	0.07	0	0	0	0.88	0.91	0.88	0	0.83	0	0.89	0	0.88
CaO	12.97	13.27	11.38	14.29	5.8	5.79	14.06	13.57	17.2	16.94	13.44	13.33	9.7	17.41	15.73
BaO	0	0	0	0	0	0	0	0	0	0	0	0	0	0	0
Na_2O	3.46	3.21	4.35	2.45	7.68	7.8	3.43	3.85	1.75	1.58	3.67	3.45	6.06	1.38	2.49
K_2O	0.5	0.37	0.41	0.31	0.28	0.4	0.39	0.29	0.18	0.22	0.39	0.37	0.27	0.14	0.29
Total	100	100	100	100	100	100	100	100	100	100	100	100	100	100	100
Si	2.38	2.37	2.47	2.36	2.79	2.75	2.25	2.28	2.08	2.18	2.28	2.36	2.47	2.20	2.17
Ti	0.01	0.02	0.01	0.01	0.00	0.00	0.01	0.01	0.01	0.01	0.01	0.01	0.00	0.00	0.01
Al	1.58	1.59	1.52	1.65	1.24	1.25	1.64	1.62	1.81	1.78	1.62	1.60	1.45	1.78	1.73
Cr	0.01	0.01	0.01	0.01	0.00	0.01	0.00	0.00	0.00	0.00	0.01	0.00	0.00	0.00	0.00
Fe^{3+}	0.00	0.00	0.00	0.00	0.00	0.00	0.00	0.00	0.00	0.00	0.00	0.00	0.00	0.00	0.00
Fe^{2+}	0.04	0.04	0.03	0.03	0.00	0.01	0.03	0.02	0.03	0.04	0.03	0.03	0.00	0.02	0.02
Mn	0.00	0.01	0.01	0.01	0.00	0.01	0.00	0.00	0.01	0.00	0.00	0.01	0.01	0.00	0.00
Mg	0.01	0.01	0.00	0.00	0.00	0.00	0.06	0.06	0.06	0.00	0.06	0.00	0.06	0.00	0.06
Ca	0.64	0.65	0.55	0.71	0.28	0.28	0.68	0.66	0.84	0.84	0.65	0.65	0.46	0.86	0.77
Ba	0.00	0.00	0.00	0.00	0.00	0.00	0.00	0.00	0.00	0.00	0.00	0.00	0.00	0.00	0.00
Na	0.31	0.29	0.38	0.22	0.67	0.68	0.30	0.34	0.16	0.14	0.32	0.31	0.53	0.12	0.22
K	0.03	0.02	0.02	0.02	0.02	0.02	0.02	0.02	0.01	0.01	0.02	0.02	0.02	0.01	0.02
Total															
	mole %	mole %	mole %	mole %	mole %	mole %	mole %	mole %	mole %	mole %	mole %	mole %	mole %	mole %	mole %
An	65.4	68.0	57.6	74.8	29.0	28.4	67.8	65.0	83.6	84.4	65.4	66.6	46.2	86.7	76.4
Ab	31.6	29.8	39.9	23.2	69.4	69.3	29.9	33.4	15.4	14.3	32.3	31.2	52.3	12.4	21.9
Or	3.0	2.3	2.5	1.9	1.7	2.3	2.2	1.7	1.0	1.3	2.3	2.2	1.5	0.8	1.7

Area	Marshall Valley			Marshall Valley											
Sample	21-01-15 P21b			21-01-15 P21d											
Clast N°	Clast 14	Clast 7	Clast 11	Clast 11	Clast 6		Clast 5		Clast 7		Clast 8		Clast 10		Clast 13
	Pl1	Pl2	Pl3	Pl5	Pl2	Pl3	Pl4	Pl6	Pl1	Pl4	Pl4	Pl3	Pl8	Pl9	Pl3
Oxides (Wt%)															
SiO_2	51.96	50.56	53.89	49.96	55.27	66.01	65.99	66.53	63.94	63.24	51.02	48.48	65.37	47.67	52.94
TiO_2	0.26	0.4	0.19	0.41	0.41	0.26	0.36	0.2	0.51	0.59	0.17	0.31	0.18	0.21	0.3
Al_2O_3	29.6	29.84	28.72	30.58	27.02	18.68	19.05	18	21.43	21.62	30.83	29.67	19.58	30.51	28.6
Cr_2O_3	0.11	0.12	0.15	0.18	0.1	0.12	0.04	0.12	0.09	0.21	0.1	0.29	0.09	0.15	0.13
Fe_2O_3	0	0	0	0	0	0	0	0	0	0	0	0	0	0	0
FeO	0.59	0.76	0.71	0.67	0.61	0.41	0.26	0.67	0.1	0.78	0.82	1.03	0.41	0.76	0.5
MnO	0.05	0.15	0.15	0.18	0.13	0.2	0.06	0.06	0.05	0.14	0.15	0.29	0.11	0.12	0
MgO	0.21	0.82	0.83	0.79	0.85	0.65	0.66	0.7	0.72	0.77	0.91	0.7	0.68	0.73	0.87
CaO	13.26	13.34	10.01	13.48	9.03	0.58	0.74	0.28	2.23	2.65	12.38	0.33	0.75	0.64	11.57
BaO	0	0	0	0	0	0	0	0	0	0	0	0	0	0	0
Na_2O	3.58	3.59	5.03	3.41	4.96	7.37	7.49	7.19	7.86	7.54	3.36	16.34	4.99	16.42	4.56
K_2O	0.38	0.41	0.32	0.35	1.63	5.72	5.35	6.26	3.07	2.46	0.26	2.56	7.83	2.79	0.52
Total	100	100	100	100.01	100.01	100	100	100.01	100	100	100	100	99.99	100	99.99
Si	2.37	2.30	2.43	2.27	2.50	2.95	2.94	2.97	2.84	2.83	2.32	2.00	2.96	1.96	2.39
Ti	0.01	0.01	0.01	0.01	0.01	0.01	0.01	0.01	0.02	0.02	0.01	0.01	0.01	0.01	0.01
Al	1.59	1.60	1.53	1.64	1.44	0.98	1.00	0.95	1.12	1.14	1.65	1.44	1.04	1.48	1.52
Cr	0.00	0.00	0.01	0.01	0.00	0.00	0.00	0.00	0.00	0.01	0.00	0.01	0.00	0.00	0.00
Fe^{3+}	0.00	0.00	0.00	0.00	0.00	0.00	0.00	0.00	0.00	0.00	0.00	0.00	0.00	0.00	0.00
Fe^{2+}	0.02	0.03	0.03	0.03	0.02	0.02	0.01	0.03	0.00	0.03	0.03	0.04	0.02	0.03	0.02
Mn	0.00	0.01	0.01	0.01	0.00	0.01	0.00	0.00	0.00	0.01	0.01	0.01	0.00	0.00	0.00
Mg	0.01	0.06	0.06	0.05	0.06	0.04	0.04	0.05	0.05	0.05	0.06	0.04	0.05	0.04	0.06
Ca	0.65	0.65	0.48	0.66	0.44	0.03	0.04	0.01	0.11	0.13	0.60	0.01	0.04	0.03	0.56
Ba	0.00	0.00	0.00	0.00	0.00	0.00	0.00	0.00	0.00	0.00	0.00	0.00	0.00	0.00	0.00
Na	0.32	0.32	0.44	0.30	0.43	0.64	0.65	0.62	0.68	0.65	0.30	1.31	0.44	1.31	0.40
K	0.02	0.02	0.02	0.02	0.09	0.33	0.30	0.36	0.17	0.14	0.02	0.13	0.45	0.15	0.03
Total															
	mole %	mole %	mole %	mole %	mole %	mole %	mole %	mole %	mole %	mole %	mole %	mole %	mole %	mole %	mole %
An	65.7	65.6	51.4	67.2	45.3	2.8	3.6	1.3	11.1	13.8	66.0	1.9	3.9	1.9	56.6
Ab	32.1	32.0	46.7	30.8	45.0	64.3	65.6	62.7	70.7	71.0	32.4	88.2	47.3	88.2	40.4
Or	2.2	2.4	2.0	2.1	9.7	32.9	30.8	35.9	18.2	15.2	1.6	9.9	48.8	9.9	3.0

Area	Miers Valley							Taylor Valley				
Sample	21-01-15 P16c							22-01-15-P15b				
Clast N°	Clast 8		Clast 10	Clast 6	Clast 1		Clast 5	Clast1	Clast2			Clast5
	Pl4	Pl5	Pl5	Pl3	Pl1	Pl3	Pl3	Pl1	Pl1		Pl2	Pl1
Oxides (Wt%)									core	rim		
SiO_2	49.58	49.78	50.32	52.88	56.14	56.71	52.06	47.42	54.93	57.35	56.39	54.47
TiO_2	0.31	0.31	0.49	0.49	0.42	0.23	0.46	0.22	0.23	0.26	0	0
Al_2O_3	30.49	30.82	29.89	28.5	26.3	26.35	28.86	33.25	27.72	24.67	26.77	27.51
Cr_2O_3	0.13	0.1	0.13	0.15	0.13	0.13	0.28	0				
Fe_2O_3	0	0	0	0	0	0	0	0	0	0	0	0
FeO	0.93	0.77	0.95	1.06	0.52	0.49	0.85	0.35	0.58	2.52	0.93	0.67
MnO	0.18	0.13	0.37	0.16	0.23	0.11	0.4	0.15	0	0	0.21	0
MgO	0.91	0.89	0.97	0.42	0.72	0.7	1	0	0	1.28	0	0.88
CaO	13.78	13.49	12.88	12.34	9	8.51	11.29	17.22	11.73	7	11.29	10.86
BaO	0	0	0	0	0	0	0	0	0	0	0	0
Na_2O	3.23	3.35	3.52	3.64	5.52	5.91	4.17	1.23	4.34	6.52	3.99	5.11
K_2O	0.46	0.36	0.48	0.37	1.03	0.88	0.64	0.15	0.48	0.41	0.42	0.5
Total	100	100	100	100	100	100	100	100	100	100	100	100
Si	2.26	2.26	2.29	2.42	2.53	2.55	2.36	2.19	2.50	2.58	2.58	2.45
Ti	0.01	0.01	0.02	0.02	0.01	0.01	0.02	0.01	0.01	0.01	0.00	0.00
Al	1.64	1.65	1.60	1.54	1.40	1.40	1.54	1.81	1.49	1.31	1.44	1.46
Cr	0.00	0.00	0.00	0.01	0.00	0.00	0.01	0.00	0.00	0.00	0.00	0.00
Fe^{3+}	0.00	0.00	0.00	0.00	0.00	0.00	0.00	0.00	0.00	0.00	0.00	0.00
Fe^{2+}	0.04	0.03	0.04	0.04	0.02	0.02	0.03	0.01	0.02	0.09	0.04	0.03
Mn	0.01	0.01	0.01	0.01	0.01	0.00	0.02	0.01	0.00	0.00	0.01	0.00
Mg	0.06	0.06	0.07	0.03	0.05	0.05	0.07	0.00	0.00	0.09	0.00	0.06
Ca	0.67	0.66	0.63	0.60	0.43	0.41	0.55	0.85	0.57	0.34	0.55	0.52
Ba	0.00	0.00	0.00	0.00	0.00	0.00	0.00	0.00	0.00	0.00	0.00	0.00
Na	0.29	0.30	0.31	0.32	0.48	0.51	0.37	0.11	0.38	0.57	0.35	0.45
K	0.03	0.02	0.03	0.02	0.06	0.05	0.04	0.01	0.03	0.02	0.02	0.03
Total												
	mole %	mole %	mole %	mole %	mole %	mole %	mole %	mole %	mole %	mole %	mole %	mole %
An	68.3	67.5	65.0	63.7	44.5	42.0	57.6	87.7	58.2	36.3	59.4	52.5
Ab	29.0	30.3	32.1	34.0	49.4	52.8	38.5	11.3	39.0	61.2	38.0	44.7
Or	2.7	2.1	2.9	2.3	6.1	5.2	3.9	0.9	2.8	2.5	2.6	2.9

Area	Wright Valley									
Sample	20-01-15-P1b									
Clast N°	Clast8	Clast 7	Clast5	Clast6	Clast16	Clast3	Clast4	Clast10	Clast9	Clast13
	pl1	pl1	pl1	pl1	pl2	pl1	pl1	pl1	pl1	pl1
Oxides (Wt%)										
SiO_2	60.07	59.83	59.46	60.26	60.72	57.64	57.53	56.07	49.93	56.93
TiO_2	0.37	0.25	0.19	0.21	0.12	0	0	0.15	0	0.23
Al_2O_3	24.59	25.01	24.64	24.29	23.91	26.33	26.12	27.31	31.87	26.22
Cr_2O_3	0.12	0.09	0.25	0.17	0.15	0.07	0.15	0.13	0	0.12
Fe_2O_3	0	0	0	0	0	0	0	0	0	0
FeO	0.23	0.32	0.44	0.28	0.28	0.05	0.23	0.33	0.17	0.22
MnO	0.07	0	0.21	0.19	0.21	0	0.16	0.13	0	0.26
MgO	0	0	0	0.17	0.69	0.87	0.79	0	0	0.7
CaO	7.54	7.1	7.58	6.97	5.73	8.2	8.35	10.44	15.53	8.42
BaO	0	0	0	0	0	0	0	0	0	0
Na_2O	6.85	6.92	6.94	7.08	8.05	6.67	6.48	5.11	2.42	6.53
K_2O	0.16	0.48	0.29	0.38	0.15	0.17	0.19	0.33	0.07	0.37
Total	100	100	100	100	100	100	100	100	100	100
Si	2.70	2.68	2.67	2.70	2.70	2.57	2.58	2.54	2.29	2.55
Ti	0.01	0.01	0.01	0.01	0.00	0.00	0.00	0.01	0.00	0.01
Al	1.30	1.32	1.30	1.28	1.25	1.39	1.38	1.46	1.72	1.38
Cr	0.00	0.00	0.01	0.01	0.01	0.00	0.01	0.00	0.00	0.00
Fe^{3+}	0.00	0.00	0.00	0.00	0.00	0.00	0.00	0.00	0.00	0.00
Fe^{2+}	0.01	0.01	0.02	0.01	0.01	0.00	0.01	0.01	0.01	0.01
Mn	0.00	0.00	0.01	0.01	0.01	0.00	0.01	0.00	0.00	0.01
Mg	0.00	0.00	0.00	0.01	0.05	0.06	0.05	0.00	0.00	0.05
Ca	0.36	0.34	0.36	0.33	0.27	0.39	0.40	0.51	0.76	0.40
Ba	0.00	0.00	0.00	0.00	0.00	0.00	0.00	0.00	0.00	0.00
Na	0.60	0.60	0.60	0.62	0.69	0.58	0.56	0.45	0.22	0.57
K	0.01	0.03	0.02	0.02	0.01	0.01	0.01	0.02	0.00	0.02
Total										
	mole %	mole %	mole %	mole %	mole %	mole %	mole %	mole %	mole %	mole %
An	37.5	35.2	37.0	34.4	28.0	40.1	41.1	52.0	77.7	40.7
Ab	61.6	62.0	61.3	63.3	71.1	59.0	57.8	46.1	21.9	57.1
Or	0.9	2.8	1.7	2.2	0.9	1.0	1.1	2.0	0.4	2.1